

Encyclopædia Inflationaris

Jérôme Martin,^a Christophe Ringeval^b and Vincent Vennin^a

^aInstitut d'Astrophysique de Paris, UMR 7095-CNRS, Université Pierre et Marie Curie, 98bis boulevard Arago, 75014 Paris (France)

^bCentre for Cosmology, Particle Physics and Phenomenology, Institute of Mathematics and Physics, Louvain University, 2 Chemin du Cyclotron, 1348 Louvain-la-Neuve (Belgium)

E-mail: jmartin@iap.fr, christophe.ringeval@uclouvain.be, vennin@iap.fr

Abstract. The current flow of high accuracy astrophysical data, among which are the Cosmic Microwave Background (CMB) measurements by the Planck satellite, offers an unprecedented opportunity to constrain the inflationary theory. This is however a challenging project given the size of the inflationary landscape which contains hundreds of different scenarios. A reasonable approach is to consider the simplest models first, namely the slow-roll single field models with minimal kinetic terms, unless the data drive us to more complicated ones. This still leaves us with a very populated landscape, the exploration of which requires new and efficient strategies. It has been customary to tackle this problem by means of approximate model independent methods while a more ambitious alternative is to study the inflationary scenarios one by one. We have developed the new publicly available runtime library **ASPIC**¹ to implement this last approach. The **ASPIC** code provides all routines needed to quickly derive reheating consistent observable predictions within this class of scenarios. **ASPIC** has been designed as an evolutive code which presently supports 64 different models, a number that may be compared with three or four representing the present state of the art. In this paper, for each of the **ASPIC** models, we present and collect new results in a systematic manner, thereby constituting the first *Encyclopædia Inflationaris*. Finally, we discuss how this procedure and **ASPIC** could be used to determine the best model of inflation by means of Bayesian inference.

Keywords: Cosmic Inflation, Slow-Roll, Reheating, Cosmic Microwave Background, Asplic

¹<http://cp3.irmp.ucl.ac.be/~ringeval/aspic.html>

Contents

1	Introduction	1
1.1	Methodology	3
1.2	The ASPIC library	10
1.3	New results	11
2	Basic Equations	16
2.1	The slow-roll phase	16
2.2	The reheating phase	20
3	Zero Parameter Models	23
3.1	Higgs Inflation (HI)	23
4	One Parameter Models	29
4.1	Radiatively Corrected Higgs Inflation (RCHI)	29
4.2	Large Field Inflation (LFI)	36
4.3	Mixed Large Field Inflation (MLFI)	38
4.4	Radiatively Corrected Massive Inflation (RCMI)	42
4.5	Radiatively Corrected Quartic Inflation (RCQI)	45
4.6	Natural Inflation (NI)	47
4.7	Exponential SUSY Inflation (ESI)	50
4.8	Power Law Inflation (PLI)	52
4.9	Kähler Moduli Inflation I (KMII)	55
4.10	Horizon Flow Inflation at first order (HF1I)	60
4.11	Coleman-Weinberg Inflation (CWI)	63
4.12	Loop Inflation (LI)	68
4.13	$(R + R^p)$ Inflation (RpI)	71
4.14	Double-Well Inflation (DWI)	74
4.15	Mutated Hilltop Inflation (MHI)	78
4.16	Radion Gauge Inflation (RGI)	81
4.17	MSSM Inflation (MSSMI)	83
4.18	Renormalizable Inflection Point Inflation (RIPI)	87
4.19	Arctan Inflation (AI)	91
4.20	Constant n_s A Inflation (CNAI)	95
4.21	Constant n_s B Inflation (CNBI)	99
5	Two Parameters Models	103
5.1	Small Field Inflation (SFI)	103
5.2	Intermediate Inflation (II)	106
5.3	Kähler Moduli Inflation II (KMIII)	111
5.4	Logamediate Inflation (LMI)	116
5.5	Twisted Inflation (TWI)	120
5.6	Generalized MSSM Inflation (GMSSMI)	124
5.7	Brane SUSY breaking Inflation (BSUSYBI)	128
5.8	Tip Inflation (TI)	131

5.9	β exponential inflation (BEI)	134
5.10	Pseudo Natural Inflation (PSNI)	136
5.11	Non Canonical Kähler Inflation (NCKI)	140
5.12	Constant Spectrum Inflation (CSI)	143
5.13	Orientifold Inflation (OI)	145
5.14	Constant n_s C Inflation (CNCI)	147
5.15	Supergravity Brane Inflation (SBI)	150
5.16	Spontaneous Symmetry Breaking Inflation (SSBI)	153
6	Three parameters Models	159
6.1	Running-mass Inflation (RMI)	159
6.2	Valley Hybrid Inflation (VHI)	163
6.3	Dynamical Supersymmetric Inflation (DSI)	167
6.4	Generalized Mixed Inflation (GMLFI)	171
6.5	Logarithmic Potential Inflation (LPI)	173
6.6	Constant n_s D Inflation (CNDI)	175
7	Conclusions	178
A	Reheating consistent slow-roll predictions	181
A.1	Higgs Inflation (HI)	181
A.2	Radiatively Corrected Higgs Inflation (RCHI)	182
A.3	Large Field Inflation (LFI)	183
A.4	Mixed Large Field Inflation (MLFI)	184
A.5	Radiatively Corrected Massive Inflation (RCMI)	185
A.6	Radiatively Corrected Quartic Inflation (RCQI)	186
A.7	Natural Inflation (NI)	188
A.8	Exponential SUSY Inflation (ESI)	189
A.9	Power Law Inflation (PLI)	191
A.10	Kähler Moduli Inflation I (KMII)	192
A.11	Horizon Flow Inflation at first order (HF1I)	193
A.12	Coleman-Weinberg Inflation (CWI)	194
A.13	Loop Inflation (LI)	196
A.14	Double Well Inflation (DWI)	198
A.15	Mutated Hilltop Inflation (MHI)	199
A.16	Radion Gauge Inflation (RGI)	200
A.17	MSSM Inflation (MSSMI)	201
A.18	Renormalizable Inflection Point Inflation (RIPI)	202
A.19	Arctan Inflation (AI)	203
A.20	Constant n_s A Inflation (CNAI)	204
A.21	Constant n_s B Inflation (CNBI)	205
A.22	Small Field Inflation (SFI)	206
A.23	Intermediate Inflation (II)	209
A.24	Kähler Moduli Inflation II (KMIII)	210
A.25	Logamediate Inflation (LMI)	211
A.26	Twisted Inflation (TWI)	217
A.27	GMSSM Inflation (GMSSMI)	218

A.28 Brane SUSY breaking Inflation (BSUSYBI)	220
A.29 Tip Inflation (TI)	221
A.30 β Exponential Inflation (BEI)	224
A.31 Pseudo Natural Inflation (PSNI)	225
A.32 Non Canonical Kähler Inflation (NCKI)	226
A.33 Constant Spectrum Inflation (CSI)	228
A.34 Orientifold Inflation (OI)	230
A.35 Constant n_s C Inflation (CNCI)	231
A.36 Supergravity Brane Inflation (SBI)	232
A.37 Spontaneous Symmetry Breaking Inflation 1 (SSBII)	234
A.38 Spontaneous Symmetry Breaking Inflation 2 (SSBI2)	237
A.39 Spontaneous Symmetry Breaking Inflation 3 (SSBI3)	238
A.40 Spontaneous Symmetry Breaking Inflation 4 (SSBI4)	241
A.41 Spontaneous Symmetry Breaking Inflation 5 (SSBI5)	244
A.42 Spontaneous Symmetry Breaking Inflation 6 (SSBI6)	247
A.43 Running Mass Inflation 1 (RMI1)	250
A.44 Running Mass Inflation 2 (RMI2)	251
A.45 Running Mass Inflation 3 (RMI3)	252
A.46 Running Mass Inflation 4 (RMI4)	253
A.47 Valley Hybrid Inflation (VHI)	254
A.48 Dynamical Supersymmetric Inflation (DSI)	259
A.49 Generalized Mixed Inflation (GMLFI)	262
A.50 Logarithmic Potential Inflation 1 (LPI1)	265
A.51 Logarithmic Potential Inflation 2 (LPI2)	268
A.52 Logarithmic Potential Inflation 3 (LPI3)	271
A.53 Constant n_s D Inflation (CNDI)	274

1 Introduction

The theory of inflation [1–4] represents a cornerstone of the standard model of modern cosmology (the “hot Big-Bang model” of Lemaître and Friedmann) [5–8]. By definition, it is a phase of accelerated expansion which is supposed to take place in the very early universe, at very high energy (between 200 and 10^{15} GeV). Inflation allows us to understand several puzzles that plagued the pre-inflationary standard model (before 1981) and that could not be understood otherwise. Without inflation, the standard model of cosmology would remain incomplete and highly unsatisfactory. The most spectacular achievement of inflation is that, combined with quantum mechanics, it provides a convincing mechanism for the origin of the cosmological fluctuations (the seeds of the galaxies and of the Cosmic Microwave Background - CMB - anisotropies) and predicts that their spectrum should be almost scale invariant (i.e. equal power on all spatial scales) [9–17] which is fully consistent with the observations. Let us notice in passing that this part of the scenario is particularly remarkable since it combines General Relativity and Quantum Mechanics [7, 8, 18–24]. Given all these spectacular successes and given the fact that, despite many efforts, inflation has not been superseded by its various challengers [25–53], this scenario has gradually become a crucial part of modern cosmology. As can be seen in Fig. 1, the number of papers devoted to this topic and published each year is inflating since the advent of inflation.

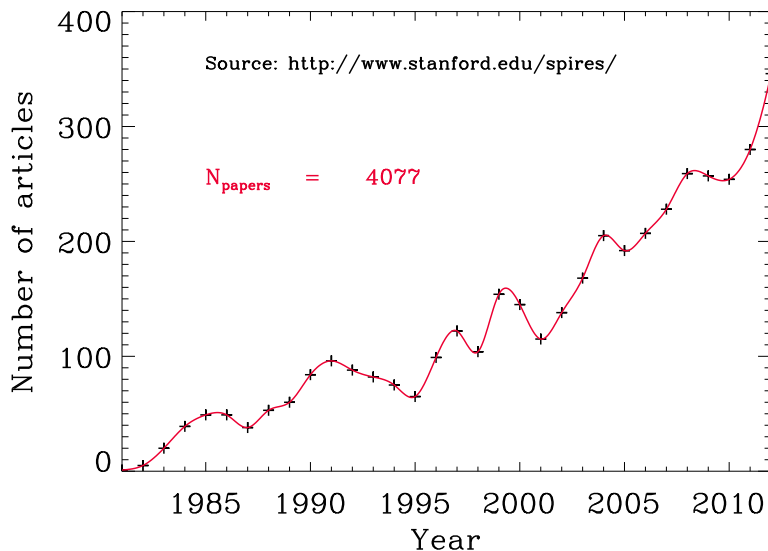


Figure 1. Number of articles containing the word “inflation” and its variations (i.e. “inflating”, “inflationary”, etc . . .) in its title published each year since the advent of inflation. The total number is estimated to be 4077 papers.

In order to produce a phase of inflation within General Relativity, the matter content of the universe has to be dominated by a fluid with negative pressure. At very high energy, the correct description of matter is field theory, the prototypical example being a scalar field since it is compatible with the symmetries implied by the cosmological principle. Quite remarkably, if the potential of this scalar field is sufficiently flat (in fact, more precisely, its logarithm) so that the field moves slowly, then the corresponding pressure is negative. This is why it is believed that inflation is driven by one (or several) scalar field(s). For obvious reasons, this scalar field was given the name “inflaton”. However, the physical nature of the inflaton and its relation with the standard model of particle physics and its extensions remain elusive. Moreover the shape of its potential is not known except, of course, that it must be sufficiently flat. This is not so surprising since, as mentioned above, the inflationary mechanism is supposed to take place at very high energies in a regime where particle physics is not known and has not been tested in accelerators.

Another crucial aspect of the inflationary scenario is how it ends and how it is connected to the subsequent hot Big-Bang phase. It is believed that, after the slow-roll period, the field oscillates at the bottom of its potential, or undergoes tachyonic preheating, but finally decays into radiation. In this way, inflation is smoothly connected to the radiation-dominated epoch [54–63]. Unfortunately, very little is observationally known on this so-called reheating period. Let us stress that adiabatic initial conditions, as favored from the current CMB measurements, naturally stem from such a setup within single field models. Another constraint is that the reheating temperature, T_{reh} , must be higher than the nucleosynthesis scale (i.e. a few MeV). If, however, one restricts oneself to specific models, then one can obtain better bounds on T_{reh} , as was recently shown for the first time in Ref. [64]. But, so far, these constraints concern a few models only.

We see that, despite the fact that it has become a cornerstone, inflation is not as observationally known as the other parts of the standard model of Cosmology. However, there is now a flow of increasingly accurate astrophysical data which gives us a unique opportunity to learn more about inflation. In particular, the Planck satellite [65], data should play a crucial role in this process. The mission complements and improves upon observations made by the NASA WMAP satellite [66, 67] and is a major source of information relevant to several cosmological issues and, of course, to inflation. But the flow of new data does not only concern the CMB. The Supernovae projects [68–71] continue to measure the distances to the nearby exploding SN1A stars while the large scale galaxy surveys such as the Sloan Digital Sky Survey (SDSS) [72, 73] are providing an unprecedented picture of the structure of the universe. SDSS is planned till 2014 and has recently provided the measure of the so-called Baryonic Acoustic Oscillations (BAO). They are the red-shifted version of the acoustic oscillations observed in the CMB anisotropies which have been transferred to the galaxy power spectrum. The “level arm” in length scales between CMB and galaxy power spectra increases the sensitivity to the small deviations from scale invariance, and thus should be extremely powerful to constrain inflationary models. For this reason, the future Euclide satellite will be another step forward in our understanding of inflation [74]. The CMB small angular scales of Planck are also complemented by balloon-borne and ground-based microwave telescopes such as the Atacama Cosmology Telescope (ACT) [75, 76] or the South Pole Telescope (SPT) [77, 78]. In a foreseeable future, the last bit of yet unexplored length scales are expected to be unveiled by the 21cm cosmological telescopes. These ones will be sensitive to the red-shifted 21cm line absorbed by hydrogen clouds before the formation of galaxies [79–85]. With such data, we will have a complete tomography of the universe history from the time of CMB emission at the surface of last scattering to the distribution of galaxies today.

The main goal of this article is to develop methods that will allow us to constrain the inflationary scenario at a level matching the accuracy of these new data. Since we have now entered the era of massive multi-data analysis, the project aims at a change of scale compared to previous approaches. In particular, one way to deal with this question is to perform systematic and “industrial” studies of this issue. Our ability to see through the inflationary window turns the early universe into a laboratory for ultra-high energy physics, at scales entirely inaccessible to conventional experimentation. In other words, this window offers a unique opportunity to learn about the very early universe and about physics in a regime that cannot be tested otherwise, even in accelerators such as the Large Hadron Collider (LHC).

1.1 Methodology

Let us now discuss how, in practice, the above described goals can be reached. One issue often raised is that, since there are (literally) a few hundreds different scenarios, it is difficult to falsify inflation. This is, however, not a very convincing argument since different models belong to different classes and usually do differ in their observable predictions. They can thus be observationally distinguished. A natural way to proceed is therefore to test inflationary models step by step, starting with the simplest scenarios. This is consistent with the Occam’s razor point of view and the way inference is achieved within Bayesian statistics (see below). With this in mind, we can classify models in three different broad categories: single-field inflation (category I), multiple-field inflation (category II) and models where matter is not described by a scalar field as, for instance, vector inflation [86] and/or

chromo-natural inflation [87] (category III). Within each category, one could further identify various sub-categories. For example, within category I, the scalar field can possess a minimal kinetic term and a smooth potential (category IA), a minimal kinetic term and a potential with features (category IB), a non-minimal kinetic term with a smooth potential (category IC) or a non-minimal kinetic term and a potential with features (category ID). The same four sub-categories can also be defined within category II (for instance, multiple Dirac Born Infeld -DBI- field inflation [88–90] belongs to category IIC) and so on. As already mentioned, each category leads to different predictions. For instance, all models of category IA predict a negligible level of non-Gaussianities [91–95] while, on the contrary, models of categories IB-ID yield non-negligible non-Gaussianities [96–110]; models belonging to IB and to IC, or II, may not predict exactly the same type of non-Gaussianities [111, 112], etc . . . In this context, a reasonable method is to start with the IA-models, unless the data force us to directly consider more complicated scenarios. That should be the case if, for instance, a non-vanishing primordial f_{NL} , the parameter characterizing the amplitude of the bispectrum, is detected. This is not the case at the time of writing. Following category IA, one should then treat categories IB-ID, then category II and so on. In this way, one can falsify inflation step by step, in a Bayesian motivated fashion.

Bayesian inference for inflation requires some cosmological data that are sensitive to it, such as the ones enumerated above. For the purpose of illustration, let us consider the CMB angular power spectrum. Cosmological measurements give us a set of numbers, C_ℓ^{meas} , that we are able to calculate theoretically within an inflationary model. This means that we know the functions $C_\ell^{\text{th}} \equiv C_\ell^{\text{th}}(\theta_{\text{stand}}, \theta_{\text{inf}})$, where θ_{stand} represents a set of parameters describing post-inflationary physics, i.e. $\theta_{\text{stand}} = (h, \Omega_\Lambda, \Omega_{\text{dm}}, \dots)$ and θ_{inf} a set of parameters describing inflationary physics. We are interested in constraining the values of those parameters, especially the θ_{inf} 's. Within a given experiment, one is given a likelihood, or an effective chi-squared $\chi^2(\theta_{\text{stand}}, \theta_{\text{inf}})$, encoding all the underlying uncertainties. In a frequentist approach, the searched values of θ_{stand} and θ_{inf} would be chosen at the best fit, i.e. those verifying $\partial\chi^2/\partial\theta = 0$. In a Bayesian approach [113], we are interested in determining the posterior distributions of the parameters, using Bayes's theorem

$$P(\theta_{\text{stand}}, \theta_{\text{inf}} | C_\ell^{\text{meas}}) = \frac{1}{\mathcal{N}} \mathcal{L}(C_\ell^{\text{meas}} | \theta_{\text{stand}}, \theta_{\text{inf}}) \pi(\theta_{\text{stand}}, \theta_{\text{inf}}), \quad (1.1)$$

where $\mathcal{L}(C_\ell^{\text{meas}} | \theta_{\text{stand}}, \theta_{\text{inf}}) = e^{-\chi^2(\theta_{\text{stand}}, \theta_{\text{inf}})/2}$ is the likelihood function, $\pi(\theta_{\text{stand}}, \theta_{\text{inf}})$ the prior distribution, describing our prejudices about the values of the parameters before our information is updated, and \mathcal{N} a normalization factor, also called Bayesian evidence. Because we are interested in the inflationary parameters, one has to integrate over the post-inflationary parameters in order to obtain the marginalized probability distribution $P(\theta_{\text{inf}} | C_\ell^{\text{meas}}) = \int P(\theta_{\text{stand}}, \theta_{\text{inf}} | C_\ell^{\text{meas}}) d\theta_{\text{stand}}$. CMB physics also tells us that the multipole moment C_ℓ^{th} can be written as

$$C_\ell^{\text{th}}(\theta_{\text{stand}}, \theta_{\text{inf}}) = \int_0^{+\infty} \frac{dk}{k} j_\ell(kr_{\text{LSS}}) T(k; \theta_{\text{stand}}) \mathcal{P}_\zeta(k; \theta_{\text{inf}}), \quad (1.2)$$

where j_ℓ is a spherical Bessel function, $T(k; \theta_{\text{stand}})$ is the transfer function which describes the evolution of cosmological perturbations during the standard Friedmann-Lemaître eras and \mathcal{P}_ζ is the inflationary power spectrum. As a result, the process of constraining inflation from the C_ℓ^{meas} reduces to the calculation of \mathcal{P}_ζ . The same lines of reasoning could be generalized to any other cosmological observables sourced during inflation, such as higher order correlation functions.

At this stage, there are, a priori, two possibilities. Either one uses a model-independent, necessarily approximate, shape for \mathcal{P}_ζ or, on the contrary, one scans the inflationary landscape, model by model, and for each of them, calculates \mathcal{P}_ζ exactly.

The advantage of working with a model-independent technique is obvious. However, it often requires an approximation scheme that may not be available for all models. In practice, an approximate method, the slow-roll approach, is known for the category IA and for the category IC, see the recent papers [114, 115]. In this case, the set of inflationary parameters θ_{inf} becomes the Hubble flow functions: $\theta_{\text{inf}} = \{\epsilon_n\}$ where the ϵ_n are defined in Eq. (2.3) and the corresponding expression of $\mathcal{P}_\zeta(k; \epsilon_n)$ is provided in Eqs. (2.18), (2.20), (2.21) and (2.22). Assuming some priors $\pi(\epsilon_n)$ on the Hubble flow functions, this method yields the posterior distributions $P(\epsilon_n | C_\ell^{\text{meas}})$ for the Hubble flow functions evaluated at the pivot scale. This approach has already been successfully implemented for the WMAP data in Refs. [64, 116–119].

The second approach is more ambitious. It consists in treating exactly all the inflationary models that have been proposed so far and in a systematic manner. For each model, the power spectrum is determined exactly by means of a mode by mode numerical integration, for instance using the `FieldInf` code¹. Such an approach can also be used with the higher correlation functions with, for instance, the recent release of the `BINGO` code calculating the inflationary bispectrum [120].

In this case, the set of parameters θ_{inf} differs according to the model considered. For instance, Large Field Inflation (LFI) for which $V(\phi) = M^4 (\phi/M_{\text{Pl}})^p$, has $\theta_{\text{inf}} = (M, p)$ while Small Field Inflation (SFI) with $V(\phi) = M^4 [1 - (\phi/\mu)^p]$ has $\theta_{\text{inf}} = (M, p, \mu)$. From `FieldInf` one can then compute $\mathcal{P}_\zeta(k; M, p)$ for LFI and $\mathcal{P}_\zeta(k; M, p, \mu)$ for SFI without any other assumptions than linear perturbation theory and General Relativity. Starting from some priors on the model parameters, e.g. in the case of LFI, $\pi(M)$ and $\pi(p)$, this method allows us to determine the posterior distributions $P(M | C_\ell^{\text{meas}})$ and $P(p | C_\ell^{\text{meas}})$, thereby providing parameter inference about the corresponding inflationary model. This approach, which was successfully implemented for the first time in Refs. [117, 121–123], and subsequently used in Ref. [124], has several advantages that we now discuss.

Firstly, the most obvious advantage is that the result is exact. The slow-roll method is an approximation and, for this reason, remains somehow limited. As mentioned before, there are plethora of models, such as single field models with features or multiple field scenarios, for which a numerical integration is mandatory.

A second reason is that a full numerical approach permits a new treatment of reheating. In the standard approach, the influence of the reheating is only marginally taken into account. Any observable predictions depend on the number of e-folds associated with a reheating era. From the fact that the reheating must proceed after the end of inflation and before the electroweak scale, one can put an order of magnitude bound on this number of e-folds [125]. This causes small uncertainties in the inflationary predictions that were not crucial in the past. However, with the accuracy of the present and future data this question now matters. This is illustrated in Fig. 2 which represents the slow-roll predictions of LFI for which $V(\phi) \propto \phi^p$. Each colored segment represents the range of observable predictions for a given value of p , each point within a segment corresponding to a given number of e-folds for the reheating or, equivalently, to a given reheating temperature T_{reh} . We see that, for relatively small values of p , it is necessary to know the number of e-folds the Universe reheated to decide

¹See <http://theory.physics.unige.ch/~ringeval/fieldinf.html>.

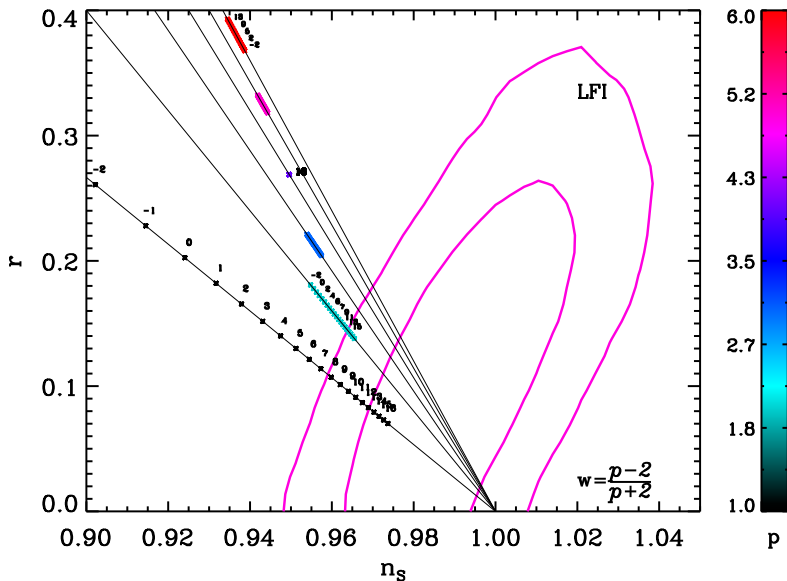


Figure 2. Observational predictions for the LFI models, $V(\phi) \propto \phi^p$, in the plane (n_s, r) (i.e. scalar spectral index and gravity wave contribution) compared to the WMAP data. Each continuous line and each color represent a different value of p . Along each line, each point (i.e. each small “cross”) denotes a different reheating temperature compatible with the constraint $\rho_{\text{end}} > \rho_{\text{reh}} > \rho_{\text{nuc}}$ (the annotations give the logarithm of the reheating temperature in GeV). We see that the details of the reheating stage now matter: along a given line, some reheating temperatures are compatible with the observational constraints while others are not. This means that the CMB observations can now put constraints on T_{reh} .

whether the model is compatible with the data or not. Conversely, the data are becoming so accurate that one can start constraining the reheating epoch. Therefore, instead of viewing the reheating parameters as external source of uncertainties, it is more accurate to include them in the numerical approach and consider they are part of the inflationary model. In its simplest description, the reheating epoch can be modeled as a cosmological fluid with a mean equation of state $\bar{w}_{\text{reh}} > -1/3$. For a simple quadratic potential, one would have $\bar{w}_{\text{reh}} = 0$. In this way, both \bar{w}_{reh} and T_{reh} are added to the inflationary parameters, e.g. we now have $\theta_{\text{inf}} = (M, p, T_{\text{reh}}, \bar{w}_{\text{reh}})$ for LFI, and `FieldInf` computes $\mathcal{P}_\zeta(k; M, p, T_{\text{reh}}, \bar{w}_{\text{reh}})$. Starting from some priors $\pi(T_{\text{reh}})$ and $\pi(\bar{w}_{\text{reh}})$ one can then obtain the corresponding posterior distributions $P(T_{\text{reh}}|C_\ell^{\text{meas}})$ and $P(\bar{w}_{\text{reh}}|C_\ell^{\text{meas}})$. The feasibility of this method has already been demonstrated in Refs. [64, 117] where constraints on the reheating temperature for LFI and SFI have been derived for the first time (see also Ref. [126]). In view of the expected accuracy for the future data, the preheating/reheating era should become a compulsory element of inflationary model testing. This issue plays an important role in the proposal put forward in this article. In addition, let us also emphasize that a proper treatment of the reheating and preheating stages is mandatory in multiple field inflation because they can affect the evolution of \mathcal{P}_ζ on large scales. Only a numerical approach can deal with this problem.

A third advantage of the numerical approach is to address the question of the priors choice in a particularly well-defined way. A crucial aspect of the Bayesian method is that

the result depends on the choice of the priors. Therefore, these ones must be chosen and discussed carefully. In the slow-roll (approximated) approach described before, the priors are chosen on the slow-roll parameters themselves. For instance, a Jeffrey’s prior is typically chosen on ϵ_1 (i.e. uniform prior on $\log \epsilon_1$), as appropriate when the order of magnitude of a parameter is not known. However, from a physical point of view, it is better to choose the priors directly on the parameters of the model, i.e. the parameters of the potential. For instance, several potentials that we will treat are the results of a one-loop calculation, namely a perturbative calculation with the coupling constant playing the role of the small parameter. It is clear that the prior must encode the fact that this parameter is small. With the numerical approach, this is very conveniently done since we directly compute the power spectrum from the potential itself. As another example, let us consider the case of LFI where $\epsilon_1 \simeq p/(4\Delta N_* + p/4)$ (ΔN_* is the number of e-folds between Hubble exit and the end of inflation, see below). Owing to the non-trivial relation between the first slow-roll parameter and p , a Jeffreys’ prior $\pi(\epsilon_1)$ on ϵ_1 implies a complicated prior $\pi(p)$ on p while a natural choice would be a flat prior. Again, implementing the priors directly on the parameters of the model is a more theoretically justified choice. Conversely, who could dispute that, beside the posterior $P(\epsilon_1|C_\ell^{\text{meas}})$, it is theoretically interesting to know the posterior distribution of p , i.e. $P(p|C_\ell^{\text{meas}})$. The exact numerical integration is a reliable technique to obtain such distributions.

The numerical approach, however, has also some disadvantages. Firstly, one needs to specify the inflationary scenarios explicitly and, therefore, the constraints obtained are not model-independent. Although this shortcoming can in fact never be avoided (we always need to make some assumptions even in the slow-roll approach) it may be partially overcome by scanning the complete inflationary landscape. Secondly, and more importantly, it is time consuming since the exact integration of the cosmological perturbations and of the corresponding correlation functions is heavy and can take up to a few minutes for complicated models. Finally, one should expect multiple degeneracies for models having a high number of inflationary parameters since the data have a limited sensitivity to the shape of the primordial observables.

Based on the previous considerations, we conclude that it would be very interesting to have an intermediate method that would allow us to get most of the results that can be derived using the exact numerical approach while being less time consuming and immune to high parameter degeneracies. This is what we suggest in the following. Our strategy is to use the slow-roll approximation in order to skip the numerical calculation of the power spectrum, but, combined with a systematic scan of the whole inflationary landscape and reheating properties. Moreover, since we have argued that inflation should be tested starting with the simplest models first (unless the data force us to move on to more complicated scenarios), our method needs to be implemented for the class of scenarios IA only. More precisely, instead of inferring the posterior distributions of the Hubble flow parameters ϵ_n only, as one would naturally do in the approximate approach discussed before, we take advantage of the fact that the ϵ_n ’s can be computed in terms of the parameters describing the reheating and $V(\phi)$. In particular, for each model, this permits a quick and efficient extraction of the posterior distributions of those parameters.

In our opinion, however, this third technique should not be viewed as a competitor of the two other ones mentioned earlier but rather as complementary and the corresponding results should be compared. Let us also notice that, if, in order to scan all the inflationary scenarios, the full exact numerical approach needs to be carried out at some point, this would

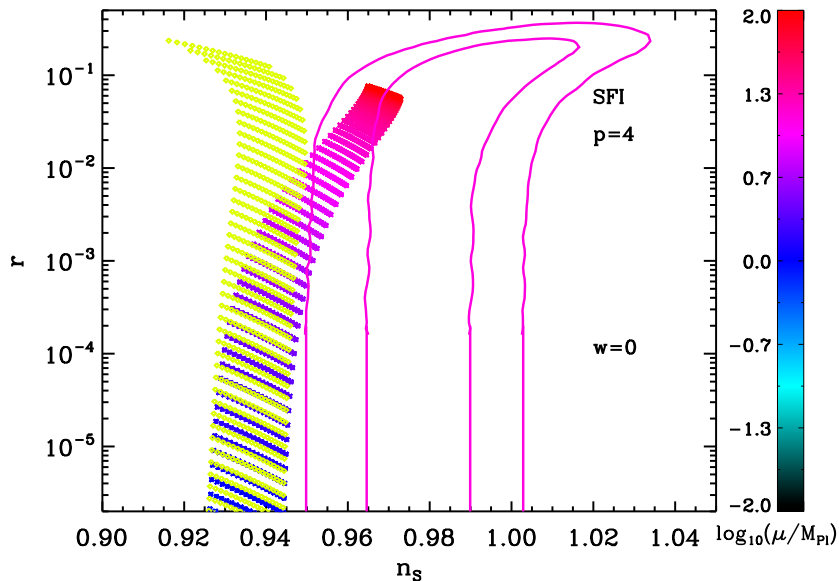


Figure 3. Exact slow-roll predictions for SFI models, $V(\phi) \propto 1 - (\phi/\mu)^4$, compared to the WMAP data. Each colored segment represents a different value of μ , the color bar giving the corresponding range of variation. Each segment is made of different points associated with different reheating temperatures. The yellow-only segments on the left represent the approximated slow-roll predictions. We see that they coincide with the exact predictions for $\mu/m_{\text{Pl}} \ll 1$ but differ in the regime $\mu/m_{\text{Pl}} \gg 1$ where the approximation becomes inaccurate. Moreover, the approximation would indicate that this class of models is disfavored while the correct slow-roll predictions show that, on the contrary, they remain compatible with the data.

by no means render the results derived in the present article useless. Indeed, the slow-roll approach is often a very useful guide of which kind of physics one should expect for a given model (initial conditions, range of the parameters, etc ...). In particular it allows us to understand any eventual parameter degeneracies within the primordial observables. In other words, the slow-roll method is an ideal tool to prepare a full numerical study.

At this point, it is worth making the following remark. The method put forward in this article uses an approximate shape for the power spectrum, namely (k_* is the pivot scale)

$$\mathcal{P}_\zeta(k) \propto a_0(\epsilon_n) + a_1(\epsilon_n) \ln\left(\frac{k}{k_*}\right) + \frac{1}{2}a_2(\epsilon_n) \ln^2\left(\frac{k}{k_*}\right) + \dots, \quad (1.3)$$

in order to shortcut a numerical integration of \mathcal{P}_ζ but is otherwise exact. In other words, once the slow-roll approximation is accepted, no additional approximation should be made. But it is important to realize that this may require additional numerical calculations in order to determine the coefficients a_i exactly, or more precisely the explicit expression, at Hubble crossing, of $a_i = a_i[\epsilon_n(\theta_{\text{inf}})]$. This issue is now very important given the accuracy of the data. This point is illustrated in Fig. 3 and more about this question can also be found in Ref. [117]. In this figure, we have represented the slow-roll predictions of a SFI model, $V(\phi) \propto 1 - (\phi/\mu)^4$. Each colored segment represents the *exact* slow-roll predictions of a model given the parameter μ and for different numbers of e-folds during the reheating.

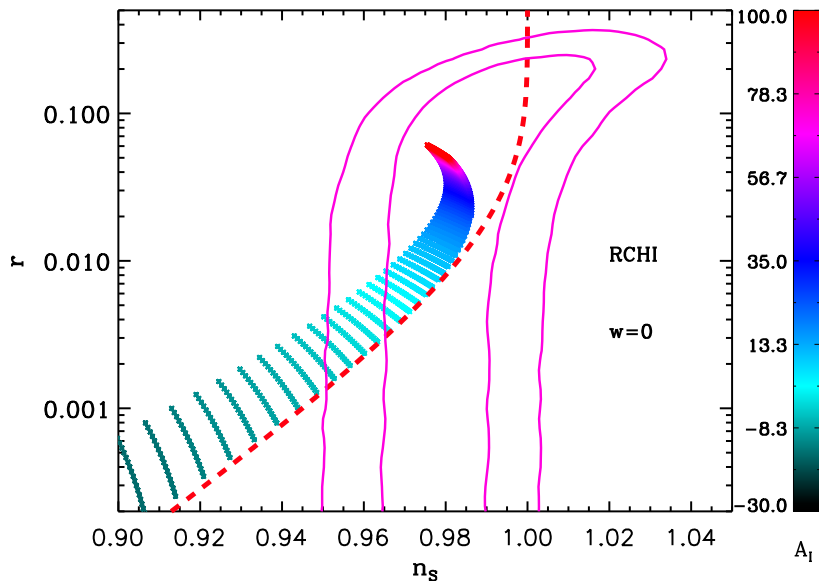


Figure 4. Predictions of the RCHI model in the plane (n_s, r) . These predictions depend on one free parameter, A_1 , for details see section 4.1. The colored segments represent the exact predictions (same conventions as in Fig. 3), obtained when the coefficients $a_i = a_i[\epsilon_n(\theta_{\text{inf}})]$ are numerically evaluated. On the contrary, the thick red dashed line indicates some approximated predictions. We see that there is a significant difference for $A_1 \gtrsim 15$.

These predictions have been computed by solving numerically the slow-roll equations. But, in the same plot, there are also other segments, on the left, and represented in yellow only. They are the slow-roll predictions for different values of μ but based on widespread *approximate* slow-roll formulas used in the literature. We see that, given the accuracy of the data, the approximated formulas are no longer accurate enough: the approximate results would predict that models with $\mu/M_{\text{Pl}} > 1$ are strongly disfavored while the correct slow-roll results show that they are still compatible with the data. Another textbook example is provided by Higgs inflation with radiative corrections (RCHI) and is presented in Fig. 4. This scenario is studied in detail in section 4.1 and depends on one free parameter, A_1 . The colored segments represent the exact predictions for different values of A_1 (see the color bar on the side of the plot). The red dashed line indicates predictions based on a commonly used approximate equation for the coefficients $a_i = a_i(\epsilon_n)$ at Hubble crossing during inflation. We see that this is no longer sufficient in the range $A_1 \gtrsim 15$. From these two examples, we conclude that it is safer to use the slow-roll approximation (which is usually extremely good) and nothing else, in particular no extra approximation on top of the slow-roll approximation. The fact that we still need to use numerical calculations to establish the observational predictions of a model does not make our approach useless. Indeed, the numerical calculations needed to estimate the $a_i = a_i[\epsilon_n(\theta_{\text{inf}})]$ are, by far, much easier than those needed to exactly compute \mathcal{P}_ζ . Therefore, the gain in computational time mentioned above is huge and allows for a fast and reliable method to constrain the inflationary landscape.

1.2 The ASPIC library

The project described before contains many different aspects that we intend to publish in several companion articles. We now explain the purpose of the present paper and put it in context with the other works that are in preparation. We have coded a public runtime library, named ASPIC for “Accurate Slow-roll Predictions for Inflationary Cosmology”, which is supposed to contain all the inflationary models that can be treated with the method described above. ASPIC already has 64 different inflationary scenarios, a number that should be compared to the three or four models that are usually considered. The ASPIC library is an open source evolutive project and, although it already contains all the most popular inflationary scenarios, aims at including more models. In this way, it will converge towards a situation where all the category IA models published since the advent of inflation are implemented thereby allowing us to exhaustively scan this part of the inflationary landscape. This article describes the ASPIC project and presents its first release and others will follow. The list of the 64 ASPIC models, as well as their acronym, is presented in Table 1 at the end of this introduction. If future cosmological data force us to move to more complicated scenarios, the ASPIC library will be upgraded accordingly. It can, moreover, already be interfaced with `FieldInf` thereby allowing for a full numerical approach, if needed. This would be especially relevant for all the single field models with modified kinetic terms (category IB) such as DBI models, models with features (category IC) such as the Starobinsky model [127] or multiple field inflationary scenarios (category II) such as double inflation [128–131], double inflation with an interaction term [132], the different versions of hybrid inflation [57, 133, 134] and more [121]. However, if the data turns out to favor simple models, such as those producing negligible non-Gaussianities and isocurvature perturbations, the ASPIC library in its present form already contains the most relevant inflationary scenarios. The ASPIC library is publicly available at <http://cp3.irmp.ucl.ac.be/~ringeval/aspic.html>.

The ASPIC library contains the numerical codes that allow us to compare the predictions of any of the 64 different models to high-accuracy data. The present article presents the general architecture of the ASPIC project and the calculations needed to understand and write these codes. In practice, for each model, we give the calculation of the three first slow-roll parameters, a discussion of how inflation ends, a discussion of the priors, a calculation of the relevant range of variation of the reheating temperature and an exact integration of the slow-roll trajectory. Then, we work out the theoretical predictions and compare them to the WMAP data in the planes (ϵ_1, ϵ_2) and (n_s, r) . Let us stress again that, beside slow-roll, no other approximation is used in the numerical codes of ASPIC.

Of course, the ASPIC models have already been partially studied in the literature but it is crucial to emphasize that, for each of them, this paper contains new results. In other words, it does not aim at being a review and, therefore, the presentation of already derived results have been kept to the minimal. Firstly, we should stress that, for all the models studied here, this is the first time that their observational predictions are worked out when the constraints on the reheating phase are accurately taken into account. As explained in Ref. [64], and briefly reviewed in section 2, it has become too inaccurate to derive the predictions of a model by simply assuming a fixed range for ΔN_* . For instance, this could lead to a reheating energy density larger than the energy density at the end of inflation which is physically irrelevant. Therefore, the predictions have been re-worked in such a consistent fashion (except for the LFI and SFI models which had been studied before [64]). This already constitutes a significant result which goes beyond the current state-of-the-art. Secondly, in the appendix, we present a series of plots which give the predictions of the various ASPIC models in the planes (n_s, r)

and (ϵ_1, ϵ_2) for different values of the free parameters characterizing each potential. Most often, this is the first time that these predictions are worked out for such a wide range of parameters and, moreover, this is the first time that these predictions are presented in this fashion. In some sense, our paper can be viewed as the first *Encyclopædia Inflationaris*.

1.3 New results

In order to be completely clear about the fact that this paper is not a review, we now highlight, in a non-exhaustive way, some of the new results obtained in this paper. In this way, we hope it gives a taste of all the new findings described later and the methods advocated earlier.

In the case of Higgs Inflation (HI), for instance, we have found an exact expression of the slow-roll trajectory and discuss the reheating parameter in the case of scalar-tensor theories of gravity. The exact trajectory is also found for radiatively corrected inflation (RCHI) and we show that the exact predictions can differ from the commonly used ones in a certain regime, see also Fig. 4. In the case of Mixed Large Field Inflation (MLFI), the exact expressions of the slow-roll parameters ϵ_2 and ϵ_3 are new. We also calculate exactly ϕ_{end} , the *vev* at which inflation stops, as well as the exact trajectory $N(\phi)$ and its inverse, $\phi(N)$. Interestingly, since the potential is the sum of a quadratic and a quartic term, one would expect the corresponding predictions to be located between the two lines in the plane (n_s, r) representing the quadratic LFI and the quartic LFI models, see for instance Fig. 2. We show that this is not the case. For Natural Inflation (NI), we provide the exact expression of ϕ_{end} , of the trajectory and its inverse. In addition, it is often claimed that, in the limit $f/M_{\text{Pl}} \gg 1$, the model is indistinguishable from a quadratic one (LFI with $p = 2$). We show that it is true for n_s and r but is not accurate for ϵ_3 , that is to say for the running α_s . For the Kähler Moduli Inflation I (KMII) and Kähler Moduli Inflation II (KMIII) models, all our results are basically new. We present, for the first time, the exact expressions of the slow-roll parameters, of the trajectories, their inverses, the possible values of α , a free parameter characterizing the shape of the potentials (not to be confused with the running). We also emphasize the role played by the running in this model: n_s and r are perfectly compatible with the data while α_s seems to constrain the model more efficiently. However, contrary to what is commonly claimed in the literature, we demonstrate that this does not rule out these models. Within the Logamediate inflation scenario, we have derived an analytic expression for the trajectory in terms of hypergeometric functions and exhibited a new inflationary domain LMI2, which is however like almost a pure de Sitter era and currently disfavored. We also have new results for the Coleman Weinberg Inflation (CWI) scenario. We find exact expressions for ϵ_3 and an exact determination of the end of inflation. We discuss, for the first time, the predictions of the model in the full parameter space. In the case of Double Well Inflation (DWI), we present a clear slow-roll analysis. The expressions of ϵ_3 , ϕ_{end} , the slow-roll trajectory, its inverse are all new. Moreover, a detailed comparison with SFI is made and we show that the corresponding predictions actually differ, contrary to what is sometimes written in the literature. In the case of the Minimal Super-Symmetric Model (MSSMI) scenario, we demonstrate several new results. We give the exact expression of the slow-roll parameters ϵ_2 and ϵ_3 , the location and the value of the maximum of the first slow-roll parameter ϵ_1 , an approximated formula for ϕ_{end} , the exact slow-roll trajectory and a useful approximated version of it. We also provide a parameter independent treatment of the quantum diffusion regime: usually this is always done using specific values of the parameters whereas we show that the corresponding conclusions are in fact completely general. We also explain why the model is quite strongly disfavored due to the observational constraints on the spectral index. For the Renormalizable

Inflection Point Inflation (RIPI) scenario, the slow roll parameters ϵ_2 and ϵ_3 , the location and the value of the maximum of ϵ_1 , the approximated determination of ϕ_{end} , the exact slow-roll trajectory and a useful approximated version of it are all new. We also discuss the CMB normalization and calculate the energy scale of inflation very accurately. Last but not the least, we show that the model is strongly disfavored by the data. We have also explored the Generalized MSSM Inflation (GMSSMI) scenario. We provide new formulas for ϵ_2 , ϵ_3 and the trajectory. We also give new bounds on the parameters characterizing the potential from the requirement of having a sufficient number of e-folds during inflation. Finally, we show that the model is disfavored by the data. Concerning the Brane Susy Breaking Scenario (BSUSYBI), we have studied the effects coming from the the field value at which inflation ends, in the slow-roll regime. For the ArcTan Inflation (AI) scenario, we work out the slow-roll analysis beyond the approximation of vacuum domination and give an exact expression for ϵ_3 and the slow-roll trajectory. For the class of models leading to a constant spectral index, CNAI, CNBI, CNCI and CNDI, we show how to calculate ϕ_{end} and the trajectory exactly. We also demonstrate that the spectral index is in fact constant only in a limited region of the parameter space which turns out to be already disfavored by the data. In the case of Intermediate Inflation (II), we present an analysis which takes into account the two terms of the potential while it is common to keep only the dominant one. We give new expressions for ϵ_3 , the slow-roll trajectory and its relation with the exact, non slow-roll, one. In the case of Twisted Inflation (TWI), we study this model for the first time in a regime where it is not equivalent to DSI. We give new expressions for ϵ_3 , the exact trajectory and the CMB normalization. We also discuss how inflation ends and show, contrary to a naive expectation, that it cannot happen by violation of the slow-roll conditions. For the Pseudo Natural Inflation (PSNI) scenario, we present new formulas for ϵ_2 , ϵ_3 , ϕ_{end} and the trajectory. This is the first time that a slow-roll analysis of Orientifold Inflation (OI) is made. As a consequence, all the corresponding results are new. In particular, we demonstrate that the model is in bad shape because it predicts a too important amount of gravitational waves. The scenario of Spontaneous Symmetry Breaking Inflation (SSBI) is important because it can cover many physically different situations. This model actually contains six different sub-models. The third slow-roll parameter, the trajectory and the CMB normalization are new results obtained for the first time in this paper. In the case of Dynamical Symmetric Inflation (DSI), we present new expressions for ϵ_3 , the trajectory and the CMB normalization. Another important result is also a careful analysis of the prior space and the limits derived on the parameters of the model which are such that it is disfavored by observations due to its blue tilt. For the Generalized Mixed Large Field Inflation (GMLFI) model, we present new equations for ϵ_2 and ϵ_3 and the trajectory. Concerning the LPI models, we have exhibited three domains in which inflation could take place, thereafter denoted by LPI1, LPI2 and LPI3. For the Non Canonical Kähler Inflation model (NCKI), we provide new results for ϵ_2 and ϵ_3 , the trajectory and the CMB normalization. We also analyze the predictions for different values of β , a parameter characterizing the potential. We show that the case $\beta < 0$ is ruled out while $\beta > 0$ is disfavored by the observations. We have also studied Loop Inflation (LI). For this model, we give new expressions of ϵ_3 , ϕ_{end} , the trajectory and its inverse in terms of a Lambert function. Also, the slow-roll analysis is carried out in the case where the correcting term is negative which we could not find elsewhere. In the case of Tip Inflation (TI), we also give ϵ_3 , ϕ_{end} and the trajectory. We also study which amounts of fine tuning is required by the model and finally show that it is ruled out because its spectrum deviates too strongly from scale invariance. Many other new results are given in this article but, as

mentioned above, we do not summarize all of them here due to space limitation. They can be found in the sections devoted to the various models listed in Table 1.

Before concluding this introduction, let us remark that this article and the ASPIC library represent important tools to carry out our final goal which consists in assessing how good is a model and in comparing the various inflationary models. This problem can be dealt within Bayesian inference for model comparison. For this purpose, one has to calculate, for each model, the global likelihood which is obtained by integrating the usual likelihood over all of the model parameter values, weighted by their respective prior probability distribution. The resulting quantity is a number associated with each model which gives the “evidence” that the model explains the data [this is the number \mathcal{N} in Eq. (1.1)]. Their respective ratios give the odds that one model explains all data compared to the others. Bayesian methods have the advantage to automatically incorporate the “Occam’s razor”: complicated inflationary models will be assigned large probability only if the complexity is required by the data. On the practical side, these two steps can be implemented by the use of Markov–Chains–Monte–Carlo (MCMC) methods, which is especially well suited with the exact numerical approach advocated before. These techniques have already been successfully implemented first in Ref. [135], and later on in Ref. [126], and we plan to extend them to all the models of the ASPIC library. As a matter of fact, this will allow us to scan the inflationary landscape in a statistically well-defined way and to address the question of “the best model of inflation”.

This article is organized as follows. In the next section, section 2, we briefly summarize slow-roll inflation and give the equations needed for the rest of this article. We also discuss the reheating stage and explains how it can be implemented. Then, in section 3, we study inflationary models which, up to the potential normalization, do not contain any free parameter (concretely, at this stage, Higgs inflation). In sections 4, 5 and 6, we analyze scenarios characterized by one, two and three free parameters, respectively. Finally, in section 7, we present our conclusions and discuss future works. In the appendix A, we give, in the planes (n_s, r) and (ϵ_1, ϵ_2) , the predictions of all the 64 ASPIC models.

Name	Parameters	Sub-models	$V(\phi)$
HI	0	1	$M^4 \left(1 - e^{-\sqrt{2/3}\phi/M_{\text{Pl}}} \right)$
RCHI	1	1	$M^4 \left(1 - 2e^{-\sqrt{2/3}\phi/M_{\text{Pl}}} + \frac{A_1}{16\pi^2} \frac{\phi}{\sqrt{6}M_{\text{Pl}}} \right)$
LFI	1	1	$M^4 \left(\frac{\phi}{M_{\text{Pl}}} \right)^p$
MLFI	1	1	$M^4 \frac{\phi^2}{M_{\text{Pl}}^2} \left 1 + \alpha \frac{\phi^2}{M_{\text{Pl}}^2} \right $
RCMI	1	1	$M^4 \left(\frac{\phi}{M_{\text{Pl}}} \right)^2 \left[1 - 2\alpha \frac{\phi^2}{M_{\text{Pl}}^2} \ln \left(\frac{\phi}{M_{\text{Pl}}} \right) \right]$
RCQI	1	1	$M^4 \left(\frac{\phi}{M_{\text{Pl}}} \right)^4 \left[1 - \alpha \ln \left(\frac{\phi}{M_{\text{Pl}}} \right) \right]$
NI	1	1	$M^4 \left 1 + \cos \left(\frac{\phi}{f} \right) \right $
ESI	1	1	$M^4 \left(1 - e^{-q\phi/M_{\text{Pl}}} \right)$
PLI	1	1	$M^4 e^{-\alpha\phi/M_{\text{Pl}}}$
KMII	1	2	$M^4 \left(1 - \alpha \frac{\phi}{M_{\text{Pl}}} e^{-\phi/M_{\text{Pl}}} \right)$
HFII	1	1	$M^4 \left(1 + A_1 \frac{\phi}{M_{\text{Pl}}} \right)^2 \left[1 - \frac{2}{3} \left(\frac{A_1}{1+A_1\phi/M_{\text{Pl}}} \right)^2 \right]$
CWI	1	1	$M^4 \left 1 + \alpha \left(\frac{\phi}{Q} \right)^4 \ln \left(\frac{\phi}{Q} \right) \right $
LI	1	2	$M^4 \left 1 + \alpha \ln \left(\frac{\phi}{M_{\text{Pl}}} \right) \right $
RpI	1	3	$M^4 e^{-2\sqrt{2/3}\phi/M_{\text{Pl}}} \left e^{\sqrt{2/3}\phi/M_{\text{Pl}}} - 1 \right ^{2p/(2p-1)}$
DWI	1	1	$M^4 \left[\left(\frac{\phi}{\phi_0} \right)^2 - 1 \right]^2$
MHI	1	1	$M^4 \left 1 - \text{sech} \left(\frac{\phi}{\mu} \right) \right $
RGI	1	1	$M^4 \frac{(\phi/M_{\text{Pl}})^2}{\alpha + (\phi/M_{\text{Pl}})^2}$
MSSMI	1	1	$M^4 \left[\left(\frac{\phi}{\phi_0} \right)^2 - \frac{2}{3} \left(\frac{\phi}{\phi_0} \right)^6 + \frac{1}{5} \left(\frac{\phi}{\phi_0} \right)^{10} \right]$
RIPI	1	1	$M^4 \left[\left(\frac{\phi}{\phi_0} \right)^2 - \left(\frac{\phi}{\phi_0} \right)^3 + \frac{9}{32} \left(\frac{\phi}{\phi_0} \right)^4 \right]$
AI	1	1	$M^4 \left 1 - \frac{2}{\pi} \arctan \left(\frac{\phi}{\mu} \right) \right $
CNAI	1	1	$M^4 \left 3 - (3 + \alpha^2) \tanh^2 \left(\frac{\alpha}{\sqrt{2}} \frac{\phi}{M_{\text{Pl}}} \right) \right $
CNBI	1	1	$M^4 \left[(3 - \alpha^2) \tan^2 \left(\frac{\alpha}{\sqrt{2}} \frac{\phi}{M_{\text{Pl}}} \right) - 3 \right]$
SFI	2	1	$M^4 \left 1 - \left(\frac{\phi}{\mu} \right)^p \right $
II	2	1	$M^4 \left(\frac{\phi - \phi_0}{M_{\text{Pl}}} \right)^{-\beta} - M^4 \frac{\beta^2}{6} \left(\frac{\phi - \phi_0}{M_{\text{Pl}}} \right)^{-\beta-2}$
KMIII	2	1	$M^4 \left 1 - \alpha \frac{\phi}{M_{\text{Pl}}} \exp \left(-\beta \frac{\phi}{M_{\text{Pl}}} \right) \right $

LMI	2	2	$M^4 \left(\frac{\phi}{M_{\text{Pl}}} \right)^\alpha \exp[-\beta(\phi/M_{\text{Pl}})^\gamma]$
TWI	2	1	$M^4 \left 1 - A \left(\frac{\phi}{\phi_0} \right)^2 e^{-\phi/\phi_0} \right $
GMSSMI	2	1	$M^4 \left \left(\frac{\phi}{\phi_0} \right)^2 - \frac{2}{3} \alpha \left(\frac{\phi}{\phi_0} \right)^6 + \frac{\alpha}{5} \left(\frac{\phi}{\phi_0} \right)^{10} \right $
BSUSYBI	2	1	$M^4 \left(e^{\sqrt{6} \frac{\phi}{M_{\text{Pl}}}} + e^{\sqrt{6} \gamma \frac{\phi}{M_{\text{Pl}}}} \right)$
TI	2	3	$M^4 \left(1 + \cos \frac{\phi}{\mu} + \alpha \sin^2 \frac{\phi}{\mu} \right)$
BEI	2	1	$M^4 \exp_{1-\beta} \left(-\lambda \frac{\phi}{M_{\text{Pl}}} \right)$
PSNI	2	1	$M^4 \left 1 + \alpha \ln \left(\cos \frac{\phi}{f} \right) \right $
NCKI	2	2	$M^4 \left 1 + \alpha \ln \left(\frac{\phi}{M_{\text{Pl}}} \right) + \beta \left(\frac{\phi}{M_{\text{Pl}}} \right)^2 \right $
CSI	2	1	$\frac{M^4}{\left(1 - \alpha \frac{\phi}{M_{\text{Pl}}} \right)^2}$
OI	2	1	$M^4 \left(\frac{\phi}{\phi_0} \right)^4 \left \left(\ln \frac{\phi}{\phi_0} \right)^2 - \alpha \right $
CNCI	2	1	$M^4 \left (3 + \alpha^2) \coth^2 \left(\frac{\alpha}{\sqrt{2}} \frac{\phi}{M_{\text{Pl}}} \right) - 3 \right $
SBI	2	2	$M^4 \left\{ 1 + \left[-\alpha + \beta \ln \left(\frac{\phi}{M_{\text{Pl}}} \right) \right] \left(\frac{\phi}{M_{\text{Pl}}} \right)^4 \right\}$
SSBI	2	6	$M^4 \left 1 + \alpha \left(\frac{\phi}{M_{\text{Pl}}} \right)^2 + \beta \left(\frac{\phi}{M_{\text{Pl}}} \right)^4 \right $
RMI	3	4	$M^4 \left 1 - \frac{c}{2} \left(-\frac{1}{2} + \ln \frac{\phi}{\phi_0} \right) \frac{\phi^2}{M_{\text{Pl}}^2} \right $
VHI	3	1	$M^4 \left 1 + \left(\frac{\phi}{\mu} \right)^p \right $
DSI	3	1	$M^4 \left 1 + \left(\frac{\phi}{\mu} \right)^{-p} \right $
GMLFI	3	1	$M^4 \left(\frac{\phi}{M_{\text{Pl}}} \right)^p \left 1 + \alpha \left(\frac{\phi}{M_{\text{Pl}}} \right)^q \right $
LPI	3	3	$M^4 \left(\frac{\phi}{\phi_0} \right)^p \left(\ln \frac{\phi}{\phi_0} \right)^q$
CNDI	3	3	$\frac{M^4}{\left\{ 1 + \beta \cos \left[\alpha \left(\frac{\phi - \phi_0}{M_{\text{Pl}}} \right) \right] \right\}^2}$

Table 1: Models contained in the first release of the ASPIC library. For each model, we give the corresponding acronym, the number of free parameters characterizing the potential, the number of sub-models and the shape of the potential. The total number of models is 64.

2 Basic Equations

In this section, we very briefly recall the theoretical foundations of inflation and we present the main tools and equations that will be used in the rest of this paper. We start with reviewing the slow-roll phase, where the cosmological fluctuations are generated and, then, we describe how the end of inflation and the transition to the standard hot Big Bang phase can be modeled.

2.1 The slow-roll phase

Let us consider a single-field inflationary model with a minimal kinetic term and a potential $V(\phi)$. The behavior of the system is controlled by the Friedmann-Lemaître and Klein-Gordon equations, namely

$$H^2 = \frac{1}{3M_{\text{Pl}}^2} \left[\frac{\dot{\phi}^2}{2} + V(\phi) \right], \quad (2.1)$$

$$\ddot{\phi} + 3H\dot{\phi} + V_\phi = 0, \quad (2.2)$$

where $H \equiv \dot{a}/a$ denotes the Hubble parameter, $a(t)$ being the Friedmann-Lemaître-Robertson Walker (FLRW) scale factor and \dot{a} its derivative with respect to cosmic time t . $M_{\text{Pl}} = 8\pi G$ denotes the reduced Planck mass. A subscript ϕ means a derivative with respect to the inflaton field. In order to describe the evolution of the background, it is convenient to introduce the Hubble flow functions ϵ_n defined by

$$\epsilon_{n+1} \equiv \frac{d \ln |\epsilon_n|}{dN}, \quad n \geq 0, \quad (2.3)$$

where $\epsilon_0 \equiv H_{\text{ini}}/H$ and $N \equiv \ln(a/a_{\text{ini}})$ is the number of e-folds. By definition, inflation is a phase of accelerated expansion, $\ddot{a}/a > 0$, or, equivalently, $\epsilon_1 < 1$. As a consequence, the end of inflation is defined by the condition $\epsilon_1 = 1$. On the other hand, the slow-roll conditions (or slow-roll approximation) refer to a situation where all the ϵ_n 's satisfy $\epsilon_n \ll 1$. If this is the case, then the parameters ϵ_n can also be expressed in terms of the successive derivatives of the potential, namely [17]

$$\epsilon_1 \simeq \frac{M_{\text{Pl}}^2}{2} \left(\frac{V_\phi}{V} \right)^2, \quad (2.4)$$

$$\epsilon_2 \simeq 2M_{\text{Pl}}^2 \left[\left(\frac{V_\phi}{V} \right)^2 - \frac{V_{\phi\phi}}{V} \right], \quad (2.5)$$

$$\epsilon_2 \epsilon_3 \simeq 2M_{\text{Pl}}^4 \left[\frac{V_{\phi\phi\phi} V_\phi}{V^2} - 3 \frac{V_{\phi\phi}}{V} \left(\frac{V_\phi}{V} \right)^2 + 2 \left(\frac{V_\phi}{V} \right)^4 \right]. \quad (2.6)$$

Therefore, a measurement of the ϵ_n 's also provides information with regards to the shape of the inflationary potential.

In terms of the number of e-folds, one can decouple Eqs. (2.1) and (2.2) to only the field evolution

$$\frac{1}{3 - \epsilon_1} \frac{d^2 \phi}{dN^2} + \frac{d\phi}{dN} = -M_{\text{Pl}}^2 \frac{d \ln V}{d\phi}, \quad (2.7)$$

showing that the potential driving the field in FLRW spacetime is $\ln[V(\phi)]$. This equation can be further simplified by using the definition of ϵ_1 and ϵ_2 to get rid of the second order derivatives. From

$$\epsilon_1 = \frac{1}{2M_{\text{Pl}}^2} \left(\frac{d\phi}{dN} \right)^2, \quad (2.8)$$

one gets

$$\left(1 + \frac{\epsilon_2}{6 - 2\epsilon_1} \right) \frac{d\phi}{dN} = -M_{\text{Pl}}^2 \frac{d \ln V}{d\phi}. \quad (2.9)$$

As a result, in the slow-roll approximation, one gets

$$\frac{d\phi}{dN} \simeq -M_{\text{Pl}}^2 \frac{d \ln V}{d\phi}. \quad (2.10)$$

This equation can be integrated to give an explicit expression of the classical trajectory. One arrives at

$$N - N_{\text{ini}} = -\frac{1}{M_{\text{Pl}}^2} \int_{\phi_{\text{ini}}}^{\phi} \frac{V(\chi)}{V_{,\chi}(\chi)} d\chi. \quad (2.11)$$

In this article, for each model, we provide the expressions of the first three Hubble flow parameters, a determination of ϕ_{end} , the value of the field at which inflation comes to an end (and the corresponding discussion) and an explicit expression of the slow-roll trajectory Eq. (2.11).

Let us now consider the behavior of inflationary cosmological perturbations. The evolution of scalar (density) perturbations can be reduced to the study of a single variable, the so-called Mukhanov–Sasaki variable $v_{\mathbf{k}}$. In Fourier space, its equation of motion can be expressed as [6–8, 16]

$$v_{\mathbf{k}}'' + \left[k^2 - \frac{(a\sqrt{\epsilon_1})''}{a\sqrt{\epsilon_1}} \right] v_{\mathbf{k}} = 0. \quad (2.12)$$

Here, a prime denotes a derivative with respect to conformal time and the quantity k is the comoving wave number of the Fourier mode under consideration. This equation is the equation of a parametric oscillator, i.e. an oscillator with a time-dependent frequency. The time-dependence of the effective frequency is controlled by the dynamics of the background, more precisely by the scale factor and its derivatives (up to fourth order). The quantity $v_{\mathbf{k}}$ is related to the curvature perturbation $\zeta_{\mathbf{k}}$ through the following expression:

$$\zeta_{\mathbf{k}} = \frac{1}{M_{\text{Pl}}} \frac{v_{\mathbf{k}}}{a\sqrt{2\epsilon_1}}. \quad (2.13)$$

The importance of $\zeta_{\mathbf{k}}$ lies in the fact that it can be viewed as a “tracer” of the fluctuations on super-Hubble scales, i.e. for all $k\eta \ll 1$, where η denotes the conformal time. Indeed, in the case of single-field inflation, this quantity becomes constant in this limit. Therefore, it can be used to “propagate” the perturbations from inflation to the subsequent cosmological eras. The statistical properties of the fluctuations can be characterized by the n -point correlation functions of $\zeta_{\mathbf{k}}$. In particular, the two-point correlation function can be written as an integral over wave numbers (in a logarithmic interval) of the power spectrum $\mathcal{P}_{\zeta}(k)$, which can be expressed as

$$\mathcal{P}_{\zeta}(k) \equiv \frac{k^3}{2\pi^2} |\zeta_{\mathbf{k}}|^2 = \frac{k^3}{4\pi^2 M_{\text{Pl}}^2} \left| \frac{v_{\mathbf{k}}}{a\sqrt{\epsilon_1}} \right|^2. \quad (2.14)$$

In order to calculate $\mathcal{P}_\zeta(k)$, one needs to integrate Eq. (2.12), which requires the knowledge of the initial conditions for the mode function $v_{\mathbf{k}}$. Since, at the beginning of inflation, all the modes of cosmological interest today were much smaller than the Hubble radius, the initial conditions are chosen to be the Bunch-Davis vacuum which amounts to

$$\lim_{k\eta \rightarrow +\infty} v_{\mathbf{k}} = \frac{1}{\sqrt{2k}} e^{-ik\eta}, \quad (2.15)$$

where $\mathcal{H} = aH$ is the conformal Hubble parameter.

The evolution of tensor perturbations (or primordial gravity waves) can also be reduced to the study of a parametric oscillator. The amplitude of each transverse Fourier mode of the gravity wave, $\mu_{\mathbf{k}}(\eta)$, obeys the following equation

$$\mu_{\mathbf{k}}'' + \left(k^2 - \frac{a''}{a} \right) \mu_{\mathbf{k}} = 0. \quad (2.16)$$

We notice that the time-dependence of the effective frequency differs from that of the scalar case and now involves the derivative of the scale factor up to second order only. It is then straightforward to determine the resulting power spectrum. From a calculation of the two-point correlation function, one obtains

$$\mathcal{P}_h(k) = \frac{2k^3}{\pi^2} \left| \frac{\mu_{\mathbf{k}}}{a} \right|^2. \quad (2.17)$$

In order to calculate this quantity, the equation of motion Eq. (2.16) needs to be solved. As it is the case for density perturbations, the initial state is chosen to be the Bunch-Davies vacuum.

The power spectra can be computed exactly by means of a mode by mode integration of Eqs. (2.12) and (2.16), which also requires an exact integration of the background, i.e. of Eqs. (2.1) and (2.2). As discussed in the introduction, this can be done with the help of publicly available codes such as `FieldInf`. We have seen above that the slow-roll approximation can be used to calculate the classical background trajectory. Quite remarkably, the same approximation also permits the derivation of the scalar and tensor power spectra. This involves a double expansion. The power spectra are expanded around a chosen pivot scale k_* such that

$$\frac{\mathcal{P}(k)}{\mathcal{P}_0(k_*)} = a_0 + a_1 \ln \left(\frac{k}{k_*} \right) + \frac{a_2}{2} \ln^2 \left(\frac{k}{k_*} \right) + \dots, \quad (2.18)$$

where

$$\mathcal{P}_{\zeta_0} = \frac{H^2}{8\pi^2 \epsilon_1 M_{\text{Pl}}^2}, \quad \mathcal{P}_{h_0} = \frac{2H^2}{\pi^2 M_{\text{Pl}}^2}, \quad (2.19)$$

and, then, the coefficients a_i are determined in terms of the Hubble flow functions. For scalar perturbations, one gets [114, 115, 136–140, 140–142]

$$\begin{aligned} a_0^{(S)} &= 1 - 2(C+1)\epsilon_1 - C\epsilon_2 + \left(2C^2 + 2C + \frac{\pi^2}{2} - f \right) \epsilon_1^2 \\ &+ \left(C^2 - C + \frac{7\pi^2}{12} - g \right) \epsilon_1 \epsilon_2 + \left(\frac{1}{2}C^2 + \frac{\pi^2}{8} - 1 \right) \epsilon_2^2 \\ &+ \left(-\frac{1}{2}C^2 + \frac{\pi^2}{24} \right) \epsilon_2 \epsilon_3, \end{aligned} \quad (2.20)$$

$$a_1^{(S)} = -2\epsilon_1 - \epsilon_2 + 2(2C+1)\epsilon_1^2 + (2C-1)\epsilon_1\epsilon_2 + C\epsilon_2^2 - C\epsilon_2\epsilon_3, \quad (2.21)$$

$$a_2^{(S)} = 4\epsilon_1^2 + 2\epsilon_1\epsilon_2 + \epsilon_2^2 - \epsilon_2\epsilon_3, \quad (2.22)$$

where $C \equiv \gamma_E + \ln 2 - 2 \approx -0.7296$, γ_E being the Euler constant, $f = 5$ and $g = 7$. For the gravitational waves, the coefficients a_i read

$$a_0^{(T)} = 1 - 2(C + 1)\epsilon_1 + \left(2C^2 + 2C + \frac{\pi^2}{2} - f\right)\epsilon_1^2 + \left(-C^2 - 2C + \frac{\pi^2}{12} - 2\right)\epsilon_1\epsilon_2, \quad (2.23)$$

$$a_1^{(T)} = -2\epsilon_1 + 2(2C + 1)\epsilon_1^2 - 2(C + 1)\epsilon_1\epsilon_2, \quad (2.24)$$

$$a_2^{(T)} = 4\epsilon_1^2 - 2\epsilon_1\epsilon_2. \quad (2.25)$$

The Hubble flow functions are time-dependent quantities such that in the above expression, it is understood that they should be evaluated at the time at which the pivot scale crosses the Hubble radius during inflation, i.e. at a time η_* such that $k_* = \mathcal{H}(\eta_*)$. Let us notice that setting the pivot at another time affects the previous expression. For instance, setting η_* such that $k_*\eta_* = -1$ would set $f = 3$ and $g = 6$. We will see below that this introduces a dependence in the parameters describing the reheating stage.

The properties of the power spectra can also be characterized by the spectral indices and their “running”. They are defined by the coefficients of the Taylor expansions of the power spectra logarithm with respect to $\ln k$, evaluated at the pivot scale k_* . This gives

$$n_S - 1 \equiv \left. \frac{d \ln \mathcal{P}_\zeta}{d \ln k} \right|_{k_*}, \quad n_T \equiv \left. \frac{d \ln \mathcal{P}_h}{d \ln k} \right|_{k_*}. \quad (2.26)$$

For the runnings, one similarly has the two following expressions

$$\alpha_S \equiv \left. \frac{d^2 \ln \mathcal{P}_\zeta}{d(\ln k)^2} \right|_{k_*}, \quad \alpha_T \equiv \left. \frac{d^2 \ln \mathcal{P}_h}{d(\ln k)^2} \right|_{k_*}, \quad (2.27)$$

and, in principle, we could also define the running of the running and so on. The slow-roll approximation allows us to calculate the quantities defined above. For instance, we have at first order in the Hubble flow parameters

$$n_S = 1 - 2\epsilon_1 - \epsilon_2, \quad n_T = -2\epsilon_1. \quad (2.28)$$

Let us also notice that the tensor-to-scalar ratio at leading order can be expressed as

$$r \equiv \frac{\mathcal{P}_h}{\mathcal{P}_\zeta} = 16\epsilon_1. \quad (2.29)$$

In the rest of this article, we give the observational predictions of each inflationary model of the ASPIC library in the planes (ϵ_1, ϵ_2) but also (n_S, r) .

Each inflationary model must also be CMB normalized, that is to say the amplitude of the power spectra, say at $k = k_*$, is completely fixed by the amplitude of the CMB anisotropies measured today. On the largest length scales, this is given to a good approximation by the CMB quadrupole $Q_{\text{rms-PS}}/T \equiv \sqrt{5C_2/(4\pi)} \simeq 6 \times 10^{-6}$, where $T \simeq 2.725$ K is the CMB blackbody temperature. This is achieved if $\mathcal{P}_{\zeta_0} \simeq 60 Q_{\text{rms-PS}}^2/T^2$. Using the slow-roll approximation of the Friedmann-Lemaître equation and writing the potential as $V(\phi) = M^4 v(\phi)$, such that the mass scale M is singled out, one arrives at

$$\left(\frac{M}{M_{\text{Pl}}}\right)^4 = 1440\pi^2 \frac{\epsilon_{1*}}{v(\phi_*)} \frac{Q_{\text{rms-PS}}^2}{T^2}. \quad (2.30)$$

This is a model-dependent expression (it depends on v) in which we have rendered explicit the dependence in the pivot time. On a more robust basis, CMB data are strongly constraining the value of $P_* \equiv \mathcal{P}_\zeta(k_*)$ and using the WMAP nine years data one gets the one-sigma confidence interval [66, 67]

$$\ln [10^{10} P_*] = 3.08 \pm 0.03. \quad (2.31)$$

This constraint and the one- and two-sigma contours in the planes (ϵ_1, ϵ_2) and (n_s, r) represented in all the figures have been obtained from a slow-roll analysis of the WMAP nine years data. Since the analysis is in all point identical to the one of the WMAP seven years data performed in Ref. [64], we do not repeat it here. The interested reader can find all the details in the appendix B of Ref. [64]. Let us just stress that we have used only the WMAP9 data together with the Hubble Space Telescope bound on H_0 [143]. Moreover, in order to get a robust inference, we have used the second order expression for the power spectra. Therefore, all the results presented below are marginalized over the second order slow-roll parameters.

Since at leading order in the slow-roll expansion we have $P_* \simeq H_*^2 / (8\pi^2 \epsilon_{1*} M_{\text{Pl}}^2)$, the Friedmann–Lemaître equation allows us to derive the relation

$$\left(\frac{M}{M_{\text{Pl}}} \right)^4 = 24\pi^2 \frac{\epsilon_{1*}}{v(\phi_*)} P_*, \quad (2.32)$$

which is, as expected, formally identical to Eq. (2.30) with

$$\frac{Q_{\text{rms-PS}}^2}{T^2} = 60 P_*. \quad (2.33)$$

It has however the advantage of using P_* which is a well inferred quantity because it is fitted against all the C_ℓ . In the following we will make no-distinction between the so-called COBE normalisation and the CMB normalisation, both being identical provided the above equation is used. For each inflationary model, these expressions will completely fix the allowed values for M .

We have shown how to calculate the two point correlation functions in the slow-roll approximation. The next logical step would be to determine the higher correlation functions. However, for the type of models considered here (i.e. category IA models), it is well-known that the corresponding signal is so small that it will stay out of reach for a while [91–95]. Therefore, we now consider the question of how to calculate the values of ϵ_1 and ϵ_2 when the pivot scale exits the Hubble radius and how this result depends on the details of the reheating period.

2.2 The reheating phase

In the last subsection, we have seen that the power spectrum (2.18) can be calculated with the help of the slow-roll approximation and expressed in terms of the Hubble flow parameters evaluated at Hubble radius crossing. Here, we briefly explain how these Hubble flow parameters can be determined. It is easy to calculate ϵ_1 , ϵ_2 and ϵ_3 as a function of ϕ from Eqs. (2.4), (2.5) and (2.6). Then, from the trajectory (2.11), one can calculate N_{end} , the total number of e-folds during inflation and N_* , the number of e-folds at the point when the pivot scale crosses the Hubble radius. If we denote by \mathcal{I} the following primitive

$$\mathcal{I}(\phi) = \int^\phi \frac{V(\psi)}{V_\psi(\psi)} d\psi, \quad (2.34)$$

which is also the slow-roll trajectory of Eq. (2.11), then we have

$$N_{\text{end}} = -\frac{1}{M_{\text{Pl}}^2} [\mathcal{I}(\phi_{\text{end}}) - \mathcal{I}(\phi_{\text{ini}})], \quad N_* = -\frac{1}{M_{\text{Pl}}^2} [\mathcal{I}(\phi_*) - \mathcal{I}(\phi_{\text{ini}})], \quad (2.35)$$

where ϕ_* is the vacuum expectation value of the field, again evaluated when the pivot scale crosses the Hubble radius. From these two expressions, it follows that

$$\phi_* = \mathcal{I}^{-1} [\mathcal{I}(\phi_{\text{end}}) + M_{\text{Pl}}^2 \Delta N_*], \quad (2.36)$$

where $\Delta N_* \equiv N_{\text{end}} - N_*$. Inserting this formula into the expressions of the Hubble flow parameters allows us to find ϵ_{n_*} and, therefore, r and n_s .

However, in order to make the above-described calculation concrete, we need to say something about the quantity ΔN_* . As was explained in details in Ref. [64], this requires to take into account the reheating stage. Let ρ and P be the energy density and pressure of the effective fluid dominating the Universe during reheating. Conservation of energy implies that

$$\rho(N) = \rho_{\text{end}} \exp \left\{ -3 \int_{N_{\text{end}}}^N [1 + w_{\text{reh}}(n)] dn \right\}, \quad (2.37)$$

where $w_{\text{reh}} \equiv P/\rho$ is the “instantaneous” equation of state during reheating. One can also define the mean equation of state parameter, \bar{w}_{reh} , by²

$$\bar{w}_{\text{reh}} \equiv \frac{1}{\Delta N} \int_{N_{\text{end}}}^{N_{\text{reh}}} w_{\text{reh}}(n) dn, \quad (2.38)$$

where

$$\Delta N \equiv N_{\text{reh}} - N_{\text{end}}, \quad (2.39)$$

is the total number of e-folds during reheating, N_{reh} being the number of e-folds at which reheating is completed and the radiation dominated era begins. Then, one introduces a new parameter

$$R_{\text{rad}} \equiv \frac{a_{\text{end}}}{a_{\text{reh}}} \left(\frac{\rho_{\text{end}}}{\rho_{\text{reh}}} \right)^4, \quad (2.40)$$

where ρ_{reh} has to be understood as the energy density at the end of the reheating era, i.e. $\rho(N_{\text{reh}})$. This definition shows that R_{rad} encodes any deviations the reheating may have compared to a pure radiation era. In fact, R_{rad} completely characterizes the reheating stage and can be expressed in terms of

$$\ln R_{\text{rad}} \equiv \frac{\Delta N}{4} (-1 + 3\bar{w}_{\text{reh}}), \quad (2.41)$$

which renders explicit that if $\bar{w}_{\text{reh}} = 1/3$, i.e. the effective fluid during reheating is equivalent to radiation, then reheating cannot be distinguished from the subsequent radiation dominated era. In this case, one simply has $R_{\text{rad}} = 1$. Let us notice that it is also possible to express (or define) $\ln R_{\text{rad}}$ as

$$\ln R_{\text{rad}} = \frac{1 - 3\bar{w}_{\text{reh}}}{12(1 + \bar{w}_{\text{reh}})} \ln \left(\frac{\rho_{\text{reh}}}{\rho_{\text{end}}} \right). \quad (2.42)$$

²In the figures, \bar{w}_{reh} has been denoted by w for simplicity.

Using entropy conservation till the beginning of the radiation era, the redshift at which inflation ended can be expressed in terms of R_{rad} as

$$1 + z_{\text{end}} = \frac{1}{R_{\text{rad}}} \left(\frac{\rho_{\text{end}}}{\tilde{\rho}_\gamma} \right)^{1/4}, \quad \tilde{\rho}_\gamma \equiv \mathcal{Q}_{\text{reh}} \rho_\gamma. \quad (2.43)$$

The quantity $\rho_\gamma = 3H_0^2 M_{\text{Pl}}^2 \Omega_\gamma$ is the total energy density of radiation today ($\Omega_\gamma \simeq 2.471 \times 10^{-5} h^{-2}$) while $\mathcal{Q}_{\text{reh}} \equiv q_0^{4/3} g_{\text{reh}} / (q_{\text{reh}}^{4/3} g_0)$ is the measure of the change of relativistic degrees of freedom between the reheating epoch and today. In this expression q and g respectively denotes the number of entropy and energetic relativistic degrees of freedom. In view of the current CMB data, the precise value for \mathcal{Q}_{reh} is unimportant as this factor has only a minimal effect. At most it can shift the values of $\ln R_{\text{rad}}$ by a $\mathcal{O}(1)$ number.

Then, straightforward considerations [64, 144] show that the quantities ΔN_* and R_{rad} are related by

$$\Delta N_* = \ln R_{\text{rad}} - N_0 - \frac{1}{4} \ln \left[\frac{9}{\epsilon_{1*} (3 - \epsilon_{1\text{end}})} \frac{V_{\text{end}}}{V_*} \right] + \frac{1}{4} \ln(8\pi^2 P_*). \quad (2.44)$$

where we have defined

$$N_0 \equiv \ln \left[\frac{k_*/a_0}{\tilde{\rho}_\gamma^{1/4}} \right], \quad (2.45)$$

which roughly measures the number of e-folds of deceleration of the Friedmann-Lemaître model. From Eq. (2.42), we see that the quantity $\ln R_{\text{rad}}$ is not arbitrary since $-1/3 < \bar{w}_{\text{reh}} < 1$ and $\rho_{\text{nuc}} < \rho_{\text{reh}} < \rho_{\text{end}}$. As a consequence, the quantity ΔN_* is also constrained to vary in a given range, i.e. $\Delta N_* \in [\Delta N_*^{\text{nuc}}, \Delta N_*^{\text{end}}]$. Moreover, this range is model-dependent since ρ_{end} or V_{end}/V_* differ for different inflationary scenarios. In fact, for each allowed value of $\ln R_{\text{rad}}$, Eq. (2.44) must be viewed as an algebraic equation allowing us to determine the corresponding ϕ_* . Explicitly, using Eq. (2.35), this equation reads

$$-\frac{1}{M_{\text{Pl}}^2} [\mathcal{I}(\phi_*) - \mathcal{I}(\phi_{\text{end}})] = \ln R_{\text{rad}} - N_0 - \frac{1}{4} \ln \left\{ \frac{9}{\epsilon_1(\phi_*) [3 - \epsilon_1(\phi_{\text{end}})]} \frac{V(\phi_{\text{end}})}{V(\phi_*)} \right\} + \frac{1}{4} \ln(8\pi^2 P_*). \quad (2.46)$$

Of course, in general, this equation can not be solved explicitly (except for LFI models, see Ref. [64]) and we have to rely on numerical calculations. Solving for each allowed value of $\ln R_{\text{rad}}$, one can determine the range of variation of $\phi_* \in [\phi_*^{\text{nuc}}, \phi_*^{\text{end}}]$ and, therefore, find the corresponding dispersion in r and n_s . In this paper, this task is carried out for all the models of the ASPIC library. Let us notice that it is compulsory to do so otherwise, assuming blindly say $\Delta N_* \in [40, 60]$, would lead to inconsistent reheating energy densities, either larger than ρ_{end} or smaller than ρ_{nuc} . Clearly, this method also allows us to put model-dependent constraints on the reheating temperature. Indeed, for some values of ρ_{reh} , the corresponding ϵ_{n*} will turn out to be outside the 1σ or 2σ contours (depending on the criterion one wishes to adopt) thus signaling an inconsistency with the data, see the discussion in the Introduction and Fig. 2.

Before closing this section, let us remind that, for each inflationary model, ASPIC gives the expression of the first three Hubble flow parameters, a discussion of the mechanism that ends inflation and the value of ϕ_{end} , the classical trajectory $\mathcal{I}(\phi)$, the CMB normalization M/M_{Pl} and a determination of the exact range $[\phi_*^{\text{nuc}}, \phi_*^{\text{end}}]$. Then all these informations are compared to CMB data in the planes (ϵ_1, ϵ_2) and (n_s, r) . This provides a powerful tool to

systematically derive the predictions for the ASPIC models and, therefore, to exactly scan the inflationary landscape. In the next section, we start the systematic exploration of the category IA models that have been studied in the literature since the advent of inflation.

3 Zero Parameter Models

3.1 Higgs Inflation (HI)

This model postulates that the inflaton field is the Higgs field h (recently discovered at the Large Hadron Collider, see Refs. [145, 146]) non-minimally coupled to gravity, see Refs. [147–149]. Indeed, one can argue that, in curved spacetime, the simplest model compatible with our knowledge of particle physics is described by a Lagrangian which is the standard model Lagrangian plus an extra term of the form $\xi H^\dagger H R$. This last term is compulsory since, in curved spacetime, it will automatically be generated by quantum corrections, see Ref. [150]. In the Jordan frame, the action of the model can be written as

$$S = \frac{\bar{M}^2}{2} \int d^4 \mathbf{x} \sqrt{-\bar{g}} [F(h) \bar{R} - Z(h) \bar{g}^{\mu\nu} \partial_\mu h \partial_\nu h - 2U(h)]. \quad (3.1)$$

The quantity \bar{M} is a mass scale that, for the moment, is not identified with the Planck scale and the tensor $\bar{g}_{\mu\nu}$ denotes the metric in the Jordan frame (in what follows, all the quantities with a bar denote quantities evaluated in the Jordan frame; quantities without a bar are quantities evaluated in the Einstein frame). The three functions $F(h)$, $Z(h)$ and $U(h)$ completely characterize the model and are chosen to be

$$F(h) = 1 + \xi h^2, \quad Z(h) = 1, \quad U(h) = \bar{M}^2 \frac{\lambda}{4} \left(h^2 - \frac{v^2}{\bar{M}^2} \right)^2, \quad (3.2)$$

where ξ is a new dimensionless parameter and $U(h)$ is the standard Higgs boson potential with v the Higgs (current) vacuum expectation value and λ the self-interacting coupling constant. Here, the field h is dimensionless (as the functions F and Z) while the potential U is of dimension two. The effective gravitational constant (measured in Cavendish-type experiments) is given by Ref. [151]

$$\frac{1}{M_{\text{Pl}}^2} = \frac{1}{\bar{M}^2} \frac{2(1 + \xi h^2) + 16\xi^2 h^2}{(1 + \xi h^2)[2(1 + \xi h^2) + 12\xi^2 h^2]}. \quad (3.3)$$

Since, today, one has $h \simeq v/\bar{M} \ll 1$, it follows that $\bar{M} \simeq M_{\text{Pl}}$ with very good accuracy and, from now on, we will always consider that this identification is valid.

The above-described model can also be written in the Einstein frame where the corresponding slow-roll analysis is easier. Denoting the metric tensor in this frame by $g_{\mu\nu}$, the action now takes the form

$$S = 2M_{\text{Pl}}^2 \int d^4 \mathbf{x} \sqrt{-g} \left[\frac{R}{4} - \frac{1}{2} g^{\mu\nu} \partial_\mu \chi \partial_\nu \chi - W(\chi) \right], \quad (3.4)$$

where the fields h and χ are related by

$$\frac{d\chi}{dh} = \frac{\sqrt{1 + \xi(1 + 6\xi)h^2}}{\sqrt{2}(1 + \xi h^2)}, \quad (3.5)$$

and the potential is given $V \equiv 2M_{\text{Pl}}^2 W = M_{\text{Pl}}^2 U/F^2$. Notice also that the canonically normalized field in the Einstein frame can be expressed as $\phi \equiv \sqrt{2}M_{\text{Pl}}\chi$. It is also important to recall that, in the Einstein frame, matter is now explicitly coupled to the scalar field ϕ . This has of course important consequences for the description of the reheating period, see Refs. [152–154] and below. The differential equation (3.5) can be integrated exactly and the result reads

$$\chi = \sqrt{\frac{1+6\xi}{2\xi}} \operatorname{arcsinh} \left[h\sqrt{\xi(1+6\xi)} \right] - \sqrt{3} \operatorname{arctanh} \left[\frac{\xi\sqrt{6}h}{\sqrt{1+\xi(1+6\xi)h^2}} \right]. \quad (3.6)$$

The inverse hyperbolic tangent is always well-defined since its argument is always smaller than one. This exact formula between the Einstein and Jordan frame fields was also derived in Ref. [152]. In fact, we are interested in the regime $\xi \gg 1$ and $\xi h \gg 1$. In this case, one can derive an approximated expression for χ . Notice that this limit must be carefully calculated because if one just replaces $1+6\xi$ with ξ in the above expression, one finds that $\chi = 0$! Using the identity $\operatorname{arcsinh} x = \ln \left(x + \sqrt{1+x^2} \right)$, the first term in Eq. (3.6) can be approximated as $\simeq \sqrt{3} \ln(2\xi\sqrt{6}h)$. Then, one can use the identity $\operatorname{arctanh} x = 1/2 \ln [(1+x)/(1-x)]$ and expand the argument of this logarithm in $1/\xi$ and $1/(\xi h)^2$. One finds that the latter reduces to $\sim 24\xi^2 h^2/(1+\xi h^2)$. Finally, combining the two terms in Eq. (3.6), one arrives at

$$\chi = \frac{\sqrt{3}}{2} \ln(1+\xi h^2). \quad (3.7)$$

The same expression can also be directly derived from Eq. (3.5) which, in the regime studied here, can be approximated as

$$\frac{d\chi}{dh} \simeq \frac{\sqrt{6}\xi h}{\sqrt{2}(1+\xi h^2)}. \quad (3.8)$$

The solution to this equation is exactly Eq. (3.7). The last step consists in inserting the expression of h in terms of χ (and, therefore, in terms of ϕ) into the definition of the potential V in the Einstein frame. This leads to the following expression

$$V(\phi) = \frac{M_{\text{Pl}}^4 \lambda}{4\xi^2} \left(1 - e^{-\sqrt{2/3}\phi/M_{\text{Pl}}} \right)^2. \quad (3.9)$$

Interestingly enough, the parameters ξ and λ enter the potential only through its overall amplitude. In the following, we define M by $M^4 \equiv M_{\text{Pl}}^4 \lambda / (4\xi^2)$. In this sense, Higgs inflation is a “zero parameter model” since the scale M is entirely determined by the amplitude of the CMB anisotropies.

Having established the shape of the potential in the Einstein frame, we can now proceed to the slow-roll analysis. For convenience, let us define x by $x \equiv \phi/M_{\text{Pl}}$. Then, the first three slow-roll parameters are given by

$$\begin{aligned} \epsilon_1 &= \frac{4}{3} \left(1 - e^{\sqrt{2/3}x} \right)^{-2}, & \epsilon_2 &= \frac{2}{3} \left[\sinh \left(\frac{x}{\sqrt{6}} \right) \right]^{-2}, \\ \epsilon_3 &= \frac{2}{3} \left[\coth \left(\frac{x}{\sqrt{6}} \right) - 1 \right] \coth \left(\frac{x}{\sqrt{6}} \right). \end{aligned} \quad (3.10)$$

These quantities are represented in Fig. 5 (left and right bottom panels) together with the potential.

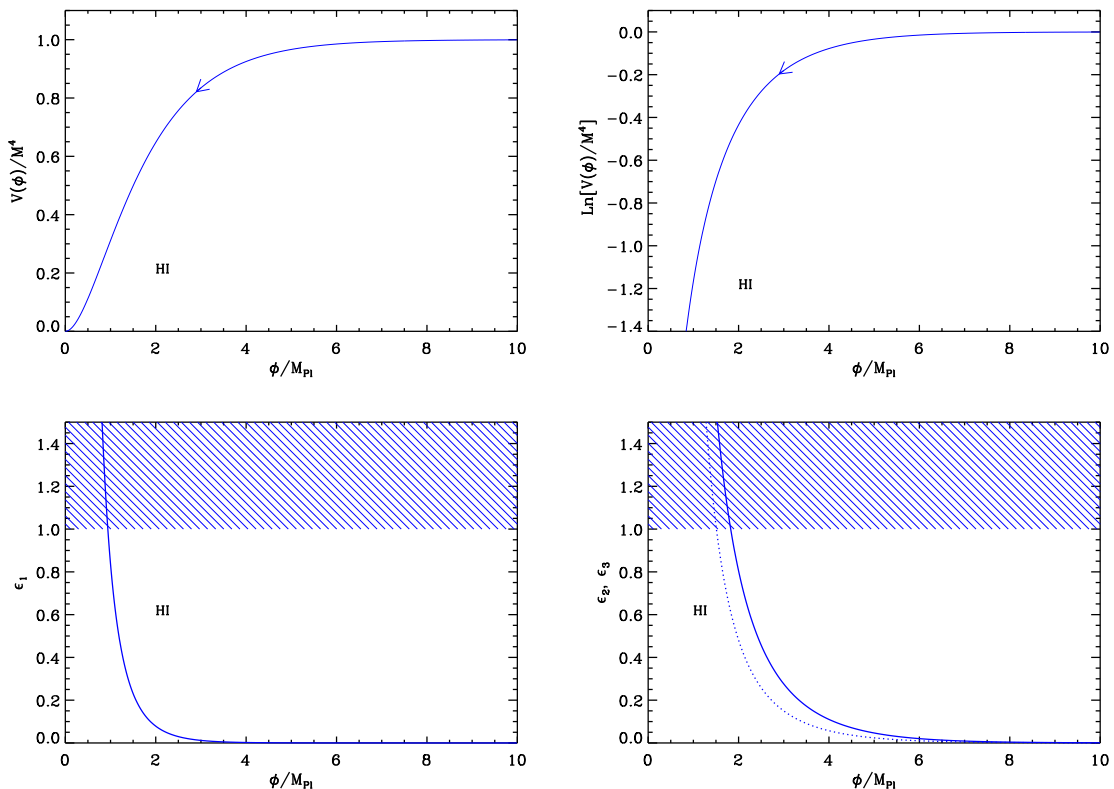


Figure 5. Higgs Inflation (HI). Top left panel: Higgs potential corresponding to Eq. (3.9). Top right panel: logarithm of the Higgs potential. It is clear from these two plots that inflation proceeds from the left to the right. Bottom left panel: slow-roll parameter ϵ_1 as a function of the field ϕ . The shaded area indicates the breakdown of the slow-roll inflation (strictly speaking when the acceleration stops) and we see that, in this model, the end of inflation occurs by violation of the slow-roll condition. Bottom right panel: slow-roll parameters ϵ_2 (solid line) and ϵ_3 (dotted line) for the same potential.

In this model, as can be noticed on these plots, inflation stops by violation of the slow-roll conditions. The condition $\epsilon_1 = 1$ occurs for $x = x_{\text{end}}$ where x_{end} can be expressed as

$$x_{\text{end}} = \sqrt{\frac{3}{2}} \ln \left(1 + \frac{2}{\sqrt{3}} \right) \simeq 0.94. \quad (3.11)$$

In fact, before the end of inflation, the slow-roll approximation breaks down when ϵ_2 becomes greater than 1. This happens for $x = x_{\epsilon_2=1}$ where

$$x_{\epsilon_2=1} = \sqrt{6} \operatorname{arcsinh} \left(\sqrt{\frac{2}{3}} \right) \simeq 1.83. \quad (3.12)$$

The third slow-roll parameter ϵ_3 also becomes greater than 1 before the end of inflation (but after the second slow-roll parameter has become unity). The corresponding vacuum expectation value can be written as

$$x_{\epsilon_3=1} = \sqrt{6} \operatorname{arctanh} \left(\frac{2}{1 + \sqrt{7}} \right) \simeq 1.51. \quad (3.13)$$

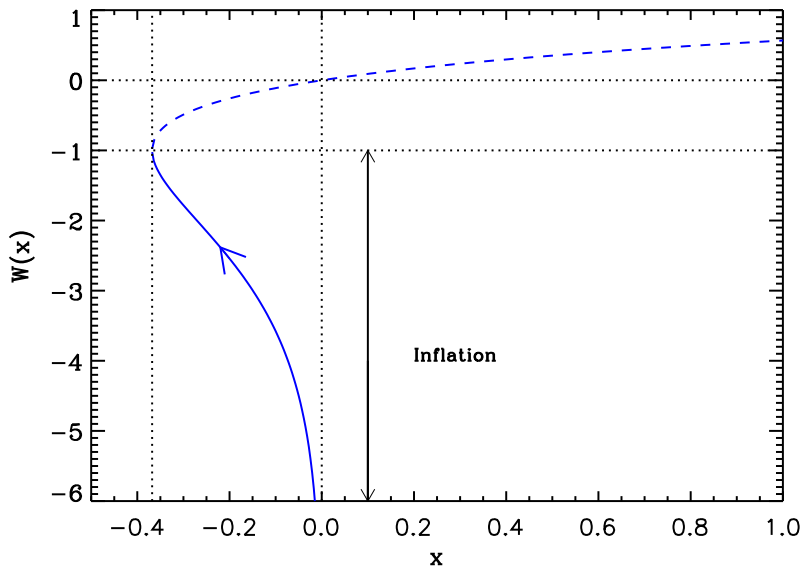


Figure 6. Lambert functions $W_0(x)$ (dashed line) and $W_{-1}(x)$ (solid line). During Higgs inflation, inflation proceeds along the “-1” branch in the direction specified by the arrow in the figure.

Of course, these three vacuum expectation values do not depend on the parameter ξ since this parameter is “hidden” in the mass scale M .

We are now in a position where one can calculate the slow-roll trajectory. Using Eq. (3.9), it can be integrated exactly and yields to

$$N - N_{\text{ini}} = \frac{1}{2} \sqrt{\frac{3}{2}} (x - x_{\text{ini}}) - \frac{3}{4} \left(e^{\sqrt{\frac{2}{3}}x} - e^{\sqrt{\frac{2}{3}}x_{\text{ini}}} \right). \quad (3.14)$$

In the regime where $x \gg 1$, the last term is dominant and this is the one usually considered in the literature, see Ref. [147]. The trajectory can be inverted and expressed in term of the “-1-branch” of the Lambert function W_{-1} , leading to

$$x = \sqrt{\frac{3}{2}} \left\{ \frac{4}{3} N + \sqrt{\frac{2}{3}} x_{\text{ini}} - e^{\sqrt{\frac{2}{3}}x_{\text{ini}}} - W_{-1} \left[-\exp \left(\frac{4}{3} N + \sqrt{\frac{2}{3}} x_{\text{ini}} - e^{\sqrt{\frac{2}{3}}x_{\text{ini}}} \right) \right] \right\}. \quad (3.15)$$

The fact that inflation proceeds on the -1 branch of the Lambert function W_{-1} , as can be seen in Fig. 6, can be justified by the following considerations. When $N = 0$, the value taken by the Lambert function is $-\exp(\sqrt{2/3}x_{\text{ini}})$, which is smaller than -1 . On the other hand, if $x = 0$, the value given for N by Eq. (3.14) can be inserted in Eq. (3.15) and one finds that the argument of the Lambert function is -1 , i.e. the connection point between the -1 branch and the 0 branch. Therefore inflation takes place between these two points.

Finally, the value of the inflaton field, x_* , calculated $\Delta N_* = N_{\text{end}} - N_*$ e-folds before

the end of inflation reads

$$x_* = \sqrt{\frac{3}{2}} \left(-\frac{4}{3} \Delta N_* + \ln \left(1 + \frac{2}{\sqrt{3}} \right) - \left(1 + \frac{2}{\sqrt{3}} \right) - W_{-1} \left\{ -\exp \left[-\frac{4}{3} \Delta N_* + \ln \left(1 + \frac{2}{\sqrt{3}} \right) - \left(1 + \frac{2}{\sqrt{3}} \right) \right] \right\} \right). \quad (3.16)$$

In principle, inserting this formula into the expressions of the slow-roll parameters (3.10) allows us to determine the observational predictions of the model.

At this stage, however, a comment is in order about reheating. As explained above, all the previous considerations are derived in the Einstein frame. In this frame, matter is not universally coupled to the metric tensor and, therefore, it is compulsory to re-consider the parametrization presented in section 2.2. In the Einstein frame, the matter action is given by $S_{\text{mat}}[\psi, A^2(\phi)g_{\mu\nu}]$, where ψ denotes some generic matter field and $g_{\mu\nu} \equiv F(h)\bar{g}_{\mu\nu}$ with $A \equiv F^{-1/2}$, see Ref. [151] (recall that quantities in the Jordan frame are denoted with a bar). In the Jordan frame, the energy density of a (conserved) fluid with equation of state $w = \bar{p}/\bar{\rho}$ scales as $\bar{\rho} \propto \bar{a}^{-3(1+w)}$ while, in the Einstein frame, $\rho \propto A^4 \bar{\rho} \propto A^{1-3w} a^{-3(1+w)}$ since the scale factors in the two frames are related by $\bar{a} = Aa$ (here, we have assumed a constant w , see the discussion below). As explained in Ref. [64] and briefly reviewed in section 2.2, the dependence of the observational predictions on reheating originates from the gradient term k/\mathcal{H} present in the Mukhanov-Sasaki variable equation of motion. In order to evaluate concretely this term, one must relate the comoving wave-number k during inflation with physical scales measured now. Clearly, this depends on the whole history of the Universe and, therefore, explains why the final result depends on the reheating duration. In the Einstein frame, one can show that the gradient term takes the standard form, namely

$$\frac{k}{\mathcal{H}} = \frac{e^{N_{\text{end}}-N}}{H} \frac{k}{a_0} \left(\frac{\rho_{\text{end}}}{\rho_\gamma} \right)^{1/4} \frac{1}{R_{\text{rad}}}, \quad (3.17)$$

with

$$\ln R_{\text{rad}} = \frac{1-3w_{\text{reh}}}{12(1+w_{\text{reh}})} \ln \left(\frac{\rho_{\text{reh}}}{\rho_{\text{end}}} \right) - \frac{1-3w_{\text{reh}}}{3(1+w_{\text{reh}})} \ln \left(\frac{A_{\text{reh}}}{A_{\text{end}}} \right), \quad (3.18)$$

where w_{reh} is the equation of state of the effective dominant fluid during reheating. In the above expressions, it is important to emphasize that all the quantities are defined in the Einstein frame and that the non-standard scaling of the various energy densities (pressureless matter and radiation) has been systematically taken into account. All the extra terms cancel out except in the definition of the parameter R_{rad} where there is an additional term depending on the function A . Remarkably, this additional term is exactly such that the parameter R_{rad} in the Einstein frame can be re-expressed in terms of the energy densities in the Jordan frame only, namely

$$\ln R_{\text{rad}} = \frac{1-3w_{\text{reh}}}{12(1+w_{\text{reh}})} \ln \left(\frac{\bar{\rho}_{\text{reh}}}{\bar{\rho}_{\text{end}}} \right). \quad (3.19)$$

Let us stress again that the above equation has an unusual form: it is a quantity in the Einstein frame expressed in terms of quantities defined in the Jordan frame.

It is also important to notice an additional limitation compared to the standard case: in presence of non-minimal coupling to gravity, our parametrization of the reheating stage works only for a constant equation of state w_{reh} while in Ref. [64] it was valid for any w_{reh} .

We now explain the origin of this limitation. In the Einstein frame, the general expression of the parameter R_{rad} is given by

$$\frac{1}{R_{\text{rad}}} = \left(\frac{\rho_{\text{reh}}}{\rho_{\text{end}}} \right)^{1/4} \frac{a_{\text{reh}}}{a_{\text{end}}}. \quad (3.20)$$

In order to obtain Eq. (3.18) from that formula, one should express the Einstein frame scale factor in term of the energy density ρ . If the equation of state w_{reh} is a constant, then $a \propto A^{(1-3w_{\text{reh}})/(3+3w_{\text{reh}})} a^{-1/(3+3w_{\text{reh}})}$. This what what has been used above and this led to Eqs. (3.18) and (3.19). But let us now assume that w_{reh} is not a constant (notice that one always has $w = \bar{w}$ since the energy density and the pressure scales with the same power of the function A in the Einstein frame). Then, ρ and a are related by

$$\frac{d\rho}{\rho} = (1 - 3w_{\text{reh}}) \frac{dA}{A} - 3(1 + w_{\text{reh}}) \frac{da}{a}. \quad (3.21)$$

If A is a constant, as explained in Ref. [64], one can always write

$$\frac{a_{\text{reh}}}{a_{\text{end}}} = \left(\frac{\rho_{\text{reh}}}{\rho_{\text{end}}} \right)^{-1/(3+3\bar{w}_{\text{reh}})}, \quad (3.22)$$

where \bar{w}_{reh} is the mean equation of state during reheating, namely

$$\bar{w}_{\text{reh}} \equiv \frac{1}{N_{\text{reh}} - N_{\text{end}}} \int_{N_{\text{end}}}^{N_{\text{reh}}} w_{\text{reh}}(n) dn. \quad (3.23)$$

If A and w_{reh} , however, are not constant, it is no longer possible to express the final formula in terms of \bar{w}_{reh} . In particular, we do not obtain a term $A^{1-3\bar{w}_{\text{reh}}}$ as desired. Therefore, in what follows, we restrict our considerations to the case where the effective fluid dominating the matter content of the Universe has a constant equation of state.

Then, from Eq. (3.17), one can re-express R_{rad} in terms of quantities defined at Hubble radius crossing. One obtains

$$\Delta N_* = \ln R_{\text{rad}} - \ln \left(\frac{k/a_0}{\rho_\gamma^{1/4}} \right) + \frac{1}{4} \ln \left(\frac{H_*^2}{M_{\text{Pl}}^2 \epsilon_{1*}} \right) - \frac{1}{4} \ln \left(\frac{3}{\epsilon_{1*}} \frac{V_{\text{end}}}{V_*} \frac{3 - \epsilon_{1*}}{3 - \epsilon_{1\text{end}}} \right). \quad (3.24)$$

Of course, this equation resembles a lot Eq. (2.44) but one has to realize that it involves quantities defined in the Einstein frame only. The term $\ln \left[(k/a_0) / \rho_\gamma^{1/4} \right] = \ln \left[(k/\bar{a}_0) / \bar{\rho}_\gamma^{1/4} \right]$ and, therefore, its numerical value remains unchanged. The other quantities appearing in this equation are obtained using our standard procedures since they refer to the inflaton sector only. Then, the range of variation of ΔN_* in Eq. (3.24) is determined by putting limits on $\ln R_{\text{rad}}$ coming from the fact that reheating must proceed between the end of inflation and the BBN. This means that the physical value of the energy density, that is to say $\bar{\rho}_{\text{reh}}$, must be such that $\bar{\rho}_{\text{nuc}} \equiv (10\text{MeV})^4 < \bar{\rho}_{\text{reh}} < \bar{\rho}_{\text{end}}$. We emphasize that physical limits must of course refer to quantities defined in the Jordan frame. But, precisely, we have shown that $\ln R_{\text{rad}}$ in the Einstein frame can be expressed according to the standard formula, provided the energy densities in the argument of the logarithm are Jordan frame energy densities. Therefore, in practice, we have $\Delta N_* \in [\Delta N_*^{\text{nuc}}, \Delta N_*^{\text{end}}]$ with

$$\Delta N_*^{\text{end}} = -N_0 + \ln \left(\frac{H_*}{M_{\text{Pl}}} \right) - \frac{1}{4} \ln \left(\frac{\rho_{\text{end}}}{M_{\text{Pl}}^4} \right), \quad (3.25)$$

where all the quantities in the above equation are calculated in the Einstein frame and, hence, are directly available since they are, by definition, the outcomes of the ASPIC library code. The other limit can be expressed as

$$\Delta N_*^{\text{nuc}} = -N_0 + \ln\left(\frac{H_*}{M_{\text{Pl}}}\right) - \frac{1}{3(1+w)} \ln\left(\frac{\bar{\rho}_{\text{end}}}{M_{\text{Pl}}^4}\right) - \frac{1-3w}{12(1+w)} \ln\left(\frac{\bar{\rho}_{\text{nuc}}}{M_{\text{Pl}}^4}\right). \quad (3.26)$$

The quantity $\bar{\rho}_{\text{nuc}}$ is defined in the Jordan frame but its value is explicitly known, see above. On the other hand, we need to evaluate $\bar{\rho}_{\text{end}}$ since the code only delivers ρ_{end} . By definition, we have

$$\bar{\rho}_{\text{end}} = \frac{\rho_{\text{end}}}{A_{\text{end}}^4} = F_{\text{end}}^2 \rho_{\text{end}} = (1 + \xi h_{\text{end}}^2)^2 \rho_{\text{end}}. \quad (3.27)$$

But $1 + \xi h_{\text{end}}^2 = e^{2\chi_{\text{end}}/\sqrt{3}}$ and $\chi_{\text{end}} = \phi_{\text{end}}/(\sqrt{2}M_{\text{Pl}}) = \sqrt{3}/2 \ln(1 + 2/\sqrt{3})$. As a consequence, the relation between the two final energy densities in the two frames can be written as

$$\bar{\rho}_{\text{end}} = \left(1 + \frac{2}{\sqrt{3}}\right)^2 \rho_{\text{end}} \simeq 2.15 \rho_{\text{end}}. \quad (3.28)$$

Therefore, the lower bound is only slightly modified (recall that $\bar{\rho}_{\text{end}}$ appears in a logarithmic term). Anyway, given the uncertainty in the definition of $\bar{\rho}_{\text{nuc}}$, it is irrelevant to include this tiny correction in our determination of ΔN_* . Consequently, we conclude that the range of variation of ΔN_* can be obtained without modifying anything to our usual way to calculate it and one can use the ASPIC code without introducing these negligible corrections.

The reheating consistent observational predictions of Higgs inflation are represented in Fig. 73 where we have displayed their dependence in the reheating temperature defined in the Jordan frame by $g_*^{1/4} \bar{T}_{\text{reh}} = (30\bar{\rho}_{\text{reh}}/\pi^2)^{1/4}$. Notice that, a priori, the reheating temperature can be calculated exactly in Higgs inflation since all the couplings between the Higgs and the other fields in the standard model are known. This gives a spectral index which is in good agreement with the data and a small contribution of gravity waves. At this stage, we do not have constraints on the parameter ξ since it is hidden in the mass scale M . Its observational value therefore comes from the amplitude of the CMB anisotropies and reads

$$\frac{M^4}{M_{\text{Pl}}^4} = 1920\pi^2 \left(1 - e^{\sqrt{\frac{2}{3}}x_*}\right)^{-4} e^{2\sqrt{\frac{2}{3}}x_*} \frac{Q_{\text{rms-PS}}^2}{T^2}. \quad (3.29)$$

Upon using the trajectory given by Eq. (3.16), the mass scale M can be written as $M/M_{\text{Pl}} \simeq 0.02(\Delta N_*)^{-3/2}$, which for the fiducial value $\Delta N_* = 55$, implies that $M \simeq 4 \times 10^{-5} M_{\text{Pl}}$, i.e., roughly speaking, inflation takes place at the GUT scale in this model. Then, using this expression of M , one obtains the following numerical value for the parameter ξ ,

$$\xi \simeq 49000\sqrt{\lambda}, \quad (3.30)$$

where we have considered $\lambda = m_{\text{H}}/v$, with $v \simeq 175\text{GeV}$ and $m_{\text{H}} \simeq 125\text{GeV}$ (see Refs. [145, 146]). These considerations are in agreement with the conclusions obtained in Refs. [147–149].

4 One Parameter Models

4.1 Radiatively Corrected Higgs Inflation (RCHI)

Let us consider again the model given by Eq. (3.1). The three functions describing this action are modified when quantum corrections are taken into account. As a consequence,

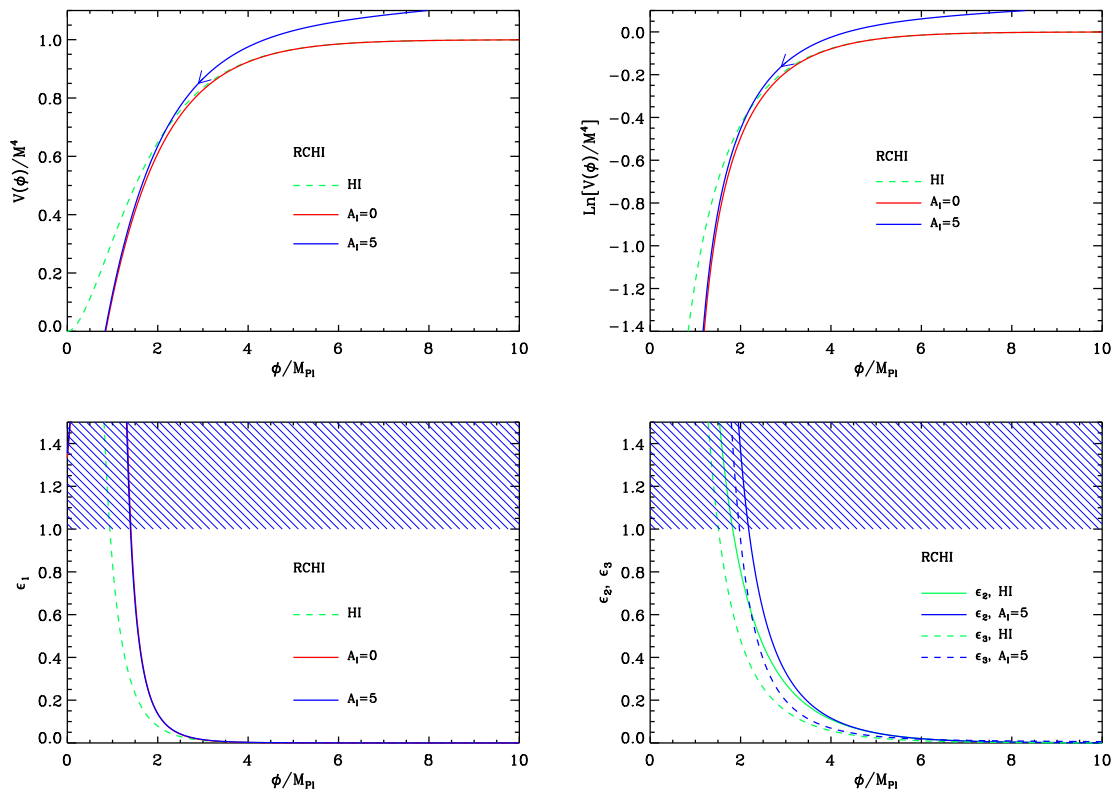


Figure 7. Top left panel: the solid blue line represents the radiatively corrected Higgs potential, see Eq. (4.11), with $A_1 = 5$. It is compared to the tree level potential given by Eq. (3.9) (dashed green line) and to Eq. (4.11) with $A_1 = 0$ (solid red line) which is supposed to be a good approximation of the tree level potential. It is obvious that this is indeed the case in the regime of interest, where the v_{ev} of the Higgs field is not too small. Top right panel: logarithm of potential, the three lines and the color code having the same meaning as in the top left panel. Bottom left panel: slow-roll parameter ϵ_1 as a function of the field ϕ , still with the same convention. As can be seen in this plot, even in presence of radiative corrections, the end of inflation occurs by violation of the slow-roll condition. Bottom right panel: slow-roll parameters ϵ_2 (solid blue line) and ϵ_3 (dashed blue line) for $A_1 = 5$ compared to their tree level counter parts (solid and dashed green lines, respectively).

the potential which supports inflation is also modified and this leads to a new inflationary scenario that we call Radiatively Corrected Higgs Inflation (RCHI). This scenario has been studied in Refs. [155] and [156–159]. At first order, the corrections to the function $Z(h)$ can be neglected while the corrections to $F(h)$ and to $U(h)$ read

$$F(h) = 1 + \xi h^2 + \frac{C}{16\pi^2} h^2 \ln\left(\frac{M_{Pl}^2 h^2}{\mu^2}\right), \quad (4.1)$$

$$U(h) = M_{Pl}^2 \frac{\lambda}{4} \left(h^2 - \frac{v^2}{M_{Pl}^2}\right)^2 + \frac{\lambda A}{128\pi^2} M_{Pl}^2 h^4 \ln\left(\frac{M_{Pl}^2 h^2}{\mu^2}\right), \quad (4.2)$$

where μ is the renormalization scale and A and C are two new constants given by

$$A = \frac{3}{8\lambda} [2g^4 + (g^2 + g'^2) - 16y_t^4] + 6\lambda + \mathcal{O}(\xi^{-2}), \quad (4.3)$$

$$C = 3\xi\lambda + \mathcal{O}(\xi^0), \quad (4.4)$$

y_t being the Yukawa coupling of the top quark and g and g' the coupling constants of the $SU(2)_L$ and $U(1)_Y$ groups. The presence of quantum corrections modifies the relation between the Jordan and the Einstein frames and changes the shape of the potential in the Einstein frame. Assuming the smallness of $A/(32\pi^2) \ll 1$ and $C/(8\pi^2\xi) \ll 1$, which is necessary for the consistence of the one-loop calculation (the second condition is in fact equivalent to $C\lambda/(8\pi^2) \ll 1$ because C is proportional to ξ), one obtains the following expression

$$V \simeq \frac{M_{\text{Pl}}^4 \lambda}{4\xi^2} \frac{\xi^2 h^4}{(1 + \xi h^2)^2} \left[1 - \frac{\xi h^2}{1 + \xi h^2} \frac{C}{8\pi^2 \xi} \ln \left(\frac{M_{\text{Pl}}^2 h^2}{\mu^2} \right) + \frac{A}{32\pi^2} \ln \left(\frac{M_{\text{Pl}}^2 h^2}{\mu^2} \right) \right]. \quad (4.5)$$

Of course, if $A = C = 0$, one checks that this potential reduces to the potential of the previous section. Notice that, at this stage, we have not assumed that $\xi h^2 \gg 1$. If we further postulate that $\xi h^2 \gg 1$ and approximate $\xi^2 h^4 / (1 + \xi h^2)^2 \simeq 1 - 2/(\xi h^2)$, then the above formula reduces to

$$V \simeq \frac{M_{\text{Pl}}^4 \lambda}{4\xi^2} \left[1 - \frac{2}{\xi h^2} + \frac{A_1}{16\pi^2} \ln \left(\frac{M_{\text{Pl}} h}{\mu} \right) \right], \quad (4.6)$$

where $A_1 \equiv A - 12\lambda$ is the inflationary anomalous scaling. This formula coincides with Eq. (6) of Ref. [157] and Eq. (9) of Ref. [159]. Although the above formulas give V in the Einstein frame, it is still expressed in term of h . The expression for the field in the Einstein frame, χ , remains to be established. Assuming the smallness of the loop corrections (but, here, we do not assume that $\xi h^2 \gg 1$), we obtain

$$\frac{d\chi}{dh} \simeq \frac{\sqrt{3}h\xi}{(1 + \xi h^2)} \left[1 + \frac{C}{16\pi^2 \xi} + \frac{C}{8\pi^2 \xi} \frac{1}{1 + \xi h^2} \ln \left(\frac{M_{\text{Pl}} h}{\mu} \right) \right]. \quad (4.7)$$

Notice that, in order to obtain this equation, we have also neglected a term proportional to $1/(\xi h)^2 \ll 1$. Contrary to the assumption $\xi h^2 \gg 1$, the condition $(\xi h)^2 \gg 1$ was also used in section 3.1. Then, it is easy to integrate this differential equation and this leads to

$$\chi \simeq \frac{\sqrt{3}}{2} \ln(1 + \xi h^2) + \frac{\sqrt{3}C}{16\pi^2 \xi} \left[\ln h - \frac{1}{1 + \xi h^2} \ln \left(\frac{M_{\text{Pl}} h}{\mu} \right) \right]. \quad (4.8)$$

In the limit $\xi h^2 \gg 1$, this expression reduces to

$$\chi \simeq \frac{\sqrt{3}}{2} \ln(\xi h^2) + \frac{\sqrt{3}C}{16\pi^2 \xi} \ln h. \quad (4.9)$$

As expected the relation between the Jordan frame field h and the Einstein frame field χ is modified by the quantum corrections. Inverting the above formula gives

$$\xi^{1/2} h \simeq e^{\chi/\sqrt{3}} - \frac{C}{16\pi^2 \xi} e^{\chi/\sqrt{3}} \left(\frac{\chi}{\sqrt{3}} - \frac{1}{2} \ln \xi \right). \quad (4.10)$$

This equation allows us to find the expression of the potential in the Einstein frame. Inserting Eq. (4.10) into Eq. (4.6) and introducing the canonically normalized field $\phi \equiv \sqrt{2}M_{\text{Pl}}\chi$, one obtains

$$\begin{aligned}
V(\phi) &\simeq \frac{M_{\text{Pl}}^4 \lambda}{4\xi^2} \left[1 - 2e^{-2\phi/(\sqrt{6}M_{\text{Pl}})} - \frac{C}{4\pi^2 \xi} e^{-2\phi/(\sqrt{6}M_{\text{Pl}})} \left(\frac{\phi}{\sqrt{6}M_{\text{Pl}}} - \frac{1}{2} \ln \xi \right) \right. \\
&\quad \left. + \frac{A_1}{16\pi^2} \ln \left(\frac{M_{\text{Pl}}}{\mu\sqrt{\xi}} \right) + \frac{A_1}{16\pi^2} \frac{\phi}{\sqrt{6}M_{\text{Pl}}} \right] \\
&\simeq \frac{M_{\text{Pl}}^4 \lambda}{4\xi^2} \left[1 - 2e^{-2\phi/(\sqrt{6}M_{\text{Pl}})} + \frac{A_1}{16\pi^2} \frac{\phi}{\sqrt{6}M_{\text{Pl}}} \right]. \tag{4.11}
\end{aligned}$$

We see that we now deal with a ‘‘one parameter model’’, A_1 , since, as usual, the mass scale $M^4 \equiv M_{\text{Pl}}^4 \lambda / (4\xi^2)$ will be determined by the COBE normalization. In the case $A_1 = 0$, it is also interesting to compare the above potential with the one given by Eq. (3.9). We see that this corresponds to assuming that the exponential $e^{-2\phi/(\sqrt{6}M_{\text{Pl}})} \ll 1$ (or, equivalently, $\phi/M_{\text{Pl}} \gg 1$) and to expand the corresponding expression at first order in this small parameter. This leads to the following formula: $V \simeq M^4 [1 - 2e^{-2\phi/(\sqrt{6}M_{\text{Pl}})}]$, i.e. exactly Eq. (4.11) for $A_1 = 0$. It is worth remarking that this approximation is not very good towards the end of inflation. Indeed, it is easy to show that (see below), for the potential (4.11) with $A_1 = 0$, $\phi_{\text{end}}/M_{\text{Pl}} = \sqrt{3/2} \ln(2 + 2/\sqrt{3}) \simeq 1.4$ which should be compared with Eq. (3.11) for the potential (3.9) according to which $\phi_{\text{end}}/M_{\text{Pl}} \simeq 0.94$. The potential (4.11) is represented and compared with its tree level counterpart in Fig. 7.

Given the potential (4.11), we can now proceed to the slow-roll analysis. Defining $x \equiv \phi/M_{\text{Pl}}$, the three first slow-roll parameters can be written as

$$\epsilon_1 = \frac{1}{12} \left[\frac{4e^{-\sqrt{2/3}x} + A_1/(16\pi^2)}{1 - 2e^{-\sqrt{2/3}x} + A_1/(32\pi^2)\sqrt{2/3}x} \right]^2, \tag{4.12}$$

$$\epsilon_2 = \frac{1}{3} \frac{8e^{-\sqrt{2/3}x} \left[1 + A_1/(16\pi^2) + A_1/(32\pi^2)\sqrt{2/3}x \right] + A_1^2/(256\pi^4)}{\left[1 - 2e^{-\sqrt{2/3}x} + A_1/(32\pi^2)\sqrt{2/3}x \right]^2}, \tag{4.13}$$

and

$$\begin{aligned}
\epsilon_3 &= 12 \left(4 + \frac{A_1}{16\pi^2} e^{\sqrt{2/3}x} \right) \left\{ 48 + 8 \frac{A_1}{16\pi^2} (9 + \sqrt{6}x) + 3 \frac{A_1^3}{4096\pi^6} e^{2\sqrt{2/3}x} \right. \\
&\quad \left. + 2e^{\sqrt{2/3}x} \left[12 + 18 \frac{A_1}{16\pi^2} \left(1 + \frac{A_1}{16\pi^2} \right) + \sqrt{6} \frac{A_1}{16\pi^2} \left(4 + 3 \frac{A_1}{16\pi^2} \right) x + 2 \frac{A_1^2}{256\pi^4} x^2 \right] \right\} \\
&\quad \times \left[24 + \frac{A_1}{16\pi^2} \left(24 + 4\sqrt{6}x + 3 \frac{A_1}{16\pi^2} e^{\sqrt{2/3}x} \right) \right]^{-1} \left[-12 + e^{\sqrt{2/3}x} \left(6 + \sqrt{6} \frac{A_1}{16\pi^2} x \right) \right]^{-2}. \tag{4.14}
\end{aligned}$$

These three slow-roll parameters are represented in Fig. 7 (bottom panels). It is interesting to compare these formulas with the expressions derived in Ref. [155] [see Eqs. (22) and (23) of that paper]. An approximate equation for the first slow-roll parameter is obtained by

neglecting the second and third terms in the denominator of Eq. (4.12), which, as a matter of fact, consists in writing $V(\phi) \simeq M^4$. Then, it follows that

$$\epsilon_1 \simeq \frac{4}{3} e^{-2\sqrt{2/3}x} \left(1 + \frac{A_1}{64\pi^2} e^{\sqrt{2/3}x} \right)^2 \simeq \frac{4}{3} \frac{1}{\xi^2 h^4} \left(1 + \frac{h^2}{h_1^2} \right)^2, \quad (4.15)$$

where we have defined $h_1^2 \equiv 64\pi^2/(\xi A_1)$ in agreement with Ref. [155]. The same approximation is made for the second slow-roll parameter (except that Ref. [155] calculates $\hat{\eta} \equiv M_{\text{Pl}}^2 V_{\phi\phi}/V$ rather than ϵ_2). The second field derivative of the potential can be written as $V_{\phi\phi} = -4M^4 e^{-\sqrt{2/3}x}/(3M_{\text{Pl}}^2)$ and, therefore, if one considers that $V(\phi) \simeq M^4$, then $\hat{\eta} \simeq -4/(3\xi h^2)$. We conclude that our expressions of ϵ_1 and ϵ_2 reproduce Eqs. (22) and (23) of Ref. [155] in the limit where $V(\phi) \simeq M^4$.

Let us now study how inflation ends in this model. From Fig. 7, it is clear that this occurs by violation of the slow-roll conditions. Working out the condition $\epsilon_1 = 1$, it follows that

$$x_{\text{end}} = \frac{1}{\sqrt{2}} - \sqrt{\frac{3}{2}} \frac{32\pi^2}{A_1} + \sqrt{\frac{3}{2}} W_{-1} \left[\frac{64\pi^2}{A_1} \left(1 + \frac{1}{\sqrt{3}} \right) e^{32\pi^2/A_1 - 1/\sqrt{3}} \right], \quad (4.16)$$

where, if $A_1 > 0$, $W_{-1} = W_0$ while, if $A_1 < 0$, $W_{-1} = W_{-1}$.

We now turn to the slow-roll trajectory. It can be integrated exactly and straightforward manipulations lead to the following expression

$$\begin{aligned} N - N_{\text{ini}} &= \sqrt{\frac{3}{2}} x - \frac{48\pi^2}{A_1} \left[1 + \frac{A_1}{32\pi^2} \left(1 + \sqrt{\frac{2}{3}} x \right) \right] \ln \left(1 + \frac{A_1}{64\pi^2} e^{\sqrt{2/3}x} \right) \\ &\quad - \frac{3}{2} \text{Li}_2 \left(-\frac{A_1}{64\pi^2} e^{\sqrt{2/3}x} \right) - \sqrt{\frac{3}{2}} x_{\text{ini}} + \frac{48\pi^2}{A_1} \left[1 + \frac{A_1}{32\pi^2} \left(1 + \sqrt{\frac{2}{3}} x_{\text{ini}} \right) \right] \\ &\quad \times \ln \left(1 + \frac{A_1}{64\pi^2} e^{\sqrt{2/3}x_{\text{ini}}} \right) + \frac{3}{2} \text{Li}_2 \left(-\frac{A_1}{64\pi^2} e^{\sqrt{2/3}x_{\text{ini}}} \right), \end{aligned} \quad (4.17)$$

where Li_2 denotes the dilogarithm function [160, 161]. Let us also notice that if we use the approximation $V(\phi) \simeq M^4$ already discussed before, then one can obtain a much simpler formula, namely

$$N - N_{\text{ini}} = -\frac{48\pi^2}{A_1} \ln \left(1 + \frac{A_1}{64\pi^2} e^{\sqrt{2/3}x} \right) + \frac{48\pi^2}{A_1} \ln \left(1 + \frac{A_1}{64\pi^2} e^{\sqrt{2/3}x_{\text{ini}}} \right). \quad (4.18)$$

This expression is in agreement with Eq. (24) of Ref. [155]. In this case, the trajectory can even be inverted and the corresponding expression for the field ϕ reads

$$x = \sqrt{\frac{3}{2}} \ln \left[\left(\frac{64\pi^2}{A_1} + e^{\sqrt{2/3}x_{\text{ini}}} \right) e^{A_1(N-N_{\text{ini}})/(48\pi^2)} - \frac{64\pi^2}{A_1} \right]. \quad (4.19)$$

We are now in a position where the predictions of the models can be calculated. They are presented in Fig. 73. We see that very negative values of A_1 are incompatible with the CMB while large values of A_1 fall right in the center of the allowed contours. Of course $|A_1|$ cannot be too large since we have required $A_1/(64\pi^2) \ll 1$. We have chosen the upper bound in Fig. 73 to be $A_1 = 100$ for which $A_1/(64\pi^2) \simeq 0.16$, i.e. still a reasonable number. It

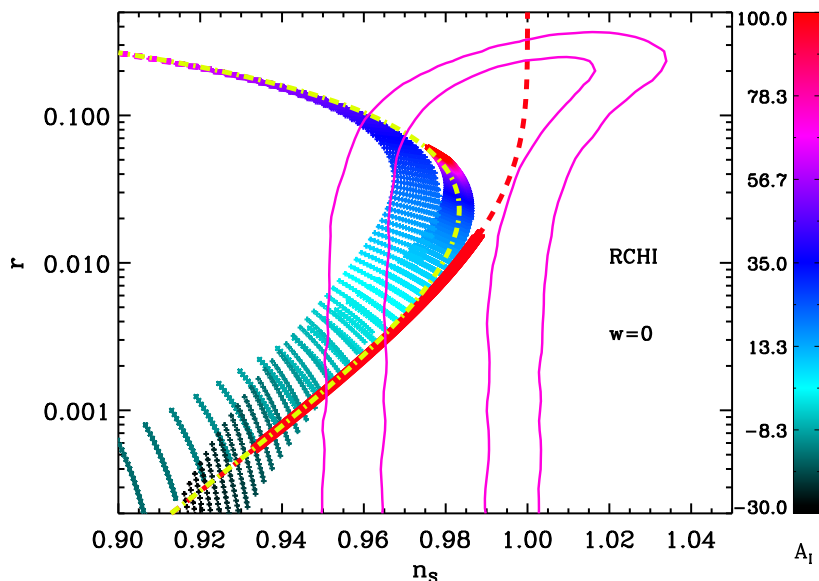


Figure 8. Predictions of the RCHI model in the plane (n_s, r) . The exact slow-roll predictions (colored segments starting in black/green at the bottom/left part of the plot and ending in red right in the middle of the allowed contours) are compared to various approximations represented by the second collection of colored segments, by the red thick dashed line and by the yellow dotted-dashed line, see the text for a detailed explanation. In the regime $10 < A_I < 100$, the exact predictions significantly differ from the approximate ones.

is interesting to compare these findings with the existing literature. Using the approximate trajectory (4.18) and neglecting the contribution originating from the end of inflation, one obtains

$$x_* = \sqrt{\frac{3}{2}} \ln \left[\frac{64\pi^2}{A_I} (e^{x_{\text{BKS}}} - 1) \right], \quad (4.20)$$

where $x_{\text{BKS}} \equiv A_I \Delta N_*/(48\pi^2)$, not to be confused with x (x_{BKS} is denoted x in Ref. [155]). The above formula giving x_* is in agreement with Eq. (27) of Ref. [155]. Then, from Eq. (4.15) and the fact that $\epsilon_2 = 4\epsilon_1 - 2\hat{\eta}$, it follows that

$$\epsilon_1 = \frac{4}{3} \left(\frac{A_I}{64\pi^2} \right)^2 \left(\frac{e^{x_{\text{BKS}}}}{e^{x_{\text{BKS}}} - 1} \right)^2 = \frac{3}{4\Delta N_*^2} \left(\frac{x_{\text{BKS}} e^{x_{\text{BKS}}}}{e^{x_{\text{BKS}}} - 1} \right)^2, \quad (4.21)$$

$$\epsilon_2 = 4\epsilon_1 + \frac{8}{3} \frac{A_I}{64\pi^2} \frac{1}{e^{x_{\text{BKS}}} - 1} = 4\epsilon_1 + \frac{2}{\Delta N_*} \frac{x_{\text{BKS}}}{e^{x_{\text{BKS}}} - 1}. \quad (4.22)$$

From these two expressions, one deduces that

$$n_s = 1 - \frac{2}{\Delta N_*} \frac{x_{\text{BKS}}}{e^{x_{\text{BKS}}} - 1}, \quad r = \frac{12}{\Delta N_*^2} \left(\frac{x_{\text{BKS}} e^{x_{\text{BKS}}}}{e^{x_{\text{BKS}}} - 1} \right)^2. \quad (4.23)$$

Notice that, in the formula giving the spectral index, the contribution originating from ϵ_1 has been neglected since it scales $\propto 1/\Delta N_*^2$. These expressions are exactly similar to Eqs. (32) and (34) of Ref. [155]. For $\Delta N_* = 60$, they can be represented as a line $r = r(n_s)$ in the

plane (n_s, r) , the parameter along the curve being A_1 . This line has been plotted in Fig. 8 for $-30 < A_1 < 100$ (red dashed line; notice that, for this line, the color code indicated by the bare on the side does not apply). Requiring $0.934 < n_s < 0.988$, which is the 2σ range coming from combining the WMAP data, the Baryon Acoustic Oscillations (BAO) data and the Supernovae measurements (notice that this range is obtained from different data sets and this is why it slightly differs from the range one might infer from the CMB contours only in Fig. 8), one obtains the solid thick red segment. It follows that $-12 \lesssim A_1 \lesssim 14$, again in agreement with Ref. [155]. These predictions are compared to the exact slow-roll predictions of Fig. 73. As usual, the exact predictions are represented by a collection of segments, each segment corresponding to different values of A_1 (that can be read by means of the color code) and each point of a given segment being in one-to-one correspondence with a given reheating temperature. The exact predictions are such that, for $A_1 < 0$, the black/green segments go to the bottom left side of the figure while for $A_1 \rightarrow 100$, the pink/red segments fall right in the middle of the allowed contours. If one wants to identify even better the exact predictions, one can also directly look at Fig. 73 and then compare it with Fig. 8. We see on this last plot that, in the limit of “large” positive values of A_1 , the exact slow-roll predictions and the predictions based on Eqs. (4.23) significantly differ. While, in order to remain inside the allowed contour, Eqs. (4.23) tell us that $A_1 \lesssim 14$, the exact predictions show that it is in fact the case for any positive values of $A_1 \lesssim 100$ [let us stress once more that $A_1/(64\pi^2)$ must remain a small quantity; values of $A_1 \lesssim 100$ are fine while values such that $A_1 > 100$ are probably meaningless, see the discussion above]. We conclude that the upper bound $A_1 \lesssim 14$ is inaccurate and is just an artifact due to the inaccurate nature of the “approximation to the slow-roll approximation”. Let us try to identify the origin of this discrepancy more precisely. In order to investigate this issue, we have also represented in Fig. 8, the predictions obtained when the approximate trajectory (4.18), the approximate expression of the first slow-roll parameter (4.15) and the relation $\epsilon_2 = 4\epsilon_1 - 2\hat{\eta}$ (but, now, without neglecting ϵ_1) are used together with an exact expression for ϕ_{end} . They are represented by the second collections of segments in Fig. 8. We see that for $A_1 \gtrsim 0$, they differ from the red thick solid line and bend toward the upper left part of the plot which is also the direction taken by the exact predictions. This suggests that neglecting the term $4\epsilon_1$ in the expression of ϵ_2 causes a non-negligible error. This is confirmed if, instead of using Eq. (4.23) for n_s , we now take

$$n_s = 1 - \frac{3}{2\Delta N_*^2} \left(\frac{x_{\text{BKS}} e^{x_{\text{BKS}}}}{e^{x_{\text{BKS}}} - 1} \right)^2 - \frac{2}{\Delta N_*} \frac{x_{\text{BKS}}}{e^{x_{\text{BKS}}} - 1}, \quad (4.24)$$

and plot again the line $r = r(n_s)$. This gives the yellow dotted-dashed curve which follows the second collection of segments. If, however, we compare the red segments (namely those with A_1 “large”) corresponding the exact predictions to the approximate red ones, we see that including the term $4\epsilon_1$ is not sufficient. For $A_1 \simeq 20$, the exact predictions are perfectly compatible with the data while the segments corresponding to the approximate formulas are not (the corresponding “red region” predicts a spectrum which is too red and a too large gravity waves contribution). We conclude that RCHI represents a textbook case for ASPIC. It illustrates that, sometimes, “approximating the slow-roll approximation” can lead to too drastic conclusions, especially given the current accuracy of the data. It is therefore safer to use the slow-roll method without any other scheme of approximations and this is the essence of the ASPIC project presented in this article. A last word is in order concerning the constraints on the parameter A_1 . Particle physics implies that $-48 \lesssim A_1 \lesssim -20$. If the upper limit $A_1 < 14$ is not accurate, we see in Fig. 8 that the bound $-12 \lesssim A_1$ is. Therefore,

unfortunately, RCHI remains disfavored when particle physics and cosmological data are simultaneously taken into account in agreement with the conclusions of Ref. [155].

Finally, let us briefly discuss how the scale M can be determined. The CMB normalization leads to the following expression

$$\frac{M^4}{M_{\text{Pl}}^4} = \frac{1080\pi^2}{\Delta N_*^2} \left(\frac{x_{\text{BKS}} e^{x_{\text{BKS}}}}{e^{x_{\text{BKS}}} - 1} \right)^2 \frac{Q_{\text{rms-PS}}^2}{T^2}, \quad (4.25)$$

which, using the expression of the scale M in terms of the parameters λ and ξ , implies that

$$\frac{\lambda}{\xi^2} \simeq 0.5 \times 10^{-9} \left(\frac{x_{\text{BKS}} e^{x_{\text{BKS}}}}{e^{x_{\text{BKS}}} - 1} \right)^2. \quad (4.26)$$

This is in agreement with Eq. (31) of Ref. [155]. If, instead, one wishes to determine M exactly, then the following formula should be used

$$\frac{M^4}{M_{\text{Pl}}^4} = 120\pi^2 \frac{Q_{\text{rms-PS}}^2}{T^2} \frac{\left[4e^{-\sqrt{2/3}x_*} + A_1/(16\pi^2) \right]^2}{\left[1 - 2e^{-\sqrt{2/3}x_*} + A_1/(32\pi^2)\sqrt{2/3}x_* \right]^3}. \quad (4.27)$$

As usual, the knowledge of ϕ_* allows us to find the posterior distribution of M , that is to say of λ/ξ^2 or ξ , since the Higgs self coupling, $\lambda = m_{\text{H}}/v$, is now known.

4.2 Large Field Inflation (LFI)

Large fields models, also referred to as chaotic inflation [162], are characterized by the monomial potential [163–167]

$$V(\phi) = M^4 \left(\frac{\phi}{M_{\text{Pl}}} \right)^p. \quad (4.28)$$

The index p is usually a positive integer but various models have been proposed in which it can also be a rational number [168–171]. This is the only model parameter, in addition to the normalization M of the potential. The potential is represented in Fig. 9 for $p = 2$.

The three Hubble flow functions are straightforwardly obtained from Eqs. (2.4), (2.5) and (2.6). Defining $x \equiv \phi/M_{\text{Pl}}$, one gets

$$\epsilon_1 = \frac{p^2}{2x^2}, \quad \epsilon_2 = \frac{2p}{x^2}, \quad \epsilon_3 = \epsilon_2. \quad (4.29)$$

These functions are represented in the two bottom panels of Fig. 9. They are monotonic decreasing functions of ϕ . One can immediately deduce that, for a given p , the model in the plane (ϵ_1, ϵ_2) is contained in the line $\epsilon_1 = (p/4)\epsilon_2$.

The slow-roll trajectory is completely explicit and obtained by quadrature from Eq. (2.11)

$$N - N_{\text{end}} = -\frac{1}{M_{\text{Pl}}^2} \int_{\phi_{\text{end}}}^{\phi} \frac{V(\chi)}{V'(\chi)} d\chi = -\frac{1}{p} \int_{\phi_{\text{end}}/M_{\text{Pl}}}^{\phi/M_{\text{Pl}}} x dx = \frac{1}{2p} (x_{\text{end}}^2 - x^2). \quad (4.30)$$

This expression can be inverted and reads

$$x = \sqrt{x_{\text{end}}^2 - 2p(N - N_{\text{end}})}. \quad (4.31)$$

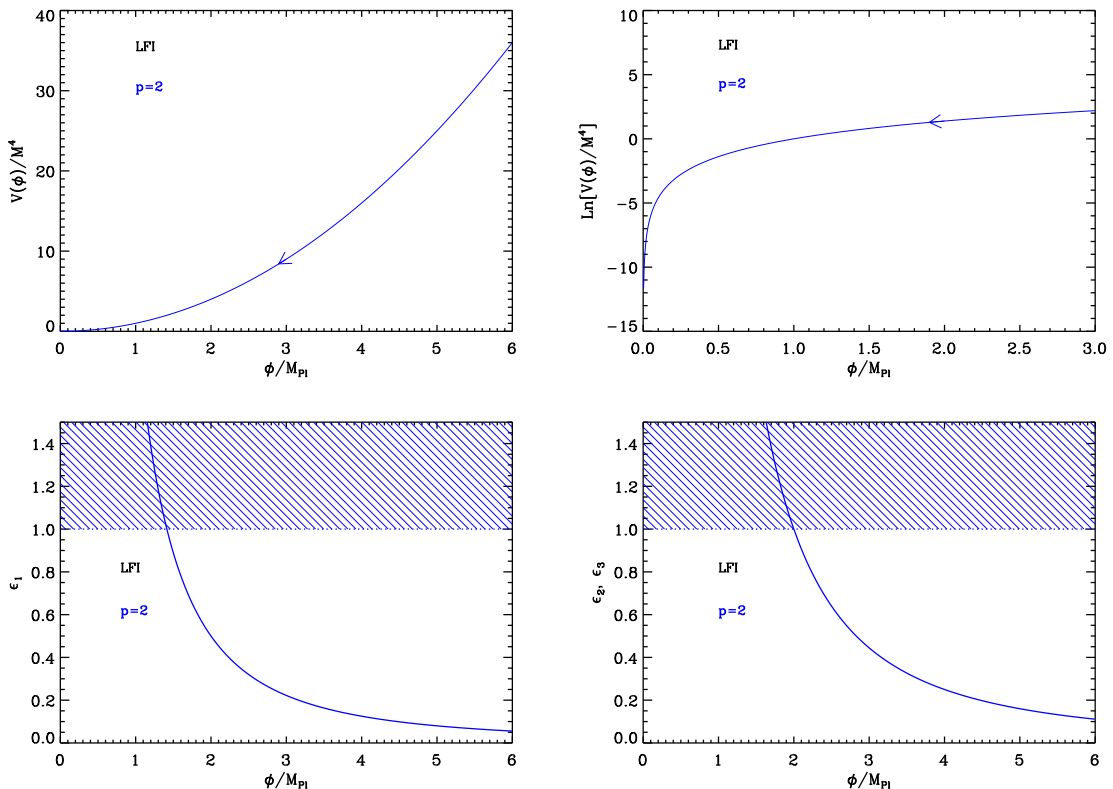


Figure 9. Large Field Inflation (LFI). Top left panel: large field potential for $p = 2$. Top right panel: logarithm of the potential for the same value of p . The required flatness of the potential becomes obvious on this plot. Bottom left panel: slow-roll parameter ϵ_1 for a large field potential with $p = 2$. The shaded area indicates where acceleration stops. Bottom right panel: slow-roll parameters ϵ_2 and ϵ_3 for a large field potential with $p = 2$. Only one curve appears because $\epsilon_2 = \epsilon_3$. On this plot, the shaded region signals the breakdown of the slow-roll approximation, which is not necessarily the end of the accelerated phase.

For the large field models, inflation ends naturally when $\epsilon_1 = 1$ (see section 1). Along the $\phi > 0$ branch of the potential, this leads to

$$x_{\text{end}} = \frac{p}{\sqrt{2}}. \quad (4.32)$$

This expression also allows us to obtain the total number of e-folds. Plugging Eq. (4.32) into Eq. (4.30), one arrives at

$$N_{\text{end}} - N_{\text{ini}} = \frac{1}{2p} x_{\text{ini}}^2 - \frac{p}{4}, \quad (4.33)$$

which can be very large if the initial field value is super-Planckian. Notice that this does not imply that the energy density is close to the Planck scale as this one is typically given by the potential and proportional to M^4 . In fact, the model remains under control only if the initial energy density is smaller than M_{Pl}^4 and this imposes a constraint on both ϕ_{ini} and M which reads

$$x_{\text{ini}} = \frac{\phi_{\text{ini}}}{M_{\text{Pl}}} \lesssim \left(\frac{M_{\text{Pl}}}{M} \right)^{4/p}. \quad (4.34)$$

Let us notice that, when the inflaton energy density approaches the Planck energy density, quantum effects become important. In this case, the stochastic inflation formalism must be used [172–178].

We now turn to the explicit determination of the slow-roll parameters. We have seen that the model is represented by the trajectory $\epsilon_1 = (p/4)\epsilon_2$ but observable models only lie in a limited portion of this straight line. Indeed, the Hubble flow parameters should be evaluated when the scales of astrophysical interest today left the Hubble radius during inflation. Following the discussion of section 2.2, we assume the pivot mode crossed the Hubble radius for $\phi = \phi_*$ at the e-fold number N_* . From the trajectory, we have

$$x_*^2 = 2p \left(\Delta N_* + \frac{p}{4} \right), \quad (4.35)$$

and the slow-roll parameters read

$$\epsilon_{1*} = \frac{p}{4(\Delta N_* + p/4)}, \quad \epsilon_{2*} = \frac{1}{\Delta N_* + p/4}, \quad \epsilon_{3*} = \epsilon_{2*}. \quad (4.36)$$

Solving Eq. (2.46) for ϕ_* yields the slow-roll predictions represented in Fig. 75. As expected, the whole family lies in the region $\epsilon_2 > 0$ and verifies $\epsilon_1 = p/4\epsilon_2$. From Fig. 75, we see that all the models with $p \gtrsim 4$ lie outside the 2σ contour. The quadratic (or massive) model remains compatible with the data and predicts quite a high contribution of gravitational waves, up to $r \sim 15\%$ level.

Finally, the parameter M can be determined from the amplitude of the CMB anisotropies, and one gets

$$\frac{Q_{\text{rms-PS}}^2}{T^2} = \frac{1}{480\pi^2\epsilon_{1*}} \frac{H_*^2}{M_{\text{Pl}}^2} = \frac{1}{1440\pi^2\epsilon_{1*}} \frac{V_*}{M_{\text{Pl}}^4}. \quad (4.37)$$

In the case of large fields model, this implies

$$\left(\frac{M}{M_{\text{Pl}}} \right)^4 = \frac{720\pi^2 p^2}{(x_*^2)^{p/2+1}} \frac{Q_{\text{rms-PS}}^2}{T^2}, \quad (4.38)$$

and given the constraints on p and ΔN_* , this leads to $M/M_{\text{Pl}} \simeq 3 \times 10^{-3}$. We recover the conclusion that, for large field models, inflation takes place close to the Grand Unified Theory (GUT) scale.

4.3 Mixed Large Field Inflation (MLFI)

This model is a generalization of the LFI model $V(\phi) \propto \phi^p$, see section 4.2, where two monomials $\propto \phi^2$ and $\propto \phi^4$ are added. The MLFI potential reads

$$V(\phi) = M^4 \frac{\phi^2}{M_{\text{Pl}}^2} \left[1 + \alpha \frac{\phi^2}{M_{\text{Pl}}^2} \right], \quad (4.39)$$

where α is a positive dimensionless parameter. If $\phi/M_{\text{Pl}} \ll 1/\sqrt{\alpha}$, then the potential is of the LFI type with $p = 2$, i.e. $V(\phi) \simeq M^4 \phi^2/M_{\text{Pl}}^2$, whereas if $\phi/M_{\text{Pl}} \gg 1/\sqrt{\alpha}$, the potential is of the LFI type with $p = 4$, i.e. $V(\phi) \simeq M^4 \alpha \phi^4/M_{\text{Pl}}^4$. Clearly, the interesting regime is when $\phi/M_{\text{Pl}} \sim 1/\sqrt{\alpha}$, where the two terms are of equal importance. The potential and its logarithm are displayed in Fig. 10. We notice that $V(\phi)$ is an increasing function of the field *vev* and, as a consequence, that inflation proceeds from the right to the left.

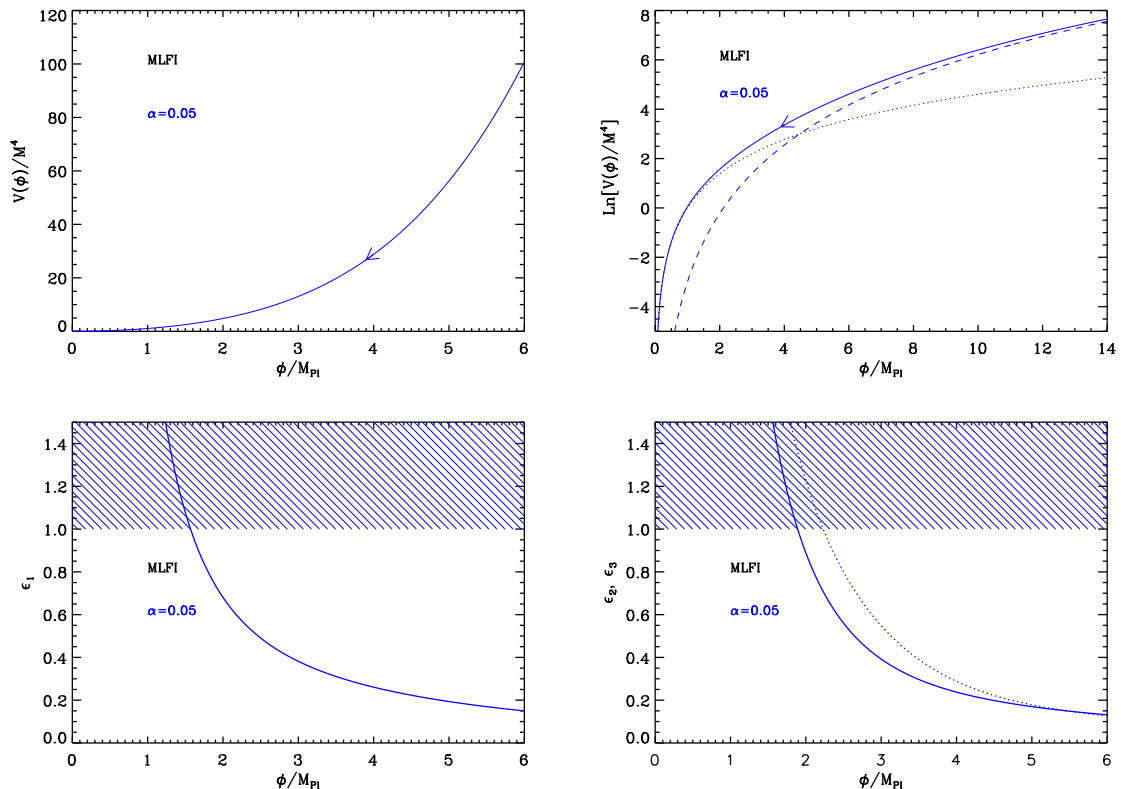


Figure 10. Top left panel: mixed large field (MLFI) potential, see Eq. (4.39), for $\alpha = 0.05$. Top right panel: logarithm of the potential for the same value of α . The dotted line indicates the potential $V(\phi) \simeq M^4 \phi^2 / M_{\text{Pl}}^2$ which is the limit of the MLFI potential in the regime $\phi / M_{\text{Pl}} \ll 1 / \sqrt{\alpha}$ while the dashed line represents the expression $V(\phi) \simeq M^4 \alpha \phi^4 / M_{\text{Pl}}^4$, the limit of $V(\phi)$ when $\phi / M_{\text{Pl}} \gg 1 / \sqrt{\alpha}$. For $\alpha = 0.05$ the two lines meet at the following value, $1 / \sqrt{\alpha} \simeq 4.5$, as can be directly checked in the figure. The arrow in the top left and right panels indicate in which direction inflation proceeds. Bottom left panel: slow-roll parameter ϵ_1 for a mixed large field potential with $\alpha = 0.05$. Bottom right panel: slow-roll parameters ϵ_2 (solid line) and ϵ_3 (dotted line) still for $\alpha = 0.05$.

This model has been investigated in different contexts. Of course, the shape of the potential appears to be natural and well-motivated since it just represents a free theory (with particles of mass $2M^4/M_{\text{Pl}}^2$) corrected by the usual self-interacting quartic term. Therefore, it does not come as a surprise that this potential has been used in many different works. In Ref. [179], this model is studied in the case where a bulk scalar field is driving inflation in large extra dimensions. In Ref. [180], it is considered in a situation where inflation is driven by highly excited quantum states. In Refs. [181, 182], the MLFI potential is utilized in the context of “fresh inflation”. The same potential was again considered in Ref. [183] where the role of inflaton is played by the Higgs triplet in a model where the type II seesaw mechanism is used to generate the small masses of left-handed neutrinos. Finally, it is also studied in Ref. [184] where supersymmetric hybrid inflation (in the framework of the Randall-Sundrum type II Braneworld model) is considered. The only constraint on the parameters of the model that is (sometimes) required is that the self-interacting term should be subdominant. This leads to the condition $\alpha M^4 / M_{\text{Pl}}^4 \ll 1$. Given the typical values imposed by

CMB normalization, i.e. $M/M_{\text{Pl}} \simeq 10^{-3}$ [see Eq. (4.38)], this is not very stringent and α can in fact vary in a quite large range of values.

Let us now define x by $x \equiv \phi/M_{\text{Pl}}$. Then, the three first slow-roll parameters can be expressed as

$$\epsilon_1 = \frac{2}{x^2} \left(\frac{1 + 2\alpha x^2}{1 + \alpha x^2} \right)^2, \quad \epsilon_2 = \frac{4}{x^2} \frac{1 + \alpha x^2 + 2\alpha^2 x^4}{(1 + \alpha x^2)^2}, \quad (4.40)$$

and

$$\epsilon_3 = \frac{M_{\text{Pl}}^2}{x^2} \frac{1 + 2\alpha x^2}{(1 + \alpha x^2)^2} \frac{4 + 12\alpha x^2 + 8\alpha^3 x^6}{1 + \alpha x^2 + 2\alpha^2 x^4}. \quad (4.41)$$

They are displayed in Fig. 10. We see that the three slow-roll parameters are decreasing functions of the field $v\phi$, which means that they are all increasing functions during inflation. As a consequence, inflation can stop by violation of the slow-roll conditions at x_{end} given by $\epsilon_1 = 1$ (see below). We also notice that ϵ_2 and ϵ_3 are larger than one at x_{end} . This means that the slow-roll approximation breaks down slightly before the end of inflation and that the few last e -folds of inflation may be not properly described by the slow-roll approximation.

Let us now study the slow-roll trajectory. It is given by

$$N_{\text{end}} - N = -\frac{1}{8} \left[x_{\text{end}}^2 + \frac{1}{2\alpha} \ln(1 + 2\alpha x_{\text{end}}^2) - x^2 - \frac{1}{2\alpha} \ln(1 + 2\alpha x^2) \right], \quad (4.42)$$

where N_{end} is the number of e -folds at the end of inflation. One can check that this expression is asymptotically correct. Indeed, when $\alpha \ll 1$, the slow-roll trajectory reduces to

$$x_{\text{end}}^2 = x^2 - 4(N_{\text{end}} - N), \quad (4.43)$$

which is the trajectory in the massive case, i.e. LFI with $p = 2$, see Eq. (4.30). On the other hand, in the limit $\alpha \rightarrow \infty$, one obtains

$$x_{\text{end}}^2 = x^2 - 8(N_{\text{end}} - N), \quad (4.44)$$

which is, as expected, the slow-roll trajectory in the quartic case, i.e. LFI with $p = 4$.

In general, the trajectory can be inverted and expressed in terms of the Lambert function. Straightforward manipulations lead to

$$x = \frac{1}{\sqrt{2\alpha}} \sqrt{-1 + \text{W}_0 \left[e^{1+2\alpha x_{\text{end}}^2} (1 + 2\alpha x_{\text{end}}^2) e^{-16\alpha(N-N_{\text{end}})} \right]}. \quad (4.45)$$

The corresponding Lambert function is displayed in Fig. 11, together with the region where inflation proceeds.

We have seen that, in MLFI, inflation stops by violation of the slow-roll condition. Let us therefore determine the corresponding $v\phi$ of the field. The condition $\epsilon_1 = 1$ leads to

$$\alpha x_{\text{end}}^3 - 2\sqrt{2}\alpha x_{\text{end}}^2 + x_{\text{end}} - \sqrt{2} = 0. \quad (4.46)$$

This is a cubic algebraic equation that can be solved exactly. In the limit $\alpha \gg 1$, the solution reads $x_{\text{end}} \simeq 2\sqrt{2}$ which is indeed the solution for the quartic case, see Eq. (4.32). On the

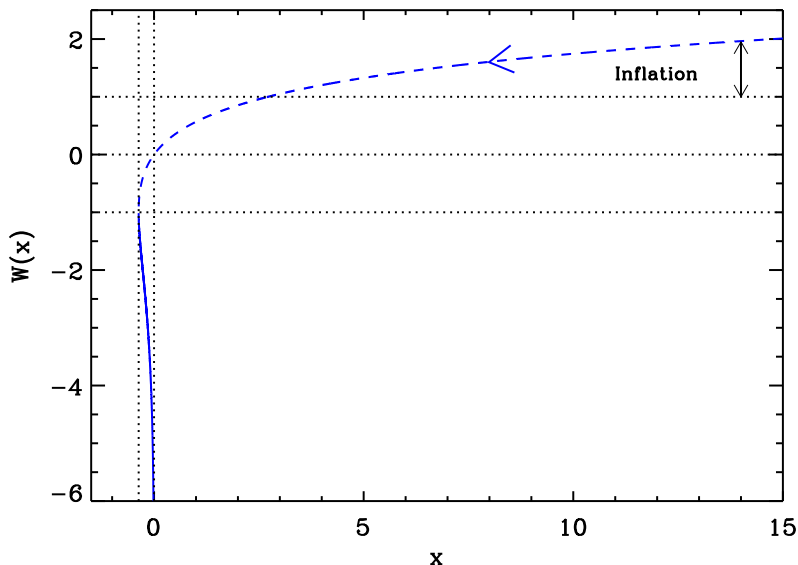


Figure 11. Lambert functions $W_0(x)$ (dashed line) and $W_{-1}(x)$ (solid line). During Mixed Large Field inflation, inflation proceeds along the “0” branch above the line $W = 1$ in the direction specified by the arrow.

other hand, if $\alpha \ll 1$, then $x_{\text{end}} \simeq \sqrt{2}$ which is also the correct result for the quadratic case. The general solution writes

$$x_{\text{end}} = \frac{2\sqrt{2}}{3} + \frac{1}{3\alpha} \left\{ \frac{1}{4\sqrt{2}} \left[4\alpha^2 (32\alpha + 9) + 2\alpha \sqrt{4\alpha^2 (32\alpha + 9)^2 - 8\alpha (8\alpha - 3)^3} \right] \right\}^{1/3} + \frac{1}{3} (8\alpha - 3) \left\{ \frac{1}{4\sqrt{2}} \left[4\alpha^2 (32\alpha + 9) + 2\alpha \sqrt{4\alpha^2 (32\alpha + 9)^2 - 8\alpha (8\alpha - 3)^3} \right] \right\}^{-1/3}. \quad (4.47)$$

Numerically, it is especially convenient to have an exact solution and ASPIC makes use of the above one.

Finally, the parameter M can be determined from the amplitude of the CMB anisotropies, and one gets

$$\left(\frac{M}{M_{\text{Pl}}} \right)^4 = \frac{2880\pi^2 (1 + 2\alpha x_*^2)^2 Q_{\text{rms-PS}}^2}{x^4 (1 + \alpha x_*^2)^3 T^2}. \quad (4.48)$$

Similarly to LFI (see section 4.2), this gives rise to $M/M_{\text{Pl}} \sim 10^{-3}$.

The reheating consistent slow-roll predictions for the MLFI models are displayed in Fig. 76. The reheating equation of state parameter \bar{w}_{reh} has been taken to 0 which is consistent with the fact that the potential is quadratic close to its minimum. As expected, when $\alpha \ll 1$ the predictions of the model match those of LFI with $p = 2$ and are aligned along the $\epsilon_1 = \epsilon_2/2$ line. On the other hand, if $\alpha \gg 1$, then the predictions are consistent with those of LFI with $p = 4$ and are aligned along the $\epsilon_1 = \epsilon_2$ line. In the intermediate regime, it is interesting to notice that the MLFI predictions continuously interpolate between these

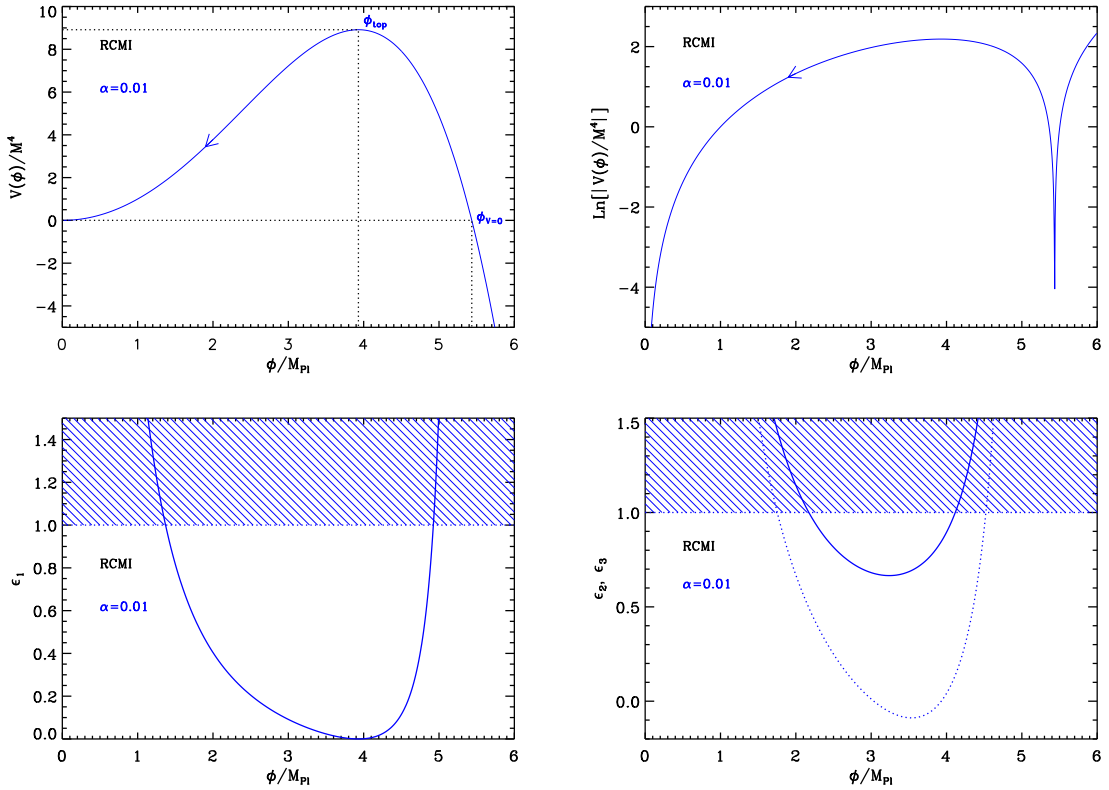


Figure 12. Radiatively Corrected Massive Inflation (RCMI) for $\alpha = 0.01$. Top panels: potential (left) and logarithm of the potential (right). Bottom left panel: slow-roll parameter ϵ_1 with respect to field values. The shaded area indicates where inflation stops. Bottom right panel: slow-roll parameters ϵ_2 (solid line) and ϵ_3 (dotted line).

two asymptotic solutions but do not remain inside the domain delimited by the two lines $\epsilon_1 = \epsilon_2/2$ and $\epsilon_1 = \epsilon_2/2$. Indeed, when α is larger than some value, one has $\epsilon_1 > \epsilon_2$. This means that, if one starts from a pure quartic potential (LFI with $p = 4$) and adds a small quadratic term, this extra term has the effect of increasing the “effective value” of p , which is quite counter intuitive. On the other hand, however, since the quadratic model better fits the data than the quartic one, small values for the parameter α are favored (all the models with $\alpha > 10^{-3}$ lie outside the 2σ contour of the WMAP data). High reheating temperatures are also preferred.

4.4 Radiatively Corrected Massive Inflation (RCMI)

This model is based on Ref. [185] and implements radiative corrections due to fermion couplings over the massive ($p = 2$) large field model (see section 4.2). With an appropriate choice of the renormalization scale $\mu = gM_{\text{Pl}}$, g denoting the Yukawa coupling, the potential is given by

$$V(\phi) = \frac{1}{2}m^2\phi^2 - \frac{g^4}{16\pi^2}\phi^4 \ln\left(\frac{\phi}{M_{\text{Pl}}}\right) = M^4 \left(\frac{\phi}{M_{\text{Pl}}}\right)^2 \left[1 - 2\alpha \frac{\phi^2}{M_{\text{Pl}}^2} \ln\left(\frac{\phi}{M_{\text{Pl}}}\right)\right], \quad (4.49)$$

where

$$M^4 \equiv \frac{1}{2} m^2 M_{\text{Pl}}^2, \quad \alpha \equiv \frac{g^4 M_{\text{Pl}}^2}{16\pi^2 m^2}. \quad (4.50)$$

This expression is obtained in the large field regime $\phi \gg m/g$, i.e. assuming that the inflationary regime takes place under the condition

$$\frac{\phi^4}{M_{\text{Pl}}^4} \gg \frac{1}{8\pi^2 \alpha} \frac{M^4}{M_{\text{Pl}}^4}. \quad (4.51)$$

Defining $x \equiv \phi/M_{\text{Pl}}$, the Hubble flow functions are given by

$$\epsilon_1 = \frac{2}{x^2} \left[\frac{1 - \alpha x^2 - 4\alpha x^2 \ln(x)}{1 - 2\alpha x^2 \ln(x)} \right]^2, \quad (4.52)$$

$$\epsilon_2 = \frac{4}{x^2} \frac{(1 + \alpha x^2)(1 + 2\alpha x^2) - 2\alpha x^2 \ln x (1 - \alpha x^2 - 4\alpha x^2 \ln x)}{(1 - 2\alpha x^2 \ln x)^2}, \quad (4.53)$$

and

$$\begin{aligned} \epsilon_3 &= \frac{4}{x^2} \frac{1 - \alpha x^2 - 4\alpha x^2 \ln x}{(1 - 2\alpha x^2 \ln x)^2} \\ &\times \frac{1 - \alpha x^2 [\alpha x^2 (4\alpha x^2 + 9) + 1] - \alpha x^2 \ln x [4\alpha^2 x^4 \ln x (4 \ln x + 1) + (\alpha x^2 + 3)(6\alpha x^2 + 2)]}{(1 + \alpha x^2)(1 + 2\alpha x^2) - 2\alpha x^2 \ln x (1 - \alpha x^2 - 4\alpha x^2 \ln x)}. \end{aligned} \quad (4.54)$$

If $\alpha = 0$, one recovers the slow-roll parameters of the massive case (namely LFI with $p = 2$, see section 4.2) as expected.

Let us now discuss the field domains in which inflation can take place. It is clear that the above potential is not positive definite for all field values. It becomes negative at the point

$$x_{V=0} = \frac{\phi_{V=0}}{M_{\text{Pl}}} = \sqrt{\frac{1}{\alpha W_0(1/\alpha)}}, \quad (4.55)$$

where W_0 is the 0-branch of the Lambert function. The model is defined only in the regime $\phi < \phi_{V=0}$. On the other hand, the top of the potential, where $V' = 0$ (or equivalently $\epsilon_1 = 0$), is given by

$$x_{\text{top}} = \frac{\phi_{\text{top}}}{M_{\text{Pl}}} = \sqrt{\frac{1}{2\alpha W_0\left(\frac{\sqrt{e}}{2\alpha}\right)}}. \quad (4.56)$$

As the model makes sense only if the logarithmic terms do not dominate the potential, the acceptable regime is $\phi < \phi_{\text{top}} < \phi_{V=0}$, and a large field region only exists for $\phi_{\text{top}}/M_{\text{Pl}} \gg 1$. From the above expression, this means that we must be in the regime $\alpha \ll 1$. This is the potential validity range as for $\phi < \phi_{\text{top}}$ one can check from Eqs. (4.49) and (4.56) that the loop corrections never exceed α/e .

Let us now turn to the slow-roll trajectory. It is given by

$$N - N_{\text{end}} = -\frac{1}{2} \int_{\phi_{\text{end}}/M_{\text{Pl}}}^{\phi/M_{\text{Pl}}} \frac{x - 2\alpha x^3 \ln x}{1 - \alpha x^2 - 4\alpha x^2 \ln x} dx, \quad (4.57)$$

an integral that cannot be performed analytically. For the purpose of this section, we can nevertheless make an expansion in α to obtain an approximate expression

$$N - N_{\text{end}} = -\frac{x^2}{4} \left[1 + \alpha \frac{x^2}{4} (1 + 4 \ln x) \right] + \frac{x_{\text{end}}^2}{4} \left[1 + \alpha \frac{x_{\text{end}}^2}{4} (1 + 4 \ln x_{\text{end}}) \right] + \mathcal{O}(\alpha^2). \quad (4.58)$$

Inflation stops close to the minimum of the potential when $\epsilon_1 = 1$. This last equation cannot be solved analytically but we can also perform an expansion at first order in α and one gets

$$x_{\text{end}} = \frac{\phi_{\text{end}}}{M_{\text{Pl}}} \simeq \frac{1}{\sqrt{2\alpha W_0 \left[\frac{e^{1+1/(4\alpha)}}{2\alpha} \right]}} \simeq \sqrt{2} - 2\sqrt{2}\alpha. \quad (4.59)$$

In the limit $\alpha \rightarrow 0$, we recover the large field result for $p = 2$, i.e. $x_{\text{end}} \rightarrow \sqrt{2}$. The maximum total number of e-folds one can realize between $\phi = \phi_{\text{top}}$ and $\phi = \phi_{\text{end}}$ can be calculated from the previous expressions. It reads

$$\begin{aligned} \Delta N_{\text{max}} = N_{\text{end}} - N_{\text{top}} &= \frac{5}{32\alpha W_0 \left(\frac{\sqrt{e}}{2\alpha} \right)} + \frac{1 + 2\alpha - 20\alpha W_0 \left[\frac{e^{1+1/(4\alpha)}}{2\alpha} \right]}{128\alpha^2 W_0^2 \left[\frac{e^{1+1/(4\alpha)}}{2\alpha} \right]} \\ &\simeq -\frac{5}{32\alpha \ln(\alpha)}. \end{aligned} \quad (4.60)$$

This is a decreasing function of α , so that α has to be small enough if one wants a sufficiently high number of e-folds to take place. Indeed, if one wants at least ΔN_{min} e-folds to occur, one needs to work with

$$\alpha < \frac{5}{32\Delta N_{\text{min}} \ln \left(\frac{32\Delta N_{\text{min}}}{10} \right)}. \quad (4.61)$$

For example, $\Delta N_{\text{min}} = 50$ imposes $\alpha < 6 \times 10^{-4}$. The fact that α is bounded from above can be directly checked in Fig. 77. The field ϕ_* value at which the pivot mode crossed the Hubble radius during inflation is obtained from Eq. (2.46) whereas the corresponding e-fold number can be obtained from the trajectory.

Finally, the parameter M can be determined from the amplitude of the CMB anisotropies, and one gets

$$\left(\frac{M}{M_{\text{Pl}}} \right)^4 = \frac{2880\pi^2}{x_*^4} \frac{(1 - 2\alpha x_*^2 \ln x_*)^3}{(1 - \alpha x_*^2 - 4\alpha x_*^2 \ln x_*)^2} \frac{Q_{\text{rms-PS}}^2}{T^2}. \quad (4.62)$$

The reheating consistent slow-roll predictions for the RCMi models are represented in Fig. 77. As expected, the LFI quadratic model case is properly recovered for $\alpha \rightarrow 0$. From this figure, we see that all models having $\alpha > 10^{-3.5}$ lie outside the 2σ contour. Let us emphasize that the value of α cannot be infinitely small due to Eq. (4.51). At zero order, one has $\phi > \phi_{\text{end}} \simeq \sqrt{2}M_{\text{Pl}}$ such that Eq. (4.51) can be recast into

$$\alpha > \frac{M^4}{8\pi^2 M_{\text{Pl}}^4} = \frac{m^2}{16\pi^2 M_{\text{Pl}}^2}. \quad (4.63)$$

From the COBE normalization, and in the limit of small α , one gets $M/M_{\text{Pl}} \gtrsim 10^{-3}$ and the lower bound reads $\alpha > 10^{-15}$.

4.5 Radiatively Corrected Quartic Inflation (RCQI)

This model is similar to RCMi discussed in section 6.1 but implements radiative corrections due to fermion couplings over a quartic ($p = 4$) large field model [185] (see section 4.2). The potential is given by

$$V = \lambda\phi^4 - \frac{g^4}{16\pi^2}\phi^4 \ln\left(\frac{\phi}{M_{\text{Pl}}}\right) = M^4 \left(\frac{\phi}{M_{\text{Pl}}}\right)^4 \left[1 - \alpha \ln\left(\frac{\phi}{M_{\text{Pl}}}\right)\right], \quad (4.64)$$

where

$$M^4 = \lambda M_{\text{Pl}}^4, \quad \alpha \equiv \frac{g^4}{16\pi^2\lambda}. \quad (4.65)$$

Defining $x = \phi/M_{\text{Pl}}$, the Hubble flow functions in the slow-roll approximation read

$$\epsilon_1 = \frac{8}{x^2} \left[\frac{1 - \frac{\alpha}{4} - \alpha \ln x}{1 - \alpha \ln x} \right]^2, \quad \epsilon_2 = \frac{8}{x^2} \frac{1 + \frac{\alpha}{4}(\alpha - 1) + \alpha \left(\frac{\alpha}{4} - 2\right) \ln x + \alpha^2 \ln^2 x}{(1 - \alpha \ln x)^2}, \quad (4.66)$$

and

$$\epsilon_3 = \frac{8}{x^2} \frac{(1 - \frac{\alpha}{2} - \alpha \ln x)(1 - \frac{\alpha}{4} - \alpha \ln x) \left[1 + \frac{\alpha^2}{2} + \frac{\alpha}{4} - \alpha \left(2 + \frac{\alpha}{4} - \alpha \ln x\right) \ln x\right]}{(1 - \alpha \ln x)^2 \left[1 + \frac{\alpha}{4}(\alpha - 1) - \alpha \left(2 - \frac{\alpha}{4} - \alpha \ln x\right) \ln x\right]}. \quad (4.67)$$

The shape of the potential and the Hubble flow functions are very similar to the ones of the RCMi model and have been represented in Fig. 13. In particular, the potential is vanishing and maximal at the field values

$$x_{V=0} = \frac{\phi_{V=0}}{M_{\text{Pl}}} = e^{1/\alpha}, \quad x_{\text{top}} = \frac{\phi_{\text{top}}}{M_{\text{Pl}}} = e^{1/\alpha - 1/4}, \quad (4.68)$$

respectively. As the model makes sense only if the corrections are small compared to the quartic term, one should consider $\alpha \ll 1$ and not too large super-Planckian field values.

The slow-roll trajectory can be integrated analytically from Eqs. (2.11) and (4.64) and one gets

$$N - N_{\text{end}} = -\frac{1}{16} \left[2x^2 - e^{-1/2+2/\alpha} \text{Ei}\left(\frac{1}{2} - \frac{2}{\alpha} + 2 \ln x\right) - 2x_{\text{end}}^2 + e^{-1/2+2/\alpha} \text{Ei}\left(\frac{1}{2} - \frac{2}{\alpha} + 2 \ln x_{\text{end}}\right) \right], \quad (4.69)$$

where the exponential integral function is defined by

$$\text{Ei}(x) \equiv - \int_{-x}^{+\infty} \frac{e^{-t}}{t} dt. \quad (4.70)$$

The quartic limit $\alpha \rightarrow 0$ is recovered by noticing that

$$\text{Ei}(-2/\alpha) \underset{\alpha \rightarrow 0}{\sim} -\frac{\alpha}{2} e^{-2/\alpha}. \quad (4.71)$$

Contrary to the RCMi model, the top of the potential is flat enough to support inflation. Indeed, one sees from Eq. (4.68) that the argument of the exponential integral function

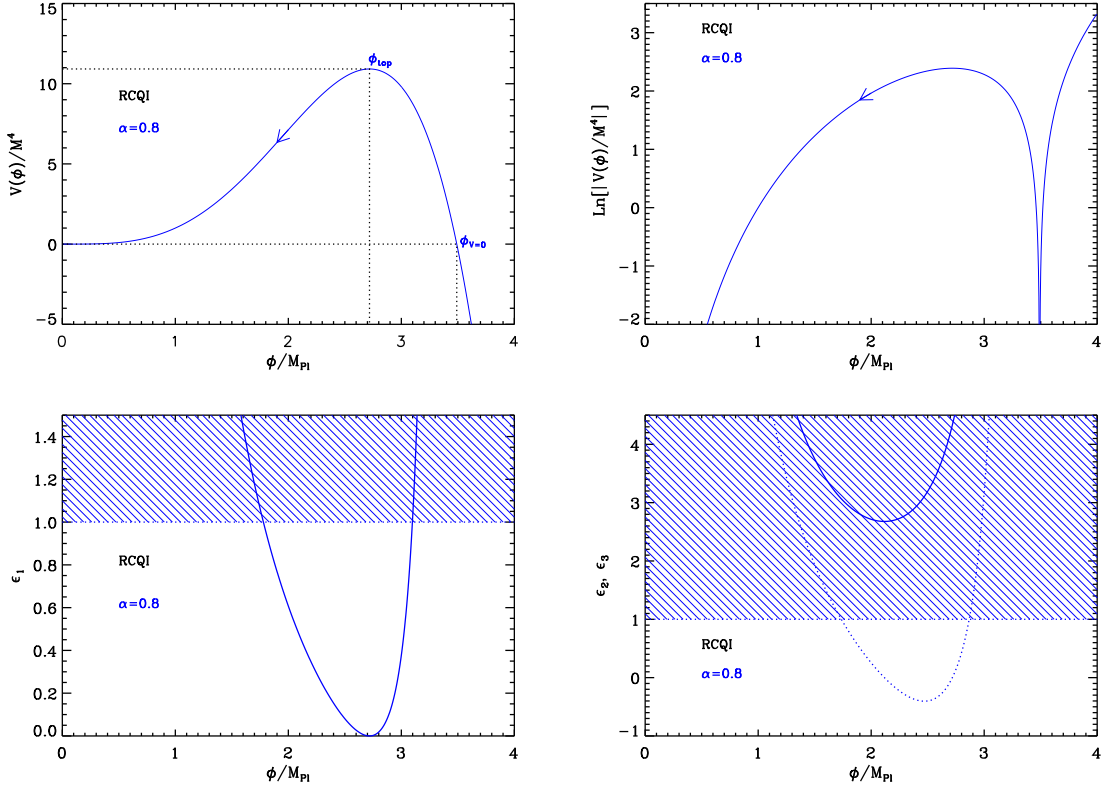


Figure 13. Radiatively Corrected Quartic Inflation (RCQI) for $\alpha = 0.8$. Top panels: the potential and its logarithm as a function of the field values. Bottom left panel: slow-roll parameter ϵ_1 . The shaded area indicates where inflation stops. Bottom right panel: slow-roll parameters ϵ_2 (solid line) and ϵ_3 (dotted line). The shaded region for ϵ_2 and ϵ_3 shows where the slow-roll approximation is violated for that value of α .

vanishes at $x = x_{\text{top}}$. Since for $y \rightarrow 0$, one has $\text{Ei}(y) \sim \gamma + \ln y$, whatever the value of x_{end} the total number of e-folds is divergent. This means that it is always possible to realize the required ΔN_* number of e-folds provided inflation starts close enough to the top of the potential.

As for RCMI, inflation stops at $\epsilon_1 = 1$ but this equation can only be solved numerically. For illustrative purpose, one can nevertheless solve it at first order in α to get

$$x_{\text{end}} = \frac{\phi_{\text{end}}}{M_{\text{Pl}}} \simeq 2\sqrt{2} - \frac{\sqrt{2}}{2}\alpha. \quad (4.72)$$

The link between ϕ_* and ΔN_* is given by the slow-roll trajectory with ϕ_* given by Eq. (2.46).

Finally, the parameter M can be determined from the amplitude of the CMB anisotropies, and one gets

$$\lambda = \frac{M^4}{M_{\text{Pl}}^4} = \frac{11520\pi^2}{x_*^6} \frac{(1 - \frac{\alpha}{4} - \alpha \ln x_*)^2}{(1 - \alpha \ln x_*)^3} \frac{Q_{\text{rms-PS}}^2}{T^2}. \quad (4.73)$$

The slow-roll predictions for RCQI are represented in Fig. 78 and 79. As expected, the quartic model case is properly recovered in the limit $\alpha \rightarrow 0$. From Fig. 78, we see that all

the models seem to lie outside the 2σ contour for $\bar{w}_{\text{reh}} = 0$. As the reheating phase takes place at the bottom of a quartic-like potential, we have also represented the prediction for $\bar{w}_{\text{reh}} = 1/3$ in Fig. 79. For a radiation-dominated reheating, ΔN_* is fixed and for each value of α one has only a single point. In that situation, all these models are still disfavored at the two-sigma level.

4.6 Natural Inflation (NI)

Natural inflation was first proposed as an attempt to solve the so-called “fine tuning” problem of inflation. Indeed, to satisfy the usual constraints on inflationary models, in particular, sufficient inflation and microwave background anisotropies, the potential V of the inflaton must be sufficiently flat. It is argued that such a flatness is not robust under radiative corrections, unless it is protected by some symmetry. This is why it was proposed in Ref. [186, 187] an approach, Natural Inflation, in which the inflaton potential is flat due to shift symmetries. Nambu-Goldstone bosons are made use of, which arise whenever a global symmetry is spontaneously broken. When the shift symmetry $\phi(x) \rightarrow \phi(x) + \text{constant}$ of their potential is broken by some additional shift symmetry breaking, these particles become pseudo-Nambu Goldstone bosons [188, 189], with nearly flat potentials, exactly as required by inflation, protected from radiative corrections, and thus generated in a “natural” way. In practice, a decay constant f determines the periodicity of the canonically normalized field, which is now invariant under $\phi \rightarrow \phi + 2\pi f$ (the continuous shift symmetry has left the floor to a discrete symmetry). More precisely, the pseudo-Nambu Goldstone boson potential resulting from explicit breaking of a shift symmetry in single field models (in four spacetime dimensions) is generally of the form

$$V(\phi) = M^4 \left[1 + \cos \left(\frac{\phi}{f} \right) \right]. \quad (4.74)$$

This model has been widely studied in Refs. [190–205]. Many types of candidates have subsequently been explored for natural inflation. For example, in Ref. [206], it was suggested to use a pseudo-Nambu Goldstone boson as the rolling field in double field inflation. Then, NI potentials generated by radiative corrections in models with explicitly broken Abelian [207] and non-Abelian [208] symmetries were considered, showing that NI models with $f \sim M_{\text{Pl}}$ and $f \ll M_{\text{Pl}}$ can both be generated. In Refs. [209, 210], shift symmetries in Kähler potentials enabled to obtain a flat potential and drive natural chaotic inflation in supergravity. Additionally, Refs. [211, 212] examined natural inflation in the context of extra dimensions and Ref. [213] used pseudo-Nambu Goldstone bosons from little Higgs models to drive hybrid inflation. Also, Refs. [214, 215] used the natural inflation idea of pseudo-Nambu Goldstone bosons in the context of braneworld scenarios to drive inflation, and in Ref. [216], it was studied in 5- D warped backgrounds. The same potential has also been obtained and studied in Ref. [217] when studying instantons in non linear sigma models, and in Ref. [218] as providing quintessential inflation. In some of these references the potential is sometimes found with the minus sign in front of the cosine term, which is, up to a shift in the field $v_{\text{ev}} \phi/f \rightarrow \phi/f + \pi$, the same potential. This model was also derived and studied in Refs. [211, 212, 219] in the context of orbifold GUT inflation, where the potential is given by

$$V(\phi) = M^4 \left[f \left(\frac{\phi}{\phi_0} \right) + f \left(2\frac{\phi}{\phi_0} \right) + \frac{f(0)}{2} \right], \quad (4.75)$$

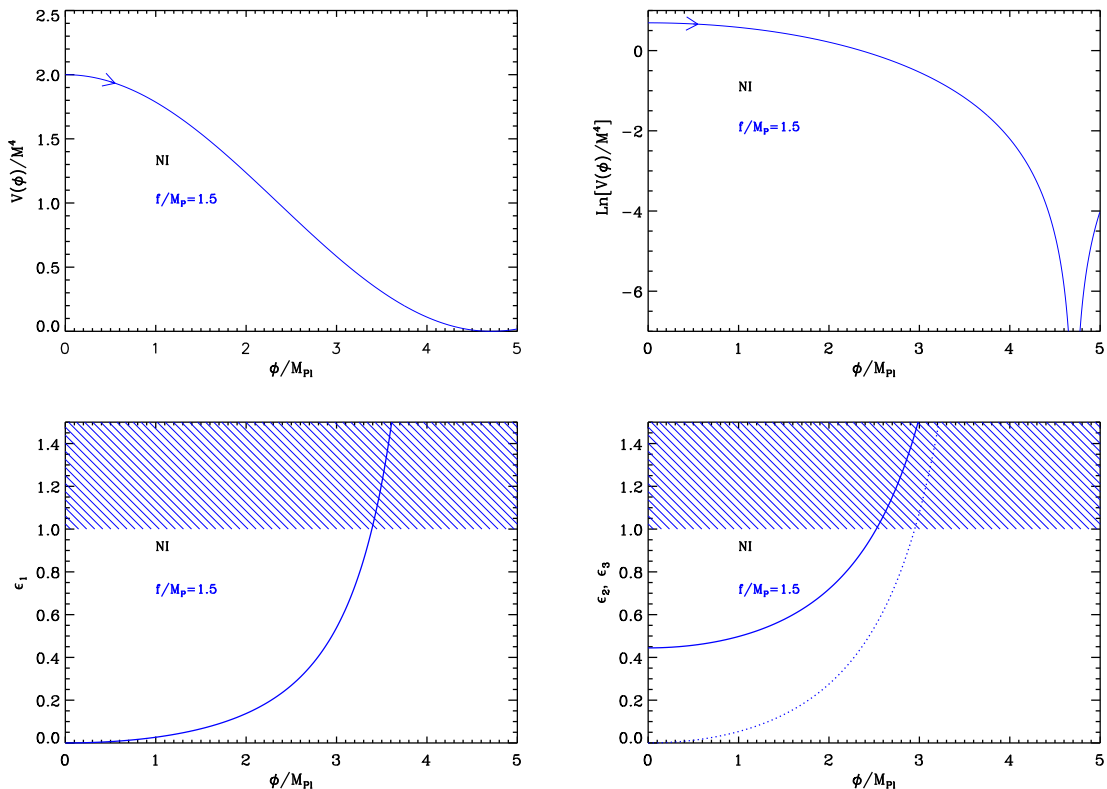


Figure 14. Natural Inflation (NI). Top left panel: potential for $f/M_{\text{Pl}} = 1.5$. Top right panel: logarithm of the potential for the same value of f . Bottom left panel: slow-roll parameter ϵ_1 for a potential with $f/M_{\text{Pl}} = 1.5$. The shaded area indicates the breakdown of the slow-roll inflation (strictly speaking when the acceleration stops). Bottom right panel: slow-roll parameters ϵ_2 (solid line) and ϵ_3 (dotted line) for a potential with $f/M_{\text{Pl}} = 1.5$.

with

$$f(x) = - \sum_{n=1}^{\infty} \frac{\cos(n\pi x)}{n^5}. \quad (4.76)$$

This potential aims at being studied in its increasing branch, and in the small field limit. At leading order, one recovers the natural inflation form of Eq. (4.74). In Refs. [220–222], it is argued that because the axion is very weakly coupled, the energy density stored in the classical axion field does not dissipate rapidly during preheating when the field classically oscillates at the bottom of its potential, and that it exceeds the critical density needed to close the universe unless $f \lesssim 10^{12} \text{GeV}$. However, as pointed out in Ref. [223] on general grounds, this constraint may not apply in the context of cosmological inflation. More precisely, in Ref. [224], it was explained how the mechanism of N -flation [225] can produce an effective potential with $f \gg M_{\text{Pl}}$ from two or more axions, each with sub-Planckian scales. For these reasons, we will assume that f can take values in a wide range, above and below the Planck mass M_{Pl} .

The potential of Eq. (4.74) is displayed with its logarithm in Fig. 14. Since it is a periodic and even function of the field *vev* ϕ , it is enough to study it in the range $\phi \in [0, \pi f]$ where

inflation proceeds from the left to the right. If one lets $x \equiv \phi/f$, the slow-roll parameters can be expressed as

$$\epsilon_1 = \frac{M_{\text{Pl}}^2}{2f^2} \frac{\sin^2(x)}{[1 + \cos(x)]^2}, \quad \epsilon_2 = \frac{2M_{\text{Pl}}^2}{f^2} \frac{1}{1 + \cos(x)}, \quad \epsilon_3 = 2\epsilon_1. \quad (4.77)$$

They are displayed in Fig. 14, where one can see that they are all increasing functions of the field vev , which means that they all increase during inflation. Inflation stops at the position x_{end} given by $\epsilon_1 = 1$ (see below), and one can see that ϵ_2 and ϵ_3 are already greater than one at this point. This means that the slow-roll approximation stops being valid slightly before the end of inflation, and the few last e-folds may not be properly described in this frame of approximations. Another remark to be made is the fact that one generically has

$$\epsilon_2 > \frac{M_{\text{Pl}}^2}{f^2}. \quad (4.78)$$

This means that in order for the slow-roll approximation to be valid, one must require $f/M_{\text{Pl}} \gg 1$, which makes the above discussion about having this condition satisfied in the framework of N -flation, of crucial importance.

The end of inflation occurs when $\epsilon_1 = 1$, i.e. at a position given by

$$x_{\text{end}} = \arccos\left(\frac{1 - 2f^2/M_{\text{Pl}}^2}{1 + 2f^2/M_{\text{Pl}}^2}\right). \quad (4.79)$$

From this expression, one can calculate the value of the other slow roll parameters at the end of inflation, namely $\epsilon_2^{\text{end}} = 2 + M_{\text{Pl}}^2/f^2$ and $\epsilon_3^{\text{end}} = 2\epsilon_2^{\text{end}}$, which confirms that the last few e-folds may not be described properly in the slow-roll approximation.

Let us now calculate the slow-roll trajectory. It is given by

$$N_{\text{end}} - N = \frac{f^2}{M_{\text{Pl}}^2} \ln \left[\frac{1 - \cos(x_{\text{end}})}{1 - \cos(x)} \right], \quad (4.80)$$

where N_{end} is the number of e-folds at the end of inflation, and N is the number of e-folds at some point when the scaled field vev is x . This trajectory can be inverted and one obtains

$$x = \arccos \left\{ 1 - [1 - \cos(x_{\text{end}})] \exp \left[-\frac{M_{\text{Pl}}^2}{f^2} (N_{\text{end}} - N) \right] \right\}. \quad (4.81)$$

Replacing x_{end} by its value [see Eq. (4.79)] gives

$$x = \arccos \left\{ 1 - \frac{4f^2}{M_{\text{Pl}}^2 + 2f^2} \exp \left[-\frac{M_{\text{Pl}}^2}{f^2} (N_{\text{end}} - N) \right] \right\}. \quad (4.82)$$

Finally, the amplitude of the CMB anisotropies fixes the parameter M to

$$\left(\frac{M}{M_{\text{Pl}}} \right)^4 = 720\pi^2 \frac{Q_{\text{rms-PS}}^2}{T^2} \frac{M_{\text{Pl}}^2}{f^2} \frac{\sin^2(x_*)}{[1 + \cos(x_*)]^3}. \quad (4.83)$$

If $f \sim \mathcal{O}(1)$, this expression simplifies to

$$\left(\frac{M}{M_{\text{Pl}}} \right)^4 \simeq 720\pi^2 \frac{Q_{\text{rms-PS}}^2}{T^2} \frac{e^{-2M_{\text{Pl}}^2/f^2 \Delta N_*}}{1 + 2f^2/M_{\text{Pl}}^2}, \quad (4.84)$$

which gives rise to $M/M_{\text{Pl}} \sim 10^{-13}$. On the contrary, if $f/M_{\text{Pl}} \gg 1$ one has

$$\left(\frac{M}{M_{\text{Pl}}}\right)^4 \simeq 360\pi^2 \frac{Q_{\text{rms-PS}}^2}{T^2} \left(\frac{f}{M_{\text{Pl}}}\right)^2 \frac{1}{\Delta N_*^2}, \quad (4.85)$$

and the potential energy scale goes up. For instance, if $f/M_{\text{Pl}} = 10^2$ one has $M/M_{\text{Pl}} \sim 10^{-2}$.

The reheating consistent slow-roll predictions for the natural inflation models are displayed in Fig. 80. The reheating equation of state parameter \bar{w}_{reh} has been taken to 0 since the potential is quadratic close to its minimum. In the limit $f/M_{\text{Pl}} \rightarrow \infty$, the quadratic model predictions (LFI with $p = 2$, see section 4.2) seem to be recovered. Indeed, from the above formula, one can check that in this limit both x_{end} and x_* approach π and the potential is, at leading order, a parabola. More precisely, one can check from Eq. (4.82) that in the limit $f/M_{\text{Pl}} \rightarrow \infty$, one has $\cos(x_*) \simeq -1 + (1 + 2\Delta N_*) M_{\text{Pl}}^2/f^2$, from which one deduces that $\epsilon_{1*} \simeq 1/(1 + 2\Delta N_*)$ and $\epsilon_{2*} \simeq 2/(1 + 2\Delta N_*) \simeq 2\epsilon_{1*}$. This relations are characteristic of the LFI quadratic models, see Eq. (4.36). However, one has $\epsilon_{3*} = 2\epsilon_{2*}$ which differs from the LFI quadratic relationship $\epsilon_{3*} = \epsilon_{2*}$, and therefore quantities sensitive to ϵ_3 , such as the running α_s , would break the degeneracy between NI and the LFI quadratic model. As expected, large values of f/M_{Pl} seem to be favored by the data (as well as high reheating temperatures), and in practice, $f/M_{\text{Pl}} < 4$ appears to be disfavored at the 2σ level by the WMAP data.

4.7 Exponential SUSY Inflation (ESI)

This model has been discussed in Ref. [226] in the context of spin-driven inflation and derived in Ref. [227] in the context of supergravity and superstrings. The potential is given by

$$V(\phi) = M^4 \left(1 - e^{-q\phi/M_{\text{Pl}}}\right), \quad (4.86)$$

where q is a positive dimensionless parameter and inflation proceeds at decreasing field values in the region where $\phi/M_{\text{Pl}} > 0$. The same potential also appears in Ref. [228] in the context of brane inflation, in Ref. [229] in the context of type IIB string compactification as fiber inflation and more recently in Ref. [230] as unitarized Higgs inflation models.

Defining $x \equiv \phi/M_{\text{Pl}}$, the Hubble flow functions in the slow-roll approximation read

$$\epsilon_1 = \frac{q^2}{2} \frac{e^{-2qx}}{(1 - e^{-qx})^2}, \quad \epsilon_2 = 2q^2 \frac{e^{-qx}}{(1 - e^{-qx})^2}, \quad \epsilon_3 = q^2 \frac{e^{-qx}(1 + e^{-qx})}{(1 - e^{-qx})^2}. \quad (4.87)$$

The potential and the Hubble flow functions with respect to the field values are represented in Fig. 15.

The slow-roll trajectory can be integrated analytically from Eq. (2.11) and one finds

$$N - N_{\text{end}} = -\frac{e^{qx} - qx}{q^2} + \frac{e^{qx_{\text{end}}} - qx_{\text{end}}}{q^2}. \quad (4.88)$$

This equation can also be inverted in terms of the Lambert function to get the field value in terms of the number of e-folds:

$$x = q(N - N_{\text{end}}) - \frac{e^{qx_{\text{end}}} - qx_{\text{end}}}{q} - \frac{1}{q} W_{-1} \left\{ -\exp \left[q^2(N - N_{\text{end}}) - (e^{qx_{\text{end}}} - qx_{\text{end}}) \right] \right\}. \quad (4.89)$$

The fact that one should choose the branch W_{-1} is justified below. The argument of the Lambert function is always negative as the exponential is always positive. Moreover, since

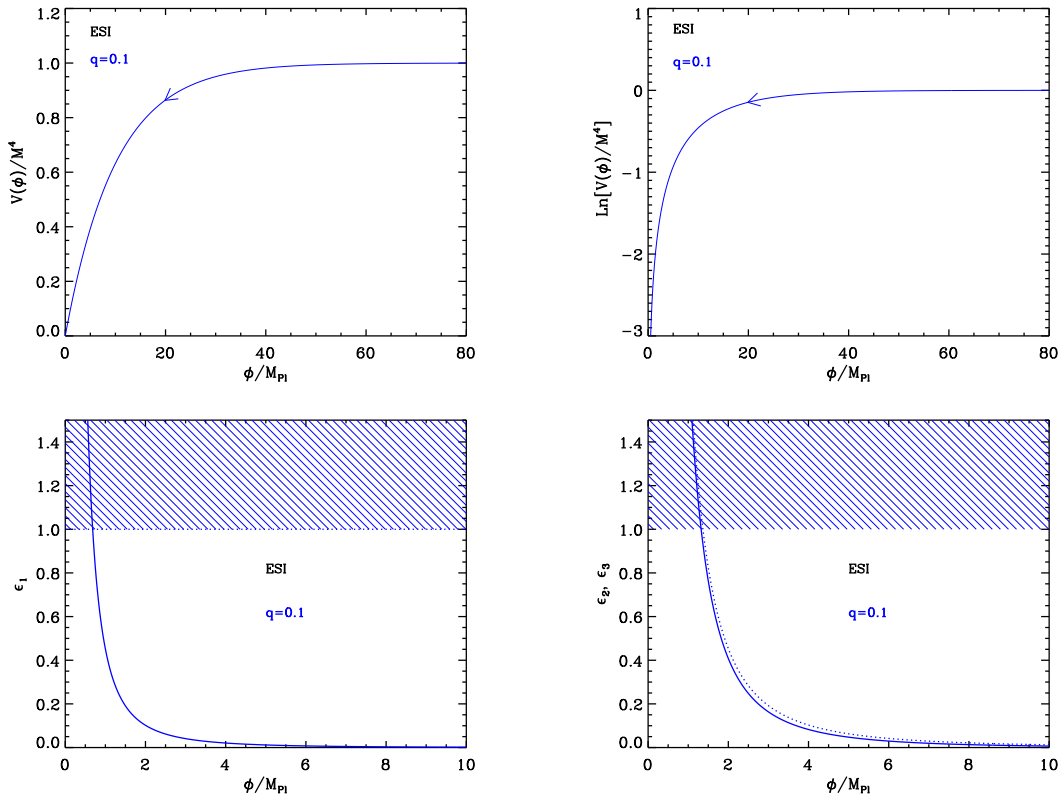


Figure 15. Exponential SUSY Inflation (ESI) for $q = \sqrt{2}$. Top panels: the potential and its logarithm. Bottom left panel: slow-roll parameter ϵ_1 . The shaded area indicates where acceleration stops. Bottom right panel: slow-roll parameters ϵ_2 (solid line) and ϵ_3 (dotted line). For those, the shaded region signals the breakdown of the slow-roll approximation but not necessarily the end of the accelerated expansion.

$x_{\text{end}} > 0$ and $N < N_{\text{end}}$, the maximal value of exponential argument is saturated for $x_{\text{end}} \rightarrow 0$, i.e. for a Lambert function argument equals to $-1/e$. As the result the Lambert function argument varies, at most, in $[-1/e, 0]$. Finally, since $x > 0$, we see directly from Eq. (4.89) that the Lambert function values have to be negative thereby ensuring that inflation proceeds only along the “ -1 ”-branch (see Fig. 16).

With such a potential, inflation ends naturally at $\epsilon_1 = 1$, i.e. at the field value

$$x_{\text{end}} = \frac{1}{q} \ln \left(1 + \frac{q}{\sqrt{2}} \right). \quad (4.90)$$

From this equation and the trajectory, we have an explicit relation between the field value ϕ_* at which the pivot mode crossed the Hubble radius during inflation and the corresponding e-fold number ΔN_* .

Finally, the parameter M can be determined from the amplitude of the CMB anisotropies, and one gets

$$\left(\frac{M}{M_{\text{Pl}}} \right)^4 = 720 q^2 \pi^2 \frac{e^{-2qx_*}}{(1 - e^{-qx_*})^3} \frac{Q_{\text{rms-PS}}^2}{T^2}, \quad (4.91)$$

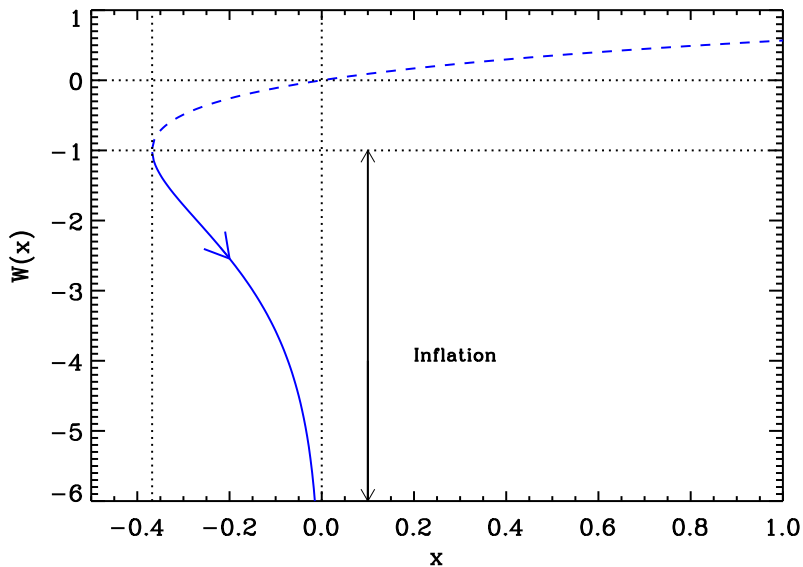


Figure 16. Lambert functions $W_0(x)$ (dashed line) and $W_{-1}(x)$ (solid line). During Exponential SUSY inflation, inflation proceeds along the “-1” branch in the direction specified by the arrow on the figure.

where the value of ϕ_* (or ΔN_*) is obtained from Eq. (2.46). The reheating consistent slow-roll prediction for the exponential Susy models are represented in Figs. 81 and 82. In the limit $q \rightarrow 0$, we recover the same prediction as a linear large field model. From Fig. 81, we see that all the models remains compatible with the current data. These figures correspond to $\bar{w}_{\text{reh}} = 0$, but one could argue that $\bar{w}_{\text{reh}} \gtrsim -1/3$ make more sense if a parametric reheating would feel the linear shape of the potential. This quite extreme situation is represented in Fig. 82. In that case, the low reheating temperatures are clearly disfavored.

4.8 Power Law Inflation (PLI)

These models refer to inflationary potentials of the form

$$V(\phi) = M^4 e^{-\alpha\phi/M_{\text{Pl}}}, \quad (4.92)$$

where α is a dimensionless parameter. They have been intensively studied as test cases because they provide an exact inflationary dynamics, of the power law form, hence their name.

It was first introduced in Ref. [231, 232] as providing quintessential inflation, i.e. models in which the energy of the scalar field redshifts as a power law with respect to the scale factor $\rho \propto a^{-q}$. In that case $\alpha = \sqrt{q/2}$. The same potential has also been studied in Ref. [233, 234] as arising when implementing large field inflation (LFI, see section 4.2) with non minimal coupling of the inflaton with the gravity sector. In Ref. [235], a cosmic no-hair theorem for Bianchi models was proven assuming that the potential of the inflaton is of type (4.92). It was shown that one must have $0 < \alpha < \sqrt{2/3}$ so that the isotropic power law solution is the unique attractor for any initially expanding Bianchi type model (except type IX). In

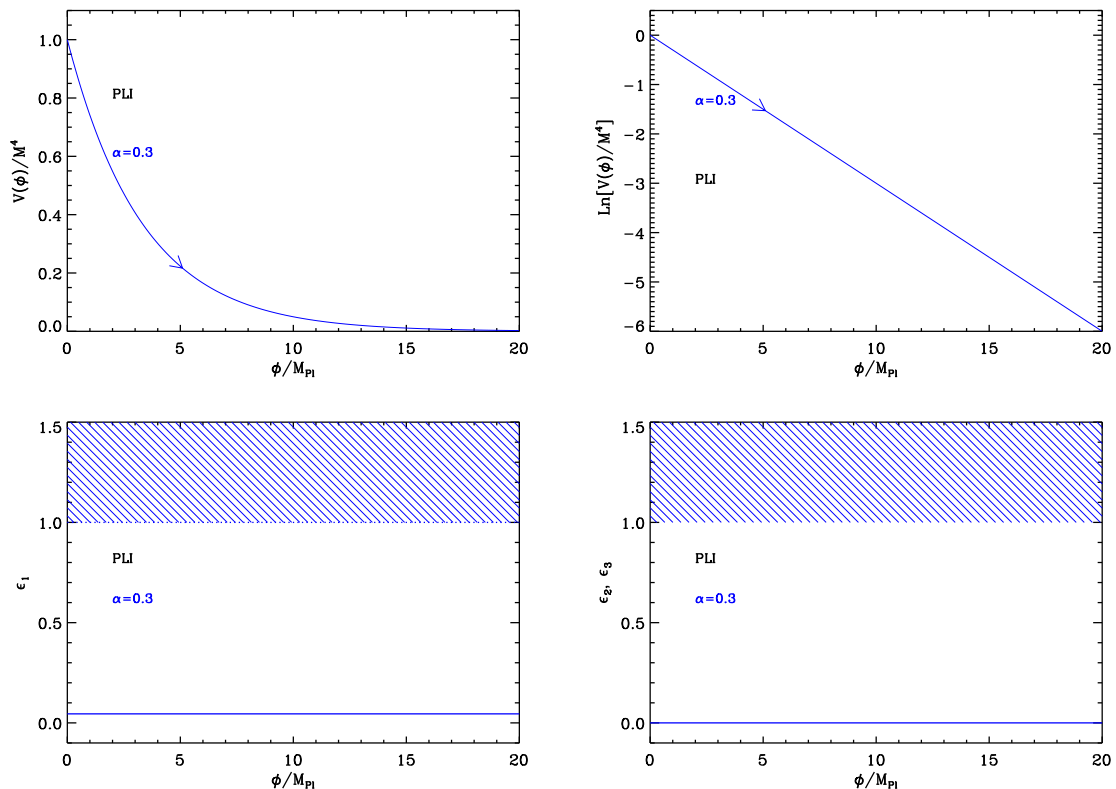


Figure 17. Power Law Inflation (PLI) for $\alpha = 0.3$. Top panels: power law potential (left) and its logarithm (right). Bottom left panel: slow-roll parameter ϵ_1 . Bottom right panel: slow-roll parameters $\epsilon_2 = \epsilon_3 = 0$. On these plots, the shaded area indicates the region where slow-roll is violated.

Ref. [236], the potential (4.92) has been studied in the Kantowski-Sachs metric, and it was found that the production of particles by the scalar field act as viscous forces which enlarge the range of initial conditions leading to successful inflation. In Ref. [237], the nature of the potential $V(\phi)$ relevant to having inflation in a minimally coupled scalar field cosmology along with a causal viscous fluid was investigated using the same potential. In Ref. [238–240], it was used to describe the dynamics of a tachyonic matter field. In Ref. [241], the general transformations that leave unchanged the form of the field equations for Bianchi V cosmologies were investigated, and it was found that they admit asymptotic stable points that lead to power law solutions of the type (4.92). In Ref. [242], inflation was studied in the context of M-theory on S^1/\mathbb{Z}_2 via the non-perturbative dynamics of M5-branes. The open membrane instanton interactions between the branes give rise to potentials of the type (4.92). Ref. [243] has used the exponential potential (4.92) in the context of Randall-Sandrum type II Braneworld model. Finally, the general dynamics of power law inflation was widely studied in Refs. [244–253], where various aspects of its phenomenology were highlighted.

The potential and its logarithm are displayed in Fig. 17. They are decreasing functions of the field, hence inflation proceeds from the left to the right. The slow-roll parameters take a simple form given by

$$\epsilon_1 = \frac{\alpha^2}{2}, \quad \epsilon_{i>1} = 0. \quad (4.93)$$

Since the first slow-roll parameter is constant, inflation cannot stop by slow-roll violation but at some point ϕ_{end} where e.g. a tachyonic instability is triggered. A priori, this provides the model with a new free parameter. However, because the slow-roll parameters do not depend on ϕ , as well as all the inflationary dynamics features, even outside the slow-roll approximation (see below), the predictions of the model cannot depend on ϕ_{end} and this parameter is irrelevant for the observable predictions.

The slow-roll hierarchy being almost trivial, the whole dynamics of the model can be worked out even out of the slow-roll approximation. Indeed, let us first notice that the slow-roll trajectory can be explicitly integrated, and gives

$$\phi/M_{\text{Pl}} = \phi_{\text{end}}/M_{\text{Pl}} + \alpha(N_{\text{end}} - N). \quad (4.94)$$

Now, one can notice that this trajectory is also a solution of the exact Klein-Gordon equation of motion, which writes, in terms of the number of e-folds N ,

$$H^2 \frac{\partial^2 \phi}{\partial N^2} + \left(3H^2 + H \partial \frac{\partial H}{\partial N} \right) \frac{\partial \phi}{\partial N} + \frac{dV}{d\phi} = 0. \quad (4.95)$$

Indeed, the first term vanishes, and the second term requires to compute

$$H^2 = \frac{V + \dot{\phi}^2/2}{3M_{\text{Pl}}^2} = \frac{V + \frac{H^2}{2} \left(\frac{\partial \phi}{\partial N} \right)^2}{3M_{\text{Pl}}^2} = \frac{V + \frac{H^2}{2} \alpha^2 M_{\text{Pl}}^2}{3M_{\text{Pl}}^2}, \quad (4.96)$$

from which one gets

$$H^2 = \frac{V}{3M_{\text{Pl}}^2} \frac{1}{1 - \frac{\alpha^2}{6}}. \quad (4.97)$$

From there, one can evaluate all terms in the Klein-Gordon equation, and verify that Eq. (4.94) is indeed a solution of Eq. (4.95). Since it is a second order differential equation, other solutions exist, but it can be shown [231, 232] that the exact solution is an attractor of all the possible solutions. Let us also notice that combining Eq. (4.97) with Eq. (4.94) gives rise to

$$H = H_{\text{end}} \left(\frac{a_{\text{end}}}{a} \right)^{\alpha^2/2}, \quad (4.98)$$

which can be integrated and gives

$$a(t) = a_{\text{end}} \left(\frac{t}{t_{\text{end}}} \right)^{2/\alpha^2}. \quad (4.99)$$

Finally, the equation of state $w = P/\rho$ can also be worked out exactly and one gets

$$w = -1 + \frac{\alpha^2}{3}. \quad (4.100)$$

Again, all the previous expressions are valid outside the slow-roll approximation. One can see that pure de Sitter corresponds to $\alpha = 0$, in this case the potential is constant, the equation of state is -1 and the scale factor expands exponentially.

Another nice feature of power-law inflation is that the spectrum of the perturbations can be computed exactly without relying on any approximation. Defining the parameter $\beta \leq -2$ by $\alpha^2/2 = (\beta + 2)/(\beta + 1)$, it is given by

$$\mathcal{P}_\zeta = \frac{H_*^2}{\pi\epsilon_1(8\pi M_{\text{Pl}}^2)} f(\beta) \left(\frac{k}{k_*}\right)^{2\beta+4}, \quad (4.101)$$

where

$$f(\beta) \equiv \frac{1}{\pi} \left[\frac{(1+\beta)^{1+\beta}}{2^{1+\beta}} \Gamma\left(\frac{1}{2} + \beta\right) \right]^2. \quad (4.102)$$

In particular, $f(\beta = -2) = 1$. The power spectrum of gravitational waves can also be deduced from the definitions of the power spectra

$$\mathcal{P}_\zeta = \frac{k^3}{8\pi^2} \left| \frac{\mu_S}{a\sqrt{\epsilon_1}} \right|^2, \quad \mathcal{P}_h = \frac{2k^3}{\pi^2} \left| \frac{\mu_T}{a} \right|^2. \quad (4.103)$$

For power law inflation, we have $\mu_S = \mu_T$, and therefore

$$r \equiv \frac{\mathcal{P}_h}{\mathcal{P}_\zeta} = 16\epsilon_1 = \frac{16n_T}{n_T - 2}, \quad (4.104)$$

since $n_T = n_S - 1 = 2\beta + 4$.

Finally, the COBE normalization gives

$$\left(\frac{M}{M_{\text{Pl}}}\right)^4 = 720\pi^2 \alpha^2 e^{\alpha\phi_*/M_{\text{Pl}}} \frac{Q_{\text{rms-PS}}^2}{T^2}. \quad (4.105)$$

Obviously, this normalization depends on the value of ϕ_{end} , and it is more relevant to express it in terms of the potential energy, say, at the end of inflation:

$$\frac{V_{\text{end}}}{M_{\text{Pl}}^4} = 720\pi^2 \alpha^2 e^{-\alpha^2 \Delta N_*} \frac{Q_{\text{rms-PS}}^2}{T^2}, \quad (4.106)$$

from which one typically gets $V_{\text{end}}^{1/4}/M_{\text{Pl}} \sim 10^{-4}$.

The reheating consistent slow-roll predictions for the power law inflation models are displayed in Fig. 83. Because the slow-roll parameters are constant during inflation, one can check that the predictions of the models do not depend on the energy scale at which the power law reheating ends. One has $n_s = 1 - \alpha^2$ and $r = 8\alpha^2$, and from the WMAP constraints, the models with $\alpha > 0.2$ are excluded at two sigma confidence level.

4.9 Kähler Moduli Inflation I (KMII)

These models are stringy models and arise when type IIB string theories via Calabi-Yau flux compactification are used. KMII scenarios have been derived and studied in Refs. [254–260]. More specifically, when internal spaces are weighted projective spaces, one of the Kähler moduli can play the role of an inflaton field and its potential, in the large field limit, reads

$$V(\phi) = M^4 \left(1 - \alpha \frac{\phi}{M_{\text{Pl}}} e^{-\phi/M_{\text{Pl}}} \right), \quad (4.107)$$

α being a positive dimensionless parameter. Actually, since we deal with a modulus, ϕ usually possesses a non-minimal kinetic term. Then, once the inflaton field has been canonically

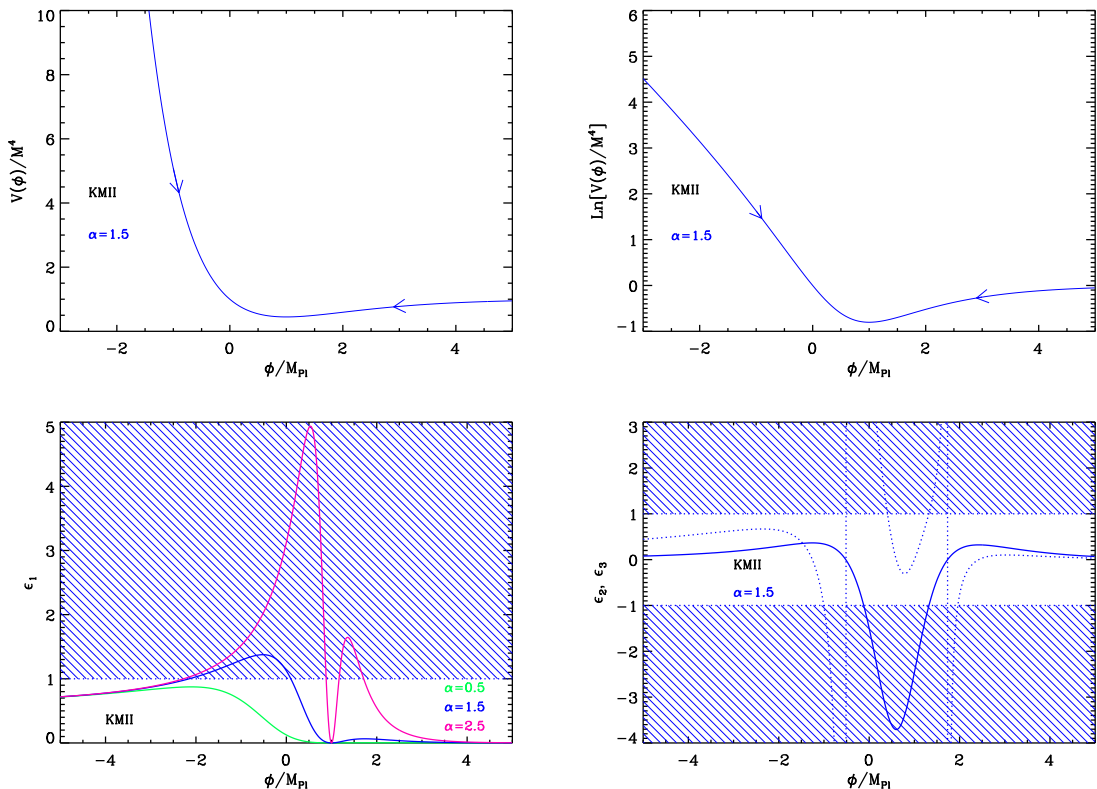


Figure 18. Top left panel: Kähler moduli inflation (KMII) potential for $\alpha = 1.5$. The two arrows indicate the two regions of the potential where inflation can take place. Top right panel: logarithm of the potential for the same value of α . Bottom left panel: slow-roll parameter ϵ_1 for $\alpha = 0.5$ (solid green line), $\alpha = 1.5$ (solid blue line) and $\alpha = 2.5$ (solid pink line). Obviously, the number of solutions of the equation $\epsilon_1 = 1$ depends on the value of α . Bottom right panel: slow-roll parameters ϵ_2 (solid line) and ϵ_3 (dotted line) for $\alpha = 1.5$.

normalized, ϕ has to be replaced with $\propto \phi^{4/3}$. The corresponding corrected potential is studied as “Kähler Moduli Inflation II” (KMIII) in section 5.3. However, sometimes, the potential (4.107) (with ϕ already canonically normalized) is also studied as a toy model (notably in Ref. [260]), the hope being that it can give a simpler description of the physics that naturally appears in the context of moduli inflation. Therefore, in this section, we also consider this scenario.

The potential in Eq. (4.107) depends on one free parameter, α . A priori, there does not exist any bound on its value. However, as explained below, in order for slow-roll inflation to occur, one must restrict the range of possible values for α . Within this range, we will show that the predictions of the model turn out to be almost independent of α (in fact, they logarithmically depend on α). The potential (4.107) and its logarithm are displayed in Fig. 18. It decreases from $\phi = 0$ (where it blows up), reaches a minimum at $\phi = M_{\text{Pl}}$, and then increases to the asymptotic value $V = M^4$ when $\phi \rightarrow +\infty$. Therefore, two regimes of inflation may a priori exist: either inflation proceeds from the left to the right in the decreasing $\phi < M_{\text{Pl}}$ branch of the potential (in this branch the *vev* ϕ increases during inflation) or it proceeds from the right to the left in the increasing $\phi > M_{\text{Pl}}$ branch of the potential (and

the *vev* decreases during inflation). However, one should keep in mind that the potential is derived under the large field assumption and, consequently, only the second regime is in fact meaningful. As a toy model, one might nevertheless want to study both regimes but it turns out that, in the first one, inflation could not stop by violation of the slow-roll conditions. This is why we will mainly focus on the second regime in the rest of this section. Let us also notice that the minimum value of the potential is located at $\phi = M_{\text{Pl}}$ and is $V_{\text{min}} = M^4 (1 - \alpha/e)$. Therefore, if one requires the potential to be positive definite everywhere, then one must have $0 < \alpha < e \simeq 2.72$. However, this condition may also be ignored if one considers that the potential (4.107) is in any case not valid at $\phi/M_{\text{Pl}} \lesssim 1$.

Defining x by $x \equiv \phi/M_{\text{Pl}}$, the three first slow-roll parameters can be expressed as

$$\epsilon_1 = \frac{\alpha^2}{2} e^{-2x} \frac{(1-x)^2}{(1-\alpha e^{-x}x)^2}, \quad \epsilon_2 = \frac{2\alpha e^{-x}}{(1-\alpha e^{-x}x)^2} (\alpha e^{-x} + x - 2), \quad (4.108)$$

and

$$\epsilon_3 = \frac{\alpha e^{-x} (x-1)}{(1-\alpha e^{-x}x)^2 (\alpha e^{-x} + x - 2)} \left[x - 3 + \alpha e^{-x} (x^2 - 3x + 6) - 2\alpha^2 e^{-2x} \right]. \quad (4.109)$$

Let us now study in more detail how inflation stops in this model. Let us first solve the equation $\epsilon_1 = 1$. As can be seen in Fig. 18, the number of solutions depends on the value of α . We now define the numbers α_1 and α_2 by

$$\alpha_1 \equiv \frac{\sqrt{2}}{\sqrt{2}-1} e^{\frac{2-\sqrt{2}}{1-\sqrt{2}}} \simeq 0.83, \quad \alpha_2 \equiv \frac{\sqrt{2}}{\sqrt{2}+1} e^{\frac{2+\sqrt{2}}{1+\sqrt{2}}} \simeq 2.41. \quad (4.110)$$

If $0 < \alpha < \alpha_1$, then there is no solution (this corresponds to the green line in the bottom left panel in Fig. 18). The inflaton field eventually oscillates around the minimum of its potential but remains in a region where inflation continues forever. In this case, in order to stop inflation, one must add an auxiliary field to the model such that a tachyonic instability is triggered at some value x_{end} . This of course increases the number of parameters of this model. If $\alpha_1 < \alpha < \alpha_2$ (which corresponds to the blue line in Fig. 18), then two solutions appear:

$$x_{\epsilon_1=1}^-|_{x<1} = x_{\text{end}}|_{x<1} = \frac{1}{1-\sqrt{2}} - W_0 \left[\frac{\sqrt{2}}{1-\sqrt{2}} \frac{e^{\frac{1}{1-\sqrt{2}}}}{\alpha} \right] \simeq -2.4 - W_0 \left(-\frac{0.3}{\alpha} \right), \quad (4.111)$$

$$x_{\epsilon_1=1}^+|_{x<1} = \frac{1}{1-\sqrt{2}} - W_{-1} \left[\frac{\sqrt{2}}{1-\sqrt{2}} \frac{e^{\frac{1}{1-\sqrt{2}}}}{\alpha} \right] \simeq -2.4 - W_{-1} \left(-\frac{0.3}{\alpha} \right), \quad (4.112)$$

where W_0 and W_{-1} denotes the “0-branch” and the “-1-branch” of the Lambert function respectively. These two solutions are both smaller than one so that they both lie in the decreasing branch of the potential. Correspondingly, two regimes of inflation exist. The first one proceeds from the left to the right and stops at $x_{\text{end}}|_{x<1}$. However, using the expression for the slow-roll parameters (4.108), it is easy to see that ϵ_1 is always larger than 1/2 in this domain. Therefore, the slow-roll approximation breaks down in this case. The second regime takes place in the $\phi/M_{\text{Pl}} > 1$ branch of the potential but inflation cannot stop by slow-roll violation. Finally, if $\alpha_2 < \alpha$ (this situation corresponds to the pink line in the bottom left

panel in Fig. 18), then four solutions exist: two were already given in Eqs. (4.111), (4.112) and the two new ones read

$$x_{\epsilon_1=1}^-|_{x>1} = \frac{1}{1+\sqrt{2}} - W_0 \left[-\frac{\sqrt{2}}{1+\sqrt{2}} \frac{e^{\frac{1}{1+\sqrt{2}}}}{\alpha} \right] \simeq 0.4 - W_0 \left(\frac{-0.9}{\alpha} \right), \quad (4.113)$$

$$x_{\epsilon_1=1}^+|_{x>1} = x_{\text{end}}|_{x>1} = \frac{1}{1+\sqrt{2}} - W_{-1} \left[-\frac{\sqrt{2}}{1+\sqrt{2}} \frac{e^{\frac{1}{1+\sqrt{2}}}}{\alpha} \right] \simeq 0.4 - W_{-1} \left(\frac{-0.9}{\alpha} \right) \quad (4.114)$$

The two new solutions are greater than one and therefore lie in the increasing branch of the potential. Thus two regimes exist in this situation. The first one is the same as before, proceeds again from the left to right, stops at $x_{\text{end}}|_{x<1}$ and suffers from the fact that ϵ_1 is always larger than $1/2$. The second one proceeds from the right to the left and ends at $x_{\text{end}}|_{x>1}$. We conclude that this regime is the regime of interest for the KMII model and that we must therefore require $\alpha > \alpha_2$.

Let us now study the slow-roll trajectory. It can be integrated exactly and its expression can be written as

$$N_{\text{end}} - N = x_{\text{end}} - \frac{e}{\alpha} \text{Ei}(x_{\text{end}} - 1) + \ln(x_{\text{end}} - 1) - x + \frac{e}{\alpha} \text{Ei}(x - 1) - \ln(x - 1), \quad (4.115)$$

where Ei is the exponential integral function [160, 161]. At this point, a few remarks are in order. First, let us notice that N goes to ∞ when x tends to 1. This means that, in the slow-roll approximation, the field can never cross the minimum of its potential. In particular, if $\alpha < \alpha_2$, that is to say if one starts from the $\phi/M_{\text{Pl}} < 1$ branch and rolls down from the left to the right, then one can never reach the physical $\phi/M_{\text{Pl}} > 1$ branch of the potential and inflation can never come to an end. Second, when $x \gg 1$, the trajectory can be approximated by

$$N_{\text{end}} - N \simeq \frac{e}{\alpha} \left(\frac{e^x}{x} - \frac{e^{x_{\text{end}}}}{x_{\text{end}}} \right). \quad (4.116)$$

Moreover, in this approximation, it can be inverted exactly and one obtains

$$x \simeq -W_{-1} \left[-\frac{1}{\alpha (N_{\text{end}} - N)/e + e^{x_{\text{end}}/x_{\text{end}}}} \right], \quad (4.117)$$

in agreement with what was obtained in Ref. [260]. In the above expression, W_{-1} is the -1 branch of the Lambert function. Let us also notice that, in Ref. [260], the branch of the Lambert function was in fact incorrectly chosen. The fact that the -1 branch of the Lambert function has to be considered comes from the following argument. When $N_{\text{end}} - N \rightarrow \infty$, the argument of the Lambert function goes to 0^- and, therefore, since x must tend towards $+\infty$ in this limit, the -1 branch must be chosen. In addition, if $N_{\text{end}} - N \rightarrow 0$, then one must have $x \rightarrow x_{\text{end}} > 1$ which is also the case if the -1 branch is retained. This is represented in Fig. 19 where the arrow indicates the direction along which inflation proceeds. Third, since, when $x \rightarrow \infty$, one has $N_{\text{end}} - N \rightarrow \infty$, a sufficient number of e -folds can always be realized in this model. Four, in fact, it is inaccurate to assume that $x_{\text{end}} \gg 1$ and, therefore, the above approximated trajectory is not so useful. However, if one only assumes that $x \gg 1$ (which can be checked to be a good approximation, especially at $x = x_*$) but not $x_{\text{end}} \gg 1$, then one can write

$$N_{\text{end}} - N \simeq \frac{e}{\alpha} \frac{e^x}{x} + x_{\text{end}} - \frac{e}{\alpha} \text{Ei}(x_{\text{end}} - 1), \quad (4.118)$$

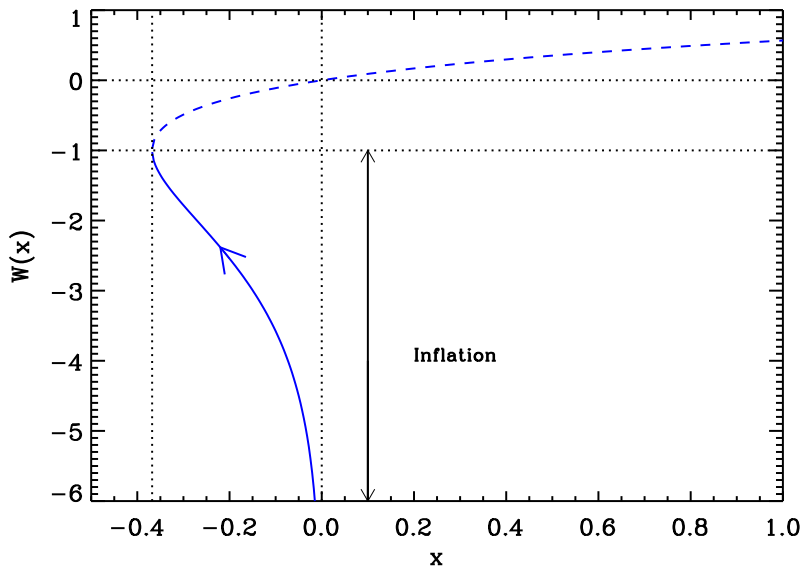


Figure 19. Lambert functions $W_0(x)$ (dashed line) and $W_{-1}(x)$ (solid line). During Kähler moduli inflation, inflation proceeds along the “-1” branch in the direction specified by the arrow.

which, moreover, can be inverted into

$$x \simeq -W_{-1} \left[-\frac{1}{\alpha (N_{\text{end}} - N) e + \text{Ei}(x_{\text{end}} - 1) - \alpha x_{\text{end}}/e} \right], \quad (4.119)$$

and which is valid whenever $x \gg 1$. However, one should keep in mind that, now, and contrary to the former approximated trajectory, taking the limit $N \rightarrow N_{\text{end}}$ in the above expression is meaningless.

Finally, it is interesting to determine the energy scale M . Using the CMB normalization, one obtains the following expression

$$\left(\frac{M}{M_{\text{Pl}}} \right)^4 = 720 \pi^2 \alpha^2 \frac{(1 - x_*)^2}{(1 - \alpha x_* e^{-x_*})^3} e^{-2x_*} \frac{Q_{\text{rms-PS}}^2}{T^2}. \quad (4.120)$$

If one uses the $x_* \gg 1$ approximation, then Eq. (4.119) tells us that $x_* \simeq \log(\alpha \Delta N_*)$ and Eq. (4.120) can be re-written as

$$\left(\frac{M}{M_{\text{Pl}}} \right)^4 = \mathcal{O}(1) 720 \frac{\pi^2}{\Delta N_*^2} \frac{Q_{\text{rms-PS}}^2}{T^2}. \quad (4.121)$$

It is remarkable that this equation does not depend on α . Using a fiducial value for ΔN_* , one typically gets $M/M_{\text{Pl}} \sim 10^{-3}$.

The predictions of KMII models are displayed in Fig. 84, for $\alpha > \alpha_2$. The reheating equation of state parameter \bar{w}_{reh} has been taken to 0 since the potential is quadratic close to its minimum [but, it should be reminded that, in principle, the potential Eq. (4.107) cannot be trusted close to its minimum]. One can see that, as announced at the beginning of this section, the predictions depend on α in a very mild way, a conclusion which is in agreement

with Refs. [254, 260]. This can be understood as follows. If one assumes that $x_* \gg 1$, then we have already noticed that Eq. (4.119) implies that $x_* \simeq \log(\alpha\Delta N_*)$. From this result, one obtains that

$$\epsilon_{1*} \simeq \frac{1}{2\Delta N_*^2} \ln^2(\alpha\Delta N_*), \quad \epsilon_{2*} \simeq \frac{2}{\Delta N_*} \ln(\alpha\Delta N_*), \quad \epsilon_{3*} \simeq \frac{1}{\Delta N_*} \ln(\alpha\Delta N_*). \quad (4.122)$$

In these expressions, we notice that the slow-roll parameters (at Hubble crossing) logarithmically depend on α . This explains the weak α dependence observed in Fig. 84. Of course, one can also calculate the corresponding expressions of the spectral index, tensor to scalar ratio and running. One arrives at

$$n_s \simeq 1 - 2\frac{\ln(\alpha\Delta N_*)}{\Delta N_*}, \quad r \simeq 8\frac{\ln^2(\alpha\Delta N_*)}{\Delta N_*^2}, \quad \alpha_s \simeq -2\frac{\ln^2(\alpha\Delta N_*)}{\Delta N_*^2}. \quad (4.123)$$

These expressions are in accordance with the estimates derived in Refs. [254, 260]. However, contrary to what is claimed in Refs. [260], the predicted value of the running is not excluded by the CMB observations since, according to WMAP9 [66, 67], one has $\alpha_s = -0.019 \pm 0.025$.

4.10 Horizon Flow Inflation at first order (HF1I)

The horizon flow models have been introduced in Ref. [261] and consist into designing field potentials to exactly produce a truncated Taylor expansion of the Hubble parameter with respect to the field. As such they constitute a whole class of phenomenological inflationary models. Here, we are considering a potential designed such that $H(\phi) = H_0(1 + A_1\phi/M_{\text{Pl}})$, where A_1 is a free dimensionless parameter. The shape of the potential reads [261]

$$V(\phi) = M^4 \left(1 + A_1 \frac{\phi}{M_{\text{Pl}}}\right)^2 \left[1 - \frac{2}{3} \left(\frac{A_1}{1 + A_1 \frac{\phi}{M_{\text{Pl}}}}\right)^2\right]. \quad (4.124)$$

Denoting $x \equiv \phi/M_{\text{Pl}}$, the potential admits a global minimum at $x_{V=\min} = -1/A_1$, which is negative

$$V_{\min} = V(\phi_{V=\min}) = -\frac{2}{3}M^4 A_1^2 < 0. \quad (4.125)$$

As a result, there are two disconnected field domains in which the potential remains definite positive, either $x > x_{V=0}^+$ or $x < x_{V=0}^-$ where $x_{V=0}^\pm$ are the two roots of $V(x_{V=0}^\pm) = 0$, i.e.

$$x_{V=0}^+ = \sqrt{\frac{2}{3}} - \frac{1}{A_1}, \quad x_{V=0}^- = -\sqrt{\frac{2}{3}} - \frac{1}{A_1}. \quad (4.126)$$

An interesting consequence of the horizon flow approach is that the Hubble flow functions can be calculated exactly, i.e. out of the slow-roll approximation because $H(\phi)$ is exactly known. As discussed in Ref. [17, 262], one could compare them with the other hierarchy of parameters, ϵ_i^V , that are defined over the successive logarithmic derivatives of the potential. In the slow-roll approximation, one precisely uses the potential derivatives to approximate the Hubble flow functions, and this consists into identifying both hierarchies at a given order of approximation. From $H \propto 1 + A_1 x$, one gets the exact Hubble flow functions

$$\epsilon_1 = 2 \left(\frac{A_1}{1 + A_1 x}\right)^2, \quad \epsilon_2 = \epsilon_3 = 2\epsilon_1, \quad (4.127)$$

whereas the slow-roll functions associated with the potential are

$$\epsilon_1^V = \frac{18A_1^2(A_1x+1)^2}{[3+6A_1x+A^2(3x^2-2)]^2}, \quad \epsilon_2^V = \frac{12A_1^2[3+6A_1x+A_1^2(3x^2+2)]}{[3+6A_1x+A_1^2(3x^2-2)]^2}, \quad (4.128)$$

and

$$\epsilon_3^V = \frac{108A_1^2(A_1x+1)^2[1+2A_1x+A_1^2(x^2+2)]}{[3+6A_1x+A_1^2(3x^2-2)]^2[3+6A_1x+A_1^2(3x^2+2)]}. \quad (4.129)$$

As shown in Ref. [17], the link between the two hierarchies can be made explicit and one has

$$\epsilon_1^V = \epsilon_1 \left(\frac{1-\eta/3}{1-\epsilon_1/3} \right)^2. \quad (4.130)$$

The η parameter is defined as

$$\eta \equiv \frac{2}{H} \frac{d^2H}{dx^2}, \quad (4.131)$$

and vanishes in our case. As a result, provided $\epsilon_1 \ll 1$, i.e. we are in the slow-roll approximation, both hierarchies give the same results at first order. In order to establish Eq. (4.130), one has to show first that

$$\eta = \epsilon_1 + \frac{1}{\sqrt{2\epsilon_1}} \frac{d\epsilon_1}{dx}, \quad (4.132)$$

and then that³

$$\frac{d\epsilon_1}{dx} = (\epsilon_1 - 3) \left(\frac{d \ln V}{dx} - \sqrt{2\epsilon_1} \right). \quad (4.133)$$

The potential and the exact Hubble flow functions have been represented in Fig. 20.

Inflation can take place inside the two positive definite domains of the potential, i.e. at negative or positive field values. However, the Hubble parameter has to be positive such that H_0 has to be chosen negative if $1 + A_1x < 0$ along the field trajectory. Since the potential is completely symmetric with respect to its minimum $x_{V=\min}$, we can study in full generality only the $x > x_{V=0}^+$ branch. In particular, as the Hubble flow functions are exact, we can also derive the exact field trajectory

$$N - N_{\text{end}} = -\frac{1}{2A_1} \left(x + \frac{1}{2}A_1x^2 - x_{\text{end}} - \frac{1}{2}A_1x_{\text{end}}^2 \right). \quad (4.134)$$

Let us notice that, in the slow-roll approximation, one would have derived the trajectory from ϵ_1^V . Doing so, one would have obtained

$$N - N_{\text{end}} = -\frac{1}{2A_1} \left(x + \frac{1}{2}A_1x^2 - x_{\text{end}} - \frac{1}{2}A_1x_{\text{end}}^2 - \frac{2}{3}A_1 \ln \left| \frac{1+A_1x}{1+A_1x_{\text{end}}} \right| \right). \quad (4.135)$$

It is amusing to remark that here, the simplest formula is not given by the slow-roll derived one, but rather by the exact one. From this remark one should keep in mind that, in order to simplify trajectories integration, one can always add factors of order $\mathcal{O}(\epsilon_1)$. The exact trajectory (4.134) can be inverted and one finds

$$x = -\frac{1}{A_1} + \frac{1}{A_1} \sqrt{1 + 2A_1x_{\text{end}} + A_1^2[x_{\text{end}}^2 - 4(N - N_{\text{end}})]}. \quad (4.136)$$

³A sign in these two equations differs from the ones typeset in Ref. [17], most probably due to a misprint.

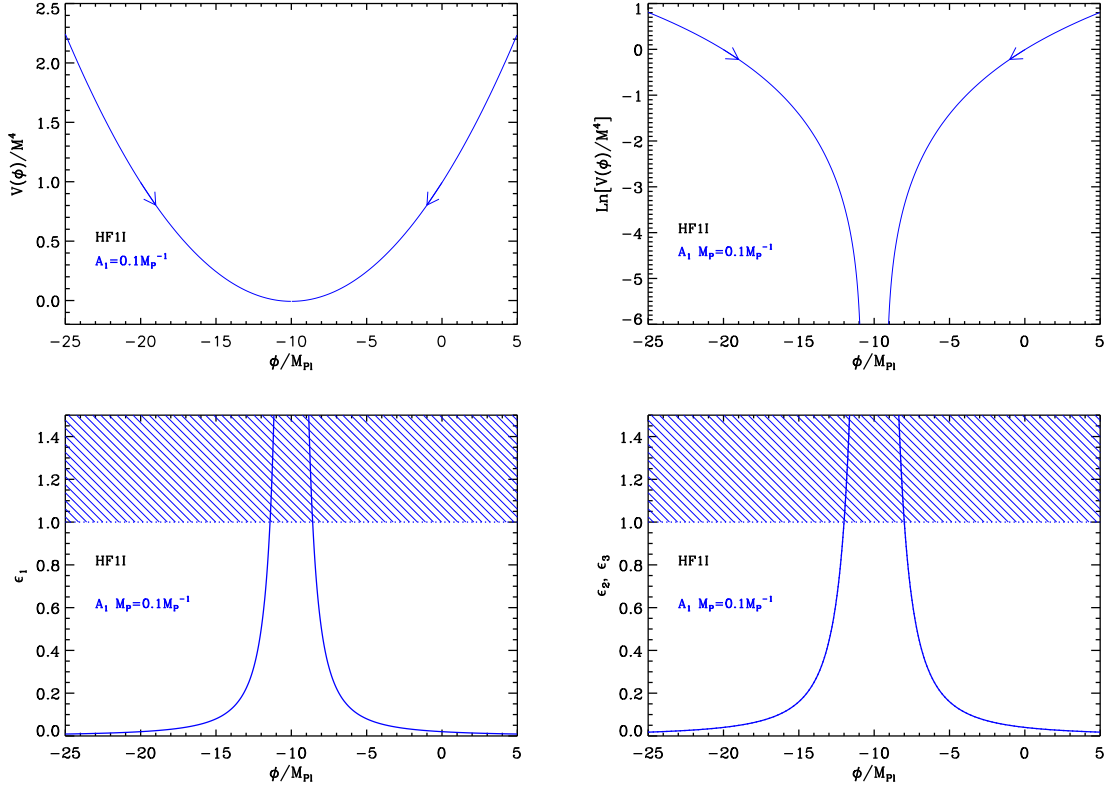


Figure 20. Top left panel: Horizon Flow Inflation at first order potential for $A_1 = 0.1$. Top panels: the potential and its logarithm with respect to the field values. Bottom left panel: the first Hubble flow function ϵ_1 (exact) and the corresponding shaded area where inflation stops. Bottom right panel: Hubble flow functions ϵ_2 (solid line) and ϵ_3 (dotted line) for the same potential. These two functions are equal to $2\epsilon_1$.

Along both the positive and negative branch of the potential, inflation ends naturally at $\epsilon_1 = 1$, that is at

$$x_{\epsilon_1=1}^{\pm} = \frac{1 \pm \sqrt{2}A_1}{A_1}. \quad (4.137)$$

Along the positive branch we are interested in, we therefore have

$$x_{\text{end}} = x_{\epsilon_1=1}^+ = \frac{1 + \sqrt{2}A_1}{A_1}. \quad (4.138)$$

Plugging this expression into Eq. (4.136) gives the field value x_* at which the pivot mode crossed the Hubble radius during inflation in terms of the e-fold number $\Delta N_* = N_{\text{end}} - N_*$. Let us remember that solving for x_* (or ΔN_*) is made through Eq. (2.46). From Eq. (4.127), one gets

$$\epsilon_{1*} = \frac{1}{1 + 2\Delta N_*} \quad (4.139)$$

which, together with $\epsilon_2 = 2\epsilon_1$, yields

$$n_s - 1 = 2n_T, \quad r = 4(1 - n_s). \quad (4.140)$$

Notice that this relation is different from the power law case and consistent with Ref. [263]. In that reference, the authors mention that the horizon flow models predicts $r \simeq 4.8(1 - n_s)$ as a result of Monte-Carlo simulations.

Finally, the potential parameter M can be determined from the COBE normalization

$$\left(\frac{M}{M_{\text{Pl}}}\right)^4 = 960\pi^2 \frac{A_1^2}{(1 + A_1 x_*)^4} \frac{Q_{\text{rms-PS}}^2}{T^2}. \quad (4.141)$$

The reheating consistent (exact) predictions for the horizon flow inflation I models are represented in Fig. 85. As expected, the relation $\epsilon_2 = 2\epsilon_1$, which is the same as for the LFI quadratic case, is properly recovered. Clearly, the predictions do not depend much on the potential parameter A_1 .

4.11 Coleman-Weinberg Inflation (CWI)

The potential of this model was first introduced by Coleman and Weinberg in Ref. [264], in the context of spontaneous symmetry breaking generated by radiative corrections. The starting point of this work is to calculate the effective potential for a massless charged meson minimally coupled to the electrodynamic field.

In that reference, the effective action is explicitly constructed from a Legendre transform of the partition function, and expanded into one-particle-irreducible Feynman diagrams with n external lines (and summing up over n). The exact knowledge of the effective potential requires an infinite summation of all these Feynman diagrams, which is in practice intractable. It is thus made use of the one loop expansion method where all diagrams with no closed loops are first summed, then all diagrams with one closed loop are added, and all higher loops diagrams neglected. Starting with a quartic interacting scalar field, and requiring that the renormalized mass vanishes, one obtains a potential of the form

$$V(\phi) = M^4 \left[1 + \alpha \left(\frac{\phi}{Q}\right)^4 \ln\left(\frac{\phi}{Q}\right) \right]. \quad (4.142)$$

Let us emphasize that another useful frame of approximation is the Gaussian effective potential method. The Gaussian effective potential is a non perturbative approach to quantum field theory [265–273], originally developed in the context of quantum mechanics, and generalized to field theory afterwards. In quantum mechanics, when studying systems governed by Hamiltonians of the form $H = p^2/2 + V(\phi)$, the idea is to calculate an effective potential V_{GEP} defined as

$$V_{\text{GEP}}(\phi_0) = \min_{\Omega} \left[\langle \psi | H | \psi \rangle, \psi(\phi) = \left(\frac{\Omega}{\hbar\pi}\right)^{1/4} e^{-\Omega(\phi-\phi_0)^2/(2\hbar)} \right], \quad (4.143)$$

i.e. the minimum possible quantum mean energy of a Gaussian wavefunction centered over ϕ_0 . Such an object turns out to be a powerful tool to addressing the effects of quantum fluctuations on the physical behavior of a system in a non perturbative way. It can be easily generalized to quantum field theories, expanding the field operator Φ only over Ω -massive excitations around the classical value Φ_0 in d dimensions,

$$\Phi(t, \mathbf{x}) = \Phi_0 + (2\pi)^{(1-d)/2} \int \frac{d^{d-1}\mathbf{k}}{\sqrt{2\sqrt{k^2 + \Omega^2}}} \left(a_{\mathbf{k}} e^{-i\sqrt{k^2 + \Omega^2}t + i\mathbf{k}\cdot\mathbf{x}} + a_{\mathbf{k}}^\dagger e^{i\sqrt{k^2 + \Omega^2}t - i\mathbf{k}\cdot\mathbf{x}} \right), \quad (4.144)$$

where $a_{\mathbf{k}}^\dagger$ and $a_{\mathbf{k}}$ are the usual creation and annihilation operators, and minimizing the quantum mean value of the Hamiltonian density over Ω . In Ref. [266], the quartic interacting scalar field has been worked out with this method, i.e. starting from $V(\phi) = m^2\phi^2/2 + \lambda\phi^4$. The Gaussian effective potential V_{GEP} obtained in this way can be expanded in power of \hbar to show that the first order terms match with the potential of Coleman and Weinberg. This is not surprising as this is equivalent to performing a one loop expansion over the effective action. However, it should be stressed that the Gaussian effective potential method provides a much more general expression for the potential, that is valid beyond this perturbative limit and that can address regimes where quantum diffusion dominates the dynamics of the scalar field.

The model is defined such that inflation ends by violation of the slow-roll conditions, and is followed by a preheating stage in which the inflaton field oscillates at the bottom of its potential. Therefore this potential minimum must be set to zero, which implies

$$\alpha = 4e. \quad (4.145)$$

One is thus left with one mass parameter, Q , which sets the typical vev at which inflation takes place, and which is related to the bare initial mass of the scalar field and to its self quartic coupling constant. The value taken for Q thus depends on the physical initial embodiment of the quartic massless theory.

The CWI potential appears in various other contexts. In Ref. [2], the $SU(5) \rightarrow SU(3) \times SU(2) \times U(1)$ phase transition in GUTs is investigated and it is shown that if the temperature T is smaller than the inflaton vev ϕ_0 at the minimum of the potential, the potential takes the form

$$V(\phi) = \frac{5325}{512}\pi^2 g^4 \left[\phi^4 \ln\left(\frac{\phi}{\phi_0}\right) - \frac{\phi^4}{4} + \frac{\phi_0^4}{4} \right], \quad (4.146)$$

where $\phi_0 \simeq 10^{14} - 10^{15}$ GeV, and $g^2 \simeq 1/3$ is the gauge coupling constant. In this context, inflation proceeds along the decreasing branch of the potential, from the left to the right. Mapping back to our notations, one gets $M^4 = 5625\pi^2 g^4 \phi_0^4 / 2048 \simeq (10^{-13} - 10^{-17}) M_{\text{Pl}}^4$, $Q/M_{\text{Pl}} = e^{1/4} \phi_0 / M_{\text{Pl}} \simeq 5 \times 10^{-5} - 5 \times 10^{-4}$, and the condition $\alpha = 4e$ is ensured. However, the value of M^4/M_{Pl}^4 is in principle fixed by the amplitude of the CMB anisotropies and contrary to what arises from Eq. (4.146), $M = \mathcal{O}(Q)$, one should have instead [see Eq. (4.153)] $M^2/M_{\text{Pl}}^2 = \mathcal{O}(M_{\text{Pl}}/Q)$, which a priori contradicts the previous considering the typical values given for Q . The same problem is present in Ref. [274], where a gravitational coupling $-R\phi^2$ in the lagrangian drives the same $SU(5)$ breaking phase transition at a temperature of about 10^{10} GeV. The same Coleman-Weinberg potential is studied, with the same typical value for Q , but where the value suggested for M^4 is closer to $M^4/M_{\text{Pl}}^4 \simeq 10^{-20}$. Again, in Refs. [3, 275, 276], the same phase transition is discussed and the inflaton field ϕ arises as a specific direction of the adjoint Higgs field. The potential is still the same with an identical typical value for Q . However, the value of M is relaxed to be a free parameter (except in Ref. [276] where $M^4/M_{\text{Pl}}^4 \simeq 10^{-20}$).

In Ref. [277] the same model is studied but in a supersymmetric context instead of conventional GUTs. Then, in Ref. [278], still with the same $SU(5)$ breaking scheme, the CWI potential is studied and the remark that without fine tuned small couplings, it cannot satisfy the COBE normalization, is explicitly made. The typical value for Q which arises in that work is closer to $Q \simeq 10^{18}$ GeV. In Ref. [279] the same issue is investigated and the typical value for Q is revisited as in the original works, i.e. $Q \simeq 10^{15}$ GeV. In Ref. [280], the

CWI potential is obtained in the context of Kaluza-Klein inflation, i.e. in higher dimensions and with higher derivative terms and logarithmic dependence on the curvature scalar. Again, the typical value for $Q \simeq 10^{15}$ GeV.

In Ref. [281] the same potential is studied, but the value used for Q is rather different, $Q = 0.223M_{\text{Pl}}$, and is fine tuned in order to have two phases of inflation, a “chaotic inflationary” phase followed by a “new inflationary” phase. In Ref. [282], the Coleman-Weinberg potential is studied in the framework of Einstein-Brans-Dicke gravity, with the same typical value for $Q \simeq 10^{15}$ GeV and the same typical value for $M^4/M_{\text{Pl}}^4 \simeq 10^{-15}$ as in the original paper. Finally, in Ref. [283] the same potential is studied as arising in non supersymmetric GUTs such as SU(5) and SO(10), and the constraint on Q is relaxed to compare the predictions of the Coleman-Weinberg potential with the WMAP observations on more general grounds. It is found that the inflationary energy scale should be of the order $M \simeq 10^{16}$ GeV, and that $Q \simeq 10 M_{\text{Pl}}$ in order to match $n_s \sim 0.96$.

Considering these developments, the parameter Q/M_{Pl} shall be taken in the range $[10^{-5}, 10^{-3}]$, and the mass parameter M will be let free to allow for a normalization with respect to the amplitude of the CMB anisotropies. The potential is displayed Fig. 21 for $\alpha = 4e$. It starts decreasing with the inflaton vev at $\phi = 0$, reaches a minimum at $\phi/Q = e^{-1/4}$ where it vanishes, and then increases and diverges as ϕ goes to ∞ . As mentioned above, inflation proceeds along the decreasing branch of the potential, in the direction specified by the arrow in the figure.

Let us compute the first slow-roll parameters. Defining $x \equiv \phi/Q$, they are given by

$$\epsilon_1 = \frac{M_{\text{Pl}}^2}{Q^2} \frac{\alpha^2}{2} x^6 \left[\frac{1 + 4 \ln(x)}{1 + \alpha x^4 \ln(x)} \right]^2, \quad (4.147)$$

while

$$\epsilon_2 = 2 \frac{M_{\text{Pl}}^2}{Q^2} \alpha x^2 \frac{-7 - 12 \ln(x) + \alpha x^4 + \alpha x^4 \ln(x) + 4\alpha x^4 \ln(x)^2}{[1 + \alpha x^4 \ln(x)]^2}, \quad (4.148)$$

and finally

$$\begin{aligned} \epsilon_3 = & \frac{M_{\text{Pl}}^2}{Q^2} \left[-26\alpha x^2 + 21\alpha^2 x^6 - 2\alpha^3 x^{10} - 128\alpha x^2 \ln(x) \right. \\ & + 152\alpha^2 x^6 \ln(x) - 11\alpha^3 x^{10} \ln(x) - 96\alpha x^2 \ln(x)^2 \\ & + 368\alpha^2 x^6 \ln(x)^2 - 14\alpha^3 x^{10} \ln(x)^2 + 384\alpha^2 x^6 \ln(x)^3 \\ & \left. - 16\alpha^3 x^{10} \ln(x)^3 - 32\alpha^3 x^{10} \ln(x)^4 \right] [1 + \alpha x^4 \ln(x)]^{-2} \\ & \times \left[7 - \alpha x^4 + 12 \ln(x) - \alpha x^4 \ln(x) - 4\alpha x^4 \ln(x)^2 \right]^{-1}. \end{aligned} \quad (4.149)$$

The three of them have the same general behavior. They vanish at $x = 0$, increase with x in the decreasing branch of the potential and diverge at the minimum of the potential. Then they decrease from diverging values in the increasing branch of the potential, and reach asymptotically vanishing values when the field vev goes to infinity. Inflation stops by slow-roll violation when $\epsilon_1 = 1$. The value of x at which this happens needs to be determined numerically, but in the limit $Q/M_{\text{Pl}} \ll 1$ (remember that $Q/M_{\text{Pl}} \simeq 10^{-4}$) where one expects $x_{\text{end}} \ll 1$, one can derive an analytic approximated formula, namely

$$x_{\text{end}} \simeq e^{-1/4} \exp \left[\text{W}_{-1} \left(-\frac{3\sqrt{2}}{4\alpha} \frac{Q}{M_{\text{Pl}}} e^{3/4} \right) \right], \quad (4.150)$$

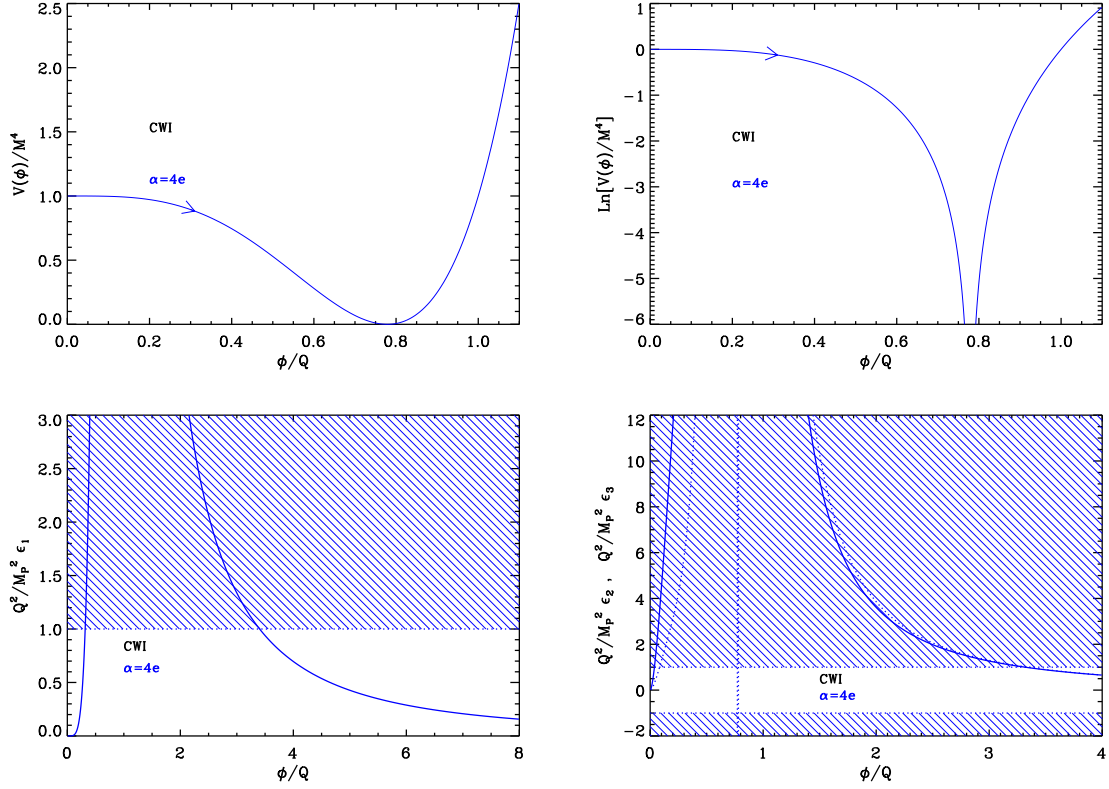


Figure 21. Coleman-Weinberg Inflation (CWI) for $\alpha = 4e$. Top left panel: Coleman-Weinberg Inflation potential as a function of ϕ/Q . Top right panel: logarithm of the potential for the same value of α . Bottom left panel: normalized first slow-roll parameter $Q^2/M_{\text{Pl}}^2 \epsilon_1$. The shaded area indicates the where inflation stops if $Q = M_{\text{Pl}}$. Bottom right panel: normalized second and third slow-roll parameters $Q^2/M_{\text{Pl}}^2 \epsilon_2$ (solid line) and $Q^2/M_{\text{Pl}}^2 \epsilon_3$ (dotted line) for the same potential.

where W_{-1} is the -1 branch of the Lambert function. A comparison between this approximated formula and the numerical solution for x_{end} is displayed in Fig. 22. The agreement is excellent.

Let us now calculate the slow-roll trajectory from Eq. (2.11). It is given by

$$\begin{aligned}
N_{\text{end}} - N &= \frac{Q^2}{M_{\text{Pl}}^2} \frac{\sqrt{e}}{4\alpha} \left\{ \text{Ei} \left[-\frac{1}{2} - 2 \ln(x) \right] - \text{Ei} \left[-\frac{1}{2} - 2 \ln(x_{\text{end}}) \right] \right\} \\
&+ \frac{Q^2}{M_{\text{Pl}}^2} \frac{1}{16\sqrt{e}} \left\{ \text{Ei} \left[\frac{1}{2} + 2 \ln(x_{\text{end}}) \right] - \text{Ei} \left[\frac{1}{2} + 2 \ln(x) \right] \right\} \\
&+ \frac{1}{8} \frac{Q^2}{M_{\text{Pl}}^2} (x^2 - x_{\text{end}}^2),
\end{aligned} \tag{4.151}$$

where Ei is the exponential integral function, N_{end} is the number of e-folds at the end of inflation and N is the number of e-folds at some point when the scaled field vev is x . In the $Q/M_{\text{Pl}} \ll 1$ limit where $x \ll 1$, the first term of this expression dominates. Since $\alpha = 4e$, the

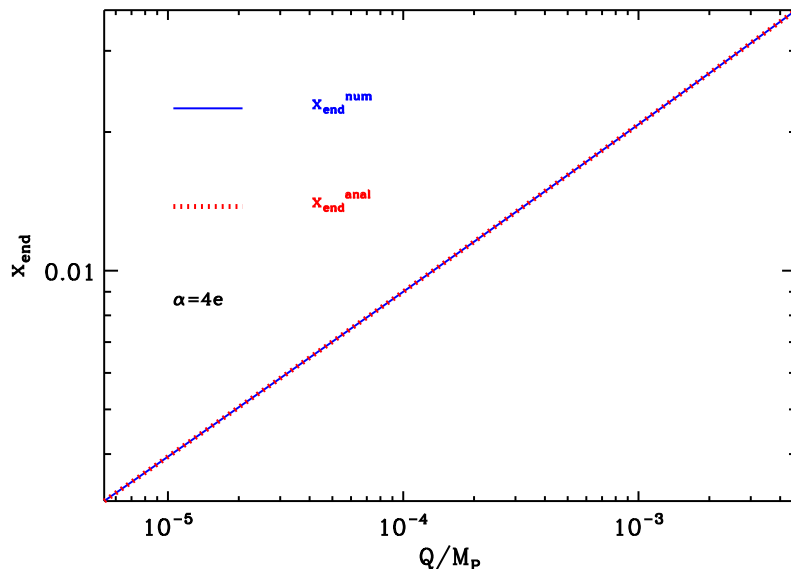


Figure 22. End of inflation in Coleman-Weinberg inflation. The approximated formula of Eq. (4.150) for x_{end} (red dashed line) is compared with the exact numerical solution of $\epsilon_1 = 1$ (blue solid line), for $\alpha = 4e$, in the physically relevant range of values for Q/M_{Pl} . The agreement is obviously excellent.

previous expression can be slightly simplified:

$$N_{\text{end}} - N = \frac{Q^2}{M_{\text{Pl}}^2} \frac{1}{16\sqrt{e}} \left\{ \text{Ei} \left[-\frac{1}{2} - 2 \ln(x) \right] - \text{Ei} \left[-\frac{1}{2} - 2 \ln(x_{\text{end}}) \right] \right. \\ \left. + \text{Ei} \left[\frac{1}{2} + 2 \ln(x_{\text{end}}) \right] - \text{Ei} \left[\frac{1}{2} + 2 \ln(x) \right] \right\} + \frac{1}{8} \frac{Q^2}{M_{\text{Pl}}^2} (x_{\text{end}}^2 - x^2). \quad (4.152)$$

After having solved the previous equation for x_* , the field value at which the pivot scale crossed the Hubble radius during inflation, M is fixed by the amplitude of the CMB anisotropies to

$$\left(\frac{M}{M_{\text{Pl}}} \right)^4 = 720\pi^2 \alpha^2 \frac{M_{\text{Pl}}^2}{Q^2} x_*^6 [1 + 4 \ln(x_*)]^2 [1 + \alpha x_*^4 \ln(x_*)]^{-3} \frac{Q_{\text{rms-PS}}^2}{T^2}. \quad (4.153)$$

The reheating consistent slow-roll predictions of the Coleman-Weinberg models are displayed Fig. 86 in the physical range $Q/M_{\text{Pl}} \in [10^{-5}, 10^{-3}]$. The reheating equation of state parameter \bar{w}_{reh} has been taken to 0 since the potential is quadratic close to its minimum $V(x) \simeq 2\alpha M^4 e^{-1/2} (x - e^{-1/4})^2$. The typical predicted amount of gravitational waves is extremely small, and a non negligible deviation from $n_s = 1$ is noticed. Also, one could choose to relax the constraint on the parameter Q and study the Coleman-Weinberg potential in general. This was done for instance in Ref. [283] where the Coleman-Weinberg potential predictions are compared with the WMAP observations on general grounds. It is found that the potential normalization should be of the order $M \simeq 10^{16}$ GeV, and that $Q \simeq 10 M_{\text{Pl}}$ in order to match $n_s \sim 0.96$. For this reason the reheating consistent slow-roll predictions are displayed in Fig. 87 in the extended range $Q/M_{\text{Pl}} \in [1, 100]$. In the limit $Q/M_{\text{Pl}} \gg 1$, the model

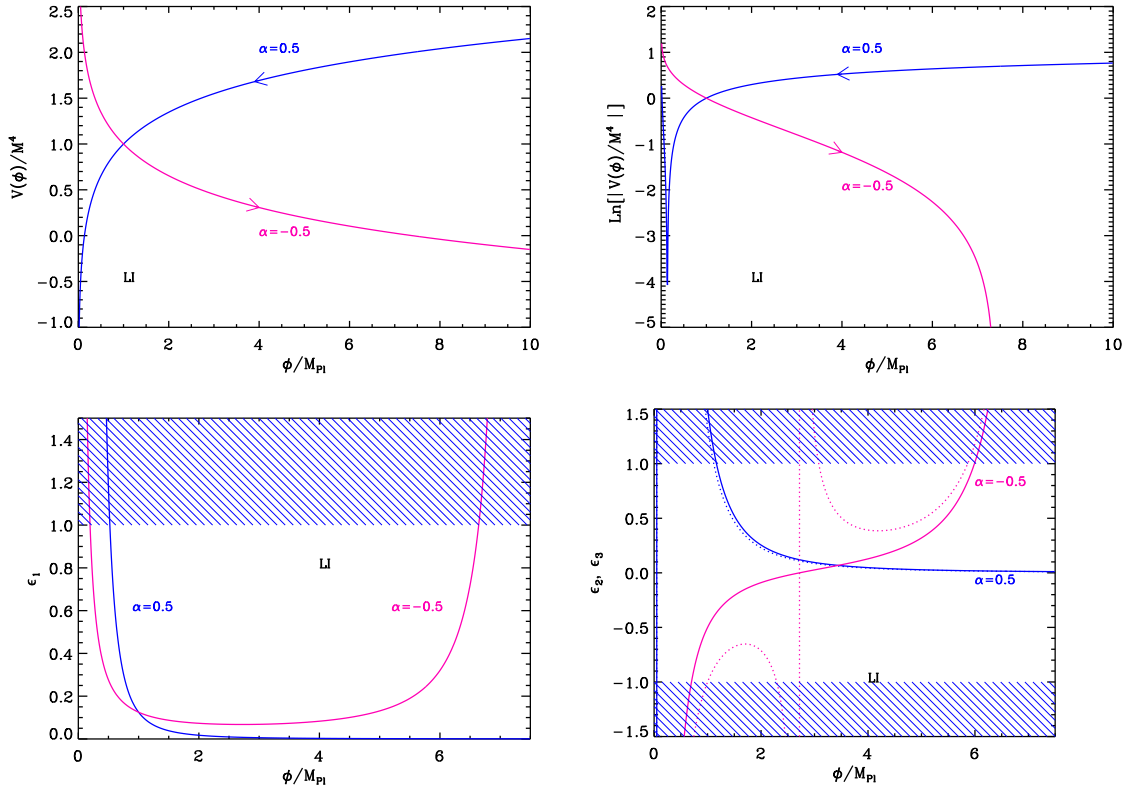


Figure 23. Loop Inflation (LI). Top left panel: Loop Inflation potential for $\alpha = \pm 0.5$, the case $\alpha = 0.5$ being displayed in blue and the case $\alpha = -0.5$ being displayed in pink. Top right panel: logarithm of the potential for the same values of α . Bottom left panel: slow-roll parameter ϵ_1 with the same values of α . The shaded area indicates where inflation stops. Bottom right panel: slow-roll parameters ϵ_2 (solid line) and ϵ_3 (dotted line) for the same values of α .

is well approximated by a quadratic potential around its minimum, and one asymptotically approaches the LFI predictions with $p = 2$ (see section 4.2).

4.12 Loop Inflation (LI)

The flatness of an inflationary potential is in general altered by radiative corrections. One loop order corrections generically take the form of a logarithmic function, $\log(\phi/\mu)$, where μ is the renormalization scale. Starting from a perfectly flat potential, one obtains a potential of the form

$$V(\phi) = M^4 \left[1 + \alpha \ln \left(\frac{\phi}{M_{\text{Pl}}} \right) \right], \quad (4.154)$$

where α is a dimensionless parameter, that can a priori be either positive or negative, and that tunes the strength of the radiative effects. Studying such potentials is therefore a simple way to discuss in which cases the quantum correction “spoil” the flatness of a potential, and how this happens.

Since this potential is very general, it has been derived and studied in various contexts. In Ref. [284], it is obtained in a supersymmetric model, where the coupling constant α is

explicitly negative and can depend on temperature. In Ref. [285] it is investigated in the context of supersymmetric cosmic string theories, in Ref. [286] in the context of spontaneous susy breaking in hybrid inflation, in Refs. [287–290] in the context of brane inflation, in Refs. [291–305] in the context of D-term inflation, in Ref. [306] in the context of F-term inflation, in Refs. [184, 307] in the context of fluxbrane inflation, in Refs. [212, 308] in the context of pseudonatural inflation, and in Ref. [309] in the context of Wess- Zumino models.

Let us define $x \equiv \phi/M_{\text{Pl}}$. The potential Eq. (4.154), as well as its logarithm, is displayed in Fig. 23. If $\alpha > 0$, it is an increasing function of the field vev , and vanishes at

$$x_{V=0} = e^{-1/\alpha}. \quad (4.155)$$

Hence inflation proceeds from the right to the left at $x > x_{V=0}$ in that case. If $\alpha < 0$ however, the potential is a decreasing function of the field, which vanishes at $x_{V=0}$, still given by Eq. (4.155), hence inflation proceeds from the left to the right at $x < x_{V=0}$ in that case.

The three first Hubble flow functions in the slow-roll approximation are given by

$$\epsilon_1 = \frac{\alpha^2}{2} \frac{1}{x^2} [1 + \alpha \ln(x)]^{-2}, \quad \epsilon_2 = 2\alpha \frac{1}{x^2} \frac{1 + \alpha + \alpha \ln(x)}{[1 + \alpha \ln(x)]^2}, \quad (4.156)$$

and

$$\begin{aligned} \epsilon_3 = & 2\alpha \frac{1}{x^2} [1 + \alpha \ln(x)]^{-2} \left[1 + \alpha + \alpha \ln(x) \right]^{-1} \times \\ & \left[1 + \frac{3\alpha}{2} + \alpha^2 + \left(2\alpha + \frac{3}{2}\alpha^2 \right) \ln(x) + \alpha^2 \ln^2(x) \right]. \end{aligned} \quad (4.157)$$

If $\alpha > 0$, the first slow-roll parameter is a decreasing function of the field vev , which diverges at $x_{V=0}$ and vanishes when $x \rightarrow \infty$. Therefore inflation stops by slow-roll violation in that case, at the point x_{end} satisfying $\epsilon_1 = 1$ and given by

$$x_{\text{end}} = \frac{1}{\sqrt{2}} \left[W_0 \left(\frac{e^{1/\alpha}}{\sqrt{2}} \right) \right]^{-1}, \quad (4.158)$$

where W_0 is the 0-branch of the Lambert function. One can check that since $W_0(y) < y$ for any y , one always has $x_{\text{end}} > x_{V=0}$, as required. When $\alpha \ll 1$, one has $x_{\text{end}} \simeq \alpha/\sqrt{2}$. If $\alpha < 0$ on the other hand, the first slow-roll parameter diverges at $x = 0$, decreases with x , reaches a minimum at $x_{\epsilon_2=0} = \exp(-1 - 1/\alpha)$, then increases with x and diverges at $x_{V=0}$. The minimum value of ϵ_1 equals $\epsilon_1(x_{\epsilon_2=0}) = \exp(2 + 2/\alpha)/2$ and it smaller than unity only if $\alpha > 2/(\log 2 - 2) \simeq -1.53$. Otherwise $\epsilon_1(x) > 1$ all over the domain and inflation cannot take place. If $\alpha > 2/(\log 2 - 2)$, the inflationary domain lies between $x_{\epsilon_1=1}^-$ and $x_{\text{end}} = x_{\epsilon_1=1}^+$, with

$$x_{\epsilon_1=1}^- = -\frac{1}{\sqrt{2}} \left[W_{-1} \left(\frac{-e^{1/\alpha}}{\sqrt{2}} \right) \right]^{-1} \quad \text{and} \quad x_{\text{end}} = x_{\epsilon_1=1}^+ = -\frac{1}{\sqrt{2}} \left[W_0 \left(\frac{-e^{1/\alpha}}{\sqrt{2}} \right) \right]^{-1}, \quad (4.159)$$

and where W_{-1} is the -1 -branch of the Lambert function. When $|\alpha| \ll 1$, one has $x_{\text{end}} \simeq e^{-1/\alpha} - 1/\sqrt{2} \gg 1$. Let us notice that the end of inflation occurs in the region $\phi \gg M_{\text{Pl}}$, where

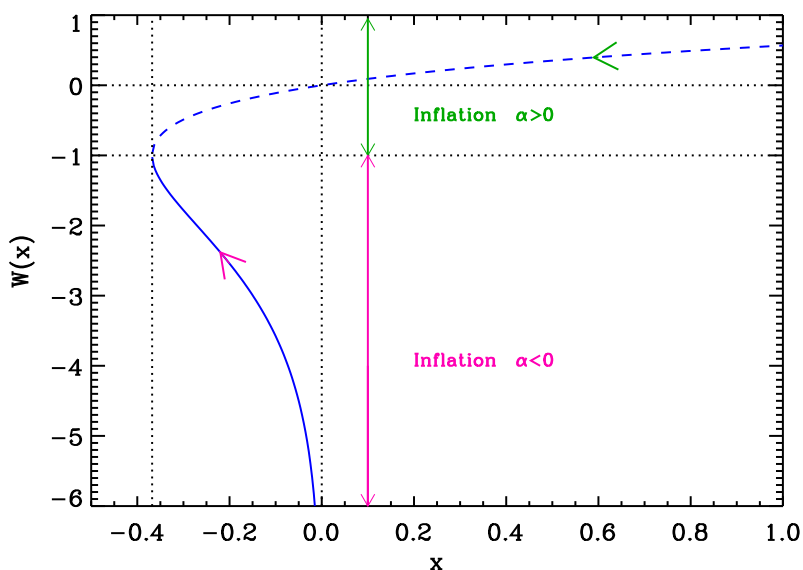


Figure 24. Lambert functions $W_0(x)$ (dashed line) and $W_{-1}(x)$ (solid line). During loop inflation, inflation proceeds along the “0” branch in the direction specified by the green arrow on the figure if $\alpha > 0$, and along the “-1” branch in the direction specified by the pink arrow on the figure if $\alpha < 0$.

Eq. (4.154) may not be well defined. Therefore, depending on the underlying theoretical setting, the end of inflation by slow-roll violation may not be meaningful.

Let us now turn to the slow-roll trajectory. It can be integrated, giving rise to

$$N_{\text{end}} - N = \frac{x^2}{2} \left[\ln(x) + \frac{1}{\alpha} - \frac{1}{2} \right] - \frac{x_{\text{end}}^2}{2} \left[\ln(x_{\text{end}}) + \frac{1}{\alpha} - \frac{1}{2} \right]. \quad (4.160)$$

When $|\alpha| \ll 1$, it approximately takes the form $2\alpha(N_{\text{end}} - N) = x^2 - x_{\text{end}}^2$. The trajectory Eq. (4.160) can be inverted making use of the Lambert function, and one obtains

$$x^2 = \frac{4(N_{\text{end}} - N) - x_{\text{end}}^2 \left[1 - \frac{2}{\alpha} - \ln(x_{\text{end}}^2) \right]}{W_{-1} \left\{ 4(N_{\text{end}} - N) e^{-(1-2/\alpha)} - \left[1 - \frac{2}{\alpha} - \ln(x_{\text{end}}^2) \right] \exp \left[-1 + \frac{2}{\alpha} + \ln(x_{\text{end}}^2) \right] \right\}}, \quad (4.161)$$

where the 0 branch of the Lambert function must be chosen if $\alpha > 0$, while the -1 branch must be chosen if $\alpha < 0$. The Lambert function is displayed in Fig. 24, together with the regions where inflation proceeds.

Let us now comment and check that this expression is valid. Firstly, if $N = N_{\text{end}}$, the Lambert function is of the form $W(-z_{\text{end}} e^{-z_{\text{end}}}) = -z_{\text{end}}$, where $z \equiv (1 - 2/\alpha) - \ln(x^2)$, and this automatically cancels the numerator such that one has indeed $x = x_{\text{end}}$. Secondly, if $\alpha > 0$, the condition $x_{\text{end}} > x_{V=0}$ implies that $z_{\text{end}} < 1$, and the Lambert function at N_{end} is equal to $-z_{\text{end}} > -1$. Therefore, at the end of inflation, one should use the zero branch of the Lambert function.

Finally, as inflation is under way, the argument of the Lambert function is decreasing which implies that the whole inflationary stage takes place on the zero branch. On the other hand, if $\alpha < 0$ using similar arguments, the whole inflationary stage can be shown to take place on the -1 branch.

Then, making use of the approximated trajectories and expressions for x_{end} the predictions for the models can be derived in the case $\alpha > 0$. The observable field value x_* , and its associated number of e-folds $\Delta N_* = N_{\text{end}} - N_*$ at which the pivot mode crossed the Hubble radius during inflation are obtained from the above equations together with Eq. (2.46). In the limit $\alpha \ll 1$, one obtains the approximate expressions

$$\epsilon_{1*} \simeq \frac{\alpha}{4\Delta N_*}, \quad \epsilon_{2*} \simeq \epsilon_{3*} \simeq \frac{1}{\Delta N_*}, \quad (4.162)$$

hence

$$r \simeq \frac{\alpha}{64\Delta N_*}, \quad n_s - 1 \simeq -\frac{1}{\Delta N_*}, \quad \text{and} \quad \alpha_s \simeq \frac{1}{\Delta N_*^2}. \quad (4.163)$$

Finally, the parameter M can be determined from the amplitude of the CMB anisotropies, and one gets

$$\left(\frac{M}{M_{\text{Pl}}}\right)^4 = 720\pi^2 \frac{\alpha^2 Q_{\text{rms-PS}}^2}{x_*^2 T^2} [1 + \alpha \ln(x_*)]^{-3}. \quad (4.164)$$

In the small $|\alpha|$ limit, for $\alpha > 0$, one obtains $M^4/M_{\text{Pl}}^4 \simeq 360\pi^2\alpha/\Delta N_* Q_{\text{rms-PS}}^2/T^2$, and for $\alpha < 0$, $M^4/M_{\text{Pl}}^4 \simeq 720\pi^2\alpha^2 e^{2/\alpha} Q_{\text{rms-PS}}^2/T^2$.

The reheating consistent slow-roll predictions of the loop inflation models are displayed in Fig. 88 for $\alpha > 0$, and in Fig. 89 for $\alpha < 0$. For $\alpha > 0$ and $\alpha \ll 1$, the approximations Eqs. (4.162) give a good description of what is obtained, namely a deviation from scale invariance which almost does not depend on α , and an amount of gravitational waves which grows linearly with α . For $\alpha < 0$, the typical predicted amount of gravitational waves is very small, and the predictions almost do not depend on the energy scale at which reheating ends (hence on ΔN_*). Interestingly enough, the parameter α does not seem to be much constrained when it is positive, whereas close-to-zero values seem to be favored when it is negative.

4.13 $(R + R^p)$ Inflation (RpI)

This model is the Einstein frame description of a scalar-tensor theory equivalent to $f(R) = R + \epsilon R^{2p}/\mu^{4p-2}$, where μ is some mass scale, and $\epsilon = \pm 1$. It generalizes the original Starobinski model [310] obtained for $p = 1$. Such theories are quite generic and appear as limiting cases of more general modified gravity theories [311–315] (see Ref. [316] for a review).

Following Ref. [313, 316], one can introduce the scalar degree of freedom

$$\frac{\phi}{M_{\text{Pl}}} = \sqrt{\frac{3}{2}} \ln(|F(R)|), \quad (4.165)$$

where $F(R) \equiv \partial f/\partial R$. The quantity $F = \Omega^2$, is also the conformal factor squared inducing the transformation from the Jordan frame to the Einstein frame. In the Einstein frame, the field ϕ evolves in a potential given by

$$V(\phi) = \frac{M_{\text{Pl}}^2}{2} \frac{|F|}{F} \frac{RF - f}{F^2}. \quad (4.166)$$

In our case, one has

$$F(R) = 1 + 2\epsilon p \left(\frac{R}{\mu^2} \right)^{2p-1}, \quad (4.167)$$

which, for small departures with respect to the Einstein-Hilbert action $R \ll \mu^2$, implies that $F(R) > 0$ as needed. Let us notice that in the opposite situation, accelerated (and super-accelerated) solutions have been shown to exist [316]. Defining

$$y \equiv \sqrt{\frac{2}{3}} \frac{\phi}{M_{\text{Pl}}}, \quad (4.168)$$

and plugging Eq. (4.167) into Eq. (4.166) one finally gets the Einstein frame potential

$$V = M^4 e^{-2y} |e^y - 1|^{2p/(2p-1)}. \quad (4.169)$$

The normalization constant M^4 is related to the modified gravity scale μ through

$$M^4 = \frac{2p-1}{4p} \frac{M_{\text{Pl}}^2 \mu^2}{(2p)^{1/(2p-1)}}. \quad (4.170)$$

For $F(R) > 0$, Eq. (4.165) implies that for $\epsilon = 1$, the model is defined in the domain $y > 0$, whereas for $\epsilon = -1$ one should consider only the domain $y < 0$. Such a potential has also been studied in Ref. [317] for $p = 1$, in Ref. [313, 318] for $p = 4$ and in Ref. [319] for $p = 2$. Let us notice that the case $p = 1$ is also the Higgs inflation potential studied in section 3.1. Taking the limit $p \rightarrow \infty$, the potential asymptotes $V \rightarrow M^4 e^{-2y} |e^y - 1|$ such that varying p allows to explore intermediate potential shapes.

Considering first the case $y > 0$ ($\epsilon = 1$), the potential admits a maximum at

$$y_{\text{max}} = \ln \left(\frac{2p-1}{p-1} \right), \quad (4.171)$$

such that inflation can proceed either for $0 < y < y_{\text{max}}$ or $y > y_{\text{max}}$. The Hubble flow functions in the slow-roll approximation read

$$\epsilon_1 = \frac{4}{3} \frac{[1 + (p-1)e^y - 2p]^2}{(2p-1)^2 (e^y - 1)^2}, \quad \epsilon_2 = \frac{8}{3} \frac{p e^y}{(2p-1)(e^y - 1)^2}, \quad (4.172)$$

and

$$\epsilon_3 = -\frac{4}{3} \frac{(e^y + 1)[1 + (p-1)e^y - 2p]}{(2p-1)(e^y - 1)^2}. \quad (4.173)$$

The potential and the Hubble flow functions for $y > 0$ have been represented in Fig. 25. As one can check on these figures, inflation never stops along the branch $y > y_{\text{max}}$ and one needs to complement the model by an ending mechanism, as for instance with an extra-field and a tachyonic instability. Although this adds one additional parameter to the model, it is not expected to affect the observable predictions. Indeed, in the large field limit, all the three Hubble flow functions admit asymptotically constant values:

$$\lim_{y \rightarrow \infty} \epsilon_1 = \frac{4}{3} \left(\frac{p-1}{2p-1} \right)^2, \quad \lim_{y \rightarrow \infty} \epsilon_2 = 0, \quad \lim_{y \rightarrow \infty} \epsilon_3 = -\frac{4}{3} \frac{p-1}{2p-1}. \quad (4.174)$$

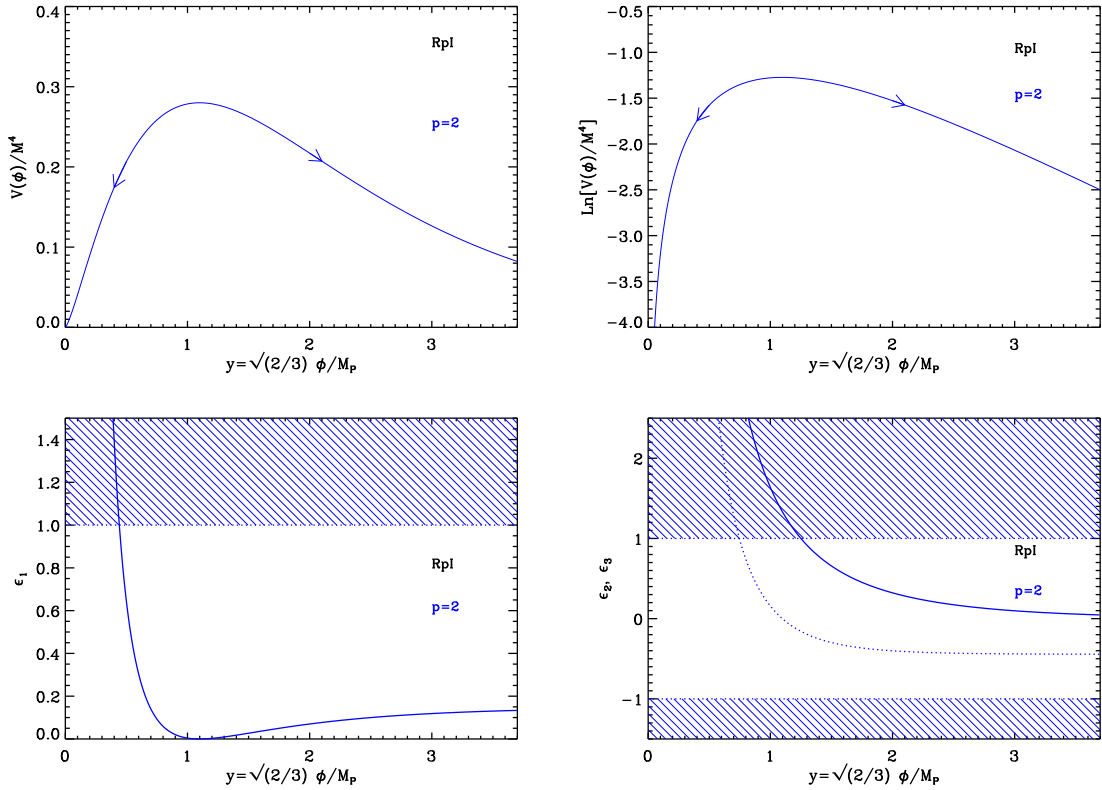


Figure 25. $(R + R^p)$ Inflation (RpI) in the Einstein frame for $p = 2$. Top panels: the potential and its logarithm. The potential admits a maximum at $y = y_{\max}$ such that inflation can take place either for $y > y_{\max}$ or $0 < y < y_{\max}$. Bottom left panel: slow-roll parameter ϵ_1 with the region in which inflation stops (shaded area). For $y > y_{\max}$, inflation never stops and one has to consider an extra-mechanism to end inflation. Bottom right panel: slow-roll parameters ϵ_2 (solid line) and ϵ_3 (dotted line). Other values of p would give similar curves.

Except for the special case $p = 1$ (see section 3.1), these values are always smaller than unity, but not particularly small. As such, all these models predict large deviation from scale invariance. As a consequence, the spectral index at first order is given by

$$n_s - 1 = -\frac{8}{3} \left(\frac{p-1}{2p-1} \right)^2, \quad (4.175)$$

which, for $p \geq 2$, remains always smaller than $-8/27 \simeq -0.3$. This is strongly disfavored by current CMB measurements.

Along the other branch, namely $0 < y < y_{\max}$, inflation stops naturally when $\epsilon_1 = 1$, i.e. at the field value

$$y_{\text{end}} = \ln \left[(2p-1) \frac{1 + 2p(\sqrt{3} + 1)}{8p^2 - 4p - 1} \right]. \quad (4.176)$$

However, the second Hubble flow function can only take relatively large value. From Eq. (4.172), since $y < y_{\max}$, one gets

$$\epsilon_2 > \epsilon_2(y_{\max}) = \frac{8}{3} \frac{p-1}{p}. \quad (4.177)$$

For $p \geq 2$, we are in the situation where $\epsilon_2 > 4/3$ and the slow-roll approximation is violated. As a result, one should not trust the slow-roll results and in particular the field value y_{end} . On the other hand, this also suggests that the spectral index is again far from scale invariance and therefore the model is certainly not compatible with CMB data. We have directly checked that this is indeed the case by means of an exact numerical integration.

For completeness, we give the slow-roll trajectory for the branch $y > y_{\text{max}}$ (in which slow-roll is still applicable)

$$N - N_{\text{end}} = \frac{3}{4} \left\{ \frac{p}{p-1} \ln \left[\frac{(p-1)e^y + 1 - 2p}{(p-1)e^{y_{\text{end}}} + 1 - 2p} \right] + y - y_{\text{end}} \right\}. \quad (4.178)$$

This expression is not properly defined for $p = 1$ but, as before, this case is dealt within the Higgs inflation model. If $y = y_{\text{max}}$, the argument of the logarithm vanishes and the total number of e-folds diverges. As a result, provided inflation starts close enough to the top of the potential, it is always possible to find a long enough inflationary period. The slow-roll trajectory cannot be analytically inverted, but using the same reheating model as in section 3.1, one can solve for the field value y_* at which the pivot mode crossed the Hubble radius. The associated number of e-fold $\Delta N_* = N_{\text{end}} - N_*$ being given by Eq. (4.178).

Concerning the case $\epsilon = -1$, i.e. the domain $y < 0$, all of the previous formula still apply but the potential is now a monotonic decreasing function of the field vev which is too steep to support inflation. In particular, over the whole negative domain, Eq. (4.172) implies that $\epsilon_1(y < 0) > \epsilon_1(y \rightarrow -\infty) = 4/3$.

Finally, the constant M can be determined from the amplitude of the CMB anisotropies. Using the COBE normalization, one has

$$\frac{M^4}{M_{\text{Pl}}^4} = 1920\pi^2 \frac{[1 + (p-1)e^{y_*} - 2p]^2 e^{2y_*} Q_{\text{rms-PS}}^2}{(2p-1)^2 (e^{y_*} - 1)^{\frac{6p-2}{2p-1}}} \frac{1}{T^2}. \quad (4.179)$$

As those models are far from being in the two-sigma confidence region for the spectral index, we do not have represented their reheating-consistent predictions in the appendix.

4.14 Double-Well Inflation (DWI)

In this section, we study the famous ‘‘Mexican hat’’ potential given by

$$V(\phi) = M^4 \left[\left(\frac{\phi}{\phi_0} \right)^2 - 1 \right]^2. \quad (4.180)$$

Except for the mass M determined by the CMB normalization, it depends on one parameter, the vev ϕ_0 . Historically, this potential was first introduced by Goldstone in Ref. [320] as a toy model for dynamical symmetry breaking. In cosmology, it is of course utilized to investigate the formation and the microscopic structure of topological defects. In the context of inflation, it was first used to construct scenarios of topological inflation, see Refs. [321, 322]. In this case, it is made use of the fact that the discrete \mathbb{Z}_2 symmetry, $\phi \rightarrow -\phi$, makes the state $\phi = 0$ unstable. Therefore, the Universe will split into two different regions separated by a domain wall. One can then show that inflation takes place within this topological defect. The potential (4.180) was also used in Refs. [323, 324] in the context of open inflation. In a rather different theoretical framework, Eq. (4.180) was studied in Refs. [325, 326] where it was derived in $N = 1$ supergravity coupled to matter. It is also interesting to notice that

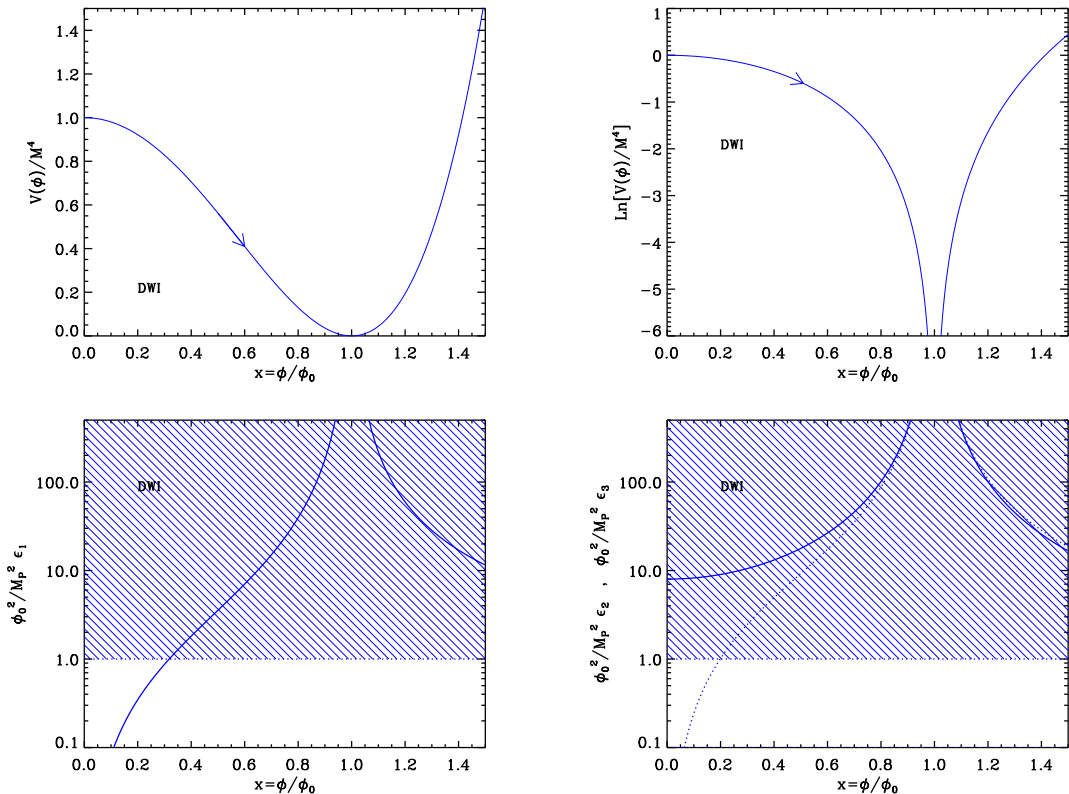


Figure 26. Top left panel: Double Well Inflation (DWI) potential as a function of ϕ/ϕ_0 . Only the $\phi > 0$ region is displayed since the potential is symmetric under $\phi \rightarrow -\phi$. Top right panel: logarithm of the potential. The arrow indicates in which direction inflation can proceed. Bottom left panel: slow-roll parameter ϵ_1 , rescaled by the quantity M_{Pl}^2/ϕ_0^2 , such that the corresponding expression becomes universal, i.e. independent of ϕ_0 . Bottom right panel: slow-roll parameters ϵ_2 (solid line) and ϵ_3 (dotted line), rescaled by M_{Pl}^2/ϕ_0^2 for the same reason as mentioned before.

it was obtained using various stringy constructions as early as the 80's, see Refs. [327, 328]. More recently, this potential was found to be relevant in a large number of different physical situations, see Refs. [283, 329–339]. Let us also mention that this model is sometimes viewed as a realistic version of Small Field Inflation (SFI) with $p = 2$ (see section 5.1), the extra quartic term preventing the potential from becoming negative. However, as will be shown in the following, these two classes of models should actually be described separately since their predictions differ in the relevant range of parameters.

The parameter ϕ_0 sets the typical vev at which inflation proceeds and depends on the symmetry breaking scale one considers. In principle, it could vary over a wide range of values, from $\phi_0 \sim 10^{15}$ GeV for GUT symmetry breaking schemes to super-Planckian vev in a stringy or supergravity context. As will be shown in the following, it is in fact constrained to be large (super-Planckian) in order for the predictions of the model to be compatible with the CMB data. The DWI potential is displayed in Fig. 26 together with its logarithm. One has represented the region $\phi > 0$ only because the potential is symmetric under $\phi \rightarrow -\phi$. We see that it decreases for $\phi < \phi_0$, vanishes at ϕ_0 and then increases for $\phi > \phi_0$. As was already mentioned before, this potential is used to describe dynamical symmetry breaking

and, as a consequence, inflation should proceed from the left to the right at $\phi < \phi_0$, in the direction specified by the arrow in Fig. 26.

Let us now calculate the slow-roll parameters. If one defines x by $x \equiv \phi/\phi_0$, then they are given by

$$\epsilon_1 = \left(\frac{M_{\text{Pl}}}{\phi_0}\right)^2 \frac{8x^2}{(x^2-1)^2}, \quad \epsilon_2 = \left(\frac{M_{\text{Pl}}}{\phi_0}\right)^2 \frac{8(1+x^2)}{(x^2-1)^2}, \quad \epsilon_3 = \left(\frac{M_{\text{Pl}}}{\phi_0}\right)^2 \frac{8(x^4+3x^2)}{(x^2-1)^2(x^2+1)}. \quad (4.181)$$

The behavior of these parameters is represented in Fig. 26. The first slow-roll parameter ϵ_1 is an increasing function of ϕ in the range $x \in [0, 1]$. It vanishes at $x = 0$ and blows up at $x = 1$. Then, for $x > 1$, it becomes a decreasing function going to zero when x goes to infinity. Clearly, we see in Fig. 26 that inflation stops by violation of the slow-roll conditions. The slow roll parameters ϵ_2 and ϵ_3 have similar behaviors, except that ϵ_2 does not vanish when $x = 0$ but is equal to $\epsilon_2(x=0) = 8(M_{\text{Pl}}/\phi_0)^2$. Therefore, in order for slow-roll to be valid, this last value should be less than one, which amounts to

$$\frac{\phi_0}{M_{\text{Pl}}} > 2\sqrt{2}. \quad (4.182)$$

This constraint on the parameter ϕ_0 shows that the symmetry breaking scale needs to be super-Planckian. If this last condition is verified, then ϵ_2 becomes greater than one during inflation at $\phi_{\epsilon_2=1}$ defined by

$$\frac{\phi_{\epsilon_2=1}}{\phi_0} = \sqrt{1 + 4 \left(\frac{M_{\text{Pl}}}{\phi_0}\right)^2 \left[1 - \sqrt{1 + \left(\frac{\phi_0}{M_{\text{Pl}}}\right)^2}\right]}. \quad (4.183)$$

This happens before the end of inflation ($\epsilon_1 = 1$) which occurs at the following value of the field

$$\frac{\phi_{\text{end}}}{M_{\text{Pl}}} = \sqrt{2 + \left(\frac{\phi_0}{M_{\text{Pl}}}\right)^2} - \sqrt{2}. \quad (4.184)$$

Let us now turn to the slow-roll trajectory. It can be integrated exactly and yields the following formula

$$N_{\text{end}} - N = \frac{1}{4} \left(\frac{\phi_0}{M_{\text{Pl}}}\right)^2 \left[\ln \left(\frac{x_{\text{end}}}{x}\right) - \frac{1}{2} (x_{\text{end}}^2 - x^2) \right], \quad (4.185)$$

where N_{end} is the number of e -folds at the end of inflation. Using the 0-branch of the Lambert function W_0 , this trajectory can be inverted. One obtains

$$x = \sqrt{-W_0 \left[-x_{\text{end}}^2 e^{-x_{\text{end}}^2} e^{8 \left(\frac{M_{\text{Pl}}}{\phi_0}\right)^2 (N - N_{\text{end}})} \right]}. \quad (4.186)$$

The fact that the 0-branch of the Lambert function should be chosen comes from the requirement that $x < 1$. The corresponding ‘‘trajectory’’ along the Lambert curve is displayed in Fig. 27, the arrow indicating in which direction inflation proceeds. This trajectory is remarkably similar to the one of SFI with $p = 2$, see section 5.1 and Eq. (5.6), the only difference being that the factor 8 in front of $N - N_{\text{end}}$ is just 4 in the case of SFI. Therefore

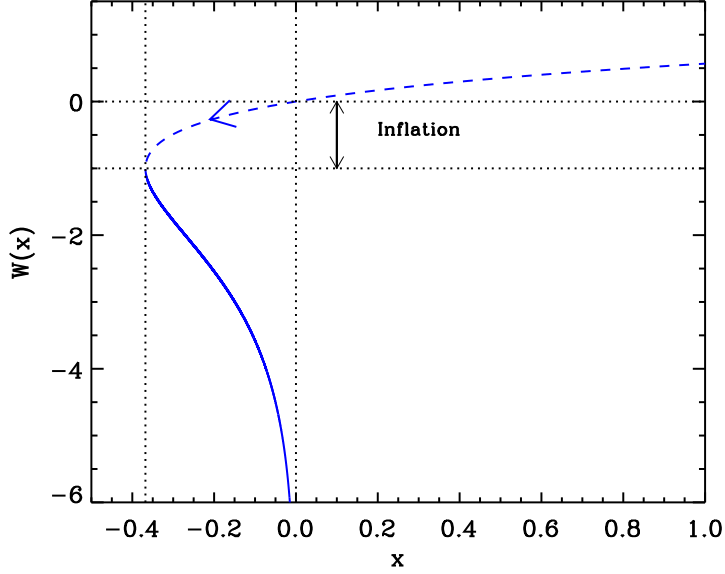


Figure 27. Lambert functions $W_0(x)$ (dashed line) and $W_{-1}(x)$ (solid line). In DWI, inflation proceeds along the negative part of the “0” branch in the direction specified by the arrow.

not only these two potentials coincide at small fields, but they also give rise to the same kind of slow-roll trajectory. This is why these two models are sometimes identified, DWI being considered as a realistic realization of SFI. However, as shown below, the observations favors super-Planckian values of ϕ_0 and, in this limit, the two models are not equivalent (of course, this also has something to do with the debate about whether having super-Planckian vev is meaningful or not). In fact, in the regime $\phi_0/M_{\text{Pl}} \gg 1$, one can write

$$x_* \simeq 1 - \sqrt{2} \frac{M_{\text{Pl}}}{\phi_0} \sqrt{1 + 2\Delta N_*} + \frac{1}{3} \left(\frac{M_{\text{Pl}}}{\phi_0} \right)^2 \left(1 + 2\Delta N_* + \frac{2}{\sqrt{1 + 2\Delta N_*}} \right) + \dots \quad (4.187)$$

From this expression it is clear that, for super-Planckian values of ϕ_0 , ϕ_* is close to the minimum of the potential where the quartic term plays an important role and, consequently, where the SFI potential is not a good approximation. A calculation of the Hubble flow parameters at Hubble crossing confirms this conclusion. They are given by

$$\epsilon_{1*} \simeq \frac{1}{1 + 2\Delta N_*}, \quad \epsilon_{2*} \simeq \frac{2}{1 + 2\Delta N_*}, \quad \epsilon_{3*} \simeq \frac{2}{1 + 2\Delta N_*}. \quad (4.188)$$

This allows us to establish the corresponding expressions of the tensor to scalar ratio, spectral index and running. One obtains

$$r \simeq \frac{16}{1 + 2\Delta N_*}, \quad n_s - 1 \simeq -\frac{4}{1 + 2\Delta N_*}, \quad \alpha_s \simeq -\frac{8}{1 + 2\Delta N_*}. \quad (4.189)$$

These expressions should be compared with Eqs. (5.17). We see that the first Hubble flow parameter for SFI and DWI differ by a factor of $\simeq 4$ and that the ϵ_2 differ by a factor of $\simeq 2$. As a consequence, as can be checked in Fig. 90, the DWI predictions are such that

$\epsilon_{2*} = 2\epsilon_{1*}$ [or equivalently, $r = 4(1 - n_s)$], whereas, as can be checked in Fig. 99, we have $\epsilon_{2*} = 4\epsilon_{1*}$ for SFI [or equivalently, $r = 8/3(1 - n_s)$]. This explains why the two models can in fact lead to quite different predictions and why DWI cannot be simply viewed as a mere realistic continuation of SFI.

Finally, it is also interesting to constrain the energy scale M . For this purpose, we use the CMB normalization which gives

$$\frac{M^4}{M_{\text{Pl}}^4} = 11520\pi^2 \left(\frac{M_{\text{Pl}}}{\phi_0}\right)^2 \frac{x_*^2}{(x_*^2 - 1)^4} \frac{Q_{\text{rms-PS}}^2}{T^2}. \quad (4.190)$$

Then, using the approximated trajectory $x_* \simeq 1 - \sqrt{2 + 4\Delta N_*} M_{\text{Pl}}/\phi_0$ in the above formula, one obtains the following expression

$$\frac{M^4}{M_{\text{Pl}}^4} \simeq 1440\pi^2 \left(\frac{\phi_0}{M_{\text{Pl}}}\right)^2 \frac{1}{(1 + 2\Delta N_*)^2} \frac{Q_{\text{rms-PS}}^2}{T^2}. \quad (4.191)$$

Then, requiring that $M < M_{\text{Pl}}$ leads to the following upper bound on the value of ϕ_0 , $\phi_0/M_{\text{Pl}} \lesssim 1.5 \times 10^5$. Combined with the lower limit (4.182), we see that the possible range of variation of ϕ_0 is quite large.

The reheating consistent slow-roll predictions for the DWI models are displayed in Fig. 90. The reheating equation of state parameter \bar{w}_{reh} has been chosen to be 0 since the potential is quadratic close to its minimum $V(\phi) \simeq 4M^4/\phi_0^2 (\phi - \phi_0)^2$. As claimed before, one can check that only super-Planckian values of the symmetry breaking scale ϕ_0 are compatible with the data. Actually, this is also true for the SFI models, see section 5.1 and Fig. 99. As already mentioned before, in this regime, the two models differ while, as expected, they are very similar for sub-Planckian values of the field *vev*.

4.15 Mutated Hilltop Inflation (MHI)

This model is a variant of the hilltop model [340, 341], referred to as small field inflation in section 5.1. From supergravity motivations, it was first introduced and discussed in Refs. [342, 343]. The potential is given by

$$V = M^4 \left[1 - \text{sech} \left(\frac{\phi}{\mu} \right) \right], \quad (4.192)$$

with $\text{sech}(x) = 1/\cosh(x)$. From its supergravity motivations, reasonable values of the parameter μ are such that $\mu < M_{\text{Pl}}$ but in other contexts such a bound may not be necessary. This is why the model is studied here on general grounds, for any value of μ , but approximated formula are also derived in the $\mu \ll M_{\text{Pl}}$ for discussion.

Defining $x \equiv \phi/\mu$, the three first Hubble flow functions in the slow-roll approximation are given by

$$\epsilon_1 = \frac{M_{\text{Pl}}^2}{2\mu^2} \coth^2 \left(\frac{x}{2} \right) \text{sech}^2(x), \quad \epsilon_2 = \frac{M_{\text{Pl}}^2}{\mu^2} \left[\text{csch}^2 \left(\frac{x}{2} \right) + 2 \text{sech}^2(x) \right], \quad (4.193)$$

$$\epsilon_3 = \frac{M_{\text{Pl}}^2}{\mu^2} \frac{\cosh(x) \coth^2 \left(\frac{x}{2} \right) + 2 \tanh^2(x)}{\cosh(x) + \sinh^2(x)}. \quad (4.194)$$

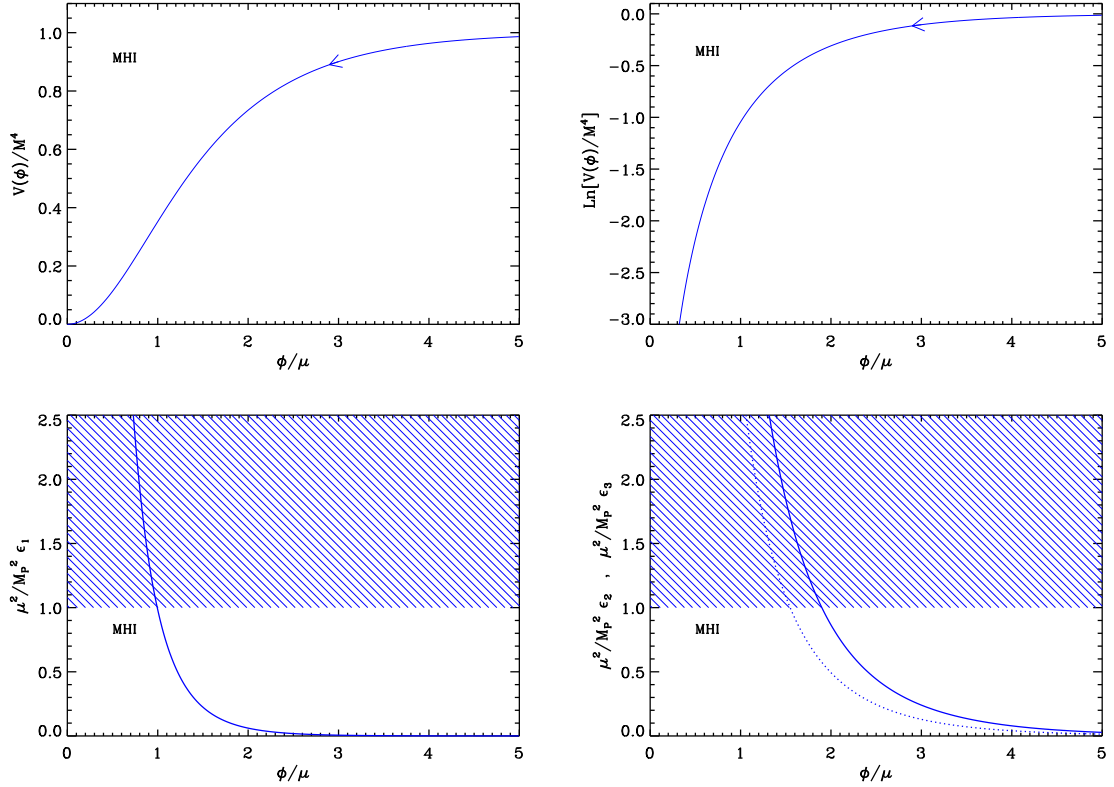


Figure 28. Mutated Hilltop Inflation (MHI). The top panels show the potential and its logarithm as a function of $x = \phi/\mu$. Bottom left panel: Rescaled slow-roll parameter ϵ_1 (divided by M_{Pl}^2/μ^2). The shaded area represents the region in which inflation stops if $\mu = M_{\text{Pl}}$. It should be accordingly rescaled for other values of μ . Bottom right panel: slow-roll parameters ϵ_2 (solid line) and ϵ_3 (dotted line), again rescaled by M_{Pl}^2/μ^2 together with the region of slow-roll violation for $\mu = M_{\text{Pl}}$.

where $\text{csch}(x) = 1/\sinh(x)$. These three quantities are monotonically decreasing functions of the field values and inflation proceeds from large field values towards small field values. Together with the potential, they are represented as a function of x in Fig. 28.

The slow-roll trajectory can be integrated exactly from Eq. (2.11) and reads

$$N - N_{\text{end}} = \frac{\mu^2}{M_{\text{Pl}}^2} \left\{ 2 \ln \left[\frac{\cosh(x/2)}{\cosh(x_{\text{end}}/2)} \right] - \cosh(x) + \cosh(x_{\text{end}}) \right\}. \quad (4.195)$$

It can also be inverted analytically to give the field values in terms of the number of e-folds using the Lambert function W_{-1} . One obtains

$$x = \text{arccosh} \left(-1 - W_{-1} \left\{ -[1 + \cosh(x_{\text{end}})] \exp \left[\frac{M_{\text{Pl}}^2}{\mu^2} (N - N_{\text{end}}) - 1 - \cosh(x_{\text{end}}) \right] \right\} \right). \quad (4.196)$$

Since $N - N_{\text{end}} < 0$ and the function ye^{-y} has a global maximum equals to $1/e$, inflation proceeds along the -1 branch of the Lambert function as represented in Fig. 29. Note that in the $\mu \ll M_{\text{Pl}}$ limit, this trajectory simply becomes $N - N_{\text{end}} \simeq \mu^2/(2M_{\text{Pl}}^2)(e^{x_{\text{end}}} - e^x)$.

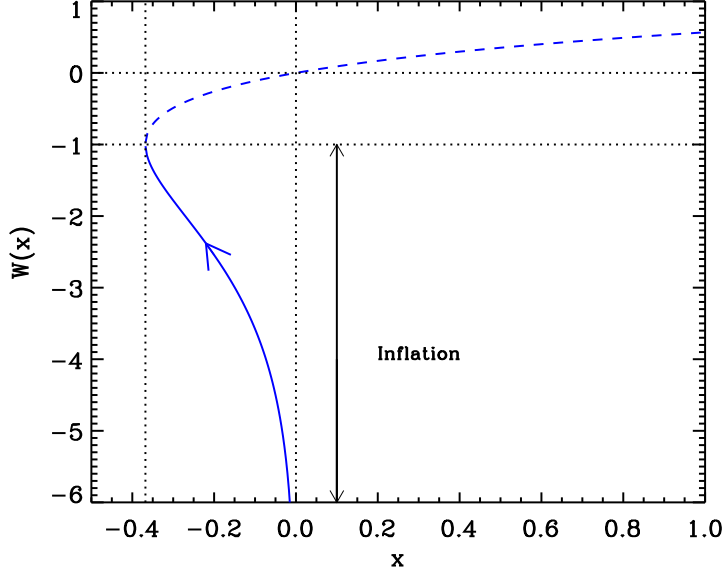


Figure 29. Lambert functions $W_0(x)$ (dashed line) and $W_{-1}(x)$ (solide line). During Mutated Hilltop inflation, inflation proceeds along the “-1” branch in the direction specified by the arrow on the figure.

For MHI, inflation naturally stops when $\epsilon_1 = 1$, which has an unique solution given by

$$x_{\text{end}} = \text{arcsech} \left[-\frac{1}{3} + \frac{1}{3} \left(1 - 6 \frac{\mu^2}{M_{\text{Pl}}^2} \right) \left(-1 + 36 \frac{\mu^2}{M_{\text{Pl}}^2} + 3\sqrt{6} \frac{\mu}{M_{\text{Pl}}} \sqrt{4 \frac{\mu^4}{M_{\text{Pl}}^4} + 22 \frac{\mu^2}{M_{\text{Pl}}^2} - 1} \right)^{-1/3} + \frac{1}{3} \left(-1 + 36 \frac{\mu^2}{M_{\text{Pl}}^2} + 3\sqrt{6} \frac{\mu}{M_{\text{Pl}}} \sqrt{4 \frac{\mu^4}{M_{\text{Pl}}^4} + 22 \frac{\mu^2}{M_{\text{Pl}}^2} - 1} \right)^{1/3} \right], \quad (4.197)$$

and with $\text{arcsech}(x) = \text{arccosh}(1/x)$. One should note that the previous equation is always well defined, regardless of the sign of the square root argument by analytic continuation. Let us notice that from Eq. (4.193) one has

$$\epsilon_2 - \epsilon_1 = \frac{1}{2} \text{csch}^2 \left(\frac{x}{2} \right) + \text{sech}(x) + \frac{5}{2} \text{sech}^2(x) > 0. \quad (4.198)$$

Consequently, the slow-roll approximation may become inaccurate before the end of inflation because $\epsilon_2 > 1$ occurs just before $\epsilon_1 = 1$. However, one can check that this happens during a negligible number of e-folds and the observable predictions for MHI remain mostly unaffected. Also, in the limit $\mu \ll M_{\text{Pl}}$, Eq. (4.197) gives $x_{\text{end}} \simeq \ln(\sqrt{2} M_{\text{Pl}}/\mu)$.

The value $x_* = \phi_*/\mu$ at which the pivot mode crossed the Hubble radius during inflation is obtained by solving Eq. (2.46) for a given reheating energy. In terms of ΔN_* , and in the limit $\mu \ll M_{\text{Pl}}$, one has $x_* \simeq \ln(2\Delta N_* M_{\text{Pl}}^2/\mu^2)$. This enables to give estimates for the slow-roll parameters at Hubble crossing, namely

$$\epsilon_{1*} \simeq \frac{1}{2\Delta N_*^2} \left(\frac{\mu}{M_{\text{Pl}}} \right)^2, \quad \epsilon_{2*} \simeq \frac{6}{\Delta N_*}, \quad \epsilon_{3*} \simeq \frac{1}{\Delta N_*}, \quad (4.199)$$

hence, at first order in slow-roll

$$r \simeq \frac{8}{\Delta N_*^2} \left(\frac{\mu}{M_{\text{Pl}}} \right)^2, \quad n_s - 1 \simeq -\frac{6}{\Delta N_*}, \quad \alpha_s \simeq -\frac{6}{\Delta N_*^2}. \quad (4.200)$$

One can see that for $\mu/M_{\text{Pl}} \ll 1$, the typical predicted amount of gravitational waves is very small, and the deviation from scale invariance almost does not depend on μ .

Finally, the constant M can be determined from the amplitude of the CMB anisotropies

$$\frac{M^4}{M_{\text{Pl}}^4} = 90\pi^2 \frac{M_{\text{Pl}}^2}{\mu^2} \text{csch}^6 \left(\frac{x_*}{2} \right) \sinh(x_*) \tanh(x_*) \frac{Q_{\text{rms-PS}}^2}{T^2}. \quad (4.201)$$

In the $\mu/M_{\text{Pl}} \ll 1$ limit, one obtains

$$\frac{M^4}{M_{\text{Pl}}^4} \simeq \frac{720\pi^2}{\Delta N_*^2} \frac{\mu^2}{M_{\text{Pl}}^2} \frac{Q_{\text{rms-PS}}^2}{T^2}. \quad (4.202)$$

Typically, for $\mu/M_{\text{Pl}} \sim 10^{-2}$, one has $M/M_{\text{Pl}} \sim 10^{-4}$.

The reheating consistent slow-roll predictions for MHI have been represented in Fig. 91. As expected, for small values of μ/M_{Pl} , the predicted amount of gravitational waves is extremely small and the deviation from scale invariance almost does not depend on μ .

4.16 Radion Gauge Inflation (RGI)

This model was studied in Ref. [344]. It is an extension of the gauge inflation scenario in which the radius modulus field around which the Wilson loop is wrapped assists inflation as it shrinks [186]. Assuming that the radion field value is such that the potential energy is minimal, for each value of the inflaton field ϕ , one can derive an effective potential

$$V(\phi) = M^4 \frac{(\phi/M_{\text{Pl}})^2}{\alpha + (\phi/M_{\text{Pl}})^2}, \quad (4.203)$$

where α is a dimensionless positive parameter. In the context of Ref. [344], the model is natural for $\alpha < 1$ but larger than unity values are not forbidden. The same potential has been obtained in Ref. [345] in the context of S-dual superstring models. In that case, α represents a typical *vev* for the inflaton, in Planck units. Defining $x = \phi/M_{\text{Pl}}$, the first three slow-roll parameters read

$$\epsilon_1 = \frac{2\alpha^2}{x^2(\alpha + x^2)^2}, \quad \epsilon_2 = 4\alpha \frac{\alpha + 3x^2}{x^2(\alpha + x^2)^2}, \quad \epsilon_3 = 4\alpha \frac{\alpha^2 + 3\alpha x^2 + 6x^4}{x^2(\alpha + x^2)^2(\alpha + 3x^2)}. \quad (4.204)$$

The potential, its logarithm, and the Hubble flow functions are represented in Fig. 30.

The slow-roll trajectory can be integrated analytically from Eq. (2.11) to obtain

$$N - N_{\text{end}} = \frac{x_{\text{end}}^2}{4} + \frac{x_{\text{end}}^4}{8\alpha} - \frac{x^2}{4} - \frac{x^4}{8\alpha}. \quad (4.205)$$

Moreover, it can be inverted explicitly to give the field values in terms of the number of e-folds as

$$x = \sqrt{-\alpha + \sqrt{-8\alpha(N - N_{\text{end}}) + (\alpha + x_{\text{end}}^2)^2}}. \quad (4.206)$$

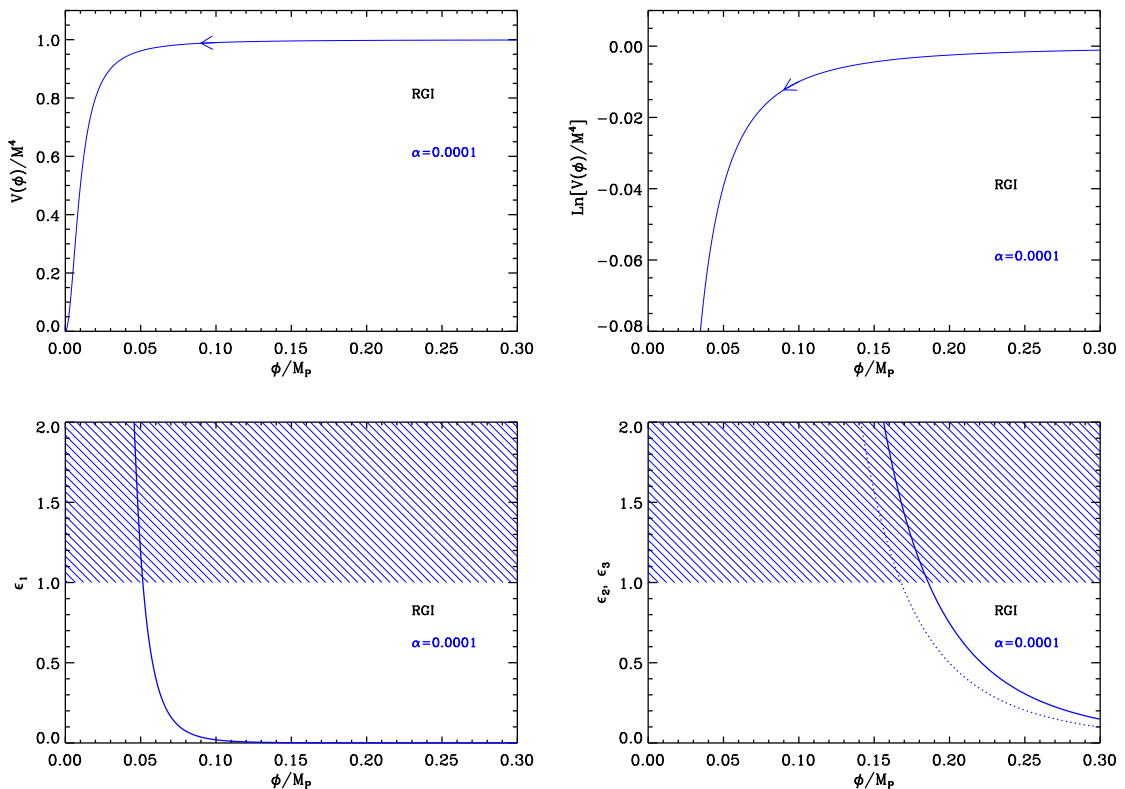


Figure 30. Radion Inflation (RGI) for $\alpha = 10^{-4}$. Top frames: the potential and its logarithm. Bottom left panel: slow-roll parameter ϵ_1 and the shaded area in which inflation stops ($\epsilon_1 > 1$). Bottom right panel: slow-roll parameters ϵ_2 (solid line) and ϵ_3 (dotted line).

The end of inflation naturally occurs for $\epsilon_1 = 1$, i.e., from Eq. (4.204), at the field value x_{end} given by

$$x_{\text{end}} = \frac{-\sqrt[3]{6}\alpha + \left[9\alpha + \sqrt{3\alpha^2(2\alpha + 27)}\right]^{2/3}}{162^{1/6} \left[9\alpha + \sqrt{3\alpha^2(2\alpha + 27)}\right]^{1/3}}. \quad (4.207)$$

As for the MHI models, one should pay attention that

$$\epsilon_2 - \epsilon_1 = 2\alpha \frac{\alpha + 6x^2}{x^2(\alpha + x^2)^2} > 0, \quad (4.208)$$

for any positive values of α . As a result, slow-roll violation, i.e. $\epsilon_2 > 1$, occurs in RGI before inflation ends. However, since the first Hubble flow function is monotonic, this is not very problematic as it happens only during a negligible number of e-folds and only around N_{end} . The slow-roll observable predictions therefore remain accurate.

As before, the observable field value x_* is obtained by solving Eq. (2.46) for a given reheating model and allows the determination of the parameter M from the amplitude of the CMB anisotropies. One gets

$$\frac{M^4}{M_{\text{Pl}}^4} = \frac{2880\pi^2\alpha^2}{x_*^4(\alpha + x_*^2)} \frac{Q_{\text{rms-PS}}^2}{T^2}. \quad (4.209)$$

The reheating consistent slow-roll predictions for these models are displayed in Fig. 92. Large values of α give back the same predictions as the large field models with $p = 2$ (see section 4.2) having $\epsilon_{2*} = 2\epsilon_{1*}$.

4.17 MSSM Inflation (MSSMI)

The Minimal Supersymmetric Standard Model (MSSM) is an extension of the Standard Model with nearly 300 gauge invariant flat directions made up of squarks, sleptons, and Higgses, whose potentials are vanishing in the supersymmetric (SUSY) limit. However, they are lifted by a soft supersymmetry breaking mass term and by superpotential corrections at scales below the Planck scale. Flat directions do exist in the resulting potential, and in Ref. [346], a catalog of the flat directions of the renormalizable and supersymmetry-preserving part of the scalar potential of the MSSM is presented. These directions are made of combinations of squarks, sleptons, and Higgses. Among them, it was found in Ref. [347] that two combinations, namely **LLe** and **udd**, could provide promising candidates for the inflaton. Starting from a superpotential of the form $W = \lambda_n/n\Phi^n M_{\text{Pl}}^{3-n}$, where $\Phi = \phi e^{i\theta}$ is the superfield which contains the flat direction, the following potential was worked out,

$$V(\phi) = \frac{1}{2}m_\phi^2\phi^2 + A \cos(n\theta + \theta_0) \frac{\lambda_n}{n} \frac{\phi^n}{M_{\text{Pl}}^{n-3}} + \lambda_n^2 \frac{\phi^{2(n-1)}}{M_{\text{Pl}}^{2(n-3)}}, \quad (4.210)$$

where the first term corresponds to a soft SUSY breaking mass term, the second term involves the angular part of the superfield via a term $\cos(n\theta + \theta_0)$, which in practice is fixed at -1 to maximize its contribution. The third term is a non renormalizable correction to the superpotential, the amplitude of which is generically such that $\lambda_n \lesssim 1$. As explained below, the second term which appears with a negative coefficient plays a crucial role in making this scenario a credible inflationary one, and it is present only when $n \geq 6$. An interesting feature of this model is that it provides inflation at sub-Planckian vev and low scale, with typical values $m_\phi \sim 1 \text{ TeV}$ and $V \sim (10^9 \text{ GeV})^4$.

Together with the global minimum at $\phi = 0$, under the condition $A^2 \geq 8(n-1)m_\phi^2$, the potential has a secondary minimum at $\phi_0 \simeq (m_\phi M_{\text{Pl}}^{n-3})^{1/(n-2)}$. If $A^2 \gg 8(n-1)m_\phi^2$, this secondary minimum becomes the deepest and thus the true minimum, but that would break charge and/or color symmetry. The curvature of the potential at this minimum is of the scale m_ϕ^2 . If inflation occurs there, one gets $H \simeq m_\phi (m_\phi/M_{\text{Pl}})^{1/(n-2)}$, which is much smaller than the potential curvature for $m_\phi \ll M_{\text{Pl}}$. This implies that the potential is too steep for quantum effects during inflaton to kick ϕ out of the false minimum. Such a situation is similar to the old inflationary scenario. However, this barrier disappears if one saturates the previous inequality and takes $A^2 = 8(n-1)m_\phi^2$. In that case, the potential has a flat inflection point at ϕ_0 and inflation can proceed between this plateau and $\phi = 0$.

As noticed in Ref. [347], higher indexes than $n = 6$ would produce too small amplitude for the scalar perturbations. This is why the model is commonly studied with $n = 6$ (with $n = 3$, this is RIPI, see section 4.18). The typical field vev put forward in Ref. [347] approaches $\phi_0 \simeq 10^{14} \text{ GeV}$.

In order to summarize the constraints the parameters have to verified we rewrite the potential of Eq. (4.210) with the new parameters

$$M^8 = \frac{M_{\text{Pl}}^3 m_\phi^5}{4\sqrt{10}\lambda_6}, \quad \phi_0^8 = \frac{M_{\text{Pl}}^6 m_\phi^2}{10\lambda_6^2}. \quad (4.211)$$

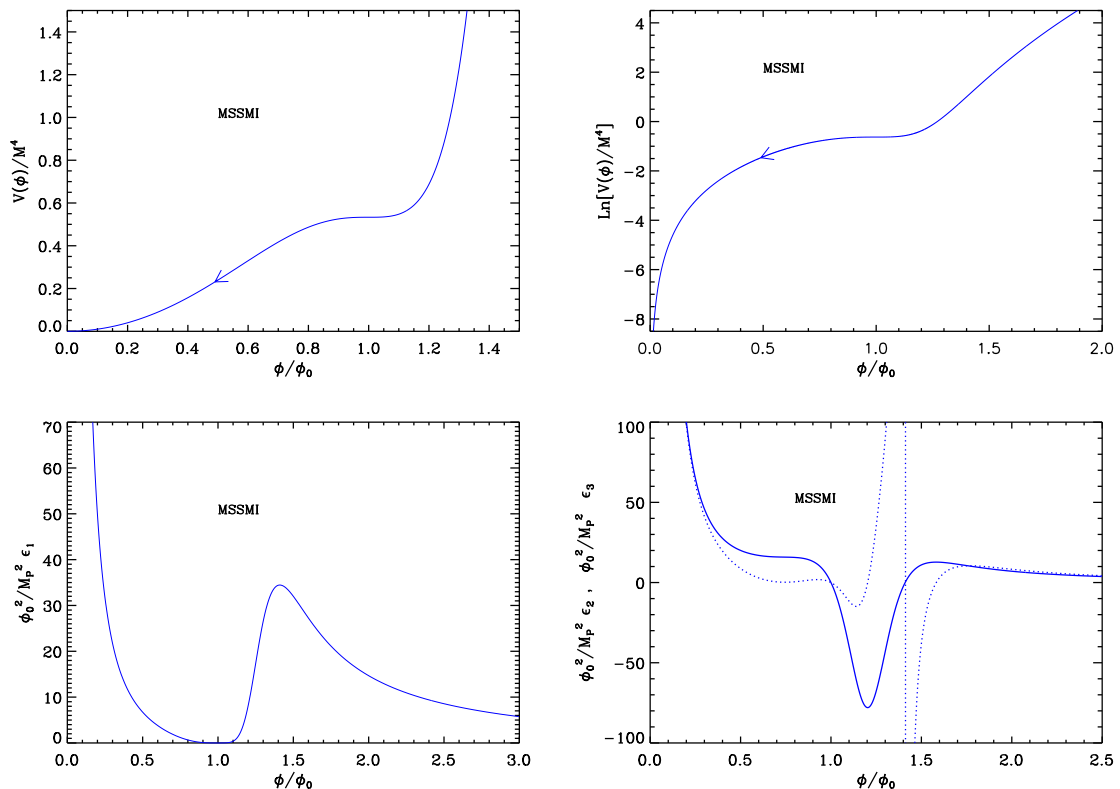


Figure 31. MSSM Inflation (MSSMI). Top left panel: MSSM Inflation potential Eq. (4.212) as a function of ϕ/ϕ_0 . Top right panel: logarithm of the potential. Bottom left panel: slow-roll parameter ϵ_1 scaled by ϕ_0^2/M_{Pl}^2 . Bottom right panel: slow-roll parameters ϵ_2 (solid line) and ϵ_3 (dotted line) scaled by ϕ_0^2/M_{Pl}^2 .

This definition ensures that ϕ_0 is the inflection point and one obtains

$$V(\phi) = M^4 \left[\left(\frac{\phi}{\phi_0} \right)^2 - \frac{2}{3} \left(\frac{\phi}{\phi_0} \right)^6 + \frac{1}{5} \left(\frac{\phi}{\phi_0} \right)^{10} \right]. \quad (4.212)$$

As we will see below, taking $\phi_0 \simeq 10^{14}$ GeV, the amplitude of the CMB anisotropies typically fixes $M \simeq 10^8$ GeV.

This potential have been studied in Refs. [348–358]. Let us notice that when $p = 3$, the same potential appears in Refs. [359, 360] as “Generalized Chaotic Inflation”, and later in Refs. [361–363] as “Punctuated Inflation”. In these references, it is shown that slow-roll inflation is briefly interrupted when the inflaton crosses the flat inflection point and this can produce step-like features in the primordial power spectra. These effects are outside the scope of the following slow-roll analysis as we will be dealing with the last slow-roll inflationary stage within this scenario.

The potential Eq. (4.212) is displayed in Fig. 31, together with its logarithm. It is an increasing function of the field, the derivative of which vanishes at $\phi = 0$ and at its second inflection point $\phi = \phi_0$, the position of the first inflection point being given by

$\phi_{V''=0}^- = \phi_0/\sqrt{3}$. Inflation proceeds between $\phi = 0$ and $\phi = \phi_0$, in the direction specified by the arrow in Fig. 31.

Defining

$$x \equiv \frac{\phi}{\phi_0}, \quad (4.213)$$

the first three Hubble flow functions in the slow-roll approximation are given by

$$\epsilon_1 = 450 \frac{M_{\text{Pl}}^2}{\phi_0^2} \frac{(x^4 - 1)^4}{x^2 (3x^8 - 10x^4 + 15)^2}, \quad \epsilon_2 = 60 \frac{M_{\text{Pl}}^2}{\phi_0^2} \frac{3x^{16} - 58x^8 + 40x^4 + 15}{x^2 (3x^8 - 10x^4 + 15)^2}, \quad (4.214)$$

and

$$\begin{aligned} \epsilon_3 = & \frac{M_{\text{Pl}}^2}{\phi_0^2} \frac{60}{x^2} (-225 + 1575x^4 - 3165x^8 + 395x^{12} + 2605x^{16} - 1275x^{20} + 81x^{24} + 9x^{28}) \\ & \times (3x^8 - 10x^4 + 15)^{-2} \times (-15 - 55x^4 + 3x^8 + 3x^{12})^{-1}. \end{aligned} \quad (4.215)$$

These two slow-roll parameters diverge when the field vev goes to 0, and vanish when the field vev goes to infinity. The first slow roll parameter ϵ_1 first decreases, vanishes at the flat inflection point where ϵ_2 vanishes too, then increases to reach a local maximum where ϵ_2 vanishes again, and eventually decreases again, to vanish at infinity together with ϵ_2 . Denoting by $x_{\epsilon_2=0}^+$ the position of the second extremum, one has

$$x_{\epsilon_2=0}^+ = \left(\frac{1}{3}\right)^{1/4} \left[2^{4/3} (i\sqrt{685} - 1)^{1/3} + 14 \times 2^{2/3} (i\sqrt{685} - 1)^{-1/3} - 1 \right]^{1/4} \simeq 1.41022. \quad (4.216)$$

In between the two local extrema of ϵ_1 , the second slow-roll parameter ϵ_2 is negative whereas it is positive elsewhere. The value of ϵ_1 at its local maximum is given by

$$\epsilon_1^{\text{max}} = \epsilon_1(x_{\epsilon_2=0}^+) \simeq 34.459 \frac{M_{\text{Pl}}^2}{\phi_0^2}. \quad (4.217)$$

With the typical above-mentioned value for $\phi_0 \simeq 10^{14} \text{GeV}$, one has $M_{\text{Pl}}^2/\phi_0^2 \simeq 10^8$ and $\epsilon_1^{\text{max}} > 1$. This means that if inflation proceeds beyond the flat inflection point, it can naturally stop by slow-roll violation. However, if this happens, inflation proceeds at $x \gg 1$ and the potential is effectively very close to a large field model one (LFI, see section 4.2) with $p = 10$.

For this reason, we will be focused to the case in which inflation occurs below the flat inflection point. In this case, the value of x_{end} at which inflation stops by slow-roll violation must be determined numerically. In the limit $\phi_0/M_{\text{Pl}} \ll 1$ however, one has $x_{\text{end}} \simeq 1$ and an approximate analytic formula can be derived

$$x_{\text{end}} \simeq 1 - \frac{1}{2^{3/4}\sqrt{15}} \sqrt{\frac{\phi_0}{M_{\text{Pl}}}}. \quad (4.218)$$

A comparison between this expression and the numerical solution of $\epsilon_1 = 1$ is displayed in Fig. 32. For physical values $\phi_0 \simeq 10^{-4} M_{\text{Pl}}$, the agreement is excellent.

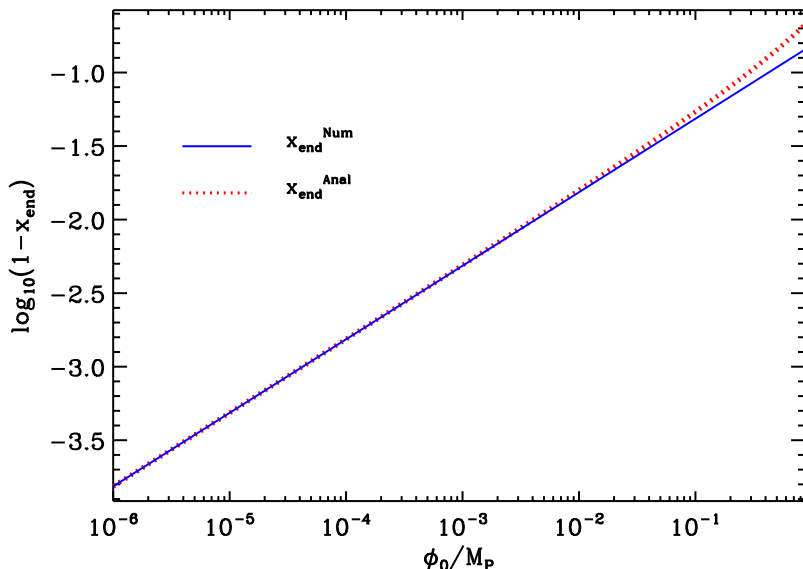


Figure 32. Location of the slow-roll violation induced end of inflation $x_{\text{end}} = \phi_{\text{end}}/\phi$ for the MSSM inflation models, as a function of ϕ_0/M_{Pl} . The blue solid curve represents a numerical solution of $\epsilon_1 = 1$, while the red dotted curve corresponds to the approximated analytic solution Eq. (4.218). For physical values $\phi_0 \sim 10^{-4}M_{\text{Pl}}$, the agreement is obviously excellent.

Let us now turn to the slow-roll trajectory. It can be integrated from Eq. (2.11) and leads to

$$N_{\text{end}} - N = \left(\frac{\phi_0}{M_{\text{Pl}}} \right)^2 \left\{ \frac{x^2 - x_{\text{end}}^2}{20} + \frac{1}{15} \left(\frac{x_{\text{end}}^2}{x_{\text{end}}^4 - 1} - \frac{x^2}{x^4 - 1} \right) - \frac{2}{15} [\text{arctanh}(x_{\text{end}}^2) - \text{arctanh}(x^2)] \right\},$$

where N_{end} is the number of e-folds at the end of inflation and N is the number of e-folds at some point when the scaled field vev is x . A few remarks are in order. Firstly, when $x \simeq 1$, the second term of the previous expression dominates, and one has $N_{\text{end}} - N \simeq 1/15 (\phi_0/M_{\text{Pl}})^2 [1/(x_{\text{end}}^4 - 1) - 1/(x^4 - 1)]$, which can be inverted and gives

$$x \simeq 1 - \frac{1}{4} \left[2^{-5/4} \sqrt{15} \sqrt{\frac{M_{\text{Pl}}}{\phi_0}} + 15 \frac{M_{\text{Pl}}^2}{\phi_0^2} (N_{\text{end}} - N) \right]^{-1}. \quad (4.219)$$

Secondly, one could wonder if a sufficient number of e-folds can be realized in the regime studied here. When $x \rightarrow 1$, the corresponding number of e-folds diverges, but in practice, the inflationary dynamics close to the flat inflection point is governed by the quantum diffusion and the classical equation of motion can not be trusted in this domain.

If one introduces the ratio η between the quantum kicks amplitude $H/(2\pi)$ and the classical drift $M_{\text{Pl}}^2 V_{\phi}/V$, when $x \simeq 1$, one has

$$\eta \simeq \frac{1}{90\sqrt{30}\pi} M^2 \phi_0 M_{\text{Pl}}^{-3} (x - 1)^{-2} \simeq \frac{4\sqrt{10}}{\pi\sqrt{3}} M^2 M_{\text{Pl}} \phi_0^{-3} (N_{\text{end}} - N)^2, \quad (4.220)$$

where the last equality comes from the approximate trajectory. In order to estimate the value of η , one needs the value of M which is fixed by the amplitude of the CMB anisotropies. With x_* the observable field value associated with $\Delta N_* = N_{\text{end}} - N_*$, one gets

$$\left(\frac{M}{M_{\text{Pl}}}\right)^4 = 2880\pi^2 \frac{M_{\text{Pl}}^2}{\phi_0^2} \frac{(1-x_*)^4}{x_*^4 \left(1 - \frac{2}{3}x_*^4 + \frac{1}{5}x_*^8\right)^3} \frac{Q_{\text{rms-PS}}^2}{T^2}. \quad (4.221)$$

In the $x_* \simeq 1$ approximation, this gives

$$\frac{M^4}{M_{\text{Pl}}^4} \simeq \frac{3}{8}\pi^2 \frac{Q_{\text{rms-PS}}^2}{T^2} \frac{\phi_0^6}{M_{\text{Pl}}^6 (N_{\text{end}} - N_*)^4}, \quad (4.222)$$

and thus

$$\eta \simeq \sqrt{20 \frac{Q_{\text{rms-PS}}^2}{T^2} \left(\frac{N_{\text{end}} - N}{\Delta N_*}\right)^2}. \quad (4.223)$$

It is quite remarkable that this formula does not depend on ϕ_0 anymore but only on the ratio $(N_{\text{end}} - N)/\Delta N_*$. From $Q_{\text{rms-PS}}/T \simeq 6 \times 10^{-6}$, one has $N_{\text{end}} - N_{\text{min}} \simeq 10^4$ in the classical regime [347]. For $\phi_0 \simeq 10^{14}$ GeV, one obtains $M \sim 10^8$ GeV, in agreement with what was announced earlier.

Finally, it can be interesting to write down the approximated slow-roll parameters at Hubble crossing and in the limit $\phi_0/M_{\text{Pl}} \ll 1$. One obtains

$$\epsilon_{1*} \simeq \left(\frac{\phi_0}{M_{\text{Pl}}}\right)^6 \frac{1}{7200\Delta N_*^4}, \quad \epsilon_{2*} \simeq \frac{4}{\Delta N_*}, \quad \epsilon_{3*} \simeq \frac{1}{\Delta N_*}, \quad (4.224)$$

hence

$$r \simeq \left(\frac{\phi_0}{M_{\text{Pl}}}\right)^6 \frac{1}{450\Delta N_*^4}, \quad n_s \simeq 1 - \frac{4}{\Delta N_*}, \quad \alpha_s \simeq -\frac{4}{\Delta N_*^2}. \quad (4.225)$$

They are similar with the typical predictions of the RIPI models [see Eq. (4.238)].

The reheating consistent slow-roll predictions of the MSSMI models are displayed in Fig. 93. The reheating equation of state parameter \bar{w}_{reh} has been taken to 0 since the potential is quadratic close to its minimum. One can check that in the limit $\phi_0/M_{\text{Pl}} \ll 1$, the first slow-roll parameter is indeed extremely small, while the second slow-roll parameter does not depend much on ϕ_0 . Remembering that $\phi_0/M_{\text{Pl}} \simeq 10^{-4}$, one can see that these models seem to be disfavored by the data since they predict a too much important deviation from scale invariance. In order to comply with the spectral index, these models should be such that $\phi_0/M_{\text{Pl}} \gg 1$, for which they are close to the large field quadratic models (LFI with $p = 2$, see section 4.2). This can be seen from the previous formula in the limit $x \ll 1$. Unfortunately, such values for ϕ_0 are, a priori, outside the range of the MSSM. Finally, comparing Fig. 94 with Fig. 93, one can see that the general features of MSSMI are very close to the RIPI ones, and that the conclusions drawn here are rather robust against the power index n appearing in Eq. (4.210).

4.18 Renormalizable Inflection Point Inflation (RIPI)

In section 4.17 inflaton is implemented within the Minimal Supersymmetric Standard Model (MSSM) around a flat inflection point. Refs. [364–366] have argued that $n = 3$, as opposed

to $n = 6$ dealt in section 4.17, is a case of interest. The potential is given by

$$V(\phi) = M^4 \left[\left(\frac{\phi}{\phi_0} \right)^2 - \left(\frac{\phi}{\phi_0} \right)^3 + \frac{9}{32} \left(\frac{\phi}{\phi_0} \right)^4 \right], \quad (4.226)$$

where ϕ_0 is the typical *vev* at which inflation occurs and is of order $\phi_0 \simeq 10^{14}$ GeV. A discussion on the fine-tuning required to get a the flat inflection point can be found in section 5.6 as only extremely small deviations from this condition are allowed. This is why in Ref. [364], an auxiliary hybrid field is introduced that dynamically uplifts the potential with a subsequent phase transition to end inflation at the necessary point in order to alleviate the fine-tuning issues. Here we study the model in its original single field form summarized in Eq. (4.226).

Let us define

$$x \equiv \frac{\phi}{\phi_0}. \quad (4.227)$$

The potential is an increasing function of the field *vev*, hence inflation proceeds from the right to the left. It has two inflection points $x_{V''=0}^\pm$, given by

$$x_{V''=0}^- = \frac{4}{9} \quad \text{and} \quad x_{V''=0}^+ = \frac{4}{3}, \quad (4.228)$$

the second one being a flat inflection point [i.e. $V'(x_{V''=0}^+) = 0$], close to which inflation takes place. This potential is displayed in Fig. 33, together with its logarithm.

Let us now turn to the slow-roll parameters. The first three Hubble flow functions in the slow-roll approximation are given by

$$\epsilon_1 = \frac{M_{\text{Pl}}^2}{\phi_0^2} \frac{8(4-3x)^4}{(9x^3 - 32x^2 + 32x)^2}, \quad \epsilon_2 = 8 \frac{M_{\text{Pl}}^2}{\phi_0^2} (3x-4) \frac{27x^3 - 108x^2 + 160x - 128}{(9x^3 - 32x^2 + 32x)^2}, \quad (4.229)$$

and

$$\begin{aligned} \epsilon_3 = & 8 \frac{M_{\text{Pl}}^2}{\phi_0^2} (3x-4) (16384 - 49152x + 62976x^2 - 45312x^3 + 20736x^4 \\ & - 5832x^5 + 729x^6) (9x^3 - 32x^2 + 32x)^{-2} (27x^3 - 108x^2 + 160x - 128)^{-1}. \end{aligned} \quad (4.230)$$

Both $\epsilon_1(x)$ and $\epsilon_2(x)$ diverge when the field *vev* goes to 0, and vanish when the field *vev* goes to infinity. The first slow-roll parameter ϵ_1 first decreases, vanishes at $x_{V''=0}^+$ where ϵ_2 vanishes too, $x_{\epsilon_2=0}^- = x_{V''=0}^+$, then increases to reach a local maximum at $x_{\epsilon_1=0}^+$ where ϵ_2 vanishes again, and eventually decreases again. The value of $x_{\epsilon_2=0}^+$ is given by

$$x_{\epsilon_2=0}^+ = \frac{4}{9} \left[3 - (9 + \sqrt{82})^{-1/3} + (9 + \sqrt{82})^{1/3} \right] \simeq 2.33. \quad (4.231)$$

In between these two local extrema of ϵ_1 , the second slow roll parameter ϵ_2 is negative, and it is positive elsewhere. The value of ϵ_1 at its local maximum, ϵ_1^{max} , is given by

$$\begin{aligned} \epsilon_1^{\text{max}} = & \frac{M_{\text{Pl}}^2}{\phi_0^2} \frac{1}{192} \left[-70 + (35030267 - 1673784\sqrt{82})^{1/3} + (35030267 + 1673784\sqrt{82})^{1/3} \right] \\ \simeq & 2.96734 \frac{M_{\text{Pl}}^2}{\phi_0^2} \end{aligned} \quad (4.232)$$

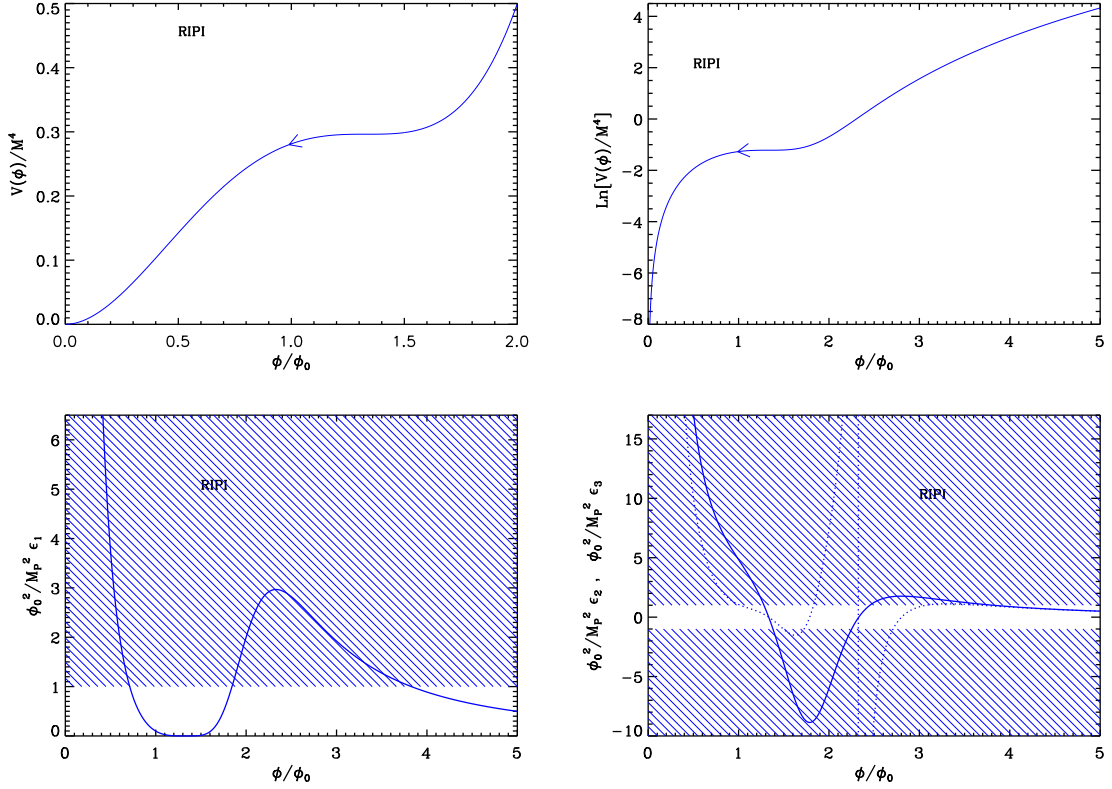


Figure 33. Renormalizable Inflection Point Inflation (RIPI). Top left panel: renormalizable inflection point inflation potential as a function of ϕ/ϕ_0 . Top right panel: logarithm of the potential, the required flatness of the potential close to its inflection point becomes obvious on this plot. Bottom left panel: slow-roll parameter ϵ_1 normalized by M_{Pl}^2/ϕ_0^2 . The shaded area indicates the region in which $\epsilon_1 > 1$ and thus where inflation stops (this has to be rescaled for $\phi_0 \neq M_{\text{Pl}}$). Bottom right panel: slow-roll parameters ϵ_2 (solid line) and ϵ_3 (dotted line), normalized by M_{Pl}^2/ϕ_0^2 .

Therefore, if $\phi_0/M_{\text{Pl}} < \sqrt{2.96734\dots} \simeq 1.72$, inflation can stop by slow-roll violation beyond the second inflection point $x_{\epsilon_2=0}^+$ if it proceeds in that part of the potential. Remembering that typically $\phi_0 \simeq 10^{14} \text{ GeV} \simeq 0.4 \times 10^{-4} M_{\text{Pl}}$, this condition is commonly satisfied. An expression for the ending point of inflation $x_{\epsilon_1=1}^+$ in that case can be obtained, but it does not add much to the discussion, since for reasonable values of ϕ_0 , it is extremely far from the flat inflection point (e.g. for $\phi_0/M_{\text{Pl}} = 10^{-4}$, one has $x_{\epsilon_1=1}^+ \simeq 71000$). Since the potential is introduced to study inflation close to a flat inflection point, it should be studied in the other regime, as it is the case for MSSM inflation (see section 4.17), i.e. when inflation takes place

between $x = 0$ and the second inflection point $x_{\epsilon_2=0}^-$. In that situation, it ends at

$$\begin{aligned}
x_{\text{end}} = x_{\epsilon_1=1}^- &= \frac{2}{27} \frac{M_{\text{Pl}}}{\phi_0} \left[9\sqrt{2} + 16 \frac{\phi_0}{M_{\text{Pl}}} + 2^{2/3} \left(-81 + 18\sqrt{2} \frac{\phi_0}{M_{\text{Pl}}} - 20 \frac{\phi_0^2}{M_{\text{Pl}}^2} \right) \right. \\
&\times \left(486 \frac{\phi_0}{M_{\text{Pl}}} - 297\sqrt{2} \frac{\phi_0^2}{M_{\text{Pl}}^2} + 544 \frac{\phi_0^3}{M_{\text{Pl}}^3} - 729\sqrt{2} \right. \\
&+ 27\sqrt{6} \sqrt{-162\sqrt{2} \frac{\phi_0^3}{M_{\text{Pl}}^3} + 99 \frac{\phi_0^4}{M_{\text{Pl}}^4} - 64\sqrt{2} \frac{\phi_0^5}{M_{\text{Pl}}^5} + 64 \frac{\phi_0^6}{M_{\text{Pl}}^6}} \left. \right)^{-1/3} \\
&- 2^{1/3} \times \left(486 \frac{\phi_0}{M_{\text{Pl}}} - 297\sqrt{2} \frac{\phi_0^2}{M_{\text{Pl}}^2} + 544 \frac{\phi_0^3}{M_{\text{Pl}}^3} - 729\sqrt{2} \right. \\
&+ 27\sqrt{6} \sqrt{-162\sqrt{2} \frac{\phi_0^3}{M_{\text{Pl}}^3} + 99 \frac{\phi_0^4}{M_{\text{Pl}}^4} - 64\sqrt{2} \frac{\phi_0^5}{M_{\text{Pl}}^5} + 64 \frac{\phi_0^6}{M_{\text{Pl}}^6}} \left. \right)^{1/3} \left. \right]. \tag{4.233}
\end{aligned}$$

For $\phi_0/M_{\text{Pl}} \ll 1$, one can numerically check that this expression is very close to the flat inflection point location $x_{\epsilon_2=0}^-$, namely

$$x_{\text{end}} \simeq \frac{4}{3} - \sqrt{\frac{16\sqrt{2}}{81} \frac{\phi_0}{M_{\text{Pl}}}}. \tag{4.234}$$

This means that in that case, the whole inflationary stage proceeds very close to this point.

The slow-roll trajectory is obtained from Eq. (2.11) and reads

$$\begin{aligned}
N_{\text{end}} - N &= \frac{\phi_0^2}{M_{\text{Pl}}^2} \left[-\frac{2x}{9} + \frac{x^2}{8} - \frac{16}{27} \frac{1}{3x-4} - \frac{4}{27} \ln(4-3x) \right. \\
&+ \left. \frac{2x_{\text{end}}}{9} - \frac{x_{\text{end}}^2}{8} + \frac{16}{27} \frac{1}{3x_{\text{end}}-4} + \frac{4}{27} \ln(4-3x_{\text{end}}) \right]. \tag{4.235}
\end{aligned}$$

Several remarks are in order. Firstly, from this expression, one can see that the number of e-folds diverges when the field goes to the inflection point of the potential. This means that this point is never crossed and if inflation proceeds beyond it, the field approaches the inflection point asymptotically. However, it turns out that an exact numerical integration of the equations of motion reveals that any deviation from slow-roll preceding the neighborhood of the flat inflection point can boost the field with a sufficient speed to cross it. On the other hand, the field dynamics at the exact location of the inflection point is dominated by quantum diffusion, and a more careful study must be carried out to describe what exactly happens there. Following the considerations of section 4.17, we will be focused on the inflationary regime only below the flat inflection, where deviations from slow-roll and quantum diffusion plays a negligible role. Then, since for $\phi_0/M_{\text{Pl}} \ll 1$ inflation takes place relatively close to the inflection point and the two last of Eq. (4.235) dominate over the two first ones. In this limit, the trajectory can be inverted to get

$$x_* \simeq \frac{4}{3} - \frac{4}{3} W_0^{-1} \left\{ 4 \exp \left[\frac{27}{4} \left(\frac{M_{\text{Pl}}}{\phi_0} \right)^2 \Delta N_* + \frac{4}{3x_{\text{end}}-4} - \log(4-3x_{\text{end}}) \right] \right\}. \tag{4.236}$$

Making use of Eq. (4.234), and keeping only the dominant terms in ϕ_0/M_{Pl} , one obtains

$$x_* \simeq \frac{4}{3} - \frac{16}{81} \left(\frac{\phi_0}{M_{\text{Pl}}} \right)^2 \frac{1}{\Delta N_*}. \quad (4.237)$$

This expression can be useful to determine typical values for the slow-roll parameters evaluated at Hubble crossing. One obtains

$$\epsilon_{1*} \simeq \frac{128}{6561} \frac{1}{\Delta N_*^4} \frac{\phi_0^6}{M_{\text{Pl}}^6}, \quad \epsilon_{2*} \simeq \frac{4}{\Delta N_*}, \quad \epsilon_{3*} \simeq \frac{1}{\Delta N_*}, \quad (4.238)$$

hence

$$r \simeq \frac{2048}{6561} \frac{1}{\Delta N_*^4} \frac{\phi_0^6}{M_{\text{Pl}}^6}, \quad n_s - 1 \simeq -\frac{4}{\Delta N_*}, \quad \alpha_s \simeq -\frac{4}{\Delta N_*^2}. \quad (4.239)$$

One can see that these models typically predict a tiny amount of gravitational waves, but a substantial deviation from scale invariance $n_s - 1 \simeq -4/\Delta N_* \sim 0.1$. The similarity with Eqs. (4.224) is obvious.

Finally, the parameter M can be determined from the amplitude of the CMB anisotropies and the observable field value $x_* = x(N_*)$ by

$$\left(\frac{M}{M_{\text{Pl}}} \right)^4 = 368640 \frac{M_{\text{Pl}}^2}{\phi_0^2} \pi^2 \frac{(4 - 3x_*)^4}{x_*^4 (9x_*^2 - 32x_* + 32)^3} \frac{Q_{\text{rms-PS}}^2}{T^2}. \quad (4.240)$$

For $\phi_0/M_{\text{Pl}} \ll 1$, one can make use of Eq. (4.237) to get the approximate expression

$$\left(\frac{M}{M_{\text{Pl}}} \right)^4 \simeq \frac{2560}{27} \frac{\pi^2}{\Delta N_*^4} \left(\frac{\phi_0}{M_{\text{Pl}}} \right)^6 \frac{Q_{\text{rms-PS}}^2}{T^2}. \quad (4.241)$$

Using the typical value $\phi_0 \simeq 10^{14}$ GeV, one gets $M/M_{\text{Pl}} \simeq 8 \times 10^{-10}$.

The reheating consistent slow-roll predictions of the renormalizable inflection point models are displayed in Fig. 94. The reheating equation of state parameter \bar{w}_{reh} has been taken to 0 since the potential is quadratic close to its minimum. One can check that in the limit $\phi_0/M_{\text{Pl}} \ll 1$, the first slow-roll parameter is indeed extremely small, while the second slow-roll parameter does not depend much on ϕ_0 . Remembering that $\phi_0/M_{\text{Pl}} \simeq 10^{-4}$, one can see that these models are disfavored by the CMB data since they predict a too large deviation from scale invariance. In order to remain inside the two-sigma confidence intervals, these models should be such that $\phi_0/M_{\text{Pl}} \gg 1$, for which they are close to quadratic models (LFI with $p = 2$, see section 4.2). However, such values for ϕ_0 are, a priori, outside the range of RIPI. Finally, comparing Fig. 94 with Fig. 93, one can see that the general features of RIPI are very close to the MSSMI ones, and that the conclusions drawn are therefore robust against the power index n of Eq. (4.210).

4.19 Arctan Inflation (AI)

This scenario was originally introduced in Ref. [367] as a toy model where the equation of state changes rapidly around $\phi = 0$. The potential reads

$$V(\phi) = M^4 \left[1 - \frac{2}{\pi} \arctan \left(\frac{\phi}{\mu} \right) \right], \quad (4.242)$$

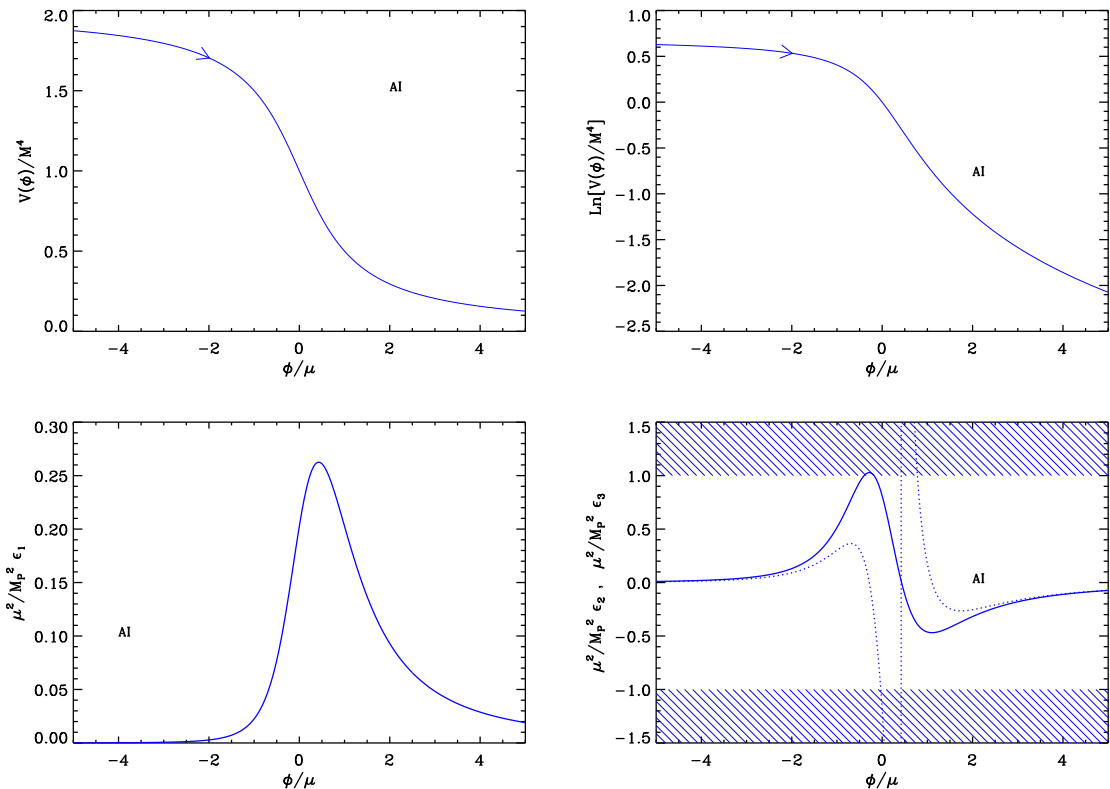


Figure 34. Top left panel: Arctan Inflation (AI) potential as a function of ϕ/μ . Top right panel: logarithm of the potential. Bottom left panel: slow-roll parameter ϵ_1 rescaled by M_{Pl}^2/μ^2 which renders the corresponding expression “universal”, i.e. independent of the free parameter μ . Bottom right panel: slow-roll parameters ϵ_2 (solid line) and ϵ_3 (dotted line) rescaled by M_{Pl}^2/μ^2 (for the same reason as mentioned before).

and depends on one free parameter, μ . This model was considered in order to test the reliability of different computational methods and schemes of approximation used in the calculations of the inflationary cosmological perturbations power spectrum, see Ref. [367]. More precisely, in Ref. [142], it was also used to study with which accuracy the first and second slow-roll order power spectra can approximate the actual power spectrum of the fluctuations in the case where the underlying model has both quite large tilt and running. This potential was considered again in Refs. [368, 369] in order to study whether it can lead to the formation of long-lived primordial black holes. In the following slow-roll analysis, μ will be viewed as a free parameter with no restricted range of variation. Let us notice, however, that since it characterizes the typical *vev* at which inflation takes place, it could also be limited to the sub-Planckian regime if one wants inflaton to proceed in a small field regime. As a matter of fact, it will be shown below that this needs to be the case if one wants inflation to end by slow-roll violation.

The potential (4.242), as well as its logarithm, are displayed in Fig. 34. They are decreasing functions of the field and, hence, inflation proceed from the left to the right, in the direction specified by the arrow in Fig. 34.

Let us now compute the three first slow-roll parameters. If one defines x by $x \equiv \phi/\mu$, their expressions are given by

$$\epsilon_1 = \frac{M_{\text{Pl}}^2}{\mu^2} \frac{2}{(1+x^2)^2 [\pi - 2 \arctan(x)]^2}, \quad \epsilon_2 = 8 \frac{M_{\text{Pl}}^2}{\mu^2} \frac{1 - \pi x + 2x \arctan(x)}{(1+x^2)^2 [\pi - 2 \arctan(x)]^2}, \quad (4.243)$$

and

$$\begin{aligned} \epsilon_3 = & 2 \frac{M_{\text{Pl}}^2}{\mu^2} [-4 + 6\pi x + \pi^2 (1 - 3x^2) + 4 (3\pi x^2 - 3x - \pi) \arctan(x) \\ & + 4 (1 - 3x^2) \arctan^2(x)] \left\{ (1+x^2)^2 [\pi - 2 \arctan(x)]^2 [-1 + \pi x - 2x \arctan(x)] \right\}^{-1}. \end{aligned} \quad (4.244)$$

They are displayed in Fig. 34. The first slow-roll parameter ϵ_1 increases during inflation, reaches a maximum at $x_{\epsilon_1^{\text{max}}}$ and then decreases. Whether inflation can stop by violation of slow-roll or not depends on the value of ϵ_1 , ϵ_1^{max} , at its maximum. This value is a solution of the following equation

$$2x_{\epsilon_1^{\text{max}}} \arctan(x_{\epsilon_1^{\text{max}}}) + 1 = \pi x_{\epsilon_1^{\text{max}}}. \quad (4.245)$$

This equation can only be solved numerically, and one obtains $x_{\epsilon_1^{\text{max}}} \simeq 0.428978$, from which one deduces that

$$\epsilon_1^{\text{max}} \simeq 0.262531 \frac{M_{\text{Pl}}^2}{\mu^2}. \quad (4.246)$$

Therefore, in order for inflation to end by slow-roll violation, one needs to work under the assumption that $\mu/M_{\text{Pl}} < 0.512378$. In that case, inflation proceeds along the plateau located at values of x such that $x < x_{\epsilon_1^{\text{max}}}$, in the direction specified by the arrow in Fig. 34 (i.e. from the left to the right). Otherwise, if one wants inflation to occur in other parts of the potential and/or for values of μ such that $\mu/M_{\text{Pl}} > 0.512378$, another mechanism needs to be considered in order to stop it (typically, we imagine a tachyonic instability in another direction in field space). This means that we also need to introduce an extra parameter x_{end} which gives the location of the *vev* at which the tachyonic instability is triggered. Let us remark that we could also consider a model where the inflaton starts at $x < x_{\epsilon_1^{\text{max}}}$, then crosses the region where ϵ_1 has its maximum and then causes the end of inflation by tachyonic instability. This case would give a bump in the power spectrum and, clearly, cannot be properly described in the slow-roll framework. In this article, we restrict ourselves to the first version of the scenario mentioned above. In this situation x_{end} is given by the smallest solution of the equation $\epsilon_1 = 1$ and needs to be computed numerically. Before inflation stops, one can see in Fig. 34 that the second slow-roll parameter ϵ_2 reaches a maximum, the location of which can be numerically computed to be $x_{\epsilon_2^{\text{max}}} \simeq -0.28539 < x_{\epsilon_1^{\text{max}}}$. At this point, one has $\epsilon_2^{\text{max}} \simeq 1.02827 M_{\text{Pl}}^2/\mu^2 > \epsilon_1^{\text{max}}$. As a consequence, the slow-roll approximation breaks down before the end of inflation. This conclusion is reinforced by the fact that ϵ_3 diverges at $x_{\epsilon_1^{\text{max}}}$. This means that the last e-folds of inflation cannot be properly described in the slow-roll framework.

Let us now turn to the slow-roll trajectory. It can be integrated exactly and yields the

following expression

$$N_{\text{end}} - N = \frac{\mu^2}{M_{\text{Pl}}^2} \left[\frac{\pi x_{\text{end}}}{2} + \frac{x_{\text{end}}^2}{6} + \frac{\pi x_{\text{end}}^3}{6} - \left(1 + \frac{x_{\text{end}}^2}{3} \right) x_{\text{end}} \arctan(x_{\text{end}}) + \frac{1}{3} \ln(1 + x_{\text{end}}^2) \right. \\ \left. - \frac{\pi x}{2} - \frac{x^2}{6} - \frac{\pi x^3}{6} + \left(1 + \frac{x^2}{3} \right) x \arctan(x) + \frac{1}{3} \ln(1 + x^2) \right], \quad (4.247)$$

where N_{end} is the number of e-folds at the end of inflation. In the vacuum dominated approximation where the potential is just given by $V(\phi) \simeq M^4$, this trajectory can be approximated by $N_{\text{end}} - N = \mu^2/M_{\text{Pl}}^2(\pi x_{\text{end}} + x_{\text{end}}^2/6 + \pi x_{\text{end}}^3/3 - \pi x - x^2/6 - \pi x^3/3)$, which can be inverted exactly if needed. This formula is valid if $\mu \ll 1$, since in that case, $x_{\text{end}} \simeq -\sqrt{M_{\text{Pl}}/(\mu\pi\sqrt{2})} \ll -1$. Under this assumption, one has $x_*^3 \simeq -3M_{\text{Pl}}^2/(\pi\mu^2)\Delta N_*$, from which one can compute the values of the three first Hubble flow parameters at Hubble radius crossing

$$\epsilon_{1*} = \frac{(\mu/M_{\text{Pl}})^{2/3}}{2(\pi\Delta N_*^2)^{2/3}}, \quad \epsilon_{2*} = \frac{4}{3\Delta N_*}, \quad \epsilon_{3*} = \frac{1}{\Delta N_*}, \quad (4.248)$$

Then, one can calculate the tensor to scalar ratio, the spectral index and the running. One obtains the following expressions

$$r = \frac{8(\mu/M_{\text{Pl}})^{2/3}}{(\pi\Delta N_*^2)^{2/3}}, \quad n_s - 1 = -\frac{4}{3\Delta N_*} \simeq -0.03, \quad \alpha_s = -\frac{4}{3\Delta N_*^2} \simeq -5 \times 10^{-4}. \quad (4.249)$$

These formulas are in agreement with the consistency relation $\alpha_s = -3/4(n_s - 1)^2$ obtained in Ref. [368].

Finally, it is interesting to estimate the energy scale M . As usual, this can be done by CMB-normalizing the model. This leads to

$$\left(\frac{M}{M_{\text{Pl}}} \right)^4 = \frac{2880\pi^3 M_{\text{Pl}}^2/\mu^2}{(1 + x_*^2)^2 [\pi - 2 \arctan(x_*)]^3} \frac{Q_{\text{rms-PS}}^2}{T^2}. \quad (4.250)$$

Under the vacuum dominated approximation ($\mu/M_{\text{Pl}} \ll 1$), the above equation can be re-expressed as

$$\left(\frac{M}{M_{\text{Pl}}} \right)^4 \simeq \frac{40 \times 3^{2/3} \pi^{4/3}}{\Delta N_*} \left(\frac{\mu}{M_{\text{Pl}}} \right)^{2/3} \frac{Q_{\text{rms-PS}}^2}{T^2}. \quad (4.251)$$

The requirement $M < M_{\text{Pl}}$ leads to an upper bound on μ , namely $\mu/M_{\text{Pl}} \lesssim 830$ (strictly speaking, this upper bound is not totally correct since the corresponding value of μ is super-Planckian while it has been derived in the vacuum dominated approximation). The typical value $M/M_{\text{Pl}} \sim 10^{-3}$ corresponds to $\mu/M_{\text{Pl}} \sim 10^{-2}$.

The slow-roll predictions of the AI models are displayed in Fig. 95, in the range $\mu/M_{\text{Pl}} < 0.512378$ (so that inflation can end by slow-roll violation). The reheating equation of state parameter \bar{w}_{reh} has been taken to be 0 but since there is no potential minimum around which the inflaton field can oscillate at the end of inflation, this parameter is a priori unspecified. One can see that this model typically predicts a small amount of gravitational waves, and a deviation from scale invariance which is in accordance with the observations. The predictions in the planes (n_s, r) are qualitatively well described by the vacuum dominated analysis (4.249) presented before.

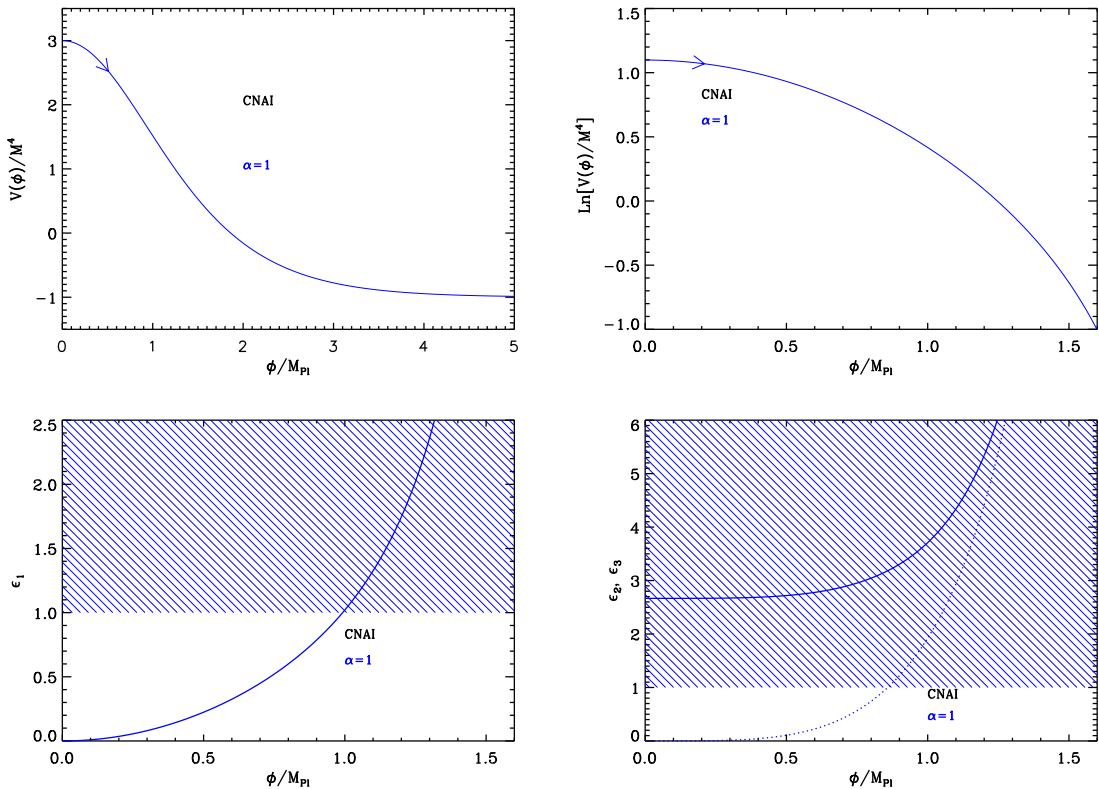


Figure 35. Constant n_s A Inflation (CNAI) potential and slow-roll parameters versus the vacuum expectation value of the inflaton field. Top left panel: Constant n_s A Inflation potential for $\alpha = 1$. Top right panel: logarithm of the potential for the same value of α . Bottom left panel: slow-roll parameter ϵ_1 (same value of α): it is clear from this plot that, in this model, inflation stops by violation of the slow-roll approximation. Bottom right panel: slow-roll parameters ϵ_2 and ϵ_3 ($\alpha = 1$).

4.20 Constant n_s A Inflation (CNAI)

This class of models is designed in order to produce power spectra with constant spectral index. It was studied for the first time in Ref. [370]. The rationale behind this approach is that, so far, no evidence for a significant running has been found in the cosmological data. Since, from a Bayesian point of view, one should avoid introducing parameters that are unnecessary in order to reproduce the observations, it makes sense to consider models which lead to exact power-law power spectra. This is of course the case for power-law inflation as discussed in section 4.8 and we will see other examples in sections 4.21, 5.14 and 6.6. In fact, in Ref. [370], a systematic analysis of potentials that yield constant spectral index was carried out. It was found that the following potential belongs to this category of models

$$V(\phi) = M^4 \left[3 - (3 + \alpha^2) \tanh^2 \left(\frac{\alpha}{\sqrt{2}} \frac{\phi}{M_{\text{Pl}}} \right) \right], \quad (4.252)$$

where α is a positive massless parameter (denoted n_0^2 in Ref. [370]) and, in this section, we study this case. This potential is represented in Fig. 35 and, since it is symmetrical under the transformation $\phi \rightarrow -\phi$, only the $\phi > 0$ part is displayed. The potential is a decreasing

function of the field vev and, therefore, inflation proceeds from the left to the right. It is positive provided $\phi < \phi_0$, where

$$\frac{\phi_0}{M_{\text{Pl}}} = \frac{\sqrt{2}}{\alpha} \operatorname{arctanh} \left(\sqrt{\frac{3}{3 + \alpha^2}} \right). \quad (4.253)$$

There is no value of α for which the potential is always positive. Defining $x = \phi/M_{\text{Pl}}$, the slow-roll parameters are given by

$$\epsilon_1 = \frac{4\alpha^2 (3 + \alpha^2)^2 \tanh^2 \left(\frac{\alpha x}{\sqrt{2}} \right)}{[6 + \alpha^2 - \alpha^2 \cosh(\sqrt{2}\alpha x)]^2}, \quad (4.254)$$

$$\epsilon_2 = \frac{2\alpha^2 (3 + \alpha^2) [12 + \alpha^2 - 2\alpha^2 \cosh(\sqrt{2}\alpha x) + \alpha^2 \cosh(2\sqrt{2}\alpha x)]}{[6 + \alpha^2 - \alpha^2 \cosh(\sqrt{2}\alpha x)]^2 \cosh^2 \left(\frac{\alpha x}{\sqrt{2}} \right)}, \quad (4.255)$$

$$\begin{aligned} \epsilon_3 = & 2\alpha^2 (3 + \alpha^2) \tanh^2 \left(\frac{\alpha}{\sqrt{2}} x \right) \left[6(-24 + 2\alpha^2 - \alpha^4) + (120\alpha^2 + 7\alpha^4) \cosh(\sqrt{2}\alpha x) \right. \\ & \left. - 2\alpha^2 (\alpha^2 - 6) \cosh(2\sqrt{2}\alpha x) + \alpha^4 \cosh(3\sqrt{2}\alpha x) \right] \\ & \times [6 + \alpha^2 - \alpha^2 \cosh(\sqrt{2}\alpha x)]^{-2} [12 + \alpha^2 - 2\alpha^2 \cosh(\sqrt{2}\alpha x) + \alpha^2 \cosh(2\sqrt{2}\alpha x)]^{-1} \end{aligned} \quad (4.256)$$

These slow-roll parameters are displayed in Fig. 35. They all increase as inflation proceeds and diverge when the field approaches ϕ_0 . Hence inflation ends by slow-roll violation. Notice that the equation $\epsilon_1 = 1$ can be solved analytically. If we define $y \equiv \sinh^2(\alpha x_{\text{end}}/\sqrt{2})$, then one has to solve the following cubic equation $\alpha^4 y^3 + (\alpha^4 - 6\alpha^2)y^2 + [9 - 6\alpha^2 - \alpha^2(3 + \alpha^2)]y + 9 = 0$. The relevant solution reads

$$y = \frac{6 - \alpha^2}{3\alpha^2} - \frac{1 - i\sqrt{3}}{3 \times 2^{1/3}} (3 + \alpha^2)^2 (1 + 3\alpha^2) P^{-1/3} - \frac{1 + i\sqrt{3}}{6 \times 2^{1/3} \alpha^4} P^{1/3}, \quad (4.257)$$

where we have defined P by

$$\begin{aligned} P \equiv & -\alpha^6 (3 + \alpha^2)^2 (6 - 52\alpha^2 + 9\alpha^4) \\ & + \sqrt{-27\alpha^{14} (3 + \alpha^2)^4 (36 - 60\alpha^2 + 96\alpha^4 + 25\alpha^6 + 4\alpha^8)}. \end{aligned} \quad (4.258)$$

Of course, ϕ_{end} can also be found numerically. The slow-roll parameters ϵ_1 and ϵ_3 both vanish when the field vev goes to 0, whereas ϵ_2 has a non vanishing minimum value, given by $\epsilon_2 \rightarrow 2\alpha^2 (3 + \alpha^2)/3$ when $x = 0$. Therefore, if α is larger than some maximum value

$$\alpha_{\text{max}} = \sqrt{\frac{1}{2} (\sqrt{15} - 3)} \simeq 0.66, \quad (4.259)$$

then ϵ_2 is larger than 1 in the whole inflationary regime and the slow-roll approximation does not hold. It is therefore necessary to work under the assumption $\alpha < \alpha_{\text{max}}$ which we assume in the following.

Let now us check that the spectral index $n_s - 1 = -2\epsilon_1 - \epsilon_2$ (at first order in slow-roll), is indeed constant, as announced previously. Expanding the slow-roll parameters ϵ_1 and ϵ_2

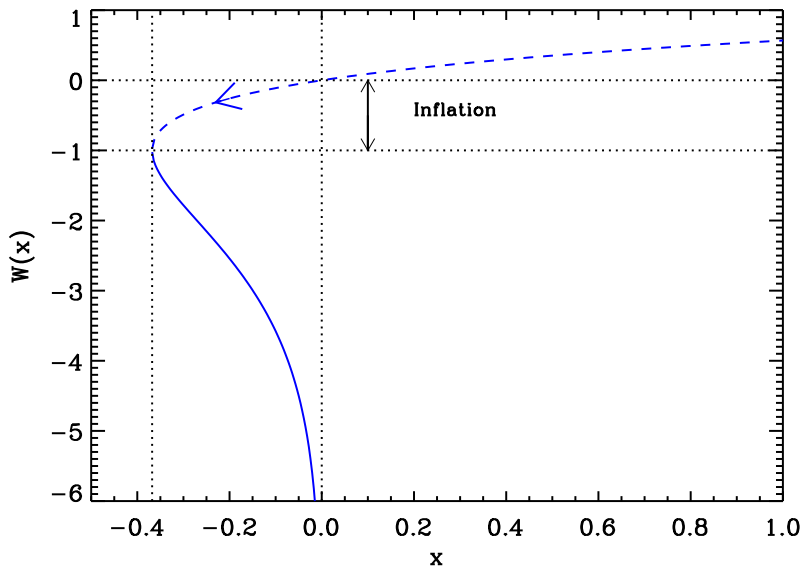


Figure 36. Lambert functions $W_0(x)$ (dashed line) and $W_{-1}(x)$ (solid line). During CNAI inflation, inflation proceeds along the “0” branch in the direction specified by the arrow on the figure.

in $\alpha \ll 1$, one obtains $\epsilon_1 = \mathcal{O}(\alpha^4)$ and $\epsilon_2 = 2\alpha^2 + \mathcal{O}(\alpha^4)$, so that $n_s - 1 = -2\alpha^2 + \mathcal{O}(\alpha^4)$. Therefore, the corresponding expression is indeed a constant (i.e. no longer depends on ϕ_*). Since we have $|n_s - 1| \ll 1$, this implies that $\alpha \ll 1$ which is consistent with the condition $\alpha < \alpha_{\max}$ derived above.

Let us now study the slow-roll trajectory of the system. This one can be integrated exactly leading to the following formula

$$N - N_{\text{ini}} = \frac{1}{\alpha^2(3 + \alpha^2)} \left\{ 3 \ln \left[\sinh \left(\frac{\alpha}{\sqrt{2}} x \right) \right] - \frac{\alpha^2}{2} \sinh^2 \left(\frac{\alpha}{\sqrt{2}} x \right) - 3 \ln \left[\sinh \left(\frac{\alpha}{\sqrt{2}} x_{\text{ini}} \right) \right] + \frac{\alpha^2}{2} \sinh^2 \left(\frac{\alpha}{\sqrt{2}} x_{\text{ini}} \right) \right\}. \quad (4.260)$$

Moreover, this trajectory can be inverted which allows us to explicitly express the *vev* of the inflaton field in terms of the e-folds number. One obtains

$$x = \frac{\sqrt{2}}{\alpha} \operatorname{arcsinh} \left[-\frac{3}{\alpha^2} W_0 \left(-\frac{\alpha^2}{3} \exp \left\{ \frac{2}{3} \alpha^2 (3 + \alpha^2) (N - N_{\text{ini}}) + 2 \ln \left[\sinh \left(\frac{\alpha}{\sqrt{2}} x_{\text{ini}} \right) \right] - \frac{\alpha^2}{3} \sinh^2 \left(\frac{\alpha}{\sqrt{2}} x_{\text{ini}} \right) \right\} \right) \right]^{1/2}, \quad (4.261)$$

where W_0 is the 0 branch of the Lambert function as required since $x(N)$ is an increasing function of N . It is displayed in Fig. 36 where the CNAI trajectory takes place between $\phi/M_{\text{Pl}} = 0$ at the origin of the plot, and $x = \phi_0/M_{\text{Pl}}$ at the junction between the -1 branch and the 0 branch.

The slow-roll predictions of the constant n_s A models are displayed in Fig. 96. When α is small (but not too small), the value of n_s is indeed constant (and compatible with

the considerations presented above) but, unfortunately, too far from scale invariance to be compatible with CMB data. When $\alpha \ll 10^{-1}$, the predictions become roughly compatible with the data but, clearly, n_s is no longer constant and no longer given by $-2\alpha^2$. At first sight, this is surprising since we expect the spectral index to tend towards $-2\alpha^2$ when α goes to zero (see above). In order to understand this point, let us remark that, in the limit where α vanishes, one can expand Eq. (4.257) to find $y \simeq 3/\alpha^2 - 3/\alpha + \mathcal{O}(\alpha)$ (the term at order α^0 is absent and this plays an important role in what follows). This leads to $\phi_{\text{end}}/M_{\text{Pl}} \simeq (\sqrt{2}/\alpha) \ln(2\sqrt{3}/\alpha) - 1/\sqrt{2} + \mathcal{O}(\alpha)$. Notice that this last equation can be easily interpreted. Indeed, the behavior of the first horizon-flow parameter (4.254) in the vicinity of ϕ_0 is given by $\epsilon_1 \simeq M_{\text{Pl}}^2/[2(\phi - \phi_0)^2]$. Therefore, the expression of ϕ_{end} found before corresponds in fact to writing $\epsilon_1 = 1$ with this approximated ϵ_1 . Then, using the slow-roll trajectory (4.261), it is easy to show that

$$\sinh^2\left(\frac{\alpha x_*}{\sqrt{2}}\right) = -\frac{3}{\alpha^2} \text{W}_0\left(-\frac{\alpha^2}{3} e^{-2A/3}\right), \quad (4.262)$$

where A is given by the following expression

$$A \equiv \alpha^2 (3 + \alpha^2) \Delta N_* - 3 \ln \left[\sinh\left(\frac{\alpha x_{\text{end}}}{\sqrt{2}}\right) \right] + \frac{\alpha^2}{2} \sinh^2\left(\frac{\alpha x_{\text{end}}}{\sqrt{2}}\right). \quad (4.263)$$

This quantity can be expanded in α using the equation for y derived above and, at leading order, one obtains

$$-\frac{2}{3}A \simeq -\frac{2}{3}\alpha^2 \Delta N_* + \ln\left(\frac{3}{\alpha^2}\right) - 1 - \frac{\alpha^2}{2}. \quad (4.264)$$

For simplicity, the last term in the previous expression can be ignored since $2\Delta N_* \gg 1/2$. It follows that, introducing the formula for $-2A/3$, Eq. (4.264), into Eq. (4.262), one arrives at

$$\sinh^2\left(\frac{\alpha x_*}{\sqrt{2}}\right) = -\frac{3}{\alpha^2} \text{W}_0\left(-\frac{1}{e} e^{-2\alpha^2 \Delta N_*}\right). \quad (4.265)$$

If we ignore the exponential in the argument of the Lambert function (since $\alpha \ll 1$) and use the identity $\text{arcsinh}(x) = \ln(x + \sqrt{x^2 + 1})$, one finally arrives at $\alpha x_* \simeq \sqrt{2} \ln(2\sqrt{3}/\alpha)$. We now understand why, in the limit $\alpha \rightarrow 0$, the spectral index is no longer constant. In order to arrive at the conclusion $n_s \simeq -2\alpha^2$, we have expanded the expressions of ϵ_1 and ϵ_2 in α , including the hyperbolic function of argument αx_* . But we have just shown that, when $\alpha \ll 1$, αx_* is not small and, therefore, the Taylor expansion of those terms is not justified. This is why, in Fig. 96, we see a deviation from the region where n_s is constant for very small values of α . In fact, this questions the interest of this model since the condition of constant spectral index is obtained only for values of n_s that are already ruled out by the CMB data. On the other hand, when $\alpha \ll 1$, the model seems compatible with the data and, therefore, represents a legitimate inflationary scenario even if the spectral index is not constant in this case.

Finally, it is also interesting to study the energy scale at which inflation takes place in this model. The COBE normalization gives

$$\left(\frac{M}{M_{\text{Pl}}}\right)^4 = \frac{11520\pi^2 \alpha^2 (\alpha^2 + 3)^2 \sinh^2\left(\frac{\alpha}{\sqrt{2}} x_*\right) Q_{\text{rms-PS}}^2}{[\alpha^2 + 6 - \alpha^2 \cosh(\sqrt{2}\alpha x_*)]^3 T^2}. \quad (4.266)$$

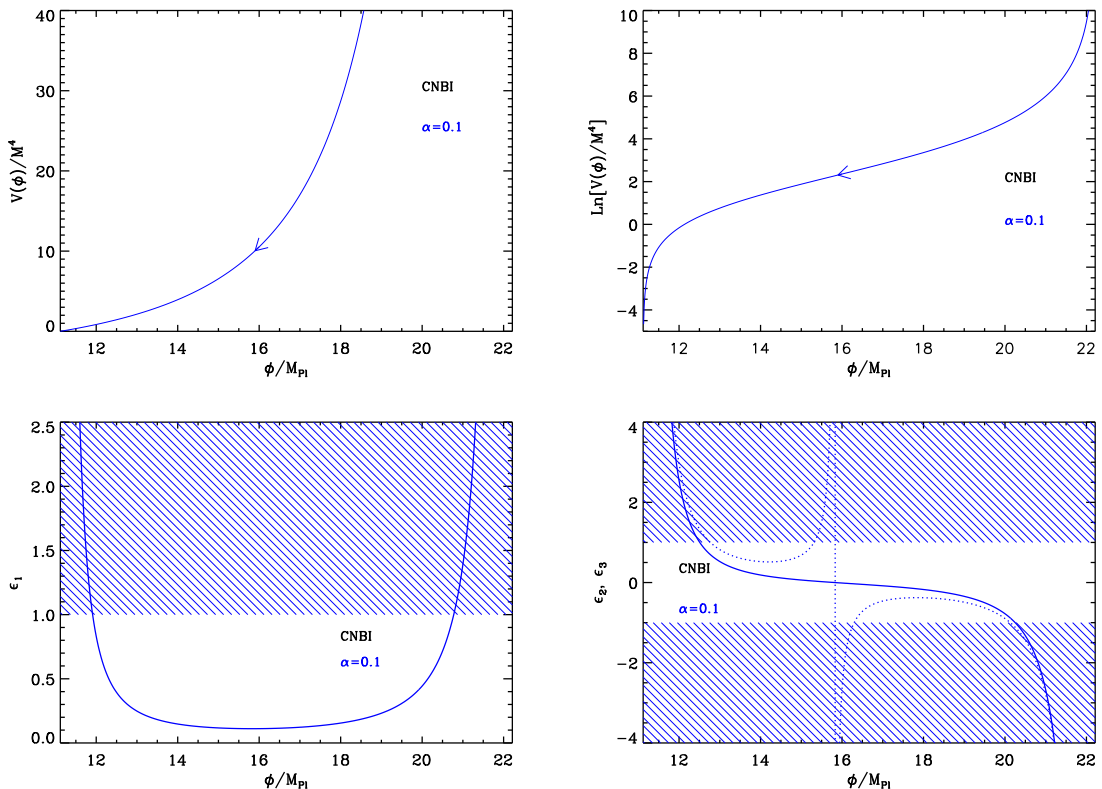


Figure 37. Top left panel: constant n_s B Inflation (CNBI) potential for $\alpha = 0.1$, see Eq. (4.268). Top right panel: logarithm of this potential (for the same value of α). Bottom left panel: slow-roll parameter ϵ_1 still for $\alpha = 0.1$. Bottom right panel: slow-roll parameters ϵ_2 and ϵ_3 again for $\alpha = 0.1$.

Since we have established the expression of x_* above, it is sufficient to use it in the above formula. We have, however, to be careful about the calculation of the denominator. Indeed, if we neglect again the exponential in the argument of the Lambert function, Eq. (4.262), then $\sinh^2(\alpha x_*/\sqrt{2}) \simeq 3/\alpha^2$ and the denominator in Eq. (4.266) vanishes. Therefore, one needs to evaluate the Lambert function more precisely and to keep the corrections proportional to ΔN_* . This can be done with the help of Eq. (33) of Ref. [371] which implies that $\sinh^2(\alpha x_*/\sqrt{2}) \simeq 3/\alpha^2 - 6\sqrt{\Delta N_*}/\alpha$. Using this expression, one arrives at

$$\frac{M}{M_{\text{Pl}}} \simeq 0.016 \alpha^{-3/4} (\Delta N_*)^{-3/8}. \quad (4.267)$$

For an order of magnitude estimate, one can use the fiducial value $\Delta N_* \simeq 55$. This leads to $M/M_{\text{Pl}} \simeq 0.0035 \alpha^{-3/4}$. Requiring $M < M_{\text{Pl}}$ puts a lower bound on the parameter α , namely $\alpha \gtrsim 5 \times 10^{-4}$. This roughly corresponds to the range studied in Fig. 96.

4.21 Constant n_s B Inflation (CNBI)

This model is another representative of the class of scenarios studied in Ref. [370]. As was already discussed in section 4.20, it is designed such that the corresponding power spectrum

has a constant spectral index. The potential is given by

$$V(\phi) = M^4 \left[(3 - \alpha^2) \tan^2 \left(\frac{\alpha}{\sqrt{2}} \frac{\phi}{M_{\text{Pl}}} \right) - 3 \right], \quad (4.268)$$

where α is a positive dimensionless parameter corresponding to $-n_0^2 > 0$ in Ref. [370]. Since the potential is periodic with period $\pi\sqrt{2}/\alpha$ and, moreover, invariant under $\phi \rightarrow -\phi$, one can restrict ourselves to the range $0 < \phi/M_{\text{Pl}} < \pi/(\sqrt{2}\alpha)$ without loss of generality. The potential is an increasing function of the field and, as a consequence, inflation proceeds from the right to the left. Finally, $V(\phi)$ is positive provided $\phi > \phi_0$, where

$$\frac{\phi_0}{M_{\text{Pl}}} = \frac{\sqrt{2}}{\alpha} \arctan \left(\sqrt{\frac{3}{3 - \alpha^2}} \right). \quad (4.269)$$

Obviously, in order for the potential not to be negative everywhere, one needs to impose that $\alpha < \sqrt{3}$ and, as a result, the previous expression is well defined. The potential (and its logarithm) is displayed in Fig. 37, in the relevant range $\phi_0/M_{\text{Pl}} < \phi/M_{\text{Pl}} < \pi/(\sqrt{2}\alpha)$.

Then, defining $x = \phi/M_{\text{Pl}}$, the slow-roll parameters are given by

$$\epsilon_1 = \frac{4\alpha^2 (\alpha^2 - 3)^2 \tan^2 \left(\frac{\alpha}{\sqrt{2}} x \right)}{[\alpha^2 + (6 - \alpha^2) \cos(\sqrt{2}\alpha x)]^2}, \quad (4.270)$$

$$\epsilon_2 = \frac{\alpha^2 (3 - \alpha^2) [6 + \alpha^2 + 2(6 - \alpha^2) \cos(\sqrt{2}\alpha x) + (\alpha^2 - 6) \cos(2\sqrt{2}\alpha x)]}{2 \cos^6 \left(\frac{\alpha}{\sqrt{2}} x \right) \left[3 + (\alpha^2 - 3) \tan^2 \left(\frac{\alpha x}{\sqrt{2}} \right) \right]^2}, \quad (4.271)$$

and

$$\begin{aligned} \epsilon_3 = & 2\alpha^2 (\alpha^2 - 3) \tan^2 \left(\frac{\alpha}{\sqrt{2}} x \right) \left[6(-72 + 14\alpha^2 - \alpha^4) + (\alpha^2 - 6)(7\alpha^2 + 78) \cos(\sqrt{2}\alpha x) \right. \\ & \left. - 2(\alpha^4 - 18\alpha^2 + 72) \cos(2\sqrt{2}\alpha x) + (\alpha^2 - 6)^2 \cos(3\sqrt{2}\alpha x) \right] \\ & \times \left[\alpha^2 + (6 - \alpha^2) \cos(\sqrt{2}\alpha x) \right]^{-2} \left[6 + \alpha^2 + 2(6 - \alpha^2) \cos(\sqrt{2}\alpha x) \right. \\ & \left. + (\alpha^2 - 6) \cos(2\sqrt{2}\alpha x) \right]^{-1}. \end{aligned} \quad (4.272)$$

These slow-roll parameters are displayed in Fig. 37 (bottom panels). The first slow-roll parameter ϵ_1 first decreases as the field vev increases and reaches a minimum value at $x_{\epsilon_2=0}$ where ϵ_2 vanishes and then increases. The value of $x_{\epsilon_2=0}$ is given by

$$x_{\epsilon_2=0} = \frac{1}{\alpha\sqrt{2}} \arccos \left[\frac{\alpha^2 - 6 + \sqrt{\alpha^4 - 36\alpha^2 + 180}}{2(\alpha^2 - 6)} \right]. \quad (4.273)$$

The second slow-roll parameter, ϵ_2 , always decreases as inflation proceeds, crossing $\epsilon_2 = 0$ at $x_{\epsilon_2=0}$. The third slow-roll parameter, ϵ_3 , is positive for $x < x_{\epsilon_2=0}$. In this domain, it decreases to reach a minimum and then increases and diverges when x approaches $x_{\epsilon_2=0}$. On the contrary, for $x > x_{\epsilon_2=0}$, ϵ_3 becomes negative. It first increases and reaches a local

maximum, then decreases and goes to $-\infty$ at $x = \pi/(\sqrt{2}\alpha)$. The three slow roll parameters diverge when ϕ goes to ϕ_0 and to $M_{\text{Pl}}\pi/(\sqrt{2}\alpha)$.

The minimum value of ϵ_1 at $x_{\epsilon_2=0}$ turns out to be smaller than 1 only if $\alpha < \alpha_{\text{max}} \simeq 0.2975$. A (rather long) analytic expression for α_{max} can be derived, but it does not provide much information to the present discussion. Therefore, one must require $\alpha < 0.2975$ in order to realize slow-roll inflation in this model. Then, assuming this is the case, it is clear from Fig. 37 and from the previous considerations that inflation ends by slow-roll violation. If we define $y \equiv \sin^2(\alpha x_{\text{end}}/\sqrt{2})$, then the condition $\epsilon_1 = 1$ is equivalent to $4(6 - \alpha^2)^2 y^3 - 4(12 - \alpha^2)(6 - \alpha^2)y^2 + 4(45 + 3\alpha^2 - 6\alpha^4 + \alpha^6)y - 36 = 0$. The relevant solution is given by

$$y = \frac{12 - \alpha^2}{3(6 - \alpha^2)} + \frac{4}{3}2^{-2/3} \left(1 - i\sqrt{3}\right) \frac{(3\alpha^2 - 1)(18 - 9\alpha^2 + \alpha^4)^2}{(6 - \alpha^2)^2} P^{-1/3} - \left(1 + i\sqrt{3}\right) \frac{2^{-1/3}}{24(6 - \alpha^2)^2} P^{1/3}, \quad (4.274)$$

where we have defined the quantity P by

$$P \equiv 64(-6 + \alpha^2)^3(-3 + \alpha^2)^2 \left(-6 + 110\alpha^2 - 9\alpha^4 + 3\alpha\sqrt{3} \times \sqrt{-36 + 408\alpha^2 - 12\alpha^4 - 25\alpha^6 + 4\alpha^8} \right). \quad (4.275)$$

If $\alpha \ll 1$, then $y \simeq 1/2$ and $x_{\text{end}} \simeq \sqrt{2}/\alpha \arcsin(1/\sqrt{2}) = \pi/(2\sqrt{2}\alpha)$.

Now, let us check that the spectral index, $n_s - 1 = -2\epsilon_1 - \epsilon_2$, at first order in slow-roll, is indeed constant as announced previously. Expanding the slow-roll parameters ϵ_1 and ϵ_2 in $\alpha \ll 1$, one obtains $\epsilon_1 = x^2\alpha^4/2 + \mathcal{O}(\alpha^6)$ and $\epsilon_2 = 2\alpha^2 + \mathcal{O}(\alpha^4)$, so that $n_s - 1 = -2\alpha^2 + \mathcal{O}(\alpha^4)$. Therefore, approximate scale-invariance, $|n_s - 1| \ll 1$, implies $\alpha^2 \ll 1$ and a first order approximation in slow-roll is in fact an expansion to second order in $\alpha \ll 1$.

Let us now turn to the slow-roll trajectory. This one can be integrated exactly, leading to the following formula

$$N - N_{\text{ini}} = \frac{1}{\alpha^2(3 - \alpha^2)} \left\{ 3 \ln \left[\sin \left(\frac{\alpha}{\sqrt{2}} x \right) \right] - \frac{6 - \alpha^2}{2} \sin^2 \left(\frac{\alpha}{\sqrt{2}} x \right) - 3 \ln \left[\sin \left(\frac{\alpha}{\sqrt{2}} x_{\text{ini}} \right) \right] + \frac{6 - \alpha^2}{2} \sin^2 \left(\frac{\alpha}{\sqrt{2}} x_{\text{ini}} \right) \right\}. \quad (4.276)$$

This formula can be inverted and x can be expressed explicitly in terms of the e-folds number. One obtains

$$x = \frac{\sqrt{2}}{\alpha} \arcsin \left[-\frac{3}{6 - \alpha^2} W_{-1} \left(-\frac{6 - \alpha^2}{3} \exp \left\{ \frac{2}{3} \alpha^2 (3 - \alpha^2) (N - N_{\text{ini}}) + 2 \ln \left[\sin \left(\frac{\alpha}{\sqrt{2}} x_{\text{ini}} \right) \right] - \frac{6 - \alpha^2}{3} \sin^2 \left(\frac{\alpha}{\sqrt{2}} x_{\text{ini}} \right) \right\} \right)^{1/2} \right], \quad (4.277)$$

where W_{-1} is the -1 branch of the Lambert function. It is displayed in Fig. 38. When $x = \pi/(\sqrt{2}\alpha)$, the argument of the Lambert function is $(\alpha^2 - 6) \exp(\alpha^2/3 - 2)/3$ which is always larger than $-1/e$ for any value of α (this expression decreases with α when $\alpha < \sqrt{3}$),

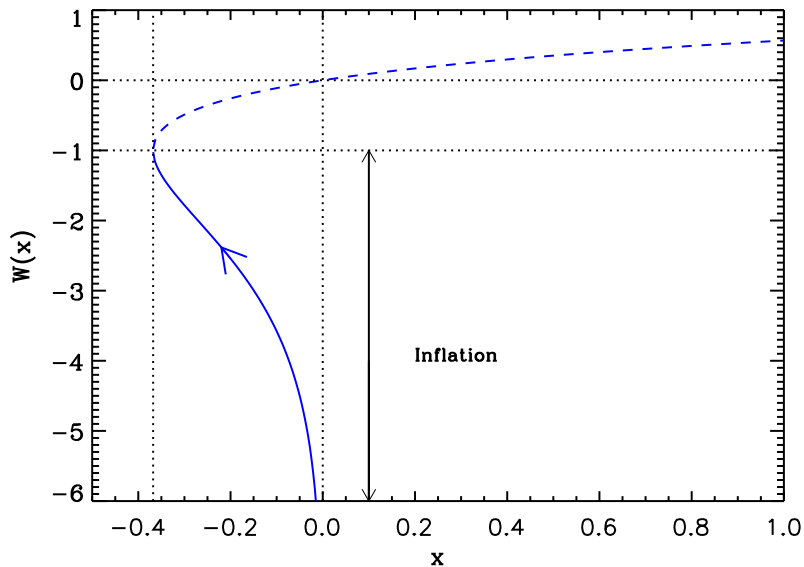


Figure 38. Lambert functions $W_0(x)$ (dashed line) and $W_{-1}(x)$ (solid line). During Constant n_s B Inflation, inflation proceeds along the “-1” branch in the direction specified by the arrow.

whereas when $x = \phi_0/M_{\text{Pl}}$, the argument of the Lambert function is just given by $-1/e$. For $x > \phi_0/M_{\text{Pl}}$, the value taken by the Lambert function must be less than -1 which indicates that the -1 branch is the relevant one. Therefore, inflation proceeds in the domain displayed in Fig. 38 in which one easily checks that the above trajectory is always well defined.

The slow-roll predictions of the constant n_s B models are displayed in Fig. 97 for the range $10^{-5} \lesssim \alpha \lesssim 10^{-1.3}$. For very small values of α , the predictions are in agreement with the data with a value of n_s centered around the constant value $n_s \simeq 0.97$ and an amount of gravitational waves such that $r \gtrsim 0.07$. But one also notices that the spectral index is not constant and, therefore, not given by $\simeq 1 - 2\alpha^2$ although one seems to approach this behavior when α increases (but, unfortunately, when the corresponding predictions leave the allowed region). In fact, it does not come as a surprise that the same phenomenon highlighted in section 4.20 is at work here. Indeed, using the slow-roll trajectory (4.276), it is easy to show that

$$\sin^2\left(\frac{\alpha x_*}{\sqrt{2}}\right) = -\frac{3}{6 - \alpha^2} W_{-1}\left(-\frac{6 - \alpha^2}{3} e^{-2A/3}\right), \quad (4.278)$$

where A is given by the following expression

$$A \equiv \alpha^2 (3 - \alpha^2) \Delta N_* - 3 \ln \left[\sin\left(\frac{\alpha x_{\text{end}}}{\sqrt{2}}\right) \right] + \frac{6 - \alpha^2}{2} \sin^2\left(\frac{\alpha x_{\text{end}}}{\sqrt{2}}\right). \quad (4.279)$$

Using the formula for x_{end} derived above, one obtains, in the limit $\alpha \ll 1$ and at this order of approximation that $x_* \simeq x_{\text{end}}$. Therefore, as in section 4.20, αx_* is not a small quantity and one cannot Taylor expand the trigonometric functions that appear in the expressions of the slow-roll parameters. This explains why, in the limit $\alpha \ll 1$, the spectral index is in fact not constant.

Finally, the COBE normalization gives

$$\left(\frac{M}{M_{\text{Pl}}}\right)^4 = \frac{11520\pi^2\alpha^2(3-\alpha^2)^2\sin^2\left(\frac{\alpha}{\sqrt{2}}x_*\right)Q_{\text{rms-PS}}^2}{[(\alpha^2-6)\cos(\sqrt{2}\alpha x_*)-\alpha^2]^3T^2}. \quad (4.280)$$

In the limit $\alpha \ll 1$ we are interested in (since we have seen that, if α is not small, then the model is ruled out), the above expression takes the form $M/M_{\text{Pl}} \simeq 0.02\alpha^{-1/4}(\Delta N_*)^{-3/8}$. We obtain almost exactly the same result as for CNAI, see Eq. (4.266), except that the power of α is different. Taking the value $\Delta N_* = 55$, it follows that $M/M_{\text{Pl}} \simeq 0.0044\alpha^{-1/4}$ and requiring $M < M_{\text{Pl}}$, one obtains the following lower bound, $\alpha \gtrsim 3.8 \times 10^{-10}$.

5 Two Parameters Models

5.1 Small Field Inflation (SFI)

This model is proto-typical of inflation occurring at the top of a flat-enough potential. As such it appears in very different contexts. It has been introduced in Ref. [2, 326] and derived in Ref. [3] in the context of radiatively induced symmetry breaking. It appears within superstring models [372], low scale symmetry breaking [208, 373], supersymmetry [286, 374] and supergravity [186, 187, 191, 207, 375–379]. It is also obtained in non-linear sigma models [217] or using moduli as inflatons [380]. It has been discussed in braneworld cosmology in Refs. [381–383] and is more recently referred to as “hilltop inflation” from Ref. [340, 341]. The potential is given by

$$V(\phi) = M^4 \left[1 - \left(\frac{\phi}{\mu} \right)^p \right], \quad (5.1)$$

and has two parameters in addition to the overall normalization M : a typical *vev* μ and the power index p . As this potential can be associated with very different physical frameworks, μ can take any values while $p > 0$ for being at the top of a potential (in the small field limit, namely $\phi \ll \mu$). In particular, we will allow super-Planckian values for μ even though, in the supergravity context, one would require $\mu < M_{\text{Pl}}$. Let us stress that Eq. (5.1) is defined only in the domain $\phi < \mu$ as one assumes that the small field potential describes only the field dynamics during inflation. The equation of state during reheating is thus not specified by Eq. (5.1). Defining

$$x \equiv \frac{\phi}{\mu}, \quad (5.2)$$

the first three Hubble flow functions read

$$\epsilon_1 = \frac{p^2}{2} \left(\frac{M_{\text{Pl}}}{\mu} \right)^2 \frac{x^{2p-2}}{(1-x^p)^2}, \quad \epsilon_2 = 2p \left(\frac{M_{\text{Pl}}}{\mu} \right)^2 x^{p-2} \frac{p-1+x^p}{(1-x^p)^2}, \quad (5.3)$$

and

$$\epsilon_3 = p \left(\frac{M_{\text{Pl}}}{\mu} \right)^2 \frac{x^{p-2} [2x^{2p} + (p-1)(p+4)x^p + (p-1)(p-2)]}{(1-x^p)^2(p-1+x^p)}. \quad (5.4)$$

They are monotonic functions of the field value but also decreasing functions of the *vev* μ . The potential, its logarithm and the Hubble flow functions are represented in Fig. 39.

The slow-roll trajectory is obtained by integrating Eq. (2.11) to get

$$N - N_{\text{end}} = \frac{1}{2p} \frac{\mu^2}{M_{\text{Pl}}^2} \left[-x^2 + x_{\text{end}}^2 + \frac{2}{2-p} (x^{2-p} - x_{\text{end}}^{2-p}) \right]. \quad (5.5)$$

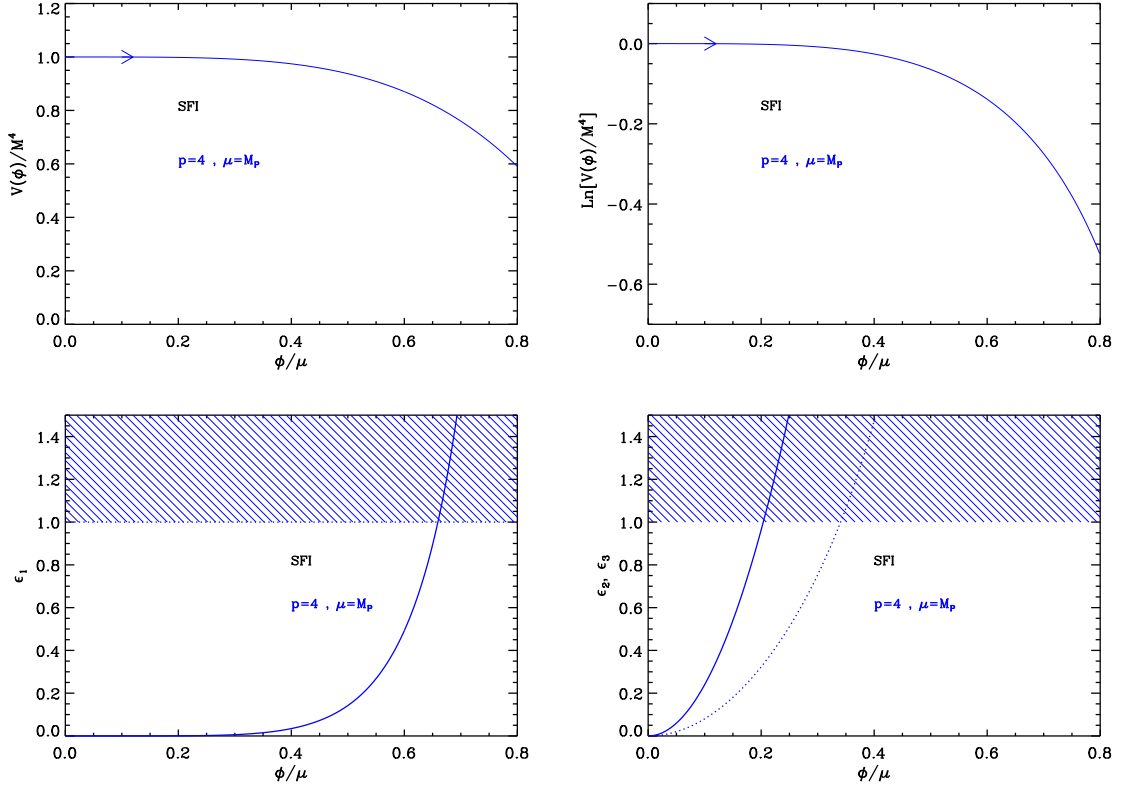


Figure 39. Small Field Inflation (SFI) for $p = 4$ and $\mu = M_{\text{Pl}}$. Upper panels: the potential and its logarithm as a function of ϕ/μ . Bottom left panel: slow-roll parameter ϵ_1 , the shaded area indicates where inflation stops. Bottom right panel: slow-roll parameters ϵ_2 (solid line) and ϵ_3 (dotted line).

This equation seems to be well-defined only for $p \neq 2$. However, the particular case $p = 2$ can be directly obtained from Eqs. (2.11) and (5.1) directly to get

$$N - N_{\text{end}} = \frac{1}{4} \frac{\mu^2}{M_{\text{Pl}}^2} \left[-x^2 + x_{\text{end}}^2 + 2 \ln \left(\frac{x}{x_{\text{end}}} \right) \right]. \quad (5.6)$$

This expression can also be viewed as the limit of Eq. (5.5) for $p \rightarrow 2$. In general, the trajectory cannot be analytically inverted to give the field value $x(N)$ but one can find some analytical form for almost all integer values of p (e.g. for $p = 1, p = 2, p = 3, p = 4, p = 6$) that we do not write down for the sake of clarity.

From the potential Eq. (5.1), inflation can stop naturally at $\epsilon_1(x_{\text{end}}) = 1$ with $x_{\text{end}} < 1$. This condition gives the algebraic equation

$$x_{\text{end}}^p + \frac{p}{\sqrt{2}} \frac{M_{\text{Pl}}}{\mu} x_{\text{end}}^{p-1} = 1, \quad (5.7)$$

which cannot be solved analytically in full generality. As for the trajectory, there are however explicit solutions for almost all integer values of p , the first two being

$$x_{\text{end}}^{(p=1)} = 1 - \frac{M_{\text{Pl}}}{\sqrt{2}\mu}, \quad x_{\text{end}}^{(p=2)} = \frac{M_{\text{Pl}}}{\sqrt{2}\mu} \left(-1 + \sqrt{1 + 2 \frac{\mu^2}{M_{\text{Pl}}^2}} \right). \quad (5.8)$$

Together with Eq. (2.46), these equations are enough to allow the determination of the field value x_* at which the observable modes crossed the Hubble radius during inflation. This fixes the value of the parameter M to match the observed amplitude of the CMB anisotropies at

$$\frac{M^4}{M_{\text{Pl}}^4} = 720\pi^2 p^2 \frac{M_{\text{Pl}}^2}{\mu^2} \frac{x_*^{2p-2}}{(1-x_*^p)^3} \frac{Q_{\text{rms-PS}}^2}{T^2}. \quad (5.9)$$

The reheating consistent slow-roll predictions for the small field models are represented in Figs. 98 to 100 for $p = 1$, $p = 2$ and $p = 4$. The $p = 1$ case is trivial since one then has $\epsilon_{2*} = 4\epsilon_{1*}$. For $p = 2$ or $p = 4$, one sees that the reheating temperature is limited from below to fit in the observable range. For instance, with $p = 2$, values of μ such that $\mu/M_{\text{Pl}} < 10$ are clearly disfavored. Let us notice that the relation $\epsilon_{2*} = 4\epsilon_{1*}$ is recovered in the limit $\mu/M_{\text{Pl}} \gg 1$ whereas one clearly observes a systematic shift in n_s (or ϵ_2) when $\mu \ll M_{\text{Pl}}$. These behaviors can in fact be understood analytically.

Small field models in the supergravity context are commonly studied in the limit $\mu \ll M_{\text{Pl}}$. In this situation it is possible to find some approximate solution to both the trajectory and x_{end} . Keeping only the dominant term in Eq. (5.7), one gets

$$x_{\text{end}}^{(p \neq 1)} \simeq \left(\frac{\sqrt{2}}{p} \frac{\mu}{M_{\text{Pl}}} \right)^{1/(p-1)}, \quad (5.10)$$

the case $p \leq 1$ being incompatible with the limit $\mu \ll M_{\text{Pl}}$ and the consistency requirement that $x_{\text{end}} < 1$. The small *vev* limit can also be used to invert Eq. (5.5). Assuming $\mu \ll M_{\text{Pl}}$ and $x_{\text{end}} \ll 1$, neglecting the quadratic terms for $p > 1$, the approximate trajectory reads

$$N - N_{\text{end}} \simeq \frac{\mu^2}{M_{\text{Pl}}^2} \frac{x^{2-p} - x_{\text{end}}^{2-p}}{p(2-p)}, \quad (5.11)$$

which can be inverted to

$$x \simeq \left[x_{\text{end}}^{2-p} - \frac{M_{\text{Pl}}^2}{\mu^2} p(2-p) (N_{\text{end}} - N) \right]^{1/(2-p)}. \quad (5.12)$$

Notice that far from the end of inflation, i.e. $N \ll N_{\text{end}}$, the first term can be neglected (for $p > 2$) since $x_{\text{end}} < 1$ and $M_{\text{Pl}}/\mu \gg 1$. Defining $\Delta N_* = N_{\text{end}} - N_*$, one can now plug this expression for x_* into the Hubble flow functions of Eqs. (5.3) and (5.4) to get their observable values:

$$\epsilon_{1*} \simeq \frac{p^2}{2} \left(\frac{M_{\text{Pl}}}{\mu} \right)^2 \left[\Delta N_* p(p-2) \left(\frac{M_{\text{Pl}}}{\mu} \right)^2 \right]^{-\frac{2(p-1)}{p-2}}, \quad \epsilon_{2*} \simeq \frac{2}{\Delta N_*} \frac{p-1}{p-2}, \quad \epsilon_{3*} \simeq \frac{1}{\Delta N_*}. \quad (5.13)$$

It is crucial to keep in mind that the above formulas are valid only in the limit $\mu \ll M_{\text{Pl}}$ and $p > 2$. As before, the limiting case $p \rightarrow 2$ has to be taken with care and, starting with Eq. (5.6), one obtains

$$\epsilon_{1*}^{(p=2)} = \exp \left(-4 \frac{M_{\text{Pl}}^2}{\mu^2} \Delta N_* \right), \quad \epsilon_{2*}^{(p=2)} = 4 \frac{M_{\text{Pl}}^2}{\mu^2}, \quad \epsilon_{3*}^{(p=2)} = 6 \epsilon_{1*}^{(p=2)}. \quad (5.14)$$

Both Eqs. (5.13) and (5.14) describes the observed behavior in Figs. 98 to 100 when $\mu/M_{\text{Pl}} \rightarrow 0$ but they do fail in the intermediate region as we have discussed in the introduction (see Fig. 3).

If the theoretical motivations underlying the potential 5.1 do not require the vev to be small, one can similarly derive approximate expressions for the observables in the limit $\mu/M_{\text{Pl}} \gg 1$ (but still with $x < 1$). Defining $\varepsilon \equiv M_{\text{Pl}}/\mu$, one has $x_{\text{end}}(\varepsilon)$ and we can search for a Taylor expanded solution of Eq. (5.7) to get

$$x_{\text{end}} = 1 - \frac{\varepsilon}{\sqrt{2}} + \frac{p-1}{4}\varepsilon^2 + \mathcal{O}(\varepsilon^3). \quad (5.15)$$

Similarly one can search for a Taylor expanded solution for the trajectory Eq. (5.5), plugging in the previous expression for x_{end} . Doing so yields

$$x_* = 1 - \varepsilon \sqrt{\frac{1}{2} + 2\Delta N_*} + \mathcal{O}(\varepsilon^2). \quad (5.16)$$

From this, one gets the corresponding Hubble flow functions

$$\epsilon_{1*} \simeq \frac{1}{4\Delta N_* + 1} \quad \epsilon_{2*} \simeq 4\epsilon_{1*}, \quad \epsilon_{3*} \simeq \epsilon_1. \quad (5.17)$$

This result is quite remarkable since the observable slow-roll parameters become μ and p independent. Performing the same calculation in the singular case $p \rightarrow 2$ yields exactly the same result. The spectral index, tensor-to-scalar ratio and running are immediately obtained from Eq. (5.17) with $r = 16\epsilon_{1*}$, $n_s - 1 \simeq -3r/8$ and $\alpha \simeq -r$. Again, these expressions match with Figs. 98 to 100 when $\mu/M_{\text{Pl}} \rightarrow \infty$.

5.2 Intermediate Inflation (II)

This model was introduced in Refs. [384–387] as an implementation of an equation of state of the form

$$\rho + p = \gamma\rho^\lambda, \quad (5.18)$$

where ρ is then energy density, p the pressure. Both $\gamma > 0$ and $\lambda > 0$ are dimensionless constants. As will be made explicit, this equation of state leads to a scale factor which is given by $a(t) \propto \exp(At^f)$ where $0 < f < 1$. In some sense the expansion is thus faster than power law but slower than de Sitter, hence the name of the model. The pure de Sitter case corresponds to $f = 1$. Inserting the Friedmann-Lemaître equation, $3M_{\text{Pl}}^2 H^2 = \rho$ as well as the equation of state Eq. (5.18) into the equation of conservation $\dot{\rho} + 3H(\rho + p) = 0$, one obtains a closed equation for ρ which is solved by

$$\rho = \rho_0 \left[3\gamma(\lambda - 1) \ln \left(\frac{a}{a_0} \right) \right]^{1/(1-\lambda)}, \quad (5.19)$$

where ρ_0 and a_0 are positive constants. Making use of the Friedmann-Lemaître equation again, one deduces the behavior for a ,

$$\ln \left(\frac{a}{a_0} \right) = 3^{\lambda/(1-2\lambda)} \gamma^{1/(1-2\lambda)} \frac{(\lambda - \frac{1}{2})^{(1-\lambda)/(1-2\lambda)}}{\lambda - 1} \left(\frac{t}{t_0} \right)^{(1-\lambda)/(1-2\lambda)}, \quad (5.20)$$

i.e. the announced behavior, $a(t) \propto \exp(At^f)$, with $f = 2(1 - \lambda)/(1 - 2\lambda)$. Since $\lambda > 0$, this means that $0 < f < 1$. Then, one can notice that it is possible to reinterpret the matter

source as that of a scalar field with the potential $V(\phi)$ given by

$$V(\phi) = 3A^2 f^2 M_{\text{Pl}}^4 \left[\frac{\phi - \phi_0}{M_{\text{Pl}} \sqrt{8A(f^{-1} - 1)}} \right]^{4(1-1/f)} - M_{\text{Pl}}^4 A f (1-f) \left[\frac{\phi - \phi_0}{M_{\text{Pl}} \sqrt{8A(f^{-1} - 1)}} \right]^{2-4/f}. \quad (5.21)$$

Indeed, starting from this potential, the Klein-Gordon equation with $H = Aft^{f-1}$, has an exact non-trivial solution given by

$$\phi = \phi_0 + M_{\text{Pl}} \sqrt{8A(f^{-1} - 1)} \left(\frac{t}{t_0} \right)^{f/2}. \quad (5.22)$$

It is then straightforward to calculate $\rho = \dot{\phi}^2/2 + V$ and $p = \dot{\phi}^2/2 - V$, and to show that they satisfy the equation of state Eq. (5.18). The potential can be recast in the form

$$V(\phi) = M^4 \left(\frac{\phi - \phi_0}{M_{\text{Pl}}} \right)^{-\beta} - M^4 \frac{\beta^2}{6} \left(\frac{\phi - \phi_0}{M_{\text{Pl}}} \right)^{-\beta-2}, \quad (5.23)$$

with $\beta = 4(1/f - 1)$. The constraint $0 < f < 1$ means that $\beta > 0$. Defining

$$x \equiv \frac{\phi - \phi_0}{M_{\text{Pl}}}, \quad (5.24)$$

it is shown below that the model predictions do not depend on ϕ_0 . Therefore Intermediate Inflation is a priori a one parameter family of models, but as explained below, one needs an extra parameter x_{end} specifying the field value at which an unspecified mechanism is triggered to end of inflation. It is thus a two parameters model.

This potential appears in the earlier work of Ref. [388] as a solution for a cosmological model containing a string creation term. It is also discussed in the context of tachyon fields in Refs. [389, 390]. Warm intermediate inflation was considered in Refs. [391, 392], intermediate inflation within a Gauss-Bonnet braneworld was studied in Ref. [393], and with Jordan-Brans-Dicke theory in Refs. [394, 395].

The potential (5.23), as well as its logarithm, are displayed in Fig. 40. It is positive definite for $x > x_{V=0} \equiv \beta/\sqrt{6}$. Therefore, one must restrict the inflaton vev to lie beyond this value. The potential increases with x , reaches a maximum at $x_{V'=0} \equiv \sqrt{\beta(\beta+2)}/6$, then decreases with x to asymptotically vanish when x goes to infinity. Therefore, a priori, two regimes of inflation exist. Either inflation proceeds at $x < x_{V'=0}$ from the right to the left, either it proceeds at $x > x_{V'=0}$ from the left to the right. However, in Eq. (5.22), one can see that the inflaton vev has to increase with time. Therefore only the branch $x > x_{V'=0}$ can produce an equation of state of the form of Eq. (5.18), which is where the model will be studied in the following.

Let us now turn to the slow-roll parameters. The first three Hubble flow functions in the slow-roll approximation are given by

$$\epsilon_1 = \frac{1}{2} \left[\frac{\beta^2(\beta+2) - 6\beta x^2}{-\beta^2 x + 6x^3} \right]^2, \quad \epsilon_2 = \frac{-2\beta x^4 + \frac{\beta^2}{3}(2\beta+6)x^2 - \frac{\beta^4}{18}(\beta+2)}{\left(x^3 - \frac{\beta^2 x}{6}\right)^2}, \quad (5.25)$$

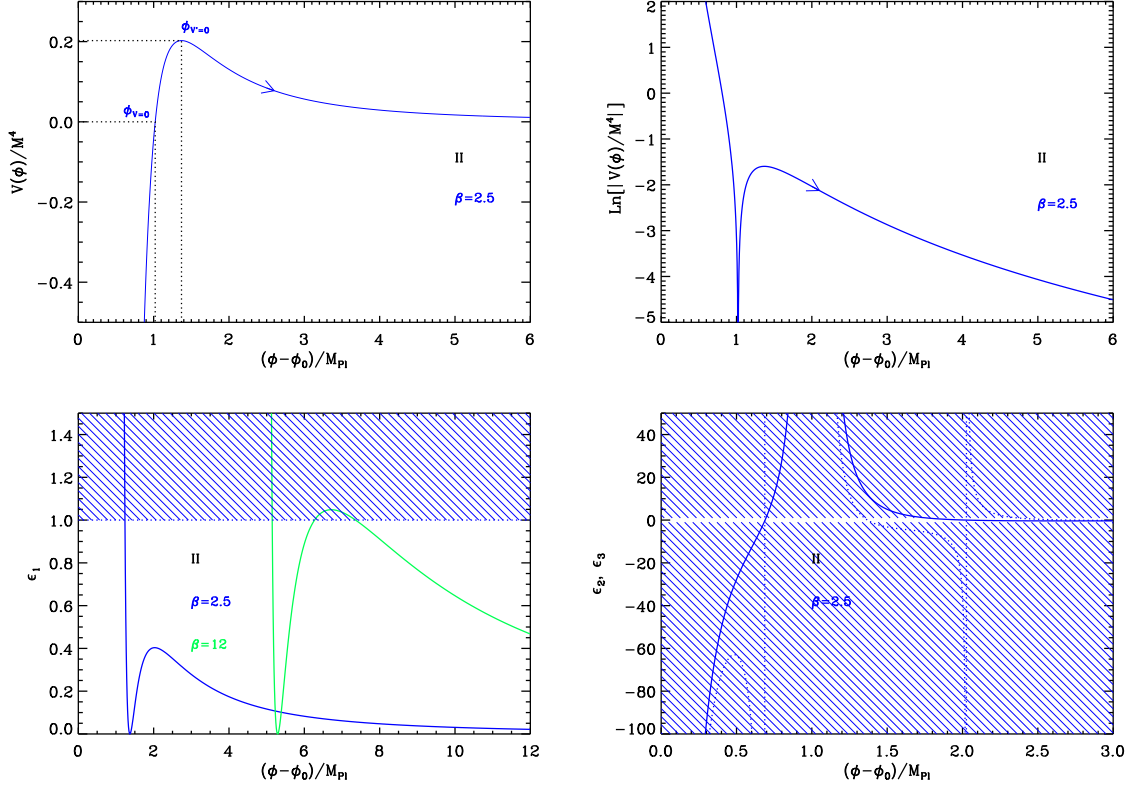


Figure 40. Intermediate Inflation (II). Upper panels: the potential and its logarithm for $\beta = 2.5$. Bottom left panel: slow-roll parameter ϵ_1 for a potential with $\beta = 2.5$ and $\beta = 12$. The position of the maximum of ϵ_1 with respect to one depends on β . The shaded area indicates where inflation stops.. Bottom right panel: slow-roll parameters ϵ_2 (solid line) and ϵ_3 (dotted line) for a potential with $\beta = 2.5$.

and

$$\epsilon_3 = \frac{\beta [6x^2 - \beta(2 + \beta)] \left[\frac{\beta^5}{18} (2 + \beta) - \beta^3 (2 + \beta) x^2 + 6\beta (4 + \beta) x^4 - 12x^6 \right]}{\left(x^3 - \frac{\beta^2}{6} x \right)^2 [\beta^3 (\beta + 2) - 12\beta (\beta + 3) x^2 + 36x^4]}. \quad (5.26)$$

They are displayed in Fig. 40. The first slow-roll parameter diverges where the potential vanishes at $x_{V=0}$, decreases from here and vanishes at the maximum of the potential $x_{V'=0}$. Then it increases again, reaches a local maximum at $x_{\epsilon_1^{\text{max}}}$, and decreases to asymptotically vanish when x goes to infinity. The location $x_{\epsilon_1^{\text{max}}}$ is given by

$$x_{\epsilon_1^{\text{max}}} = \sqrt{\frac{\beta}{2} \left(1 + \frac{\beta}{3} + \sqrt{1 + \frac{4\beta}{9}} \right)}. \quad (5.27)$$

At this point, the maximum value of ϵ_1 is

$$\epsilon_1^{\max} = \frac{\beta}{9} \frac{\left(1 + 3\sqrt{1 + 4\beta/9}\right)^2}{\left(1 + \sqrt{1 + 4\beta/9}\right)^2 \left(1 + \beta/3 + \sqrt{1 + 4\beta/9}\right)}. \quad (5.28)$$

If $\beta < 9/2(1 + \sqrt{2}) \simeq 10.86$, this maximum value is smaller than one. In this case inflation cannot stop by slow-roll violation in the decreasing branch of the potential and an extra parameter x_{end} must be added to the model to specify the location where another mechanism such as e.g. tachyonic instability could trigger the end of inflation. If $\beta > 9/2(1 + \sqrt{2}) \simeq 10.86$, the local maximum value of ϵ_1 is higher than one and in the decreasing branch of the potential, either inflation takes place between $x_{V'=0}$ and the first solution of $\epsilon_1 = 1$, either it takes place between the second solution of $\epsilon_1 = 1$ and $x = \infty$. As will be shown below, only the latter case is consistent with the exact trajectory Eq. (5.22) which allows for an equation of state of the form of Eq. (5.18).

The slow-roll trajectory of the model can be obtained from Eq. (2.11). However, as already mentioned, a non-trivial and exact field evolution is given by Eq. (5.22). Written in terms of the number of e-folds $N - N_0 = \ln(a/a_0) = A(t^f - t_0^f)$, one obtains

$$x = \sqrt{x_{\text{end}}^2 + 2\beta(N - N_{\text{end}})}. \quad (5.29)$$

This expression is exact and does not involve any approximations. It can be compared to slow-roll trajectory which reads

$$N_{\text{end}} - N = \frac{1}{2\beta}(x_{\text{end}}^2 - x^2) + \frac{1}{6} \ln \left[x_{\text{end}}^2 - \frac{\beta(\beta + 2)}{6} \right] - \ln \left[x^2 - \frac{\beta(\beta + 2)}{6} \right], \quad (5.30)$$

where N_{end} is the number of e-folds at the end of inflation and N is the number of e-folds at some point when the scaled field vev is x . As mentioned above, the slow-roll trajectory should match the exact one in the decreasing branch of the potential. For $x \rightarrow \infty$, one can neglect the logarithmic terms in Eq. (5.30) and one indeed recovers Eq. (5.29). This is expected since, in this limit, the slow-roll parameters all go to zero and the slow-roll approximation becomes increasingly accurate. As a result, the domain of validity lies at $x \gg x_{V'=0}$, i.e. between the second solution of $\epsilon_1 = 1$ and $x = \infty$ and inflation cannot stop by slow-roll violation. This justifies the need of the extra-parameter x_{end} . This parameter is thus constrained to $x_{\text{end}} > x_{V'=0}$ and should be large enough to allow for a sufficient number of e-folding. In order to get $N_{\text{end}} - N_{\text{ini}}$ e-folds, making use of Eq. (5.29), one gets

$$x_{\text{end}} = \sqrt{x_{\text{ini}}^2 + 2\beta(N_{\text{end}} - N_{\text{ini}})}. \quad (5.31)$$

If $\beta > 9/2(1 + \sqrt{2}) \simeq 10.86$, x_{ini} is bounded from below by the highest solution of the equation $\epsilon_1 = 1$. This equation admits three solutions in that case, which, from the smallest

to the biggest, are given by

$$x_{\epsilon_1=1}^0 = -\frac{\beta}{3\sqrt{2}} + \frac{\sqrt{2}}{3} \frac{\beta^{4/3}}{\sqrt[3]{9+2\beta+i\sqrt{-81-36\beta+4\beta^2}}} + \frac{\beta^{2/3}}{3\sqrt{2}} \sqrt[3]{9+2\beta+i\sqrt{-81-36\beta+4\beta^2}}, \quad (5.32)$$

$$x_{\epsilon_1=1}^\mp = \frac{\beta}{3\sqrt{2}} + \frac{1 \mp i\sqrt{3}}{3\sqrt{2}} \frac{\beta^{4/3}}{\sqrt[3]{9+2\beta+i\sqrt{-81-36\beta+4\beta^2}}} + \left(1 \pm i\sqrt{3}\right) \frac{\beta^{2/3}}{6\sqrt{2}} \sqrt[3]{9+2\beta+i\sqrt{-81-36\beta+4\beta^2}}. \quad (5.33)$$

The first solution is located below the maximum of the potential $x_{\epsilon_1=1}^0 < x_{V'=0}$, while the two other ones are located beyond it $x_{\epsilon_1=1}^\mp > x_{V'=0}$. Using the larger solution as a lower bound for x_{ini} , one gets

$$x_{\text{end}} > \sqrt{(x_{\epsilon_1=1}^+)^2 + 2\beta(N_{\text{end}} - N_{\text{ini}})}. \quad (5.34)$$

If $\beta < 9/2(1 + \sqrt{2})$, only one solution to $\epsilon_1 = 1$ exists,

$$x_{\epsilon_1=1} = -\frac{\beta}{3\sqrt{2}} + \frac{\sqrt{2}}{3} \frac{\beta^{4/3}}{\sqrt[3]{9+2\beta+\sqrt{81+36\beta-4\beta^2}}} + \frac{\beta^{2/3}}{3\sqrt{2}} \sqrt[3]{9+2\beta+\sqrt{81+36\beta-4\beta^2}}, \quad (5.35)$$

which is located below the maximum of the potential $x_{\epsilon_1=1}^0 < x_{V'=0}$. In principle x_{ini} is only bounded from below by $x_{V'=0}$ in this case and the number of e-folds given by the slow-roll trajectory Eq. (5.30) diverges close to this potential maximum. As a result, provided x_{ini} is fine-tuned close to $x_{V'=0}$, there is no bound on x_{end} . The prior space described by these relations is displayed in Fig. 41.

According to the previous discussion, the observable field value, at which the pivot mode crossed the Hubble radius during inflation, is such that $x_* \gg 1$. In this limit, it is possible to approximate the slow-roll parameters at Hubble crossing with

$$\epsilon_1^* \simeq \frac{\beta^2}{2x_*^2}, \quad \epsilon_2^* \simeq \epsilon_3^* \simeq -\frac{2\beta}{2x_*^2}, \quad (5.36)$$

hence

$$r \simeq \frac{8\beta^2}{x_*^2}, \quad n_s - 1 \simeq \frac{\beta(2-\beta)}{x_*^2}, \quad \alpha_s = \frac{2\beta^2(\beta-2)}{x_*^4}. \quad (5.37)$$

These estimates match with those of Ref. [387]. Finally, the parameter M is obtained from the amplitude of the CMB anisotropies

$$\left(\frac{M}{M_{\text{Pl}}}\right)^4 = 720\pi^2 \left[\frac{\beta^2(\beta+2)}{6} - \beta x_*^2\right]^2 \left[x_*^3 - \frac{\beta^2 x_*}{6}\right]^{-2} \left[x_*^{-\beta} - \frac{\beta^2}{6} x_*^{-\beta-2}\right] \frac{Q_{\text{rms-PS}}^2}{T^2}. \quad (5.38)$$

In the $x_* \gg 1$ limit, this gives

$$\frac{M^4}{M_{\text{Pl}}^4} \simeq 720\pi^2 \beta^2 x_*^{-2-\beta} \frac{Q_{\text{rms-PS}}^2}{T^2}, \quad (5.39)$$

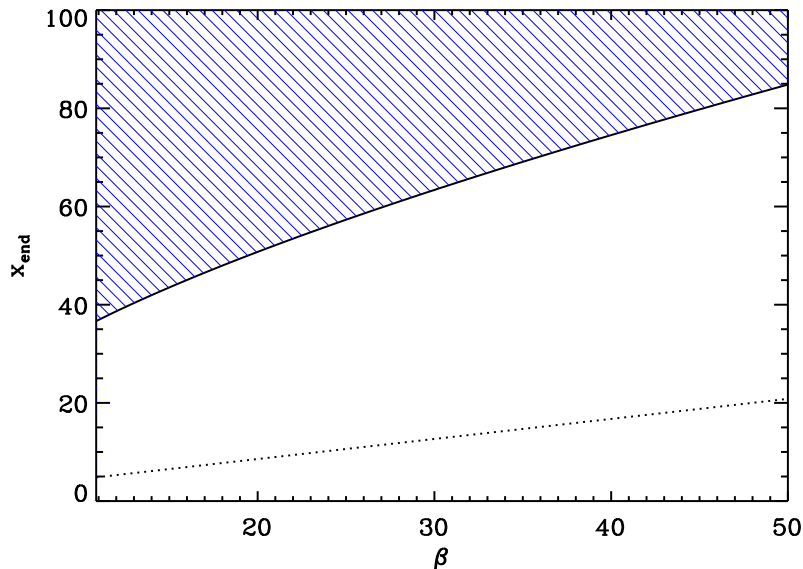


Figure 41. Prior space on x_{end} derived from Eq. (5.34) with $N_{\text{end}} - N_{\text{ini}} = 60$, as a function of $\beta > 9/2(1 + \sqrt{2})$ (black solid line). The black dotted line corresponds to $x_{V'=0}$. For $\beta < 9/2(1 + \sqrt{2})$, provided some fine-tuning on the initial conditions, x_{end} can take any values. The dashed area corresponds to parameters for the model which produce at least the required number of e-folds.

which yields $M/M_{\text{Pl}} \lesssim 10^{-2}$.

The reheating consistent slow-roll predictions for the intermediate inflation models are displayed in Fig. 101, for different values of $\beta > 0$, and for x_{end} describing the prior space displayed in Fig. 41. The reheating equation of state parameter \bar{w}_{reh} has been taken to 0 but since there is no potential minimum around which the inflaton field can oscillate at the end of inflation, this parameter is a priori unspecified and can take different values. In any case the reheating temperature is fully degenerate with the parameter x_{end} , and therefore these two parameters can not be constrained independently. However one can see that x_{end} is clearly limited from below as expected. The black solid lines represent the locus of the points such that $\epsilon_1^* = -\beta/4\epsilon_2^*$, or equivalently, $n_s - 1 = (1/\beta - 1/2)r/4$, these consistency relations arising from Eqs. (5.36). One can check that they provide a good qualitative description of the model predictions. In particular, they explain why, for $\beta < 2$, one has a blue tilt $n_s > 1$.

5.3 Kähler Moduli Inflation II (KMIII)

These models are string motivated scenarios. They arise in the context of type IIB string theory via Calabi-Yau flux compactification. They have been derived and studied in Refs. [254–260], and a two-field generalization of this model has been investigated in Refs. [255–259]. More precisely, when the internal spaces are weighted projective spaces, one of the Kähler moduli can play the role of an inflaton field, and its potential reads, in the “large field limit” (an accurate definition is given below), $V(\phi) = M^4 [1 - \alpha\phi/M_{\text{Pl}} \exp(-\beta\phi/M_{\text{Pl}})]$. This toy model potential is studied as “Kähler Moduli Inflation I (KMII)” in section 4.9. But, in fact, the field is not canonically normalized since it is a modulus. It is therefore necessary to first canonically normalize it and, then, re-derive the potential in terms of this canonically

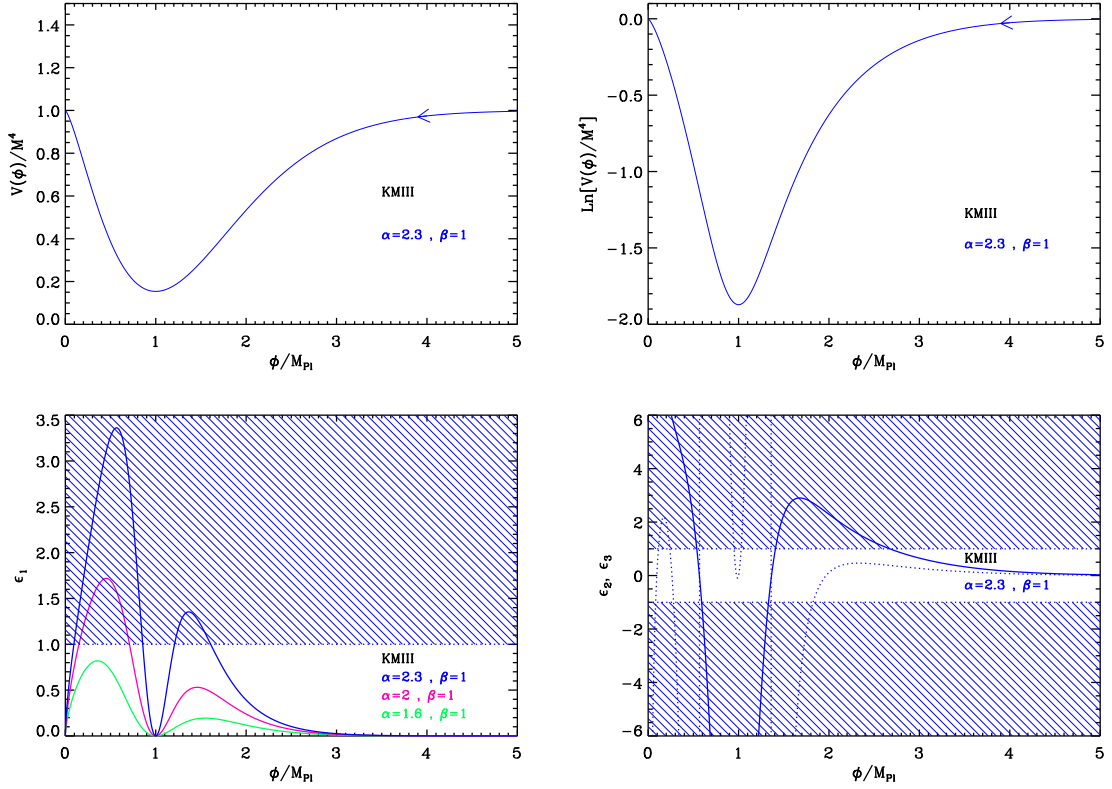


Figure 42. Top left panel: Kähler moduli inflation II (KMIII) potential for $\alpha = 2.3$ and $\beta = 1$. Top right panel: logarithm of the potential for the same value of α and β . Bottom left panel: slow-roll parameter ϵ_1 for a potential with $\alpha = 1.6$ (green solid line), 2 (pink solid line), 2.3 (blue solid line) and $\beta = 1$. Clearly, the number of solutions of the equation $\epsilon_1 = 1$ depends on the value of α and β . The shaded area indicates the breakdown of the slow-roll inflation (strictly speaking when the acceleration stops). Bottom right panel: slow-roll parameters ϵ_2 (solid line) and ϵ_3 (dotted line) for $\alpha = 2.3$ and $\beta = 1$. The values of α and β chosen here may not be physical: they have just been chosen for the sake of illustration.

normalized inflaton field. Following this procedure, one arrives at

$$V(\phi) = M^4 \left[1 - \alpha \left(\frac{\phi}{M_{\text{Pl}}} \right)^{4/3} e^{-\beta(\phi/M_{\text{Pl}})^{4/3}} \right]. \quad (5.40)$$

which is the potential that we study in this section. Let us now see what are the typical values that the parameters can take. In the context of IIB flux compactification, making use of the canonical notations used in the references cited above, they can be expressed as

$$M^4 = \frac{3}{4} \xi \frac{\hat{W}_0^2}{\mathcal{V}_s^3}, \quad \alpha = a_n \left(\frac{3\mathcal{V}_s}{4\lambda} \right)^{2/3}, \quad \beta = \frac{4\hat{W}_0 a_n \hat{A}_n}{M^4 \mathcal{V}_s^2} \left(\frac{3\mathcal{V}_s}{4\lambda} \right)^{2/3}. \quad (5.41)$$

The quantity \mathcal{V}_s represents the Calabi-Yau volume and is supposed to be such that $\mathcal{V}_s \gg 1$. In Ref. [260] the typical value $\mathcal{V}_s \sim 3 \times 10^6$ was chosen. The parameter A_n depends on the complex structure moduli and is typically of order $\mathcal{O}(1)$. One has $a_n = 2\pi/N$, where N is a

positive integer (for $D3$ -brane instantons, one has $N = 1$). The dimensionless parameter \hat{W}_0 is defined by $\hat{W}_0 = W_0/\ell_s^4$, W_0 being the tree level value of the superpotential and ℓ_s being the string length. It is usually considered that \hat{W}_0 is of order $\mathcal{O}(1)$. The dimensionless parameter λ is model dependent but is considered to be of order $\mathcal{O}(1)$. Finally, $\xi = \zeta(3)\xi(\mathcal{M})/[2(2\pi)^3]$, where $\xi(\mathcal{M})$ is the Euler number of the internal Calabi-Yau space \mathcal{M} , is also of order $\mathcal{O}(1)$. Making use of these values, one typically obtains $\alpha \sim 10^5$ and $\beta \sim 10^{12}$. More generally, to summarize this discussion, one should remember that

$$\alpha = \mathcal{O}\left(\mathcal{V}_s^{2/3}\right), \quad \beta = \mathcal{O}\left(\mathcal{V}_s^{5/3}\right), \quad (5.42)$$

where $\mathcal{V}_s \gg 1$ is the Calabi-Yau volume. Finally, the potential Eq. (5.40) is derived under the assumption that $\exp\left[\beta(\phi/M_{\text{Pl}})^{4/3}\right] \gg \mathcal{V}_s^2$, which shall be referred to as the ‘‘large field’’ condition in the following.

The potential (5.40) and its logarithm are displayed in Fig. 42. $V(\phi)$ decreases from $V/M^4 = 1$ at $\phi = 0$, reaches a minimum at $\phi/M_{\text{Pl}} = \beta^{-3/4}$, and then increases to the asymptotic value $V/M^4 = 1$ when $\phi \rightarrow +\infty$. However, since the potential is derived under the large field assumption, only the increasing branch of the potential is relevant. Inflation proceeds from the right to the left along this branch. The minimum value of the potential at $\phi = M_{\text{Pl}}\beta^{-3/4}$ is given by $V_{\text{min}} = M^4[1 - \alpha/(\beta e)]$. Therefore, if one wants the potential to be definite positive everywhere, one must have $\alpha/\beta < e$. From Eq. (5.42), we see that this condition is naturally satisfied since $\alpha/\beta = \mathcal{O}(\mathcal{V}_s^{-1}) \ll 1$. Anyway, since the potential (5.40) is only valid in the large field region, this criterion does not play a crucial role in what follows.

Let us now calculate the three first Hubble flow parameters. Defining $x \equiv \phi/M_{\text{Pl}}$, they are given by

$$\epsilon_1 = \frac{8\alpha^2}{9} x^{2/3} e^{-2\beta x^{4/3}} \left(\frac{1 - \beta x^{4/3}}{1 - \alpha x^{4/3} e^{-\beta x^{4/3}}} \right)^2, \quad (5.43)$$

$$\epsilon_2 = \frac{8\alpha}{9} x^{-2/3} e^{-2\beta x^{4/3}} \frac{3\alpha x^{4/3} + \alpha\beta x^{8/3} + e^{\beta x^{4/3}} (1 - 9\beta x^{4/3} + 4\beta^2 x^{8/3})}{(1 - \alpha x^{4/3} e^{-\beta x^{4/3}})^2}, \quad (5.44)$$

and

$$\begin{aligned} \epsilon_3 = & \left\{ 8\alpha (1 - \beta x^{4/3}) \left[\alpha^2 x^{8/3} (9 + \beta x^{4/3}) - 2\alpha e^{\beta x^{4/3}} x^{4/3} (-4 + 19\beta x^{4/3} - 9\beta^2 x^{8/3} \right. \right. \\ & \left. \left. + 4\beta^3 x^4) - e^{2\beta x^{4/3}} (1 + 11\beta x^{4/3} - 30\beta^2 x^{8/3} + 8\beta^3 x^4) \right] \right\} \left\{ 9x^{2/3} (e^{\beta x^{4/3}} - \alpha x^{4/3})^2 \right. \\ & \left. \times \left[\alpha x^{4/3} (3 + \beta x^{4/3}) + e^{\beta x^{4/3}} (1 - 9\beta x^{4/3} + 4\beta^2 x^{8/3}) \right] \right\}^{-1}. \end{aligned} \quad (5.45)$$

Let us now study how inflation ends in this model. Inflation stops by violation of the slow-roll conditions, when $\epsilon_1 = 1$. As can be seen in Fig. 42, the number of solutions to this last equation depends on the value of α and β . For $\alpha/\beta < e$ (remember that $\alpha/\beta \ll 1$ is necessary in this model), the first slow-roll parameter ϵ_1 starts increasing from $\epsilon_1 = 0$ at $x = 0$, reaches a first local maximum, and then decreases to vanish at $x = \beta^{-3/4}$. Then, it increases again, reaches a second local maximum and, finally, asymptotically vanishes when $x \rightarrow \infty$. Whether this second maximum is larger than one or not depends on the value of α

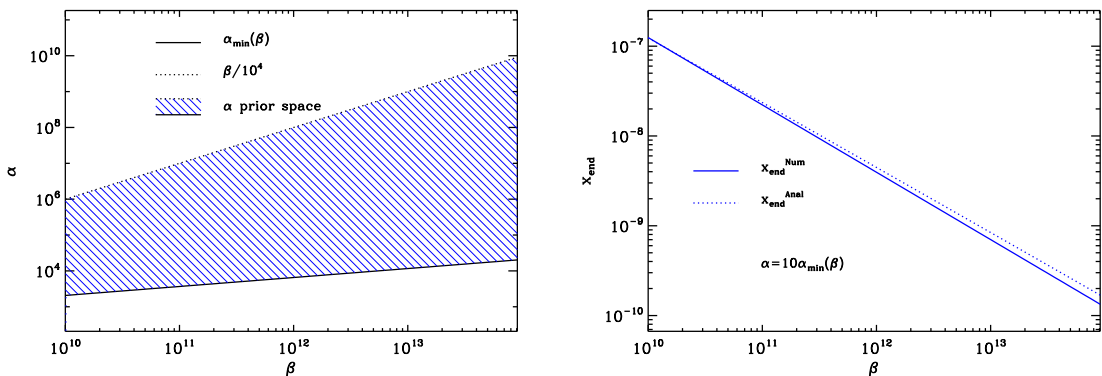


Figure 43. Left panel: allowed region (“prior space”) in the parameter plane (α, β) for the KMIII model. For a given β , the lower bound on α is determined from the condition that inflation stops by violation of the slow-roll conditions, i.e. such that a solution to the equation $\epsilon_1 = 1$ exists in the increasing branch of the potential. This lower bound must be determined numerically due to the complexity of the equation $\epsilon_1 = 1$. Recalling that $\alpha/\beta = \mathcal{O}(\mathcal{V}_s^{-1}) \sim 10^{-6} \ll 1$, the condition $\alpha < \beta/10^{-4}$ is a reasonable choice for an upper bound. It is represented by the dotted line. Therefore, the allowed region corresponds to the shaded region where the two conditions are satisfied. Right panel: comparison between the exact numerical value of $x_{\text{end}}(\beta)$ (blue solid line), and the approximated formula given by Eq. (5.46) (blue dotted line) for $\alpha = 10\alpha_{\text{min}}(\beta)$. The agreement is good enough for a qualitative discussion, but a numerical calculation of x_{end} is required for an accurate computation.

and β . It turns out that this is the case if α is large enough, $\alpha > \alpha_{\text{min}}(\beta)$, where the function $\alpha_{\text{min}}(\beta)$ needs to be computed numerically and is displayed in the left panel in Fig. 43. The condition $\alpha_{\text{min}}(\beta) < \alpha \ll \beta$ thus defines the allowed range of variation for the parameter α . For the value of x_{end} itself, it is not possible to find an exact expression due to the complexity of the equations but one can provide the following approximated formula,

$$x_{\text{end}} = x_{\epsilon_1=1}^+|_{x>1} \simeq \left[-\frac{1}{4\beta} W_{-1} \left(-\frac{81}{16\beta} \right) \right]^{3/4}, \quad (5.46)$$

where W_{-1} is the Lambert function. It is interesting to notice that the above expression is in fact independent of α . It is compared to the exact numerical solution for x_{end} in the right panel of Fig. 43. The agreement is good enough for a qualitative discussion but not sufficient for an accurate competition. In the ASPIC code, the exact solution is of course used.

Let us now turn to the slow-roll trajectory. Unfortunately, KMIII is one of the rare cases where it cannot be integrated analytically (of course, in the ASPIC code, the slow-roll trajectory is determined exactly). However, in the large field limit $x \gg \beta^{-3/4}$, one can obtain the following expression

$$N_{\text{end}} - N \simeq \frac{9}{16\alpha\beta^2} \left(\frac{e^{\beta x^{4/3}}}{x^2} - \frac{e^{\beta x_{\text{end}}^{4/3}}}{x_{\text{end}}^2} \right), \quad (5.47)$$

from which one deduces that

$$x = \left(-\frac{3}{2\beta} W_{-1} \left\{ -\frac{2}{3}\beta \left[\frac{e^{\beta x_{\text{end}}^{4/3}}}{x_{\text{end}}^2} + \frac{16\alpha\beta^2}{9} (N_{\text{end}} - N) \right]^{-2/3} \right\} \right)^{3/4}, \quad (5.48)$$

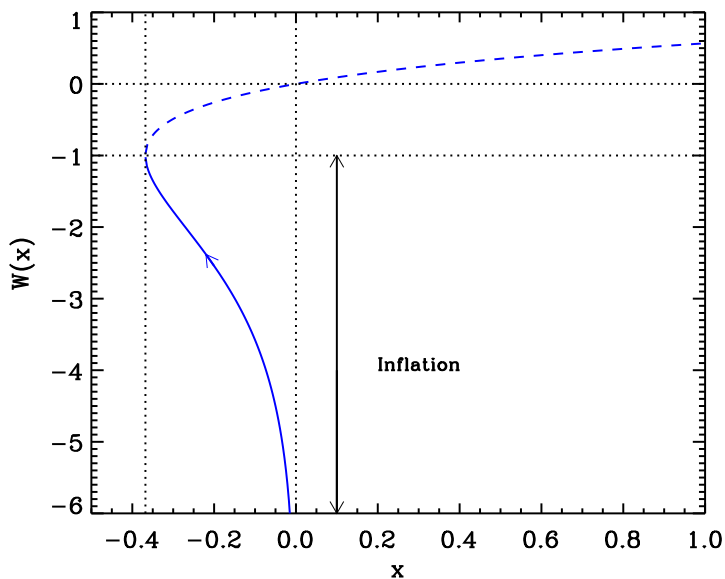


Figure 44. Lambert functions $W_0(x)$ (dashed line) and $W_{-1}(x)$ (solid line). During Kähler moduli inflation II, inflation proceeds along the “-1” branch in the direction specified by the arrow.

in agreement with what was obtained in Ref. [260] (despite the fact that, in Ref. [260], the wrong branch of the Lambert function was chosen). The Lambert function is displayed in Fig. 44 and the part of the curve where inflation proceeds is indicated by the arrow. The fact that the -1 branch of the Lambert function has to be chosen comes from the fact that, when $N_{\text{end}} - N \rightarrow \infty$, one must have $x \rightarrow \infty$. On the other hand, when $N_{\text{end}} - N \rightarrow 0$, $x \rightarrow x_{\text{end}} > \beta^{-3/4}$ and this is consistent with the choice of the -1 branch.

Finally, one can use the CMB normalization to calculate the mass scale M . Without any approximation this time, this leads to the following expression gives

$$\left(\frac{M}{M_{\text{Pl}}}\right)^4 = 1280\pi^2 \alpha^2 x_*^{2/3} e^{-2\beta x_*^{4/3}} \left(1 - \beta x_*^{4/3}\right)^2 \left(1 - \alpha x_*^{4/3} e^{-\beta x_*^{4/3}}\right)^{-2} \frac{Q_{\text{rms-PS}}^2}{T^2}. \quad (5.49)$$

Making use of the approximated trajectory, one has $x_* \propto \ln(\alpha\sqrt{\beta})/\beta$, from which one roughly obtains $M^4/M_{\text{Pl}}^4 \propto 1280\pi^2 \sqrt{\beta} Q_{\text{rms-PS}}^2/T^2$, and the scale M is of the order of the Planck mass.

The reheating consistent slow-roll predictions for the Kähler moduli inflation II models are displayed in Fig. 102, for $10^9 < \beta < 10^{15}$, and $\alpha_{\text{min}}(\beta) < \alpha < \beta/100$. For a given value of β , the slow-roll predictions do not depend significantly on α , so that the predictions are the same for different values of α within the allowed range. Also, we notice that ϵ_1 is typically extremely small and that ϵ_2 is almost independent of β . Let us see how one can get analytical estimates describing these results. Working out Eq. (5.46) and Eqs. (5.43), (5.44), and (5.45) in the large field limit, one obtains

$$\epsilon_{1*} \simeq \frac{9}{2\Delta N_* \beta^{3/2}} \ln^{-1/2} \left(\frac{16\alpha\beta^2}{9} \Delta N_* \right), \quad \epsilon_{2*} \simeq \frac{2}{\Delta N_*}, \quad \epsilon_{3*} \simeq \frac{1}{\Delta N_*}, \quad (5.50)$$

from which one deduces that

$$n_s \simeq 1 - \frac{2}{\Delta N_*}, \quad r \simeq \frac{72}{\Delta N_* \beta^{3/2}} \ln^{-1/2} \left(\frac{16\alpha\beta^2}{9} \Delta N_* \right), \quad \alpha_s \simeq -\frac{2}{\Delta N_*^2}. \quad (5.51)$$

Several comments are in order here. First, we see that the slow-roll parameters at Hubble crossing depend on α logarithmically only. This explains the weak dependence noticed in Fig. 102 and discussed before. Second, we also notice that ϵ_{2*} and ϵ_{3*} do not depend on β . Third, ϵ_1 is a very small number since it is proportional to the inverse of $\beta^{3/2}$. This also means that, when β increase, ϵ_1 decreases. All these considerations can be checked in Fig. 102. This implies that the amount of gravitational waves predicted by this model is very small. This is in agreement with the rough estimates given in Refs. [254, 257, 258, 260]. However, contrary to what is claimed in Ref. [260], the predicted value for the running of the spectral index is not excluded by observations since, according to WMAP9 [66, 67], $\alpha_s = -0.019 \pm 0.025$ while, for the fiducial value $\Delta N_* \simeq 55$, one obtains $\alpha_s \simeq -0.0006$.

5.4 Logamediate Inflation (LMI)

Logamediate inflation has been discussed in Refs. [396, 397] and refers to inflationary scenarios in which the scale factor evolves according to

$$a(t) = a_0 \exp \left[A \left(\ln \frac{t}{t_0} \right)^\lambda \right], \quad (5.52)$$

where A and λ are two dimensionless parameters and where t_0 has the dimension of a cosmic time. This evolution form for the scale factor is required to occur “at late times”, i.e. when $t \gg t_0$. If $\lambda = 1$, one recovers the power law model (see section 4.8), and in that case, t_0 can be absorbed in a rescaling of the scale factor. Otherwise, these three parameters are relevant and one therefore expects LMI to be a two parameters models according to our classification. Following Ref. [396], from Eq. (5.52), one has

$$H \equiv \frac{\dot{a}}{a} = \frac{A\lambda}{t} \left(\ln \frac{t}{t_0} \right)^{\lambda-1}, \quad (5.53)$$

from which one deduces that $A\lambda > 0$ in order to have expansion ($H > 0$). From Eq. (5.52), one can also establish that

$$\frac{\ddot{a}}{a} = \frac{A\lambda}{t^2} \left(\ln \frac{t}{t_0} \right)^{\lambda-1} \left[(\lambda-1) \left(\ln \frac{t}{t_0} \right)^{-1} - 1 + A\lambda \left(\ln \frac{t}{t_0} \right)^{\lambda-1} \right], \quad (5.54)$$

from which one deduces that in order to have inflation at late times (when $t \gg t_0$), one must have $\lambda > 1$, or if $\lambda = 1$, $A > 1$.

If this inflationary scenario is implemented within a single minimally coupled scalar field ϕ , one can derive the corresponding potential. From the Friedmann-Lemaître and Klein-Gordon equations one can show that [396]

$$\frac{\dot{\phi}(t)}{M_{\text{Pl}}} = \frac{\sqrt{2A\lambda}}{t} \left(\ln \frac{t}{t_0} \right)^{\frac{\lambda-1}{2}}. \quad (5.55)$$

This equation can easily be integrated into

$$\frac{\phi(t)}{M_{\text{Pl}}} = \frac{\phi_0}{M_{\text{Pl}}} + 2 \frac{\sqrt{2A\lambda}}{\lambda+1} \left(\ln \frac{t}{t_0} \right)^{\frac{\lambda+1}{2}}. \quad (5.56)$$

Combining the Friedmann-Lemaître equation $3M_{\text{Pl}}^2 H^2 = V(\phi) + \dot{\phi}^2/2$ and the relation $2M_{\text{Pl}}^2 \dot{H} = -\dot{\phi}^2$, one obtains $V(\phi) = 3M_{\text{Pl}}^2 H^2 + M_{\text{Pl}}^2 \dot{H}$, namely

$$V(\phi) = \frac{3M_{\text{Pl}}^2 A^2 \lambda^2}{t^2} \left(\ln \frac{t}{t_0} \right)^{2(\lambda-1)} + \frac{M_{\text{Pl}}^2 A \lambda}{t^2} (\lambda-1) \left(\ln \frac{t}{t_0} \right)^{\lambda-2} - \frac{M_{\text{Pl}}^2 A \lambda}{t^2} \left(\ln \frac{t}{t_0} \right)^{\lambda-1}. \quad (5.57)$$

Together with Eq. (5.56), this gives a parametric representation of the field potential in terms of t . It can be further simplified since the logamediate regime occurs in the limit $t \gg t_0$. If $\lambda > 1$, the first term of this expression dominates at late times and one has $V(\phi) = 3M_{\text{Pl}}^2 A^2 \lambda^2 (\ln t/t_0)^{2(\lambda-1)} / t^2$. Defining $x \equiv (\phi - \phi_0) / M_{\text{Pl}}$, one makes use of Eq. (5.56) to obtain

$$V(\phi) = M^4 x^\alpha \exp(-\beta x^\gamma), \quad (5.58)$$

where the new parameters are defined by

$$\alpha = 4 \frac{\lambda-1}{\lambda+1}, \quad \beta = 2 \left[\frac{\lambda+1}{2\sqrt{2A\lambda}} \right]^{2/(\lambda+1)}, \quad \gamma = \frac{2}{\lambda+1}, \quad (5.59)$$

and

$$\frac{M^4}{M_{\text{Pl}}^4} = \frac{3A^2 \lambda^2}{M_{\text{Pl}}^2 t_0^2} \left(\frac{\lambda+1}{2\sqrt{2A\lambda}} \right)^{4\frac{\lambda-1}{\lambda+1}}. \quad (5.60)$$

The same potential has been studied for $\alpha = 2$, $\beta = 1/8$ and $\gamma = 2$ within tachyon inflation models in Ref. [398]. The case $\lambda = 1$ is particular. At late times, the first term and the last term must be kept in Eq. (5.57), such that $V(\phi) = (3A-1)AM_{\text{Pl}}^2/t^2$. In that situation, one has $x = \sqrt{2A} \ln t/t_0$, and the derived potential shares the same expressions for α , β and γ as in Eq. (5.59) but evaluated at $\lambda = 1$. There is a difference however because M^4 now reads $M^4 = (3A-1)AM_{\text{Pl}}^2/t_0^2$. We recover explicitly that $\lambda = 1$ corresponds to power law inflation and has already been treated in section 4.8.

In the following, we will work only with the derived parameters β , γ and M^4 , noticing that

$$\alpha = 4(1-\gamma). \quad (5.61)$$

The restrictions $A\lambda > 0$ and $\lambda \geq 1$ translates into the conditions $0 < \gamma \leq 1$ and $\beta > 0$. Following Ref. [397], since there is no fundamental reasons preventing it, we will generalize this model to any possible values of these parameters supporting inflation.

The three first Hubble flow functions in the slow-roll approximation read

$$\epsilon_1 = \frac{(\alpha - \beta\gamma x^\gamma)^2}{2x^2}, \quad \epsilon_2 = \frac{2}{x^2} [\alpha + \beta(\gamma-1)\gamma x^\gamma], \quad (5.62)$$

$$\epsilon_3 = \frac{\alpha - \beta\gamma x^\gamma}{x^2} \frac{2\alpha - \beta(\gamma-2)(\gamma-1)\gamma x^\gamma}{\alpha + \beta(\gamma-1)\gamma x^\gamma}. \quad (5.63)$$

The potential and the Hubble flow functions in the slow-roll approximation have been represented in Fig. 45.

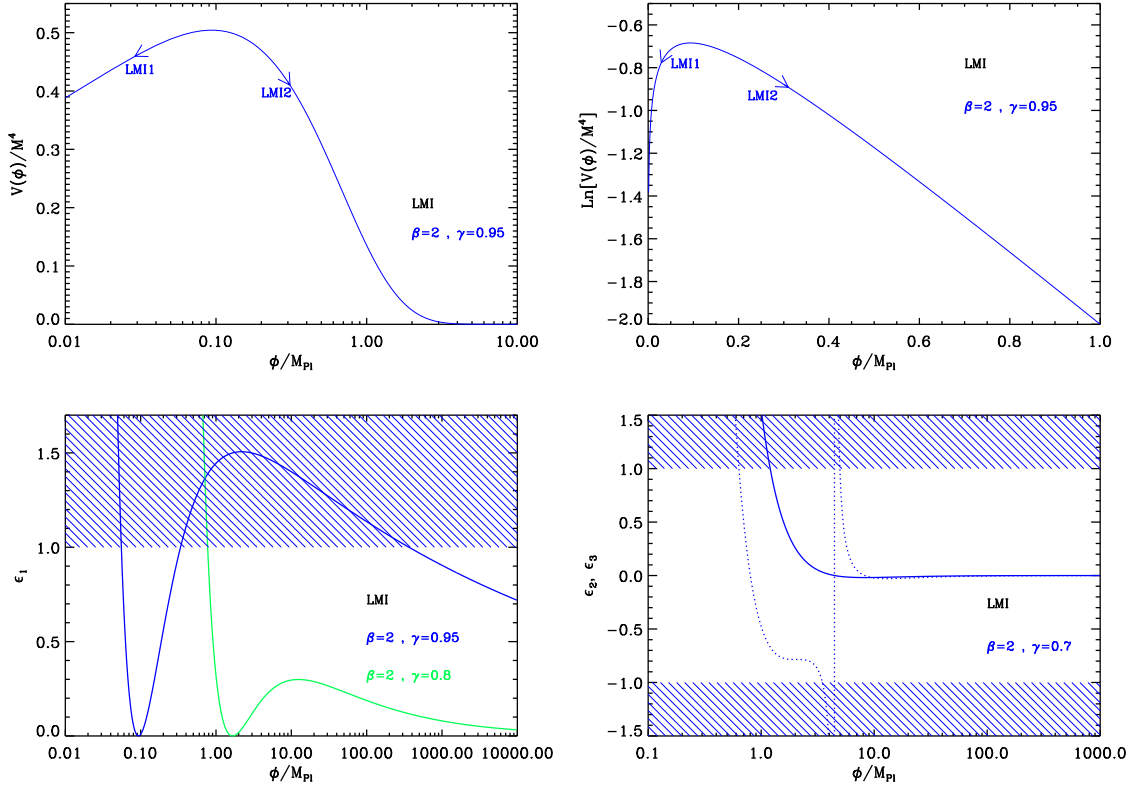


Figure 45. Logamediate Inflation (LMI). Upper panels: the potential and its logarithm for $\beta = 2, \gamma = 0.95$. Bottom left panel: Hubble flow function ϵ_1 for a potential with $\beta = 2, \gamma = 0.95$ (blue curve) and $\beta = 2, \gamma = 0.8$ (green curve). The position of the maximum of ϵ_1 with respect to one depends on γ . The shaded region indicates where inflation stops. Bottom right panel: slow-roll parameters ϵ_2 (solid line) and ϵ_3 (dotted line) for a potential with $\beta = 2, \gamma = 0.7$.

Inflation can proceed in two regimes: either at decreasing field values, left to the top of the potential (LMI1), or at increasing field values, right to the top of the potential (LMI2). Notice that from Eq. (5.56), ϕ has to increase with time to reproduce the scale factor expansion Eq. (5.52) and this happens only in the regime LMI2 for large values of x . As can be seen in Fig. 45, the slow-roll parameter ϵ_1 diverges when x approaches zero, it vanishes at the top of the potential for $x = x_{V^{\max}}$ and it is maximal at $x = x_{\epsilon_1^{\max}}$ with

$$x_{V^{\max}} \equiv \left(\frac{\alpha}{\beta\gamma} \right)^{1/\gamma}, \quad x_{\epsilon_1^{\max}} = \left[\frac{\alpha}{\beta\gamma(1-\gamma)} \right]^{1/\gamma}. \quad (5.64)$$

Finally it asymptotes to zero for large values of the field. The value of the local maximum of ϵ_1 reads

$$\epsilon_1^{\max} = \frac{\alpha^2}{2} \left[\frac{\beta\gamma(1-\gamma)}{\alpha} \right]^{\frac{2}{\gamma}} \left(\frac{\gamma}{1-\gamma} \right)^2. \quad (5.65)$$

Thus in the regime LMI1, inflation always stops naturally as ϵ_1 becomes larger than unity whereas in the regime LMI2, this may occur only if $\epsilon_1^{\max} > 1$ and if inflation has started from $x_{\text{ini}} < x_{\epsilon_1^{\max}}$. Otherwise, if inflation starts with $x_{\text{ini}} > x_{\epsilon_1^{\max}}$, or if $\epsilon_1^{\max} < 1$, one needs

to add an extra-parameter x_{end} encoding an unspecified mechanism to end inflation. In that situation, the model becomes a three parameters one. If one makes use of $\alpha = 4(1 - \gamma)$, one obtains $\epsilon_1^{\text{max}} = 8\gamma^2 (\beta\gamma/4)^{2/\gamma}$. Solving $\epsilon_1^{\text{max}} \geq 1$ for β gives

$$\beta \geq \frac{4}{\gamma(8\gamma^2)^{\gamma/2}}. \quad (5.66)$$

This condition is therefore required for the model LMI2, if one wants inflation to end naturally. As we will see below, LMI2 inflating in the domain $x_{V^{\text{max}}} < x < x_{\epsilon_1^{\text{max}}}$ is a very fine tuned situation which is strongly disfavored by the observations. Notice that if one assumes $0 < \gamma \leq 1$, this conditions translates into $\beta > \sqrt{2}$.

The slow-roll trajectory can be integrated thanks to the hypergeometric function [160, 161] ${}_2F_1$, leading to

$$N - N_{\text{end}} = \frac{x_{\text{end}}^2}{2\alpha} {}_2F_1 \left[1, \frac{2}{\gamma}, \frac{2}{\gamma} + 1, \left(\frac{x_{\text{end}}}{x_{V^{\text{max}}}} \right)^\gamma \right] - \frac{x^2}{2\alpha} {}_2F_1 \left[1, \frac{2}{\gamma}, \frac{2}{\gamma} + 1, \left(\frac{x}{x_{V^{\text{max}}}} \right)^\gamma \right]. \quad (5.67)$$

One can notice that inserting $\alpha = 4(1 - \gamma)$, as a function of $x/x_{V^{\text{max}}}$, this trajectory only involves γ . Plugging $x = x_{V^{\text{max}}}$ into Eq. (5.67) one gets an infinite number of e-folds. This means that the required number of e-folds to solve the problems of the standard Big-Bang scenario can always be realized, both in the decreasing branch of the potential and the increasing one, provided that inflation starts close enough to $x_{V^{\text{max}}}$. However, it can numerically be checked that in the case of LMI2 with $\epsilon_1^{\text{max}} > 1$ and inside the $x_{V^{\text{max}}} < x < x_{\epsilon_1^{\text{max}}}$ region, one has to fine tune x_{ini} and x_* extremely close to $x_{V^{\text{max}}}$. In that situation $n_s = 1$, with vanishing r and vanishing running of the spectral index, can be considered as generic predictions of the model. For this reason, it is more natural to consider LMI2 in the large field regime, namely $x > \max(x_{V^{\text{max}}}, x_{\epsilon_1^{\text{max}}})$, together with the extra-parameter x_{end} .

The trajectory in Eq. (5.67) cannot be inverted analytically. However, one can perform some consistency checks in the limit $x/x_{V^{\text{max}}} \gg 1$ in which

$$N - N_{\text{end}} \simeq \frac{1}{\beta\gamma(2 - \gamma)} \left(x^{2-\gamma} - x_{\text{end}}^{2-\gamma} \right), \quad (5.68)$$

and

$$x \simeq \left[x_{\text{end}}^{2-\gamma} + \beta\gamma(2 - \gamma)(N - N_{\text{end}}) \right]^{\frac{1}{2-\gamma}}. \quad (5.69)$$

These expressions can be compared to Eq. (5.56)

$$x = 2 \frac{\sqrt{2A\lambda}}{\lambda + 1} \left(\ln \frac{t}{t_0} \right)^{\frac{\lambda+1}{2}}, \quad (5.70)$$

where t in terms of the number of e-folds N can be obtained from Eq. (5.52). With $N - N_0 = A(\ln t/t_0)^\lambda$, one gets

$$x = 2 \frac{\sqrt{2A\lambda}}{\lambda + 1} \left(\frac{N - N_0}{A} \right)^{\frac{\lambda+1}{2\lambda}}. \quad (5.71)$$

The previous calculations are consistent since, making use of Eq. (5.59), Eq. (5.69) and Eq. (5.71) are the same when setting the constants $N_0 = N_{\text{ini}}$ and $x_0 = x_{\text{ini}} = 0$. This means that in the late times limit $x/x_{V^{\text{max}}} \gg 1$, the slow-roll trajectory coincides with the exact one, as expected.

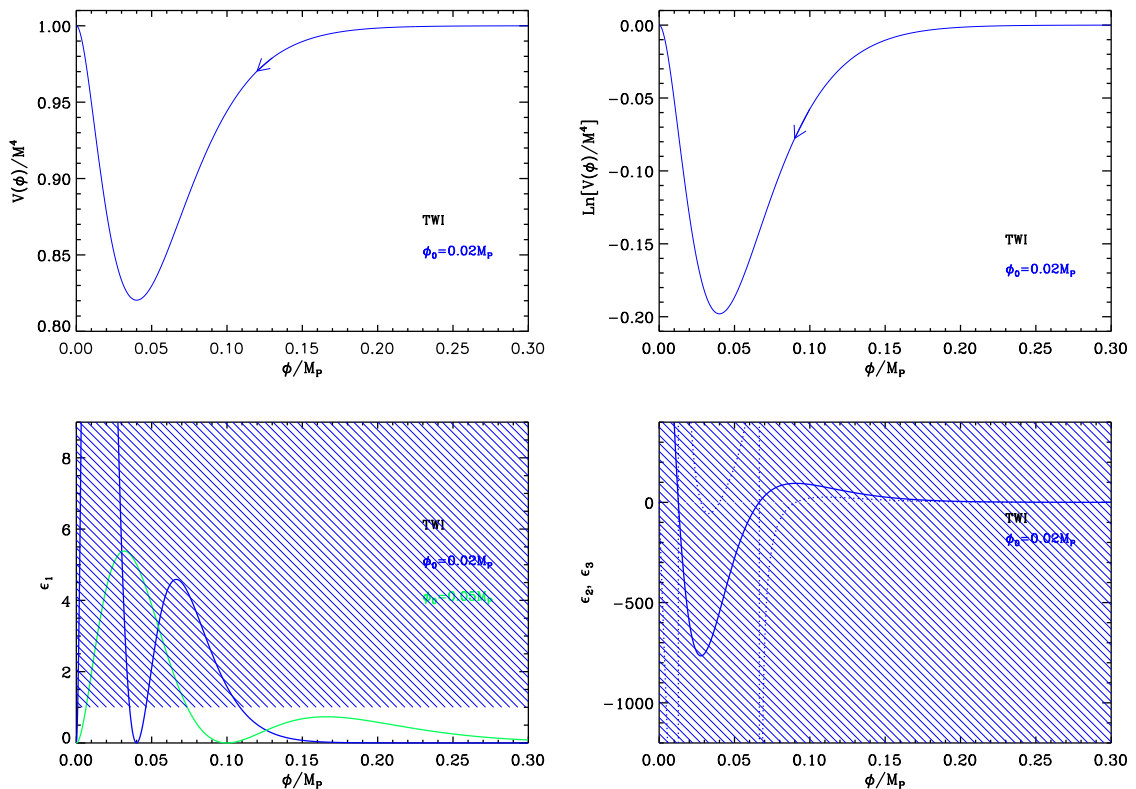


Figure 46. Top left panel: Twisted Potential Inflation (TWI) for $\phi_0 = 0.02M_{\text{Pl}}$. Top right panel: logarithm of the potential for the same value of ϕ_0 . Bottom left panel: slow-roll parameter ϵ_1 with $\phi_0 = 0.02M_{\text{Pl}}$ (solid blue line) and $\phi_0 = 0.05M_{\text{Pl}}$ (solid green line). The shaded area indicates the non-inflationary region. Bottom right panel: slow-roll parameters ϵ_2 (solid line) and ϵ_3 (dotted line) with $\phi_0 = 0.02M_{\text{Pl}}$.

The amplitude of the CMB anisotropies fixes the value of the parameter M according to

$$\frac{M^4}{M_{\text{Pl}}^4} = 720\pi^2 (\alpha - \beta\gamma x_*^\gamma)^2 e^{\beta x_*^\gamma} x_*^{-\alpha-2} \frac{Q_{\text{rms-PS}}^2}{T^2}, \quad (5.72)$$

where x_* is the observable field value obtained by solving Eq. (2.46) given some assumptions on the reheating. The reheating consistent slow-roll predictions for the models LMI1 and LMI2 (at $x > x_{e_1}^{\text{max}}$) are displayed in Figs. 103, 104, and 105 for LMI1, and in Figs. 106, 107, and 108 for LMI2. In the case of LMI2, the turning points in the plots precisely correspond to the case where inflation occurs in the fine-tuned domain $x_{V^{\text{max}}} < x_* < x_{e_1}^{\text{max}}$ and in which the model behaves like a pure de Sitter era.

5.5 Twisted Inflation (TWI)

This model was introduced in Ref. [399] and is based on higher dimensional supersymmetric gauge theory compactified to four dimensions and with twisted supersymmetry breaking boundary conditions. These boundary conditions lead to a potential for directions in field space that would have been flat if supersymmetry were not broken. If the field values in

these directions are much larger than the supersymmetry-breaking scale, then the flatness of the potential is nearly restored. In a 4 + 1 dimensional maximally supersymmetric gauge theory on a circle, with antiperiodic boundary conditions for fermions, the inflaton potential can be calculated directly in field theory by integrating out the heavy W-bosons and their superpartners (if the theory is weakly coupled at the compactification scale). This leads to the following expression

$$V(\phi) = M^4 \left[1 - A \left(\frac{\phi}{\phi_0} \right)^2 e^{-\phi/\phi_0} \right], \quad (5.73)$$

where A is a constant parameter given by

$$A \equiv \frac{32}{93\zeta(5)} \simeq 0.33, \quad (5.74)$$

and where ϕ_0 is the supersymmetry breaking scale, which must be sub-Planckian in order for Planck suppressed operators to be ignored in the derivation of the model, $\phi_0 \ll M_{\text{Pl}}$. The potential (5.73) is the small coupling limit of the model, while the strong coupling limit corresponds to a DSI model with $p = 3$, see section 6.3.

The potential Eq. (5.73), as well as its logarithm, is displayed in Fig. 46. Inflation is supposed to take place above the supersymmetry scale, at $\phi > \phi_0$, i.e. in the increasing branch of the potential. This means that it proceeds from the right to the left in the direction indicated by the arrow. The minimum of the potential is located at $\phi/\phi_0 = 2$.

Let us now turn to the calculation of the Hubble flow parameters. If one defines x by $x \equiv \phi/\phi_0$, then they are given by

$$\epsilon_1 = \frac{A^2}{2} \left(\frac{M_{\text{Pl}}}{\phi_0} \right)^2 e^{-2x} \left[\frac{x(x-2)}{1 - Ax^2 e^{-x}} \right]^2, \quad \epsilon_2 = 2A \left(\frac{M_{\text{Pl}}}{\phi_0} \right)^2 e^{-2x} \frac{2Ax^2 + e^x(x^2 - 4x + 2)}{(1 - Ax^2 e^{-x})^2}, \quad (5.75)$$

and

$$\epsilon_3 = A \left(\frac{M_{\text{Pl}}}{\phi_0} \right)^2 x(2-x) e^{-2x} \frac{4A^2 x^3 - e^{2x}(x^2 - 6x + 6) - A x e^x(x^3 - 6x^2 + 18x - 12)}{(1 - Ax^2 e^{-x})^2 [2Ax^2 + e^x(x^2 - 4x + 2)]}. \quad (5.76)$$

They are displayed in Fig. 46. The first slow-roll parameter ϵ_1 vanishes at the minimum of the potential when $x = 2$, then increases with x and reaches a maximum at $x_{\epsilon_1^{\text{max}}}$, and then decreases to zero when x goes to infinity. The value of ϵ_1 at this local maximum is larger than one if ϕ_0 is smaller than some value that can only be determined numerically. We find

$$\phi_0 < 0.04228 M_{\text{Pl}}. \quad (5.77)$$

Therefore, a priori, one could conclude that inflation can stop by slow-roll violation. However, if one numerically integrates the exact trajectory (i.e. if one does not make use of the slow-roll approximation) and computes the evolution of the first slow-roll first parameter, which is defined by $\epsilon_1^H = -\dot{H}/H^2$, then one observes that it always remains smaller than one, see Fig. 47. This is due to the fact that while the inflaton rolls down its potential and approaches its minimum, the slow-roll parameters continuously increase. When ϵ_1 becomes of order $\mathcal{O}(1)$, the slow-roll approximation breaks down. Usually, this leads only to small corrections at the end of inflation. However, in the case of twisted inflation, this leads to

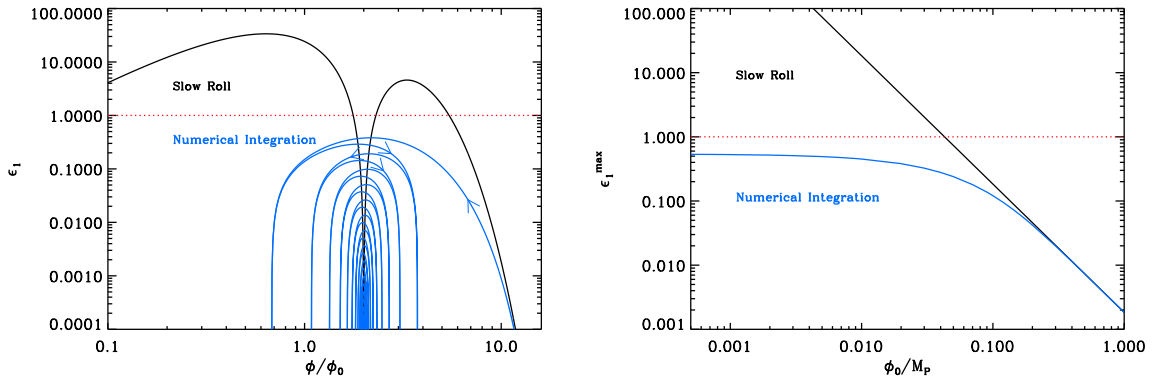


Figure 47. Left panel: slow-roll parameter ϵ_1 as a function of the field *vev* ϕ/ϕ_0 , for $\phi_0/M_{\text{Pl}} = 0.02 < 0.04228$, see Eq. (5.77). The solid black line corresponds to the approximated slow-roll formula (5.75), i.e. $\epsilon_1^V = M_{\text{Pl}}^2/2 V_\phi^2/V^2$, while the solid blue line represents the exact $\epsilon_1^H = -\dot{H}/H^2$ obtained from a numerical integration starting at $\phi_{\text{ini}}/M_{\text{Pl}} = 0.33$ and vanishing initial velocity. We see that the exact ϵ_1^H remains in fact always smaller than one and that inflation never stops. The inflaton eventually oscillates around the minimum of its potential located at $\phi = 2\phi_0$ (the arrows indicate the direction of the first oscillations). Right panel: Maximum value taken by ϵ_1^V (solid black line) and ϵ_1^H (solid blue line) for different values of ϕ_0 . One can see that ϵ_1^H remains smaller than one for any value of ϕ_0 . When ϕ_0 increases, the slow-roll parameters, which scale proportional to M_{Pl}^2/ϕ_0^2 , decrease so that the slow-roll approximation becomes more and more efficient and eventually starts matching the numerical exact predictions.

a radically different picture. The reason behind this phenomenon is just that the potential does not vanish at its minimum and, therefore, acts as a cosmological constant. In practice, the numerical calculations indicate that the field oscillate around its minimum but always such that $\epsilon_1^H < 1$ and independently on the value of ϕ_0 , see Fig. 47. This means that, in principle, inflation can never stops since the final stage of the evolution just corresponds to an inflaton field sitting for ever at the bottom of the potential and, as already mentioned, acting like a cosmological constant. However, as explained in Ref. [399], the interactions of the inflaton field with the other degrees of freedom of the standard model starts to play a role in this regime. As a consequence, the energy contained in the inflaton field is quickly transferred to other fields and a phase of reheating starts. The details of this process are complicated and are discussed in Ref. [399]. In order to model the end of inflation, one can just introduce an extra free parameter x_{end} that gives the *vev* at which inflation stops. As a consequence, TWI is in fact a two parameter model, ϕ_0 and ϕ_{end} .

Let us now turn to the slow-roll trajectory. It can be integrated exactly leads to the following expression

$$N_{\text{end}} - N = \left(\frac{\phi_0}{M_{\text{Pl}}}\right)^2 \left\{ \frac{1}{2A} [\text{Ei}(x_{\text{end}}) - \text{Ei}(x)] - \frac{e^2}{2A} [\text{Ei}(x_{\text{end}} - 2) - \text{Ei}(x - 2)] + x_{\text{end}} - x + 2 \ln\left(\frac{x_{\text{end}} - 2}{x - 2}\right) \right\}, \quad (5.78)$$

where N_{end} is the number of e-folds at the end of inflation and Ei is the exponential integral function [160, 161]. If one makes the vacuum dominated approximation, $x \gg 1$, then a simpler

formula can be derived for the trajectory, namely $N_{\text{end}} - N \simeq (\phi_0/M_{\text{Pl}})^2/A (e^x/x^2 - e^x_{\text{end}}/x_{\text{end}}^2)$. Of course, the TWI ASPIC code makes use of the exact trajectory. Then, this allows us to obtain an approximated expression for the vev of the field at Hubble radius crossing. One obtains

$$x_* \sim \ln \left[4A\Delta N_* \left(\frac{M_{\text{Pl}}}{\phi_0} \right)^2 \right], \quad (5.79)$$

which is valid if the condition $\phi_0/M_{\text{Pl}} \ll 1$ holds, i.e. precisely in the regime for which the TWI potential was derived. Using this formula, one can estimate the value of the three first Hubble flow parameters at Hubble crossing. One arrives at

$$\begin{aligned} \epsilon_{1*} &\simeq \frac{A^2}{2} \left(\frac{M_{\text{Pl}}}{\phi_0} \right)^2 e^{-2x_*} x_*^4 \sim \frac{1}{32\Delta N_*^2} \left(\frac{\phi_0}{M_{\text{Pl}}} \right)^2, \\ \epsilon_{2*} &\simeq \frac{\epsilon_{3*}}{2} \simeq 2A \left(\frac{M_{\text{Pl}}}{\phi_0} \right)^2 e^{-x_*} x_*^2 \sim \frac{1}{2\Delta N_*}. \end{aligned} \quad (5.80)$$

Finally, we can derive an expression for the tensor to scalar ratio, the spectral index

$$r \simeq 8A^2 \left(\frac{M_{\text{Pl}}}{\phi_0} \right)^2 e^{-2x_*} x_*^4 \sim \frac{1}{2\Delta N_*^2} \left(\frac{\phi_0}{M_{\text{Pl}}} \right)^2, \quad n_{\text{S}-1} \simeq -2A \left(\frac{M_{\text{Pl}}}{\phi_0} \right)^2 x_*^2 e^{-x_*} \sim \frac{1}{2\Delta N_*}, \quad (5.81)$$

and the running

$$\alpha_{\text{S}} \simeq -2A^2 \left(\frac{M_{\text{Pl}}}{\phi_0} \right)^4 x_*^4 e^{-2x_*} \sim -\frac{1}{8\Delta N_*^2}. \quad (5.82)$$

These estimates are in agreement with the ones of Ref. [399], the only difference being that the factor 4 appearing in Eq. (5.79) was not taken into account in that paper. However, we have checked that this does not affect the predictions in a significant way.

It is also interesting to discuss the value of the scale M since this is important from the model building point of view. The CMB normalization gives

$$\frac{M^4}{M_{\text{Pl}}^4} = 720\pi^2 A^2 \left(\frac{M_{\text{Pl}}}{\phi_0} \right)^2 \frac{[e^{-x_*} x_* (x_* - 2)]^2 Q_{\text{rms-PS}}^2}{(1 - Ax_*^2 e^{-x_*})^3 T^2}. \quad (5.83)$$

In vacuum dominated approximation, the above expression simplifies and gives $M^4/M_{\text{Pl}}^4 \simeq 45\pi^2/\Delta N_*^2 \phi_0^2/M_{\text{Pl}}^2 Q_{\text{rms-PS}}^2/T^2$. Typically, this leads to $M/M_{\text{Pl}} \sim 10^{-5}$ for $\phi_0/M_{\text{Pl}} \sim 10^{-4}$.

We are now in a position where we can discuss the exact predictions of the TWI model. They are presented in Fig. 109. The reheating equation of state parameter \bar{w}_{reh} has been taken to be 0 since the potential is quadratic close to its minimum. However, since the details of reheating depend on the details of the interactions between the inflaton field and the others degrees of freedom in the theory, this parameter is a priori unspecified and could very well take different values. In the ASPIC code, \bar{w}_{reh} can be freely chosen. Anyway, since the reheating temperature is in fact fully degenerate with the parameter x_{end} , these two parameters can not be constrained independently. One can check that the rough description provided by Eqs. (5.81) is correct: the model typically predicts a small amount of gravitational waves which increases with ϕ_0 , and a deviation from scale invariance which does not significantly depends on ϕ_0 . When $\phi_0/M_{\text{Pl}} \sim \mathcal{O}(1)$, however, one notices a turning point in the line representing the predictions (at fixed values of ϕ_0). This corresponds to the separation between two regimes, one where $x_* < x_{\epsilon_1^{\text{max}}}$ and ϵ_1 is an increasing function of x (hence ϵ_{1*}

increases with x_{end}) and another where $x_* > x_{\epsilon_1^{\text{max}}}$ and ϵ_1 is a decreasing function of x (hence ϵ_{1*} decreases with x_{end}). If a sufficient number of e-folds can be realized in the $2 < x < x_{\epsilon_1^{\text{max}}}$ part of the potential, then ϵ_{2*} can become negative. However, this mostly happens for values of x_{end} fine tuned around $x_{\text{end}} \simeq 2$.

5.6 Generalized MSSM Inflation (GMSSMI)

As for the MSSMI models, GMSSMI are based on the Minimal Supersymmetric Model (MSSM) in which the vanishing directions are lifted by a soft supersymmetry breaking mass term and by superpotential corrections. The potential is of the form

$$V(\phi) = \frac{1}{2}m_\phi^2\phi^2 - A\frac{\lambda_n}{n}\frac{\phi^n}{M_{\text{Pl}}^{n-3}} + \lambda_n^2\frac{\phi^{2(n-1)}}{M_{\text{Pl}}^{2(n-3)}}. \quad (5.84)$$

Details about this potential, the meaning of its parameters as well as typical values for them are given in section 4.17. There, it was discussed with $n = 6$ and in the particular case for which it contains a flat inflection point, i.e. when $A^2 = 8(n-1)m_\phi^2$. Following Refs. [351, 400–403], one may wonder whether the model is robust when this relation is not exactly satisfied, that is to say what is the amount of fine tuning involved in this flat inflection point condition. In this more general case, the potential can be reparametrized in the form

$$V(\phi) = M^4 \left[\left(\frac{\phi}{\phi_0} \right)^2 - \frac{2}{3}\alpha \left(\frac{\phi}{\phi_0} \right)^6 + \frac{\alpha}{5} \left(\frac{\phi}{\phi_0} \right)^{10} \right], \quad (5.85)$$

where $\phi_0 \simeq 10^{14}$ GeV and $M \simeq 10^8$ GeV, the later being obtained by the CMB normalization as in section 4.17. The positive dimensionless parameter α encodes any deviations from the MSSM case for which it equals unity, $\alpha_{\text{MSSM}} = 1$.

The potential is displayed in Fig. 48, where four cases can be distinguished. In the following, we define

$$x \equiv \frac{\phi}{\phi_0}. \quad (5.86)$$

If $\alpha < 9/25$, the second derivative of the potential do not vanish and the potential is convex everywhere. This corresponds to the case $\alpha = 0.1$ case in Fig. 48. If $9/25 < \alpha < 1$, the potential has two inflection points $x_{V''=0}^\pm$ and is concave in between. It remains an increasing function of the field since its first derivative never vanishes. This is illustrated with the case $\alpha = 0.7$ in Fig. 48. If $\alpha = 1$, this is the MSSM inflation models (see section 4.17) where the potential has a flat inflection point. If $1 < \alpha < 9/5$, the potential decreases in between $x_{V'=0}^\pm$ but remains positive everywhere. This is typical of the case $\alpha = 1.5$ in Fig. 48. Finally, if $\alpha > 9/5$, the potential becomes negative (hence is not properly defined) in between $x_{V=0}^\pm$ (see $\alpha = 2.5$ in Fig. 48). The values of the field *vev* appearing in this discussion are given by the following formulas:

$$x_{V''=0}^\pm = \left[\frac{5}{9} \left(1 \pm \sqrt{1 - \frac{9}{25\alpha}} \right) \right]^{1/4}, \quad x_{V'=0}^\pm = \left(1 \pm \sqrt{1 - \frac{1}{\alpha}} \right)^{1/4}, \quad (5.87)$$

and

$$x_{V=0}^\pm = \left[\frac{5}{3} \left(1 \pm \sqrt{1 - \frac{9}{5\alpha}} \right) \right]^{1/4}. \quad (5.88)$$

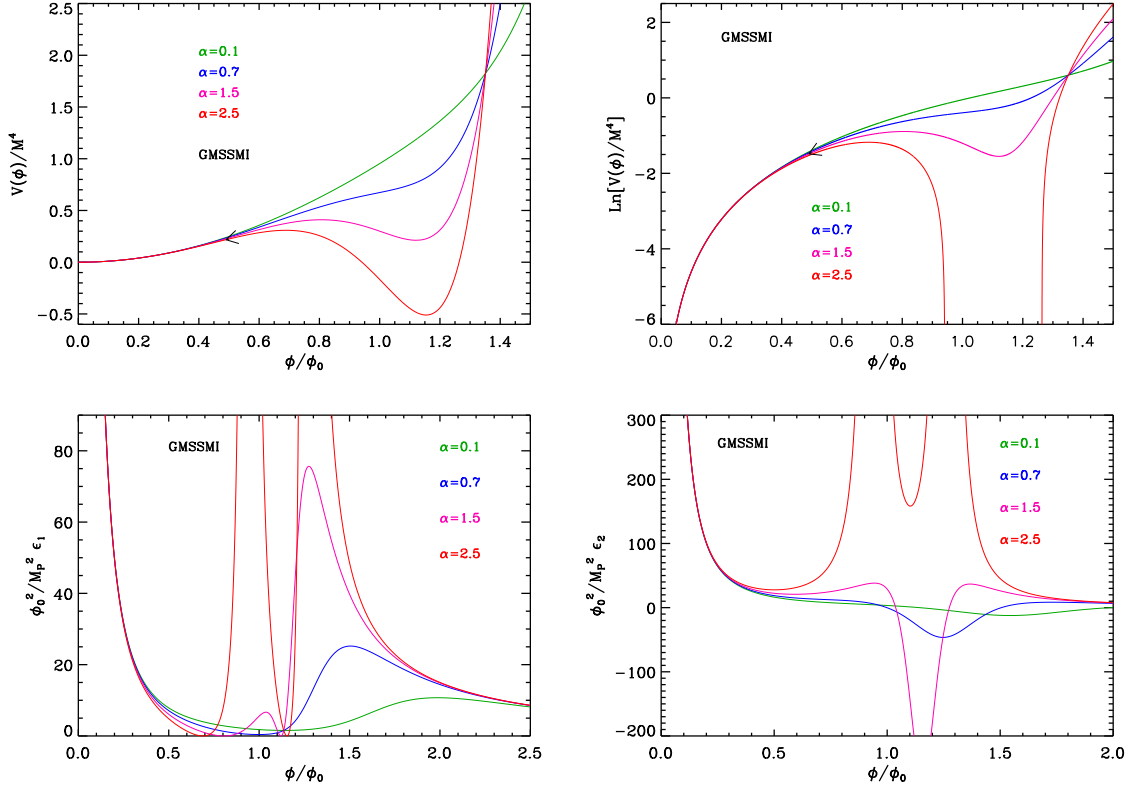


Figure 48. GMSSM Inflation (GMSSMI). Top left panel: GMSSM Inflation potential Eq. (5.85) for $\alpha = 0.1, 0.7, 1.5, 2.5$, as a function of ϕ/ϕ_0 . Top right panel: logarithm of the potentials for the same value of α . Bottom left panel: slow-roll parameter ϵ_1 for a potential with the same values of α . Bottom right panel: slow-roll parameter ϵ_2 for a potential with the same values of α . See discussion in the text body.

Let us now calculate the first Hubble flow functions in the slow-roll approximation. They are given by

$$\begin{aligned}\epsilon_1 &= 450 \left(\frac{M_{\text{Pl}}}{\phi_0} \right)^2 \frac{(1 - 2\alpha x^4 + \alpha x^8)^2}{x^2 (15 - 10\alpha x^4 + 3\alpha x^8)^2}, \\ \epsilon_2 &= 60 \left(\frac{M_{\text{Pl}}}{\phi_0} \right)^2 \frac{15 + 40\alpha x^4 + \alpha (20\alpha - 78) x^8 + 3\alpha^2 x^{16}}{x^2 (15 - 10\alpha x^4 + 3\alpha x^8)^2},\end{aligned}\tag{5.89}$$

and

$$\begin{aligned}\epsilon_3 &= 60 \left(\frac{M_{\text{Pl}}}{\phi_0} \right)^2 \left[225 - 1800\alpha x^4 + 60\alpha (69 + 10\alpha) x^8 - 40 (189 - 100\alpha) \alpha^2 x^{12} \right. \\ &\quad + 10\alpha^2 (243 - 504\alpha + 402\alpha^2) x^{16} + 40\alpha^3 (117 - 20\alpha) x^{20} + 12\alpha^3 (10\alpha - 123) x^{24} \\ &\quad + 72\alpha^4 x^{28} + 9\alpha^4 x^{32} \left. \right] \times [3375x^2 + 4500\alpha x^6 - 600\alpha (27 + 10\alpha) x^{10} \\ &\quad + 100\alpha^2 (261 - 20\alpha) x^{14} + 10\alpha^2 (200\alpha^2 - 840\alpha - 621) x^{18} + 60\alpha^3 (69 - 20\alpha) x^{22} \\ &\quad + 48\alpha^3 (10\alpha - 9) x^{26} - 180\alpha^4 x^{30} + 27\alpha^4 x^{34}]^{-1}.\end{aligned}\tag{5.90}$$

The first two slow-roll parameters diverge when $x \rightarrow 0$ and vanish asymptotically. In between, their shape depends on α as it is represented in Fig. 48. If $\alpha < 1$, ϵ_1 first decreases, reaches a local non zero minimum where ϵ_2 vanishes, then increases to reach a local maximum where ϵ_2 vanishes again, and eventually decreases again. Let $x_{\epsilon_2=0}^\pm$ be the position of these two local extrema. From Ferrari's solutions for depressed quartic equations one gets

$$x_{\epsilon_2=0}^\pm = \left[\frac{1}{2\alpha} \sqrt{\frac{5}{3}} \left(\sqrt{\Sigma} \pm 2 \sqrt{\frac{39}{5} \alpha - 2\alpha^2 - \frac{\Sigma}{4} - \frac{12}{\sqrt{15\Sigma}} \alpha^2} \right) \right]^{1/4}, \quad (5.91)$$

where

$$\begin{aligned} \delta &= \frac{736\alpha^2}{25} - \frac{208\alpha^3}{15} + \frac{16\alpha^4}{9}, \\ \Delta &= -\frac{430336\alpha^4}{625} + \frac{612352\alpha^5}{1125} - \frac{20992\alpha^6}{225} + \frac{256\alpha^8}{243}, \\ \sigma &= -\frac{12896\alpha^3}{125} + \frac{2944\alpha^4}{25} - \frac{416\alpha^5}{15} + \frac{64\alpha^6}{27} + \frac{6}{5} \sqrt{15\Delta} \alpha, \\ \Sigma &= \frac{52\alpha}{5} - \frac{8\alpha^2}{3} + \frac{\delta}{\sigma^{1/3}} + \sigma^{1/3}, \end{aligned} \quad (5.92)$$

are intermediate quantities introduced solely to reduce the size of Eq. (5.91). If $\alpha > 1$, ϵ_1 has two local minimums located at $x_{V'=0}^\pm$ where it vanishes. In between it reaches a local maximum or may even diverges for $\alpha > 9/5$ (see Fig. 48). The slow-roll parameter ϵ_2 vanishes when ϵ_1 reaches these local maxima, or diverge when ϵ_1 does (for $\alpha > 9/5$). As explained in section 4.17, inflation is meant to proceed at $\phi \lesssim \phi_0$. Let us assume that inflation ends by violation of slow-roll when $\epsilon_1 > 1$ between $x = 0$ and the position of the first minimum $x_{\epsilon_1^{\min}}$. Following the previous considerations, this latter location is defined as

$$x_{\epsilon_1^{\min}} = \begin{cases} x_{\epsilon_2=0}^- & \text{if } \alpha < 1 \\ x_{V'=0}^- & \text{if } \alpha > 1 \end{cases}, \quad (5.93)$$

and provides a numerical upper bound to determine x_{end} the solution of $\epsilon_1(x_{\text{end}}) = 1$. This one can only be determined numerically. The values of $x_{\epsilon_2=0}^\pm$ and $x_{V'=0}^\pm$ in terms of α are displayed in the left panel of Fig. 49 together with $x_{\epsilon_1^{\min}}$. The right panel of Fig. 49 represents the value of the first slow-roll parameter at this minimum, $\epsilon_1^{\min} = \epsilon_1(x_{\epsilon_1^{\min}})$. For $\alpha < 1$, one can see that $\epsilon_1^{\min} < 1$ only if the parameter $\alpha \lesssim 1$. This defines a minimum value for α , which depends on ϕ_0 , allowing for inflation to take place inside this domain. When $\alpha \simeq 1$, one can derive an approximated version of Eq. (5.91), namely, $x_{\epsilon_2=0}^- \simeq 1 - (1 - \alpha)/32$. Plugging it into the expression for ϵ_1 one obtains

$$\epsilon_1^{\min} \simeq \frac{225}{32} (\alpha - 1)^2 \frac{M_{\text{Pl}}^2}{\phi_0^2}, \quad (5.94)$$

from which one gets

$$\alpha > 1 - \frac{4\sqrt{12}}{15} \frac{\phi_0}{M_{\text{Pl}}}. \quad (5.95)$$

For the value suggested in Ref. [347], $\phi_0/M_{\text{Pl}} \simeq 10^{-4}$, one obtains $\alpha > 1 - 10^{-5}$, which is in agreement with Ref. [400], and shows that the model needs to be sufficiently fine tuned close to regular MSSM inflation in order to be a viable inflationary model.

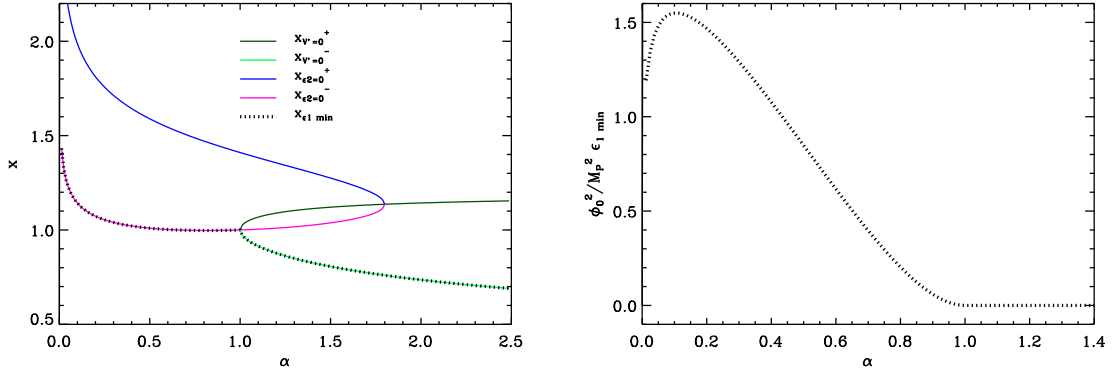


Figure 49. GMSSM Inflation (GMSSMI). Left panel: $x_{\epsilon_2=0}^{\pm}$ defined in Eq. (5.91) and $x_{V'=0}^{\pm}$ defined in Eq. (5.87) together with $x_{\epsilon_1 \min}$ (see Eq. (5.93)) as a function of α . Right panel: minimal value of the slow-roll parameter ϵ_1 (rescaled by ϕ_0^2/M_{Pl}^2) as a function of α . When it is greater than unity, inflation cannot occur.

On top of that, as shall be seen now, the constraints on α are even tighter if one wants a sufficient number of e-folds to be produced. Let us thus turn to the slow-roll trajectory. It can be integrated, and leads to

$$N_{\text{end}} - N = \frac{\phi_0^2}{M_{Pl}^2} \left\{ -\frac{x_{\text{end}}^2 - x^2}{20} - \frac{b_+}{10\sqrt{a_+}} [\arctan(\sqrt{a_+}x_{\text{end}}) - \arctan(\sqrt{a_+}x^2)] \right. \\ \left. - \frac{b_-}{10\sqrt{a_-}} [\arctan(\sqrt{a_-}x_{\text{end}}) - \arctan(\sqrt{a_-}x^2)] \right\}. \quad (5.96)$$

where

$$a_{\pm} = -\alpha \pm \sqrt{\alpha^2 - \alpha}, \quad b_{\pm} = 2 \frac{a_{\pm} + \frac{1}{3}\alpha}{a_{\pm} - a_{\mp}}, \quad (5.97)$$

A few remarks are in order. Firstly, even if the terms appearing in the previous expression are complex, their imaginary contributions cancel out and the resulting expression is truly a real quantity. Then, one can check that formally, when $\alpha \rightarrow 0$, one has $a_{\pm} \rightarrow 0$ and $b_{\pm} \rightarrow 1$, hence $N \simeq -(x^2 - x_{\text{ini}}^2)/4$, which is precisely the LFI slow-roll trajectory for $p = 2$, see section 4.2. This is just a formal check since α is meant to be tuned close to 1 within the GMSSMI scenario. Finally, let us notice that in the case $\alpha < 1$, and contrary to the MSSM models ($\alpha = 1$), the number of e-folds never diverges at a given point x . Therefore, the total number of e-folds is bounded by some maximal value all over the domain under scrutiny. Working out the limit of Eq. (5.96) when $\alpha \rightarrow 1$, one has

$$N_{\text{end}} - N_{\text{ini}} \leq \left(\frac{\phi_0}{M_{Pl}} \right)^2 \frac{\pi}{30} \frac{1}{\sqrt{1-\alpha}}. \quad (5.98)$$

Therefore, if one require to realize at least $\Delta N = N_{\text{end}} - N_{\text{ini}}$ e-folds, one has to fine tune α to

$$\alpha > 1 - \left(\frac{\phi_0}{M_{Pl}} \right)^4 \frac{\pi^2}{900\Delta N^2}. \quad (5.99)$$

Remembering that the small parameter here is ϕ_0/M_{Pl} , one can see that it is a much tighter constraint than the one of Eq. (5.95). Taking $\phi_0/M_{\text{Pl}} \simeq 10^{-4}$ and $\Delta N \simeq 50$, one obtains $\alpha > 1 - 10^{-22}$. This makes the fine-tuning even worse and the model rather difficult to track down on a numerical side. As explained below, the same condition $|\alpha - 1| < \phi_0^4/M_{\text{Pl}}^4/\Delta N^2$ also applies to the case $\alpha > 1$ to maintain a deviation from scale invariance acceptable. This makes the whole class of models fine-tuned.

Finally, the amplitude of the CMB anisotropies fixes the parameter M to

$$\left(\frac{M}{M_{\text{Pl}}}\right)^4 = 2880\pi^2 \frac{M_{\text{Pl}}^2}{\phi_0^2} \frac{(1 - 2\alpha x_*^4 + \alpha x_*^8)^2}{x_*^4 (1 - \frac{2}{3}\alpha x_*^4 + \frac{\alpha}{5}x_*^8)^3} \frac{Q_{\text{rms-PS}}^2}{T^2}. \quad (5.100)$$

As explained in section 4.17, this leads to $M/M_{\text{Pl}} \simeq 10^8$ GeV for $\phi_0/M_{\text{Pl}} \simeq 10^{-4}$.

The reheating consistent slow-roll predictions of the GMSSMI models are displayed in Figs. 110, 111, for $\alpha > 1$ and $\alpha < 1$, respectively. The reheating equation of state parameter \bar{w}_{reh} has been taken to 0 since the potential is quadratic close to its minimum. In both cases, one can see that in the limit $\alpha \rightarrow 1$, the standard MSSM predictions are recovered, see Fig. 93. The amount of gravitational waves r seems to be quite independent on α and comply with its regular MSSM counterpart, while the spectral index n_s strongly depends on α . In the case $\alpha > 1$, pushing α out of 1 worsens the spectral index problem, already present in standard MSSMI. These models are therefore strongly disfavored by the data. In the case $\alpha < 1$ however, there is a very narrow range of acceptable values for α . They are well inside the $|\alpha - 1| < \phi_0^4/M_{\text{Pl}}^4/\Delta N^2$ condition and the spectral index inside the two-sigma confidence intervals. But as can be seen in Fig. 111, the spectral index varies so quickly with α that the fine-tuning is absolute. In Refs. [351, 400–403], it is argued that since the flat saddle point condition is robust against radiative corrections, such a fine tuning may not a problem. However, as explained here, even if the flat saddle point condition is exactly satisfied, the models are disfavored by the observations, and the deviation from that condition must be set to a well defined non-zero value.

5.7 Brane SUSY breaking Inflation (BSUSYBI)

This model has been studied in Ref. [404] in the context of superstrings models⁴. The potential is a sum of two exponential terms

$$V(\phi) = M^4 \left(e^{\sqrt{6}\frac{\phi}{M_{\text{Pl}}}} + e^{\sqrt{6}\gamma\frac{\phi}{M_{\text{Pl}}}} \right), \quad (5.101)$$

one is a “hard” exponential brought about by a SUSY breaking mechanism and the other is a “slow-roll term” having $0 < \gamma < 1/\sqrt{3}$ and that dominates the eventual inflationary dynamics. It was shown in Ref. [404] that the scalar is forced to emerge from an initial singularity climbing up the mild portion of the potential in the fast-roll regime, so that at some point it experiences the hard exponential and bounces against it. The ensuing dynamics approaches rather slowly the eventual attractor and can also generate superimposed oscillations in the primordial power spectrum. Let us notice that if the term in $\sqrt{6}$ in the first exponential function is relaxed to be a free parameter, the potential becomes as in Ref. [405], i.e. a general exponential brane potential. Defining

$$x \equiv \frac{\phi}{M_{\text{Pl}}}, \quad (5.102)$$

⁴see Eq. (1.1) and Eq. (2.9) in that reference.

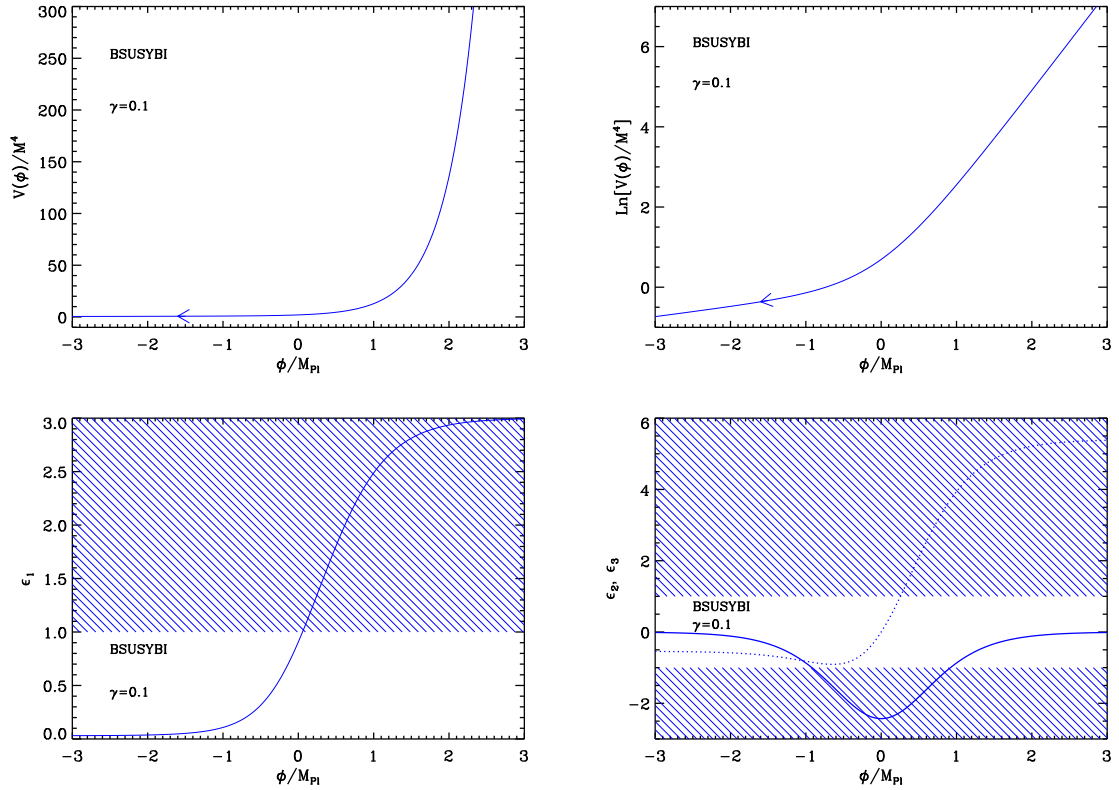


Figure 50. Brane SUSY breaking Inflation (BSUSYBI) for $\gamma = 0.1$. Upper panels: the potential and its logarithm. Bottom left panel: the first slow-roll parameter ϵ_1 as a function of the field value, the shaded area indicates where inflation stops. Bottom right panel: slow-roll parameter ϵ_2 and ϵ_3 .

the first three Hubble flow functions in the slow-roll approximation read

$$\epsilon_1 = 3 \left(\frac{e^{\sqrt{6}x} + \gamma e^{\sqrt{6}\gamma x}}{e^{\sqrt{6}x} + e^{\sqrt{6}\gamma x}} \right)^2, \quad \epsilon_2 = -12(\gamma - 1)^2 \frac{e^{\sqrt{6}(\gamma+1)x}}{(e^{\sqrt{6}x} + e^{\sqrt{6}\gamma x})^2}, \quad (5.103)$$

and

$$\epsilon_3 = 6(1 - \gamma) \frac{(e^{\sqrt{6}x} - e^{\sqrt{6}\gamma x})(e^{\sqrt{6}x} + \gamma e^{\sqrt{6}\gamma x})}{(e^{\sqrt{6}x} + e^{\sqrt{6}\gamma x})^2}. \quad (5.104)$$

These functions together with the potential are displayed in Fig. 50. The two exponential components are clearly visible on the plot of the logarithm of the potential. The required flatness of the potential is realized only along the γ branch and for negative values of x . The first Hubble flow function ϵ_1 is an increasing function of x which varies between its asymptotic values:

$$\lim_{x \rightarrow -\infty} \epsilon_1 = 3\gamma^2, \quad \lim_{x \rightarrow +\infty} \epsilon_1 = 3. \quad (5.105)$$

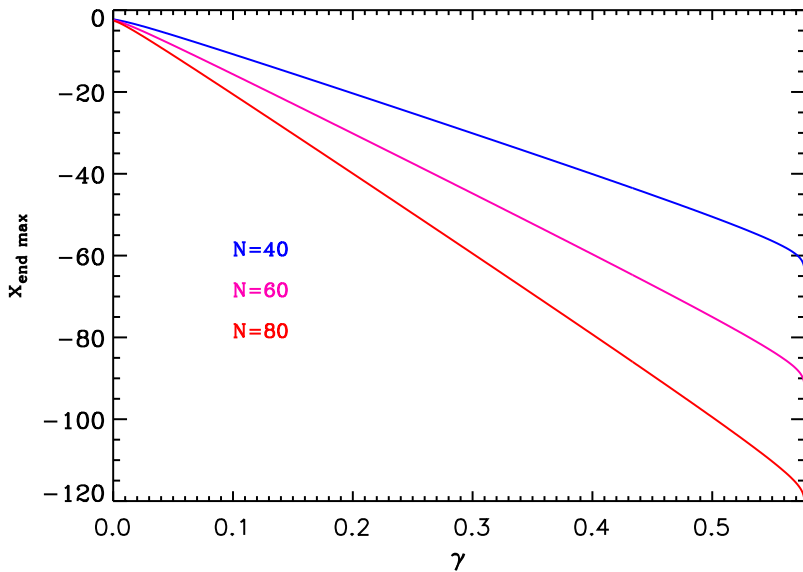


Figure 51. Maximum value of x_{end} in order to realize N e-folds of inflation between $x_{\epsilon_1=1}$ and x_{end} as a function of $0 < \gamma < 1/\sqrt{3}$. This condition defines a prior for the model parameter x_{end} , which is the region lying under the curves on the figure.

For γ small enough ($\gamma < 1/\sqrt{3}$), it is greater than unity at positive field values, i.e. for $x > x_{\epsilon_1=1}$ with

$$x_{\epsilon_1=1} = \frac{1}{\sqrt{6}(\gamma-1)} \ln \left(\frac{\sqrt{3}-1}{1-\gamma\sqrt{3}} \right). \quad (5.106)$$

As a result, inflation can only proceed in the domain $x < x_{\epsilon_1=1}$ and it never stops. Hence the need for an extra-parameter x_{end} encoding the field value at which some unspecified mechanism (such as a tachyonic instability) is triggered and stops inflation. Let us notice that the slow-roll parameter ϵ_2 is always negative and goes to zero at large $|x|$ with a local minimum in $x = 0$ equals to $\epsilon_2^{\text{min}} = -3(\gamma-1)^2$. Finally, the slow-roll parameter ϵ_3 vanishes when $x = 0$ and shares the same sign as x . Its asymptotic values are

$$\lim_{x \rightarrow -\infty} \epsilon_3 = 6\gamma(\gamma-1), \quad \lim_{x \rightarrow +\infty} \epsilon_3 = 6(1-\gamma). \quad (5.107)$$

The slow-roll trajectory can be integrated and gives

$$N - N_{\text{end}} = -\frac{1}{\sqrt{6}}(x - x_{\text{end}}) + \frac{1}{6\gamma} \ln \left[\frac{1 + \gamma e^{\sqrt{6}(\gamma-1)x}}{1 + \gamma e^{\sqrt{6}(\gamma-1)x_{\text{end}}}} \right]. \quad (5.108)$$

This equation cannot be analytically inverted but since inflation requires $x < x_{\epsilon_1=1}$, it shows that x_{end} should not be too close to $x_{\epsilon_1=1}$ in order to realize enough e-folds of inflation. This puts some upper bound on x_{end} , that can be computed numerically and that is displayed in Fig. 51. This value $x_{\text{end}}^{\text{max}}$ defines a prior for the model parameter x_{end} , which is the region lying under the curves on the figure.

Integrating Eq. (2.46) finally gives the field value x_* at which the pivot mode crossed the Hubble radius during inflation. The parameter M being fixed by the amplitude of the CMB anisotropies

$$\left(\frac{M}{M_{\text{Pl}}}\right)^4 = 4320\pi^2 \frac{\left(e^{\sqrt{6}x_*} + \gamma e^{\sqrt{6}\gamma x_*}\right)^2}{\left(e^{\sqrt{6}x_*} + e^{\sqrt{6}\gamma x_*}\right)^3} \frac{Q_{\text{rms-PS}}^2}{T^2}. \quad (5.109)$$

The reheating consistent slow-roll predictions of the BSUSYBI models have been plotted in Fig. 112. The parameter x_{end} varies between $2x_{\text{end}}^{\text{max}} < x_{\text{end}} < x_{\text{end}}^{\text{max}}$ ($x_{\text{end}}^{\text{max}} < 0$), under which the predictions of the model coincide with those of PLI (see section 4.8). Large values for the parameter γ are disfavored and it has to be smaller than $\lesssim 10^{-1}$ for the predictions to remain inside the two sigma confidence intervals. For $\gamma \lesssim 3 \times 10^{-2}$, we also see that the parameter x_{end} is bounded from below.

5.8 Tip Inflation (TI)

In Ref. [406], the motion of a space filling D3-brane at the tip of a warped deformed conifold is studied, where no anti D3-brane is present and the inflaton potential is induced by threshold corrections to the superpotential. For the canonically normalized inflaton field, this potential is given by

$$V = M^4 \left(1 + \cos \frac{\phi}{\mu} + \alpha \sin^2 \frac{\phi}{\mu}\right), \quad (5.110)$$

where inflation proceeds in the region $0 < \phi/\mu < \pi$. As ϕ describes the position of a D3-brane in some angular direction, its kinetic term comes from the DBI action. However, as explained in Ref. [406], in the slow-roll regime the DBI kinetic term reduces to the canonical one. The constant in front of the cosine has been set to 1 in order to have a vanishing cosmological constant at the end of inflation. The mass scale μ can be interpreted as an axion decay constant, when the potential is derived for an axionic field (as for the Natural Inflation model, see section 4.6). As discussed in Ref. [406], it is not possible to obtain a large axion decay constant in the underlying string theory model, hence $\mu/M_{\text{Pl}} \ll 1$ (typically $\mu/M_{\text{Pl}} \simeq 10^{-4}$). When $\alpha \ll 1$, the potential reduces to the natural inflation (NI) one. Yet, it was shown in section 4.6 that only super-Planckian decay constants $\mu/M_{\text{Pl}} > \mathcal{O}(1)$ could make the natural inflation models compatible with observations (see e.g. Fig. 80). As noticed in Ref. [406], this means that the tip inflation models with $\alpha \ll 1$ are not viable. On the other hand, it is noticed that if α is fine tuned to $\alpha \simeq 1/2$, the potential of Eq. (5.110) becomes very flat close to the top and that a phenomenologically successful slow-roll inflationary stage could occur. This is why these models are studied for $\mu/M_{\text{Pl}} \simeq 10^{-4} \ll 1$, and $\alpha \simeq 1/2$.

Defining

$$x \equiv \frac{\phi}{\mu}, \quad (5.111)$$

the potential of Eq. (5.110) and its logarithm with respect to x are displayed in Fig. 52. Its general shape depends on the value of α . If $\alpha < 1/2$, it is a decreasing function of the field vev , hence inflation proceeds from the left to the right, and it has a vanishing minimum at $x = \pi$. Its first derivative vanishes at the top of the potential for $x = 0$ while its second derivative $V''(x=0) \propto 2\alpha - 1$. It vanishes there when $\alpha = 1/2$ and the potential becomes flat enough to support inflation. If $\alpha > 1/2$, the potential maximum is not located at $x = 0$

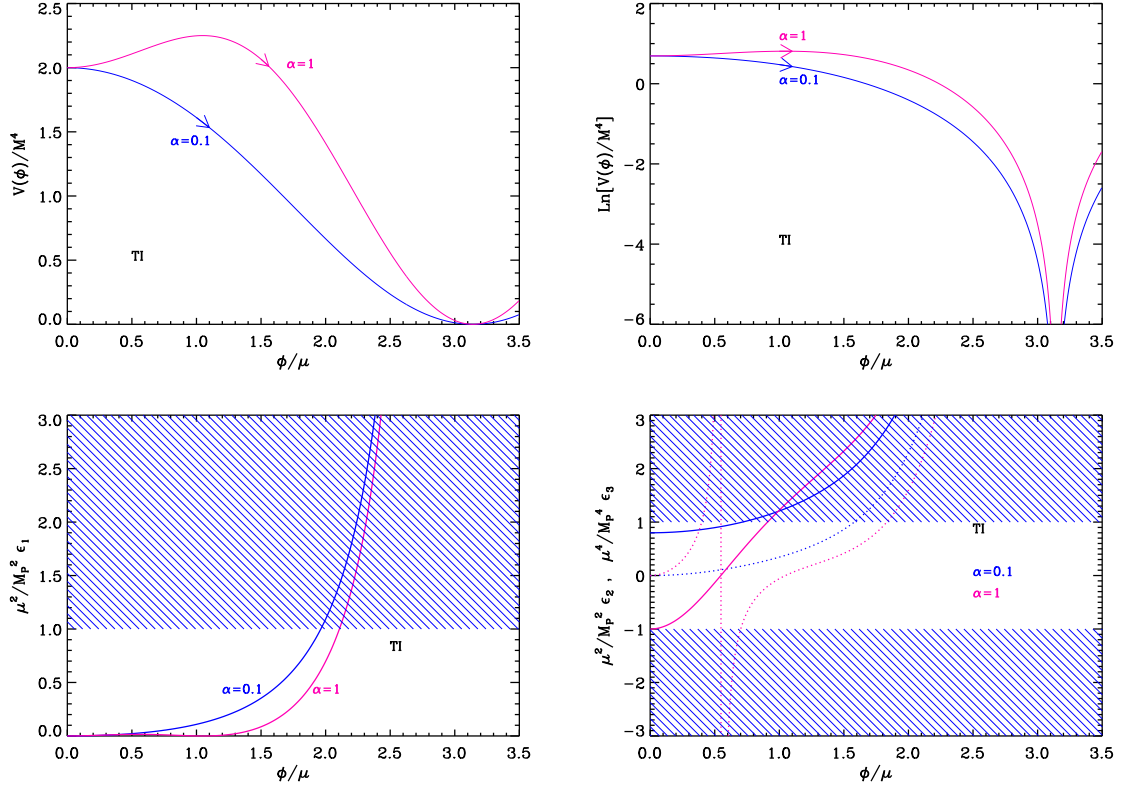


Figure 52. Tip Inflation (TI). Upper panels: Tip Inflation potential and its logarithm for $\alpha = 0.1$ (blue line) and $\alpha = 1$ (pink line), as a function of ϕ/μ . Bottom left panel: slow-roll parameter ϵ_1 normalized by M_{Pl}^2/μ^2 . The shaded area indicates the breakdown of the slow-roll inflation if $\mu = M_{\text{Pl}}$ (strictly speaking when the acceleration stops). Bottom right panel: slow-roll parameter ϵ_2 (solid line) and ϵ_3 (dotted line), again rescaled by M_{Pl}^2/μ^2 .

anymore but at $x = \arccos[1/(2\alpha)]$. Let us thus define

$$x_{V'=0} = \begin{cases} 0 & \text{if } \alpha < 1/2, \\ \arccos\left(\frac{1}{2\alpha}\right) & \text{if } \alpha > 1/2. \end{cases} \quad (5.112)$$

If $\alpha > 1/2$, the potential decreases with the field vev in the range $x_{V'=0} < x < \pi$, where inflation proceeds from the left to the right. Again, the first derivative of the potential vanishes at the top of the potential while its second derivative $V''(x = x_{V'=0}) \propto 1/(2\alpha) - 2\alpha$ again vanishes when $\alpha = 1/2$. This is why α must be close enough to $1/2$ in order for a viable slow-roll inflationary regime to take place.

Let us calculate the Hubble flow functions within the slow-roll approximation. They read

$$\epsilon_1 = \frac{M_{\text{Pl}}^2}{\mu^2} \frac{(1 - 2\alpha \cos x)^2 \sin^2 x}{2(1 + \cos x + \alpha \sin^2 x)^2}, \quad (5.113)$$

$$\epsilon_2 = \frac{M_{\text{Pl}}^2}{\mu^2} \frac{2 \cos^2 \frac{x}{2}}{(1 + \cos x + \alpha \sin^2 x)^2} [2 + \alpha(3 + 4\alpha) - 2\alpha(3 + 2\alpha) \cos x - \alpha \cos 2x], \quad (5.114)$$

and

$$\epsilon_3 = \frac{M_{\text{Pl}}^2}{\mu^2} \left\{ -2 - \frac{2+4\alpha}{(1+\alpha-\alpha\cos x)^2} + \frac{5+3\alpha}{1+\alpha-\alpha\cos x} + \frac{1}{\cos^2 \frac{x}{2}} + \frac{4(1+\alpha+3\alpha^2) - 2\alpha(7+4\alpha)\cos x}{\alpha[\cos 2x + (6+4\alpha)\cos x - 3 - 4\alpha] - 2} \right\}. \quad (5.115)$$

They are displayed in Fig. 52. They are increasing functions of the field vev in the inflationary domain $x_{V'=0} < x < \pi$, and diverge when $x \rightarrow \pi$. The first and third slow-roll parameters ϵ_1 and ϵ_3 vanish at the potential maximum. However, the second slow-roll parameter ϵ_2 takes a non vanishing positive value given by

$$\epsilon_2(x = x_{V'=0}) = \begin{cases} \frac{M_{\text{Pl}}^2}{\mu^2} (1-2\alpha) & \text{if } \alpha < 1/2, \\ 4 \frac{M_{\text{Pl}}^2}{\mu^2} \frac{2\alpha-1}{2\alpha+1} & \text{if } \alpha > 1/2. \end{cases} \quad (5.116)$$

This means that in order for a slow-rolling inflationary regime to take place, $|\epsilon_2| < 1$, one needs again to adjust α close to $1/2$, such that $|\alpha - 1/2| \ll \mu^2/M_{\text{Pl}}^2 \ll 1$ with a typically value being given by $\mu \simeq 10^{-4} M_{\text{Pl}}$.

Inflation stops by violation of slow-roll, when $\epsilon_1 = 1$ at the position x_{end} given by

$$x_{\text{end}} = \arccos \left[\Sigma + \frac{(1+i\sqrt{3})\sigma}{3 \times 2^{2/3} (\delta + \sqrt{\Delta})^{1/3}} - \frac{(1-i\sqrt{3})\sigma'}{6 \times 2^{1/3}} (\delta + \sqrt{\Delta})^{1/3} \right]. \quad (5.117)$$

In this formula, we have defined

$$\Delta = -864\alpha^6 (2\alpha+1)^3 \frac{\mu^2}{M_{\text{Pl}}^2} \left(\frac{\mu^2}{M_{\text{Pl}}^2} + 2 \right)^2 \times \left\{ (2\alpha-1)^3 + 2(2\alpha+1)[(\alpha-10)\alpha-2] \frac{\mu^2}{M_{\text{Pl}}^2} - 4(2\alpha+1)^2 \frac{\mu^4}{M_{\text{Pl}}^4} \right\}, \quad (5.118)$$

and

$$\delta = 8\alpha^3 \left[2(2\alpha-1)^3 - 3(1+2\alpha)(5+2\alpha)(1+4\alpha) \frac{\mu^2}{M_{\text{Pl}}^2} - 15(1+\alpha)(1+2\alpha)^2 \frac{\mu^4}{M_{\text{Pl}}^4} - 2(1+2\alpha)^3 \frac{\mu^6}{M_{\text{Pl}}^6} \right], \quad (5.119)$$

together with

$$\sigma = 3 + 4\alpha(1-\alpha) - 2 \frac{\mu^2}{M_{\text{Pl}}^2} (1+2\alpha)^2 - \frac{8}{2 + \frac{\mu^2}{M_{\text{Pl}}^2}}, \quad \sigma' = \frac{1}{2\alpha^2 \left(2 + \frac{\mu^2}{M_{\text{Pl}}^2} \right)}. \quad (5.120)$$

Let us now turn to the slow-roll trajectory. It can be integrated explicitly, leading to

$$N_{\text{end}} - N = \frac{\mu^2}{M_{\text{Pl}}^2} \frac{1}{2\alpha-1} \ln \left(\frac{1-\cos x}{1-\cos x_{\text{end}}} \right) - \frac{\mu^2}{2M_{\text{Pl}}^2} \frac{2\alpha+1}{2\alpha-1} \ln \left(\frac{1-2\alpha\cos x}{1-2\alpha\cos x_{\text{end}}} \right). \quad (5.121)$$

For $\alpha = 1/2$, this expression is singular, and one has

$$N_{\text{end}} - N = \frac{\mu^2}{M_{\text{Pl}}^2} \left[\frac{1}{1 - \cos x} - \frac{1}{1 - \cos x_{\text{end}}} - \frac{1}{2} \ln \left(\frac{1 - \cos x}{1 - \cos x_{\text{end}}} \right) \right]. \quad (5.122)$$

Finally, the parameter M can be determined from the amplitude of the CMB anisotropies and the observable field value x_* [see Eq. (2.46)], and one gets

$$\left(\frac{M}{M_{\text{Pl}}} \right)^4 = 720\pi^2 \frac{M_{\text{Pl}}^2}{\mu^2} \frac{(1 - 2\alpha \cos x_*)^2 \sin^2 x_*}{(1 + \cos x_* + \alpha \sin^2 x_*)^3} \frac{Q_{\text{rms-PS}}^2}{T^2}. \quad (5.123)$$

The reheating consistent slow-roll predictions of the TI models are displayed in Fig. 113 for $\alpha < 1/2$ and in Fig. 114 for $\alpha > 1/2$, with $\mu/M_{\text{Pl}} = 10^{-6}$, 10^{-4} and 10^{-2} . In both cases, one can see that α needs to be sufficiently adjusted to $1/2$, namely $|2\alpha - 1| \ll \mu^2/M_{\text{Pl}}^2$, otherwise the deviation from scale invariance is too important, as expected. The typical amount of gravitational waves is very small. To see how μ/M_{Pl} is constrained, the slow-roll predictions are displayed for $\alpha = 1/2$ in Fig. 115, and with μ varying. One can see that even if one allows values of μ larger than the typical ones ($\mu/M_{\text{Pl}} \simeq 10^{-4}$) these models are disfavored by the observations since they deviate too much from scale invariance.

5.9 β exponential inflation (BEI)

This model was introduced and studied in Ref. [407] as a phenomenological generalization of the PLI exponential potential (see section 4.8). The proposed potential is given by

$$V(\phi) = M^4 \exp_{1-\beta} \left(-\lambda \frac{\phi}{M_{\text{Pl}}} \right), \quad (5.124)$$

where the generalized exponential function $\exp_{1-\beta}$ is defined by

$$\exp_{1-\beta}(f) = \begin{cases} (1 + \beta f)^{1/\beta} & \text{for } 1 + \beta f > 0, \\ 0 & \text{otherwise.} \end{cases} \quad (5.125)$$

As discussed in Ref. [407], for $f > 0$ and $g > 0$, this function satisfies the following identities:

$$\exp_{1-\beta} [\ln_{1-\beta}(f)] = f, \quad \ln_{1-\beta}(f) + \ln_{1-\beta}(g) = \ln_{1-\beta}(fg) - \beta [\ln_{1-\beta}(f) \ln_{1-\beta}(g)], \quad (5.126)$$

where $\ln_{1-\beta}(f) = (f^\beta - 1)/\beta$ is the generalized logarithmic function. As the parameter $\beta \rightarrow 0$, all the above expressions reproduce the usual exponential and logarithm properties. The limit $\beta \rightarrow 0$ therefore matches with the PLI potential (see section 4.8), but as discussed below, this is not the case for the observable predictions which remain in a separate branch. Defining

$$x \equiv \frac{\phi}{M_{\text{Pl}}}, \quad (5.127)$$

the domain of definition depends on the sign of β . For $\beta > 0$, the field values are such that $x < 1/(\beta\lambda)$, whereas if $\beta < 0$, the potential is defined for $x > 1/(\beta\lambda)$. In both cases, inflation proceeds at increasing field values, i.e. from the left to the right. The first three Hubble flow functions in the slow-roll approximation are given by

$$\epsilon_1 = \frac{\lambda^2}{2(1 - \beta\lambda x)^2}, \quad \epsilon_2 = \frac{2\beta\lambda^2}{(1 - \beta\lambda x)^2} = 4\beta\epsilon_1, \quad \epsilon_3 = \epsilon_2. \quad (5.128)$$

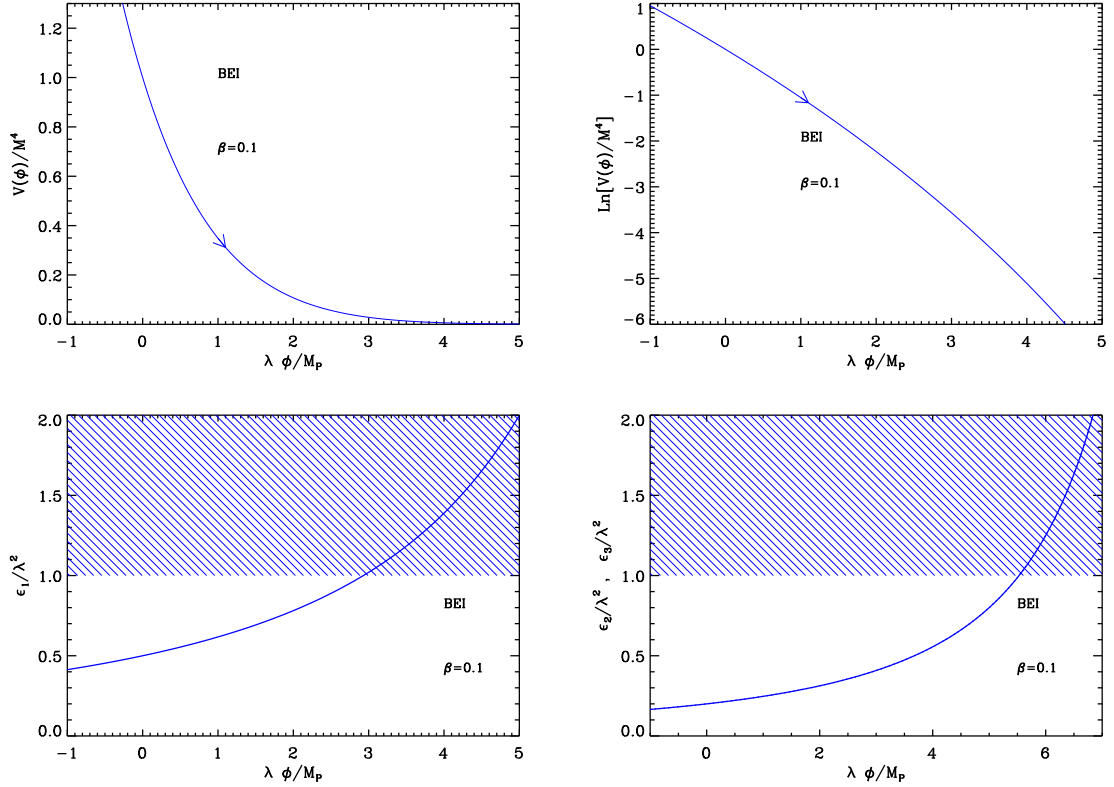


Figure 53. β exponential inflation (BEI) for $\beta = 0.1$. Upper panels: the potential and its logarithm. Bottom left panel: slow-roll parameter ϵ_1 with respect to the field values. The shaded area indicates where inflation stops if $\lambda = 1$. Bottom right panel: slow-roll parameters $\epsilon_2 = \epsilon_3$.

Together with the potential, they have been represented in Fig. 53.

One immediately sees that ϵ_1 is an increasing function of x only for the case where $\beta > 0$. Therefore inflation can naturally stop at x_{end} such that $\epsilon_1(x_{\text{end}}) = 1$. In the opposite situation, namely $\beta < 0$, inflation has to be ended by some additional mechanism and x_{end} would become an extra-parameter. Since this model is purely phenomenological, we will be focused in the following to the case $\beta > 0$ for which

$$x_{\text{end}} = \frac{1}{\beta} \left(\frac{1}{\lambda} - \frac{1}{\sqrt{2}} \right). \quad (5.129)$$

The slow-roll trajectory can be integrated explicitly and reads

$$N - N_{\text{end}} = \frac{1}{\lambda} (x - x_{\text{end}}) - \frac{\beta}{2} (x^2 - x_{\text{end}}^2). \quad (5.130)$$

It can also be inverted into

$$x = \frac{1}{\lambda\beta} - \sqrt{\left(x_{\text{end}} - \frac{1}{\lambda\beta}\right)^2 - \frac{2}{\beta}(N - N_{\text{end}})}. \quad (5.131)$$

From there, the observable field value x_* can be linked to the number of e-folds $\Delta N_* = N_{\text{end}} - N_*$ at which the pivot mode crossed the Hubble radius during inflation. Making use

of Eq. (5.129), one gets

$$x_* = \frac{1}{\lambda\beta} - \sqrt{\frac{1}{2\beta^2} + \frac{2}{\beta}\Delta N_*}. \quad (5.132)$$

Inserting this expression into the slow-roll parameters formulas yields

$$\epsilon_{1*} = \frac{1}{1 + 4\beta\Delta N_*}, \quad \epsilon_{2*} = \epsilon_{3*} = 4\beta\epsilon_{1*}. \quad (5.133)$$

Therefore, the slow-roll predictions of these models do not depend on the potential parameter λ . Moreover, the limit $\beta \rightarrow 0$ does not give the same observable predictions as for the PLI models due to the singular behavior of x_{end} . These models can therefore be viewed as a completely different class.

Finally, the amplitude of the CMB anisotropies fixes the parameter M with

$$\left(\frac{M}{M_{\text{Pl}}}\right)^4 = 720\pi^2\lambda^2(1 - \beta\lambda x_*)^{-2-\frac{1}{\beta}}\frac{Q_{\text{rms-PS}}^2}{T^2}. \quad (5.134)$$

Notice that from Eq. (5.132), the above expression can be written in terms of ΔN_* and it does not depend on λ anymore. The reheating consistent slow-roll predictions for the BEI models are displayed in Fig. 116. The potential parameter β is bounded from below $\beta \gtrsim 0.6$ for the predictions to remain inside the two-sigma confidence intervals, while the potential parameter λ is totally unconstrained.

5.10 Pseudo Natural Inflation (PSNI)

Pseudo Natural Inflation (PSNI) was introduced and studied in Ref. [212]. This model has common points with NI, see section 4.6. Indeed, in PSNI, the inflaton field is also a pseudo-Nambu Goldstone boson which appears after symmetry breaking. As is well-known, the corresponding potential is nearly flat and is, therefore, well-suited for inflation. The main ideas behind this construction are reviewed in section 4.6. The main difference with respect to natural inflation, for which the broken symmetry is a shift symmetry, is that in pseudo natural inflation the broken symmetry is now a $U(1)$ one. A concrete implementation of this idea has been proposed in Ref. [212]. Suppose that we have the following supersymmetric hybrid superpotential

$$W = \lambda_0 S (\psi_1^2 + \psi_2^2 - f^2) + \frac{\lambda_1}{2} \psi_1 \varphi^2 + \lambda_2 X (\varphi^2 - v^2), \quad (5.135)$$

with $\lambda_1^2 f^2 > 2\lambda_2^2 v^2$, where ψ_1 , ψ_2 and φ are scalar fields and λ_0 , λ_1 and λ_2 are coupling constants. The flat directions of this superpotential can be reparametrized as

$$\psi_1 + i\psi_2 \equiv (f + \sigma) e^{i\phi/f}, \quad \psi_1 - i\psi_2 \equiv (f - \sigma) e^{-i\phi/f}, \quad (5.136)$$

where ϕ is the Nambu-Goldstone boson associated to the broken $U(1)$ symmetry and σ is a modulus. One can assume that σ is stabilized and sits at $\sigma = 0$, the minimum of a potential originating from supersymmetry breaking. The field ϕ plays the role of the inflaton. Using the above expressions and the conditions $\sigma = 0$, one obtains that $\psi_1 = f \cos(\phi/f)$ and $\psi_2 = f \sin(\phi/f)$. The $U(1)$ symmetry is explicitly broken by the term proportional to λ_1 and this generates a potential for ϕ . If the initial condition in the early Universe is such that $\phi \simeq 0$, it will force $\varphi = 0$, because of the large mass (i.e. $\lambda_1 f$) it receives from ψ_1 through

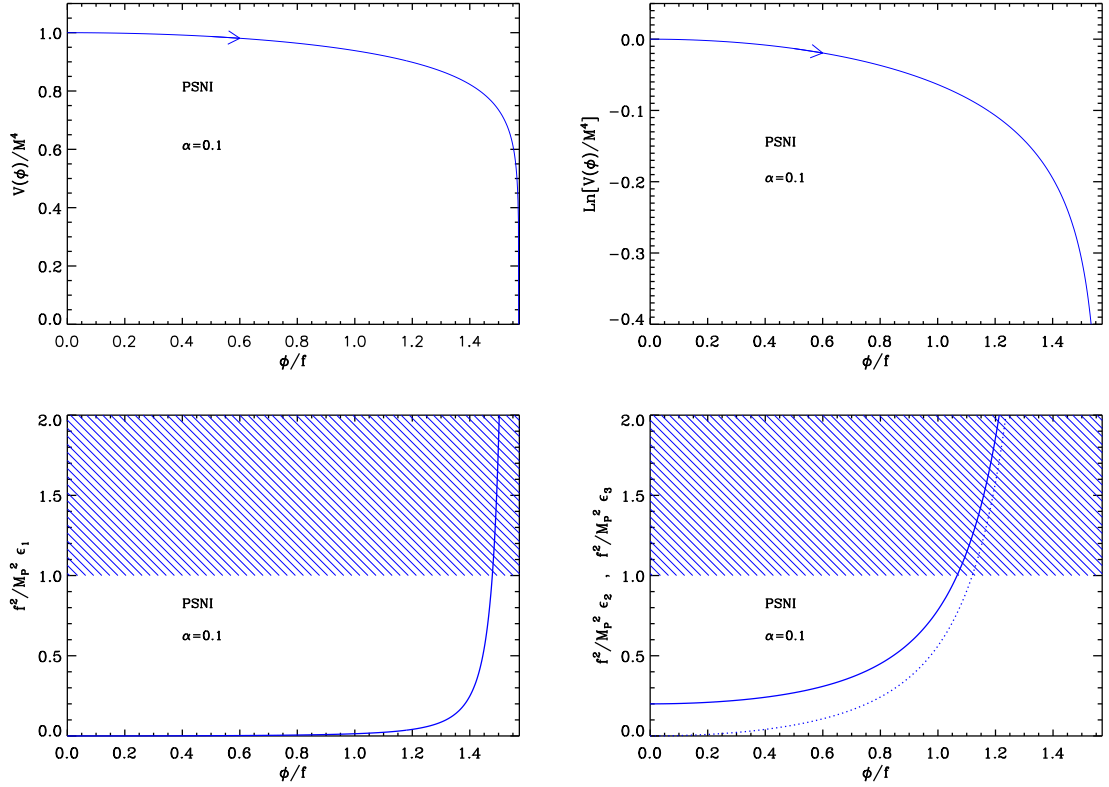


Figure 54. Top left panel: Pseudo Natural Inflation (PSNI) potential, for $\alpha = 0.1$, as a function of ϕ/f . Top right panel: logarithm of the potential for the same value of α . Bottom left panel: slow-roll parameter ϵ_1 , rescaled by the quantity M_{Pl}^2/f^2 such that it acquires a universal form, for the same value of α . Bottom right panel: slow-roll parameter ϵ_2 (solid line) and ϵ_3 (dotted line), rescaled by the quantity M_{Pl}^2/f^2 , still for the same value of α .

the coupling term $\propto \psi_1 \varphi^2$. But then SUSY is broken because $F_X \simeq \langle \partial W / \partial X \rangle \simeq \lambda_2 v^2 \neq 0$, where there is no contribution from φ since we have just shown that it vanishes. As a consequence, the corresponding vacuum energy density is given by $V_0 \simeq |F_X|^2 = \lambda_2^2 v^4$. This tree level potential is corrected by two kind of contributions. First, supergravity induces a soft SUSY breaking mass of order H for every scalar, but since ϕ is a pseudo Nambu-Goldstone boson, it only receives a potential due to the explicit breaking term proportional to λ_1 . The corresponding contribution is loop suppressed, $m_\phi^2 \sim 3\lambda_1^2 H^2 / (16\pi^2)$, as soon as $\lambda_1 \lesssim 1$ which will be assumed. Second, the potential receives a direct Yukawa mediated contribution through a φ loop and Ref. [212] has shown that it takes the form

$$V(\phi) \simeq V_0 \left(1 + \frac{\lambda_2^2}{4\pi^2} \ln \frac{\lambda_1 \psi_1}{\mu} \right) = V_0 \left[1 + \frac{\lambda_2^2}{4\pi^2} \ln \frac{\cos(\phi/f)}{\mu/f} \right]. \quad (5.137)$$

Using more friendly notations, the potential can be reexpressed as

$$V = M^4 \left[1 + \alpha \ln \left(\cos \frac{\phi}{f} \right) \right], \quad (5.138)$$

with the following definitions

$$M^4 = \lambda_2^2 v^4 \left[1 + \frac{\lambda_2^2}{4\pi^2} \ln \left(\frac{\lambda_1 f}{\mu} \right) \right], \quad \alpha = \frac{\frac{\lambda_2^2}{4\pi^2}}{1 + \frac{\lambda_2^2}{4\pi^2} \ln \left(\frac{\lambda_1 f}{\mu} \right)}. \quad (5.139)$$

Therefore, one typically has $\alpha \ll 1$, and the scale f should a priori be such that $f \lesssim M_{\text{Pl}}$ in order to avoid the usual problems of natural inflation.

The potential (5.138) as well as its logarithm are displayed in Fig. 54. Since ϕ is assumed to be such that $\phi \simeq 0$ initially, the potential must be studied in the range $\phi/f \in [0, \pi/2]$. It is positive definite in the range $\phi/f \in [0, \arccos(e^{-1/\alpha})]$. We see that it is a decreasing function of the inflaton vev , which means that inflation proceeds from the left to the right in the direction specified by the arrow in Fig. 54.

Let us now turn to the slow-roll parameters. If one defines $x \equiv \phi/f$, then the three first Hubble flow parameters are given by

$$\epsilon_1 = \frac{M_{\text{Pl}}^2}{2f^2} \frac{\alpha^2 \tan^2 x}{(1 + \alpha \ln \cos x)^2}, \quad \epsilon_2 = 2\alpha \frac{M_{\text{Pl}}^2}{f^2} \frac{1 + \alpha + \alpha \ln \cos x - \alpha \cos^2 x}{\cos^2 x (1 + \alpha \ln \cos x)^2}, \quad (5.140)$$

$$\epsilon_3 = \alpha \frac{M_{\text{Pl}}^2}{f^2} (\tan x)^2 \frac{2 + 3\alpha + \alpha^2 - \alpha^2 \cos 2x + (4 + 3\alpha) \alpha \ln \cos x + 2\alpha^2 \ln^2 \cos x}{(1 + \alpha \ln \cos x)^2 (1 + \alpha \ln \cos x + \alpha \sin^2 x)}. \quad (5.141)$$

They are displayed in Fig. 54. We see on this plot that the slow-roll parameters ϵ_1 and ϵ_3 vanish when x goes to 0 and diverge when x goes to $\pi/2$. On the other hand, the slow-roll parameter ϵ_2 has a non zero limit when x goes to 0, namely

$$\lim_{x \rightarrow 0} \epsilon_2 = 2 \frac{M_{\text{Pl}}^2}{f^2} \alpha. \quad (5.142)$$

This quantity should be small in order for slow-roll to be valid. This means that, at a fixed scale f , the parameter α needs to be smaller than $\sim f^2 M_{\text{Pl}}^2$. From the monotonous behavior of ϵ_1 , one also notices that inflation stops by violation of the slow-roll conditions when $\epsilon_1 = 1$. Unfortunately, this equation cannot be solved exactly and the solution needs to be determined numerically. However, since we are in a regime where $f/M_{\text{Pl}} \ll 1$ and $\alpha M_{\text{Pl}}^2/f^2 \ll 1$, one has that x_{end} must be close to $\pi/2$. One can derive a better approximation by solving the equation $\epsilon_1 = 1$ using an expansion in the small quantities of the problem. One arrives at

$$x_{\text{end}} \simeq \frac{\pi}{2} - \frac{\alpha}{\sqrt{2}} \frac{M_{\text{Pl}}}{f}, \quad (5.143)$$

that is to say the first correction to $\pi/2$ is linear in $\alpha M_{\text{Pl}}/f$ and, as expected, negative. As usual, the ASPIC code makes use of the exact solution.

Let us now turn to the slow-roll trajectory. It can be integrated exactly in terms of the dilogarithm function Li_2 (also referred to as Spence's function, or Jonquière function). This function was already used in this paper, for instance in section 4.1. The explicit expression of the trajectory reads

$$N_{\text{end}} - N = \frac{f^2}{\alpha M_{\text{Pl}}^2} \left[(1 + \alpha \ln \cos x_{\text{end}}) \ln \sin x_{\text{end}} + \frac{\alpha}{4} \text{Li}_2(\cos^2 x_{\text{end}}) \right] - \frac{f^2}{\alpha M_{\text{Pl}}^2} \left[(1 + \alpha \ln \cos x) \ln \sin x + \frac{\alpha}{4} \text{Li}_2(\cos^2 x) \right], \quad (5.144)$$

where N_{end} is the number of e-folds at the end of inflation. Unfortunately, this trajectory cannot be inverted due to its complexity. However, if one uses the two conditions $f/M_{\text{Pl}} \ll 1$ and $\alpha M_{\text{Pl}}^2/f^2 \ll 1$, one can simplify a lot its expression. In particular, at Hubble crossing, one can write

$$\Delta N_* \simeq \frac{f^2}{2\alpha M_{\text{Pl}}^2} \left[\left(x_* - \frac{\pi}{2} \right)^2 - \left(x_{\text{end}} - \frac{\pi}{2} \right)^2 \right], \quad (5.145)$$

from which one can obtain an explicit formula for ϕ_*

$$x_* \simeq \frac{\pi}{2} - \sqrt{2\alpha\Delta N_*} \frac{M_{\text{Pl}}}{f}. \quad (5.146)$$

Then, this also allows us to derive useful approximated equations for the first three Hubble flow parameters, namely

$$\epsilon_{1*} \simeq \frac{\alpha}{4\Delta N_*}, \quad \epsilon_{2*} \simeq \epsilon_{3*} \simeq \frac{1}{\Delta N_*}. \quad (5.147)$$

The next step is of course to establish the expressions of the tensor to scalar ratio, spectral index and running for PSNI. One arrives at

$$r \simeq \frac{4\alpha}{\Delta N_*}, \quad n_s - 1 \simeq \alpha_s \simeq -\frac{1}{\Delta N_*}, \quad (5.148)$$

These formulas are in agreement with the estimates given in Ref. [212]. Interestingly enough, we see that these predictions are independent of the scale f and that the spectral index (and the running) is even independent of α .

The last step consists in using the CMB normalization in order to derive an expression for the mass scale M . Straightforward manipulations lead to

$$\left(\frac{M}{M_{\text{Pl}}} \right)^4 = 720\pi^2 \alpha^2 \frac{M_{\text{Pl}}^2}{f^2} \frac{\tan^2 x_*}{(1 + \alpha \ln \cos x_*)^3} \frac{Q_{\text{rms-PS}}^2}{T^2}. \quad (5.149)$$

Under the two conditions $f/M_{\text{Pl}} \ll 1$ and $\alpha M_{\text{Pl}}^2/f^2 \ll 1$ and using the same method as before, this leads to

$$\left(\frac{M}{M_{\text{Pl}}} \right)^4 \simeq \frac{360\pi^2 \alpha Q_{\text{rms-PS}}^2}{\Delta N_* T^2}. \quad (5.150)$$

Requiring $M < M_{\text{Pl}}$ is easily achieved since, for the fiducial value $\Delta N_* \simeq 55$, this is equivalent to $\alpha \lesssim 2580$ whereas we have $\alpha \ll 1$. Taking the more realistic value $\alpha \sim 10^{-6}$ and $\Delta N_* \sim 55$, one typically obtains that $M/M_{\text{Pl}} \sim 10^{-3}$.

The predictions of the PSNI models are displayed in Fig. 117 for $f/M_{\text{Pl}} = 10^{-3}, 10^{-1}, 10$ respectively (although this last value is considered just for the purpose of illustration since super-Planckian values of f are not very physical). The reheating equation of state parameter w has been taken to 0 but since there is no potential minimum around which the inflaton field can oscillate at the end of inflation, this parameter is a priori unspecified and can take different values (in the ASPIC code, this parameter can be freely chosen). One can see that the rough description provided by Eqs. (5.147) is correct: when $\alpha M_{\text{Pl}}^2/f^2 \ll 1$, the deviation from scale invariance does not depend on the model parameters and is of the order of $n_s \simeq 1 - 1/\Delta N_* \simeq 0.975$, while $r \simeq 4\alpha/\Delta N_*$ is typically very small.

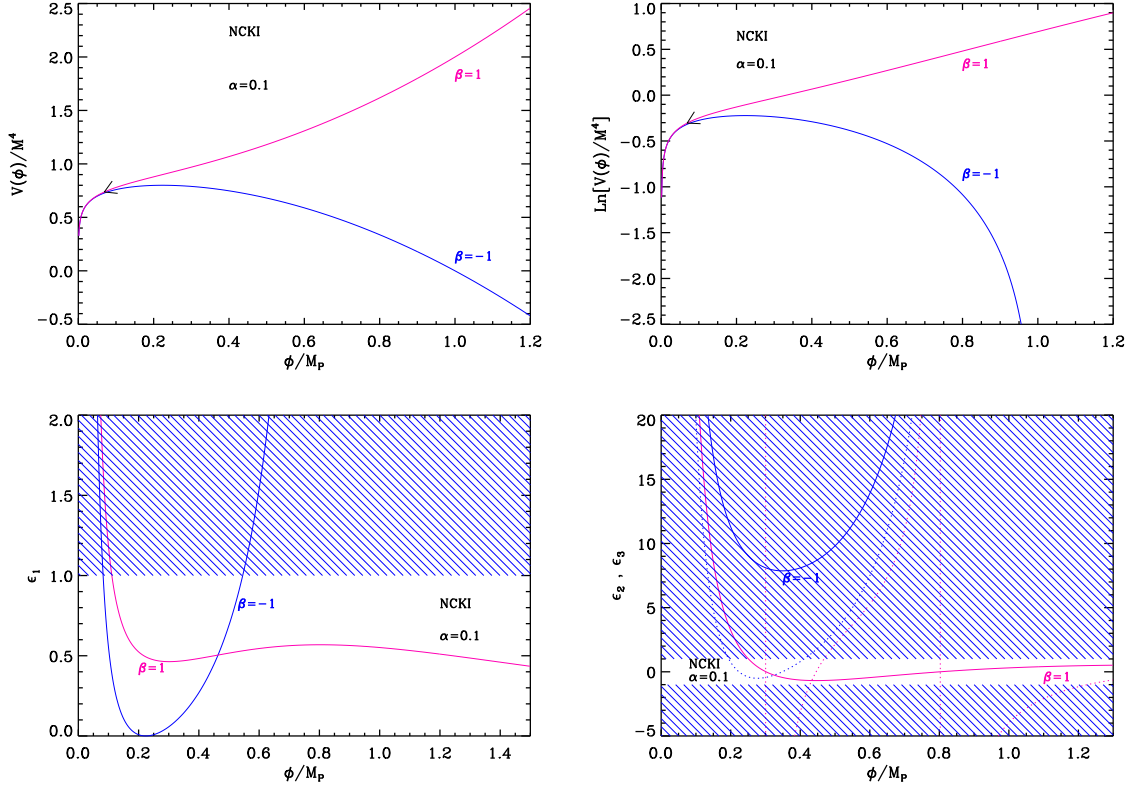


Figure 55. Top left panel: Non Canonical Kähler Inflation (NCKI) potential for $\alpha = 0.1$ and $\beta = \pm 1$. The solid blue line represents the case $\beta = -1$ while the solid pink line represents the case $\beta = 1$. Top right panel: logarithm of the potential for the same values of α and β . Bottom left panel: slow-roll parameter ϵ_1 , for a potential with the same values of α and β and the same color code. The shaded area indicates the region where inflation is not possible. Bottom right panel: slow-roll parameters ϵ_2 (solid blue and pink lines) and ϵ_3 (dotted blue and pink lines), for a potential with the values of α and β already considered in the other panels.

5.11 Non Canonical Kähler Inflation (NCKI)

This model was introduced and studied in Ref. [408]. It was also considered in Ref. [340] as a way to model hilltop inflation. Its potential is given by, see e.g. Eq.(45) of Ref. [340]

$$V = M^4 \left[1 + \alpha \ln \left(\frac{\phi}{M_{\text{Pl}}} \right) + \beta \left(\frac{\phi}{M_{\text{Pl}}} \right)^2 \right], \quad (5.151)$$

where α is a small positive dimensionless parameter and β a dimensionless parameter of order $\mathcal{O}(1)$ which can be either positive or negative. These models are supposed to arise in the context of F -term inflation with three fields, S and the pair $\psi, \bar{\psi}$ whose Kähler potential and superpotential can be written as $K(S, \psi, \bar{\psi}) = |S|^2 + |\psi|^2 + |\bar{\psi}|^2$ and $W(S, \psi, \bar{\psi}) = \lambda S(\psi\bar{\psi} - \Lambda^2)$. The pair can be seen as waterfall fields and the *vev* Λ is typically taken at the GUT scale, $\Lambda \simeq 10^{16}\text{GeV}$. The field S , or rather its canonically normalized version $\phi = \sqrt{2}|S|$, is seen as the inflaton field. For $\phi > \sqrt{2}\Lambda$, the tree level of the potential is sufficiently flat and reads $V(\phi) = \lambda^2 \Lambda^4 [1 + \lambda^2/(8\pi^2) \log(\phi/Q)]$, where Q is the renormalization scale.

Choosing this scale is a priori not obvious but, as argued in Ref. [340], Q should be taken such that the loop contribution remains a small correction at Hubble radius crossing. However, the Kähler function and the superpotential generically contains higher order terms and these terms will correct the above mentioned potential. In particular the non canonical terms in the Kähler potential will generate a mass term of the order $\lambda^2 \Lambda^4 / M_{\text{Pl}}^2$ [340]. As a consequence, the potential can be expressed in a form given by Eq. (5.151) with, as already mentioned above, $\alpha \ll 1$, and $|\beta| = \mathcal{O}(1)$. The case $\beta > 0$ has been investigated in Refs. [408, 409] as “hybrid inflation with quasi-canonical supergravity” and the case $\beta < 0$ was studied in Ref. [340]. For $\beta > 0$, the potential (5.151) can be viewed as a valley hybrid potential [VHI, see section 6.2 and Eq. (6.15)] plus radiative corrections described, as usual, by a logarithmic term. Therefore, a consistency check is that, when $\alpha \rightarrow 0$, all the formulas derived below must reproduce those derived in section 6.2. Finally, let us mention that the potential (5.151) has also been obtained in Ref. [410] for $\beta < 0$ (under the name “SUSY breaking potential”) and in Ref. [411] in the context of supersymmetric hybrid inflation.

The potential (5.151), as well as its logarithm, are displayed in Fig. 55. We now describe its shape. For this purpose, let us first define the quantity x by $x \equiv \phi / M_{\text{Pl}}$. If $\beta > 0$, the potential is definite positive provided $x > x_{V=0}^-$, where

$$x_{V=0}^- = \left[\frac{\alpha}{2\beta} W_0 \left(\frac{2\beta}{\alpha} e^{-2/\alpha} \right) \right]^{1/2}, \quad (5.152)$$

and where W_0 is the “0”-branch of the Lambert function. In this case, the potential is an increasing function of the field vev and, therefore, inflation proceeds from the right to the left in the direction indicated by the arrow in Fig. 55. Let us also notice that, in this case, the potential has an inflection point located at $x_{V''=0} = \sqrt{\alpha / (2\beta)}$. If $\beta < 0$, we must have $2\beta/\alpha \exp(1 - 2/\alpha) > -1$ in order to avoid the situation where the potential is everywhere negative. This implies that either $\beta > -1$ or $\beta < -1$ and, in this last case, $\alpha < -2/W_{-1}[1/(e\beta)]$ or $\alpha > -2/W_0[1/(e\beta)]$. If one of these conditions is satisfied (which is generically the case when $\alpha \ll 1$ which is the regime we are interested in), the potential is positive provided $x_{V=0}^- < x < x_{V=0}^+$, where $x_{V=0}^-$ is defined in Eq. (5.152) and where

$$x_{V=0}^+ = \left[\frac{\alpha}{2\beta} W_{-1} \left(\frac{2\beta}{\alpha} e^{-2/\alpha} \right) \right]^{1/2}, \quad (5.153)$$

W_{-1} being the -1 branch of the Lambert function. In this case, the potential is a concave function of the field vev , with a maximum located at $x_{V'=0} = \sqrt{-\alpha / (2\beta)}$. Typically, inflation proceeds from the right to the left at small values of the field vev compared to the Planck mass.

Let us now calculate to the Hubble flow parameters. They are given by the following expressions

$$\epsilon_1 = \frac{(\alpha + 2\beta x^2)^2}{2x^2 (1 + \alpha \ln x + \beta x^2)^2}, \quad (5.154)$$

$$\epsilon_2 = 2 \frac{\alpha(\alpha + 1) + (5\alpha - 2)\beta x^2 + 2\beta^2 x^4 + \alpha(\alpha - 2\beta x^2) \ln x}{x^2 (1 + \alpha \ln x + \beta x^2)^2}, \quad (5.155)$$

and

$$\epsilon_3 = \frac{1}{x^2} \left[\frac{2(\alpha + 2\beta x^2)^2}{(1 + \alpha \ln x + \beta x^2)^2} + \frac{\alpha - 2\beta x^2}{1 + \alpha \ln x + \beta x^2} + \frac{\alpha^2 + 8\alpha\beta x^2 - 4\beta^2 x^4}{\alpha(\alpha + 1) + (5\alpha - 2)\beta x^2 + 2\beta^2 x^4 + \alpha(\alpha - 2\beta x^2) \ln x} \right]. \quad (5.156)$$

The are displayed in the bottom panels in Fig. 55. If $\beta > 0$, the first slow-roll parameter ϵ_1 diverges when $x \rightarrow x_{V=0}^-$. For $x > x_{V=0}^-$, it first decreases, then reaches a minimum, then increases and reaches a local maximum. Finally, from this maximum, it decreases again and vanishes at infinity. Therefore, in that case, inflation stops by violation of the slow-roll conditions at a *vev* x_{end} that cannot be calculated exactly and has to be estimated by numerical calculation. If $\beta < 0$, the first slow-roll parameter diverges when $x \rightarrow x_{V=0}^-$. For $x > x_{V=0}^-$, ϵ_1 decreases, vanishes at the potential local maximum $x_{V'=0}$, and then increases and blows up when $x \rightarrow x_{V=0}^+$. At the same time, the second slow-roll parameter ϵ_2 decreases in the inflationary domain $x_{V=0}^- < x < x_{V'=0}$. Let us also notice that, since $\epsilon_2(x_{V'=0}) \propto 2\alpha - \alpha^2 + \alpha^2 \ln[-\alpha/(2\beta)]$, one has $\epsilon_2 > 0$, thanks to the condition $2\beta/\alpha \exp(1 - 2/\alpha) > -1$. As for the case $\beta > 0$, inflation ends by violation of the slow-roll conditions at a *vev* that needs to be computed numerically. These calculations are implemented in the routines of the ASPIC code.

Let us now turn to the slow-roll trajectory. This one can be integrated exactly using the dilogarithm function Li_2 . The corresponding expression reads

$$N_{\text{end}} - N = \left(1 - \frac{\alpha}{2} + \alpha \ln x\right) \frac{\ln(\alpha + 2\beta x^2)}{4\beta} + \frac{x^2}{4} - \frac{\alpha}{4\beta} \ln \alpha \ln x + \frac{\alpha}{8\beta} \text{Li}_2\left(-2\frac{\beta}{\alpha} x^2\right) - \left(1 - \frac{\alpha}{2} + \alpha \ln x_{\text{end}}\right) \frac{\ln(\alpha + 2\beta x_{\text{end}}^2)}{4\beta} - \frac{x_{\text{end}}^2}{4} + \frac{\alpha}{4\beta} \ln \alpha \ln x_{\text{end}} - \frac{\alpha}{8\beta} \text{Li}_2\left(-2\frac{\beta}{\alpha} x_{\text{end}}^2\right), \quad (5.157)$$

where N_{end} is the number of e-folds at the end of inflation. The above expression is quite complicated and a simpler expression can be derived in the limit $\alpha \ll 1$. In that case, as expected, one obtains $N_{\text{end}} - N = x^2/4 + \log(x)/(2\beta) - x_{\text{end}}^2/4 - \log(x_{\text{end}})/(2\beta)$, which is precisely the slow-roll trajectory for the VHI models with $\mu = M_{\text{Pl}}/\sqrt{\beta}$ and $p = 2$, see Eq. (6.23). Obviously, when $\alpha \neq 0$, the exact trajectory cannot be inverted analytically.

Finally, the parameter M can be determined from the CMB normalization. One obtains the following expression

$$\left(\frac{M}{M_{\text{Pl}}}\right)^4 = 720\pi^2 \frac{(\alpha + 2\beta x_*^2)^2}{x_*^2 (1 + \alpha \ln x_* + \beta x_*^2)^3} \frac{Q_{\text{rms-PS}}^2}{T^2}. \quad (5.158)$$

The exact predictions of the NCKI models are displayed in Figs. 118-119 for $\beta > 0$ and $\beta < 0$, respectively. The reheating equation of state parameter w has been taken to be 0 but, since there is no potential minimum around which the inflaton field can oscillate at the end of inflation, this parameter is in fact unspecified. Some remarks are in order at this point. First, when $\beta > 0$, we notice that ϵ_2 at Hubble crossing is either positive or negative while, when $\beta < 0$, it is always positive. This is in agreement with what we have discussed before. Second, when $\beta > 0$ and $\alpha \ll 1$, one can check that the predictions of the models are similar to the VHI ones with $p = 2$ (compare with Fig. 149). Again, this is consistent with the previous considerations. Third, when $|\beta| \gtrsim \mathcal{O}(1)$, the predictions of the models do not depend much on β . Fourth, as expected, when $\beta \rightarrow 0$, one recovers the predictions of the LI

models, see section 4.12 and Fig. 88. We conclude that all the consistency checks listed above are compatible with the considerations presented before. Now, in the regime $|\beta| = \mathcal{O}(1)$ and $\alpha \ll 1$, Figs. 118-119 indicate that the case $\beta > 0$ is disfavored by the observations. The situation is even worse for the case $\beta < 0$, the deviation from scale invariance being clearly too important to satisfy the observational constraints.

5.12 Constant Spectrum Inflation (CSI)

This potential belongs to the class of models discussed in Ref. [412] and is constructed to produce a constant power spectrum $P(k) \propto k^0$ for the primordial density fluctuations, i.e. $n_s = 1$. It reads

$$V(\phi) = \frac{M^4}{\left(1 - \alpha \frac{\phi}{M_{\text{Pl}}}\right)^2}. \quad (5.159)$$

There is a symmetry for $\phi/M_{\text{Pl}} \rightarrow 2/\alpha - \phi/M_{\text{Pl}}$ and inflation can proceed indifferently in the branch $\phi/M_{\text{Pl}} < 1/\alpha$ or in the branch $\phi/M_{\text{Pl}} > 1/\alpha$, leading to the same physical predictions. For this reason, we will be interested in the following to the branch $\phi/M_{\text{Pl}} < 1/\alpha$. Defining

$$x \equiv \frac{\phi}{M_{\text{Pl}}}, \quad (5.160)$$

the first three Hubble flow functions in the slow-roll approximation are given by

$$\epsilon_1 = \frac{2\alpha^2}{(\alpha x - 1)^2}, \quad \epsilon_2 = \epsilon_3 = -2\epsilon_1. \quad (5.161)$$

The previous relation $\epsilon_2 = -2\epsilon_1$ means that at first order in slow-roll, the spectral index is indeed equals to unity, or $n_s - 1 = 0$. Recall that the potential of this model is precisely constructed for this relation to be true. Let us notice however that at second order in slow-roll, $\epsilon_2 = \epsilon_3 = -2\epsilon_1$ yields $n_s - 1 = 4\epsilon_1^2 > 0$. One should note that another way to realize $n_s - 1 = 0$ at first order in slow-roll is to take the large field inflation potential LFI (see section 4.2) with a negative power index $p = -2$. In that case one also has $\epsilon_2 = \epsilon_3 = -2\epsilon_1$ and, at second order, $n_s - 1 = 4\epsilon_1^2$ is also verified. However, the expressions for ϵ_1 are different between the two models such that the actual value of the spectral index at second order will differ. The potential and the Hubble flow functions have been represented in Fig. 56.

As can be checked in this figure, ϵ_1 is a monotonous function of x in both branches of the potential, it diverges at $x = 1/\alpha$ and vanishes for $x \rightarrow \pm\infty$. Inflation can therefore take place in the region $x < x_{\epsilon_1=1}^-$ for the branch $x < 1/\alpha$ (or $x > x_{\epsilon_1=1}^+$ for the branch $x > 1/\alpha$), where $x_{\epsilon_1=1}^\pm$ are the field values at which $\epsilon_1 = 1$:

$$x_{\epsilon_1=1}^\pm = \frac{1 \pm \sqrt{2}\alpha}{\alpha}. \quad (5.162)$$

Since the field evolution is repelled from $x_{\epsilon_1=1}^\pm$, inflation does not stop by slow-roll violation and an extra-parameter x_{end} should be considered. As for the other models in such a situation, x_{end} gives the field value at which an unspecified mechanism stopping inflation is triggered. For this reason, CSI is a two parameters model. Let us notice that the slow-roll parameters $\epsilon_2 = \epsilon_3$ are also negative monotonous functions of x in both branches of the potential and cross the line $\epsilon_2 = \epsilon_3 = -1$ at

$$x_{\epsilon_2=-1}^\pm = x_{\epsilon_3=-1}^\pm = \frac{1 \pm 2\alpha}{\alpha}. \quad (5.163)$$

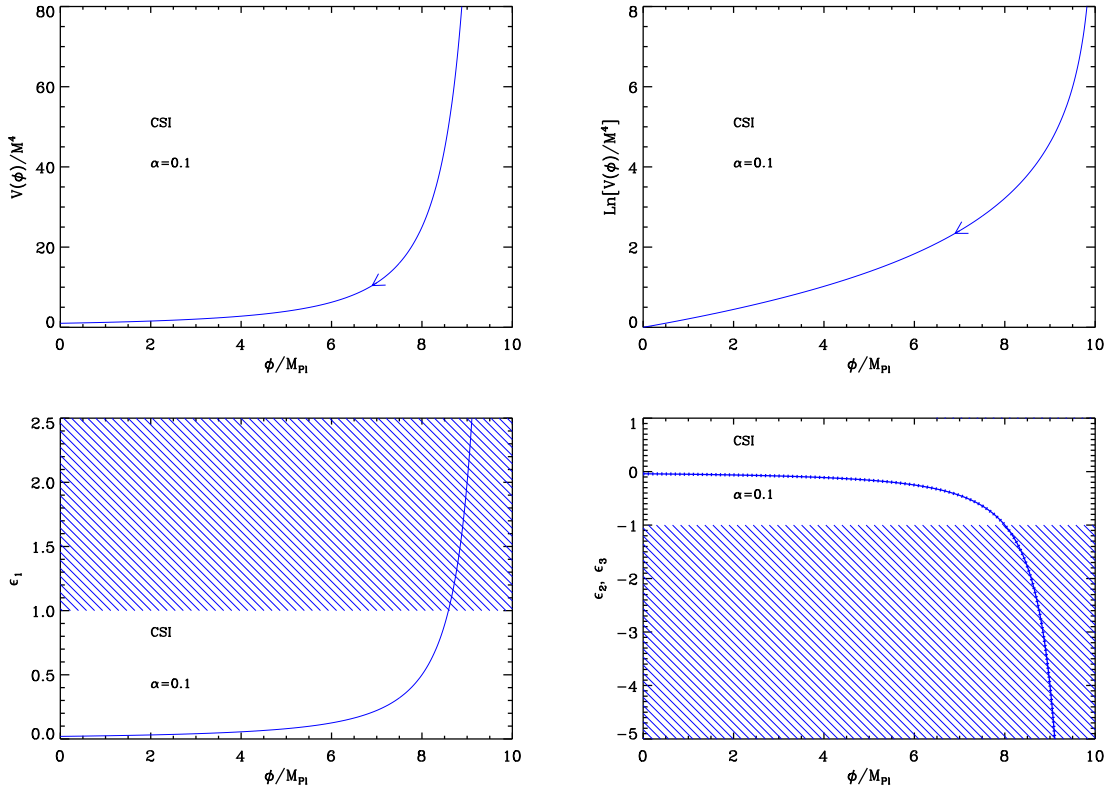


Figure 56. Constant Spectrum Inflation (CSI) for $\alpha = 0.1$. Upper panels: the potential and its logarithm along the branch $x < 1/\alpha$. Bottom left panel: slow-roll parameter ϵ_1 together with the region in which it is larger than unity and in which inflation cannot occur (shaded). Bottom right panel: slow-roll parameter $\epsilon_2 = \epsilon_3$ along the same branch $x < 1/\alpha$.

As a result, there is a small domain $x_{\epsilon_2=-1}^- < x < x_{\epsilon_1=1}^-$ during which inflation has just started but is slow-roll violating (and similarly on the other branch). This is not problematic as the field evolution is driven away from this domain towards the one in which all the Hubble flow functions become small (see Fig. 56).

The slow-roll trajectory can be integrated explicitly to

$$N - N_{\text{end}} = \frac{x^2}{4} - \frac{x}{2\alpha} + \frac{x_{\text{end}}^2}{4} - \frac{x_{\text{end}}}{2\alpha}, \quad (5.164)$$

and also inverted analytically to get

$$x = \frac{1 \pm \sqrt{1 - 2\alpha x_{\text{end}} + \alpha^2 x_{\text{end}}^2 + 4\alpha^2 (N - N_{\text{end}})}}{\alpha}. \quad (5.165)$$

The sign \mp depending on whether one is working in the $x < 1/\alpha$ branch or in the $x > 1/\alpha$ branch, respectively. A consequence of this formula is the fact that if one requires $N_{\text{end}} - N_{\text{ini}}$ e-folds to be produced, x_{end} should be smaller than some value $x_{\text{end}}^{\text{max}}$ given by

$$x_{\text{end}}^{\text{max}} = \frac{1}{\alpha} - \sqrt{2 + 4(N_{\text{end}} - N_{\text{ini}})}, \quad (5.166)$$

in the $x < 1/\alpha$ branch. Equivalently, with a minus sign in this expression, this would be $x_{\text{end}}^{\text{min}}$ for the branch $x > 1/\alpha$.

Finally, the observable field value x_* is obtained by solving Eq. (2.46) while the amplitude of the CMB anisotropies fixes the parameter M to

$$\left(\frac{M}{M_{\text{Pl}}}\right)^4 = 2880\pi^2\alpha^2\frac{Q_{\text{rms-PS}}^2}{T^2}. \quad (5.167)$$

Interestingly, it only depends on α , and not on x_* (i.e. it has no explicit dependence on the reheating). The reheating consistent slow-roll predictions for the CSI models are represented in Figs. 120 and 121 for $\alpha = 10^{-3}$ and $\alpha = 1$, respectively.

5.13 Orientifold Inflation (OI)

This model has been studied in Ref. [413] in the context of four-dimensional strongly interacting theories non minimally coupled to gravity, with composite inflation driven by orientifold field theories. When the number of colors N is large, such theories feature super Yang-Mills properties, and performing an expansion in $1/N$, an effective action can be derived in the Einstein frame. For the canonically normalized field, the inflaton potential reduces to

$$V(\phi) = M^4 \left(\frac{\phi}{\phi_0}\right)^4 \left[\left(\ln \frac{\phi}{\phi_0}\right)^2 - \alpha \right], \quad (5.168)$$

where $\alpha = \mathcal{O}(1/N) \ll 1$ and $\phi_0 \simeq 10^{16}$ GeV. The potential as well as its logarithm are displayed in Fig. 57.

Defining

$$x \equiv \frac{\phi}{\phi_0}, \quad (5.169)$$

the potential remains positive provided $x < x_{V'=0}^-$ or $x > x_{V'=0}^+$, where

$$x_{V'=0}^{\pm} = e^{\pm\sqrt{\alpha}}. \quad (5.170)$$

It vanishes at $x = 0$, then increases to reach a local maximum at $x_{V'=0}^-$, decreases again to become negative at $x_{V'=0}^-$, reaches a local minimum at $x_{V'=0}^+$, then increases again to become positive at $x_{V'=0}^+$ and diverges asymptotically. The values of $x_{V'=0}^-$ and $x_{V'=0}^+$ are given by

$$x_{V'=0}^{\pm} = e^{-\frac{1}{4} \pm \sqrt{\frac{1}{16} + \alpha}}. \quad (5.171)$$

A priori three regimes of inflation may exist: $x < x_{V'=0}^-$ and inflation proceeds from the right to the left, $x_{V'=0}^- < x < x_{V'=0}^+$ and inflation proceeds from the left to the right, $x_{V'=0}^+ < x$ and inflation proceed from the right to the left in the direction specified by the arrow in Fig. 57. As explained below, only the third domain allows for a slow-roll inflationary regime.

This is why we now turn to the slow-roll parameter values. The first three Hubble flow functions in the slow-roll approximation are given by

$$\epsilon_1 = 2\frac{M_{\text{Pl}}^2}{\phi_0^2} \left[\frac{2\ln^2(x) + \ln(x) - 2\alpha}{x\ln^2(x) - \alpha x} \right]^2, \quad (5.172)$$

$$\epsilon_2 = 4\frac{M_{\text{Pl}}^2}{\phi_0^2} \frac{2\ln^4(x) + \ln^3(x) + (1-4\alpha)\ln^2(x) - \alpha\ln(x) + \alpha + 2\alpha^2}{[x\ln^2(x) - \alpha x]^2}, \quad (5.173)$$

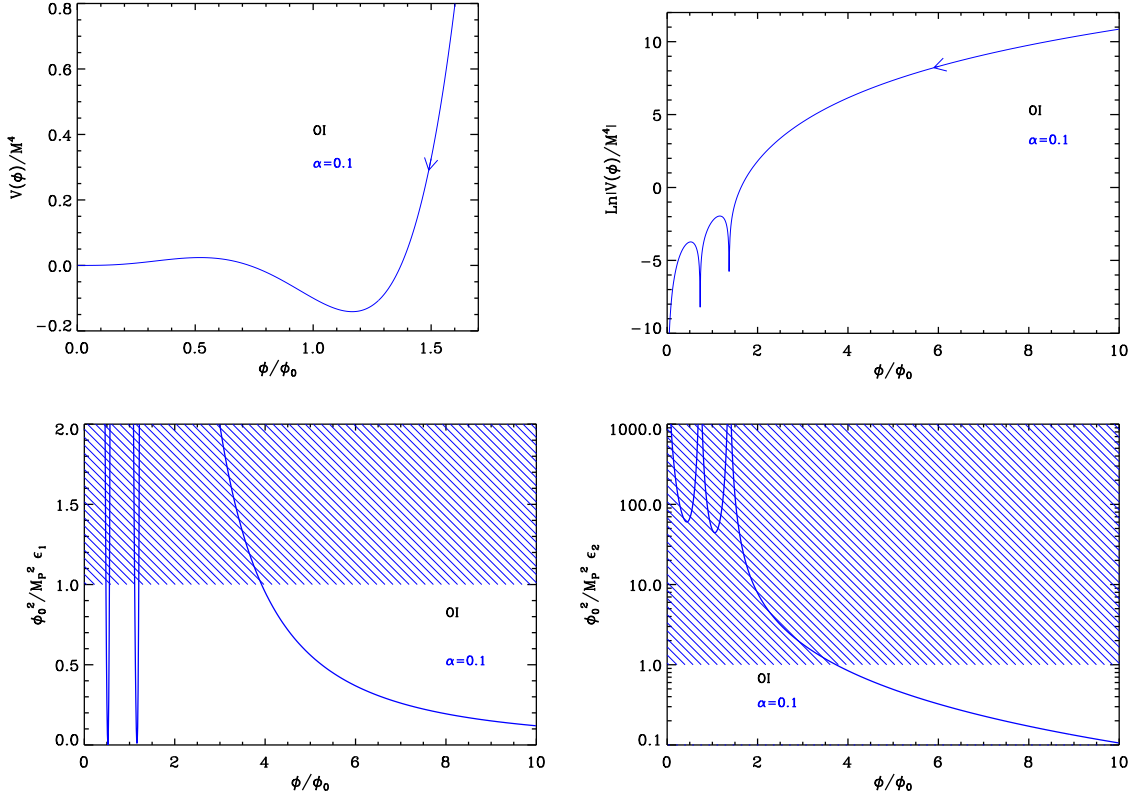


Figure 57. Orientifold Inflation (OI) for $\alpha = 0.1$. Upper panels: the potential and its logarithm. Bottom left panel: slow-roll parameter ϵ_1 , rescaled by the factor ϕ_0^2/M_{Pl}^2 . The shaded area indicates where inflation cannot occur (for $\phi = M_{\text{Pl}}$). Bottom right panel: rescaled slow-roll parameter ϵ_2 .

and

$$\begin{aligned}
\epsilon_3 = & 2 \frac{M_{\text{Pl}}^2}{\phi_0^2} \left[8\alpha^4 + 6\alpha^3 - \alpha^2 (8\alpha + 15) \ln(x) + 2\alpha (3 - 16\alpha^2 - 2\alpha) \ln^2(x) \right. \\
& + 8\alpha (3\alpha + 1) \ln^3(x) + 2(24\alpha^2 - 5\alpha + 1) \ln^4(x) + (7 - 24\alpha) \ln^5(x) + 8(1 - 4\alpha) \ln^6(x) \\
& \left. + 8 \ln^7(x) + 8 \ln^8(x) \right] [x \ln^2(x) - \alpha x]^{-2} \\
& \times \left[2\alpha^2 + \alpha - \alpha \ln(x) + (1 - 4\alpha) \ln^2(x) + \ln(x)^3 + 2 \ln(x)^4 \right]^{-1}.
\end{aligned} \tag{5.174}$$

They have been represented in Fig. 57. One can see that the slow-roll regime can only take place in the $x > x_{V=0}^+$ region, where ϵ_1 continuously increase as inflation proceeds from the right to the left, and diverges at $x_{V=0}^+$. In the other domains, ϵ_2 remains too large to support slow-rolling. Within the $x > x_{V=0}^+$ domain, inflation naturally ends by slow-roll violation, but the field value x_{end} at which this occurs has to be determined numerically. However, since $\phi_0 \simeq 10^{16}$ GeV, one can work out an approximated formula for x_{end} in the $\phi_0 \ll M_{\text{Pl}}$ limit, namely

$$x_{\text{end}} \simeq 2\sqrt{2} \frac{M_{\text{Pl}}}{\phi_0}. \tag{5.175}$$

The slow-roll trajectory stems from Eq. (2.11) and one gets

$$N_{\text{end}} - N = -\frac{\phi_0^2}{M_{\text{Pl}}^2} \left\{ \frac{x_{\text{end}}^2 - x^2}{8} + \frac{\ln^2(x_{V'=0}^+) - \alpha}{2\sqrt{1+16\alpha}} (x_{V'=0}^+)^2 \left[\text{Ei} \left(2 \ln \frac{x_{\text{end}}}{x_{V'=0}^+} \right) - \text{Ei} \left(2 \ln \frac{x}{x_{V'=0}^+} \right) \right] - \frac{\ln^2(x_{V'=0}^-) - \alpha}{2\sqrt{1+16\alpha}} (x_{V'=0}^-)^2 \left[\text{Ei} \left(2 \ln \frac{x_{\text{end}}}{x_{V'=0}^-} \right) - \text{Ei} \left(2 \ln \frac{x}{x_{V'=0}^-} \right) \right] \right\}, \quad (5.176)$$

where Ei is the exponential integral function, and where $x_{V'=0}^\pm$ have been defined in Eq. (5.171). In the $\phi_0 \ll M_{\text{Pl}}$ limit, this trajectory reduces to $\Delta N_* \simeq \phi_0 / (4M_{\text{Pl}}^2)(x_*^2 - x_{\text{end}}^2)$, where we have introduced the observable field value x_* at which the pivot mode crossed the Hubble radius during inflation. It can be inverted to give x_* in terms of $\Delta N_* = N_{\text{end}} - N_*$ and one gets

$$x_* \simeq 2 \frac{M_{\text{Pl}}}{\phi_0} \sqrt{\Delta N_* + 2}. \quad (5.177)$$

Plugging this into Eqs. (5.172), (5.173) and (5.174) gives the approximated expressions

$$\epsilon_{1*} \simeq \epsilon_{2*} \simeq \epsilon_{3*} \simeq \frac{2}{\Delta N_* + 2}, \quad (5.178)$$

hence

$$r \simeq \frac{32}{\Delta N_* + 2}, \quad n_s - 1 \simeq -\frac{6}{\Delta N_* + 2}, \quad \alpha_s \simeq -\frac{12}{(\Delta N_* + 2)^2}. \quad (5.179)$$

From x_* , the parameter M is fixed by the amplitude of the CMB anisotropies and one gets

$$\left(\frac{M}{M_{\text{Pl}}} \right)^4 = \frac{2880\pi^2 [2 \ln^2(x_*) + \ln(x_*) - 2\alpha]^2 M_{\text{Pl}}^2 Q_{\text{rms-PS}}^2}{x_*^6 [\ln^2(x_*) - \alpha]^3 \phi_0^2 T^2}. \quad (5.180)$$

In the $\phi_0 \ll M_{\text{Pl}}$ limit, this gives rise to

$$\left(\frac{M}{M_{\text{Pl}}} \right)^4 \simeq \frac{180\pi^2}{(\Delta N_* + 2)^3} \left(\frac{\phi_0}{M_{\text{Pl}}} \right)^4 \frac{1}{\ln^2 \left(2 \frac{M_{\text{Pl}}}{\phi_0} \sqrt{\Delta N_* + 2} \right)} \frac{Q_{\text{rms-PS}}^2}{T^2}. \quad (5.181)$$

With $\phi_0 \simeq 10^{16}$ GeV, this typically gives $M/M_{\text{Pl}} \simeq 5 \times 10^{-4}$.

The reheating consistent slow-roll predictions for the orientifold inflation models are displayed in Fig. 122, for $\phi_0/M_{\text{Pl}} = 10^{-4}, 10^{-2}$, and 1. Let us stress that natural values are $\phi_0 \simeq 10^{16}$ GeV) and $\alpha \in [10^{-3}, 1]$. The reheating equation of state parameter has been fixed to $\bar{w}_{\text{reh}} = 0$ since the potential is quadratic close to its minimum. According to the rough picture provided by Eq. (5.178), the predictions of these models almost do not depend on its parameters ϕ_0 and α , which is why all the prediction points are superimposed in Fig. 122. In particular, one can see that these models generically predict an important amount of gravitational waves which is disfavored by the observations.

5.14 Constant n_s C Inflation (CNCI)

This model has been obtained in Ref. [370] and is the third example of a class of scenarios already studied in sections 4.20 and 4.21. As explained in those sections, the corresponding

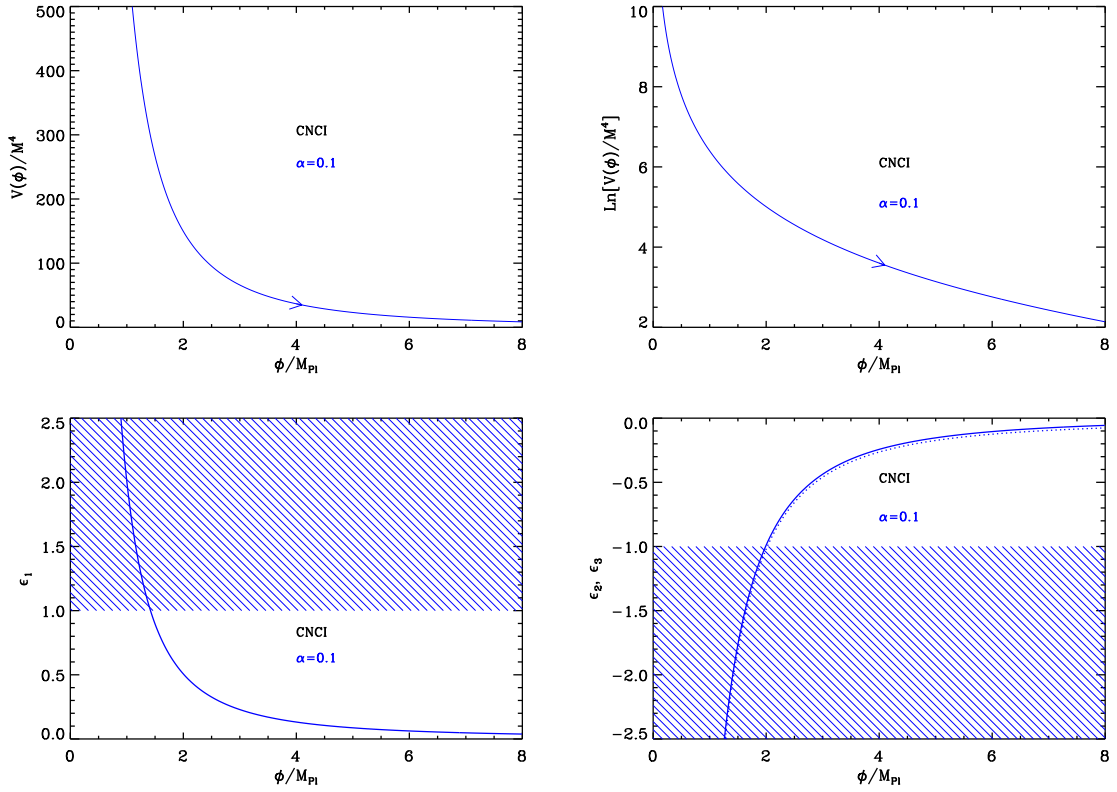


Figure 58. Top left panel: Constant n_s C inflaton potential for $\alpha = 0.1$. Inflation proceeds from the left to the right as indicated by the arrow. Top right panel: logarithm of the potential for the same value of α . Bottom left panel: the first slow-roll parameter ϵ_1 for $\alpha = 0.1$. Bottom right panel: slow-roll parameters ϵ_2 and ϵ_3 , still for $\alpha = 0.1$.

potential is designed in order to produce a power spectrum with constant spectral index. The potential studied in this section reads

$$V(\phi) = M^4 \left[(3 + \alpha^2) \coth^2 \left(\frac{\alpha}{\sqrt{2}} \frac{\phi}{M_{\text{Pl}}} \right) - 3 \right], \quad (5.182)$$

where α is a positive dimensionless parameter (denoted n_0 in Ref. [370]). The potential being symmetrical in $\phi \rightarrow -\phi$, only the $\phi > 0$ part is displayed in Fig. 58. It is a decreasing function of the field vev , and its asymptotic value when ϕ/M_{Pl} goes to infinity is given by $\alpha^2 M^4$, hence the potential is always positive. Defining $x = \phi/M_{\text{Pl}}$, the three first slow-roll parameters are given by

$$\epsilon_1 = \frac{4\alpha^2 (3 + \alpha^2)^2 \coth^2 \left(\frac{\alpha x}{\sqrt{2}} \right)}{[6 + \alpha^2 + \alpha^2 \cosh(\sqrt{2}\alpha x)]^2}, \quad (5.183)$$

$$\epsilon_2 = -\frac{2\alpha^2 (3 + \alpha^2) [12 + \alpha^2 + 2\alpha^2 \cosh(\sqrt{2}\alpha x) + \alpha^2 \cosh(2\sqrt{2}\alpha x)]}{[6 + \alpha^2 + \alpha^2 \cosh(\sqrt{2}\alpha x)]^2 \sinh^2 \left(\frac{\alpha x}{\sqrt{2}} \right)}, \quad (5.184)$$

and

$$\begin{aligned}
\epsilon_3 = & -2\alpha^2 (3 + \alpha^2) \left[6 (24 - 2\alpha^2 + \alpha^4) + (120\alpha^2 + 7\alpha^4) \cosh(\sqrt{2}\alpha x) \right. \\
& + 2\alpha^2 (\alpha^2 - 6) \cosh(2\sqrt{2}\alpha x) + \alpha^4 \cosh(3\sqrt{2}\alpha x) \left. \right] \coth^2\left(\frac{\alpha}{\sqrt{2}}x\right) \\
& \times \left[6 + \alpha^2 + \alpha^2 \cosh(\sqrt{2}\alpha x) \right]^{-2} \left[12 + \alpha^2 + 2\alpha^2 \cosh(\sqrt{2}\alpha x) + \alpha^2 \cosh(2\sqrt{2}\alpha x) \right]^{-1}.
\end{aligned} \tag{5.185}$$

These slow-roll parameters are displayed in Fig. 58 (bottom panels). We see that the first slow-roll parameters monotonously decreases during inflation. It blows up as the field vev approaches zero and tends to zero when the field vev goes to infinity. On the contrary, the second and third slow-roll parameters monotonously increase from $-\infty$ to zero as inflation proceeds.

Given the above described behavior of ϵ_1 , it is clear that inflation cannot stop by slow-roll violation. Therefore, it should be stopped by instability which means and that an extra parameter x_{end} should be added to the model.

Now let us check that the spectral index $n_s - 1 = -2\epsilon_1 - \epsilon_2$ at first order in slow-roll, is indeed constant. Expanding the slow-roll parameters ϵ_1 and ϵ_2 in $\alpha \ll 1$, one obtains $\epsilon_1 = 2/x^2 + 2\alpha^2/3 + \mathcal{O}(\alpha^4)$ and $\epsilon_2 = -4/x^2 + 2\alpha^2/3 + \mathcal{O}(\alpha^4)$, so that $n_s - 1 = -2\alpha^2 + \mathcal{O}(\alpha^4)$. One concludes that this two parameter model does produce a constant n_s power spectrum. This also implies that a first order approximation in slow-roll is an expansion to second order in $\alpha \ll 1$. We have already encountered similar calculations in sections 4.20 and 4.21. Based on our results for those sections, one should remark that, if x_{end} is such that $\alpha x_* \gtrsim 1$, the previous expansion does not hold and deviations from constant n_s may appear.

Let us now consider the slow-roll trajectory. It can be integrated exactly and is given by the following formula

$$\begin{aligned}
N - N_{\text{ini}} = & \frac{1}{\alpha^2 (3 + \alpha^2)} \left\{ 3 \ln \left[\cosh \left(\frac{\alpha}{\sqrt{2}} x \right) \right] + \frac{\alpha^2}{2} \cosh^2 \left(\frac{\alpha}{\sqrt{2}} x \right) \right. \\
& \left. - 3 \ln \left[\cosh \left(\frac{\alpha}{\sqrt{2}} x_{\text{ini}} \right) \right] - \frac{\alpha^2}{2} \cosh^2 \left(\frac{\alpha}{\sqrt{2}} x_{\text{ini}} \right) \right\}.
\end{aligned} \tag{5.186}$$

Moreover, this expression can be explicitly inverted. As a consequence, the function $x(N)$ can be written as

$$\begin{aligned}
x = & \frac{\sqrt{2}}{\alpha} \operatorname{arccosh} \left[\frac{3}{\alpha^2} W_0 \left(\frac{\alpha^2}{3} \exp \left\{ \frac{2}{3} \alpha^2 (3 + \alpha^2) (N - N_{\text{ini}}) \right. \right. \right. \\
& \left. \left. \left. + 2 \ln \left[\cosh \left(\frac{\alpha}{\sqrt{2}} x_{\text{ini}} \right) \right] + \frac{\alpha^2}{3} \cosh^2 \left(\frac{\alpha}{\sqrt{2}} x_{\text{ini}} \right) \right\} \right) \right]^{1/2},
\end{aligned} \tag{5.187}$$

where W_0 is the Lambert function. The fact that we deal with the 0-branch is obvious since the argument of this function is positive definite.

The predictions of the CNCI models are displayed in Fig. 123, for $\alpha = 10^{-3}, 0.1, 0.2$. The thin black solid lines are the lines such that $n_s - 1 = -2\alpha^2$. We see that, for very small values of α , the predictions are indeed such that the spectral index is constant. For α not too small, however, we also notice deviations from this law and the larger α the stronger these deviations, which is of course what one expects. This is reminiscent of the phenomenon observed in sections 4.20 and 4.21 for similar scenarios. We also remark that, for a given

value of α , the deviations from $n_s - 1 = -2\alpha^2$ become larger when x_{end} increase (i.e. when the line becomes redder in Fig. 123). This, of course, makes sense since, in this case, the Taylor expansion of the trigonometric functions which appear in the expressions of the slow-roll parameters is no longer valid (a larger x_{end} means a larger x_*). This has for consequence that CNCI inflation is only marginally consistent with the data. Indeed, it is precisely in the region where $n_s - 1 = -2\alpha^2$ would be compatible with the observations that the deviations play an important role and push the predictions outside the allowed contours. In fact, one can understand better the properties of this scenario if one explicitly calculates x_* . Using Eq. (5.186), it is easy to show that

$$\cosh^2\left(\frac{\alpha x_*}{\sqrt{2}}\right) = \frac{3}{\alpha^2} W_0\left(\frac{\alpha^2}{3} e^{2A/3}\right), \quad (5.188)$$

where we have defined the quantity A by

$$A \equiv -\alpha^2 (3 + \alpha^2) \Delta N_* + 3 \ln \left[\cosh\left(\frac{\alpha x_{\text{end}}}{\sqrt{2}}\right) \right] + \frac{\alpha^2}{2} \cosh^2\left(\frac{\alpha x_{\text{end}}}{\sqrt{2}}\right) \quad (5.189)$$

In the regime where $\alpha \ll 1$ and $\alpha x_{\text{end}} \ll 1$, the previous expression reduces to $x_*^2 \simeq x_{\text{end}}^2 - 4\Delta N_*$. This last formula is identical to the slow-roll trajectory for LFI provided $p = -2$, see Eq. (4.30). At the beginning of this section, we have show that, at leading order $\epsilon_1 \simeq 2/x^2$ and $\epsilon_2 \simeq -4/x^2$ and, comparing with Eqs. (4.29), we notice that these are also the slow-roll parameters for LFI with $p = -2$. In fact, expanding Eq. (5.182), one sees that $V(\phi) \propto \phi^{-2}$ which confirms the previous considerations. We conclude that, in the regime where $\alpha \ll 1$ and $\alpha x_{\text{end}} \ll 1$, the model is very close to LFI with $p = -2$. This also allows us to understand better why the spectral index is constant in this case. For LFI, Eqs. (4.29) tell us that $\epsilon_1 = p^2/(2x^2)$ and $\epsilon_2 = 2p/x^2$. If one chooses $p = -2$ then one obtains $n_s = 1$ because $-2\epsilon_1$ and $-\epsilon_2$ exactly cancel out in the expression of the spectral index. In the case of CNCI inflation, ϵ_1 and ϵ_2 have the previously quoted values at leading order plus corrections quadratic in α . Because of the cancellation mentioned before, the leading term is absent and one is left with the quadratic corrections only. This explains and justifies the formula $n_s = 1 - 2\alpha^2$.

Finally, we conclude this section by discussing how the mass scale M can be chosen. The COBE normalization gives

$$\left(\frac{M}{M_{\text{Pl}}}\right)^4 = \frac{11520\pi^2\alpha^2(3+\alpha^2)^2 \cosh^2\left(\frac{\alpha}{\sqrt{2}}x_*\right) Q_{\text{rms-PS}}^2}{[6 + \alpha^2 + \alpha^2 \cosh(\sqrt{2}\alpha x_*)]^3 T^2}. \quad (5.190)$$

We can obtain an order of estimate of M using the following very rough approximations. From Eq. (5.188), one deduces that $\cosh^2(\alpha x_*/\sqrt{2}) \simeq 1 - 2\alpha^2\Delta N_* + \alpha^2 x_{\text{end}}^2/2 \simeq 1$. Inserting this formula into Eq. (5.190), and taking the leading order in α , one obtains $M/M_{\text{Pl}} \simeq 0.02\sqrt{\alpha}$. This implies that $M < M_{\text{Pl}}$ if $\alpha \lesssim 2420$, which is largely the case for the predictions displayed in Fig. 123.

5.15 Supergravity Brane Inflation (SBI)

This model has been originally proposed in Refs. [414, 415] in the context of brane cosmology within a supergravity bulk spacetime. In the original works, the model is studied in the high energy regime, i.e. for inflation and reheating occurring at energy densities higher than the

brane tension and therefore with a modified Friedmann-Lemaître equation. According to our previous discussions, we will be restricted in the following to the low energy limit for which inflation occurs at an energy scale smaller than the brane tension. The potential reads

$$V(\phi) = M^4 \left\{ 1 + \left[-\alpha + \beta \ln \left(\frac{\phi}{M_{\text{Pl}}} \right) \right] \left(\frac{\phi}{M_{\text{Pl}}} \right)^4 \right\}, \quad (5.191)$$

where α and β are dimensionless one loop coupling constants. On a purely phenomenological basis, Eq. (5.191) is a typical F-term supergravity potential with loop corrections. For instance, setting $\alpha = 0$ gives back the Coleman-Weinberg CWI models (see section 4.11). Defining

$$x \equiv \frac{\phi}{M_{\text{Pl}}}, \quad (5.192)$$

the potential decreases from $x = 0$ to reach its minimum at $x = x_{V'=0}$, then increases again and diverges when x goes to infinity. The value of $x_{V'=0}$ is given by

$$x_{V'=0} = \exp \left(\frac{\alpha}{\beta} - \frac{1}{4} \right). \quad (5.193)$$

Since the logarithm terms in Eq. (5.191) are loop corrections, they should not dominate over the leading order terms. As a result, inflation can take place only in the domain $x < x_{V'=0}$. At its minimum, the potential equals

$$V_{\text{min}} = V(x_{V'=0}) = M^4 \left(1 - \frac{\beta}{4} e^{4\alpha/\beta-1} \right), \quad (5.194)$$

which is negative or null for

$$\alpha \geq \alpha_{\text{min}}(\beta) = \frac{\beta}{4} \left[1 - \ln \left(\frac{\beta}{4} \right) \right]. \quad (5.195)$$

Under this condition, inflation can proceed at increasing field values in the domain $0 < x < x_{V=0} < x_{V'=0}$, where $x_{V=0}$ is the value at which the potential vanishes. It is given by

$$x_{V=0} = \left[\frac{-4/\beta}{W_{-1}(-4/\beta e^{-4\alpha/\beta})} \right]^{1/4}, \quad (5.196)$$

where W_{-1} is the -1 branch of the Lambert function. Let us notice that if Eq. (5.195) is not satisfied, the potential would admit a positive global minimum that triggers a pure de-Sitter era without graceful exit. The first three Hubble flow functions in the slow-roll approximation are given by

$$\epsilon_1 = \frac{x^6 (-4\alpha + \beta + 4\beta \ln x)^2}{2(1 - \alpha x^4 + \beta x^4 \ln x)^2}, \quad (5.197)$$

$$\epsilon_2 = 2 \frac{(12\alpha - 7\beta - 12\beta \ln x) x^2 + (4\alpha^2 - \alpha\beta + \beta^2 + \beta^2 \ln x - 8\alpha\beta \ln x + 4\beta^2 \ln^2 x) x^6}{[1 + x^4 (-\alpha + \beta \ln x)]^2}, \quad (5.198)$$

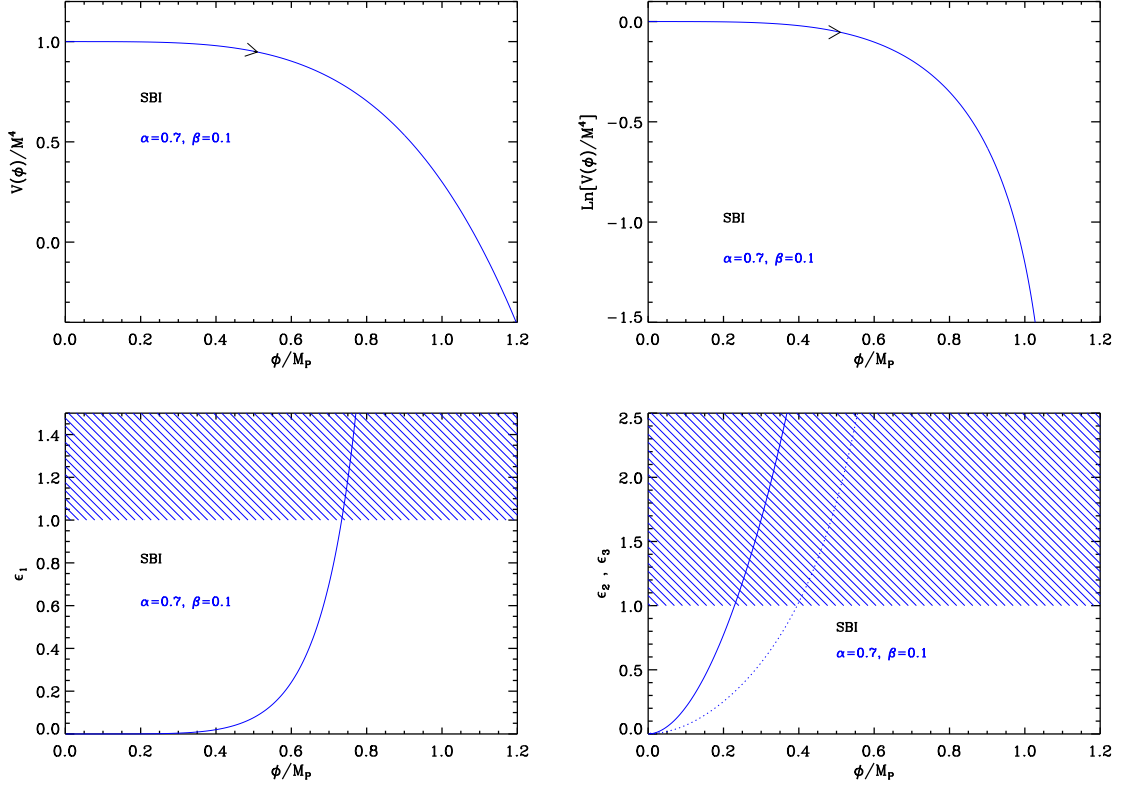


Figure 59. Supergravity Brane Inflation (SBI) for $\alpha = 0.7$ and $\beta = 0.1$. Upper panels: the potential and its logarithm in the small field branch. Bottom left panel: slow-roll parameter ϵ_1 . The shaded area indicates where inflation stops. Bottom right panel: slow-roll parameters ϵ_2 (solid line) and ϵ_3 (dotted line).

$$\epsilon_3 = \frac{8}{x^2} + 2 \frac{(-4 + \beta x^4)^2}{x^2 (1 - \alpha x^4 + \beta x^4 \ln x)^2} + \frac{1}{x^2} \frac{-52 + 9\beta x^4}{1 - \alpha x^4 + \beta x^4 \ln x} + \frac{144\alpha - 84\beta + (28\alpha - 11\beta)\beta x^4 - 4\beta(36 + 7\beta x^4) \ln x}{(12\alpha - 7\beta - 12\beta \ln x)x^2 + (4\alpha^2 - \alpha\beta + \beta^2 - 8\alpha\beta \ln x + \beta^2 \ln x + 4\beta^2 \ln^2 x)x^6}.$$
(5.199)

Together with the potential, they have been represented in Fig. 59 for the physical branch $0 < x < x_{V=0}$.

The slow-roll trajectory can be integrated analytically and one obtains

$$N - N_{\text{end}} = \frac{e^{2\frac{\alpha}{\beta} - \frac{1}{2}}}{16} \left[\text{Ei} \left(\frac{1}{2} - 2\frac{\alpha}{\beta} + 2 \ln x \right) - \text{Ei} \left(\frac{1}{2} - 2\frac{\alpha}{\beta} + 2 \ln x_{\text{end}} \right) \right] - \frac{e^{\frac{1}{2} - 2\frac{\alpha}{\beta}}}{4\beta} \left[\text{Ei} \left(-\frac{1}{2} + 2\frac{\alpha}{\beta} - 2 \ln x \right) - \text{Ei} \left(-\frac{1}{2} + 2\frac{\alpha}{\beta} - 2 \ln x_{\text{end}} \right) \right] - \frac{x^2 - x_{\text{end}}^2}{8}.$$
(5.200)

Since $\epsilon_1(x)$ is an increasing function of x , inflation stops at $x = x_{\text{end}}$ where x_{end} is the solution of $\epsilon_1(x_{\text{end}}) = 1$. From Eq. (5.197), there is no analytical solution for x_{end} and this equation has to be solved numerically. Let us stress however that since ϵ_1 diverges for $x \rightarrow x_{V=0}$, one

always has $x_{\text{end}} < x_{V=0}$.

The field value x_* at which the pivot scale crossed the Hubble radius during inflation is obtained by solving Eq. (2.46) while the parameter M is fixed by the amplitude of the CMB anisotropies, i.e.

$$\left(\frac{M}{M_{\text{Pl}}}\right)^4 = \frac{720\pi^2 (4\alpha - \beta - 4\beta \ln x_*)^2 Q_{\text{rms-PS}}^2}{(-1 + \alpha x_*^4 - \beta x_*^4 \ln x_*)^3 T^2}. \quad (5.201)$$

The reheating consistent slow-roll predictions for the SBI models are displayed in Figs. 124 and 125, for $\beta = 5 \times 10^{-5}$ and $\beta = 10^{-3}$, respectively. These plots exhibit the trend with respect of β : larger values of β produce a completely negligible amount of gravitational waves.

5.16 Spontaneous Symmetry Breaking Inflation (SSBI)

The potential that we study in this section is given by the following expression

$$V(\phi) = M^4 \left[1 + \alpha \left(\frac{\phi}{M_{\text{Pl}}}\right)^2 + \beta \left(\frac{\phi}{M_{\text{Pl}}}\right)^4 \right], \quad (5.202)$$

where α and β are two dimensionless parameters. Formally, this potential is very general since it is just made of the three first terms of a general Taylor expansion. Moreover, it arises in various different contexts that we now briefly review. In fact, these different examples usually differ in the signs for the parameters α and β . A first example is simply Ref. [276] where this potential was used as a toy model to implement “New Inflation”. Then, it was also considered in Ref. [416] (with the assumptions $\alpha < 0$ and $\beta > 0$) in the framework of models with spontaneous symmetry breaking where ϕ represents one of the components of a Higgs field. In Ref. [417], it was studied in the context of “Mixmaster inflation”. In Refs. [418, 419], it was investigated in the context of gauge mediated SUSY breaking inflation. More recently, it was also used in Refs. [420, 421] to study a model of “Spinodal Inflation”. After the 90’s, it was considered again several times: in the context of the Randall-Sundrum model in Ref. [422], in the context of pseudonatural inflation in Ref. [212], in the context of induced gravity inflation in Ref. [423], in the context of electroweak inflation in Ref. [424], in the context of Sneutrino hybrid inflation in Ref. [425], in the context of racetrack inflation in Ref. [426], in the context of minimal left-right symmetric models with spontaneous D-parity breaking in Ref. [427], in the context of hilltop supernatural inflation in Refs. [428–430], in the context of a supersymmetric B - L extension of the standard model in Refs. [431, 432] and, finally, in the context of Kähler-driven tribrid inflation in Ref. [433]. As already mentioned above, these works differ on the signs of α and β . Refs. [417, 425, 426] require $\alpha > 0$, $\beta > 0$ while Refs. [212, 276, 416, 420, 421, 423, 424, 427] assume $\alpha < 0$, $\beta > 0$. On the other hand, Refs. [428–430] consider that $\alpha > 0$ and $\beta < 0$ and Refs. [418, 419] that $\alpha < 0$, $\beta < 0$. We see that the four possible combinations have all been studied. Also, in Refs. [431, 432], one has $\alpha, \beta \lesssim \mathcal{O}(1)$ and inflation only takes place in the increasing branches of the potential (see below). Finally, in Refs. [422, 433], $\beta > 0$ is taken to be positive and the sign of α is left unspecified.

Based on this quick review of the literature, we conclude that it is necessary to study the model in full generality and, therefore, in what follows, we study all the possible situations. As mentioned above, four cases should be distinguished: $\alpha > 0$, $\beta > 0$; $\alpha < 0$, $\beta < 0$; $\alpha > 0$, $\beta < 0$ and $\alpha < 0$, $\beta > 0$, with two possible domains of inflation in the two latter cases. Therefore we have six regimes of inflation that we label SSBI1, SSBI2, SSBI3, SSBI4, SSBI5 and SSBI6. The different potentials and inflationary regimes are displayed and defined in

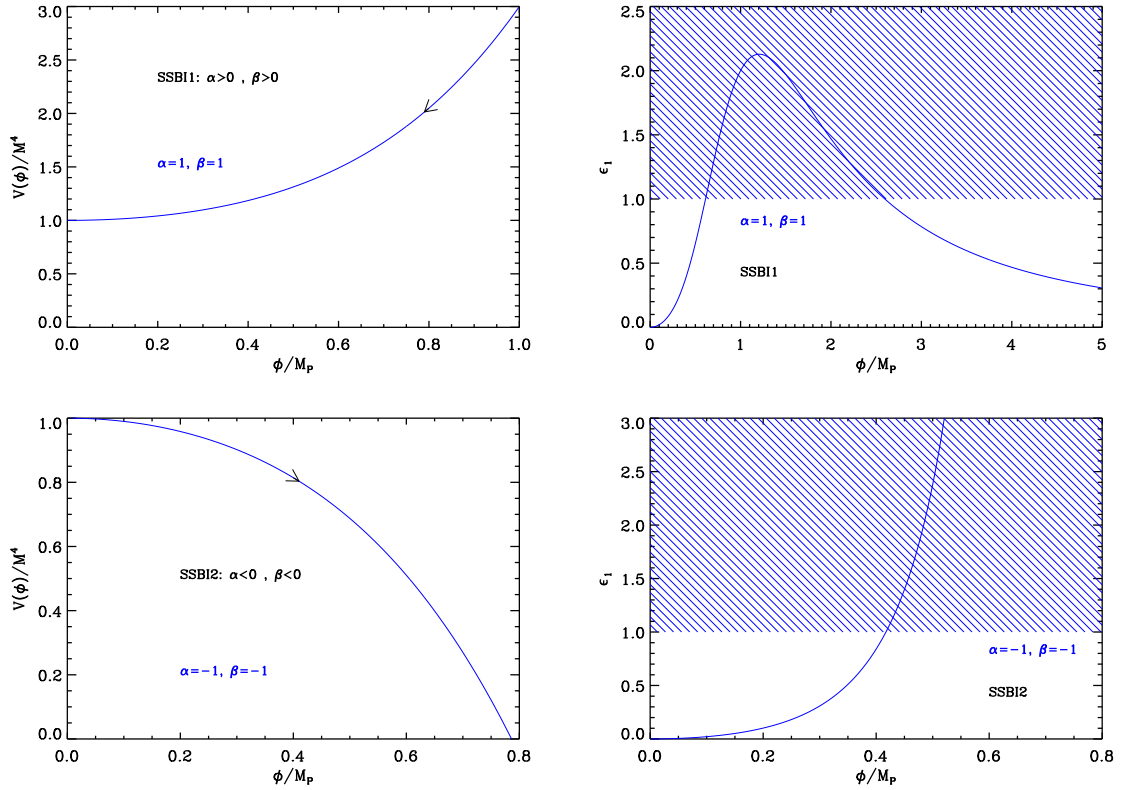


Figure 60. Spontaneous Symmetry Breaking Inflation (SSBI) potential and the corresponding Hubble flow parameter ϵ_1 for the two cases $\alpha > 0, \beta > 0$ (SSBI1), and $\alpha < 0, \beta < 0$ (SSBI2). The values of the parameters are chosen to be $\alpha, \beta = \pm 1$. The four other possibilities, namely SSBI3, SSBI4, SSBI5, SSBI6 are displayed in Fig. 61.

Fig. 60 and Fig. 61. Since the potential is symmetric under $\phi/M_{\text{Pl}} \rightarrow -\phi/M_{\text{Pl}}$, it is only displayed and studied for $\phi > 0$.

Let us now calculate the slow-roll parameters. If one defines x by $x \equiv \phi/M_{\text{Pl}}$, then the three first Hubble parameters are given by the following expressions

$$\epsilon_1 = \frac{2(\alpha x + 2\beta x^3)^2}{(1 + \alpha x^2 + \beta x^4)^2}, \quad \epsilon_2 = \frac{4[-\alpha + (\alpha^2 - 6\beta)x^2 + \alpha\beta x^4 + 2\beta^2 x^6]}{(1 + \alpha x^2 + \beta x^4)^2}, \quad (5.203)$$

and

$$\epsilon_3 = \frac{4x^2(\alpha + 2\beta x^2)[-3\alpha^2 + 6\beta + \alpha(\alpha^2 - 12\beta)x^2 + 3(\alpha^2 - 8\beta)\beta x^4 + 2\beta^3 x^8]}{(1 + \alpha x^2 + \beta x^4)^2[-\alpha + (\alpha^2 - 6\beta)x^2 + \alpha\beta x^4 + 2\beta^2 x^6]}. \quad (5.204)$$

The first slow-roll parameter ϵ_1 is displayed in the right panels of Figs. 60 and 61 while the second and third slow-roll parameters ϵ_2 and ϵ_3 are displayed in Fig. 62. Let us describe the behavior of these slow-roll parameters, for the six models under consideration. For SSBI1, ϵ_1 vanishes at $x = 0$, reaches a maximum at $x_{\epsilon_2=0}^{\text{SSBI1}}$ (where ϵ_2 vanishes and ϵ_3 diverges) and then decreases to asymptotically vanish when x goes to infinity. The value of $x_{\epsilon_2=0}^{\text{SSBI1}}$ is given

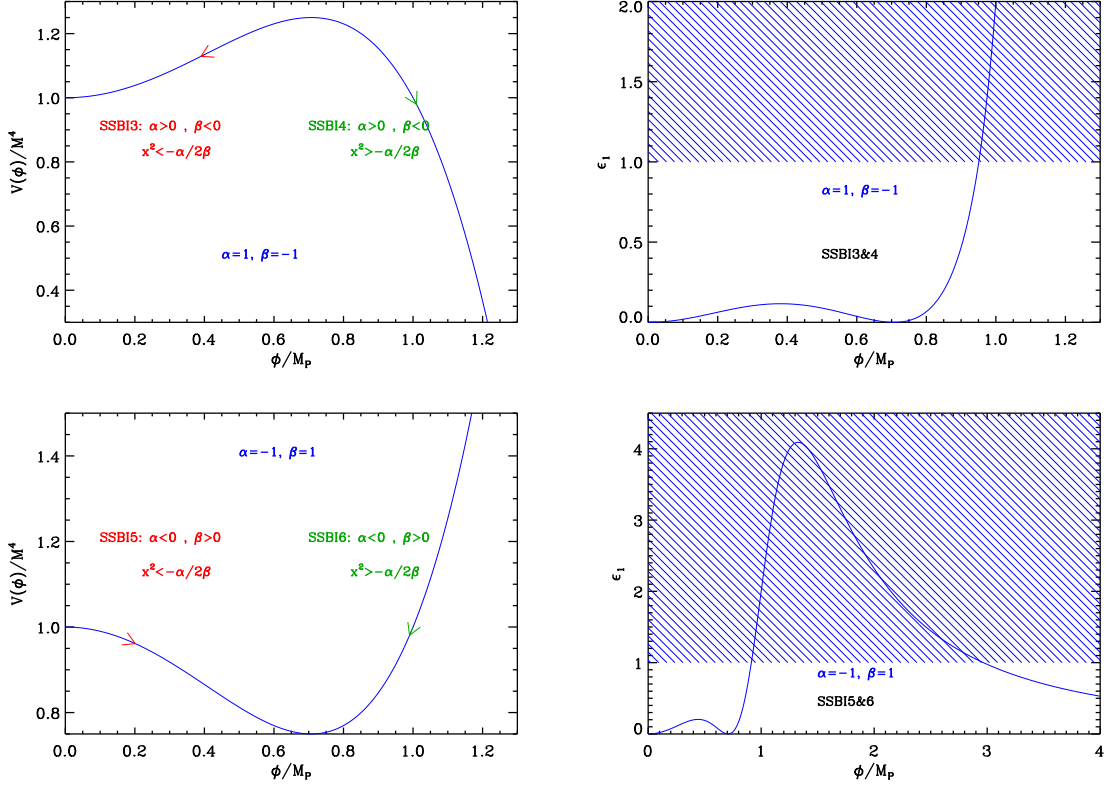


Figure 61. Spontaneous Symmetry Breaking Inflation (SSBI) potential and the corresponding Hubble flow parameter ϵ_1 for the two cases $\alpha > 0, \beta < 0$ (corresponding to SSBI3 to SSBI4) and $\alpha < 0, \beta > 0$ (corresponding to SSBI5 and to SSBI6). In each of these cases, the direction in which inflation proceeds is indicated by the arrow.

by

$$x_{\epsilon_2=0}^{\text{SSBI1}\&3\&6} = \left\{ -\frac{\alpha}{6\beta} + \frac{1}{6\beta} \left[8\alpha^3 + \sqrt{64\alpha^6 + (5\alpha^2 - 36\beta)^3} \right]^{1/3} + \frac{36\beta - 5\alpha^2}{6\beta} \left[8\alpha^3 + \sqrt{64\alpha^6 + (5\alpha^2 - 36\beta)^3} \right]^{-1/3} \right\}^{1/2}. \quad (5.205)$$

Whether the maximum of ϵ_1 at this point is larger or smaller than 1 depends on α and β . In the following, we restrict ourselves to the physical regime where $\alpha, \beta \lesssim \mathcal{O}(1)$. For each value of β , there is a minimum value of α , denoted α_{\min} , above which the maximum is larger than 1. The line $\alpha_{\min}(\beta)$ is displayed in Fig. 63 and the shaded area in this plot represents the region in the parameter space where inflation stops by slow-roll violation. When $\beta \ll 1$, $\alpha_{\min}(\beta)$ approaches 2 as can be noticed in the figure. In addition, for $\beta \gtrsim 0.25$, the maximum value for ϵ_1 becomes larger than 1 for any value of α .

For SSBI2, the three first slow-roll parameters are monotonic increasing functions of

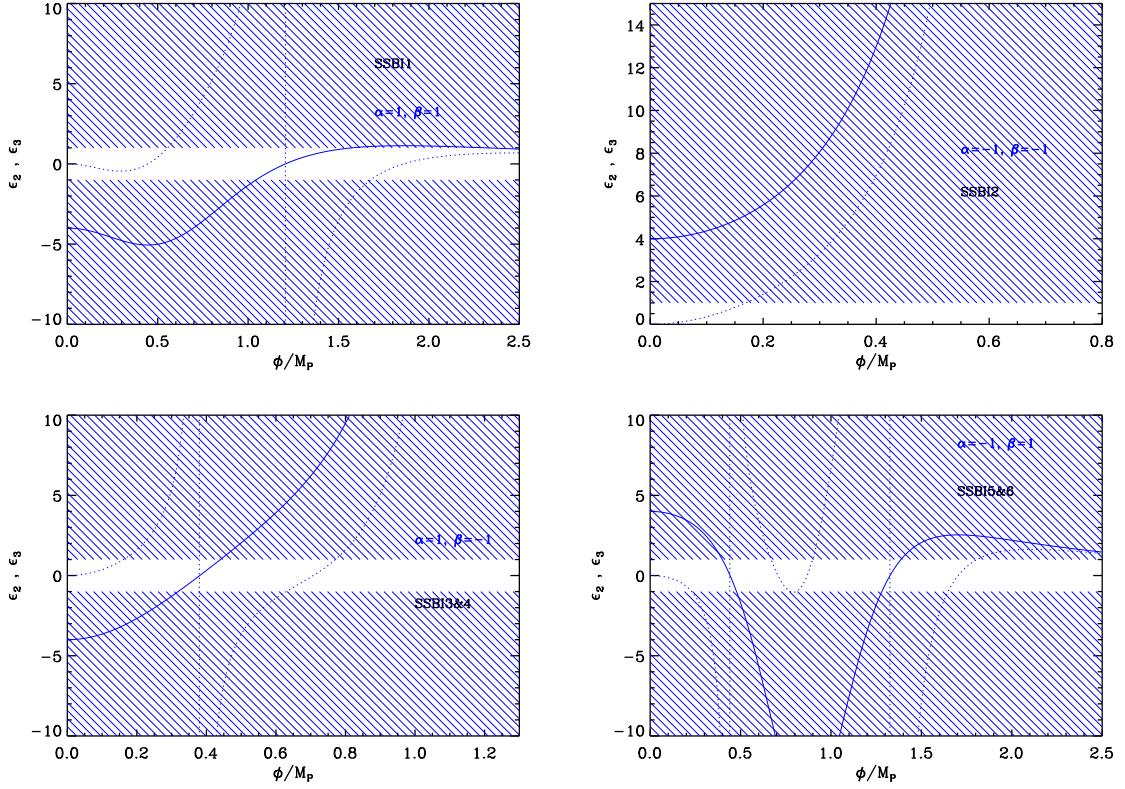


Figure 62. Second slow-roll parameter ϵ_2 (solid line) and third slow-roll parameter ϵ_3 (dotted line), for the six SSBI models studied in this section. The free parameters of the models are chosen to be $\alpha, \beta = \pm 1$.

the field vev and diverge when the potential vanishes at

$$x_{V=0}^{\text{SSBI2}\&4\&5} = \sqrt{-\frac{\alpha + \sqrt{\alpha^2 - 4\beta}}{2\beta}}. \quad (5.206)$$

Hence inflation ends by slow-roll violation at x_{end} . Unfortunately, the corresponding vev cannot be found exactly and one has to rely on numerical calculations. Let us also notice that, while the first and third slow-roll parameters ϵ_1 and ϵ_3 vanish at $x = 0$, ϵ_2 is equal to $\epsilon_2^{\text{min}} = -4\alpha$ at this point. Therefore, in order for the slow-roll approximation to be valid, one needs to work with $|\alpha| \ll 1$.

For SSBI3, the first slow-roll parameter ϵ_1 vanishes at $x = 0$ and at $x = \sqrt{-\alpha/(2\beta)}$. In between, it reaches a maximum located at

$$x_{\epsilon_2=0}^{\text{SSBI3}} = x_{\epsilon_2=0}^{\text{SSBI1}}, \quad (5.207)$$

a point where ϵ_2 vanishes and ϵ_3 diverges. Whether the maximum of ϵ_1 at this point is larger or smaller than 1 depends again on α and β . For each value of β , there is a minimum value for $\alpha = \alpha_{\text{min}}$ above which inflation stops by slow-roll violation. This discussion is in fact similar to the one presented in the SSBI1 case. The corresponding allowed region is represented in Fig. 63 (top right panel).

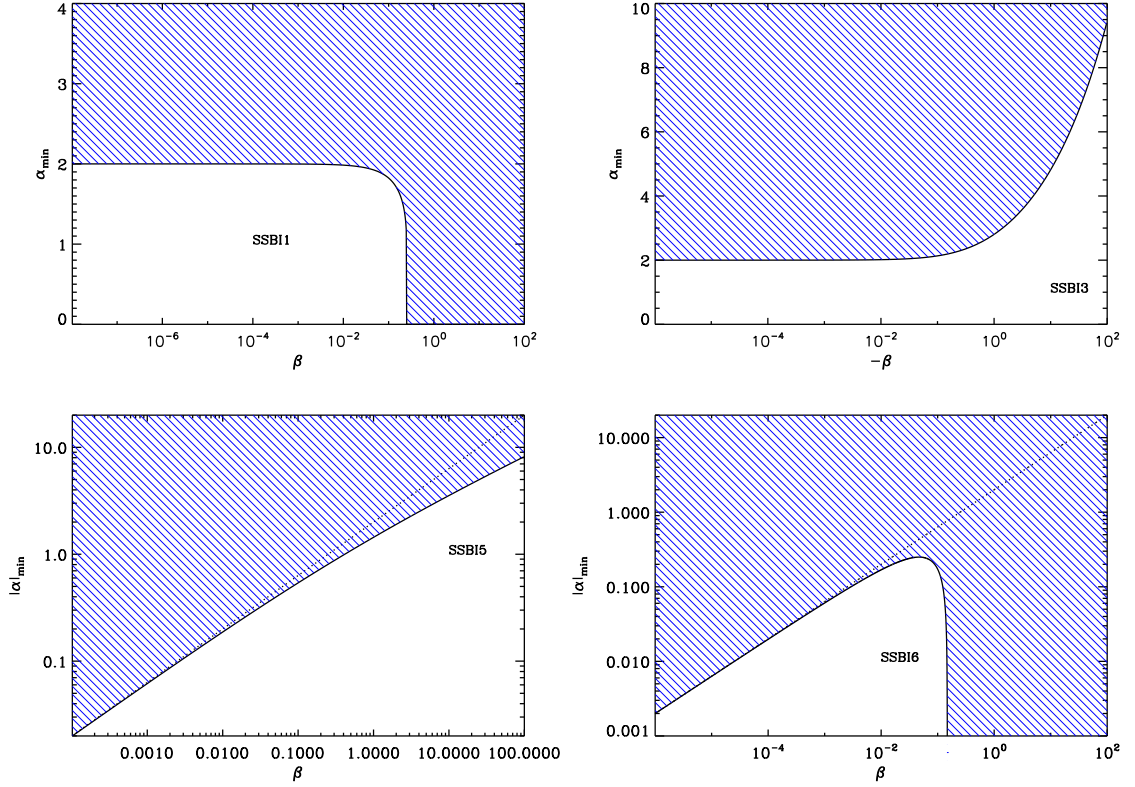


Figure 63. The solid black line gives the minimum value of $|\alpha|$, denoted here by α_{\min} , as a function of β in order for inflation to stop by slow-roll violation for SSBI1 (top left panel), SSBI3 (top right panel), SSBI5 (bottom left panel) and SSBI6 (bottom right panel). The region above the curve (shaded region) represents the allowed region (i.e. the one where inflation stops because ϵ_1 reaches one). For SSBI1, when $\beta \gtrsim 0.25$, this is always the case. For SSBI1 and SSBI3, α_{\min} approaches the asymptotic value $\alpha_{\min} = 2$ when $|\beta| \ll 1$. For SSBI5 and SSBI6, inflation stops by slow-roll violation when $\alpha < -|\alpha_{\min}|$. Finally, the dotted lines in the bottom panels corresponds $\alpha^2 = 4\beta$, see the discussion in the text.

For SSBI4, the three first slow-roll parameters are monotonic increasing functions of the field vev and diverge when the potential vanishes at $x_{V=0}^{\text{SSBI2\&4}}$. The first and third slow-roll parameters ϵ_1 and ϵ_3 vanish when $x = \sqrt{-\alpha/(2\beta)}$ while ϵ_2 has a non zero value $\epsilon_2^{\min} = 8\alpha\beta/(\beta^2 - \alpha^2/4)$ at this point. From the above discussion, it is clear that, in this version of the scenario, inflation also stops by violation of the slow-roll condition. As for SSBI2, however, the corresponding vev can not be determined exactly and a numerical calculation is needed.

For SSBI5, the behavior of the slow-roll parameters depend on α^2/β . If $\alpha^2/\beta \geq 4$, the minimum of the potential at $x = \sqrt{-\alpha/(2\beta)}$ is negative. The potential vanishes at $x_{V=0}^{\text{SSBI2\&4\&5}}$ and the three first slow-roll parameters continuously increase between $x = 0$ where they vanish (except from ϵ_2 for which $\epsilon_2^{\min} = -4\alpha$) and $x_{V=0}^{\text{SSBI2\&4\&5}}$ where they diverge. Inflation ends by slow-roll violation at some point x_{end} that needs to be determined numerically. On the other hand, if $\alpha^2/\beta \leq 4$, ϵ_1 vanishes at $x = 0$, reaches a maximum at $x_{\epsilon_2=0}^{\text{SSBI5}}$ (where ϵ_2 vanishes and ϵ_3 diverges), then decreases and finally vanishes at $x = \sqrt{-\alpha/(2\beta)}$.

The value of $x_{\epsilon_2=0}^{\text{SSBI5}}$ is given by

$$x_{\epsilon_2=0}^{\text{SSBI5}} = \left\{ -\frac{\alpha}{6\beta} - \frac{1+i\sqrt{3}}{12\beta} \left[8\alpha^3 + \sqrt{64\alpha^6 + (5\alpha^2 - 36\beta)^3} \right]^{1/3} + \frac{5\alpha^2 - 36\beta}{12\beta} (1-i\sqrt{3}) \left[8\alpha^3 + \sqrt{64\alpha^6 + (5\alpha^2 - 36\beta)^3} \right]^{-1/3} \right\}^{1/2}. \quad (5.208)$$

Whether the maximum of ϵ_1 at this point is larger or smaller than 1 depends on α and β and is again similar to what has already been discussed before. The region in the parameter space where inflation ends by slow-roll violation is displayed in Fig. 63 and corresponds to the points such that $\alpha < -|\alpha_{\min}|$. In this plot, the dotted line represents the curve $\alpha^2 = 4\beta$, above which one is sure that inflation ends by slow-roll violation since the minimum of the potential is negative in this case. For values of $\beta \ll 1$, one can see that $|\alpha_{\min}| \sim 2\sqrt{\beta}$ and the allowed region becomes negligible.

Finally the case SSBI6 remains to be treated. The behavior of the slow roll parameters depend on α^2/β in the same way as before. If $\alpha^2/\beta \geq 4$, the minimum of the potential at $x = \sqrt{-\alpha/(2\beta)}$ is negative. The potential vanishes at $x_{V=0}^{\text{SSBI6}}$ and the slow-roll parameters continuously decrease from this value (where they blow up) and go to zero at infinity. The value of $x_{V=0}^{\text{SSBI6}}$ can be expressed as

$$x_{V=0}^{\text{SSBI6}} = \sqrt{\frac{-\alpha + \sqrt{\alpha^2 - 4\beta}}{2\beta}}. \quad (5.209)$$

On the other hand, if $\alpha^2/\beta \leq 4$, ϵ_1 vanishes at $x = \sqrt{-\alpha/(2\beta)}$, reaches a maximum at $x_{\epsilon_2=0}^{\text{SSBI6}}$ and then decreases. At infinity, it goes to zero. The value of $x_{\epsilon_2=0}^{\text{SSBI6}}$ is given by

$$x_{\epsilon_2=0}^{\text{SSBI6}} = x_{\epsilon_2=0}^{\text{SSBI3}} = x_{\epsilon_2=0}^{\text{SSBI1}}. \quad (5.210)$$

Whether the maximum of ϵ_1 at this point is larger or smaller than 1 depends on α and β . The corresponding region in the parameter space is displayed in Fig. 63 and corresponds to the inequality $\alpha < -|\alpha_{\min}|$. The dotted line represents the law $\alpha^2 = 4\beta$. Above this line, one is sure that inflation can stop by slow-roll violation since, in this case, the potential becomes negative at some point. It is also interesting to notice that, when $\beta \gtrsim 1.48$, the maximum value of ϵ_1 is larger than 1 for any value of α . On the other hand, if $\beta \ll 1$, the allowed region shrinks to zero.

Let us now turn to the slow-roll trajectory. This one can be integrated exactly and the following expression is obtained

$$N_{\text{end}} - N = -\frac{1}{2\alpha} \ln \left(\frac{x_{\text{end}}}{x} \right) - \frac{x_{\text{end}}^2 - x^2}{8} - \frac{\alpha^2 - 4\beta}{16\alpha\beta} \ln \left(\frac{1 + \frac{2\beta}{\alpha} x_{\text{end}}^2}{1 + \frac{2\beta}{\alpha} x^2} \right), \quad (5.211)$$

where N_{end} is the number of e-folds at the end of inflation. It is important to notice that the argument of the logarithm is always positive.

Finally, it is interesting to constrain the value of the scale M with the CMB normalization. It follows that

$$\left(\frac{M}{M_{\text{Pl}}} \right)^4 = \frac{2880 (\alpha x_* + 2\beta x_*^3)^2 \pi^2 Q_{\text{rms-PS}}^2}{(1 + \alpha x_*^2 + \beta x_*^4)^3 T^2}. \quad (5.212)$$

We are now in a position where we can discuss the predictions of the six versions of this model. The reheating consistent slow-roll predictions for the SSBI1 models are displayed in Figs. 126, 127 and 128 for $\beta = 10^{-3}$, $\beta = 10^{-1}$ and $\beta = 10$, respectively. SSBI1 seems to be disfavored by the observations. The predictions of SSBI2 models are displayed in Fig. 129 for different values of β and α . We notice that they depend on the parameter α quite strongly. The spectral index is clearly red and, for values of β of order one, the contribution of gravity waves becomes very small. For SSBI3, the predictions are presented in Figs. 130, 131 and 132 for $\beta = -10^{-3}$, $\beta = -5 \times 10^{-3}$ and $\beta = -10^{-2}$ respectively. As we increase β , the points start spreading in the plane (n_s, r) . For this class of models, the spectrum is red and the level of gravity waves quite important. The predictions for the SSBI4 models are displayed in Figs. 133, 134, and 135 for $\beta = -10^{-5}$, -10^{-4} , -10^{-3} respectively. One can notice that the typical predicted values for ϵ_1 decrease with the absolute value of β . As before the spread of the points increases with β . The tilt is still red and the contribution of gravity waves is small for small values of α . The predictions for the SSBI5 models are displayed in Figs. 136, 137 and 138 for $\beta = 10^{-6}$, $\beta = 10^{-5}$ and $\beta = 10^{-4}$, respectively. Once again, for $\mathcal{O}(1)$ values of β , one can see that the model predict a small amount of gravitational waves but a deviation from scale invariance not really compatible with the observational constraints. Finally, the reheating consistent slow-roll predictions for the SSBI6 models are displayed in Figs. 139, 140 and 141 for $\beta = 10^{-6}$, $\beta = 10^{-1}$ and $\beta = 1$, respectively. When $\beta \ll 1$ the predictions of the model do not depend on β . Moreover, for values of β of order one, the predictions become almost independent of the two parameters of the model.

6 Three parameters Models

6.1 Running-mass Inflation (RMI)

This model has been derived and studied in Refs. [286, 434–442]. Following Ref. [437], let us briefly discuss its physical origin. At tree level, a potential can always be expanded as $V(\phi) \simeq M^4 + m^2\phi^2/2 + \lambda/4\phi^4 + \dots$. Since the potential must be flat to support inflation, quantum corrections play an important role. Typically, they modify the potential with a term of the form $(c_1 + c_2\phi^2 + c_4\phi^4) \ln(\phi/\mu)$, where μ is the renormalization scale, see Ref. [437]. In a non supersymmetric framework, the quartic term dominates and one is led to models similar to RCMI, RCQI or CWI, see section 4.4, 4.5 and 4.11. On the other hand, in a supersymmetric context, at least if supersymmetry is spontaneously broken, the quadratic and the quartic terms cancel and one is left with a model similar to LI, see sections 4.12. If, however, supersymmetry is explicitly broken by the presence of soft terms, then the most important term will be the quadratic one. This gives rise to the RMI models that we study in this section. The corresponding potential is given by

$$V(\phi) = M^4 \left[1 - \lambda \left(-\frac{1}{2} + \ln \frac{\phi}{\mu} \right) \frac{\phi^2}{\mu^2} \right], \quad (6.1)$$

which is a function of ϕ/μ only. The same potential has also been obtained in Ref. [443] in the context of quadratic supergravity. This potential is characterized by three free parameters, M , μ and λ . However it turns out to be more convenient to use a slightly different parametrization (essentially to facilitate the comparison with the existing literature). For this reason, we re-write λ as $\lambda/\mu^2 \equiv c/(2M_{\text{Pl}}^2)$, thus introducing the parameter c . Then, the

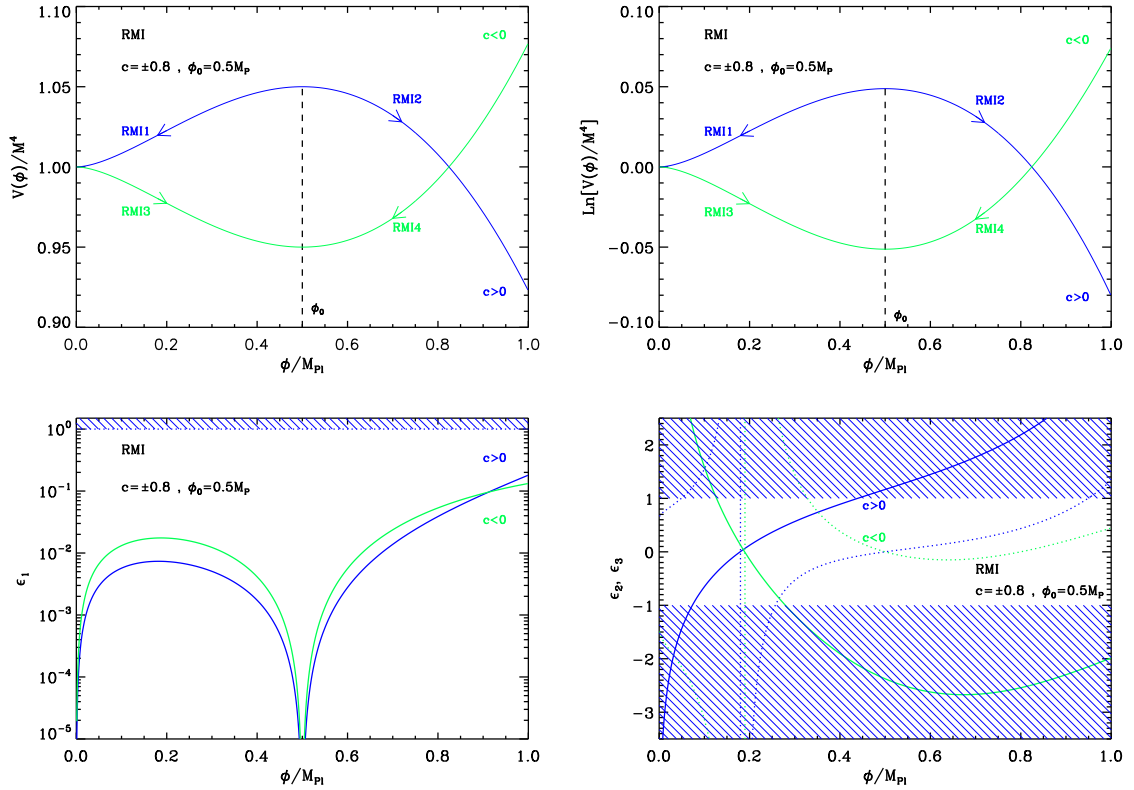


Figure 64. Top left panel: running mass potential for $c = 0.8$ (blue line) or $c = -0.8$ (green line) and $\phi_0 = 0.5M_{\text{Pl}}$. Top right panel: logarithm of the potentials for the same values of c and ϕ_0 . Bottom left panel: slow-roll parameter ϵ_1 for a potential with $c = \pm 0.8$ and $\phi_0 = 0.5M_{\text{Pl}}$. Bottom right panel: slow-roll parameters ϵ_2 (solid line) and ϵ_3 (dotted line) for $c = \pm 0.8$ and $\phi_0 = 0.5M_{\text{Pl}}$. The value $c = \pm 0.8$ may not be physical and was chosen only in order to produce a clear plot.

potential takes the form

$$V(\phi) = M^4 \left[1 - \frac{c}{2} \left(-\frac{1}{2} + \ln \frac{\phi}{\phi_0} \right) \frac{\phi^2}{M_{\text{Pl}}^2} \right], \quad (6.2)$$

where $\phi_0 \equiv \mu$. In this expression, M , c and ϕ_0 are free parameters. The dimensionless parameter c can be positive or negative. Its absolute value is typically of the order 10^{-1} to 10^{-2} , as noticed in Refs. [437, 440, 442], because a larger value of $|c|$ would not allow slow-roll inflation to take place, and a lower value would break the condition under which the loop effects can be neglected when deriving the potential Eq. (6.2). This condition allows a linear expansion of the effective mass of the inflation in logarithms, and thus implies that $|\ln(\phi/\phi_0)| \ll 1$, which defines the region in which the potential is valid. Also, this model is commonly worked out in the vacuum dominated regime (otherwise it is equivalent to a large field model, LFI, see section 4.2), which means that $c\phi_0^2/M_{\text{Pl}}^2 \ll 1$. The location $\phi = \phi_0$ is an extremum of $V(\phi)$, a maximum if $c > 0$ and a minimum if $c < 0$. The potential and its logarithm are represented in Fig. 64.

Running mass inflation can be realized in four different ways [437], denoted as RMI1, RMI2, RMI3 and RMI4 in what follows. RMI1 corresponds to the case where $c > 0$ and

$\phi < \phi_0$, see Fig. 64 (top panels). In this case, ϕ decreases during inflation. RMI2 also corresponds to $c > 0$ but with $\phi > \phi_0$ and ϕ increases during inflation. RMI3 refers to the situation where $c < 0$ and $\phi < \phi_0$ all the time. In this case, ϕ increases during inflation. Finally, RMI4 has $c < 0$ and $\phi > \phi_0$ decreases as inflation proceeds.

Using the potential (6.2), one can calculate the three slow-roll parameters ϵ_1 , ϵ_2 and ϵ_3 . One obtains the following expressions

$$\epsilon_1 = \frac{c^2}{2} \left[\frac{\frac{\phi}{M_{\text{Pl}}} \ln \frac{\phi}{\phi_0}}{1 - \frac{c}{2} \left(-\frac{1}{2} + \ln \frac{\phi}{\phi_0} \right) \frac{\phi^2}{M_{\text{Pl}}^2}} \right]^2, \quad (6.3)$$

$$\epsilon_2 = 2c \frac{1 + \frac{c}{4} \frac{\phi^2}{M_{\text{Pl}}^2} + \left(1 - \frac{c}{4} \frac{\phi^2}{M_{\text{Pl}}^2} \right) \ln \frac{\phi}{\phi_0} + \frac{c}{2} \frac{\phi^2}{M_{\text{Pl}}^2} \ln^2 \frac{\phi}{\phi_0}}{\left[1 - \frac{c}{2} \left(-\frac{1}{2} + \ln \frac{\phi}{\phi_0} \right) \frac{\phi^2}{M_{\text{Pl}}^2} \right]^2}, \quad (6.4)$$

and

$$\begin{aligned} \epsilon_3 = & \frac{c \ln \frac{\phi}{\phi_0}}{\left[1 - \frac{c}{2} \left(-\frac{1}{2} + \ln \frac{\phi}{\phi_0} \right) \frac{\phi^2}{M_{\text{Pl}}^2} \right]^2} \left[1 + \frac{c}{4} \frac{\phi^2}{M_{\text{Pl}}^2} + \left(1 - \frac{c}{4} \frac{\phi^2}{M_{\text{Pl}}^2} \right) \ln \frac{\phi}{\phi_0} + \frac{c}{2} \frac{\phi^2}{M_{\text{Pl}}^2} \ln^2 \frac{\phi}{\phi_0} \right]^{-1} \\ & \times \left[1 + \frac{c}{2} \frac{\phi^2}{M_{\text{Pl}}^2} + \frac{c^2}{16} \frac{\phi^4}{M_{\text{Pl}}^4} + c \left(2 \frac{\phi^2}{M_{\text{Pl}}^2} + \frac{c}{2} \frac{\phi^4}{M_{\text{Pl}}^4} \right) \ln \frac{\phi}{\phi_0} + c \left(3 \frac{\phi^2}{M_{\text{Pl}}^2} - \frac{c}{2} \frac{\phi^4}{M_{\text{Pl}}^4} \right) \ln^2 \frac{\phi}{\phi_0} \right. \\ & \left. + \frac{c^2}{2} \frac{\phi^4}{M_{\text{Pl}}^4} \ln^3 \frac{\phi}{\phi_0} \right]. \end{aligned} \quad (6.5)$$

The slow-roll parameters are represented in the bottom panels in Fig. 64.

Now let us examine how inflation ends in this model. The slow-roll parameter ϵ_1 has a maximum in the $\phi < \phi_0$ region and a maximum in the $\phi > \phi_0$ region, see Fig. 64. If these maxima were larger than one, inflation could in principle stop by violation of the slow-roll conditions (i.e., clearly, if ϵ_1 is always smaller than one, this can never happen). In the vacuum dominated approximation, however, we see from Eq. (6.3), that $\epsilon_1 \simeq c^2/2\phi^2/M_{\text{Pl}}^2 \ln^2(\phi/\phi_0)$. This means that the *vev* ϕ_{end} satisfies $\phi_{\text{end}}/\phi_0 \ln(\phi_{\text{end}}/\phi_0) = \pm\sqrt{2}/cM_{\text{Pl}}/\phi_0$. But we have established previously that the vacuum dominated condition precisely implies that $cM_{\text{Pl}}/\phi_0 \gg 1$. As a result, we have $\phi_{\text{end}}/\phi_0 \ln(\phi_{\text{end}}/\phi_0) \gg 1$ or $\phi_{\text{end}}/\phi_0 \gg 1$ and, hence, $\ln(\phi_{\text{end}}/\phi_0) \gg 1$ as well. But for the model to be valid, we have already mentioned that one must have $|\ln(\phi/\phi_0)| \ll 1$. We conclude that the value of ϕ_{end} obtained above lies outside the regime of validity of the potential. This means that, either the end of inflation nevertheless occurs by violation of the slow-roll but in a regime where additional unknown corrections arise and modify the shape of $V(\phi)$ (and the calculations presented here cannot describe this phase), or there is a tachyonic instability which ends inflation in the regime where our calculations are valid but we must introduce a new parameter, ϕ_{end} , the *vev* at which the instability occurs. In this article, we follow the second possibility which implies that RMI is indeed a three parameters model.

We now turn to the calculation of the physical predictions of these models. The first step is to obtain the slow-roll trajectory. One obtains

$$N - N_{\text{ini}} = \frac{1}{c} \left(\ln \left| \ln \frac{\phi}{\phi_0} \right| - \ln \left| \ln \frac{\phi_{\text{ini}}}{\phi_0} \right| \right) - \frac{1}{4} \left(\frac{\phi^2}{M_{\text{Pl}}^2} - \frac{\phi_{\text{ini}}^2}{M_{\text{Pl}}^2} \right) + \frac{1}{4} \left(\frac{\phi_0}{M_{\text{Pl}}^2} \right)^2 \left[\text{Ei} \left(2 \ln \frac{\phi}{\phi_0} \right) - \text{Ei} \left(2 \ln \frac{\phi_{\text{ini}}}{\phi_0} \right) \right], \quad (6.6)$$

where the exponential integral function Ei is defined by $\text{Ei}(x) \equiv -\int_{-x}^{+\infty} dt e^{-t}/t$ [160, 161]. This expression cannot be inverted analytically (unless numerical methods are used as done in the ASPIC library). However, in the limit $c\phi/M_{\text{Pl}} \ll 1$ (the vacuum dominated regime), the above expression can be approximated by

$$N \simeq \frac{1}{c} \left(\ln \left| \ln \frac{\phi}{\phi_0} \right| - \ln \left| \ln \frac{\phi_{\text{ini}}}{\phi_0} \right| \right), \quad (6.7)$$

from which it follows that

$$\phi(N) = \phi_0 \exp \left(e^{cN} \ln \frac{\phi_{\text{ini}}}{\phi_0} \right). \quad (6.8)$$

We are now in a position where we can discuss the observable consequences of the above considerations. The exact slow-roll predictions of the four models, RMI1, RMI2, RMI3 and RMI4 are presented in Figs. 142, 143, 144 and 145 for $|c| = 10^{-2}$, $\phi_0/M_{\text{Pl}} < 1/\sqrt{|c|}$, and $1/e < \phi_{\text{end}}/\phi_0 < e$, respectively. In order to interpret them, it is interesting to use approximations. From the trajectory (6.8), it is straightforward to calculate ϕ_* . Remembering that inflation is supposed to stop by instability at ϕ_{end} , one obtains $\phi_* = \phi_0 \exp [e^{-c\Delta N_*} \ln(\phi_{\text{end}}/\phi_0)]$. Then, using Eqs. (6.3), (6.4) and (6.5) in the vacuum dominated limit, we find that

$$\epsilon_{1*} \simeq \frac{c^2}{2} \left(\frac{\phi_0}{M_{\text{Pl}}} \right)^2 \exp \left[2e^{-c\Delta N_*} \ln \left(\frac{\phi_{\text{end}}}{\phi_0} \right) \right] e^{-2c\Delta N_*} \ln^2 \left(\frac{\phi_{\text{end}}}{\phi_0} \right), \quad (6.9)$$

$$\epsilon_{2*} \simeq 2c \left[1 + e^{-c\Delta N_*} \ln \left(\frac{\phi_{\text{end}}}{\phi_0} \right) \right]. \quad (6.10)$$

In fact, in order to compare with the existing literature, it turns out to be convenient to define the following quantity

$$s \equiv c \ln \left(\frac{\phi_0}{\phi_*} \right) = -c e^{-c\Delta N_*} \ln \left(\frac{\phi_{\text{end}}}{\phi_0} \right). \quad (6.11)$$

For RMI1 and RMI4, $s > 0$ while for RMI2 and RMI3 one has $s < 0$. This quantity can also be used to estimate ϕ_{end} since $\phi_{\text{end}} \simeq \phi_0 \exp[-s \exp(-cN_*)/c]$. Then, Eqs. (6.9) and (6.10) can be re-written as

$$\epsilon_{1*} \simeq \frac{s^2}{2} \left(\frac{\phi_0}{M_{\text{Pl}}} \right)^2 e^{-2s/c}, \quad \epsilon_{2*} \simeq 2c \left(1 - \frac{s}{c} \right). \quad (6.12)$$

The last equations means that the trajectory in the plane (ϵ_1, ϵ_2) can be expressed as $\epsilon_2 \simeq 2(c-s) + 4\epsilon_1 M_{\text{Pl}}^2/\phi_0^2$. If we neglect ϵ_{1*} (with respect to ϵ_{2*}) then one recovers the formula already derived in Refs. [437, 440, 442], namely $n_s - 1 \simeq 2(s-c)$. The same route for the third slow-roll parameter gives $\epsilon_2 \epsilon_3 \simeq -2cs$ and neglecting again ϵ_1 , one gets the scalar running

$\alpha_s \simeq 2sc$. The above analytical estimates agree well with the exact predictions in Figs. 142, 143, 144 and 145.

Finally, a few words on the mass scale M are in order. From the CMB normalization, we obtain the following expression

$$\frac{M^4}{M_{\text{Pl}}^4} = 720\pi^2 c^2 \frac{Q_{\text{rms-PS}}^2}{T^2} \frac{\phi_*^2/M_{\text{Pl}}^2 \ln^2(\phi_*/M_{\text{Pl}})}{\{1 - c/2[-1/2 + \ln(\phi_*/\phi_0)]\phi_*^2/M_{\text{Pl}}^2\}^3}. \quad (6.13)$$

A simpler formula can be derived if one uses the approximate formulas established above. In this case, one can write $M^4/M_{\text{Pl}}^4 \simeq 720\pi^2 s^2 (Q_{\text{rms-PS}}^2/T^2)(\phi_0/M_{\text{Pl}})^2 e^{-2s/c}$.

6.2 Valley Hybrid Inflation (VHI)

Hybrid inflation is a two-fields model with the potential [133, 193, 286, 444–447]

$$V(\phi, \psi) = \frac{1}{2}m^2\phi^2 + \frac{\lambda'}{4}(\psi^2 - \Delta^2)^2 + \frac{\lambda}{2}\phi^2\psi^2, \quad (6.14)$$

where ϕ is the inflaton, ψ the waterfall field and λ and λ' are two coupling constants. As a two-field models, the hybrid potential supports various inflationary domains. The standard lore is that inflation can proceed along the valley given by $\psi = 0$ and, in this case, the potential reduces to an effective single field potential that can be written as

$$V(\phi) = M^4 \left[1 + \left(\frac{\phi}{\mu} \right)^p \right], \quad (6.15)$$

with $p = 2$ and where one has used the following parameter redefinition

$$M = \frac{\lambda'^{1/4} \Delta}{\sqrt{2}}, \quad \mu = \sqrt{\frac{\lambda'}{2}} \frac{\Delta^2}{m}. \quad (6.16)$$

Inflation along the valley has been shown to be a dynamical attractor of the two-field dynamics in Refs. [448, 449]. However, as recently shown in Ref. [450], the hybrid potential can also support an inflationary phase along a mixed valley-waterfall trajectory, which is genuinely a two-fields dynamics. As we use a single field description here, those effects cannot be described by the potential of Eq. (6.15). For this reason, we will refer to the single field approximation as the valley hybrid regime. Let us stress that if the waterfall inflationary regime occurs, it will erase any observable effects coming the valley hybrid regime. As a result, Eq. (6.15) is a good description of hybrid inflation only if the model parameters are such that the waterfall regime remains sub-dominant. According to Ref. [450, 451], this is the case provided

$$\sqrt{\lambda'} \frac{\Delta^3}{m} \ll M_{\text{Pl}}^2, \quad (6.17)$$

a condition that will be assumed in the following. The effective potential Eq. (6.15) was also obtained in Ref. [452] in the context of supergravity brane inflation, and in Ref. [430] in the context of hilltop supernatural inflation. It depends on three parameters, namely M , μ and p . In fact, as mentioned before, $p = 2$ for the two-field model given in Eq. (6.14) but we will consider the most general situation by letting $p > 0$ unspecified. Let us again all multifield effects such as the generation of isocurvature modes or cosmic strings cannot be accounted within the single field dynamics [121, 453–455].

The first three Hubble flow functions in the slow-roll approximation can be derived from Eq. (6.15). Defining

$$x \equiv \frac{\phi}{\mu}, \quad (6.18)$$

they read

$$\epsilon_1 = \frac{p^2}{2} \left(\frac{M_{\text{Pl}}}{\mu} \right)^2 \frac{x^{2p-2}}{(1+x^p)^2}, \quad \epsilon_2 = 2p \left(\frac{M_{\text{Pl}}}{\mu} \right)^2 x^{p-2} \frac{x^p - p + 1}{(1+x^p)^2}, \quad (6.19)$$

and

$$\epsilon_3 = p \left(\frac{M_{\text{Pl}}}{\mu} \right)^2 x^{p-2} \frac{2x^{2p} - (p-1)(p+4)x^p + (p-1)(p-2)}{(1+x^p)^2 (x^p - p + 1)}. \quad (6.20)$$

A specific feature of hybrid inflation in comparison to large and small field models is that ϵ_2 and ϵ_3 can be negative (see Fig. 65). In particular

$$\epsilon_2 \underset{x \rightarrow 0}{\sim} -2p(p-1) \left(\frac{M_{\text{Pl}}}{\mu} \right)^2 x^{p-2}, \quad (6.21)$$

and ϵ_3 blows up in the limit $x^p \rightarrow p-1$. Together with the potential, the three Hubble flow functions have been represented in Fig. 65.

The slow-roll trajectory is obtained by integrating Eq. (2.11) with the valley hybrid potential and reads

$$N - N_{\text{end}} = \frac{1}{2p} \frac{\mu^2}{M_{\text{Pl}}^2} \left[-x^2 + x_{\text{end}}^2 + \frac{2}{2-p} \left(x_{\text{end}}^{2-p} - x^{2-p} \right) \right], \quad (6.22)$$

which is, up to a sign, the same as for the SFI models [see Eq. (5.5)]. The case $p=2$ requires a special attention, but as for SFI, it is recovered as the limit $p \rightarrow 2$ in the previous equation. One gets

$$N - N_{\text{end}} = \frac{1}{4} \frac{\mu^2}{M_{\text{Pl}}^2} \left[-x^2 + x_{\text{end}}^2 - 2 \ln \left(\frac{x}{x_{\text{end}}} \right) \right], \quad (6.23)$$

which is again very similar to SFI, up to a sign. The trajectory (6.22) cannot be inverted analytically in the general case to get $x(N)$. It is however possible to perform this inversion for almost all integer values of p , but those expressions will be omitted for the sake of clarity. We simply give an approximate solution valid only in the limit $x \ll 1$ and $p > 2$

$$x \simeq \left[x_{\text{end}}^{2-p} + p(p-2) \frac{M_{\text{Pl}}^2}{\mu^2} (N - N_{\text{end}}) \right]^{1/(2-p)}. \quad (6.24)$$

If the waterfall regime does not take place, i.e. under the condition (6.17), valley hybrid inflation ends by a tachyonic instability in the small field regime $x < 1$, also referred to as the vacuum dominated regime. From the two-fields potential (6.14), one sees that the transverse direction becomes tachyonic at the inflaton value

$$x_{\text{end}} = \frac{\lambda'}{\lambda} \Delta. \quad (6.25)$$

In the single field approach, x_{end} is therefore an extra-parameter and VHI is a three parameters model according to our classification. However, as can be seen in Fig. 65, one should

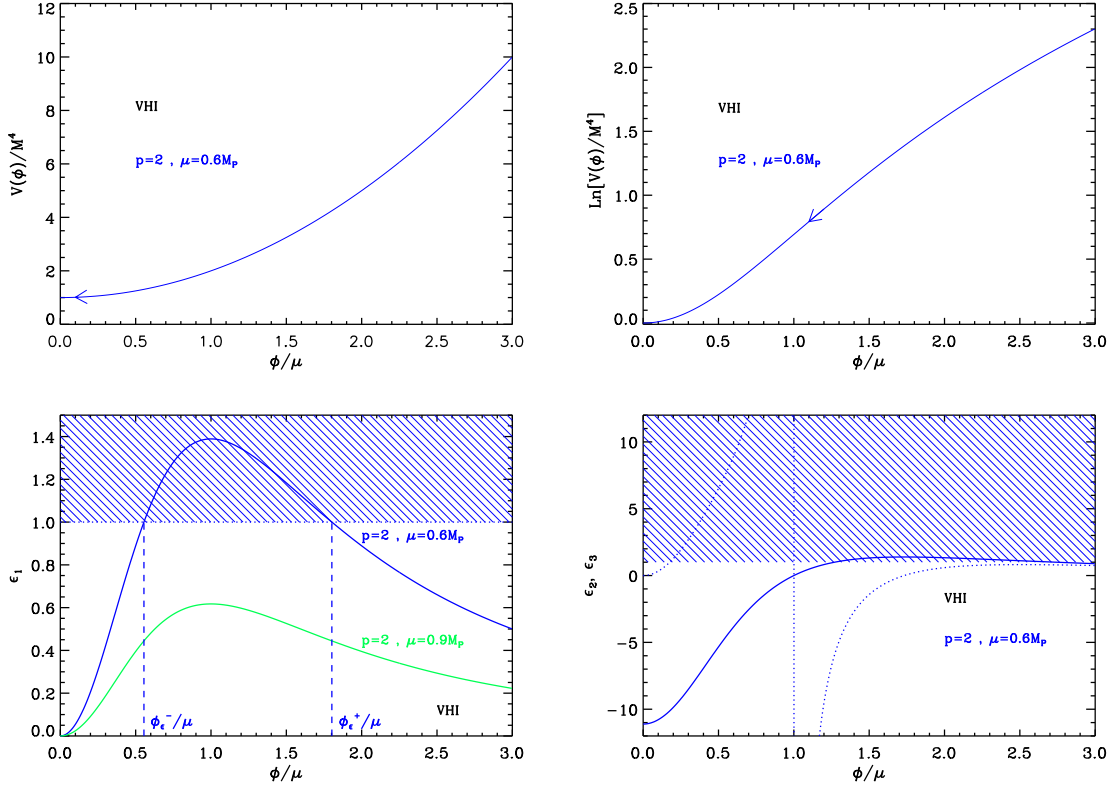


Figure 65. Valley Hybrid inflation (VHI) for $p = 2$. Upper panels: the potential and its logarithm for $\mu = 0.6M_{\text{Pl}}$. Bottom left panel: slow-roll parameter ϵ_1 for $\mu = 0.6M_{\text{Pl}}$ (blue line) and $\mu = 0.9M_{\text{Pl}}$ (green line). For small values of μ , the inflationary regions are separated into a large field one and the vacuum dominated one. The latter may not exist due to slow-roll violations if the field evolves first in the large field domain (see text). The shaded area indicates the regions in which acceleration cannot occur. Bottom right panel: slow-roll parameters ϵ_2 (solid line) and ϵ_3 (dotted line) for $\mu = 0.6M_{\text{Pl}}$.

pay attention to the various domains in which inflation can take place. They are given by the behavior of $\epsilon_1(x)$.

If $p > 1$, the slow-roll parameter ϵ_1 vanishes when the field goes to zero and at infinity while it reaches a maximum for

$$x_{\epsilon_1^{\text{max}}} = (p-1)^{1/p}, \quad (6.26)$$

equals to

$$\epsilon_1^{\text{max}} = \frac{1}{2} \left(\frac{M_{\text{Pl}}}{\mu} \right)^2 (p-1)^{\frac{2p-2}{p}}. \quad (6.27)$$

Defining

$$\mu_\epsilon \equiv \frac{M_{\text{Pl}}}{\sqrt{2}} (p-1)^{1-1/p}, \quad (6.28)$$

for all $\mu > \mu_\epsilon$, one has $\epsilon_1(x) < 1$ and inflation can proceed all over the domain $x > 0$. On the contrary, if $\mu < \mu_\epsilon$, then inflation can, a priori, proceed in two disconnected domains. Either

$0 < x < x_{\epsilon_1=1}^-$ or $x > x_{\epsilon_1=1}^+$ where $x_{\epsilon_1=1}^\pm$ are the two roots of $\epsilon_1 = 1$, i.e. the solutions of

$$x^{2p} + 2x^p - \frac{p^2}{2} \left(\frac{M_{\text{Pl}}}{\mu} \right)^2 x^{2p-2} + 1 = 0. \quad (6.29)$$

This equation cannot be solved explicitly in the general case but, as for the trajectory, there are analytical expressions for almost all integer values of p . For instance, for $p = 2$, one gets

$$x_{\epsilon_1=1}^{\pm(p=2)} = \frac{1}{\sqrt{2}} \frac{M_{\text{Pl}}}{\mu} \left(1 \pm \sqrt{1 - 2 \frac{\mu^2}{M_{\text{Pl}}^2}} \right). \quad (6.30)$$

The positive sign corresponds to the largest root while the minus one to the smallest (see Fig. 65). In the limit $\mu \ll M_{\text{Pl}}$, one has $x_{\epsilon_1=1}^+ \simeq p M_{\text{Pl}} / (\sqrt{2} \mu)$ which is also the expression of x_{end} for the large field model LFI (see section 4.2). That's not surprising since in that situation Eq. (6.15) is indeed dominated by the monomial term. In fact, the two above-mentioned domains precisely corresponds to a large field one for $x > x_{\epsilon_1=1}^+$ and a vacuum dominated one for $x < x_{\epsilon_1=1}^-$. It is a common mistake to assume that the large field domain remains unobservable due to the existence of the vacuum dominated one. Indeed, as shown in Ref. [448], the large field regime becomes observable provided $\mu \ll \mu_\epsilon$. In that situation, after having crossed $x_{\epsilon_1=1}^+$, the field goes on fast-rolling in the region $\epsilon_1(x) > 1$. Then, it enters the domain $x < x_{\epsilon_1=1}^-$ with a strong initial velocity such that it traverses the whole vacuum dominated region, still in fast-roll, to reach x_{end} and without triggering inflation. All observable predictions in such a situation are similar to the LFI models. Let us notice that if there exists a mechanism that can gently put the field without a strong initial velocity inside the $x < x_{\epsilon_1=1}^-$ domain, then inflation can still occur in the vacuum dominated region, even though $\mu < \mu_\epsilon$. But if the field is coming from the region $x > x_{\epsilon_1=1}^+$, then this regime does not exist anymore.

For $p = 1$, $\epsilon_1(x)$ is a decreasing function of the field and takes a finite value $M_{\text{Pl}}^2 / (2\mu^2)$ for $x \rightarrow 0$. The behavior is similar to the case $p > 1$ and if $\mu > M_{\text{Pl}} / \sqrt{2}$ inflation can take place all over $x > x_{\text{end}}$. However, if $\mu < M_{\text{Pl}} / \sqrt{2}$ then the vacuum dominated region does not exist anymore and $x_{\epsilon_1=1}^+ = x_{\epsilon_1=1}^- = M_{\text{Pl}} / (\sqrt{2}\mu) - 1$. One should also notice that if $p = 1$ the relation $\epsilon_2 = 4\epsilon_1$ applies.

Finally, for $p < 1$, $\epsilon_1(x)$ is a decreasing function of the field but it blows up when $x \rightarrow 0$. In that situation, inflation stops at $x = \max(x_{\epsilon_1=1}^-, x_{\text{end}})$ but the field will still fast-roll till the tachyonic instability develops at x_{end} . As a result, even if for some cases $x_{\epsilon_1=1}^- > x_{\text{end}}$, the observable predictions remain mostly the same.

According to the previous discussion, for $p > 1$, the VHI effective potential is therefore adequate to describe the vacuum dominated regime only, i.e. for $x_{\text{end}} < x < x_{\epsilon_1=1}^-$ where x_{end} is the instability point given by Eq. (6.25). In that situation, solving Eq. (2.46) together with the trajectory (6.22) gives the observable field value x_* at which the pivot mode crossed the Hubble radius during inflation. The potential parameter M is fixed from the amplitude of the CMB anisotropies

$$\frac{M^4}{M_{\text{Pl}}^4} = 720\pi^2 p^2 \frac{M_{\text{Pl}}^2}{\mu^2} \frac{x_*^{2p-2}}{(1+x_*^p)^3} \frac{Q_{\text{rms-PS}}^2}{T^2}. \quad (6.31)$$

The reheating consistent slow-roll predictions are displayed in Figs. 146, 147, 148, 149 and 150 for $p = 0.5$, $p = 1$, $p = 1.5$, $p = 2$ and $p = 3$, respectively. For $p > 1$, x_{end} is varied

between 0 and an upper bound that is such that $x_{\text{in}} < x_{\epsilon_1=1}^-$ if $x_{\epsilon_1^{\text{max}}} > 1$, and $x_{\text{end}} < 10$ in both cases since the potential is valid in its vacuum dominated regime, while for $p \leq 1$, it is varied on a wider range, with no particular constraints. For $p = 1$, the predictions lie on the contour $\epsilon_2 = 4\epsilon_1$ as expected whereas for $p > 1$ one recovers a blue spectral index when $x_{\epsilon_1^{\text{max}}} > 1$, while a red spectral index can be obtained when $x_{\epsilon_1^{\text{max}}} < 1$ and $x_* > x_{\epsilon_1^{\text{max}}}$, with $x_* < 1$.

6.3 Dynamical Supersymmetric Inflation (DSI)

This model has been derived and studied in Ref. [456, 457] in the context of supersymmetry breaking generated by gauge dynamics. Its potential is given by

$$V(\phi) = M^4 \left[1 + \left(\frac{\phi}{\mu} \right)^{-p} \right], \quad (6.32)$$

where p is a free index parameter, and μ is a scale of order $\mu \simeq 10^{10}$ GeV. In Ref. [456], it is argued that such potentials can appear generically in supersymmetric theories. As explained below, the inflationary regime takes place at large field values for which the denominator of Eq. (6.32) is always well-defined. Within the philosophy of these models, it is also argued in Ref. [456] that non-renormalizable terms of the form

$$V(\phi) = M^4 \left[1 + \left(\frac{\phi}{\mu} \right)^{-p} \right] + \frac{\phi^{q+4}}{M_{\text{Pl}}^q}, \quad (6.33)$$

may be present, but they are suppressed by powers of M_{Pl} , the only explicit scale allowed in the theory. This extra term provides the potential with an absolute minimum at a *vev* given by

$$\phi_{\text{Vmin}} = \left(\frac{p}{q+4} M^4 \mu^p M_{\text{Pl}}^q \right)^{\frac{1}{p+q+4}}. \quad (6.34)$$

This means that these extra terms can be neglected in the region $\phi \ll \phi_{\text{Vmin}}$. Also, in order for the potential Eq. (6.32) to produce inflation, $\ln V$ must be flat enough, and inflation takes place in its vacuum dominated part $\phi \gg \mu$. One concludes that the potential Eq. (6.32) should be studied in the regime

$$\mu \ll \phi \ll \phi_{\text{Vmin}}, \quad (6.35)$$

which puts interesting priors on the models parameters, as explained below. Before turning to the slow-roll analysis of the models, let us mention that the potential Eq. (6.32) is in fact quite general, and that it has been later studied in other contexts. In Ref. [193], the same potential appears with $p = 2$ in the context of mutated hybrid inflation. In Refs. [123, 287, 288, 330, 458–461, 461–471], this is a typical potential in the context of brane inflation where μ is an effective compactification scale $\mu \simeq 10^{12}$ GeV. In Refs. [472, 473], the same potential arises in the context of tachyon inflation, in Ref. [474] in the context of SQCD inflation, and in Ref. [399] as the strong coupling limit of the twisted inflation model (see TWI, section 5.5). Let us also mention that the same kind of inverse power law potential is made use of in quintessential inflation models [231, 475, 476].

The potential Eq. (6.32), as well as its logarithm, is displayed in Fig. 66. It is a decreasing function of the field, hence inflation proceeds from the left to the right. Let us calculate the slow-roll parameters. Defining

$$x \equiv \frac{\phi}{\mu}, \quad (6.36)$$

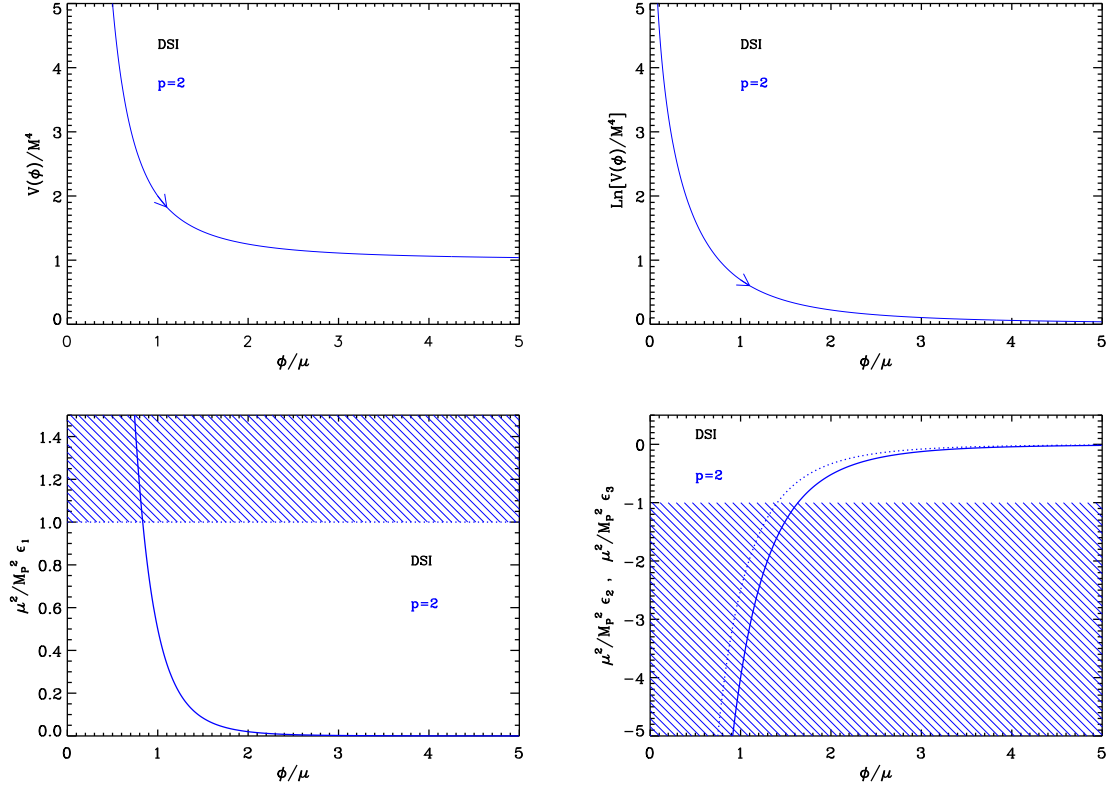


Figure 66. Dynamical Supersymmetric Inflation (DSI) for $p = 2$. Upper panels: the potential and its logarithm as a function of ϕ/μ . Bottom left panel: slow-roll parameter ϵ_1 rescaled by M_{Pl}^2/μ^2 . The shaded area indicates the region in which inflation cannot occur for $\mu = M_{\text{Pl}}$. Bottom right panel: slow-roll parameters ϵ_2 (solid line) and ϵ_3 (dotted line), rescaled by M_{Pl}^2/μ^2 .

the first three Hubble flow functions in the slow-roll approximation read

$$\epsilon_1 = \frac{p^2}{2} \left(\frac{M_{\text{Pl}}}{\mu} \right)^2 \frac{x^{-2p-2}}{(1+x^{-p})^2}, \quad \epsilon_2 = -2p \left(\frac{M_{\text{Pl}}}{\mu} \right)^2 x^{-p-2} \frac{x^{-p} + p + 1}{(1+x^{-p})^2}, \quad (6.37)$$

and

$$\epsilon_3 = -p \left(\frac{M_{\text{Pl}}}{\mu} \right)^2 x^{-p-2} \frac{[2x^{-2p} + (p+1)(p-4)x^{-p} + (p+1)(p+2)]}{(1+x^{-p})^2 (x^{-p} + p + 1)}. \quad (6.38)$$

Let us notice already that, from these expressions, one has

$$-2\epsilon_1 - \epsilon_2 = \left(\frac{M_{\text{Pl}}}{\mu} \right)^2 \frac{px^{-p-2}}{(1+x^{-p})^2} [px^{-p} + 2p(p+1)x^{-p-2}] > 0, \quad (6.39)$$

which implies a blue spectral index for the scalar power spectrum since, at first order, $n_s - 1 = -2\epsilon_{1*} - \epsilon_{2*}$. As announced before, these functions become very small at large fields $x \gg 1$. More precisely, there is a minimum value $x_{\epsilon_1=1}$ below which $\epsilon_1 > 1$ and inflation cannot take place. This value has to be determined numerically, but since generally, $\mu/M_{\text{Pl}} \ll 1$, an

approximated expression can be derived as

$$x_{\epsilon_1=1} \simeq \left(\frac{p}{\sqrt{2}} \frac{M_{\text{Pl}}}{\mu} \right)^{1/(p+1)}. \quad (6.40)$$

Because the potential is decreasing with x , inflation can only take place in the domain $x > x_{\epsilon_1=1} \gg 1$ if $\mu \ll M_{\text{Pl}}$. It cannot stop by slow-roll violation and another mechanism such as, e.g. a tachyonic instability, has to be introduced. We will denote by x_{end} the field value at which this occurs and that is an extra model parameter. Obviously, it must be such that $x_{\epsilon_1=1} < x_{\text{end}} \ll x_{V\text{-min}}$.

Let us now turn to the slow-roll trajectory. It can be integrated explicitly from Eq. (2.11) and one obtains

$$N_{\text{end}} - N = \frac{\mu^2}{2pM_{\text{Pl}}^2} \left(x_{\text{end}}^2 + \frac{2}{p+2} x_{\text{end}}^{p+2} - x^2 - \frac{2}{p+2} x^{p+2} \right). \quad (6.41)$$

In the $\mu/M_{\text{Pl}} \ll 1$ limit, one has $x > x_{\epsilon_1=1} \gg 1$, and the previous trajectory can be approximated by

$$N_{\text{end}} - N \simeq \frac{\mu^2}{p(p+2)M_{\text{Pl}}^2} \left(x_{\text{end}}^{p+2} - x^{p+2} \right). \quad (6.42)$$

This expression can be analytically inverted to get the observable field value x_* in terms of $\Delta N_* = N_{\text{end}} - N_*$ as

$$x_* \simeq \left[x_{\text{end}}^{p+2} - \frac{M_{\text{Pl}}^2}{\mu^2} p(p+2) \Delta N_* \right]^{\frac{1}{p+2}}. \quad (6.43)$$

One can notice that the total amount of e-folds is bounded because $x_{\text{end}} \ll x_{V\text{-min}}$ and cannot take infinitely large values. In order to get a number of e-folds, $\Delta N > \Delta N_{\text{min}}$, x_{end} should be sufficiently large with $x_{\text{end}} > x_{\text{end}}^{\text{min}}$. More precisely, setting $x_{\text{ini}} = x_{\epsilon_1=1}$, one has

$$x_{\text{end}}^{\text{min}} \simeq \left[p(p+2) \frac{M_{\text{Pl}}^2}{\mu^2} \Delta N_{\text{min}} + \left(\frac{p}{\sqrt{2}} \frac{M_{\text{Pl}}}{\mu} \right)^{\frac{p+2}{p+1}} \right]^{\frac{1}{p+2}} \simeq \left[p(p+2) \frac{M_{\text{Pl}}^2}{\mu^2} \Delta N_{\text{min}} \right]^{\frac{1}{p+2}}. \quad (6.44)$$

In practice one wants $\Delta N_{\text{min}} > 50$ to solve the problems of the standard Big-Bang scenario. Whether this value is compatible, or not, with the condition $x_{\text{end}} \ll x_{V\text{-min}}$ depends on the value of M^4 appearing in Eq. (6.34), which is itself determined by the amplitude of the CMB anisotropies.

From x_* , the amplitude of the CMB anisotropies fixes M such that

$$\left(\frac{M}{M_{\text{Pl}}} \right)^4 = 720\pi^2 p^2 \left(\frac{M_{\text{Pl}}}{\mu} \right)^2 x_*^{-2p-2} (1 + x_*^{-p})^{-3} \frac{Q_{\text{rms-PS}}^2}{T^2}. \quad (6.45)$$

In the limit $\mu/M_{\text{Pl}} \ll 1$, one has $x_* \gg 1$ and this expression can be approximated by

$$\frac{M^4}{M_{\text{Pl}}^4} \simeq 720\pi^2 p^2 \frac{M_{\text{Pl}}^2}{\mu^2} x_*^{-2p-2} \frac{Q_{\text{rms-PS}}^2}{T^2}. \quad (6.46)$$

Therefore, from Eq. (6.34), one has

$$x_{V\text{-min}} \simeq \left[720\pi^2 \frac{p^3}{q+4} \left(\frac{M_{\text{Pl}}}{\mu} \right)^{6+q} x_*^{-2p-2} \frac{Q_{\text{rms-PS}}^2}{T^2} \right]^{\frac{1}{p+q+4}}, \quad (6.47)$$

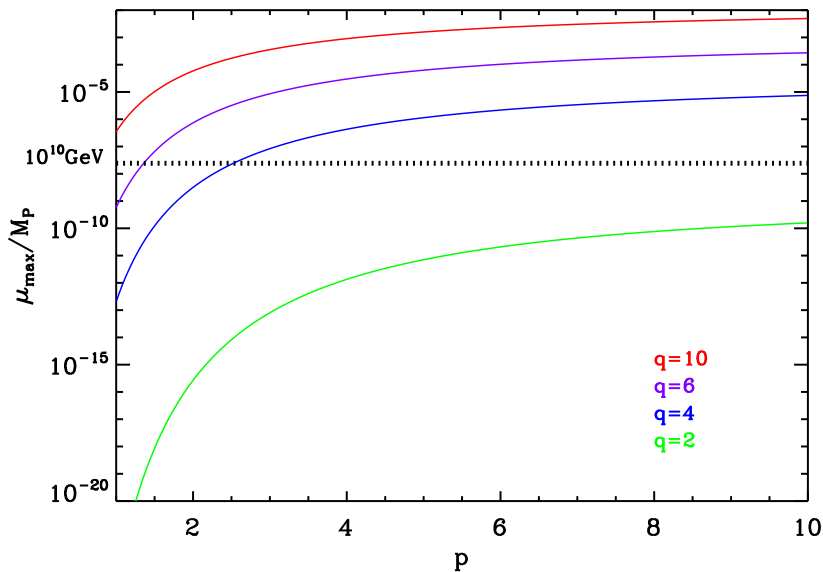


Figure 67. Dynamical Supersymmetric Inflation. Maximal value of μ/M_{Pl} with respect to p , and for different values of q , such that the condition $x_{\text{end}}^{\text{min}} < x_{\text{end}}^{\text{max}}$ is satisfied. We have fixed $\Delta N_{\text{max}} = 50$. The black dotted line show a typical value for $\mu/M_{\text{Pl}} \simeq 10^{10}$ GeV [456].

with x_* depending on x_{end} through Eq. (6.43). One can see that the previous expression decreases with x_* . As a result, $x_{\text{V-min}}$ decreases with x_{end} . The condition $x_{\text{end}} \ll x_{\text{V-min}}$ imposes an upper bound on $x_{\text{end}} < x_{\text{end}}^{\text{max}}$ with

$$x_{\text{end}}^{\text{max}} \simeq \left[720\pi^2 \frac{p^3}{q+4} \frac{Q_{\text{rms-PS}}^2}{T^2} \left(\frac{M_{\text{Pl}}}{\mu} \right)^{q+6} \right]^{1/(3p+q+6)}. \quad (6.48)$$

The prior condition on x_{end} is therefore of the type $x_{\text{end}}^{\text{min}} < x_{\text{end}} \ll x_{\text{end}}^{\text{max}}$, with $x_{\text{end}}^{\text{min}}$ defined by Eq. (6.44) and $x_{\text{end}}^{\text{max}}$ defined by Eq. (6.48). Let us notice that $x_{\text{end}}^{\text{min}} \propto (M_{\text{Pl}}/\mu)^{2/(p+2)}$ while $x_{\text{end}}^{\text{max}} \propto (M_{\text{Pl}}/\mu)^{(q+6)/(3p+q+6)}$. Therefore, for any $q > 0$, there exist a sufficiently small value of μ , say μ_{max} under which the condition $x_{\text{end}}^{\text{min}} \ll x_{\text{end}}^{\text{max}}$ is fulfilled. It reads

$$\frac{\mu_{\text{max}}}{M_{\text{Pl}}} \simeq \frac{\left(720\pi^2 \frac{p^3}{q+4} \frac{Q_{\text{rms-PS}}^2}{T^2} \right)^{(p+2)/(pq)}}{[p(p+2)\Delta N_{\text{min}}]^{(3p+q+6)/(pq)}}, \quad (6.49)$$

and has been represented in Fig. 67. One can see that a typical value $\mu/M_{\text{Pl}} \simeq 10^{10}$ GeV (see Ref. [456]) is not allowed for all realistic values of p and q . As such, the prior space for p , μ , and x_{end} is constrained and should be handled carefully.

The reheating consistent slow-roll predictions of the dynamical supersymmetric models are displayed in Figs. 151, 152 and 153 for $p = 2$, $p = 3$ and $p = 4$, respectively, and with $10^{-10} M_{\text{Pl}} < \mu < \mu_{\text{max}}$ (where μ_{max} has been calculated taking $q = 8$ and $\Delta N_{\text{min}} = 60$ to cover a large prior space). The reheating equation of state parameter \bar{w}_{reh} has been taken to 0 but since there is no potential minimum around which the inflaton field can oscillate at the end of

inflation, this parameter is a priori unspecified and can take different values. In any case the reheating temperature is strongly degenerated with the parameter $x_{\text{end}}^{\text{min}} < x_{\text{end}} < x_{\text{endmax}}$ preventing their inference. One can check that the spectral index is blue, as announced earlier, rendering these models rather disfavored by the observations. The typical amount of gravitational waves is very small, in agreement with the results of Ref. [456].

6.4 Generalized Mixed Inflation (GMLFI)

This model is a generalization of MLFI (see section 4.3), i.e. the sum of two monomial functions with arbitrary power indexes. The potential is

$$V = M^4 \left(\frac{\phi}{M_{\text{Pl}}} \right)^p \left[1 + \alpha \left(\frac{\phi}{M_{\text{Pl}}} \right)^q \right], \quad (6.50)$$

where α , p and q are three dimensionless positive parameters. It can be seen as a general extension of the large field inflation potential (LFI, see section 4.2), which is recovered when $\alpha \rightarrow 0$ or $\alpha \rightarrow \infty$. The parameter α therefore tunes the relative weight of the two terms. Since the potential is an increasing function of the inflaton vev , inflation proceeds at decreasing field value and occurs in the large field regime $\phi/M_{\text{Pl}} \gg 1$. Defining

$$x \equiv \frac{\phi}{M_{\text{Pl}}}, \quad (6.51)$$

the first three Hubble flow functions in the slow-roll approximation reads

$$\epsilon_1 = \frac{1}{2x^2} \left[\frac{p + \alpha(p+q)x^q}{1 + \alpha x^q} \right]^2, \quad (6.52)$$

$$\epsilon_2 = \frac{2p + \alpha^2(p+q)x^{2q} + \alpha(2p+q-q^2)x^q}{x^2 [1 + \alpha x^q]^2}, \quad (6.53)$$

and

$$\begin{aligned} \epsilon_3 = & \frac{1/x^2}{[1 + \alpha x^q]^2} [pq^2 + \alpha^2 q^2 (p+q)x^{2q} + \alpha q^2 (2p+q-q^2)x^q]^{-1} \\ & \times \left\{ 2q^2 [p^2 + \alpha^4 (p+q)^2] x^{4q} + \alpha^2 q^2 [12p^2 + 6pq(2-q) + (q-2)(q-1)q^2] x^{2q} \right. \\ & \left. + \alpha^3 q^3 (p+q) \left[8\frac{p}{q} + (1-q)(4+q) \right] x^{3q} + \alpha pq^2 [8p+q(4+q^2-3q)] x^q \right\}. \end{aligned} \quad (6.54)$$

They are decreasing functions of the field, vanishing when $x \rightarrow \infty$ and diverging when $x \rightarrow 0$. Together with the potential and its logarithm, the Hubble flow functions have been represented in Fig. 68.

From Fig. 68, one sees that inflation ends by slow-roll violation for $x = x_{\text{end}}$, the solution of $\epsilon_1(x_{\text{end}}) = 1$. From Eq. (6.52), one gets

$$\sqrt{2}\alpha x_{\text{end}}^{q+1} + \sqrt{2}x_{\text{end}} = \pm [p + \alpha(p+q)x_{\text{end}}^q]. \quad (6.55)$$

One can check that for $\alpha = 0$ one recovers the LFI- p result $x_{\text{end}} = p/\sqrt{2}$ (see section 4.2), and that for $\alpha \rightarrow \infty$ one gets $x_{\text{end}} = (p+q)/\sqrt{2}$, which correspond again to the LFI- $p+q$ solution.

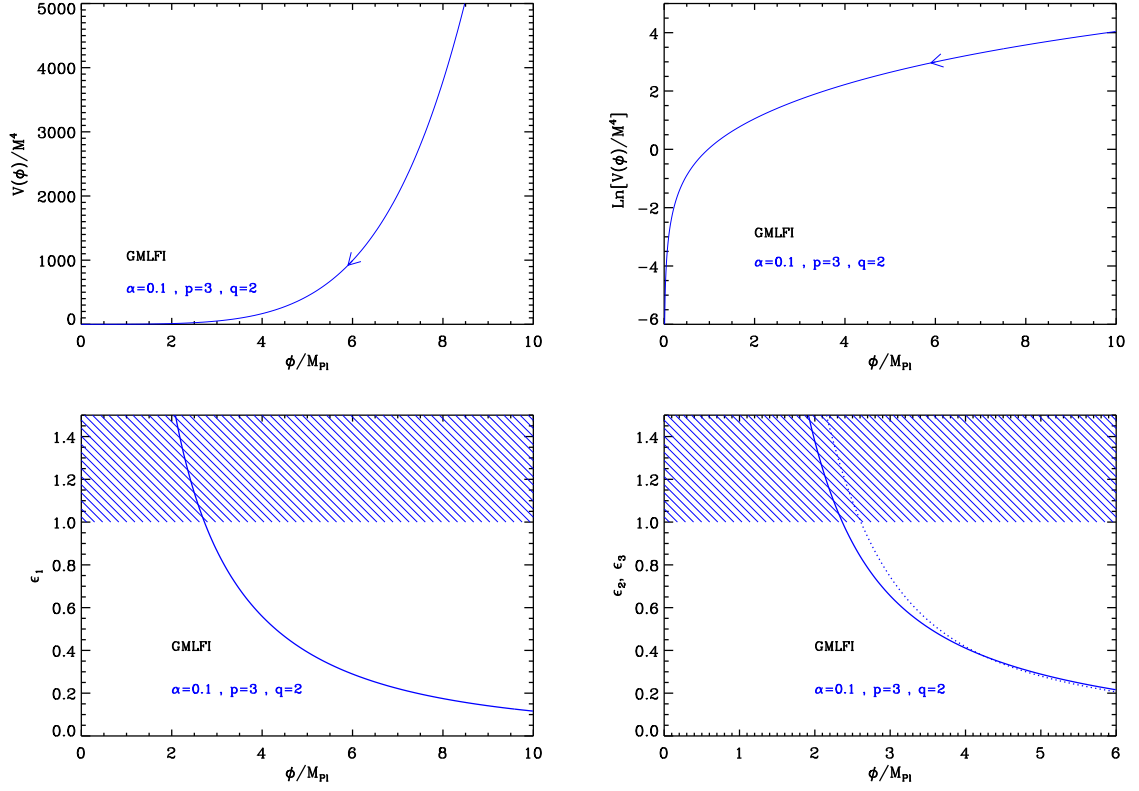


Figure 68. Generalized Mixed Inflation (GMLFI) for $p = 3, q = 2$ and $\alpha = 0.1$. Upper panels: the potential and its logarithm with respect the field value. Bottom left panel: slow-roll parameter ϵ_1 , the shaded region is where inflation stops. Bottom right panel: slow-roll parameters ϵ_2 (solid line) and ϵ_3 (dotted line).

The above equation cannot be solved analytically for arbitrary values of p, q . This is possible only in some particular cases $q = 0, q = 1$ or $q = 2$. For $q = 0$, this is LFI whereas $q = 2$ corresponds to MLFI, both solutions being given in section 4.2 and section 4.3, respectively. For $q = 1$, one obtains

$$x_{\text{end}} = \frac{\sqrt{2}}{4} (p+1) - \frac{1}{2\alpha} + \frac{\sqrt{4 + 4\sqrt{2}\alpha(p-1) + 2\alpha^2(p+1)^2}}{4\alpha}. \quad (6.56)$$

In general x_{end} has to be determined numerically.

The slow-roll trajectory can be integrated explicitly from Eq. (2.11), which gives

$$N_{\text{end}} - N = \frac{1}{2(p+q)} x^2 \left\{ 1 + \frac{q}{p} {}_2F_1 \left[1, \frac{2}{q}, 1 + \frac{2}{q}, -\alpha q \left(\frac{1}{p} + \frac{1}{q} \right) x^q \right] \right\} - \frac{1}{2(p+q)} x_{\text{end}}^2 \left\{ 1 + \frac{q}{p} {}_2F_1 \left[1, \frac{2}{q}, 1 + \frac{2}{q}, -\alpha q \left(\frac{1}{p} + \frac{1}{q} \right) x_{\text{end}}^q \right] \right\}. \quad (6.57)$$

Here ${}_2F_1$ stands for the Gauss hypergeometric function. Since it is equal to unity when its last argument vanishes, one can check that in the limit $\alpha \rightarrow 0$, one recovers the slow-roll trajectory for the LFI- p models while the limit $\alpha \rightarrow \infty$ leads to the trajectory of the

LFI- $p + q$ models. Finally, since ${}_2F_1[1, 1, 2, x] = -\ln(1-x)/x$, one can also check that the MLFI case corresponds to $p = q = 2$. The previous expression can only be inverted for $q = 0$ (LFI) and $q = 2$ (MLFI), and they have been already discussed in section 4.2 and section 4.3, respectively. The case $q = 1$ could also be simplified using ${}_2F_1[1, 2, 3, x] = -2/x - 2\log(1-x)/x^2$. In general, one has to inverse this slow-roll trajectory numerically.

Finally, Eq. (2.46) allows for the determination of the observable field value x_* once the reheating is specified. The parameter M can then be determined from the amplitude of the CMB anisotropies and verifies

$$\frac{M^4}{M_{\text{Pl}}^4} = 720\pi^2 \frac{[p + \alpha(p+q)x_*^q]^2 Q_{\text{rms-PS}}^2}{x_*^{p+2} [1 + \alpha x_*^q]^3 T^2}. \quad (6.58)$$

The reheating consistent slow-roll predictions for the generalized mixed large field models are displayed in Figs 154, 155, and 156 for $p = 2$ and $q = 1$; $p = 2$ and $q = 3$; and $p = 3$ and $q = 2$; respectively. As for MLFI, the predictions lie between the LFI- p and LFI- $p + q$ models, but can actually be out of this region for high enough values of α . This means that if one starts from a pure $V \propto \phi^{p+q}$ potential and adds a small $\propto \phi^p$ term, this extra term has the effect of increasing the “effective value” of the power index of the potential. Moreover, since for the large field inflation models, the p -model is favored with respect to the $p + q$ -one, small values for the parameter α are favored, together with high reheating temperatures.

6.5 Logarithmic Potential Inflation (LPI)

This class of models has been studied on general grounds in Ref. [477]. The inflaton is assumed to evolve in a potential of the form

$$V(\phi) = M^4 \left(\frac{\phi}{\phi_0}\right)^p \left(\ln \frac{\phi}{\phi_0}\right)^q. \quad (6.59)$$

On more fundamental grounds, such a potential appears in various contexts. For instance, for $p = 4$ and $q = 3$, one recovers the model discussed in Ref. [413] in the context of Super Yang-Mills theories. For $p = 4$ and $q = 1$, this model matches with the so-called Glueball Inflation of Ref. [478]. For both of these models, the inflaton is however non-minimally coupled to gravity. Defining

$$x \equiv \frac{\phi}{\phi_0}, \quad (6.60)$$

the potential exhibits a local maximum at $x = x_{V\text{max}}$ and a vanishing local minimum at $x = x_{V=0}$ with

$$x_{V\text{max}} = e^{-q/p}, \quad x_{V=0} = 1. \quad (6.61)$$

For $x > x_{V=0}$, $V(x)$ increases and finally diverge when x goes to infinity. The potential is always definite positive in the $x > 1$ branch, whereas it is definite positive in the $x < 1$ branch only if q is an even integer. The first three Hubble flow functions in the slow-roll approximation are given by

$$\epsilon_1 = \frac{M_{\text{Pl}}^2}{\phi_0^2} \frac{[q + p \ln(x)]^2}{2x^2 \ln(x)^2}, \quad \epsilon_2 = 2 \frac{M_{\text{Pl}}^2}{\phi_0^2} \frac{q + q \ln(x) + p \ln(x)^2}{x^2 \ln(x)^2}, \quad (6.62)$$

and

$$\epsilon_3 = \frac{M_{\text{Pl}}^2}{\phi_0^2} [q + p \ln(x)] \frac{2q + 3q \ln(x) + 2q \ln(x)^2 + 2p \ln(x)^3}{x^2 \ln(x)^2 [q + q \ln(x) + p \ln(x)^2]}. \quad (6.63)$$

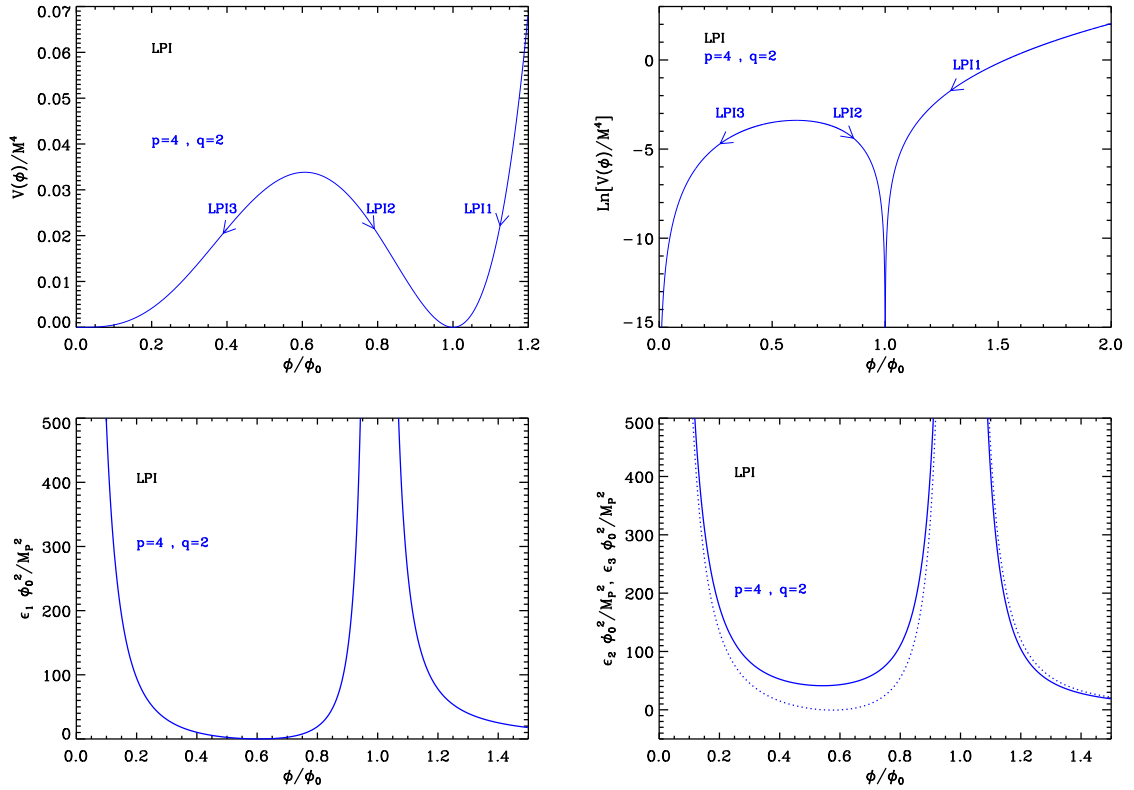


Figure 69. Logarithmic Potential Inflation (LPI) for $p = 4, q = 2$. Upper panels: the potential and its logarithm. Bottom left panel: slow-roll parameter ϵ_1 . Bottom right panel: slow-roll parameters ϵ_2 (solid line) and ϵ_3 (dotted line).

Together with the potential, they are displayed in Fig. 69.

As can be checked on this figure, and assuming q is even, the behavior of $\epsilon_1(x)$ exhibits three domains in which inflation can occur and can naturally end. Either $x > 1$ and inflation proceeds at decreasing field values (LPI1), or $x_{V\text{-max}} < x < 1$ and inflation proceeds at increasing field values (LPI2), or $0 < x < x_{V\text{-max}}$ and inflation proceeds at decreasing field values (LPI3). For these three domains, the slow-roll trajectory can be integrated analytically and one has

$$N - N_{\text{end}} = \left(\frac{\phi_0}{M_{\text{Pl}}} \right)^2 \left\{ -\frac{x^2 - x_{\text{end}}^2}{2p} + \frac{q}{p^2} e^{-2q/p} \left[\text{Ei} \left(\frac{2q}{p} + 2 \ln x \right) - \text{Ei} \left(\frac{2q}{p} + 2 \ln x_{\text{end}} \right) \right] \right\}. \quad (6.64)$$

Let us remark that for $x \rightarrow +\infty$ (LPI1), one recovers the large field inflation (LFI) trajectory of section 4.2 and where p matches the same parameter.

Along the three regimes, inflation ends at the field value x_{end} solution of $\epsilon_1(x_{\text{end}}) = 1$ in the domain of interest, i.e. verifying

$$p \ln(x_{\text{end}}) + q \mp \sqrt{2} \frac{\phi_0}{M_{\text{Pl}}} x_{\text{end}} \ln(x_{\text{end}}) = 0. \quad (6.65)$$

This is a transcendental equation that cannot be solved analytically for any values of p and q . It can nevertheless be solved numerically in each of the three above-mentioned domains.

Together with Eq. (6.64) and Eq. (2.46), it uniquely determines the observable field value x_* at which the pivot mode crossed the Hubble radius during inflation. Therefore, according to our classification, LPI is a three parameters model with p , q and ϕ_0 .

Finally, the parameter M is fixed by the amplitude of the CMB anisotropies to

$$\frac{M^4}{M_{\text{Pl}}^4} = 720\pi^2 \left(\frac{M_{\text{Pl}}}{\phi_0} \right)^2 \frac{[q + p \ln(x_*)]^2 Q_{\text{rms-PS}}^2}{x_*^{2+p} \ln(x_*)^{2+q} T^2}. \quad (6.66)$$

The reheating consistent slow-roll predictions for the LPI1 models with $p = 4$ are represented in Figs 157, 158, and 159 for $q = 2$, $q = 1$ and $q = 3$, respectively. The predictions for the LPI2 domain are displayed in Figs 160, 161, and 162 for $p = 1$, $q = 2$; $p = 2$, $q = 2$; and $p = 3$, $q = 4$; respectively. For the LPI3 domain, they have been plotted in Figs 163, 164, and 165 for $p = 1$, $q = 2$; $p = 2$, $q = 2$; and $p = 3$, $q = 4$; respectively. One can see that the current CMB data require LPI inflation to take place with super-Planckian values for ϕ_0 while some peculiar combination of p and q are already disfavored at more than two-sigma.

6.6 Constant n_s D Inflation (CNDI)

This model has been studied in Ref. [412]. Its potential is designed in order to produce a power law power spectrum $\propto k^n$ (where n is a constant). In this sense, the approach followed here is similar to the one investigated in sections 4.20, 4.21 and 5.14. The potential studied in this section is given by

$$V(\phi) = \frac{M^4}{\left\{ 1 + \beta \cos \left[\alpha \left(\frac{\phi - \phi_0}{M_{\text{Pl}}} \right) \right] \right\}^2}, \quad (6.67)$$

where α and β are two dimensionless parameters. Since the potential is an even function of $x \equiv (\phi - \phi_0)/M_{\text{Pl}}$ and is periodic with period 2π , it can be studied without loss of generality in the range $x \in [0, \pi/\alpha]$ only (with $\alpha > 0$, $\beta > 0$). $V(\phi)$ and its logarithm are displayed in Fig. 70 (top panels) for two different representative values of β . If $\beta < 1$ (blue curve), it is an increasing function of the field, hence inflation proceeds from the right to the left. On the contrary, if $\beta \geq 1$ (pink curve), it diverges at $x_{V \rightarrow \infty} = \arccos(-1/\beta)/\alpha$. Then, for $x < x_{V \rightarrow \infty}$ it is an increasing function of x and inflation proceeds from the right to the left, whereas for $x > x_{V \rightarrow \infty}$ it is a decreasing function of x and inflation proceeds from the left to the right.

The three first slow-roll parameters are given by the following expressions

$$\epsilon_1 = \frac{2\alpha^2 \beta^2 \sin^2(\alpha x)}{[1 + \beta \cos(\alpha x)]^2}, \quad \epsilon_2 = \frac{-4\alpha^2 \beta [\beta + \cos(\alpha x)]}{[1 + \beta \cos(\alpha x)]^2}, \quad (6.68)$$

and

$$\epsilon_3 = \frac{-2\alpha^2 \beta [2\beta^2 - 1 + \beta \cos(\alpha x)] \sin^2(\alpha x)}{[\beta + \cos(\alpha x)] [1 + \beta \cos(\alpha x)]^2}. \quad (6.69)$$

They are displayed in Fig. 70 (bottom panels). Let now study in more detail the behavior of ϵ_1 and ϵ_2 . This one depends on whether β is larger or smaller than 1. If $\beta < 1$, The first slow-roll parameter ϵ_1 vanishes at $x = 0$ and $x = \pi/\alpha$, and reaches a maximum in between at $x_{\epsilon_2=0}$. This maximum is larger than one provided $\alpha > \alpha_{\min}(\beta)$, where

$$\alpha_{\min}(\beta) = \sqrt{\frac{1 - \beta^2}{2\beta^2}}. \quad (6.70)$$

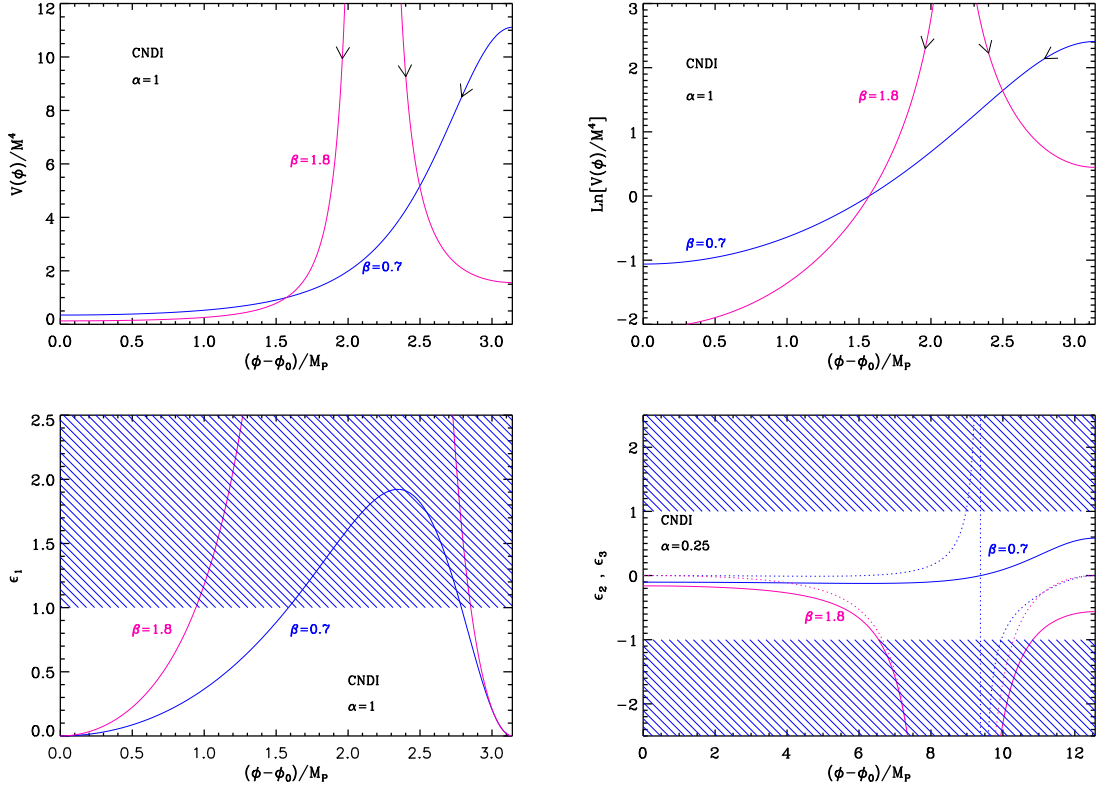


Figure 70. Top left panel: constant n_s D inflaton potential for $\alpha = 1$ and two values of β , namely $\beta = 0.7$ (solid blue line) and $\beta = 1.3$ (solid pink line). Top right panel: logarithm of the potential for the same values of α and β and with the same color code. Bottom left panel: first slow-roll parameter ϵ_1 for a potential with $\alpha = 1$ and $\beta = 0.7$ (solid blue line), $\beta = 1.8$ (solid pink line). The shaded area indicates the breakdown of slow-roll inflation (strictly speaking where acceleration cannot occur). Bottom right panel: second and third slow-roll parameters ϵ_2 and ϵ_3 for $\alpha = 0.25$ and the same values of β as in the other plots.

In that case, inflation can stop by slow-roll violation, at the position x_{end} given by

$$x_{\text{end}} = x_{\epsilon_1=1}^+ = \frac{1}{\alpha} \arccos \left[\frac{\alpha \sqrt{2\beta^2 (1 + 2\alpha^2) - 2} - 1}{\beta + 2\alpha^2 \beta} \right], \quad (6.71)$$

and inflation proceeds in the range $[x_{\text{end}}, \pi/\alpha]$ (from the right to the left). On the other hand, the second slow-roll parameter ϵ_2 is a monotonous increasing function of x , which vanishes at $x_{\epsilon_2=0} = \arccos(-\beta)/\alpha$. If $\beta \geq 1$, as can be seen in Fig. 70, the first slow-roll parameter ϵ_1 diverges at $x_{V \rightarrow \infty} = \arccos(-1/\beta)/\alpha$, so that inflation cannot stop by slow-roll violation in that case. This means that inflation must end by instability and, therefore, that the model depends on an additional parameter. The second slow-roll parameter ϵ_2 is always negative and also diverges at $x_{V \rightarrow \infty}$. Let us notice that, for $\beta < 1$ and $\alpha > \alpha_{\text{min}}(\beta)$, and for $\beta > 1$ (for any α), it can also be useful (see discussion below) to give the other solution of $\epsilon_1 = 1$. This one reads

$$x_{\epsilon_1=1}^- = \frac{1}{\alpha} \arccos \left[-\frac{\alpha \sqrt{2\beta^2 (1 + 2\alpha^2) - 2} + 1}{\beta + 2\alpha^2 \beta} \right]. \quad (6.72)$$

We are now in a position where the slow-roll trajectory can be determined. It turns out that this one can be integrated exactly and reads

$$N - N_{\text{ini}} = \frac{1}{2\alpha^2} \left\{ -\ln [\sin(\alpha x)] - \frac{1}{\beta} \ln \left[\tan \left(\alpha \frac{x}{2} \right) \right] + \ln [\sin(\alpha x_{\text{ini}})] + \frac{1}{\beta} \ln \left[\tan \left(\alpha \frac{x_{\text{ini}}}{2} \right) \right] \right\}. \quad (6.73)$$

Because of the logarithmic functions in the trajectory, a sufficient number of e-folds can be realized only if the initial conditions are fine tuned and x_{ini} is chosen to be extremely close to π/α . Concretely, it can be seen in the following way. One can calculate the function $N_{\text{end}} - N_{\text{ini}}$ by inserting Eq. (6.71) into Eq. (6.73). Then, the total number of e-folds during inflation becomes function of x_{ini} and of the two parameters α and β . For given values of those parameters, it is easy to plot $(N_{\text{end}} - N_{\text{ini}})(x_{\text{ini}})$ which always remains small compared to one unless $x_{\text{ini}} \rightarrow \pi/\alpha$ where it blows up. In order to have $N_{\text{end}} - N_{\text{ini}} \gtrsim 60$, it is therefore necessary to have $x_{\text{ini}} \simeq \pi/\alpha$. Technically, this property can be seen in the following way. Let us write x_{ini} as $\pi/\alpha + \delta x_{\text{ini}}$ where $\delta x_{\text{ini}} \ll 1$. Then, it is easy to show that $\ln [\sin(\alpha x_{\text{ini}})] + \ln [\tan(\alpha x_{\text{ini}}/2)]/\beta \simeq -\ln \left[(\alpha/2)^{1/\beta} \alpha^{-1} (\delta x_{\text{ini}})^{(1-\beta)/\beta} \right]$. Defining the constant A by $A \equiv \ln [\sin(\alpha x_{\text{end}})] + \ln [\tan(\alpha x_{\text{end}}/2)]/\beta$, one arrives at

$$\delta x_{\text{ini}} \simeq \left[\alpha \left(\frac{\alpha}{2} \right)^{-1/\beta} e^{-A} \right]^{\beta/(1-\beta)} e^{-2\alpha^2 \beta (N_{\text{end}} - N_{\text{ini}})/(1-\beta)}. \quad (6.74)$$

The coefficient between the squared brackets only depends on α and β which are, a priori, coefficients of order one. Therefore, this coefficient is also of order one. On the other hand, the argument of the exponential is $2(N_{\text{end}} - N_{\text{ini}}) > 120$ times a negative term (since $0 < \beta < 1$) of order one. This means that δx_{ini} is in fact exponentially small. We have thus recovered the fine-tuning mentioned above. Then, one can question the physical relevance of such a fine tuning, and, furthermore, it makes the numerical treatment of the model intractable with a reasonable level of accuracy. But, the typical predictions of the model in that case (taking $x_* \simeq \pi/\alpha$) are $\epsilon_1 \simeq 0$, $\epsilon_2 \simeq 4\alpha^2\beta/(1-\beta)$, and $\epsilon_3 \simeq 0$. It follows that the condition $\alpha > \alpha_{\text{min}}(\beta)$ implies $\epsilon_2 > 2(1+\beta)/\beta > 4$. Obviously, $\epsilon_2 > 4$ is completely ruled out by the observations and the case $\beta < 1$ is therefore excluded.

Let us now study the case $\beta > 1$ which remains the only viable possibility. In this case, as already discussed before, inflation cannot end by slow-roll violation and one needs to add an extra parameter x_{end} , making the model a three parameter one. In the range $\alpha x_{\text{end}} \ll 1$, one has $\epsilon_1 \ll 1$ and $\epsilon_2 \simeq -4\alpha^2\beta/(1+\beta)$ such that the spectral index is given by $n_s \simeq 1 + 4\alpha^2\beta/(\beta+1)$. Therefore, it is indeed a constant.

The predictions of CNDI inflation are displayed in Figs. 166 and 167. We see that, in the regime $\alpha x_{\text{end}} \ll 1$, the spectral index is indeed a constant. However, this occurs in a regime where the predictions are not really consistent with the observations (the spectrum is too blue). On the other hand, when αx_{end} is no longer small, we observe strong deviations from the law $n_s \simeq 1 + 4\alpha^2\beta/(\beta+1)$ but, for relatively small values of α , the predictions become compatible with the data. Obviously, these considerations bear some resemblance with the findings of sections 4.20, 4.21 and 5.14.

The last thing which remains to be done is to estimate the energy scale M . For this purpose, we calculate the COBE normalization and it follows that

$$\left(\frac{M}{M_{\text{Pl}}} \right)^4 = 2880\alpha^2\beta^2\pi^2 \sin^2(\alpha x_*) \frac{Q_{\text{rms-PS}}^2}{T^2}. \quad (6.75)$$

We are mainly interested in the regime where the predictions are in agreement with the data. In that case, as established above, αx_* is no longer small and it becomes difficult to express the term $\sin(\alpha x_*)$ as a function of α , β and x_{end} . In this situation, a numerical approach becomes the easiest method to estimate the scale M .

7 Conclusions

Let us very briefly recap our main findings and present some directions for future works.

In this article, we have discussed the question of how the inflationary theory can be constrained given that we now have at our disposal high accuracy cosmological data. We have argued that this can be done by means of the slow-roll approximation which has the advantage of being relatively model independent. Although this approximation cannot be used if one has to deal with more complicated models, it produces interesting but limited information on inflation. Concretely, it leads to the Hubble flow posterior distributions $P(\epsilon_n | C_\ell^{\text{meas}})$. This is interesting since this gives a general constraint on the derivatives of the inflaton potential. But, at the same time, this does not answer some legitimate fundamental questions one might have about the plethora of inflationary scenarios studied so far. For instance, it does not tell us rigorously which constraints exist on the parameters of a given model. Indeed, suppose that we are interested in LFI, $V(\phi) \propto \phi^p$. It is obvious that we would like to know for which values of p this class of models is compatible with the data and for which values it is not.

In order to complement the slow-roll approximation and to address the above mentioned issues, we have argued that it is interesting to scan the inflationary landscape model by model and have provided the public code `ASPIC` to do so. Of course, this has to be done for all the inflationary scenarios since it would be arbitrary to consider only a restricted class while ignoring the others. In fact, this question deserves to be discussed in more detail. One could indeed imagine that it is not necessary to consider all the models one by one and that considering a representative for each class is sufficient. Indeed, to simplify the discussion, it is common to distinguish three broad types of scenarios: large field models (LFI), small field models (SFI) and Hybrid models (VHI). Such a classification is not very precise and biased because it pushes to the front line these three models. It could be reasonably argued that a better classification is the one of Schwarz and Terrero-Escalante introduced in Ref. [479]. For a scalar field, the ratio of the kinetic energy to the total energy density is given by $\epsilon_1/3 = \dot{\phi}^2/(2\rho)$. From the definition of ϵ_2 , one sees that ϵ_1 , and thus the kinetic contribution to the total energy density, increases if $\epsilon_2 > 0$ and decreases if $\epsilon_2 < 0$. On the other hand, we also have

$$\frac{d(\dot{\phi}^2/2)}{dt} = H \frac{\dot{\phi}^2}{2} (\epsilon_2 - 2\epsilon_1), \quad (7.1)$$

and, therefore, the absolute value of the kinetic energy increases if $\epsilon_2 > 2\epsilon_1$ whereas it decreases if $\epsilon_2 < 2\epsilon_1$. This allows us to identify three different regions: $\epsilon_2 > 2\epsilon_1$ (region 1), $\epsilon_2 < 2\epsilon_1$ (region 2), $\epsilon_2 < 0 < 2\epsilon_1$ (region 3).

These three regions are identified in Fig. 71. If we use the first order slow-roll expressions, the condition $\epsilon_2 > 0$ is equivalent to $r < 8(1 - n_s)$ while $\epsilon_2 > 2\epsilon_1$ amounts to $r < 4(1 - n_s)$. These two lines are also represented in Fig. 71 (solid black lines). We have also superimposed the predictions of LFI, SFI and VHI (upper panel). We see that the three regions defined above roughly correspond to the cases large field, small field and hybrid.

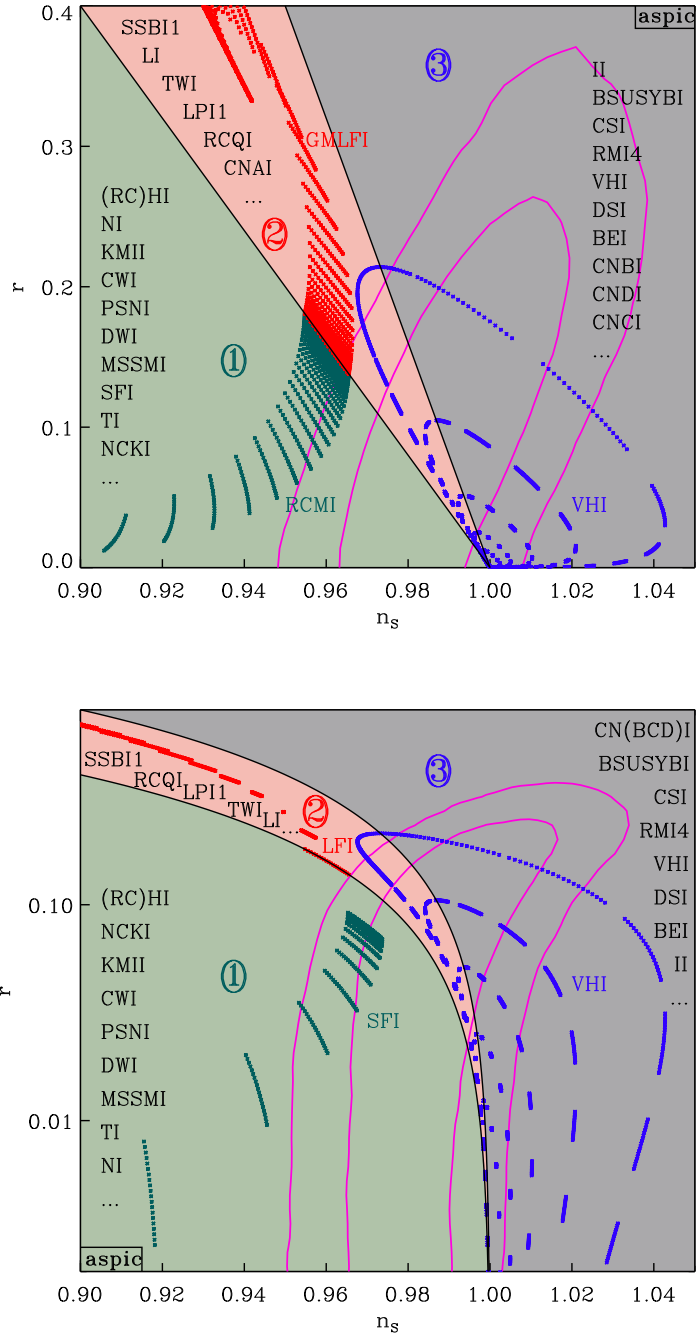


Figure 71. Upper panel: various ASPIC scenarios in the (n_s, r) plane using the Schwarz-Terrero-Escalante classification [479]. Bottom panel: same plot in logarithmic scale for another sample of models.

However, the correspondence is not perfect and we notice, for instance, that the predictions of VHI can penetrate region 2.

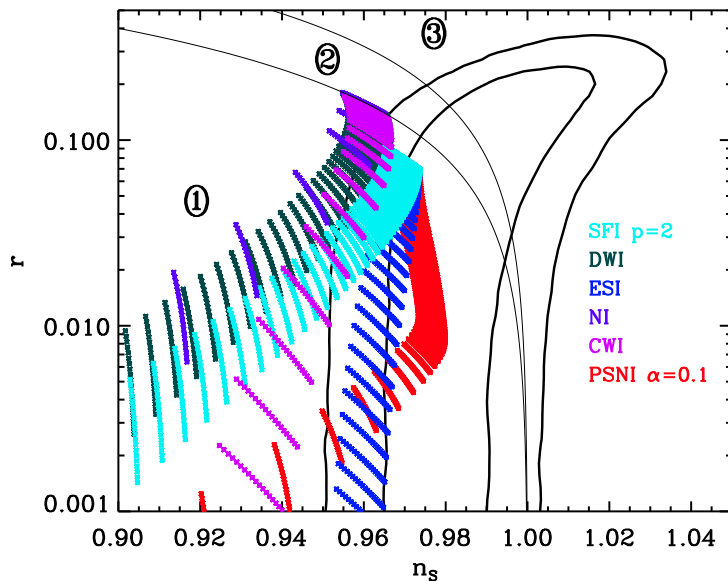


Figure 72. Observable predictions in the (n_s, r) plane for various models belonging to region 1 of the Schwarz-Terrero-Escalante classification (see Fig. 71). Despite the fact that they are in the same broad class, the accuracy of the CMB data allows us to discriminate among them thereby justifying a detailed navigation within the inflationary landscape.

Then, having identified three broad classes of scenarios, the question is whether testing only a representative model for each class would be sufficient. In Fig. 72, we have considered the predictions of six different models that all belong to region 1. This plot clearly shows that inside this region, these six models span different domains that are separated enough to be distinguishable within current and future data. We therefore conclude that, given the quality of the current data, working only with broad classes of models is no longer justified. Therefore, if one really wants to scan the inflationary landscape, it is necessary to consider the approach advocated in this paper.

With ASPIC, we have provided a new tool to treat any model of inflation and this has led us to derive observational predictions for 64 models. ASPIC is an evolutive project and therefore the next steps will be to complete and upgrade it with new models. Finally, the ultimate goal is to identify which ASPIC model is performing the best for explaining cosmological data. In order to carry out this task, an appropriate method is to use Bayesian evidence and model comparison. Then, we should be able to identify, in a statistically well-defined manner, what might be called “the best model of inflation”.

A Reheating consistent slow-roll predictions

A.1 Higgs Inflation (HI)

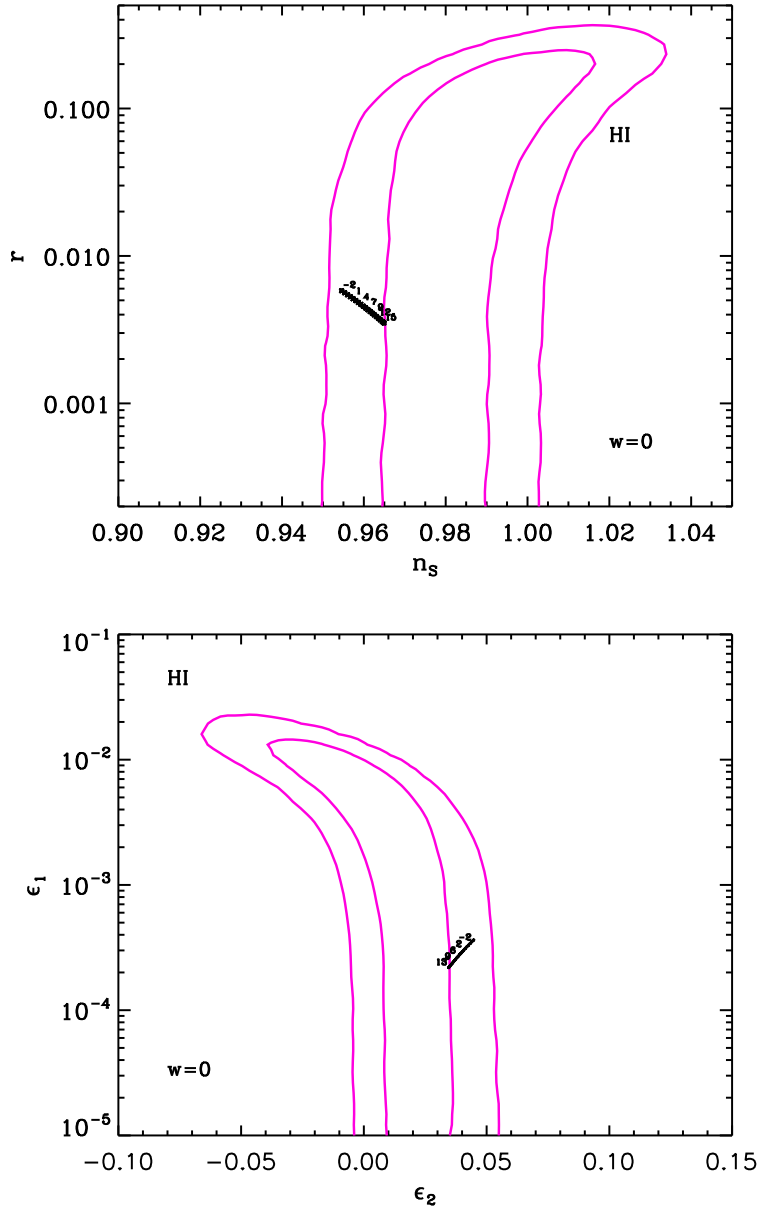


Figure 73. Reheating consistent slow-roll predictions for the Higgs model in the plane (n_s, r) (top panel) and the plane (ϵ_1, ϵ_2) (bottom panel). The two pink solid contours are the one and two-sigma WMAP confidence intervals (marginalized over second order slow-roll). The annotations trace the energy scale at which the large field reheating ends and correspond to $\log(g_*^{1/4} T_{\text{reh}}/\text{GeV})$.

A.2 Radiatively Corrected Higgs Inflation (RCHI)

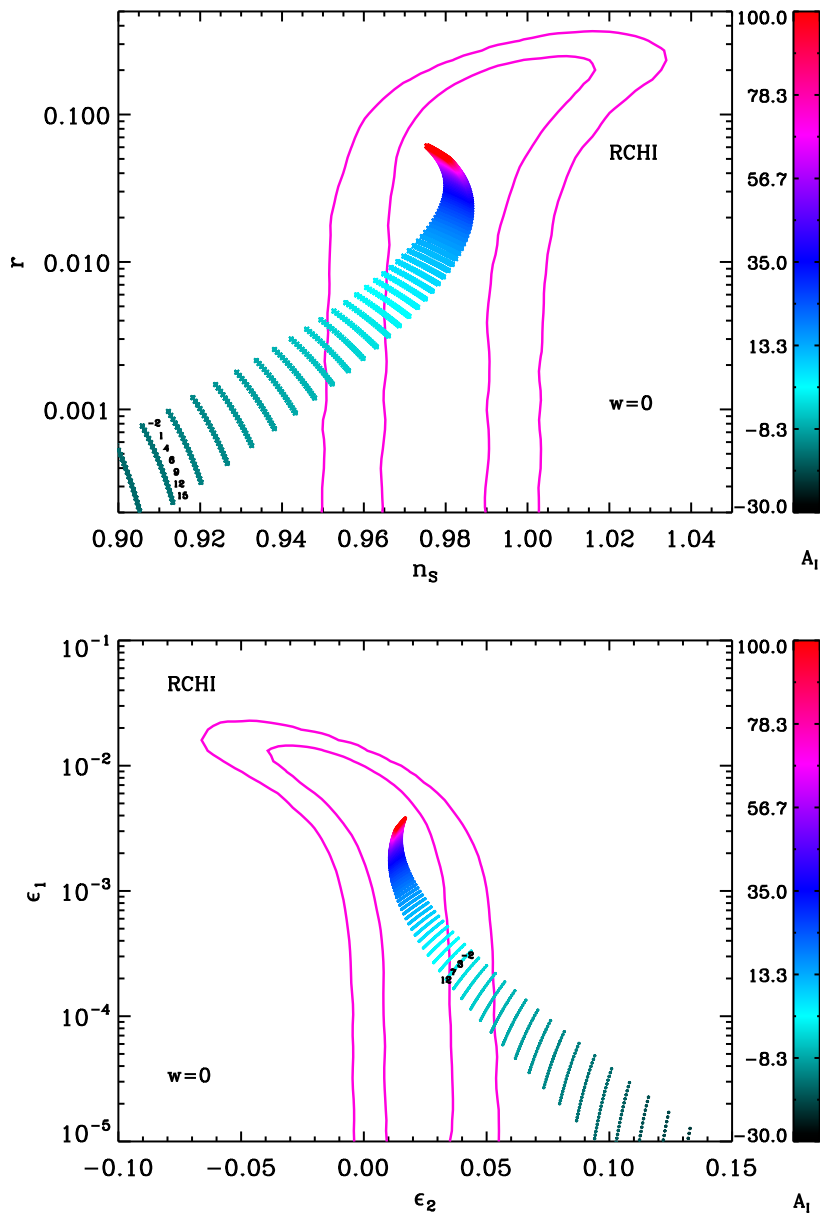


Figure 74. Reheating consistent slow-roll predictions for the radiatively corrected Higgs model in the plane (n_s, r) (top panel) and the plane (ϵ_1, ϵ_2) (bottom panel). The two pink solid contours are the one and two-sigma WMAP confidence intervals (marginalized over second order slow-roll). The annotations trace the energy scale at which the large field reheating ends and correspond to $\log(g_*^{1/4} T_{\text{reh}}/\text{GeV})$.

A.3 Large Field Inflation (LFI)

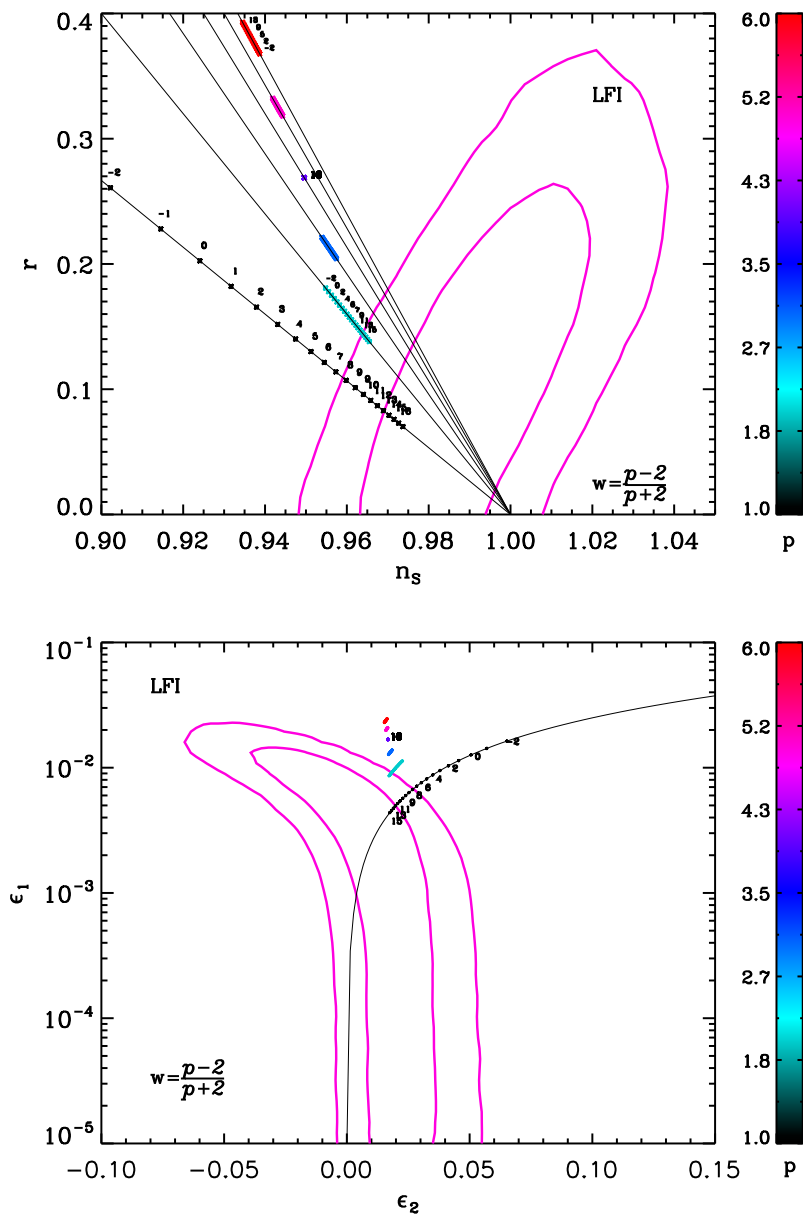


Figure 75. Reheating consistent slow-roll predictions for the large field models in the plane (n_s, r) (top panel) and the plane (ϵ_1, ϵ_2) (bottom panel). The two pink solid contours are the one and two-sigma WMAP confidence intervals (marginalized over second order slow-roll). The black solid lines represent the locus of different LFI- p models [for which $(1 + 2/p)r = 8(1 - n_s)$, ie $\epsilon_1 = (p/4)\epsilon_2$]. The annotations trace the energy scale at which the large field reheating ends and correspond to $\log(g_*^{1/4}T_{\text{reh}}/\text{GeV})$. Clearly, these values are limited from below to stay inside the two-sigma contours and models with $p > 3$ are excluded at two sigma confidence level.

A.4 Mixed Large Field Inflation (MLFI)

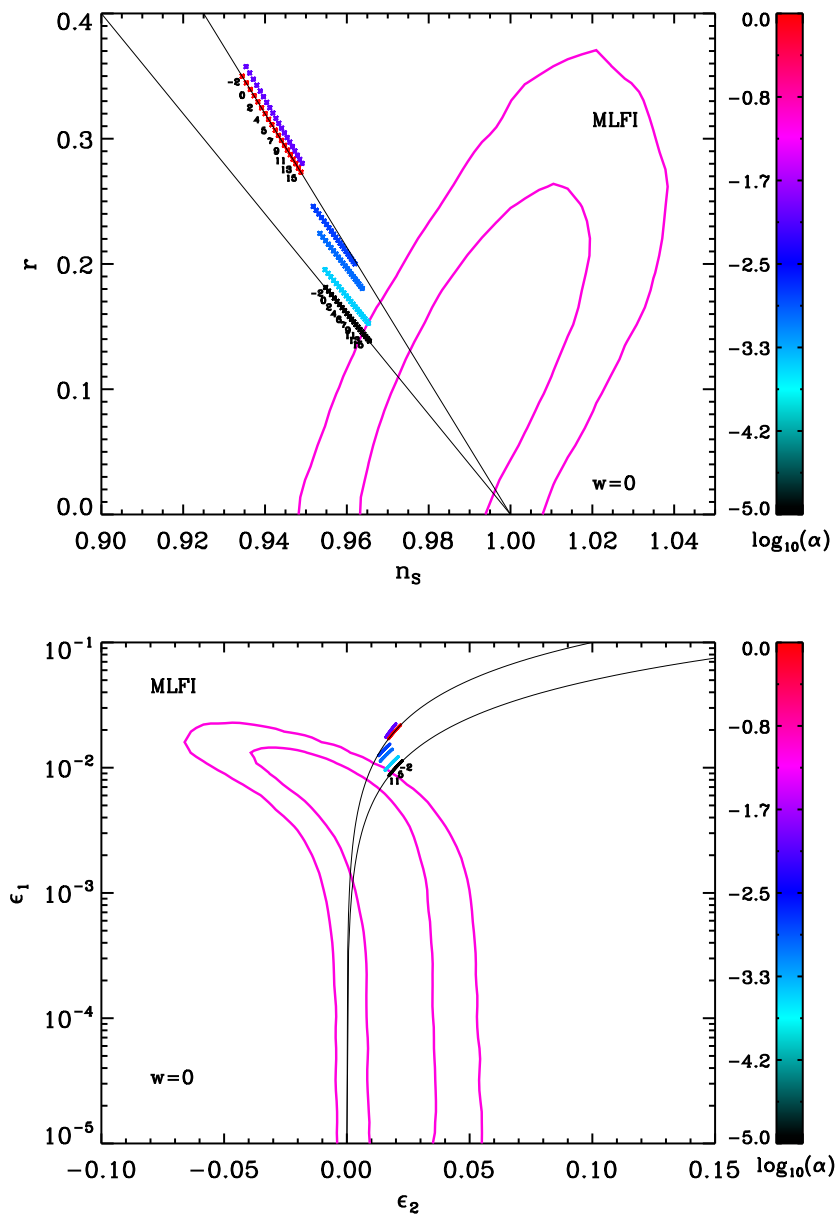


Figure 76. Reheating consistent slow-roll predictions for the mixed large field models in the plane (n_s, r) (top panel) and the plane (ϵ_1, ϵ_2) (bottom panel). The two pink solid contours are the one and two-sigma WMAP confidence intervals (marginalized over second order slow-roll). The reheating equation of state parameter \bar{w}_{reh} has been taken to 0 since the potential is quadratic close to its minimum. The black solid lines represent the locus of the quadratic model (namely LFI with $p = 2$) and of the quartic model (namely LFI with $p = 4$) [for which $(1 + 2/p)r = 8(1 - n_s)$, i.e. $\epsilon_1 = (p/4)\epsilon_2$]. The annotations trace the energy scale at which the mixed large field reheating ends and correspond to $\log(g_*^{1/4} T_{\text{reh}}/\text{GeV})$. Clearly, these values are limited from below to stay inside the two-sigma contours and models with $\alpha > 10^{-3}$ are excluded at two-sigma confidence level.

A.5 Radiatively Corrected Massive Inflation (RCMI)

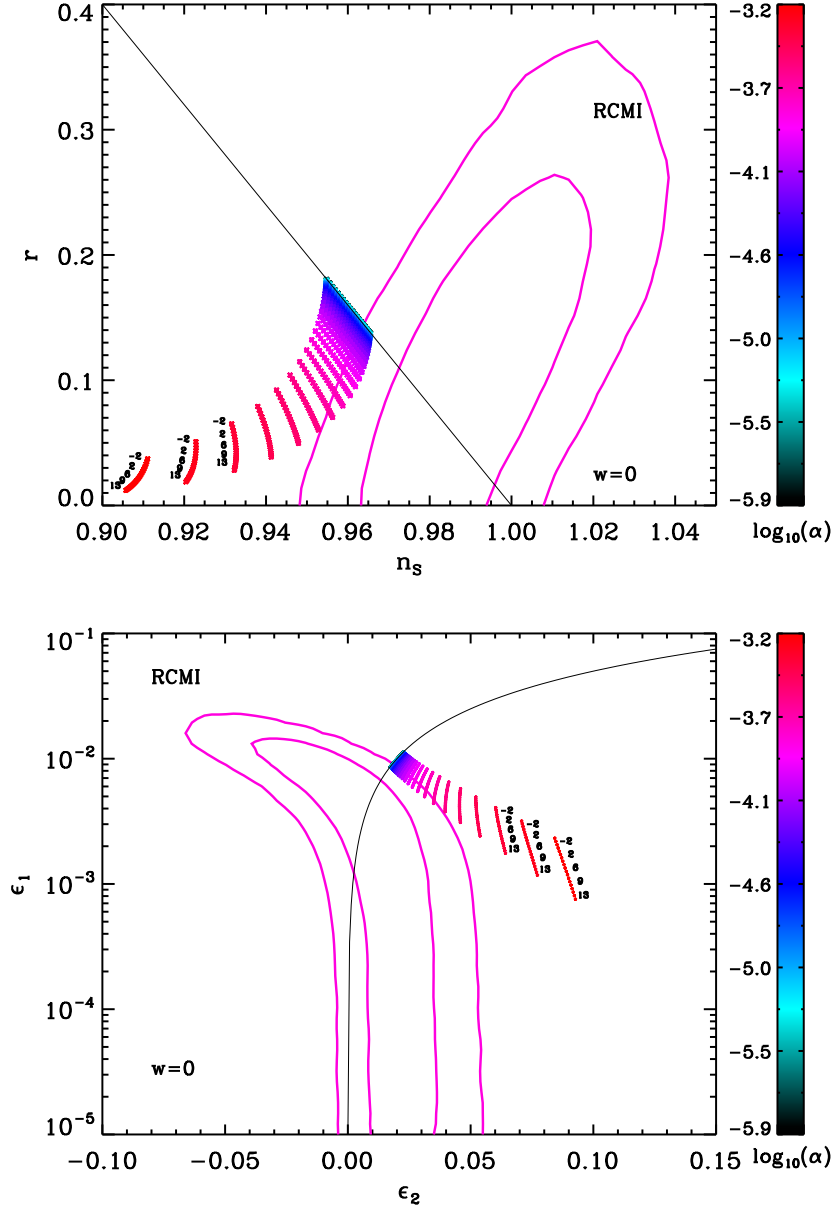


Figure 77. Reheating consistent slow-roll predictions for the radiatively corrected massive models in the plane (n_s, r) . The two pink solid contours are the one and two-sigma WMAP confidence intervals (marginalized over second order slow-roll). The black solid line represent the locus of the quadratic model [i.e. LFI with $p = 2$, for which $r = 4(1 - n_s)$, i.e. $\epsilon_1 = \epsilon_2/2$]. The annotations trace the energy scale at which the radiatively corrected massive reheating ends and correspond to $\log(g_*^{1/4} T_{\text{reh}}/\text{GeV})$. Clearly, these values are limited from below to stay inside the two-sigma contours and models with $\alpha > 10^{-3.5}$ are disfavored at two sigma confidence level.

A.6 Radiatively Corrected Quartic Inflation (RCQI)

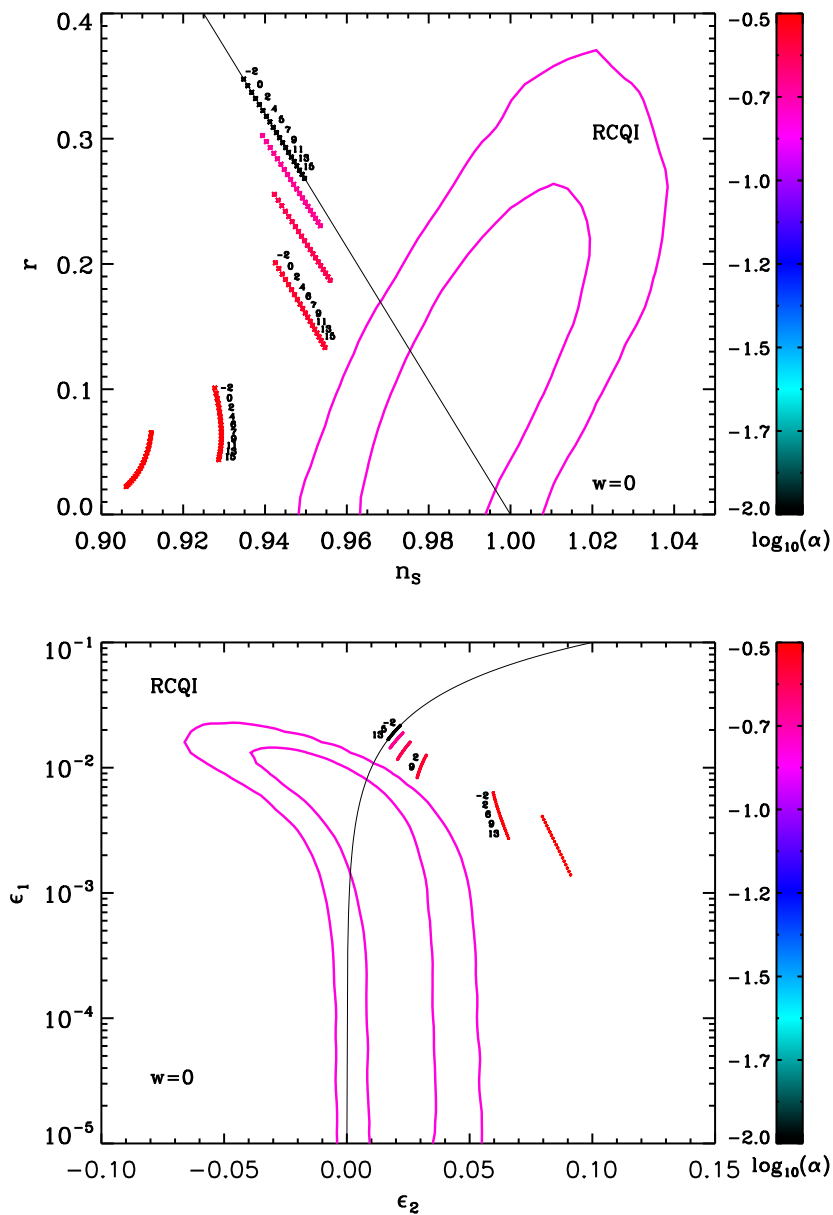


Figure 78. Reheating consistent slow-roll predictions for the radiatively corrected quartic models in the plane (n_s, r) (top panel) and the plane (ϵ_1, ϵ_2) (bottom panel), with $\bar{w}_{\text{reh}} = 0$. The two pink solid contours are the one and two-sigma WMAP confidence intervals (marginalized over second order slow-roll). The black solid line represent the locus of the quartic model [i.e. LFI with $p = 4$, for which $r = (16/3)(1 - n_s)$, i.e. $\epsilon_1 = \epsilon_2$]. The annotations trace the energy scale at which the radiatively corrected quartic reheating ends and correspond to $\log(g_*^{1/4} T_{\text{reh}}/\text{GeV})$. Clearly, these values are limited from below, and regardless of them, these models seem to be disfavored at two sigma confidence level.

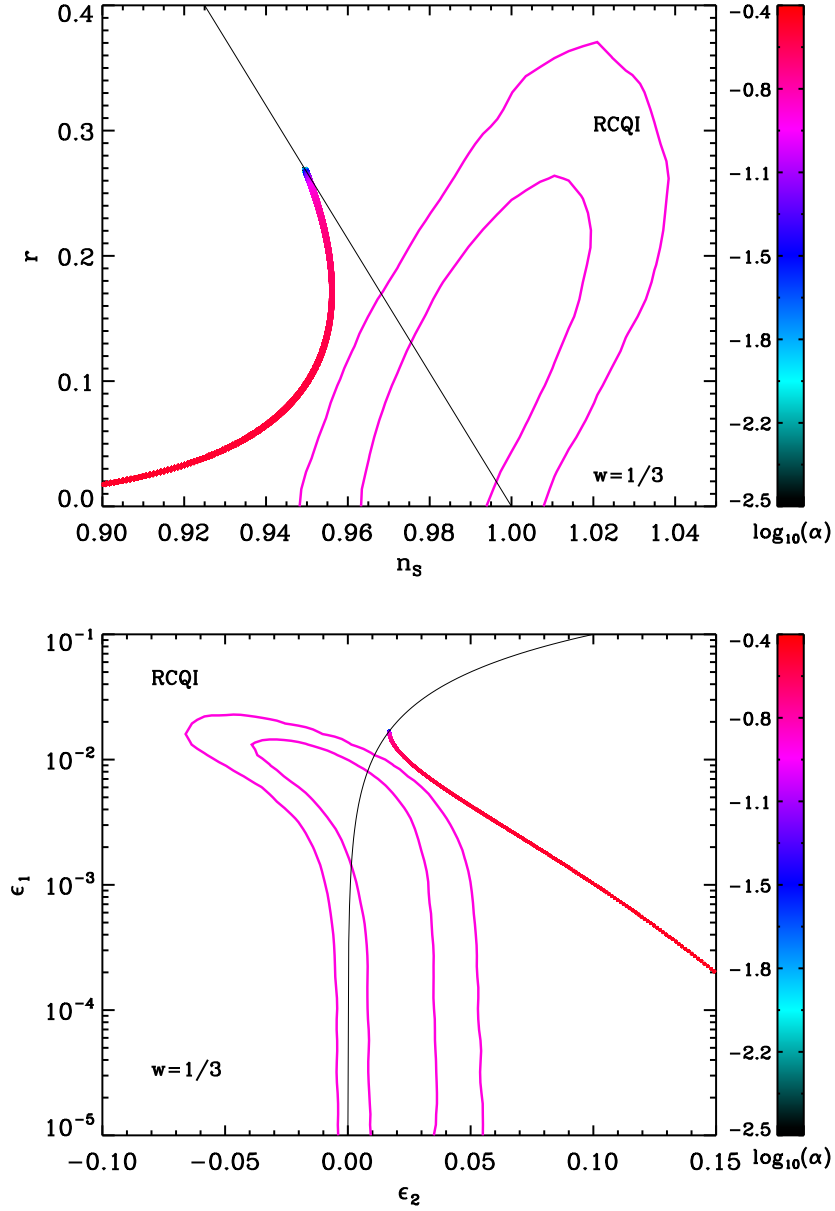


Figure 79. Reheating consistent slow-roll predictions for the radiatively corrected quartic models in the plane (n_s, r) (top panel) and the plane (ϵ_1, ϵ_2) (bottom panel), with $\bar{w}_{\text{reh}} = \frac{1}{3}$. This value of \bar{w}_{reh} may be more physically justified if the reheating phase takes place at the bottom of the potential, which is quartic in a good approximation, and for which one has $\bar{w}_{\text{reh}} = 1/3$. The two pink solid contours are the one and two-sigma WMAP confidence intervals (marginalized over second order slow-roll). The black solid line represent the locus of the quartic model [i.e. LFI with $p = 4$, for which $r = (16/3)(1 - n_s)$, i.e. $\epsilon_1 = \epsilon_2$]. The annotations trace the energy scale at which the radiatively corrected quartic reheating ends and correspond to $\log(g_*^{1/4} T_{\text{reh}}/\text{GeV})$. Clearly, these values are limited from below, and regardless of them, these models are disfavored at two sigma confidence level.

A.7 Natural Inflation (NI)

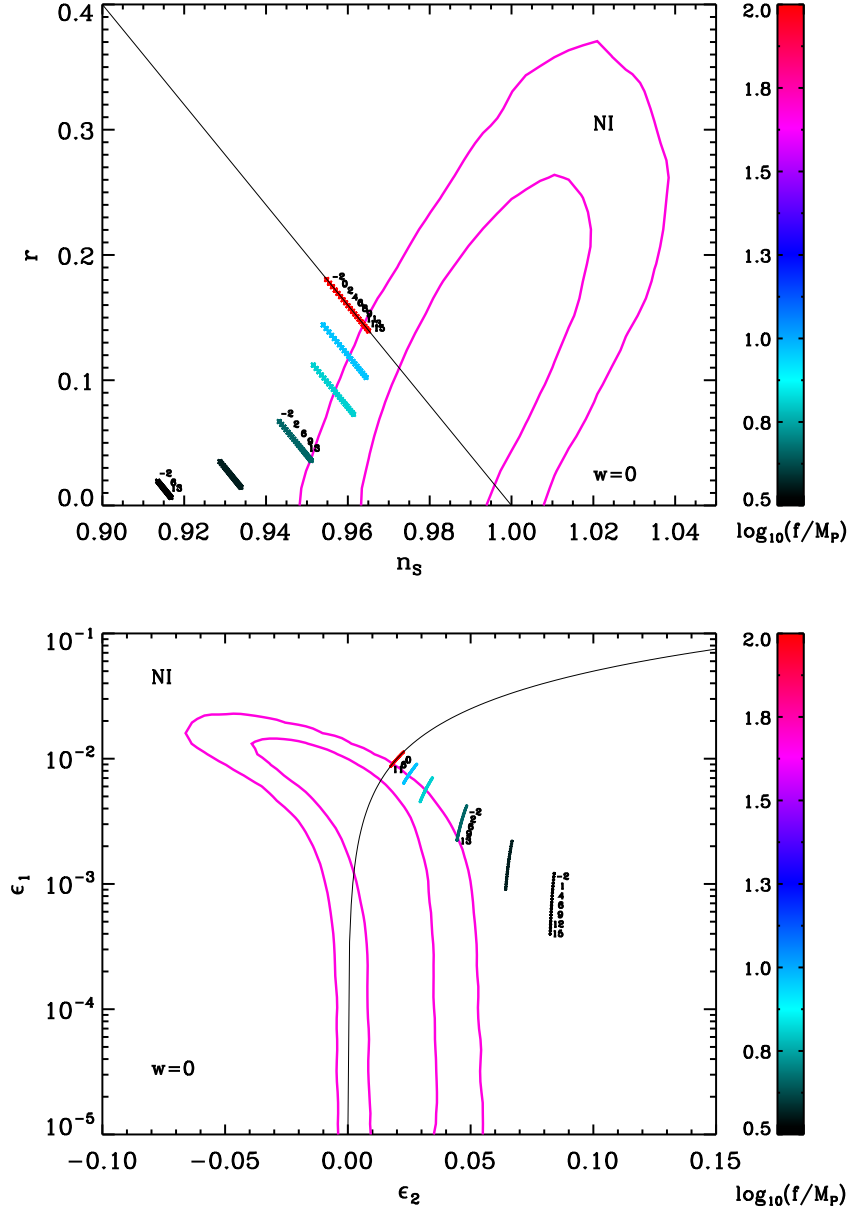


Figure 80. Reheating consistent slow-roll predictions for the natural inflation models in the plane (n_s, r) (top panel) and the plane (ϵ_1, ϵ_2) (bottom panel). The two pink solid contours are the one and two-sigma WMAP confidence intervals (marginalized over second order slow-roll). The reheating equation of state parameter \bar{w}_{reh} has been taken to 0 since the potential is quadratic close to its minimum. The black solid line represent the locus of the quadratic model points [i.e. LFI with $p = 2$, for which $r = 4(1 - n_s)$, i.e. $\epsilon_1 = \epsilon_2/2$]. The annotations trace the energy scale at which the natural reheating ends and correspond to $\log(g_*^{1/4} T_{\text{reh}}/\text{GeV})$. Clearly, high values of f/M_{Pl} seem to be favored by the data, as well as high reheating temperatures.

A.8 Exponential SUSY Inflation (ESI)

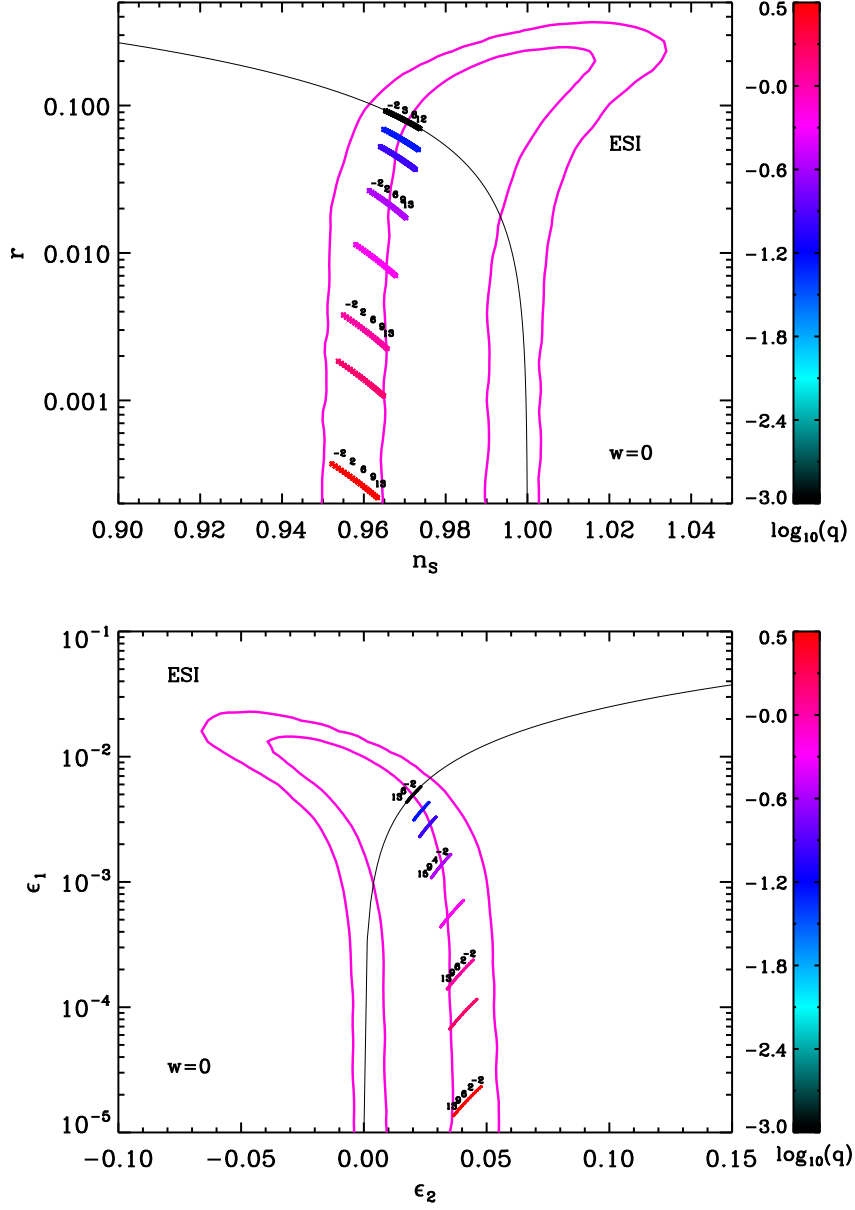


Figure 81. Reheating consistent slow-roll predictions for the exponential susy models in the plane (n_s, r) (top panel) and the plane (ϵ_1, ϵ_2) (bottom panel), with $\bar{w}_{\text{reh}} = 0$. The two pink solid contours are the one and two-sigma WMAP confidence intervals (marginalized over second order slow-roll). The black solid line represent the locus obtained from the linear large field model [with $p = 1$, for which $r = (8/3)(1 - n_s)$, i.e. $\epsilon_1 = \epsilon_2/4$]. The annotations trace the energy scale at which the exponential susy reheating ends and correspond to $\log(g_*^{1/4} T_{\text{reh}}/\text{GeV})$. Clearly, all these models seem to be consistent with observations.

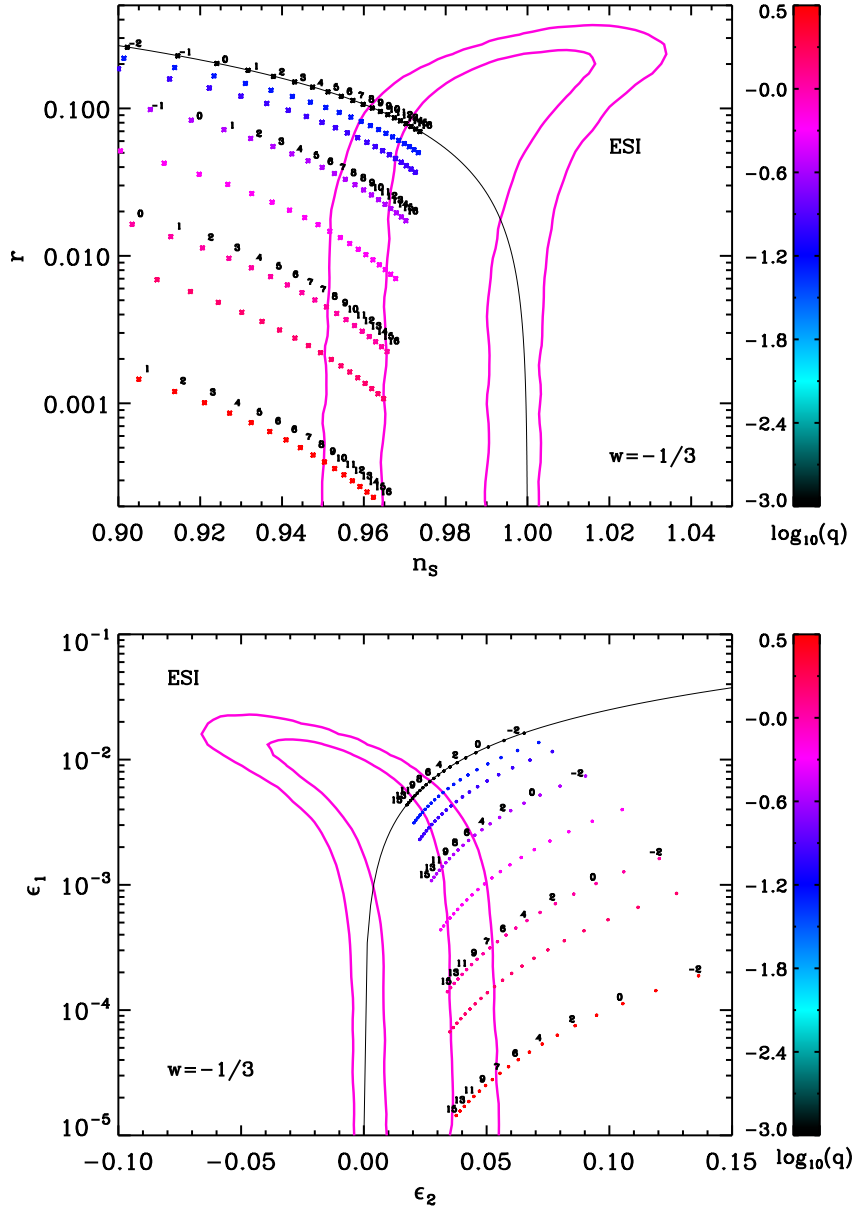


Figure 82. Reheating consistent slow-roll predictions for the exponential susy models in the plane (n_s, r) (top panel) and the plane (ϵ_1, ϵ_2) (bottom panel), with $\bar{w}_{\text{reh}} = -1/3$. This value of \bar{w}_{reh} may be more physically justified (although rather extreme) if a parametric reheating feels the bottom of the potential, which is linear in a good approximation. The two pink solid contours are the one and two-sigma WMAP confidence intervals (marginalized over second order slow-roll). The black solid line represent the locus of the linear large field model [with $p = 1$, for which $r = (8/3)(1 - n_s)$, i.e. $\epsilon_1 = \epsilon_2/4$]. The annotations trace the energy scale at which the exponential susy reheating ends and correspond to $\log(g_*^{1/4} T_{\text{reh}}/\text{GeV})$. Clearly in that case, these values are limited from below.

A.9 Power Law Inflation (PLI)

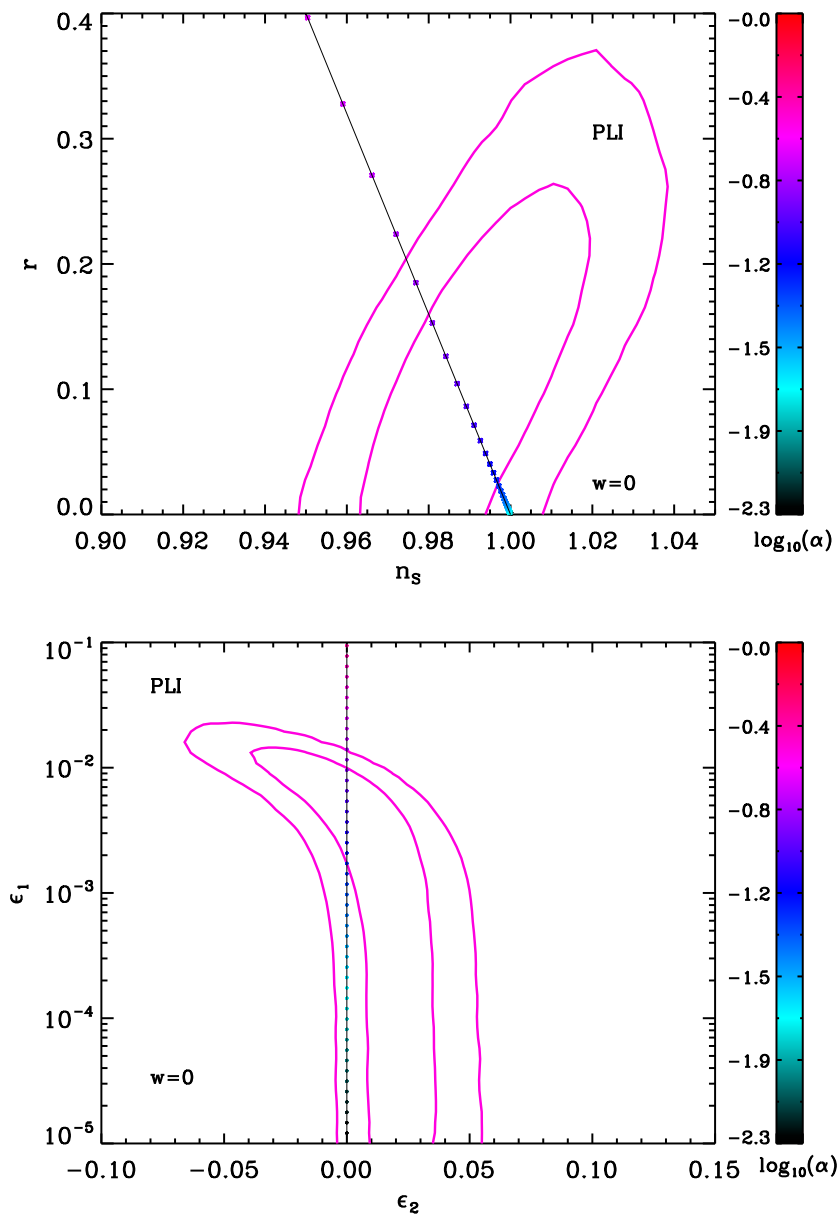


Figure 83. Reheating consistent slow-roll predictions for the power law models in the plane (n_s, r) (top panel) and the plane (ϵ_1, ϵ_2) (bottom panel). The two pink solid contours are the one and two-sigma WMAP confidence intervals (marginalized over second order slow-roll). The black solid line represents the locus of the points such that $r = -8(n_s - 1)$, i.e. $\epsilon_2 = 0$. The annotations of the energy scale at which reheating ends are not displayed since the predictions of these models do not depend on this parameter. Clearly, models with $\alpha > 0.2$ are excluded at two sigma confidence level.

A.10 Kähler Moduli Inflation I (KMII)

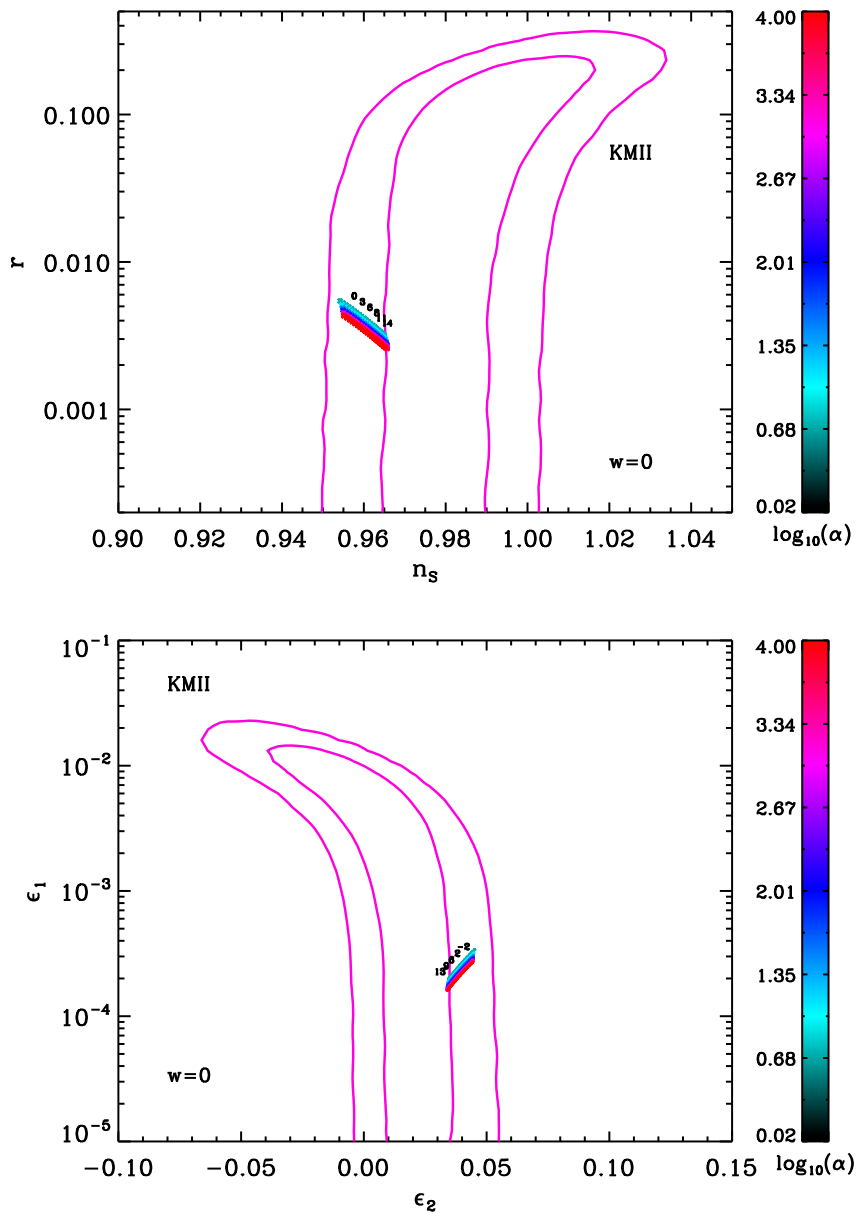


Figure 84. Reheating consistent slow-roll predictions for the Kähler Moduli I models in the plane (n_s, r) (top panel) and the plane (ϵ_1, ϵ_2) (bottom panel). The two pink solid contours are the one and two-sigma WMAP confidence intervals (marginalized over second order slow-roll). The reheating equation of state parameter $\bar{w}_{\text{reh}} = 0$ since the potential is quadratic close to its minimum. The annotations trace the energy scale at which reheating ends and correspond to $\log(g_*^{1/4} T_{\text{reh}}/\text{GeV})$.

A.11 Horizon Flow Inflation at first order (HF1I)

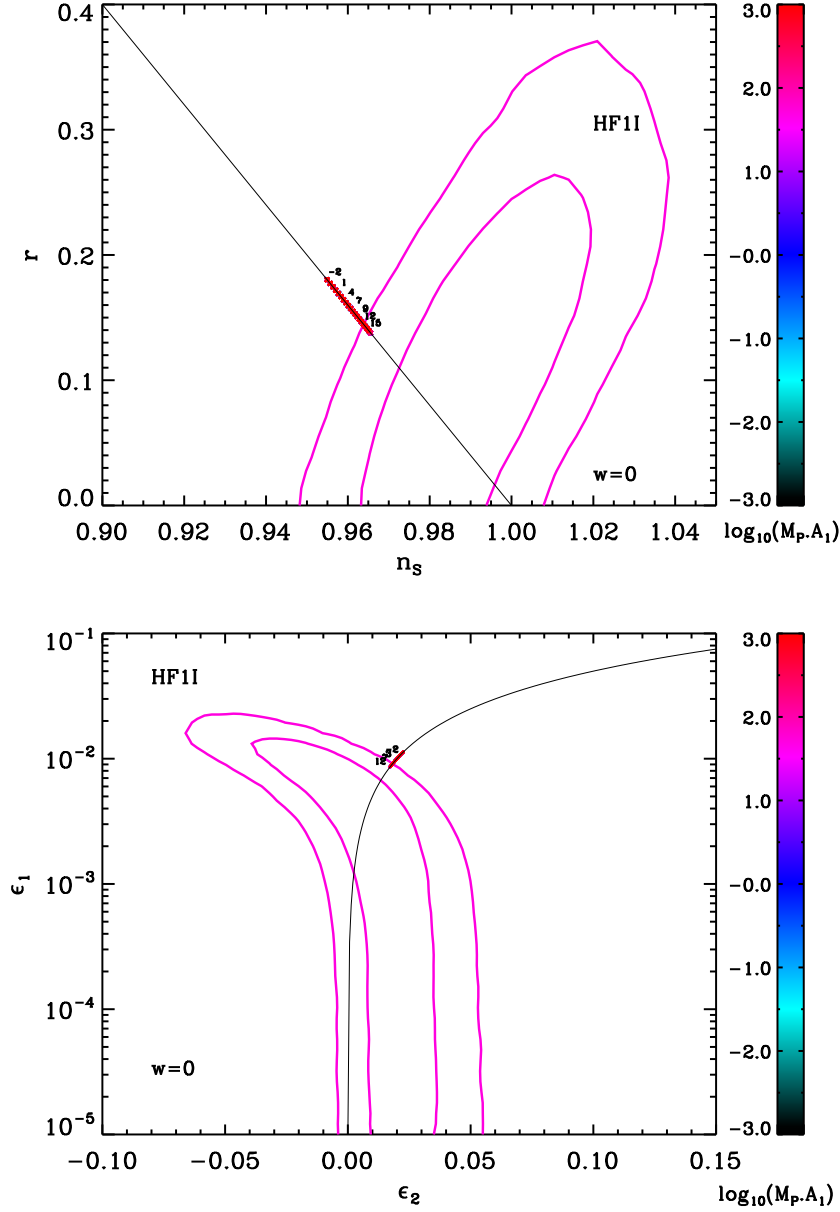


Figure 85. Reheating consistent (exact) predictions for the horizon flow inflation at first order models in the plane (n_s, r) (top panel) and the plane (ϵ_1, ϵ_2) (bottom panel). The two pink solid contours trace the two-sigma WMAP confidence intervals (marginalized over second order slow-roll). The black solid line represent the locus of the quadratic large field model [with $p = 2$, for which $r = 4(1 - n_s)$, i.e. $\epsilon_1 = \epsilon_2/2$]. The annotations trace the energy scale at which reheating ends and correspond to $\log(g_*^{1/4} T_{\text{reh}}/\text{GeV})$. Clearly, a high energy scale reheating is preferred for these models to remain inside the two-sigma contours. Notice that, up to the amplitude of the CMB anisotropies, the predictions do not depend much on A_1 as they are all superimposed.

A.12 Coleman-Weinberg Inflation (CWI)

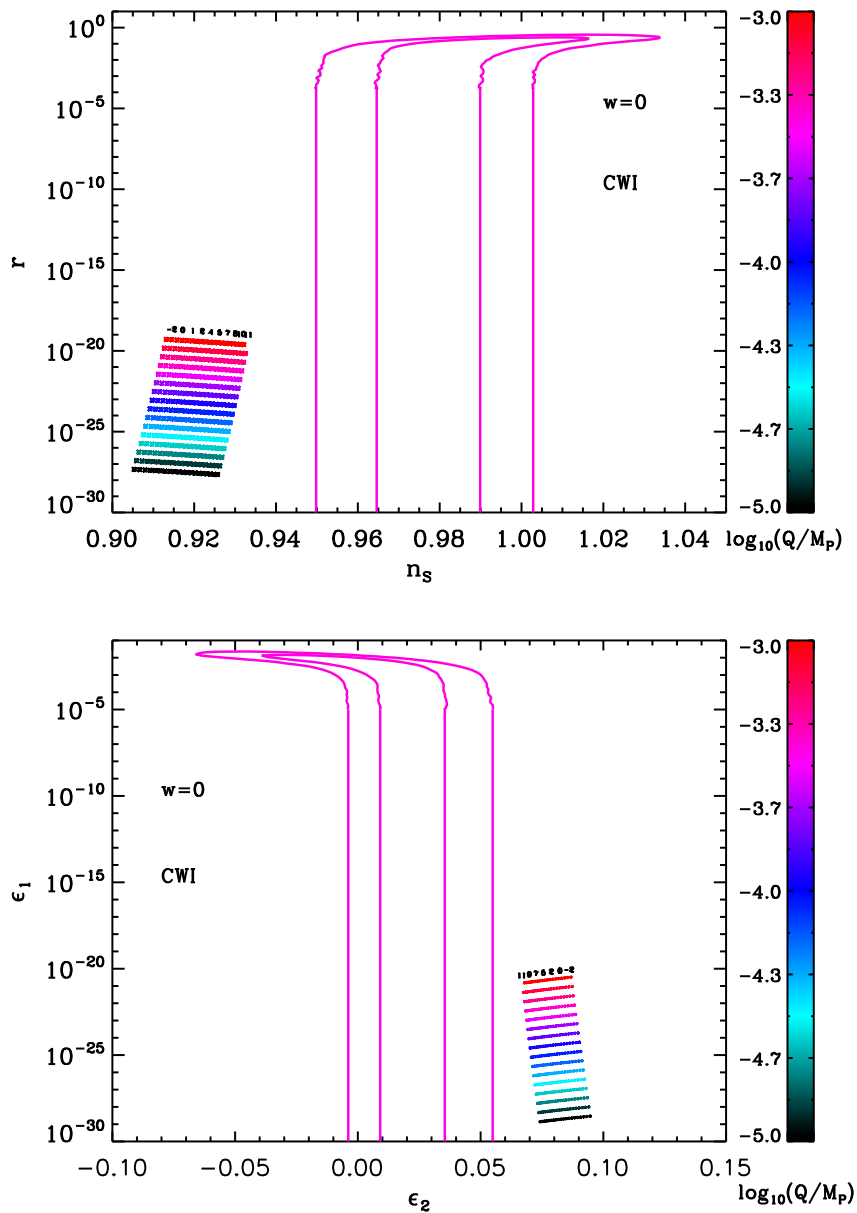


Figure 86. Reheating consistent slow-roll predictions for the Coleman-Weinberg models in the plane (n_s, r) (top panel) and the plane (ϵ_1, ϵ_2) (bottom panel), in the physical domain $Q/M_{\text{Pl}} \in [10^{-5}, 10^{-3}]$. The two pink solid contours are the one and two-sigma WMAP confidence intervals (marginalized over second order slow-roll). The annotations trace the energy scale at which reheating ends and correspond to $\log(g_*^{1/4} T_{\text{reh}}/\text{GeV})$. The typical amount of gravitational waves is extremely small.

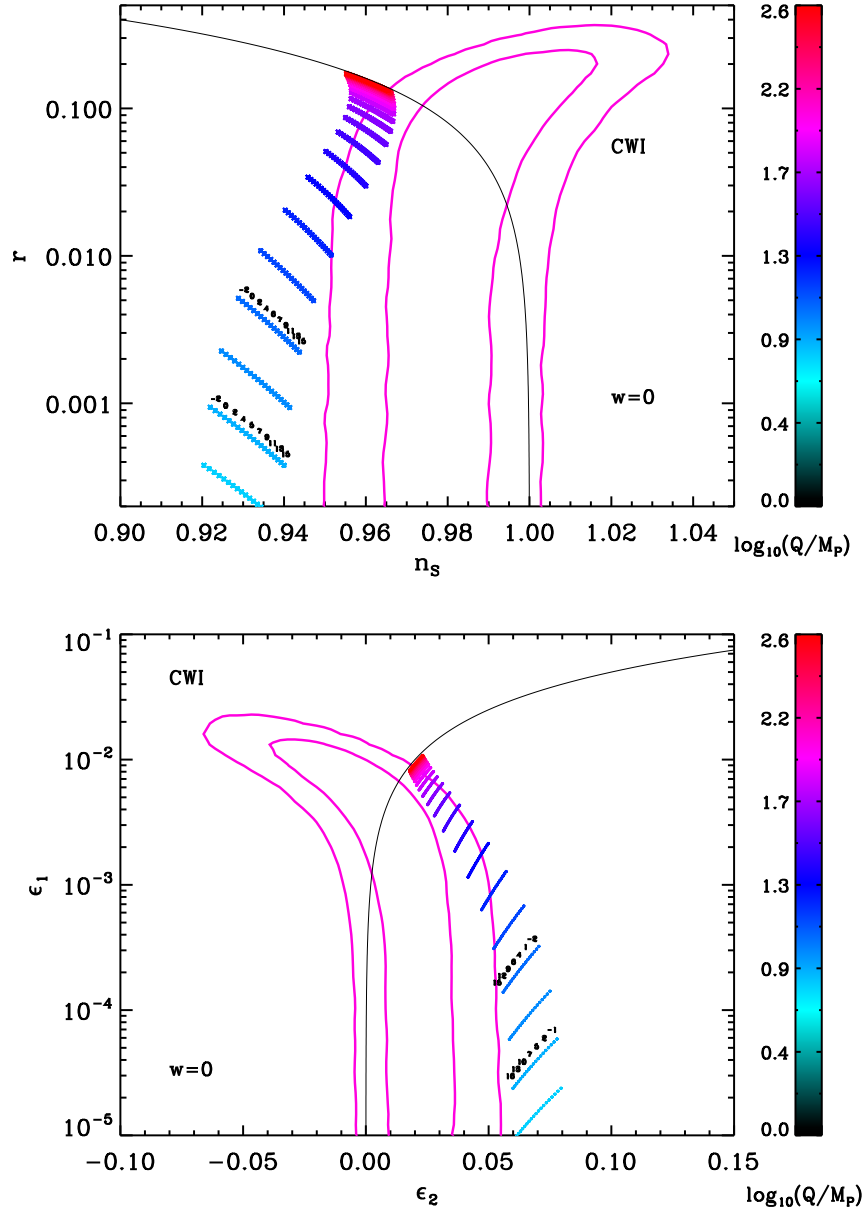


Figure 87. Reheating consistent slow-roll predictions for the Coleman-Weinberg models in the plane (n_s, r) (top panel) and the plane (ϵ_1, ϵ_2) (bottom panel), in the domain $Q/M_{\text{Pl}} \in [1, 100]$. The two pink solid contours are the one and two-sigma WMAP confidence intervals (marginalized over second order slow-roll). The annotations trace the energy scale at which reheating ends and correspond to $\log(g_*^{1/4} T_{\text{reh}}/\text{GeV})$. When $Q/M_{\text{Pl}} \gg 1$, the model is similar to a quadratic potential close to its minimum, and the predictions match the LFI $\epsilon_1 = \epsilon_2/2$ relation (see section 4.2) represented by the black lines.

A.13 Loop Inflation (LI)

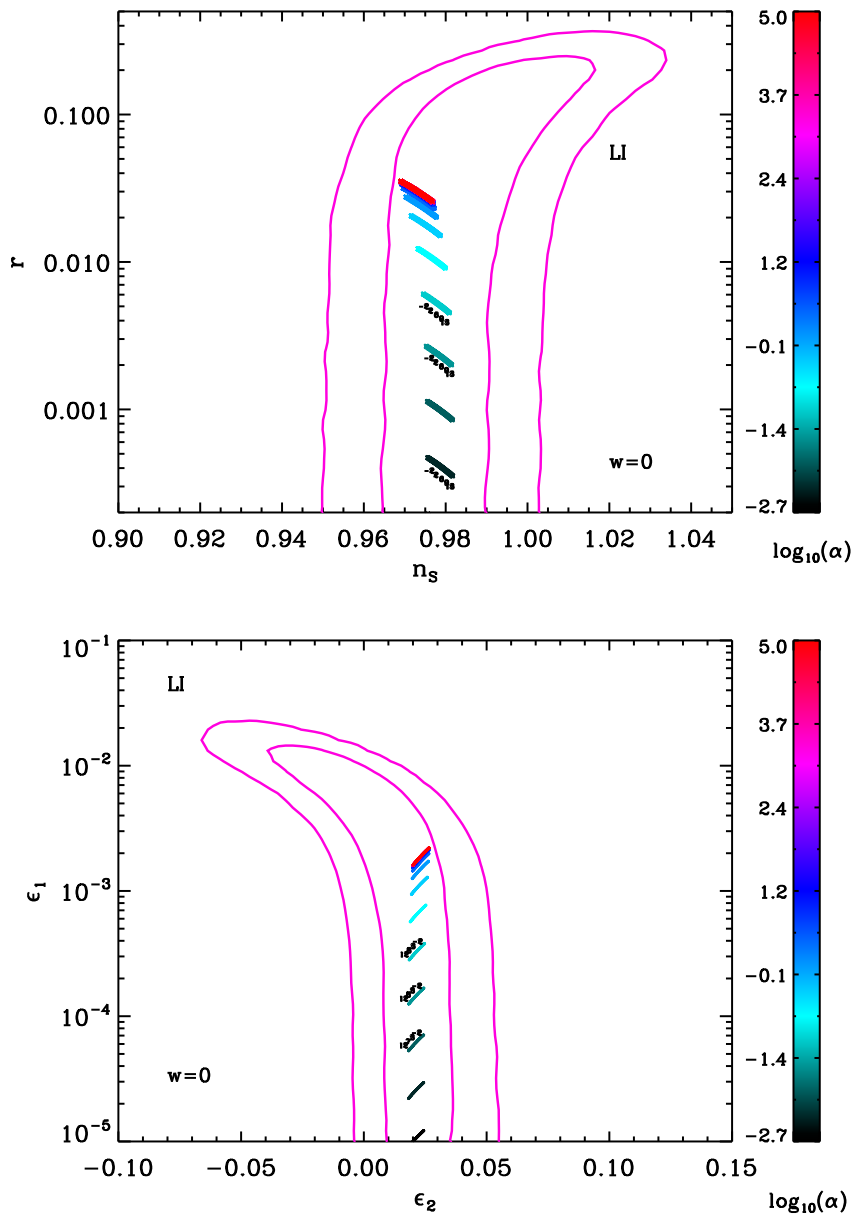


Figure 88. Reheating consistent slow-roll predictions for the loop inflation models for $\alpha > 0$, in the plane (n_s, r) (top panel), and the plane (ϵ_1, ϵ_2) (bottom panel). The two pink solid contours are the one and two-sigma WMAP confidence intervals (marginalized over second order slow-roll). The annotations trace the energy scale at which reheating ends and correspond to $\log(g_*^{1/4} T_{\text{reh}}/\text{GeV})$.

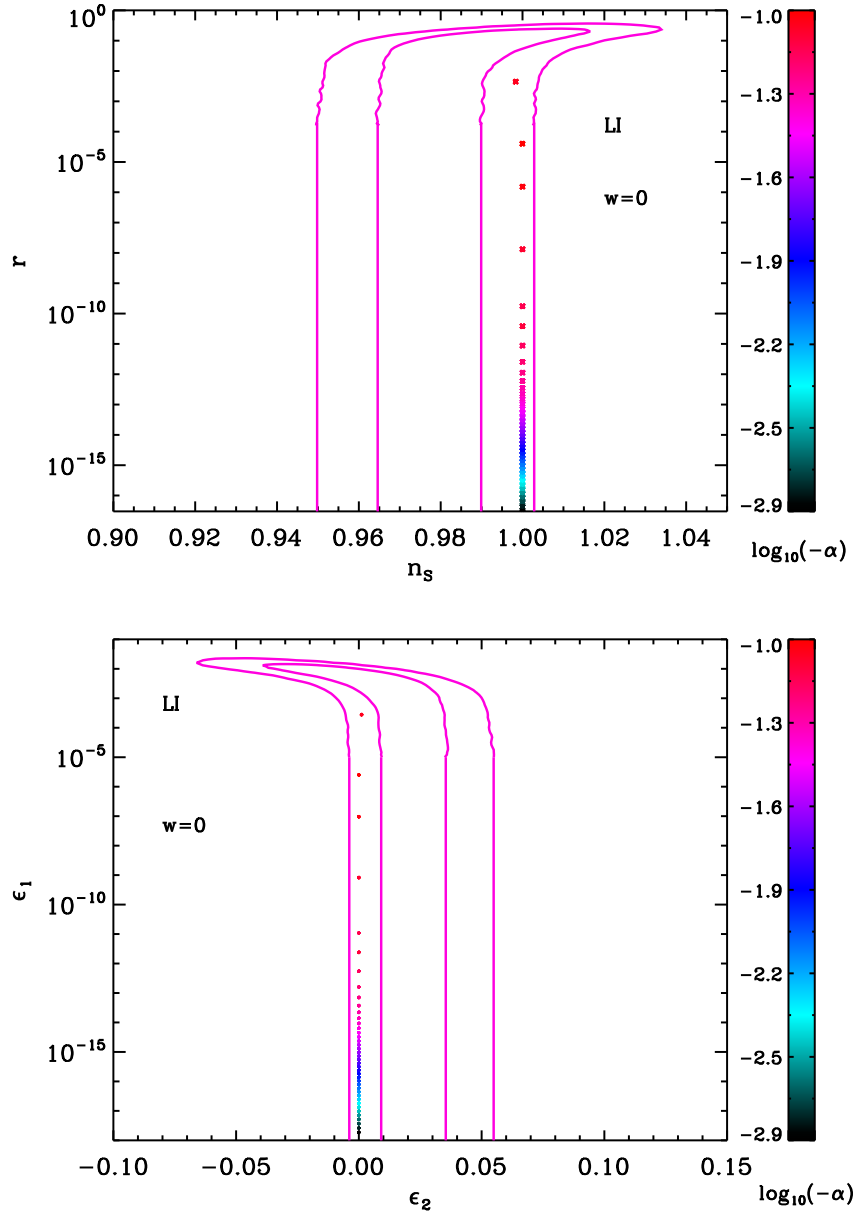


Figure 89. Reheating consistent slow-roll predictions for the loop inflation models for $\alpha < 0$, in the plane (n_s, r) (top panel), and the plane (ϵ_1, ϵ_2) (bottom panel). The two pink solid contours are the one and two-sigma WMAP confidence intervals (marginalized over second order slow-roll). Since the slow-roll predictions almost do not depend on the energy scale at which reheating ends, the usual annotations which trace $\log(g_*^{1/4} T_{\text{reh}}/\text{GeV})$ are not displayed.

A.14 Double Well Inflation (DWI)

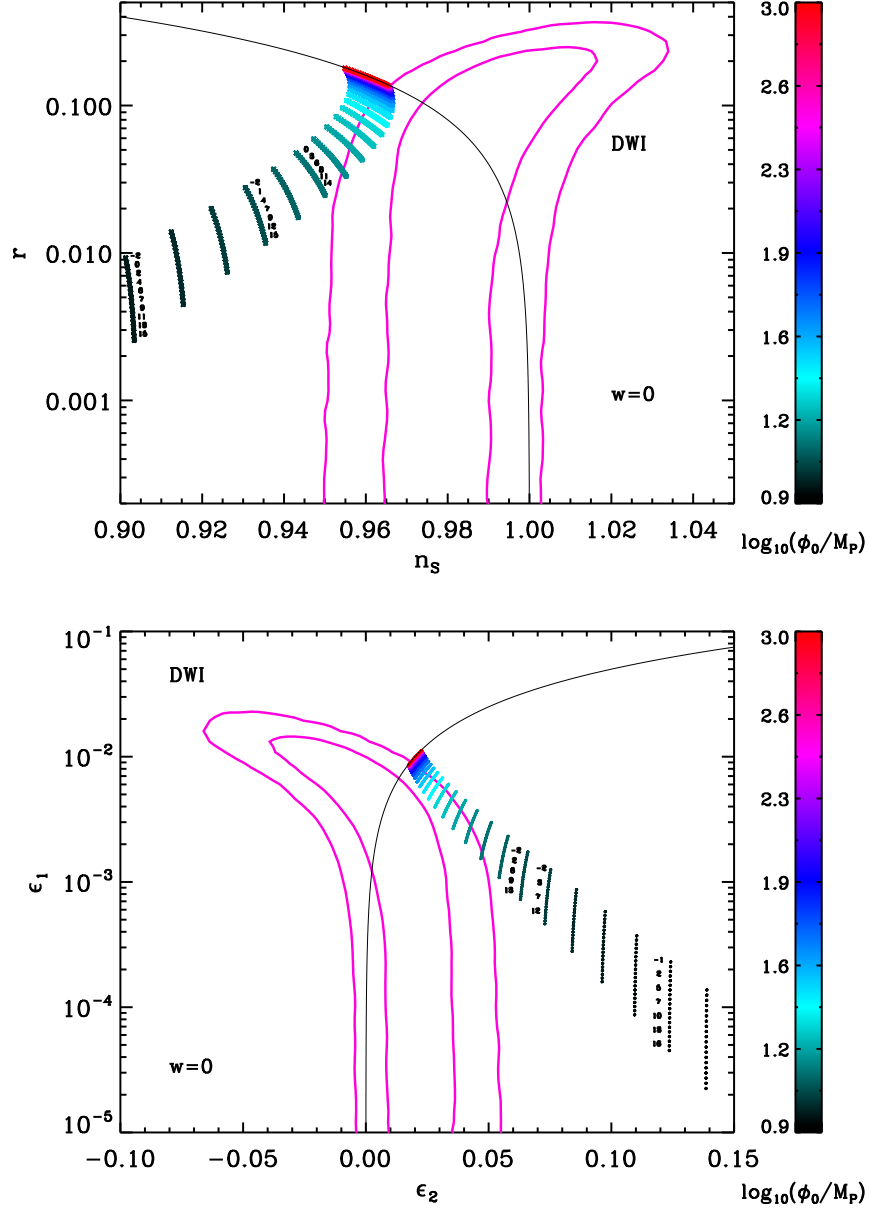


Figure 90. Reheating consistent slow-roll predictions for the double well models in the plane (n_s, r) (top panel) and the plane (ϵ_1, ϵ_2) (bottom panel). The two pink solid contours are the one and two-sigma WMAP confidence intervals (marginalized over second order slow-roll). The annotations trace the energy scale at which reheating ends and correspond to $\log(g_*^{1/4} T_{\text{reh}}/\text{GeV})$. The shape of the zone covered by the models predictions is similar to the one for Small Field Inflation (SFI, see Fig. 99), except in the domain $\phi_0 \gg M_{\text{Pl}}$, which is the one favored by the observations. The black solid line represent the locus of the points such that $r = 4(1 - n_s)$, i.e. $\epsilon_2 = 2\epsilon_1$, on which this model lies for $\phi_0/M_{\text{Pl}} \gg 1$.

A.15 Mutated Hilltop Inflation (MHI)

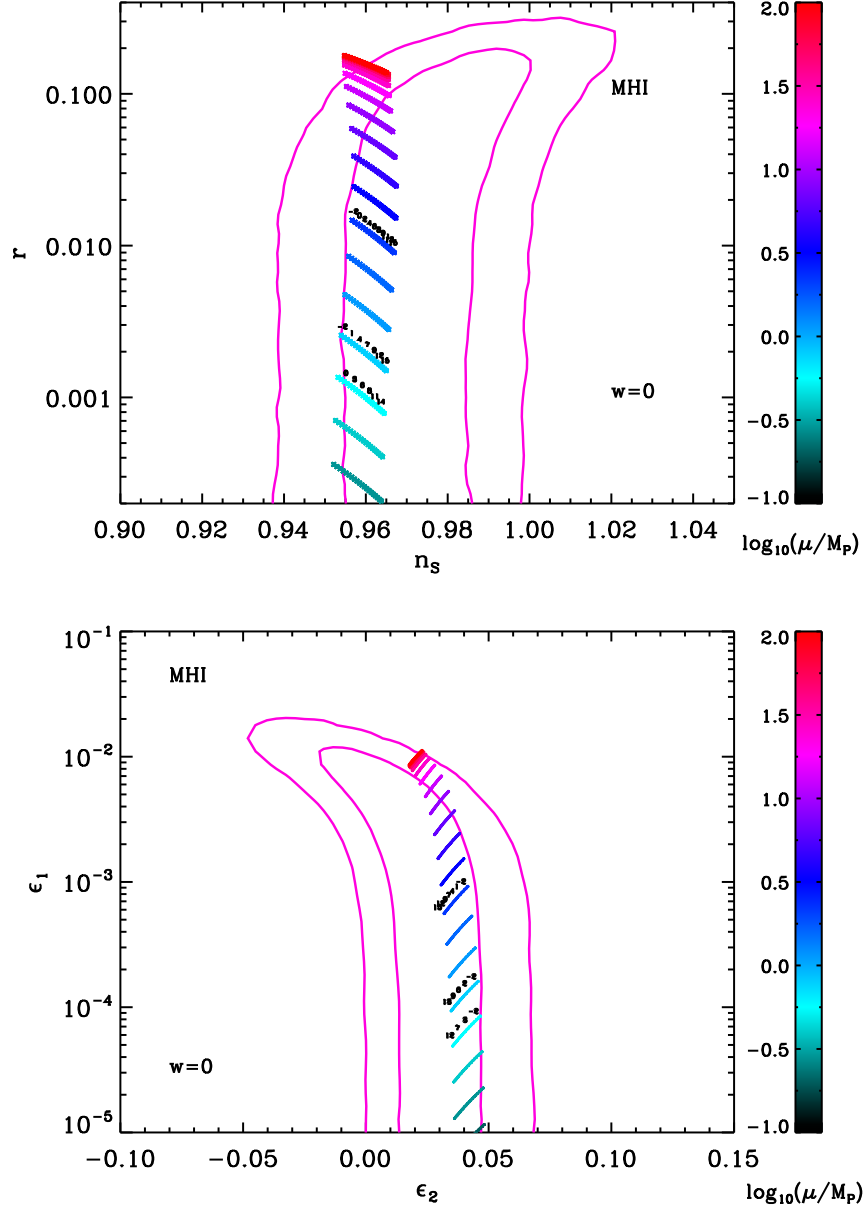


Figure 91. Reheating consistent slow-roll predictions for the mutated hilltop models in the plane (n_s, r) (top panel) and the plane (ϵ_1, ϵ_2) (bottom panel). The two pink solid contours are the one and two-sigma WMAP confidence intervals (marginalized over second order slow-roll). The annotations trace the energy scale at which reheating ends and correspond to $\log(g_*^{1/4} T_{\text{reh}}/\text{GeV})$. For small values of μ/M_{Pl} , this model predicts a very small amount of gravitational waves

A.16 Radion Gauge Inflation (RGI)

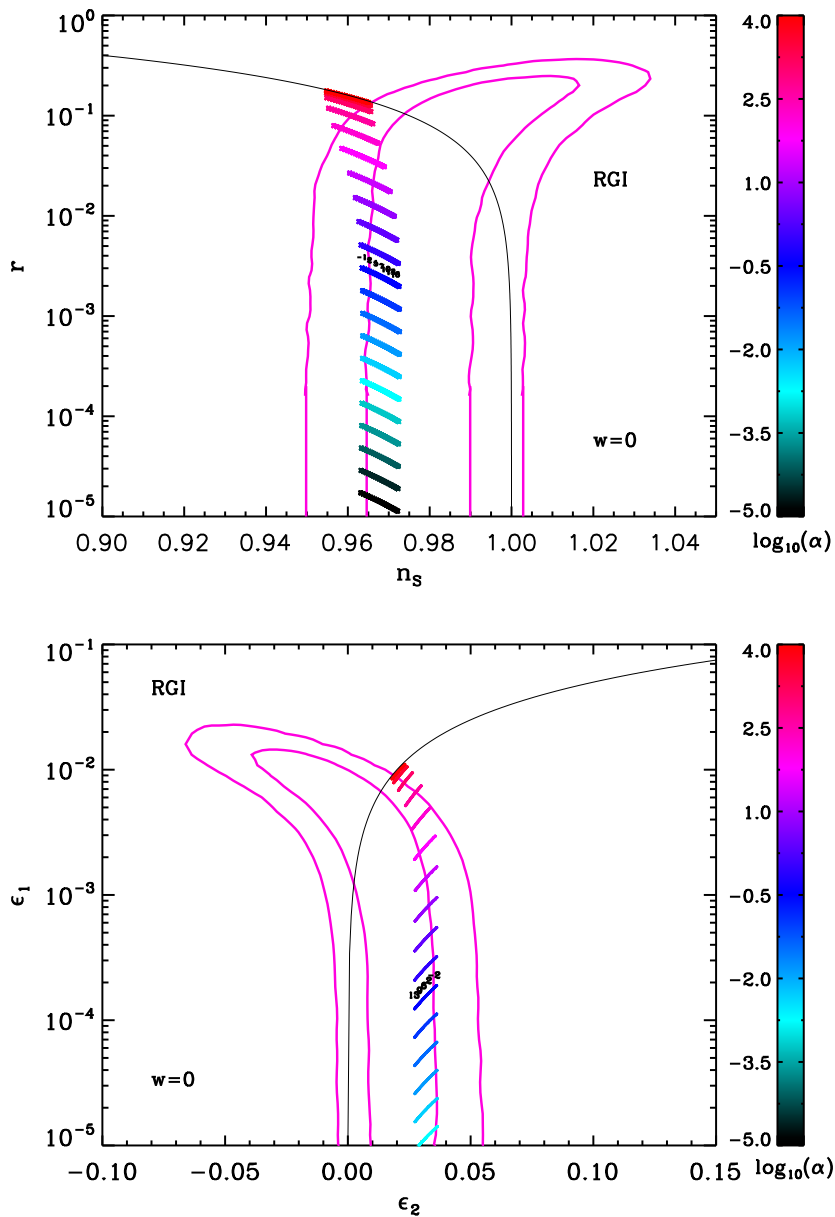


Figure 92. Reheating consistent slow-roll predictions for the radion gauge models in the plane (n_s, r) (top panel) and the plane (ϵ_1, ϵ_2) (bottom panel). The two pink solid contours are the one and two-sigma WMAP confidence intervals (marginalized over second order slow-roll). The annotations trace the energy scale at which reheating ends and correspond to $\log(g_*^{1/4} T_{\text{reh}}/\text{GeV})$. At large values of α , the predictions are the same as the large field model with $p = 2$ (see Fig. 75) for which $\epsilon_2 = 2\epsilon_1$ (black solid line).

A.17 MSSM Inflation (MSSMI)

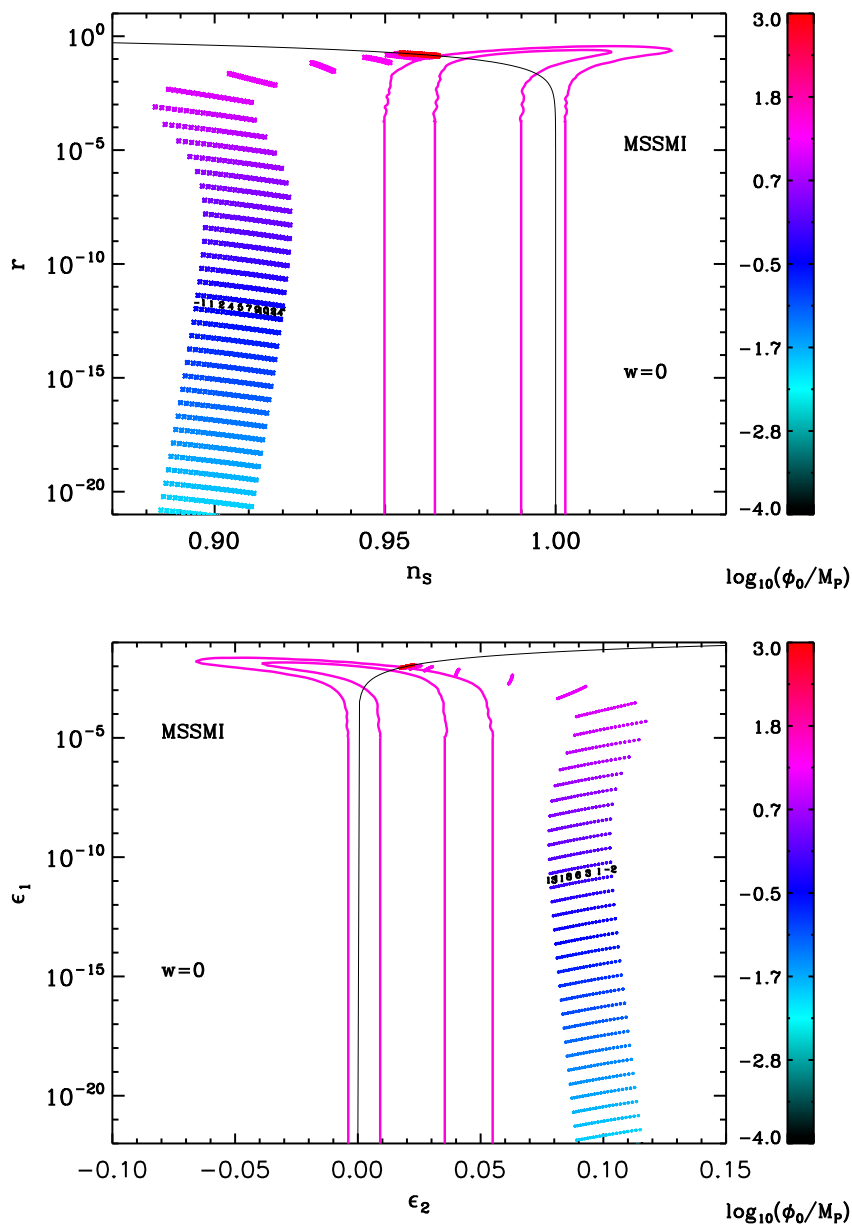


Figure 93. Reheating consistent slow-roll predictions for the MSSMI models in the plane (n_s, r) (top panel) and the plane (ϵ_1, ϵ_2) (bottom panel). The two pink solid contours are the one and two-sigma WMAP confidence intervals (marginalized over second order slow-roll). The annotations trace the energy scale at which reheating ends and correspond to $\log(g_*^{1/4} T_{\text{reh}}/\text{GeV})$. The black solid line represent the locus of the points such that $r = 4(1 - n_s)$, i.e. $\epsilon_2 = 2\epsilon_1$, on which this model lies for $\phi_0/M_{\text{Pl}} \gg 1$. However, the physical relevant value is closer to $\phi_0/M_{\text{Pl}} \simeq 10^{-4}$.

A.18 Renormalizable Inflection Point Inflation (RIPI)

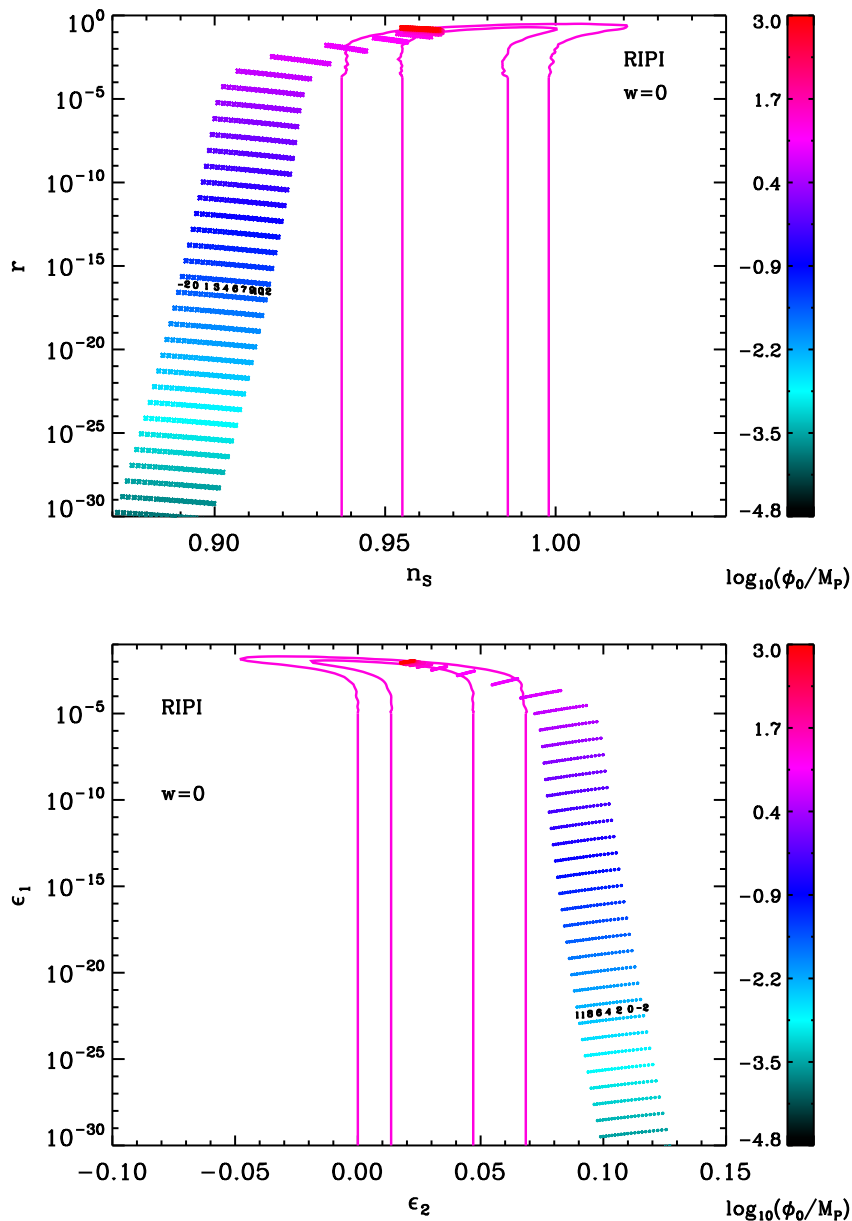


Figure 94. Reheating consistent slow-roll predictions for the renormalizable inflection point models in the plane (n_s, r) (top panel) and the plane (ϵ_1, ϵ_2) (bottom panel). The two pink solid contours are the one and two-sigma WMAP confidence intervals (marginalized over second order slow-roll). The annotations trace the energy scale at which reheating ends and correspond to $\log(g_*^{1/4} T_{\text{reh}}/\text{GeV})$.

A.19 Arctan Inflation (AI)

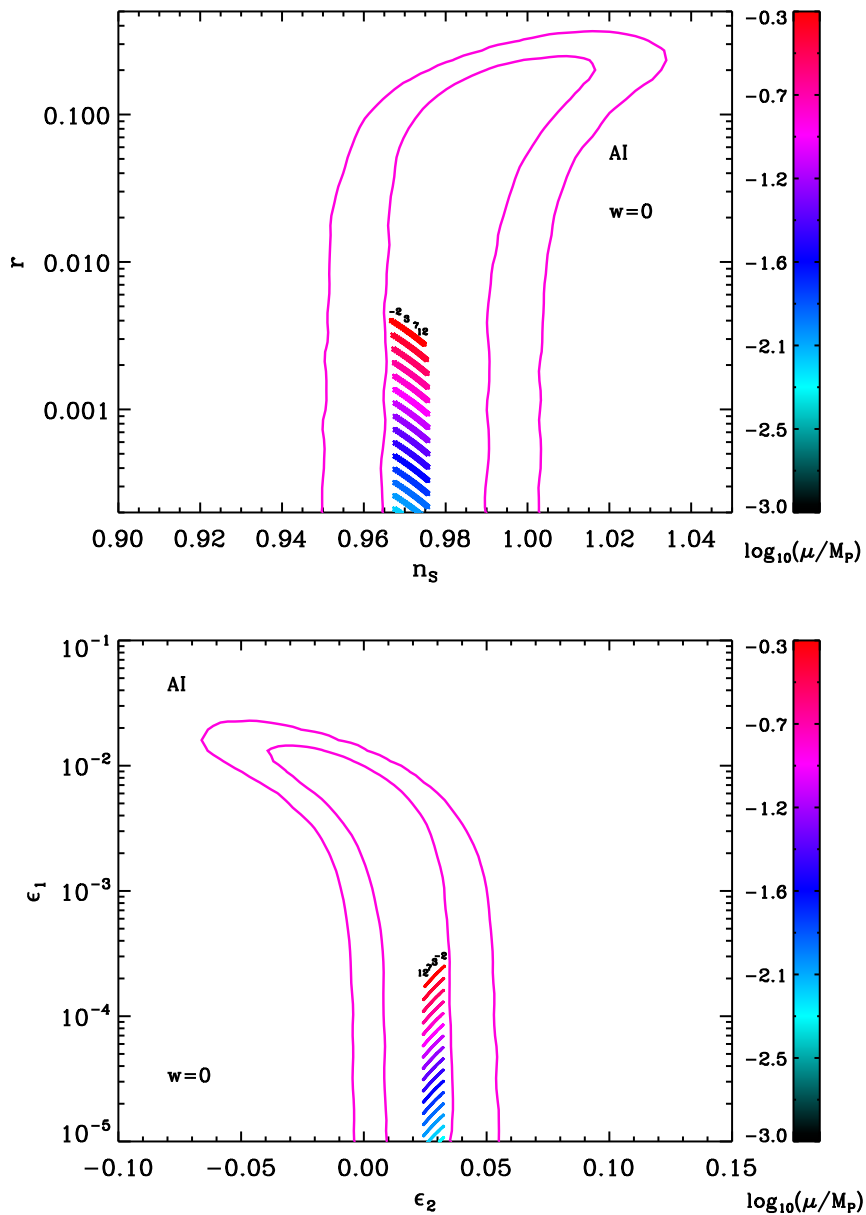


Figure 95. Reheating consistent slow-roll predictions for the arctan models in the plane (n_s, r) (top panel) and the plane (ϵ_1, ϵ_2) (bottom panel), when the reheating equation of state is $\bar{w}_{\text{reh}} = 0$. The two pink solid contours are the one and two-sigma WMAP confidence intervals (marginalized over second order slow-roll). The annotations trace the energy scale at which reheating ends and correspond to $\log(g_*^{1/4} T_{\text{reh}}/\text{GeV})$.

A.20 Constant n_s A Inflation (CNAI)

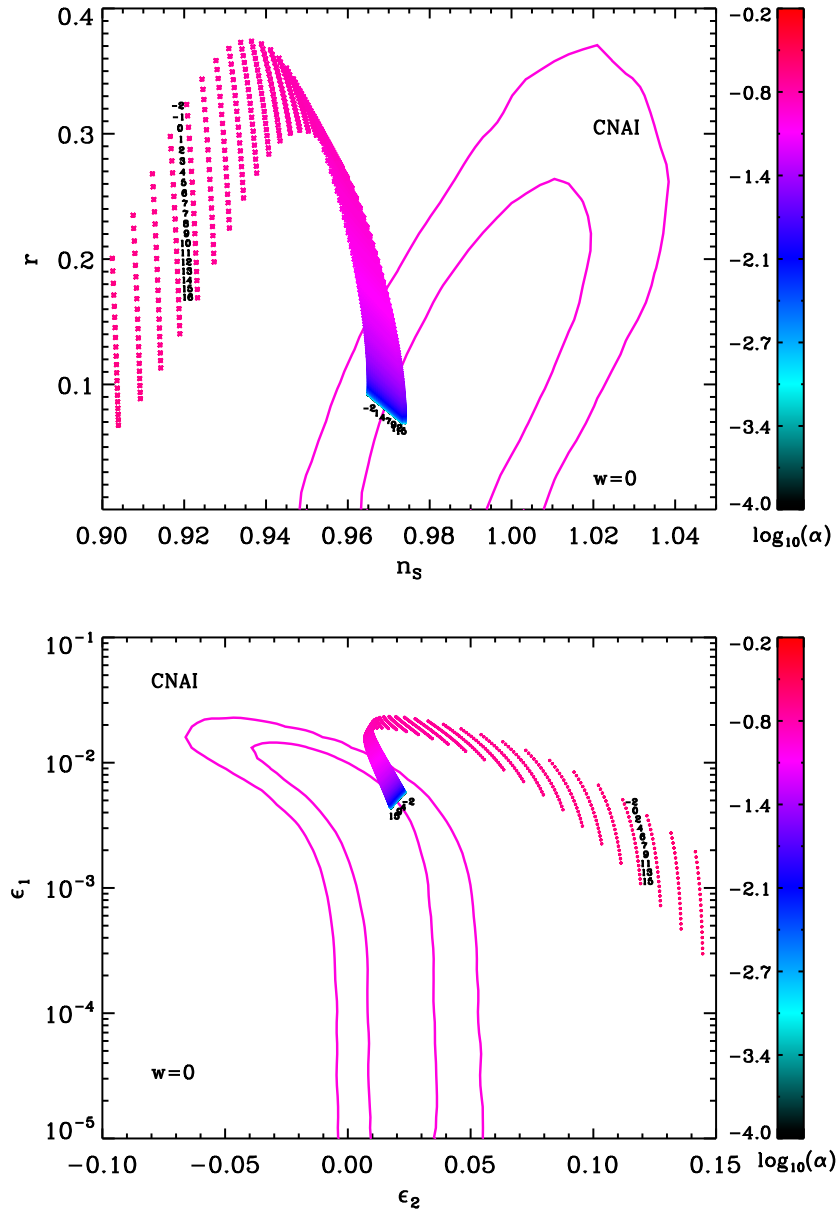


Figure 96. Reheating consistent slow-roll predictions for the constant n_s A models in the plane (n_s, r) (top panel) and the plane (ϵ_1, ϵ_2) (bottom panel). The two pink solid contours are the one and two-sigma WMAP confidence intervals (marginalized over second order slow-roll). The annotations trace the energy scale at which reheating ends and correspond to $\log(g_*^{1/4} T_{\text{reh}}/\text{GeV})$.

A.21 Constant n_s B Inflation (CNBI)

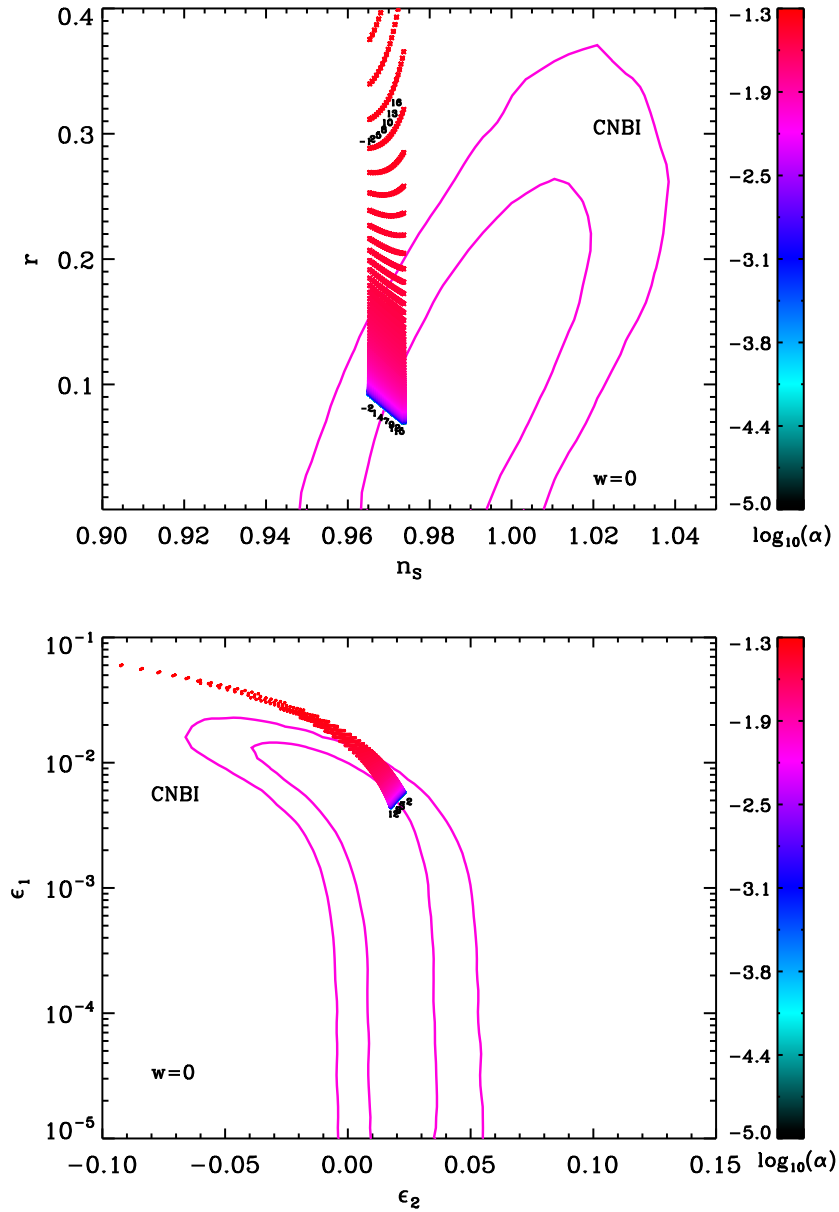


Figure 97. Reheating consistent slow-roll predictions for the constant n_s B models in the plane (n_s, r) (top panel) and the plane (ϵ_1, ϵ_2) (bottom panel). The two pink solid contours are the one and two-sigma WMAP confidence intervals (marginalized over second order slow-roll). The annotations trace the energy scale at which reheating ends and correspond to $\log(g_*^{1/4} T_{\text{reh}}/\text{GeV})$.

A.22 Small Field Inflation (SFI)

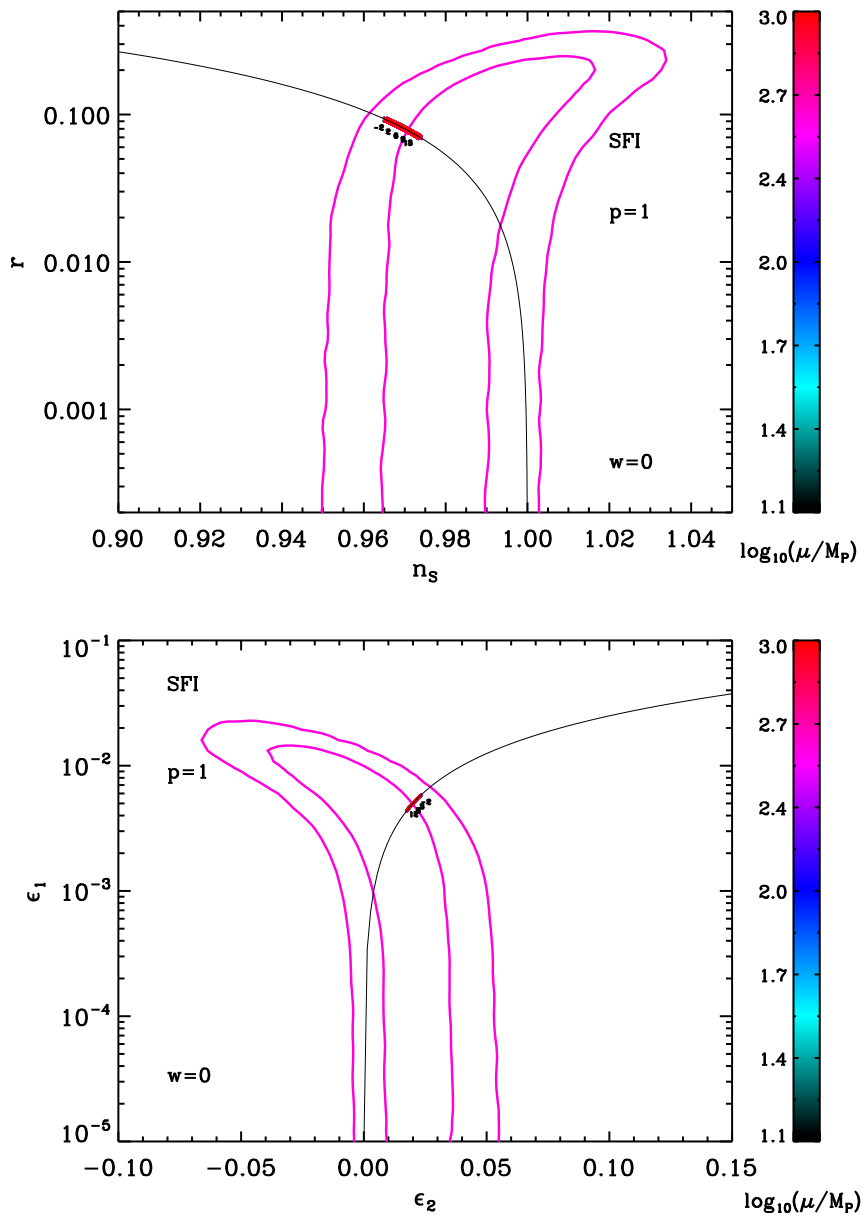


Figure 98. Reheating consistent slow-roll predictions for the small field models with $p = 1$ in the plane (n_s, r) (top panel) and the plane (ϵ_1, ϵ_2) (bottom panel). The two pink solid contours are the one and two-sigma WMAP confidence intervals (marginalized over second order slow-roll). The annotations trace the energy scale at which reheating ends and correspond to $\log(g_*^{1/4} T_{\text{reh}}/\text{GeV})$. The black solid line represent the locus of the points such that $r = (8/3)(1 - n_s)$, i.e. $\epsilon_2 = 4\epsilon_1$, on which this model must lie.

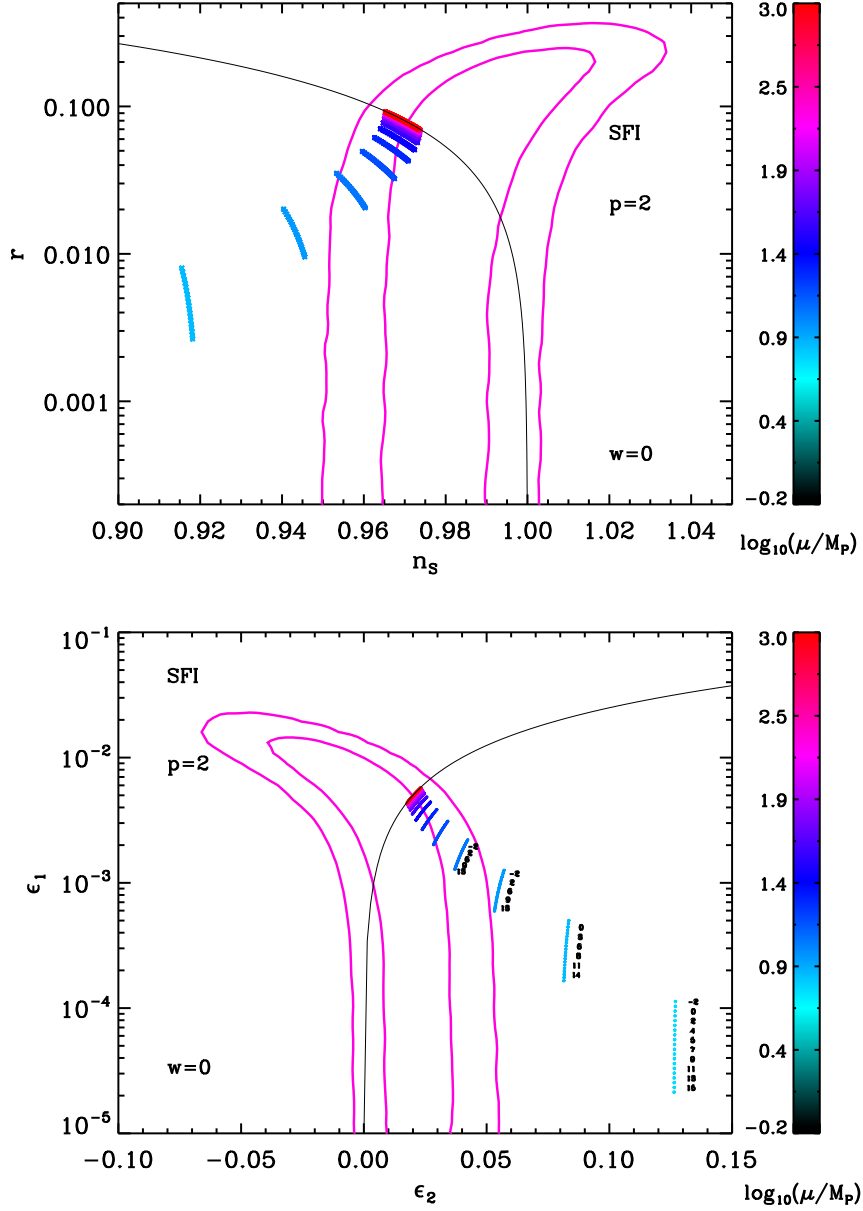


Figure 99. Reheating consistent slow-roll predictions for the small field models with $p = 2$ in the plane (n_s, r) (top panel) and the plane (ϵ_1, ϵ_2) (bottom panel). The two pink solid contours are the one and two-sigma WMAP confidence intervals (marginalized over second order slow-roll). The annotations trace the energy scale at which reheating ends and correspond to $\log(g_*^{1/4} T_{\text{reh}}/\text{GeV})$. Clearly, if μ/M_{Pl} is not too high these values are limited from below to stay inside the two-sigma contours, and $\mu/M_{\text{Pl}} < 10$ seems to be disfavored by the data. The black solid line represent the locus of the points such that $r = (8/3)(1 - n_s)$, i.e. $\epsilon_2 = 4\epsilon_1$, on which this model lies for $\mu/M_{\text{Pl}} \gg 1$.

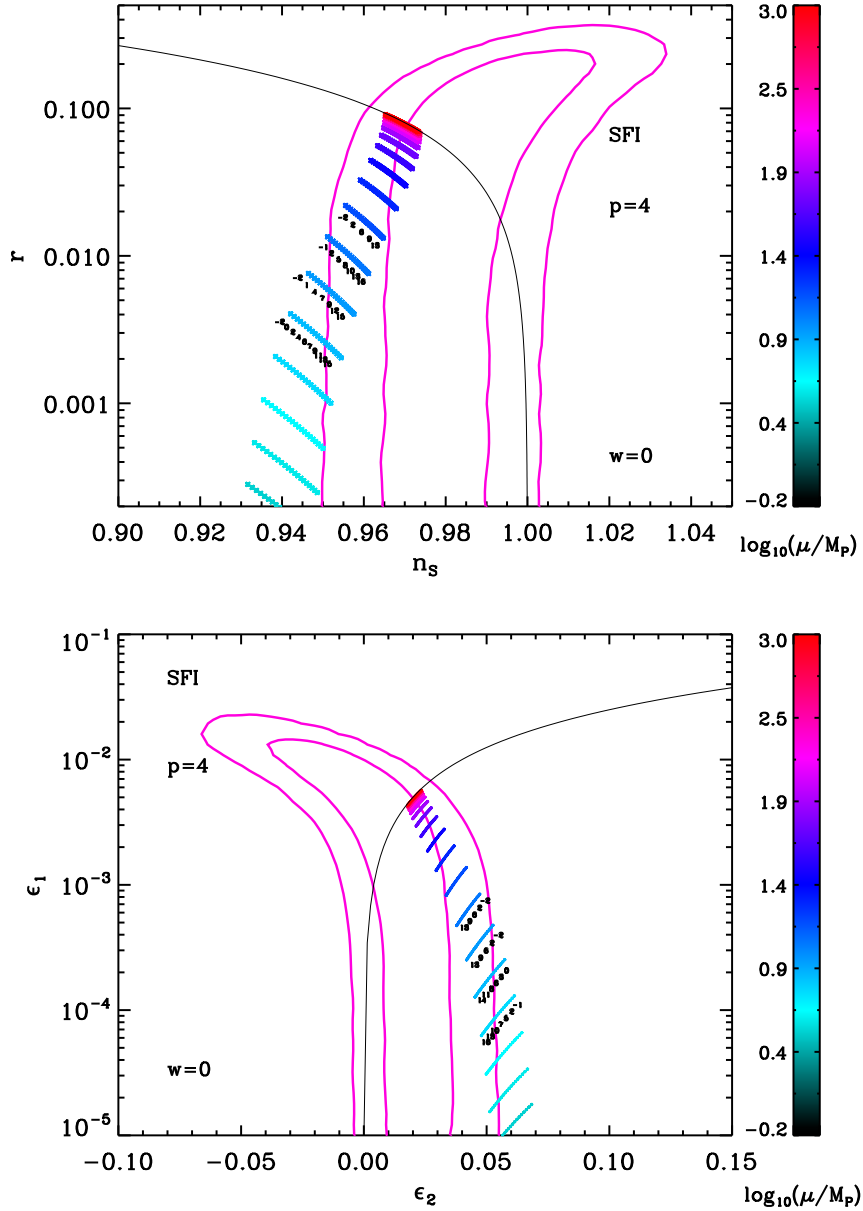


Figure 100. Reheating consistent slow-roll predictions for the small field models with $p = 4$ in the plane (n_s, r) (top panel) and the plane (ϵ_1, ϵ_2) (bottom panel). The two pink solid contours are the one and two-sigma WMAP confidence intervals (marginalized over second order slow-roll). The annotations trace the energy scale at which reheating ends and correspond to $\log(g_*^{1/4} T_{\text{reh}}/\text{GeV})$. Clearly, if μ/M_{Pl} is not too high these values are limited from below to stay inside the two-sigma contours. The black solid line represent the locus of the points such that $r = (8/3)(1 - n_s)$, i.e. $\epsilon_2 = 4\epsilon_1$, on which this model lies for $\mu/M_{\text{Pl}} \gg 1$.

A.23 Intermediate Inflation (II)

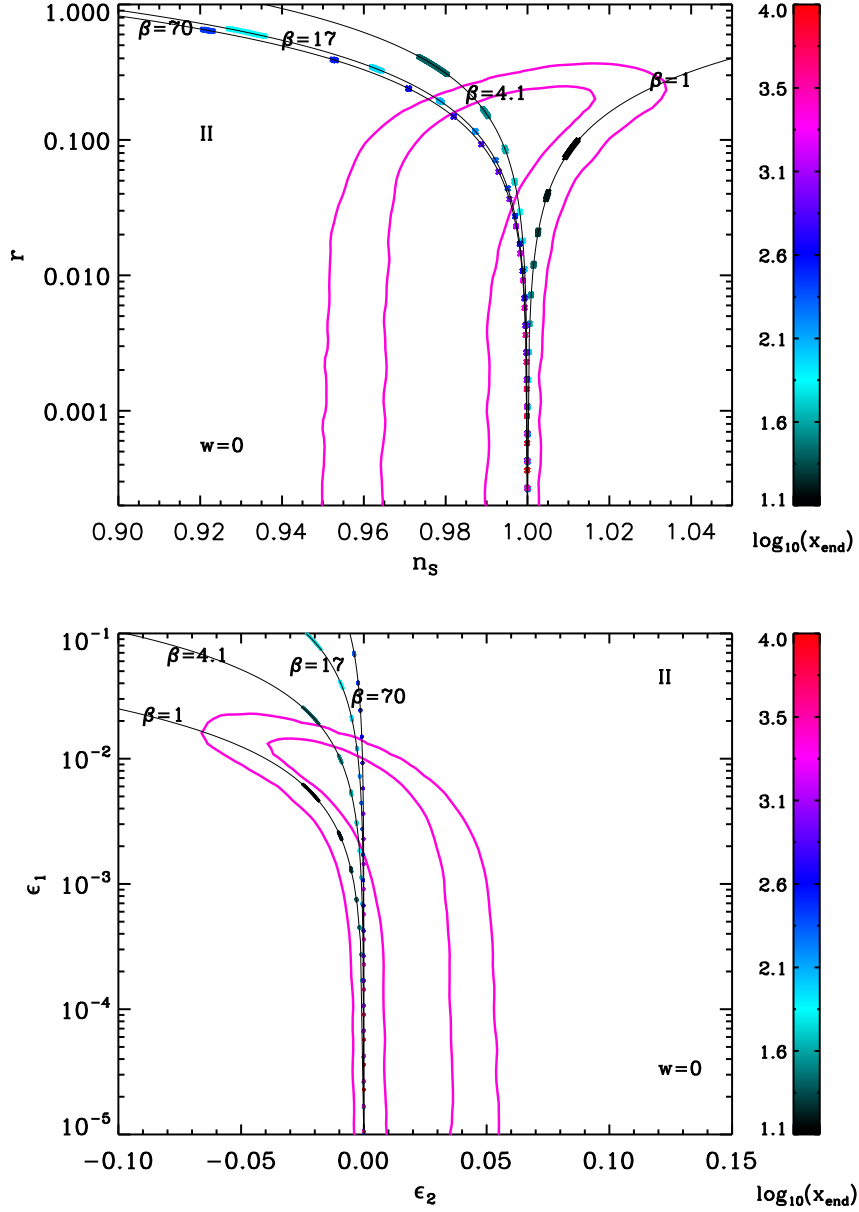


Figure 101. Reheating consistent slow-roll predictions for the intermediate inflation models in the plane (n_s, r) (top panel) and the plane (ϵ_1, ϵ_2) (bottom panel). The two pink solid contours are the one and two-sigma WMAP confidence intervals (marginalized over second order slow-roll). Four different values of β are displayed (namely $\beta = 1, 4.1, 17, 70$), and for each of them the black solid lines correspond to the points such that $\epsilon_1 = -(\beta/4)\epsilon_2$, on which the predictions should lie for $x_{\text{end}} \gg 1$, which is very well verified. The annotations of the energy scale at which reheating ends are not displayed since this parameter is degenerated with x_{end} .

A.24 Kähler Moduli Inflation II (KMIII)

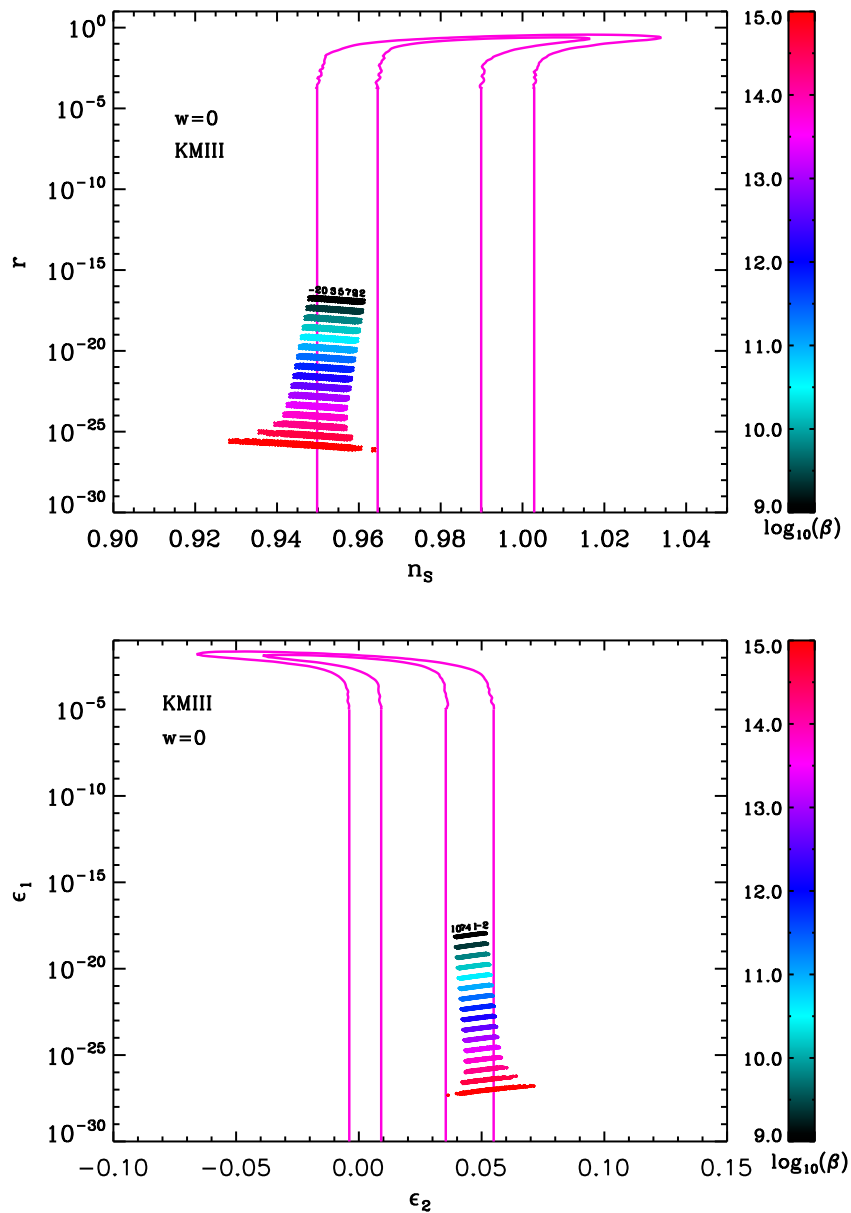


Figure 102. Reheating consistent slow-roll predictions for the Kähler moduli III models in the plane (n_s, r) (top panel) and the plane (ϵ_1, ϵ_2) (bottom panel), for $10^9 < \beta < 10^{15}$, $\alpha_{\min}(\beta) < \alpha < \beta/100$. The two pink solid contours are the one and two-sigma WMAP confidence intervals (marginalized over second order slow-roll). The predictions almost do not depend on α , which is why when β is fixed, points corresponding to different values of α can not be distinguished. The annotations trace the energy scale at which reheating ends and correspond to $\log(g_*^{1/4} T_{\text{reh}}/\text{GeV})$.

A.25 Logamediate Inflation (LMI)

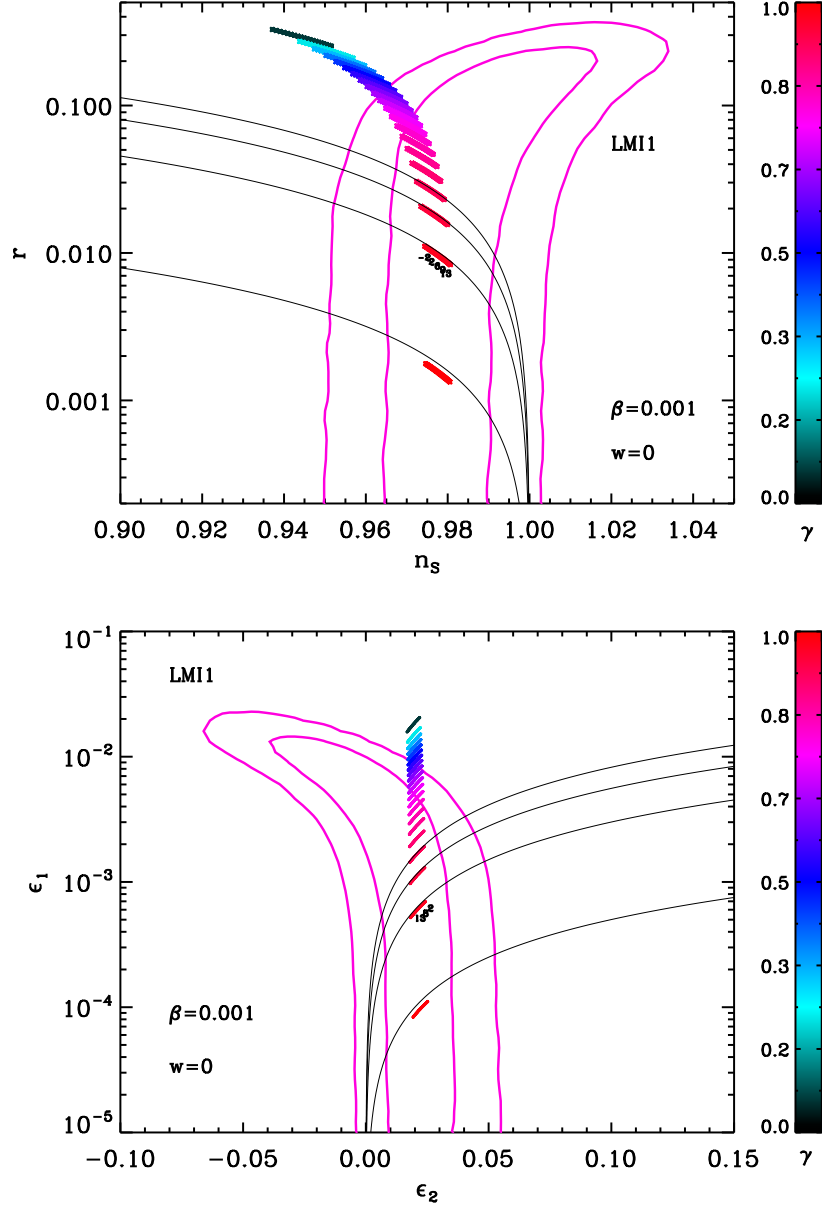


Figure 103. Reheating consistent slow-roll predictions for the Logamediate Inflation 1 models with $\beta = 10^{-3}$, in the plane (n_s, r) (top panel) and the plane (ϵ_1, ϵ_2) (bottom panel). Inflation proceeds at decreasing field values, from the right to the left and with $x < x_{V\text{-max}}$. The two pink solid contours are the one and two-sigma WMAP confidence intervals (marginalized over second order slow-roll). The annotations trace the energy scale at which reheating ends and correspond to $\log(g_*^{1/4} T_{\text{reh}}/\text{GeV})$. For $\beta \ll 1$, the exponential term in the potential Eq. (5.58) is almost constant so that the model is close to large field inflation (LFI, see section 4.2). In that limit, one has $\epsilon_1 = \alpha\epsilon_2/4 = (1 - \gamma)\epsilon_2$, which corresponds to the black solid lines.

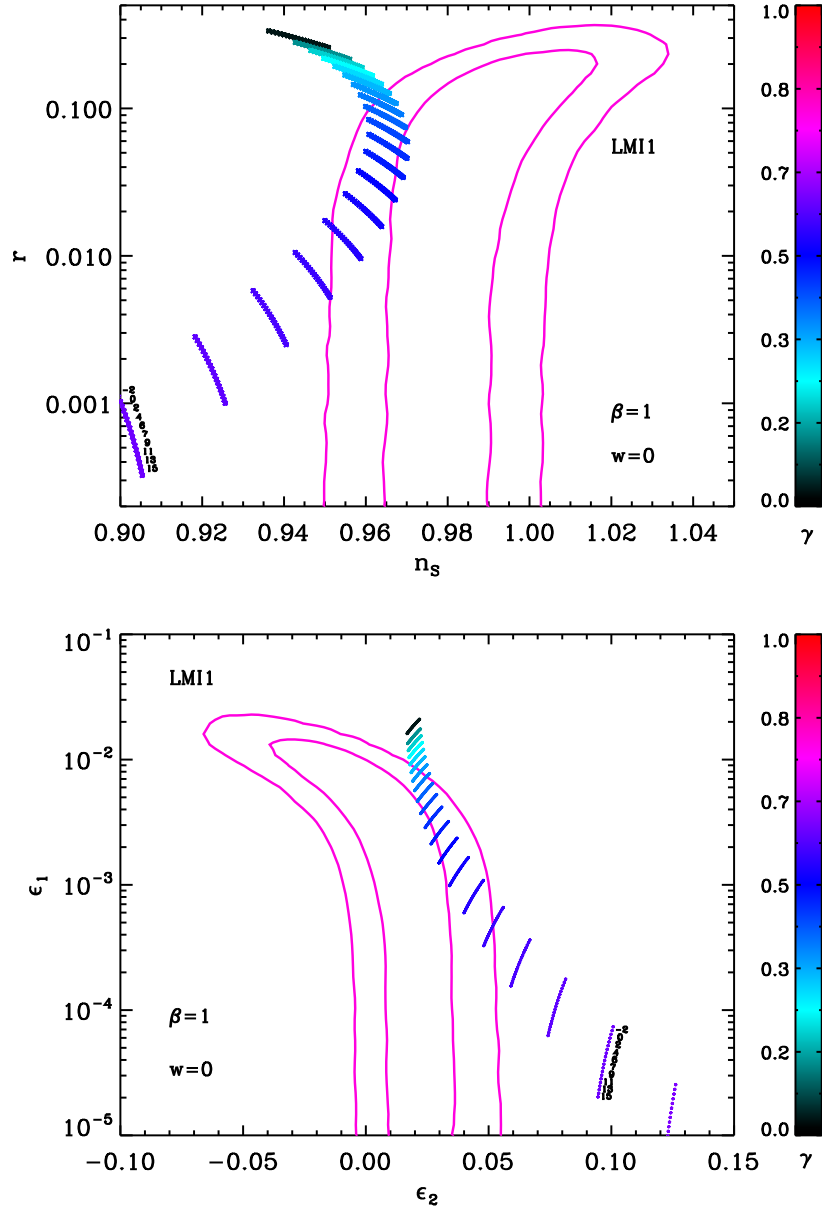


Figure 104. Reheating consistent slow-roll predictions for the Logamediate Inflation 1 models with $\beta = 1$ in the plane (n_s, r) (top panel) and the plane (ϵ_1, ϵ_2) (bottom panel). Inflation proceeds as in Fig. 103, at decreasing field values and with $x < x_{V^{\text{max}}}$. The two pink solid contours are the one and two-sigma WMAP confidence intervals (marginalized over second order slow-roll). The annotations trace the energy scale at which reheating ends and correspond to $\log(g_*^{1/4} T_{\text{reh}}/\text{GeV})$.

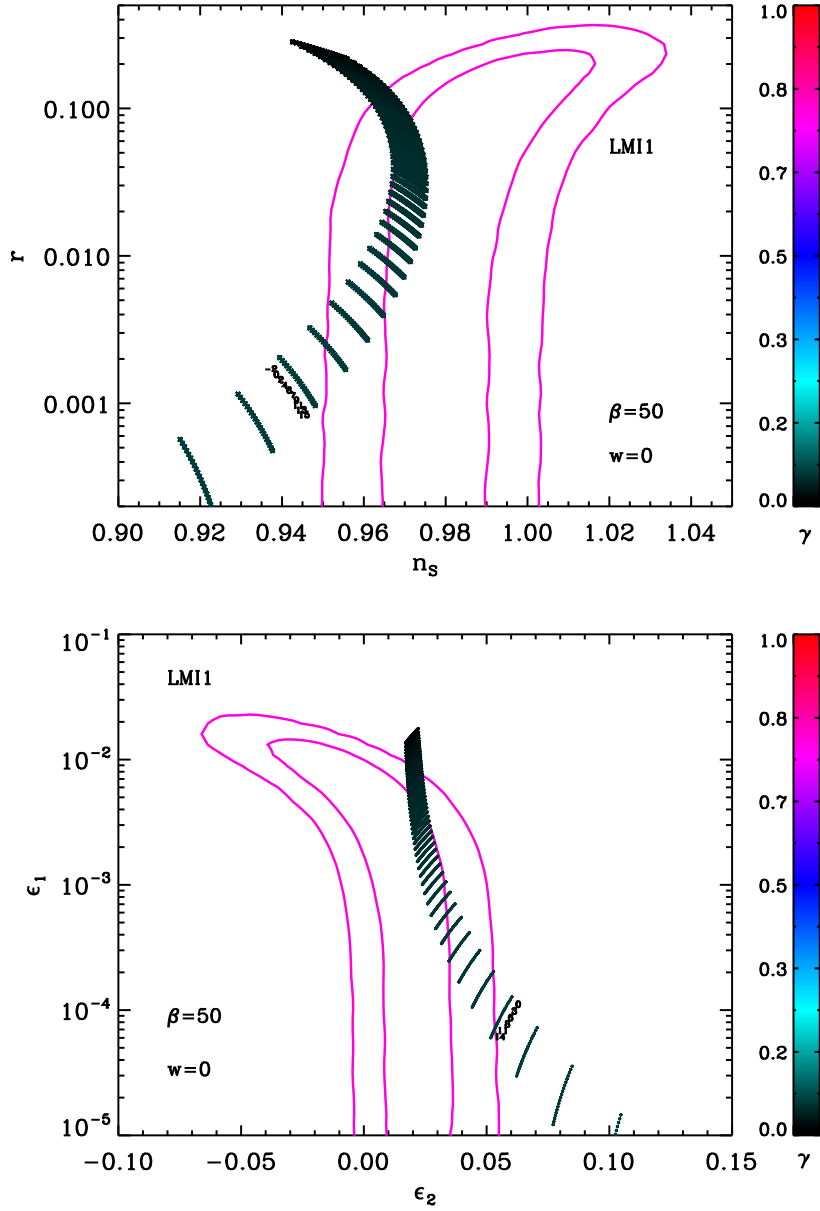


Figure 105. Reheating consistent slow-roll predictions for the Logamediate Inflation 1 models ($x < x_{V^{\max}}$) with $\beta = 50$, in the plane (n_s, r) (top panel) and the plane (ϵ_1, ϵ_2) (bottom panel). The two pink solid contours are the one and two-sigma WMAP confidence intervals (marginalized over second order slow-roll). The annotations trace the energy scale at which reheating ends and correspond to $\log(g_*^{1/4} T_{\text{reh}}/\text{GeV})$. For such high values of β , only small values of γ are in agreement with observations.

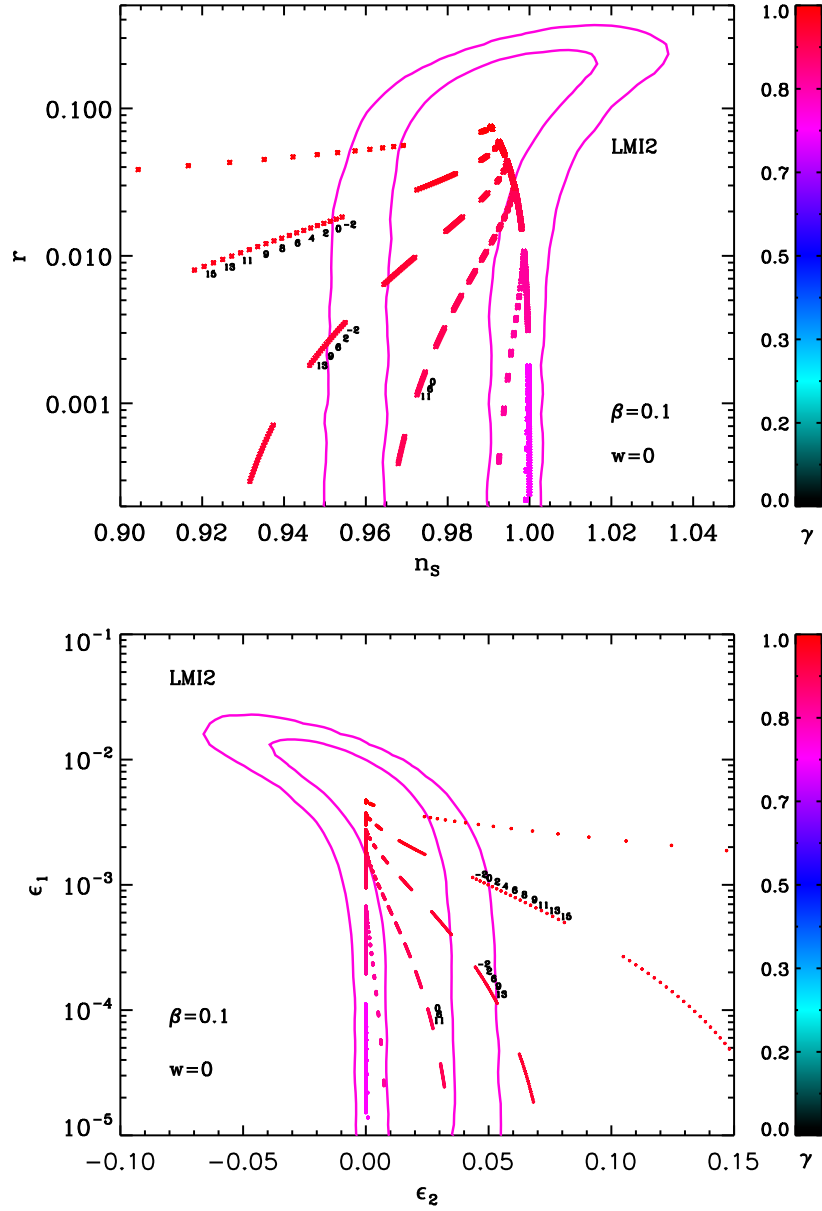


Figure 106. Reheating consistent slow-roll predictions for the Logamediate Inflation 2 models with $\beta = 0.1$, in the plane (n_s, r) (top panel) and the plane (ϵ_1, ϵ_2) (bottom panel). Inflation proceeds at increasing field values, from the left to the right, and with $x > x_{V,\text{max}}$. The color of the data points encodes the value of γ , while different data blocks correspond to different values of x_{end} . Inside a given block, the annotations trace the energy scale at which reheating ends and correspond to $\log(g_*^{1/4} T_{\text{reh}}/\text{GeV})$. The two pink solid contours are the one and two-sigma WMAP confidence intervals (marginalized over second order slow-roll).

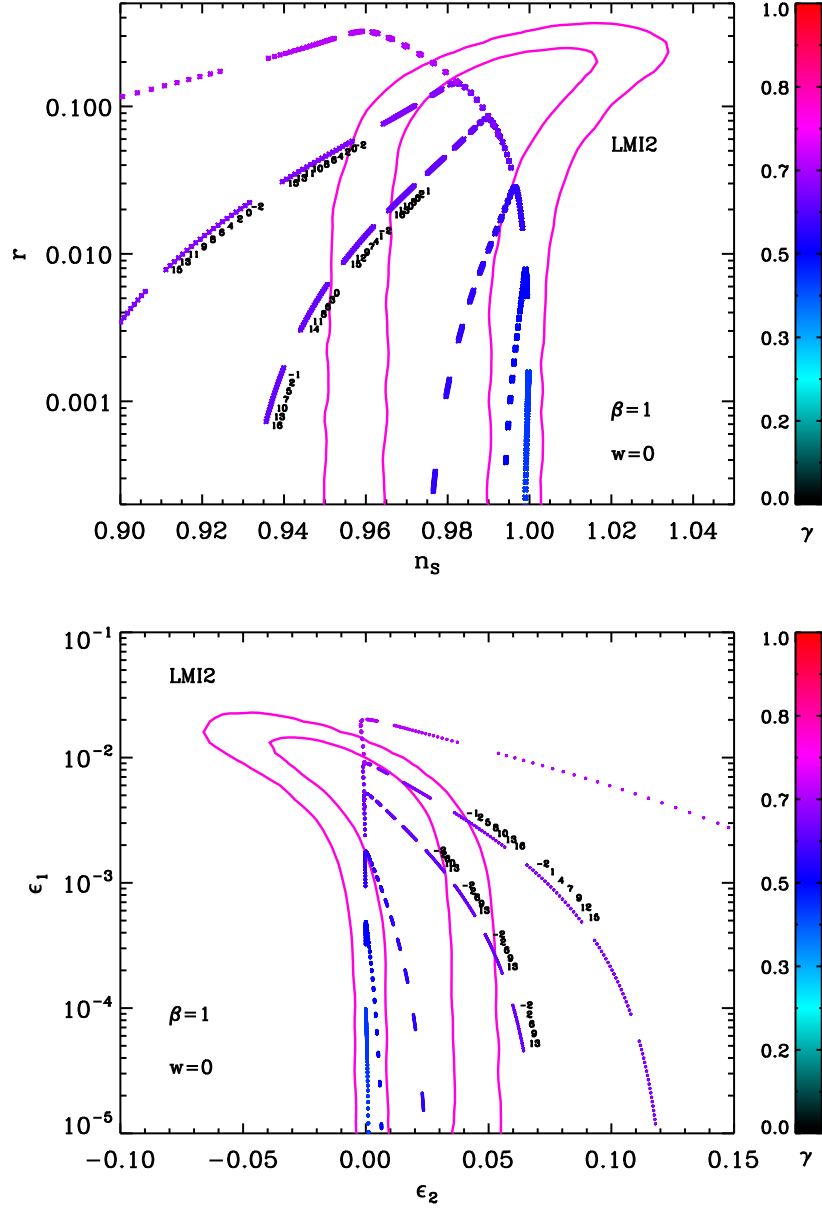


Figure 107. Reheating consistent slow-roll predictions for the Logamediate Inflation 2 models ($x > x_{V^{\text{max}}}$) with $\beta = 1$, in the plane (n_s, r) (top panel) and the plane (ϵ_1, ϵ_2) (bottom panel). The color of the data points encodes the value of γ , while different data blocks correspond to different values of x_{end} . Inside a given block, the annotations trace the energy scale at which reheating ends and correspond to $\log(g_*^{1/4} T_{\text{reh}}/\text{GeV})$. The two pink solid contours are the one and two-sigma WMAP confidence intervals (marginalized over second order slow-roll). For fixed γ , the turning point in the predictions line occurs when x_{end} lies in the fine-tuned region of LMI2, i.e. $x_{V^{\text{max}}} < x < x_{\epsilon_1^{\text{max}}}$. One sees that the predictions become infinitely close to pure de-Sitter.

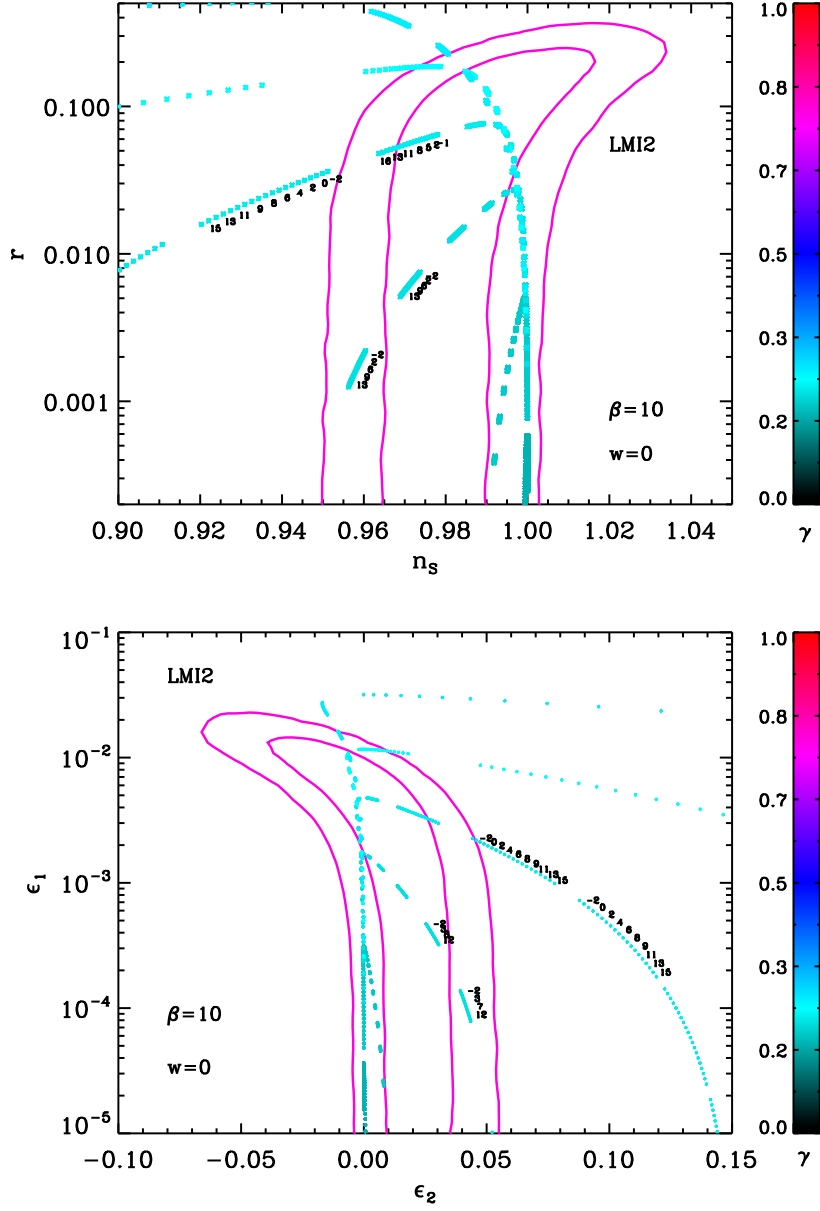


Figure 108. Reheating consistent slow-roll predictions for the Logamediate Inflation 2 models ($x > x_{V^{\max}}$) with $\beta = 10$, in the plane (n_s, r) (top panel) and the plane (ϵ_1, ϵ_2) (bottom panel). The color of the data points encodes the value of γ , while different data blocks correspond to different values of x_{end} . Inside a given block, the annotations trace the energy scale at which reheating ends and correspond to $\log(g_*^{1/4} T_{\text{reh}}/\text{GeV})$. The two pink solid contours are the one and two-sigma WMAP confidence intervals (marginalized over second order slow-roll). For fixed γ , the turning point in the predictions line occurs when $x_{V^{\max}} < x < x_{\epsilon_1^{\max}}$.

A.26 Twisted Inflation (TWI)

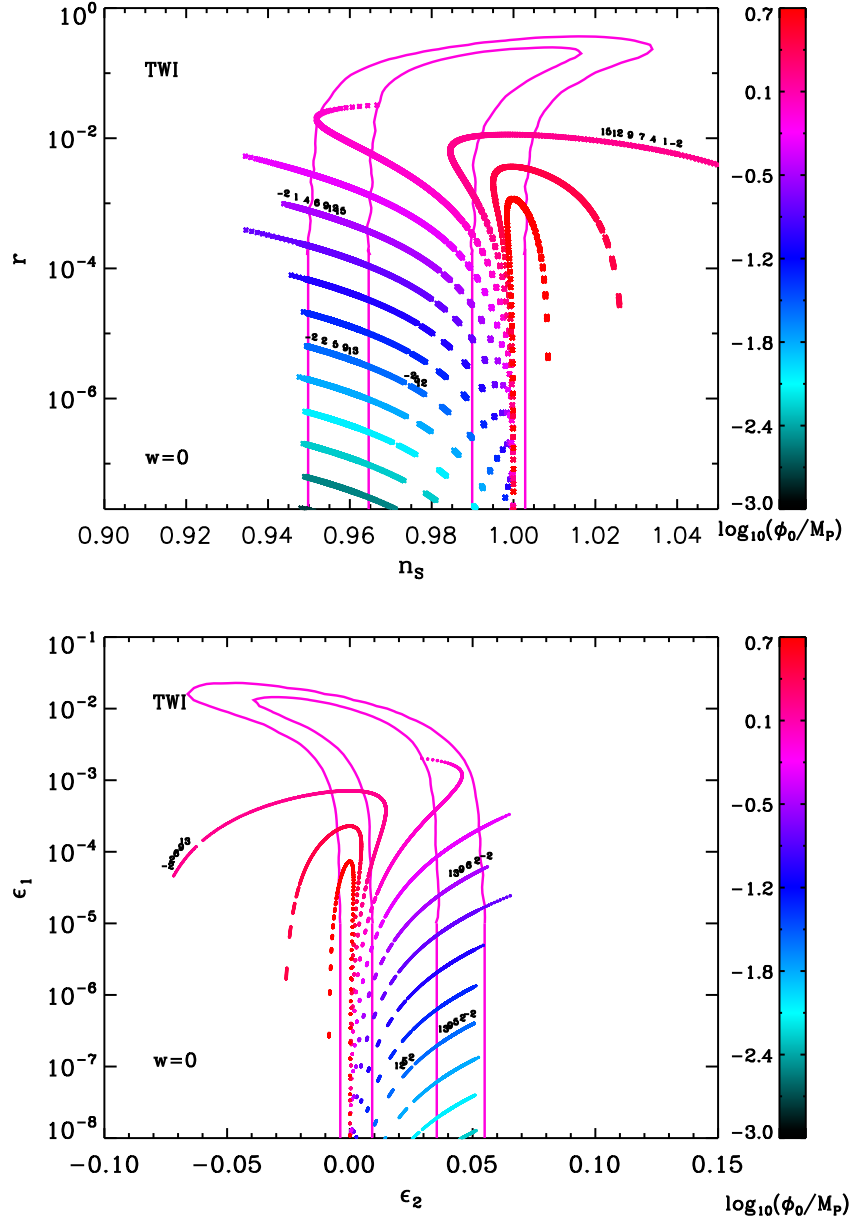


Figure 109. Reheating consistent slow-roll predictions for the twisted models in the plane (n_s, r) (top panel) and the plane (ϵ_1, ϵ_2) (bottom panel). The two pink solid contours are the one and two-sigma WMAP confidence intervals (marginalized over second order slow-roll). The color of the data points encodes the value of ϕ_0 , while different data blocks correspond to different values of x_{end} . Inside a given block, the annotations trace the energy scale at which reheating ends and correspond to $\log(g_*^{1/4} T_{\text{reh}}/\text{GeV})$.

A.27 GMSSM Inflation (GMSSMI)

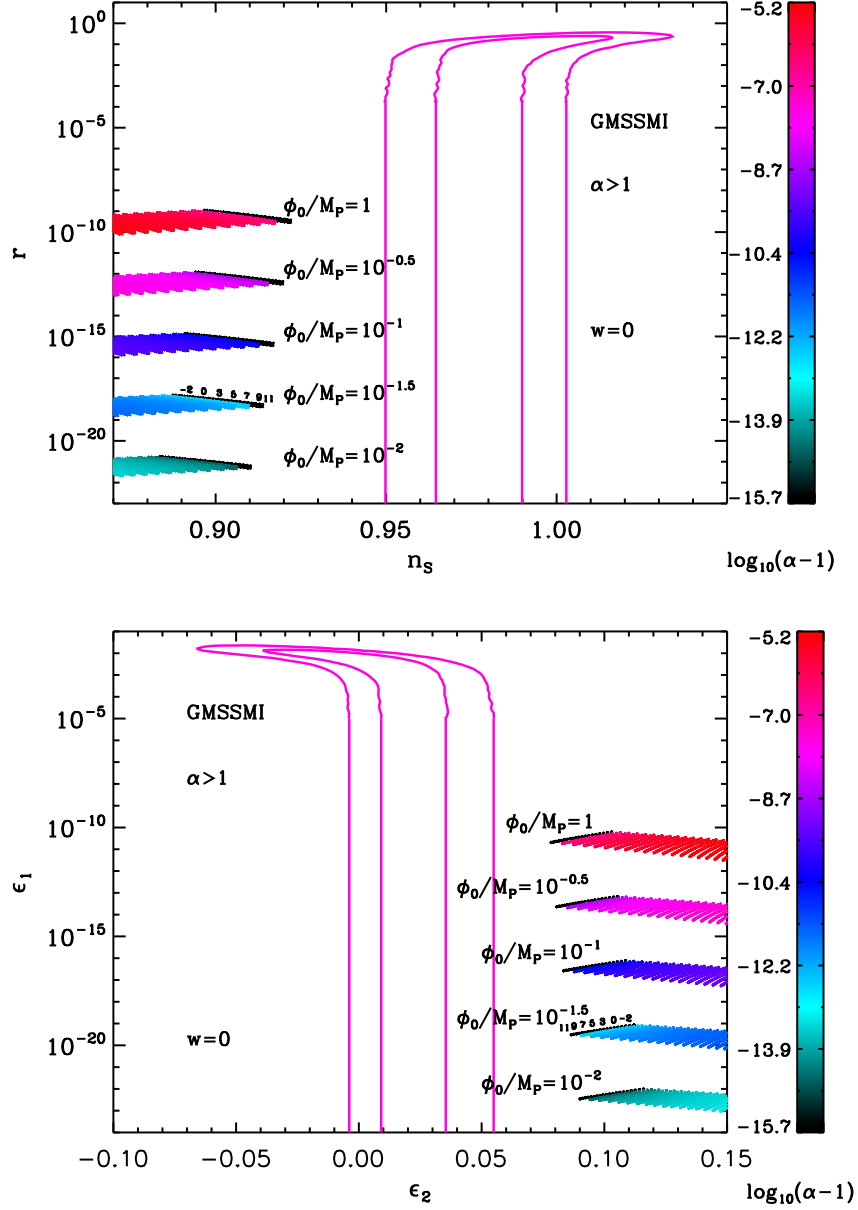


Figure 110. Reheating consistent slow-roll predictions for the GMSSMI models in the plane (n_s, r) (top panel) and the plane (ϵ_1, ϵ_2) (bottom panel), for $1 < \alpha < 1 + \phi_0^4/M_{\text{Pl}}^4 \pi^2/900/(N_{\text{end}} - N_{\text{ini}})^2$. The two pink solid contours are the one and two-sigma WMAP confidence intervals (marginalized over second order slow-roll). The annotations trace the energy scale at which reheating ends and correspond to $\log(g_*^{1/4} T_{\text{reh}}/\text{GeV})$. When $\alpha \rightarrow 1$, one recovers the standard MSSM predictions, see Fig. 93.

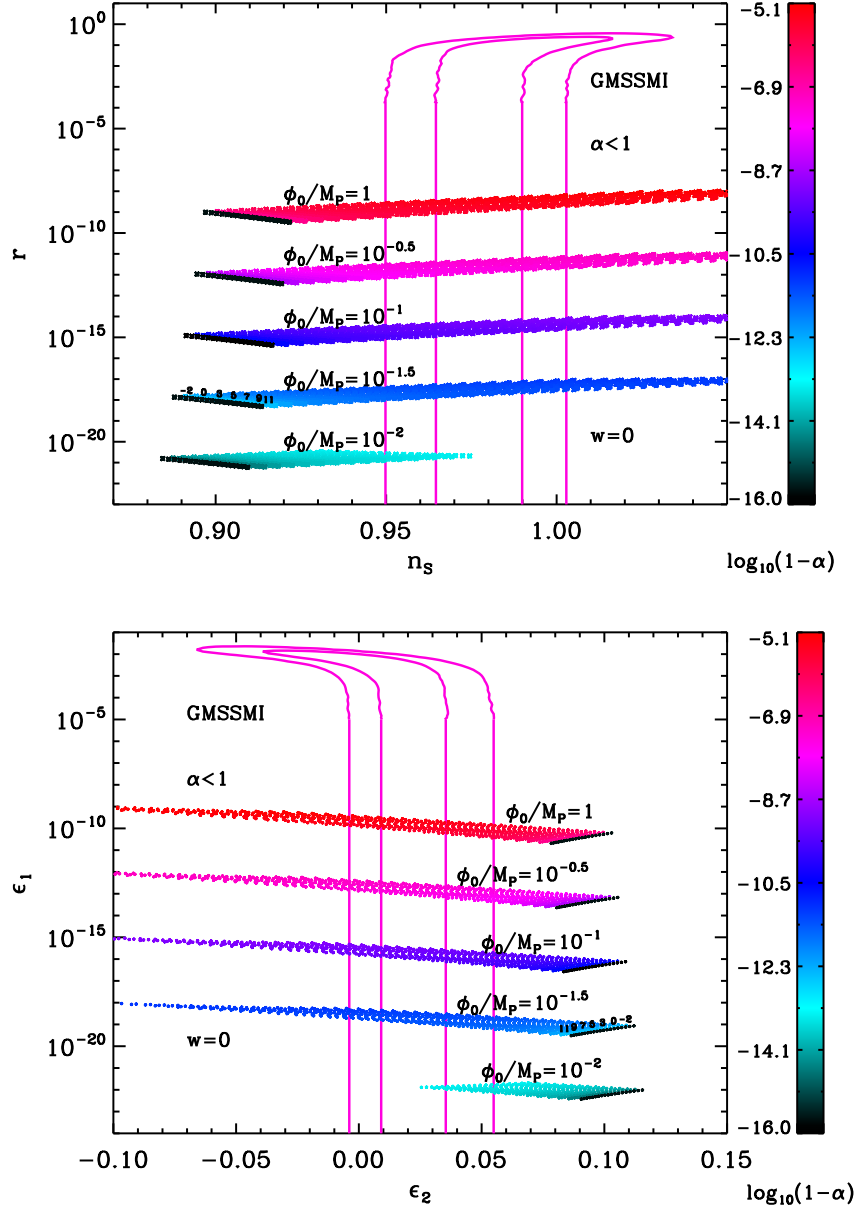


Figure 111. Reheating consistent slow-roll predictions for the GMSSMI models in the plane (n_s, r) (top panel) and the plane (ϵ_1, ϵ_2) (bottom panel), for $1 - \phi_0^4/M_{\text{Pl}}^4\pi^2/900/(N_{\text{end}} - N_{\text{ini}})^2 < \alpha < 1$. The two pink solid contours are the one and two-sigma WMAP confidence intervals (marginalized over second order slow-roll). The annotations trace the energy scale at which reheating ends and correspond to $\ln(g_*^{1/4}T_{\text{reh}}/\text{GeV})$. When $\alpha \rightarrow 1$, one recovers the standard MSSM predictions, see Fig. 93.

A.28 Brane SUSY breaking Inflation (BSUSYBI)

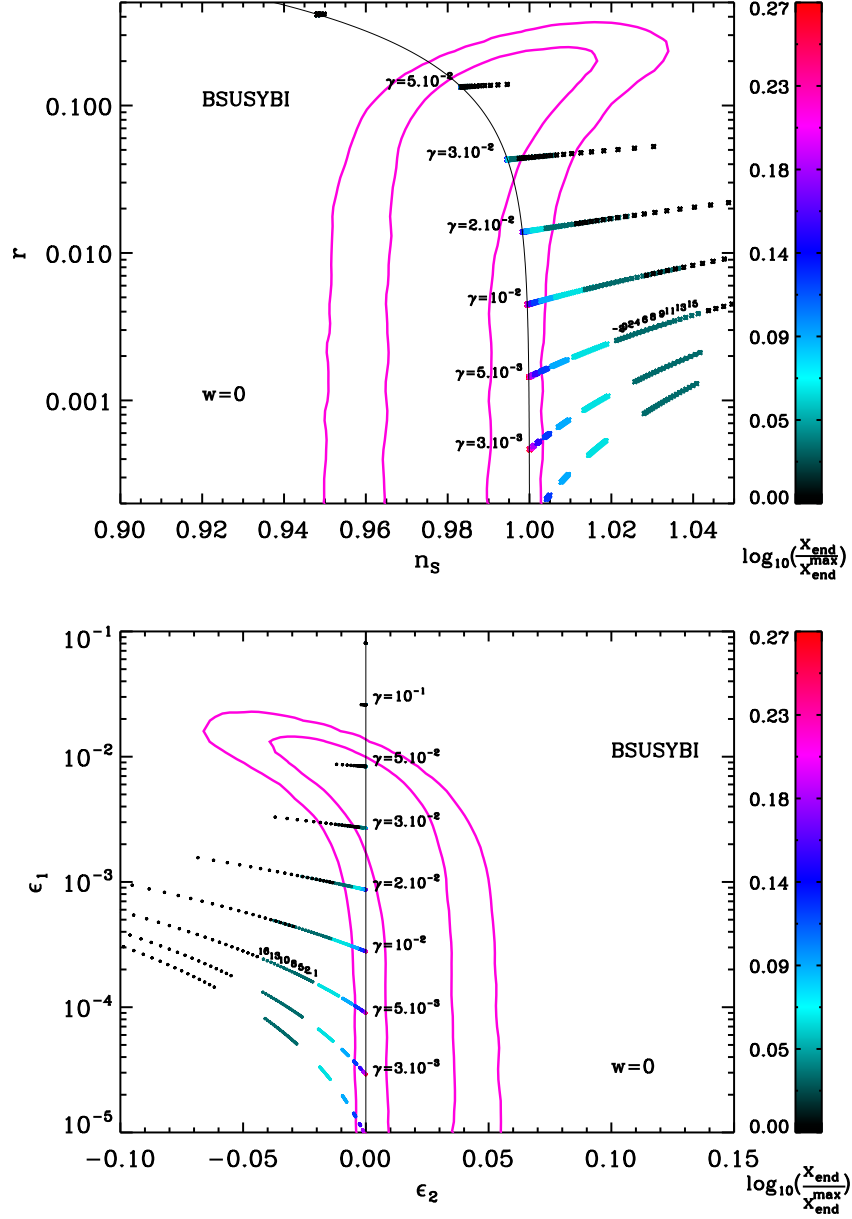


Figure 112. Reheating consistent slow-roll predictions for the BSUSYBI models in the plane (n_s, r) (top panel) and the plane (ϵ_1, ϵ_2) (bottom panel). The two pink solid contours are the one and two-sigma WMAP confidence intervals (marginalized over second order slow-roll). The parameter x_{end} varies between $2x_{\text{end}}^{\text{max}} < x_{\text{end}} < x_{\text{end}}^{\text{max}}$ ($x_{\text{end}}^{\text{max}} < 0$), under which the predictions of the model coincide with the line $\epsilon_2 = 0$ (black solid), i.e. PLI (see section 4.8). The annotations trace the energy scale at which reheating ends and correspond to $\log(g_*^{1/4} T_{\text{reh}}/\text{GeV})$. The parameter γ should be $\lesssim 10^{-1}$ for the predictions to remain inside the two sigma confidence intervals. For $\gamma \lesssim 3 \times 10^{-2}$, x_{end} is limited from below.

A.29 Tip Inflation (TI)

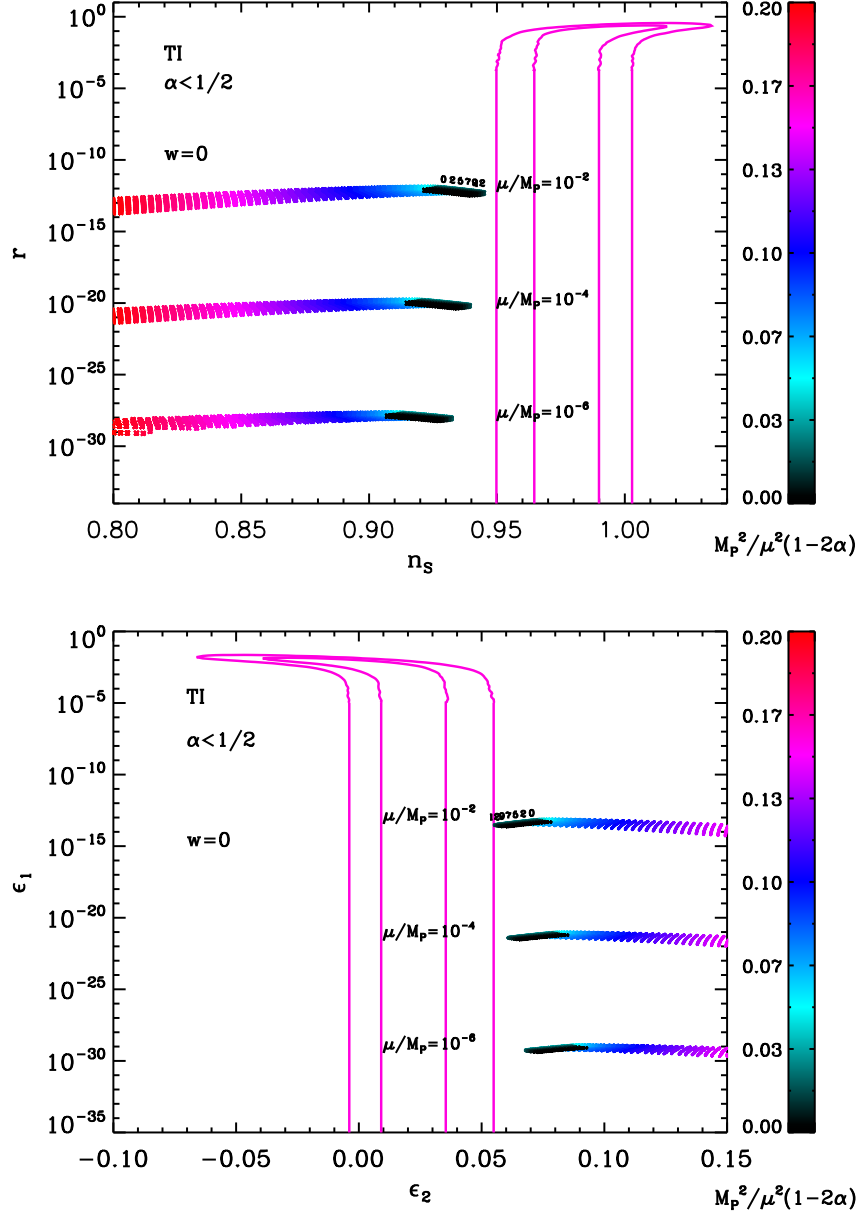


Figure 113. Reheating consistent slow-roll predictions for the tip inflation models with $\alpha < 1/2$, and for $\mu/M_{\text{Pl}} = 10^{-6}, 10^{-4}, 10^{-2}$ in the plane (n_s, r) (top panel) and the plane (ϵ_1, ϵ_2) (bottom panel). The two pink solid contours are the one and two-sigma WMAP confidence intervals (marginalized over second order slow-roll). The annotations trace the energy scale at which reheating ends and correspond to $\log(g_*^{1/4} T_{\text{reh}}/\text{GeV})$.

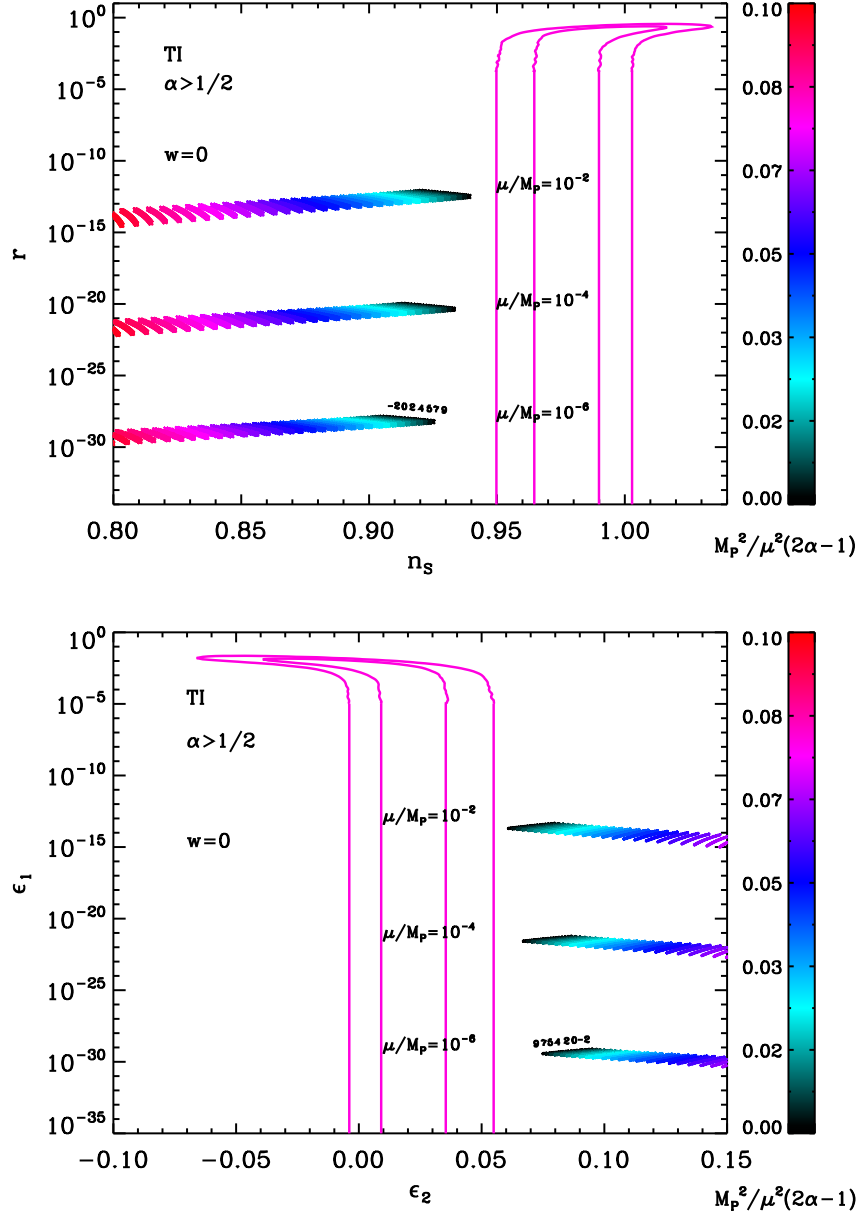


Figure 114. Reheating consistent slow-roll predictions for the tip inflation models with $\alpha > 1/2$, and for $\mu/M_{\text{Pl}} = 10^{-6}, 10^{-4}, 10^{-2}$ in the plane (n_s, r) (top panel) and the plane (ϵ_1, ϵ_2) (bottom panel). The two pink solid contours are the one and two-sigma WMAP confidence intervals (marginalized over second order slow-roll). The annotations trace the energy scale at which reheating ends and correspond to $\log(g_*^{1/4} T_{\text{reh}}/\text{GeV})$.

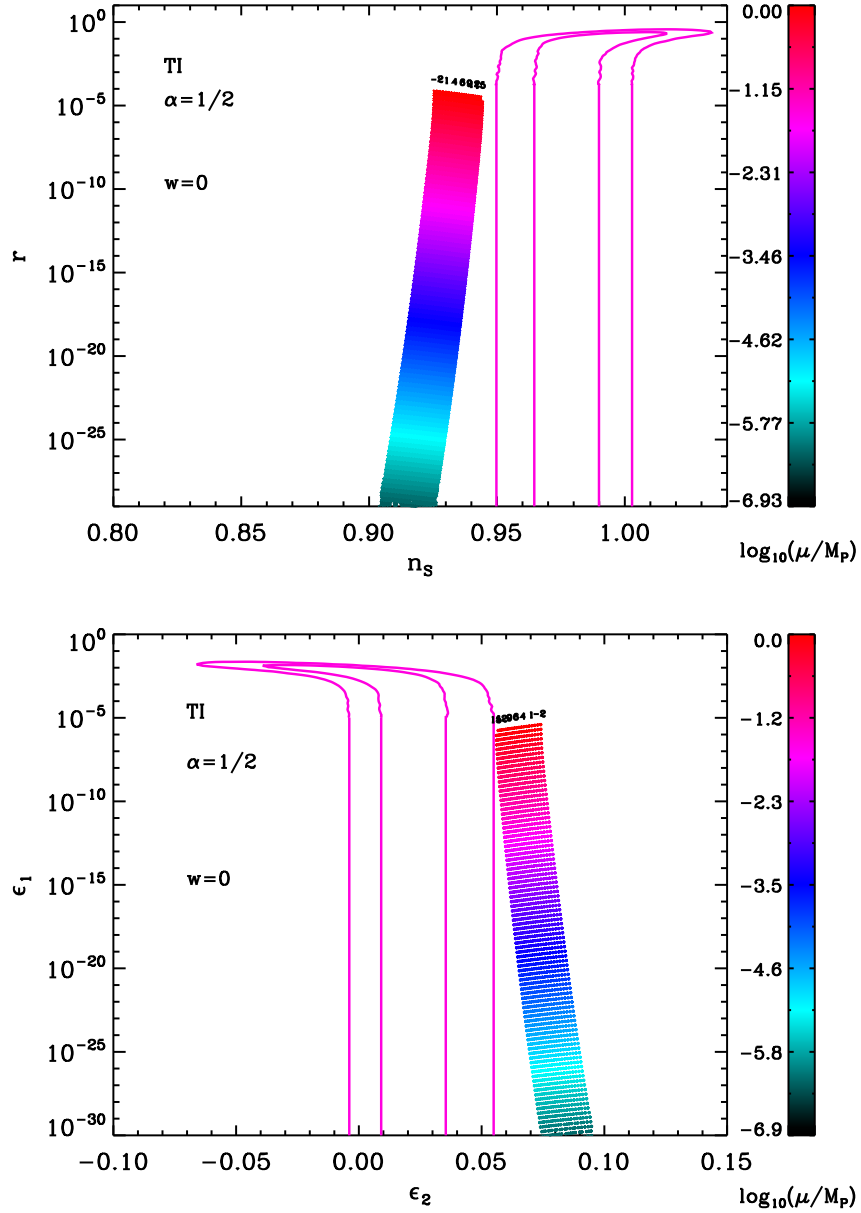


Figure 115. Reheating consistent slow-roll predictions for the tip inflation models with $\alpha = 1/2$ in the plane (n_s, r) (top panel) and the plane (ϵ_1, ϵ_2) (bottom panel). The two pink solid contours are the one and two-sigma WMAP confidence intervals (marginalized over second order slow-roll). The annotations trace the energy scale at which reheating ends and correspond to $\log(g_*^{1/4} T_{\text{reh}}/\text{GeV})$.

A.30 β Exponential Inflation (BEI)

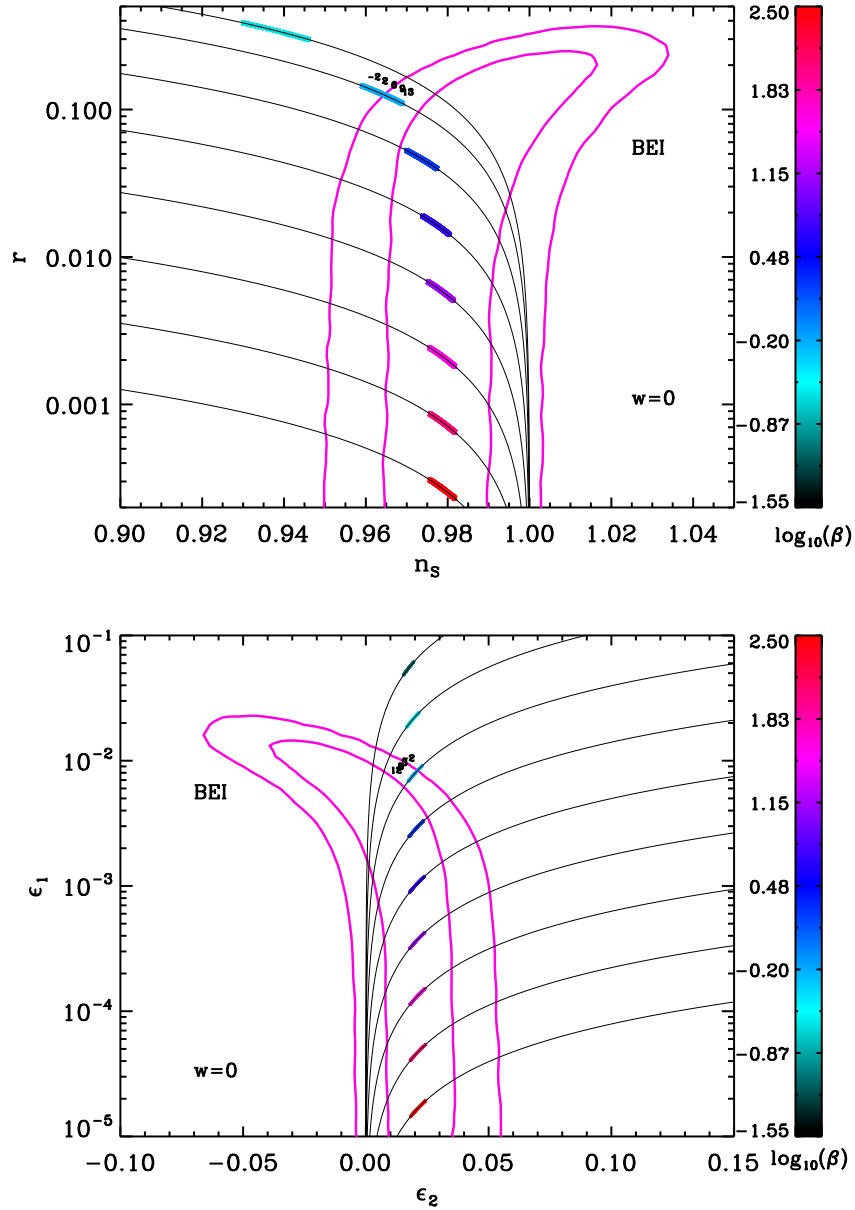


Figure 116. Reheating consistent slow-roll predictions for the β exponential inflation models in the plane (n_s, r) (top panel) and the plane (ϵ_1, ϵ_2) (bottom panel). The two pink solid contours are the one and two-sigma WMAP confidence intervals (marginalized over second order slow-roll). The black solid lines represent the locus of the points such that $\epsilon_2 = 4\beta\epsilon_1$. The annotations trace the energy scale at which reheating ends and correspond to $\log(g_*^{1/4} T_{\text{reh}}/\text{GeV})$.

A.31 Pseudo Natural Inflation (PSNI)

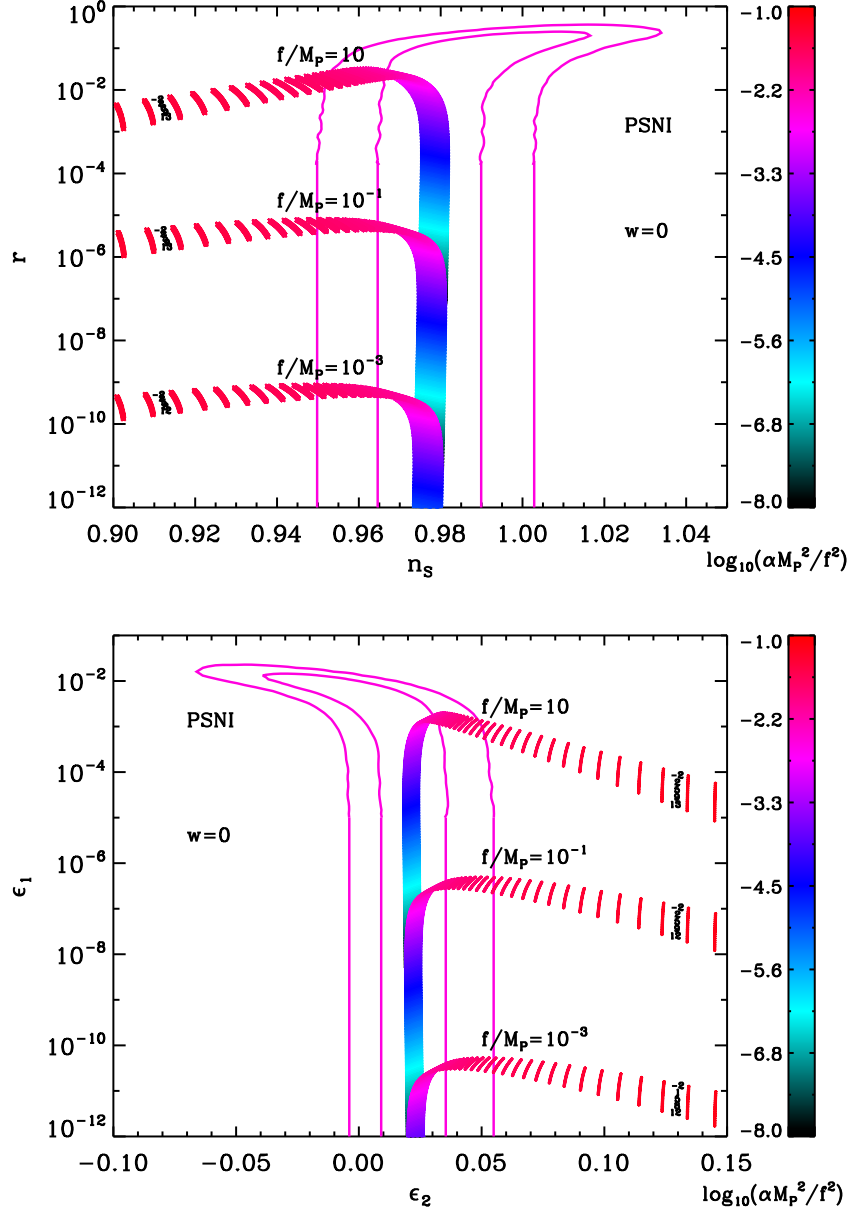


Figure 117. Reheating consistent slow-roll predictions for the pseudo natural inflation models with $\mu/M_{\text{Pl}} = 10, 10^{-1}, 10^{-3}$, in the plane (n_s, r) (top panel) and the plane (ϵ_1, ϵ_2) (bottom panel). The two pink solid contours are the one and two-sigma WMAP confidence intervals (marginalized over second order slow-roll). The annotations trace the energy scale at which reheating ends and correspond to $\log(g_*^{1/4} T_{\text{reh}}/\text{GeV})$.

A.32 Non Canonical Kähler Inflation (NCKI)

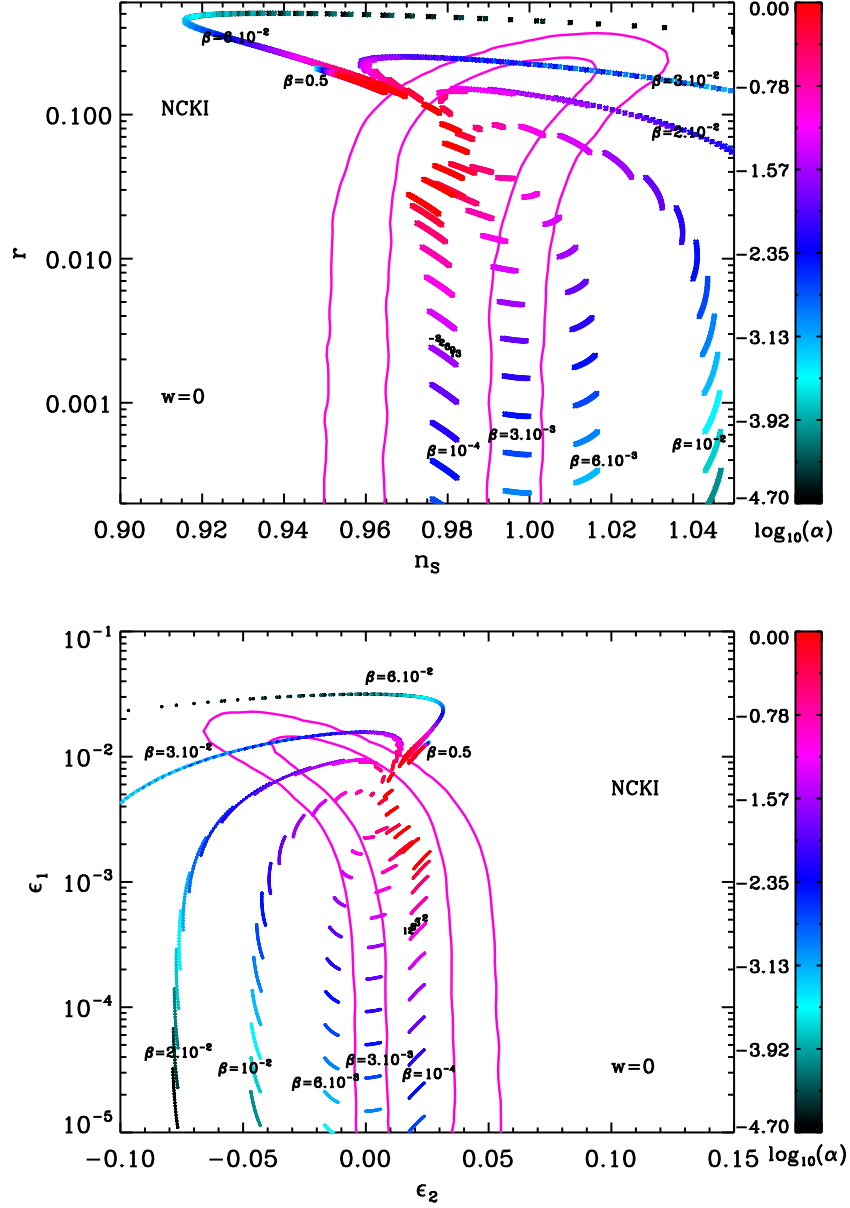


Figure 118. Reheating consistent slow-roll predictions for the non canonical Kähler inflation models with $\beta > 0$ in the plane (n_s, r) (top panel) and the plane (ϵ_1, ϵ_2) (bottom panel). The two pink solid contours are the one and two-sigma WMAP confidence intervals (marginalized over second order slow-roll). The annotations trace the energy scale at which reheating ends and correspond to $\log(g_*^{1/4} T_{\text{reh}}/\text{GeV})$. When $\beta \gtrsim 1$, the predictions are almost identical to those displayed here.

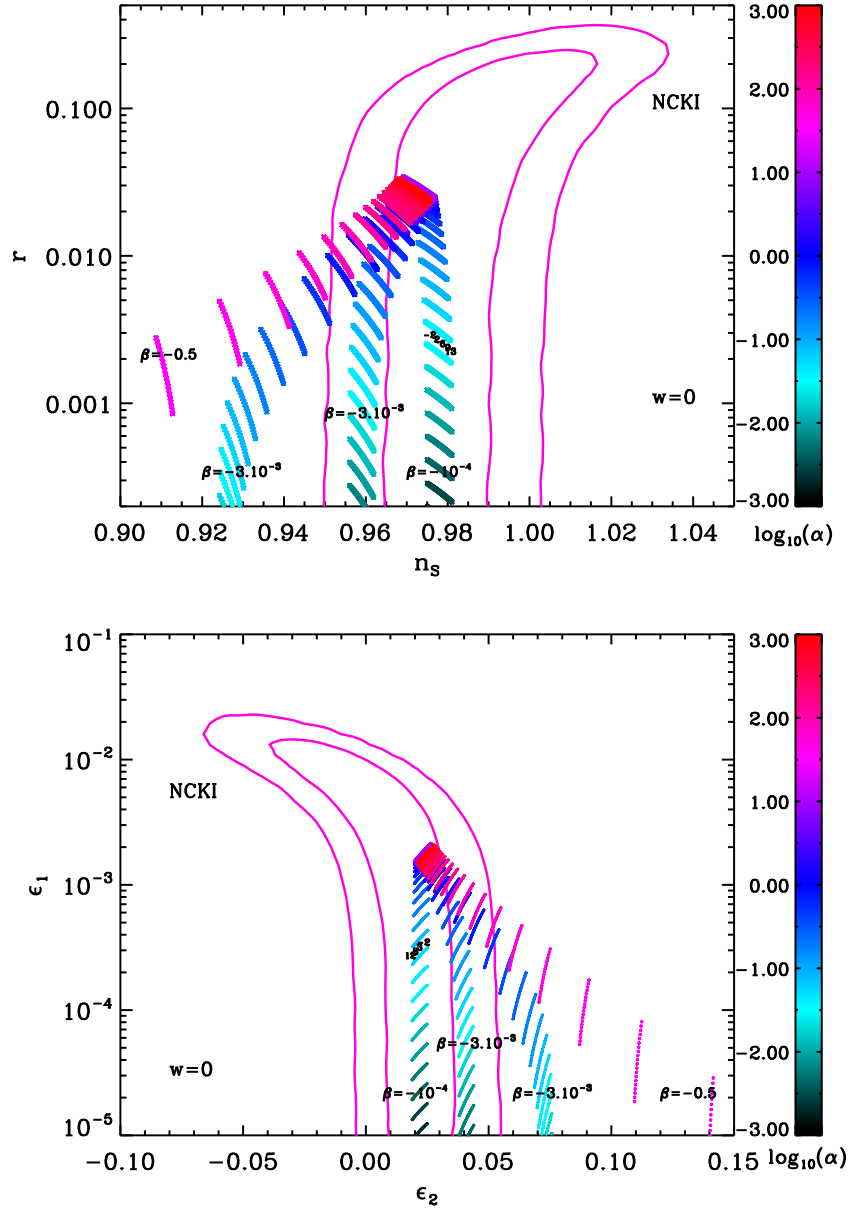


Figure 119. Reheating consistent slow-roll predictions for the non canonical Kähler inflation models with $\beta < 0$, in the plane (n_s, r) (top panel) and the plane (ϵ_1, ϵ_2) (bottom panel). The two pink solid contours are the one and two-sigma WMAP confidence intervals (marginalized over second order slow-roll). The annotations trace the energy scale at which reheating ends and correspond to $\log(g_*^{1/4} T_{\text{reh}}/\text{GeV})$. When $\beta \lesssim -1$, the predictions remain almost unchanged.

A.33 Constant Spectrum Inflation (CSI)

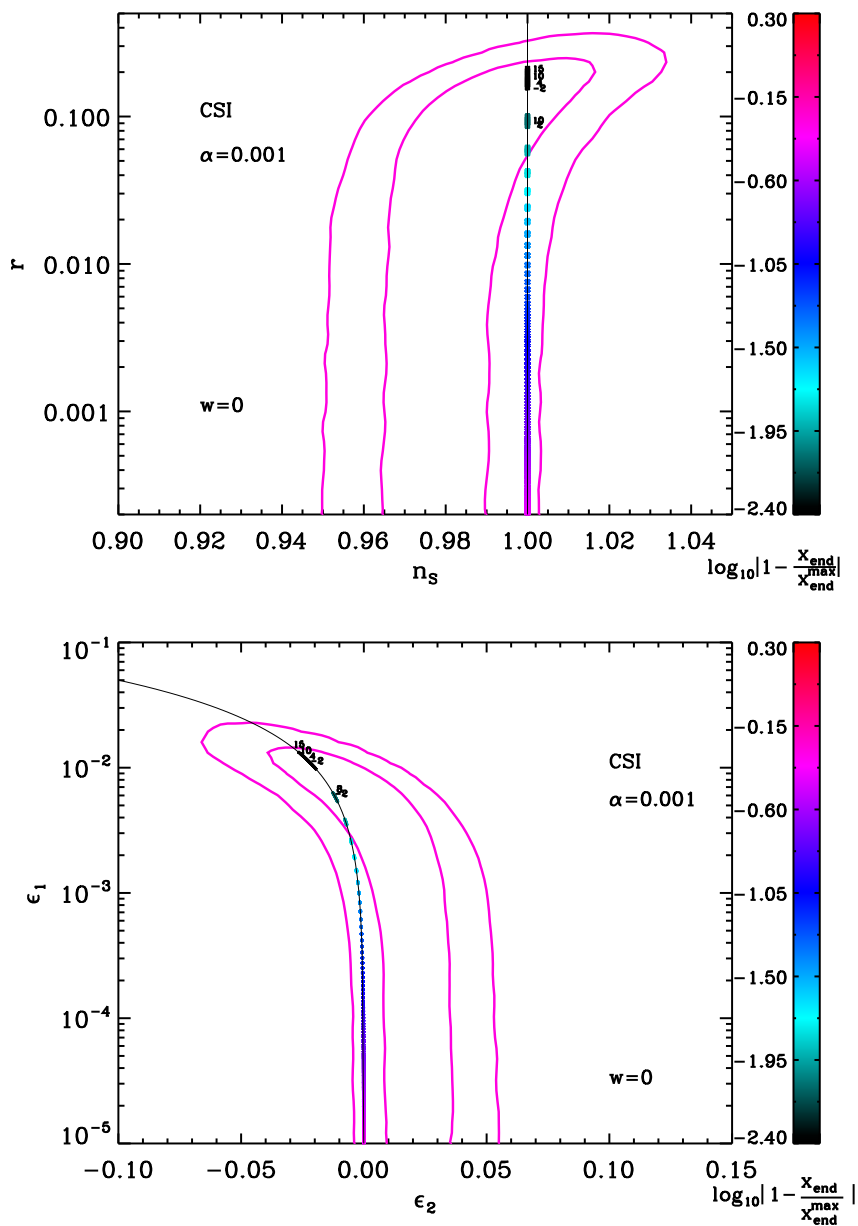


Figure 120. Reheating consistent slow-roll predictions for the Constant Spectrum models in the plane (n_s, r) (top panel) and the plane (ϵ_1, ϵ_2) (bottom panel), for $\alpha = 10^{-3}$. The two pink solid contours are the one and two-sigma WMAP confidence intervals (marginalized over second order slow-roll). The black solid lines correspond to $n_s = 1$, and the annotations trace the energy scale at which reheating ends and correspond to $\log(g_*^{1/4} T_{\text{reh}}/\text{GeV})$.

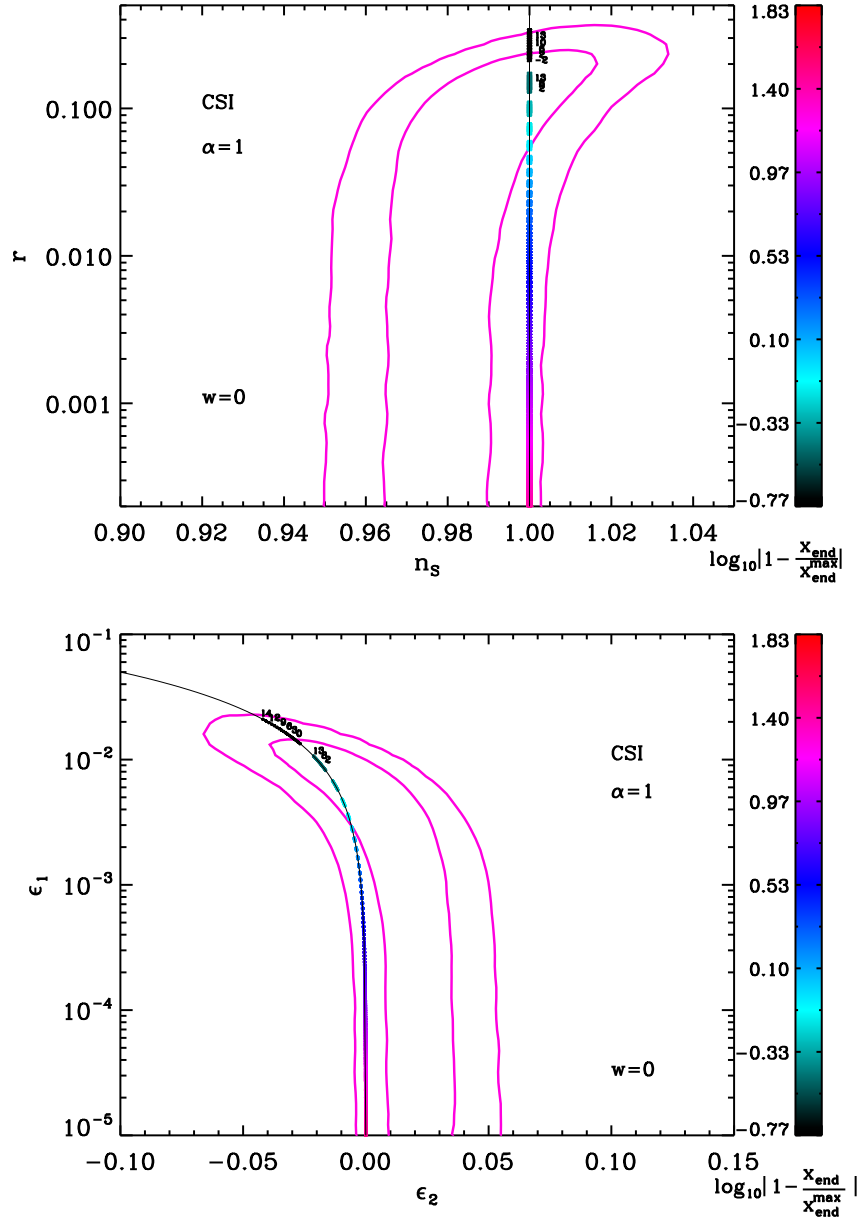


Figure 121. Reheating consistent slow-roll predictions for the Constant Spectrum models in the plane (n_s, r) (top panel) and the plane (ϵ_1, ϵ_2) (bottom panel), for $\alpha = 1$. The two pink solid contours are the one and two-sigma WMAP confidence intervals (marginalized over second order slow-roll). The black solid lines correspond to $n_s = 1$, and the annotations trace the energy scale at which reheating ends and correspond to $\log(g_*^{1/4} T_{\text{reh}}/\text{GeV})$.

A.34 Orientifold Inflation (OI)

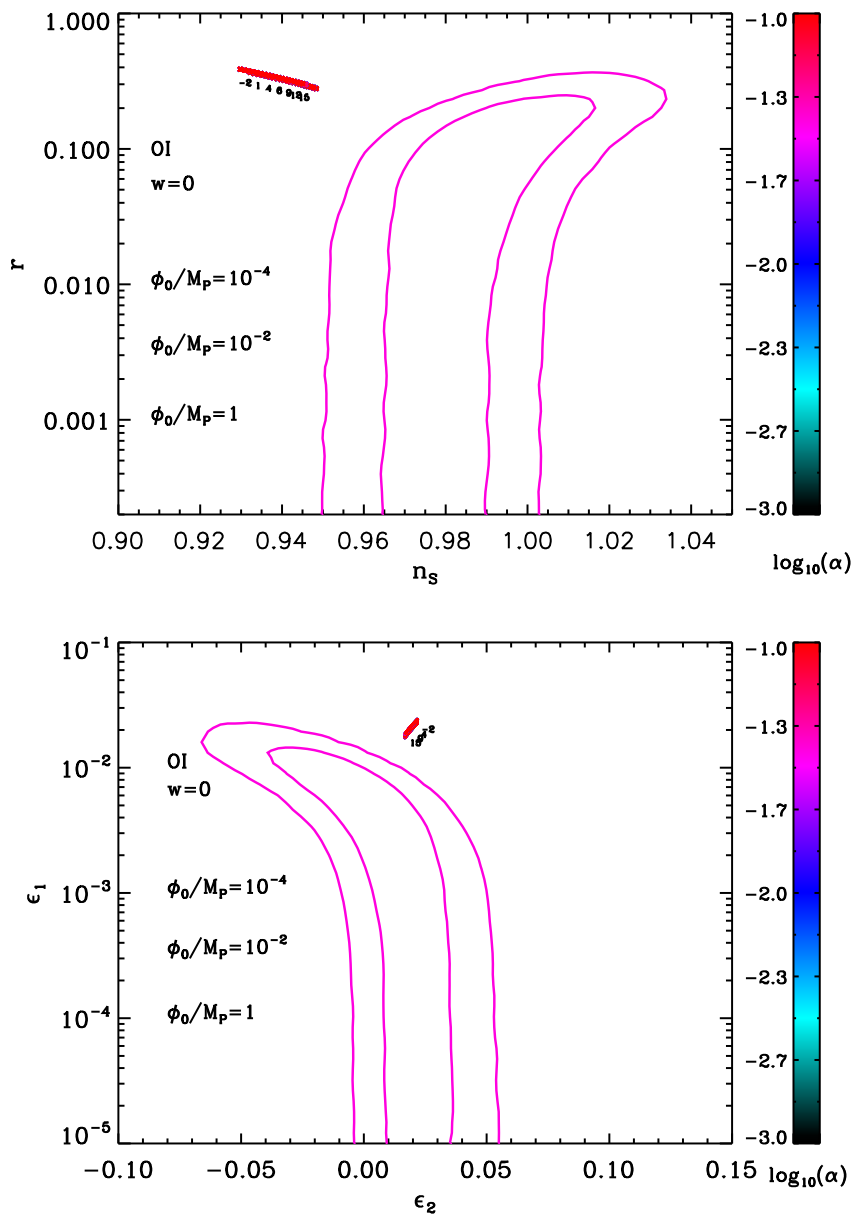


Figure 122. Reheating consistent slow-roll predictions for the orientifold inflation models for $\phi_0/M_{Pl} = 10^{-4}, 10^{-2}, 1$ and $\alpha \in [10^{-3}, 10^{-1}]$, in the plane (n_s, r) (top panel) and the plane (ϵ_1, ϵ_2) (bottom panel). The two pink solid contours are the one and two-sigma WMAP confidence intervals (marginalized over second order slow-roll). The annotations trace the energy scale at which reheating ends and correspond to $\log(g_*^{1/4} T_{\text{reh}}/\text{GeV})$. Since the predictions of these models almost do not depend on its parameters, they are all superimposed and one cannot distinguish the different values of ϕ_0 are α .

A.35 Constant n_s C Inflation (CNCI)

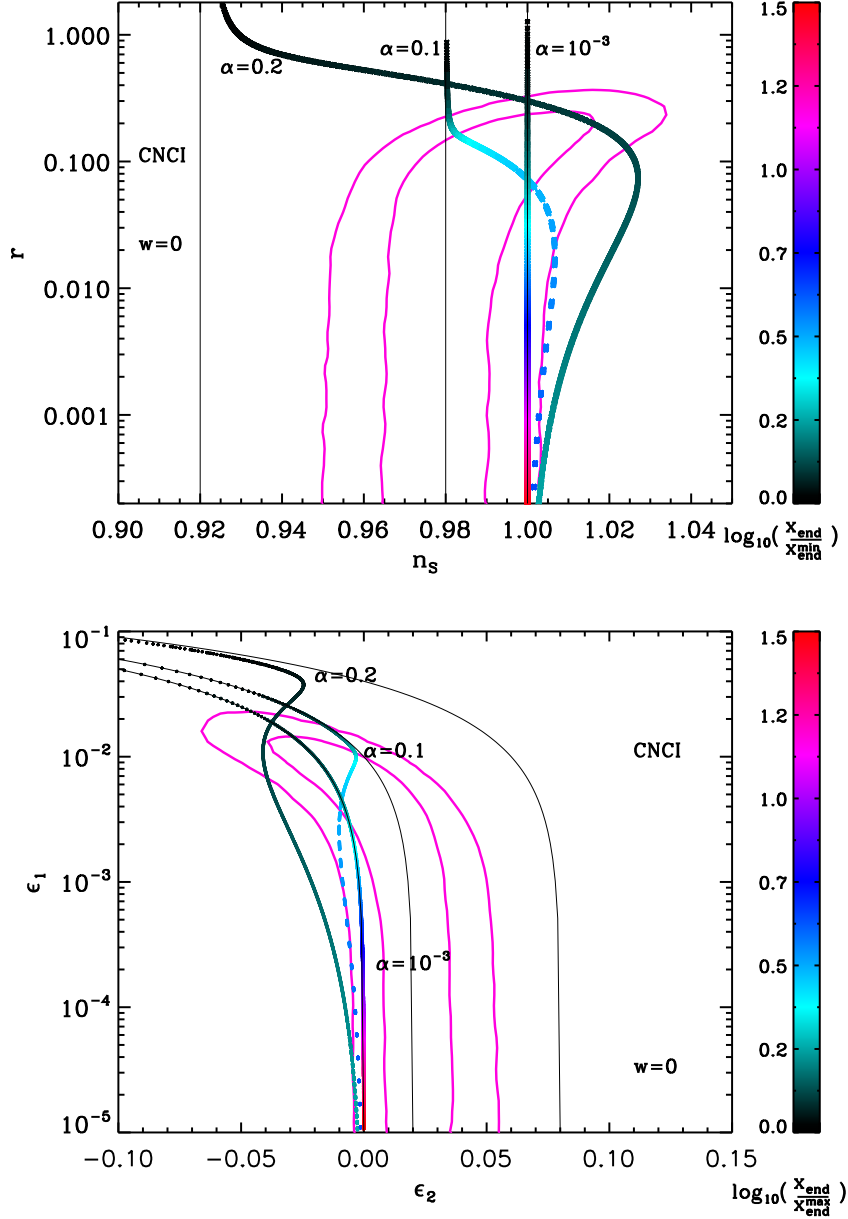


Figure 123. Reheating consistent slow-roll predictions for the constant n_s C inflation models for $\alpha = 10^{-3}, 0.1, 0.2$ in the plane (n_s, r) (top panel) and the plane (ϵ_1, ϵ_2) (bottom panel). The black solid lines are the $n_s - 1 = -2\alpha^2$ contours, for the displayed values of α . The two pink solid contours are the one and two-sigma WMAP confidence intervals (marginalized over second order slow-roll). The energy scale at which reheating ends is degenerated with the parameter x_{end} , which is why it is not labeled.

A.36 Supergravity Brane Inflation (SBI)

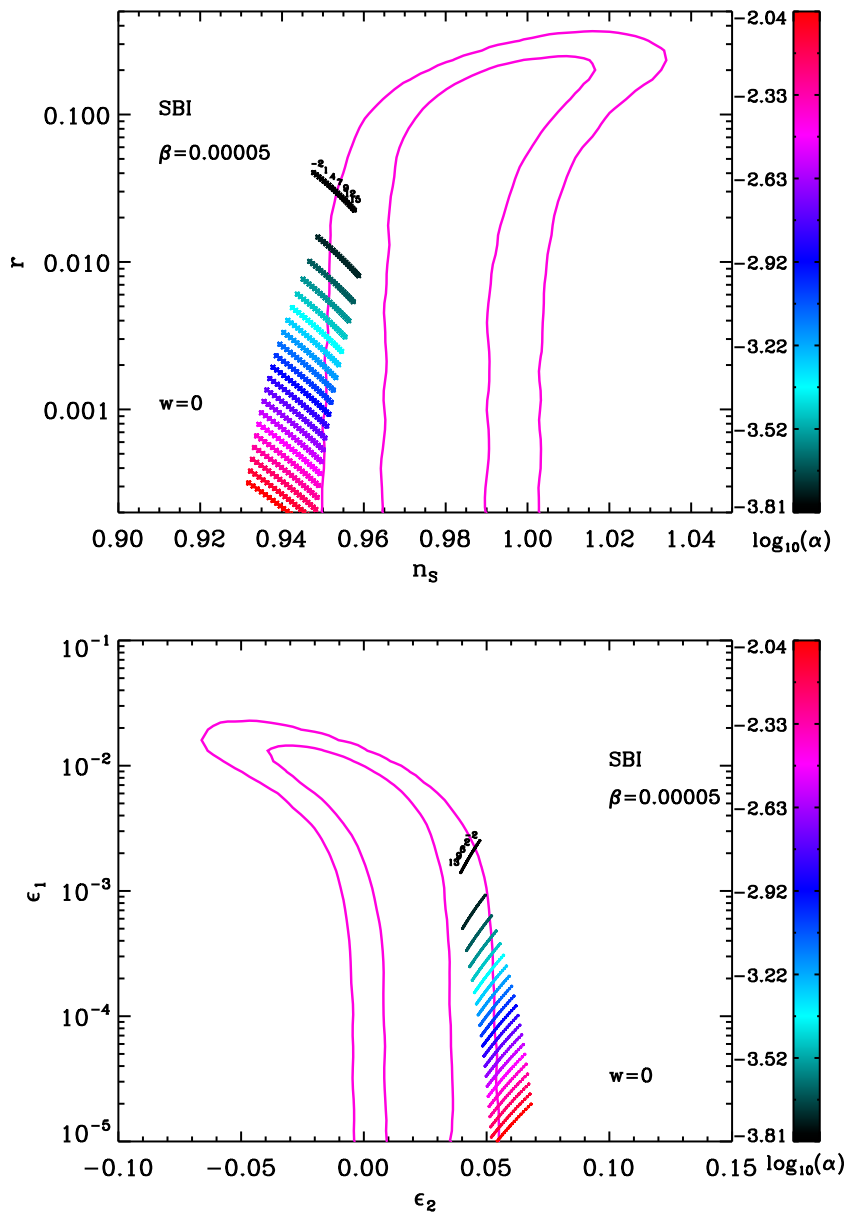


Figure 124. Reheating consistent slow-roll predictions for the supergravity brane inflation models for $\beta = 5 \times 10^{-5}$ in the plane (n_s, r) (top panel) and the plane (ϵ_1, ϵ_2) (bottom panel). The two pink solid contours are the one and two-sigma WMAP confidence intervals (marginalized over second order slow-roll). The annotations trace the energy scale at which reheating ends and correspond to $\log(g_*^{1/4} T_{\text{reh}}/\text{GeV})$.

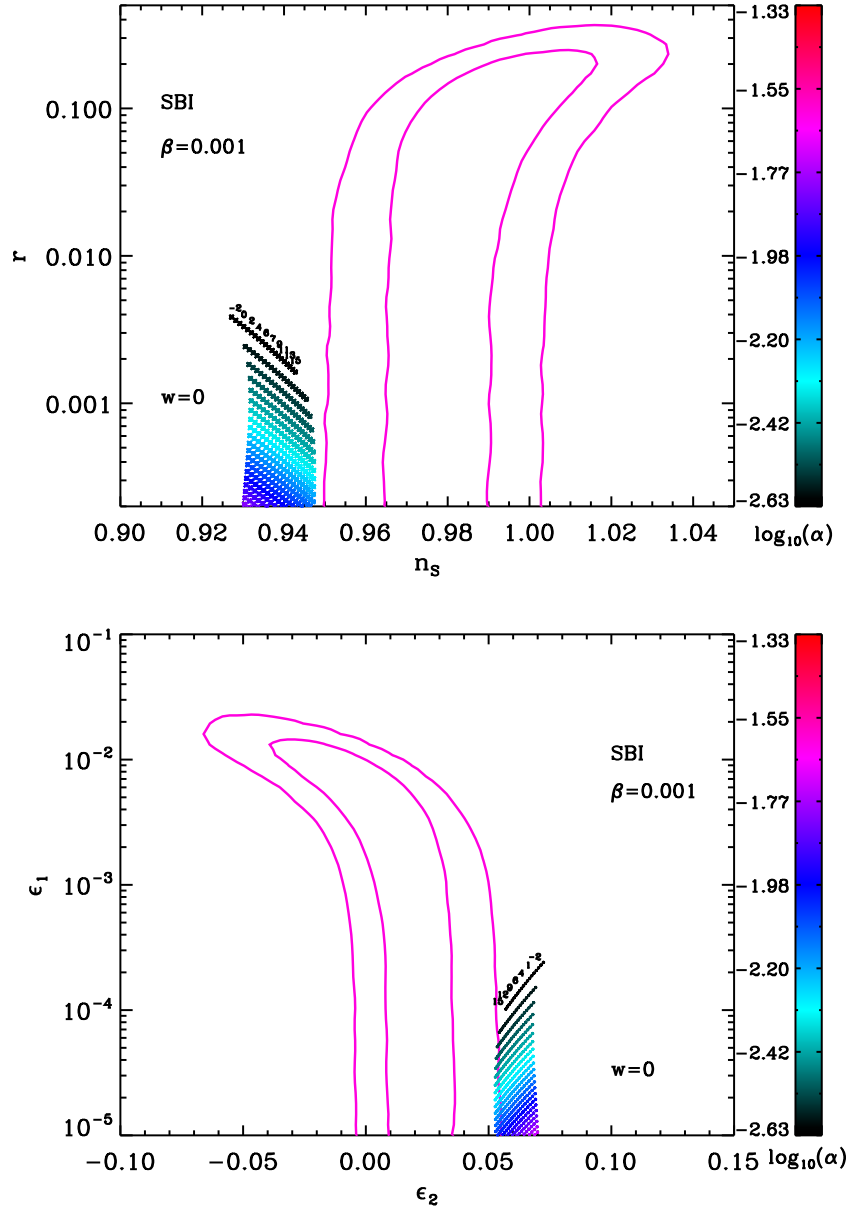


Figure 125. Reheating consistent slow-roll predictions for the supergravity brane inflation models for $\beta = 10^{-3}$ in the plane (n_s, r) (top panel) and the plane (ϵ_1, ϵ_2) (bottom panel). The two pink solid contours are the one and two-sigma WMAP confidence intervals (marginalized over second order slow-roll). The annotations trace the energy scale at which reheating ends and correspond to $\log(g_*^{1/4} T_{\text{reh}}/\text{GeV})$.

A.37 Spontaneous Symmetry Breaking Inflation 1 (SSBII)

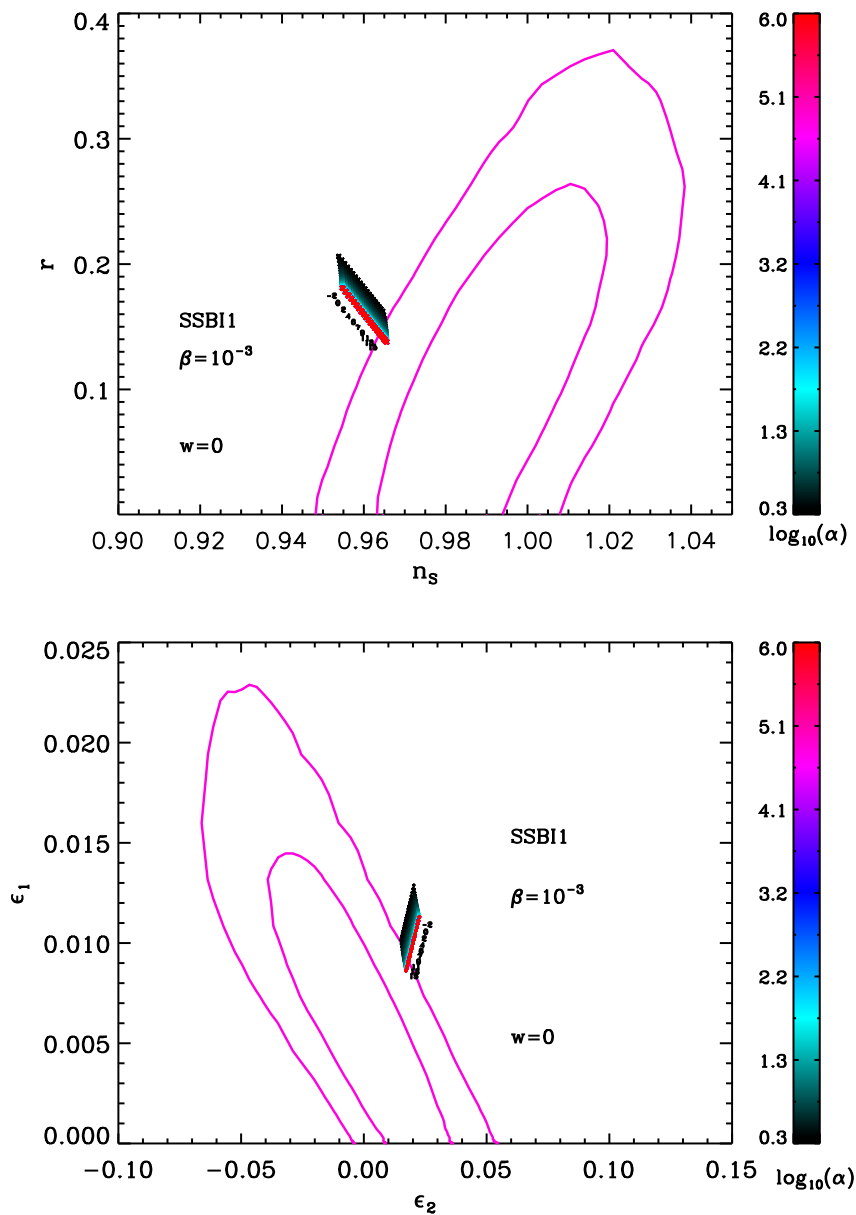


Figure 126. Reheating consistent slow-roll predictions for the spontaneous symmetry breaking 1 inflation ($\alpha > 0, \beta > 0$) models with $\beta = 10^{-3}$, in the plane (n_s, r) (top panel) and the plane (ϵ_1, ϵ_2) (bottom panel). The two pink solid contours are the one and two-sigma WMAP confidence intervals (marginalized over second order slow-roll). The annotations trace the energy scale at which reheating ends and correspond to $\log(g_*^{1/4} T_{\text{reh}}/\text{GeV})$. The parameter α is varied between $\alpha_{\text{min}}(\beta) < \alpha < 10^6 \alpha_{\text{min}}(\beta)$.

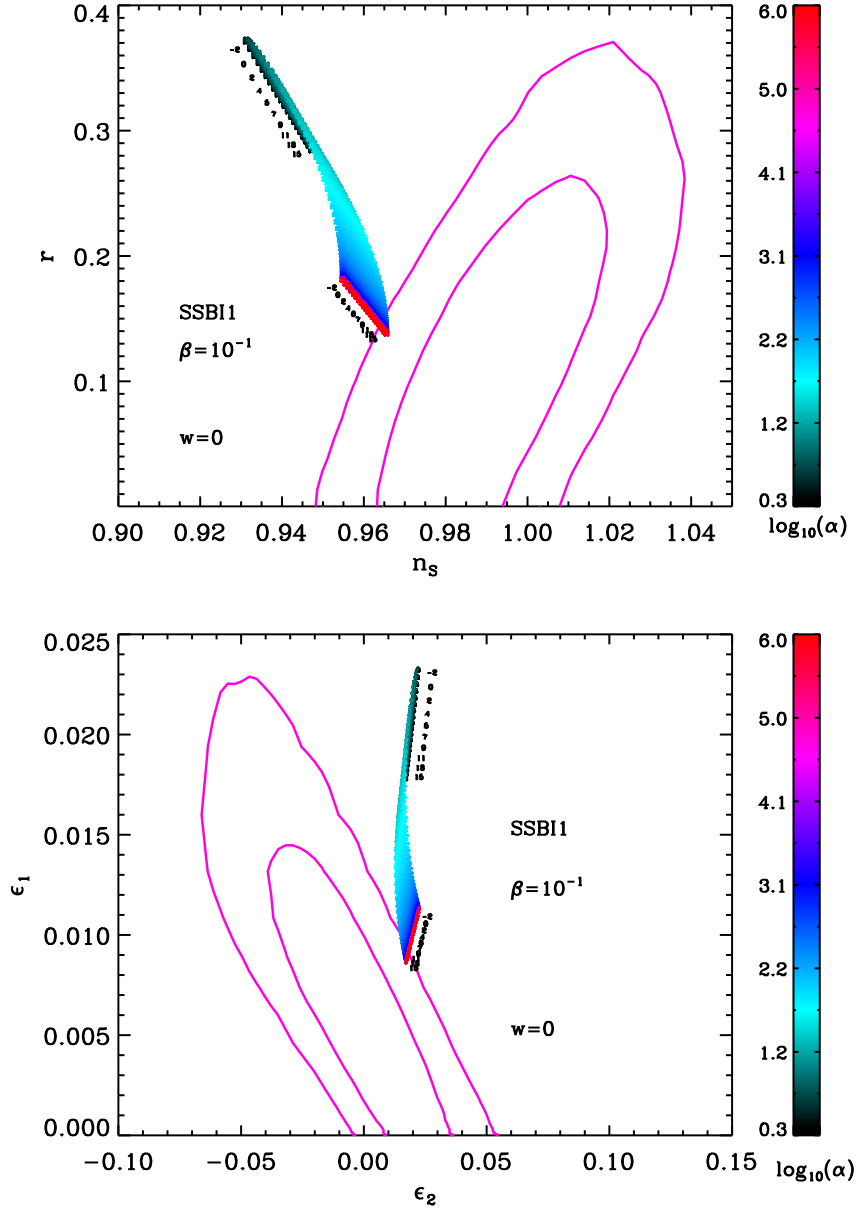


Figure 127. Reheating consistent slow-roll predictions for the spontaneous symmetry breaking 1 inflation ($\alpha > 0, \beta > 0$) models with $\beta = 10^{-1}$, in the plane (n_s, r) (top panel) and the plane (ϵ_1, ϵ_2) (bottom panel). The two pink solid contours are the one and two-sigma WMAP confidence intervals (marginalized over second order slow-roll). The annotations trace the energy scale at which reheating ends and correspond to $\log(g_*^{1/4} T_{\text{reh}}/\text{GeV})$. The parameter α is varied between $\alpha_{\text{min}}(\beta) < \alpha < 10^6 \alpha_{\text{min}}(\beta)$.

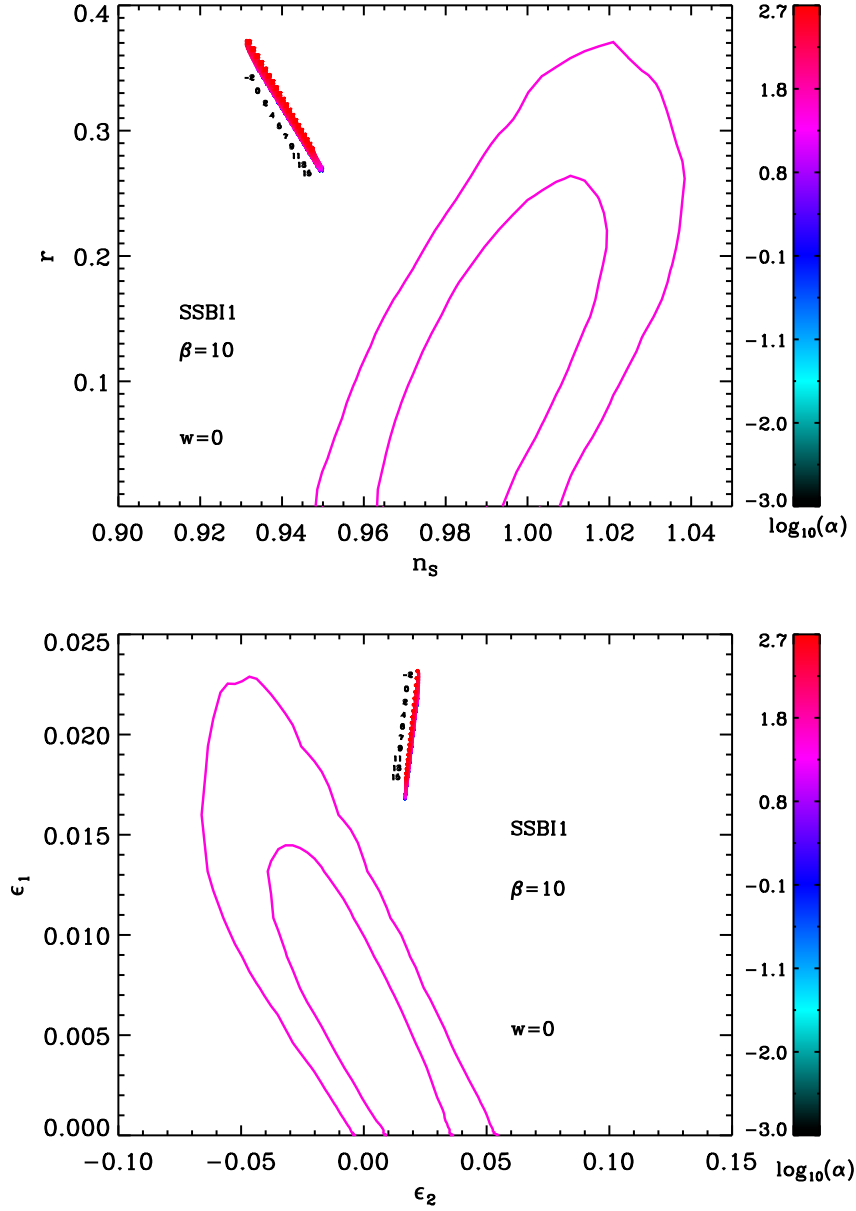


Figure 128. Reheating consistent slow-roll predictions for the spontaneous symmetry breaking 1 inflation ($\alpha > 0, \beta > 0$) models with $\beta = 10$, in the plane (n_s, r) (top panel) and the plane (ϵ_1, ϵ_2) (bottom panel). The two pink solid contours are the one and two-sigma WMAP confidence intervals (marginalized over second order slow-roll). The annotations trace the energy scale at which reheating ends and correspond to $\log(g_*^{1/4} T_{\text{reh}}/\text{GeV})$. The parameter α is varied between $\alpha_{\text{min}}(\beta) < \alpha < 10^6 \alpha_{\text{min}}(\beta)$.

A.38 Spontaneous Symmetry Breaking Inflation 2 (SSBI2)

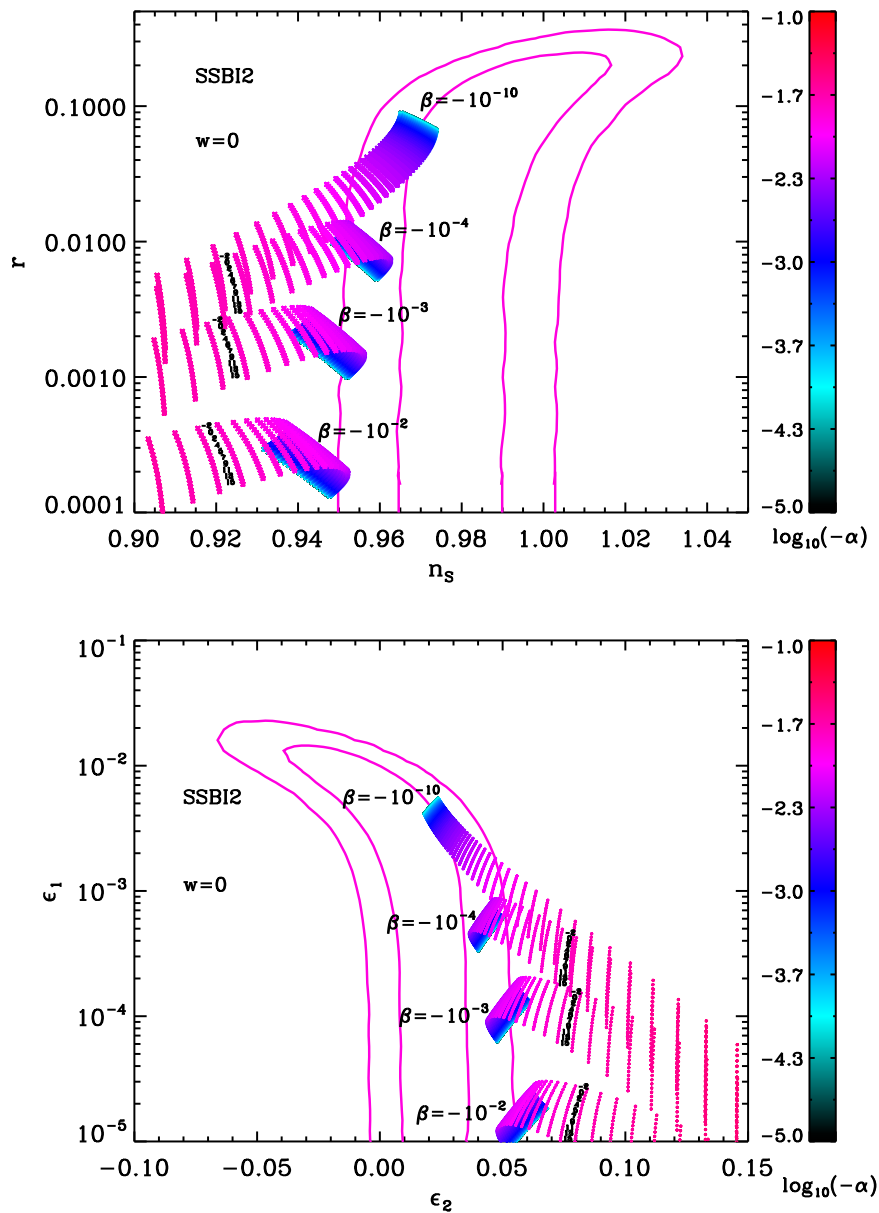


Figure 129. Reheating consistent slow-roll predictions for the spontaneous symmetry breaking 2 inflation ($\alpha < 0, \beta < 0$) models, in the plane (n_s, r) (top panel) and the plane (ϵ_1, ϵ_2) (bottom panel). The two pink solid contours are the one and two-sigma WMAP confidence intervals (marginalized over second order slow-roll). The annotations trace the energy scale at which reheating ends and correspond to $\log(g_*^{1/4} T_{\text{reh}}/\text{GeV})$.

A.39 Spontaneous Symmetry Breaking Inflation 3 (SSBI3)

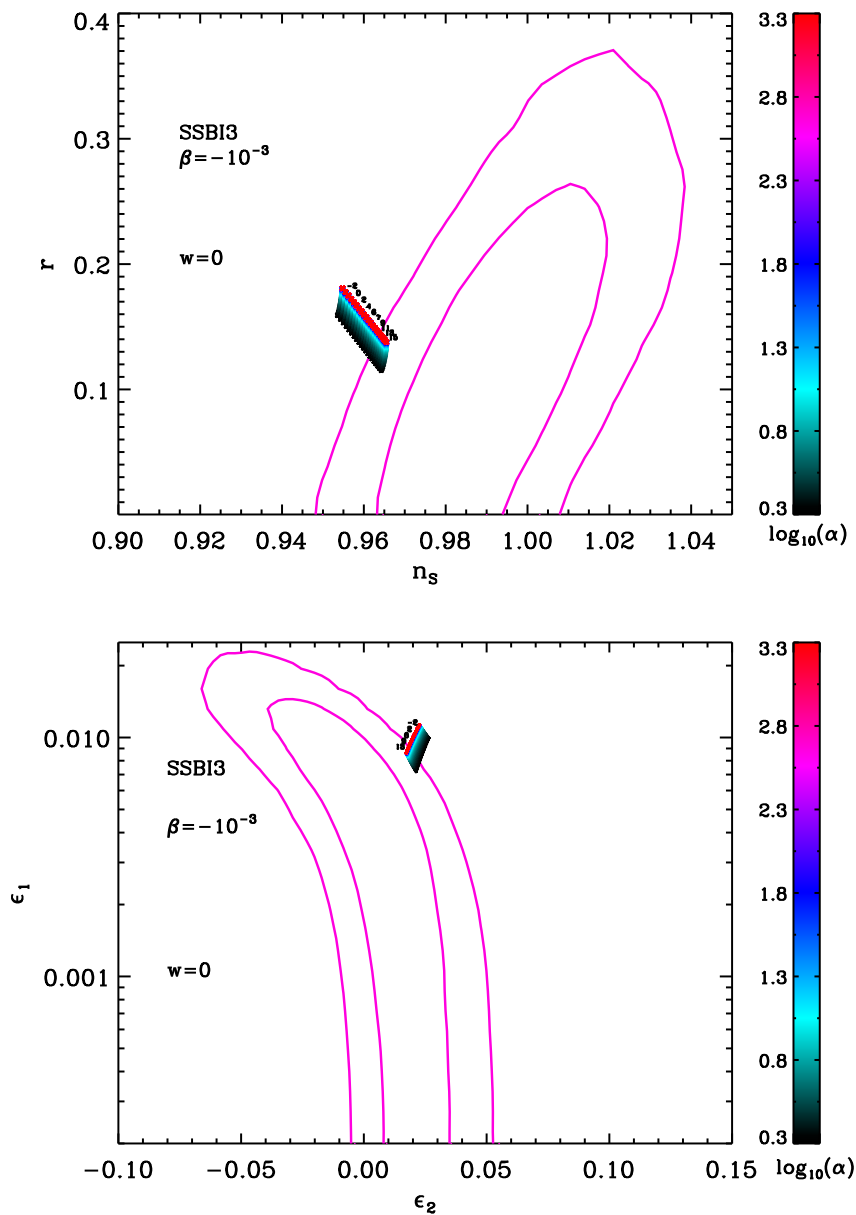


Figure 130. Reheating consistent slow-roll predictions for the spontaneous symmetry breaking 3 inflation [$\alpha > 0, \beta < 0, x^2 < -\alpha/(2\beta)$] models for $\beta = -10^{-3}$, in the plane (n_s, r) (top panel) and the plane (ϵ_1, ϵ_2) (bottom panel). The two pink solid contours are the one and two-sigma WMAP confidence intervals (marginalized over second order slow-roll). The annotations trace the energy scale at which reheating ends and correspond to $\log(g_*^{1/4} T_{\text{reh}}/\text{GeV})$. The parameter α is varied between $\alpha_{\min}(\beta) \simeq 2 < \alpha < 10^3 \alpha_{\min}(\beta)$.

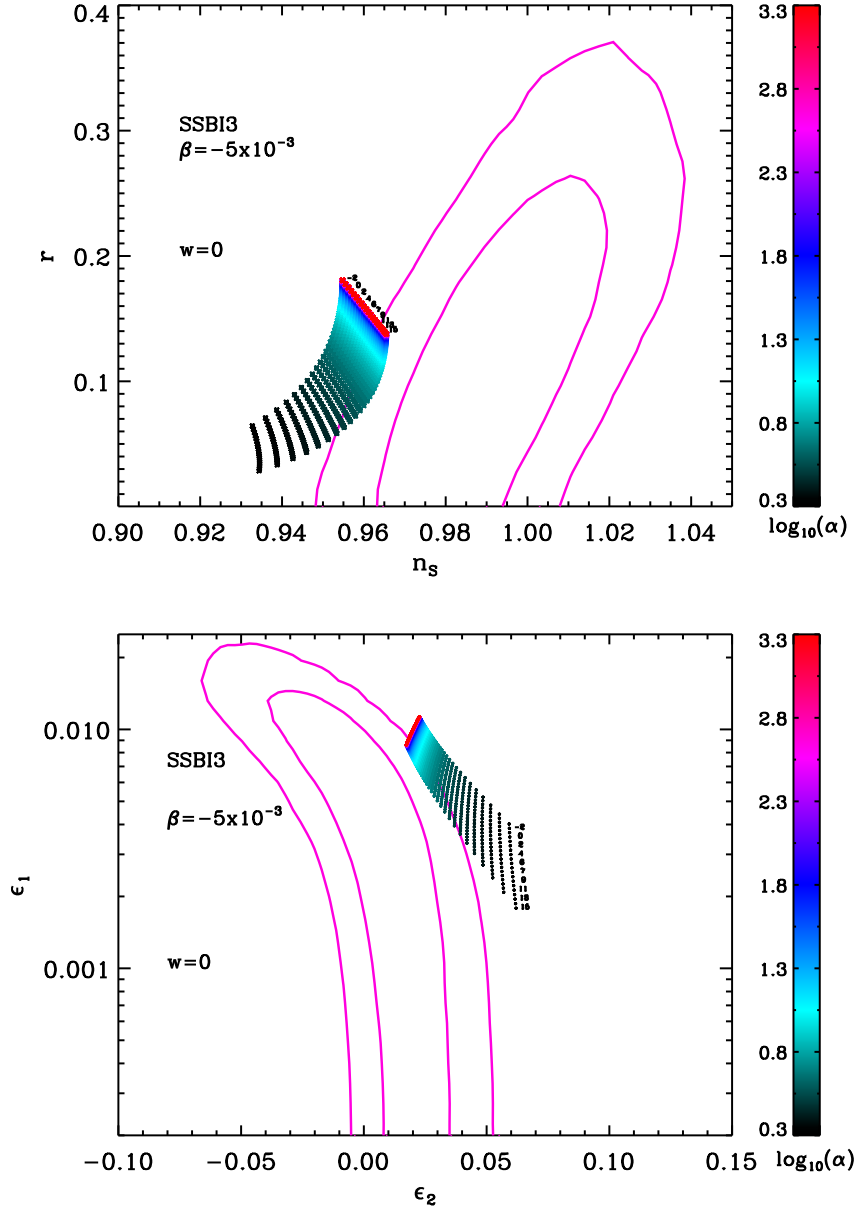


Figure 131. Reheating consistent slow-roll predictions for the spontaneous symmetry breaking 3 inflation [$\alpha > 0, \beta < 0, x^2 < -\alpha/(2\beta)$] models for $\beta = -5 \times 10^{-3}$, in the plane (n_s, r) (top panel) and the plane (ϵ_1, ϵ_2) (bottom panel). The two pink solid contours are the one and two-sigma WMAP confidence intervals (marginalized over second order slow-roll). The annotations trace the energy scale at which reheating ends and correspond to $\log(g_*^{1/4} T_{\text{reh}}/\text{GeV})$. The parameter α is varied between $\alpha_{\text{min}}(\beta) \simeq 2 < \alpha < 10^3 \alpha_{\text{min}}(\beta)$.

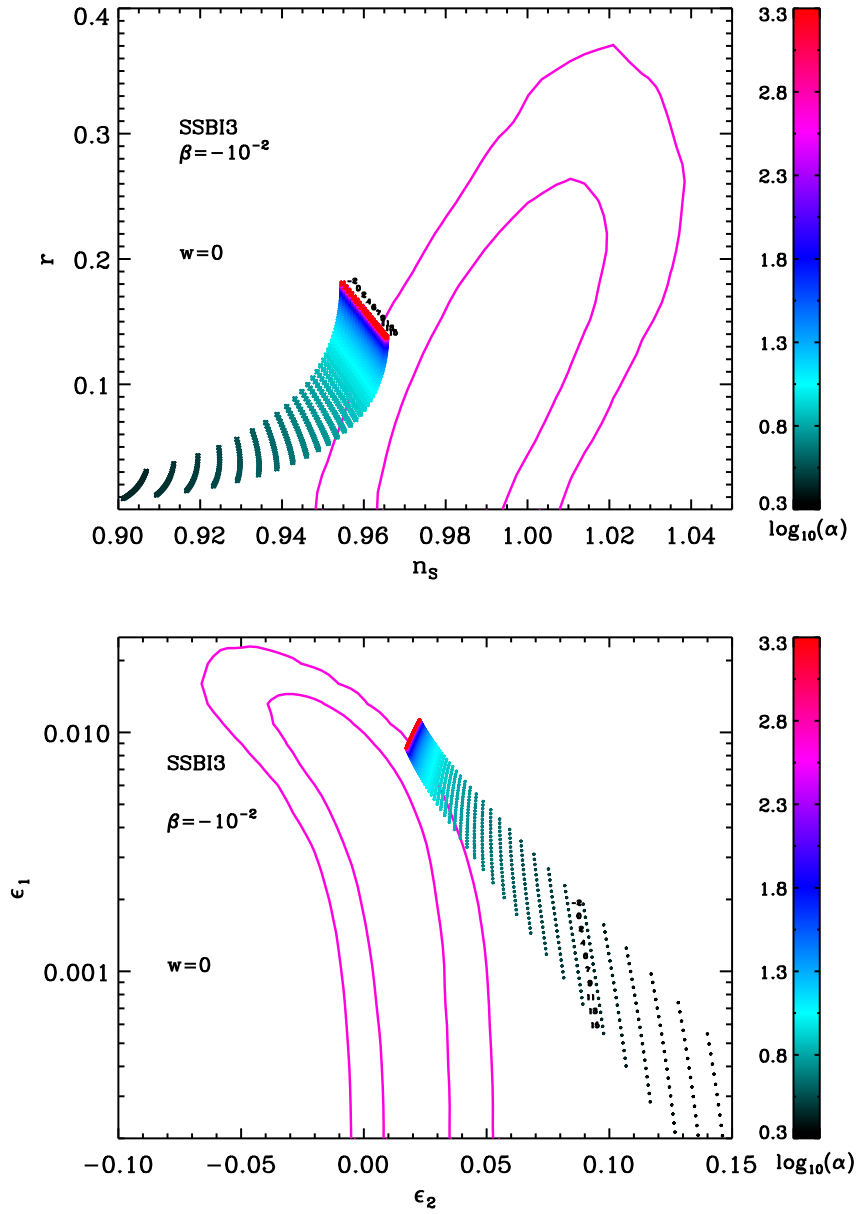


Figure 132. Reheating consistent slow-roll predictions for the spontaneous symmetry breaking 3 inflation [$\alpha > 0, \beta < 0, x^2 < -\alpha/(2\beta)$] models for $\beta = -10^{-2}$, in the plane (n_s, r) (top panel) and the plane (ϵ_1, ϵ_2) (bottom panel). The two pink solid contours are the one and two-sigma WMAP confidence intervals (marginalized over second order slow-roll). The annotations trace the energy scale at which reheating ends and correspond to $\log(g_*^{1/4} T_{\text{reh}}/\text{GeV})$. The parameter α is varied between $\alpha_{\text{min}}(\beta) \simeq 2 < \alpha < 10^3 \alpha_{\text{min}}(\beta)$.

A.40 Spontaneous Symmetry Breaking Inflation 4 (SSBI4)

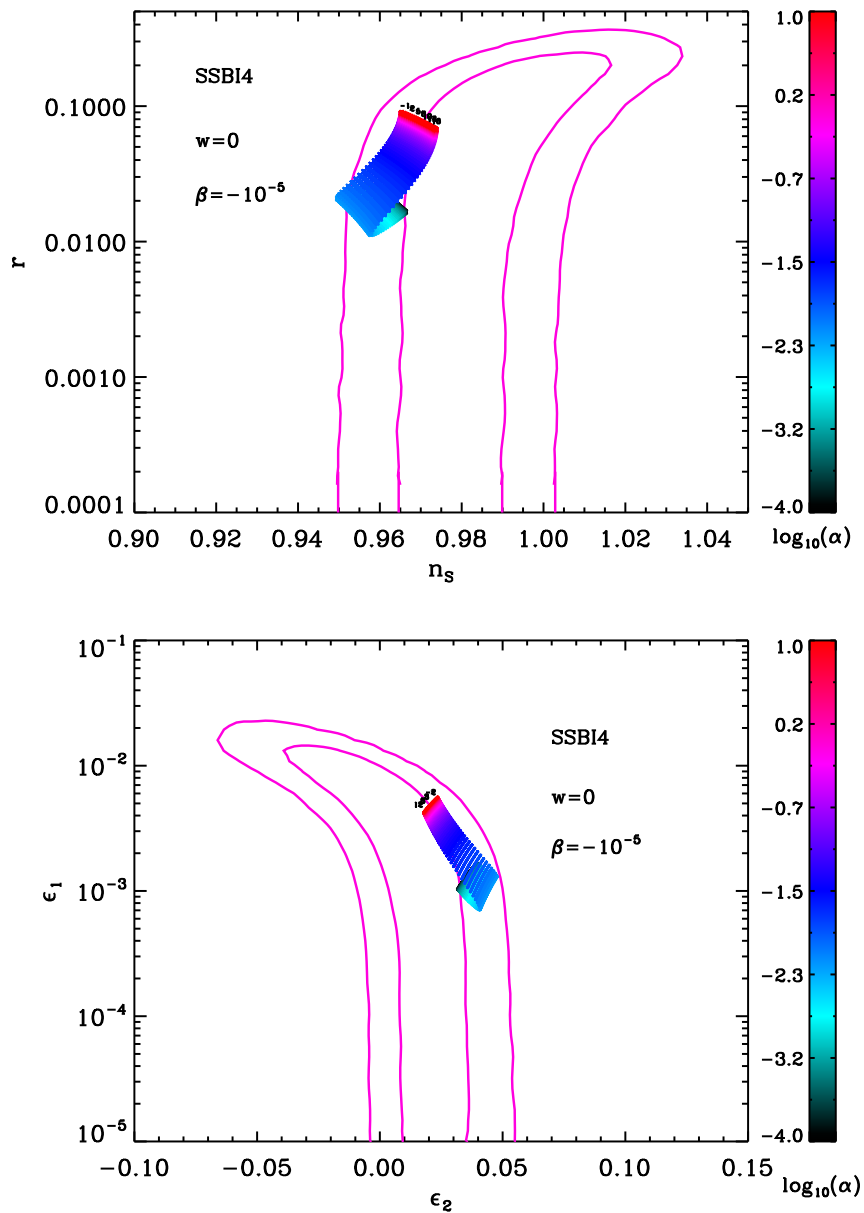


Figure 133. Reheating consistent slow-roll predictions for the spontaneous symmetry breaking 4 inflation [$\alpha > 0, \beta < 0, x^2 > -\alpha/(2\beta)$] models for $\beta = -10^{-5}$, in the plane (n_s, r) (top panel) and the plane (ϵ_1, ϵ_2) (bottom panel). The two pink solid contours are the one and two-sigma WMAP confidence intervals (marginalized over second order slow-roll). The annotations trace the energy scale at which reheating ends and correspond to $\log(g_*^{1/4} T_{\text{reh}}/\text{GeV})$.

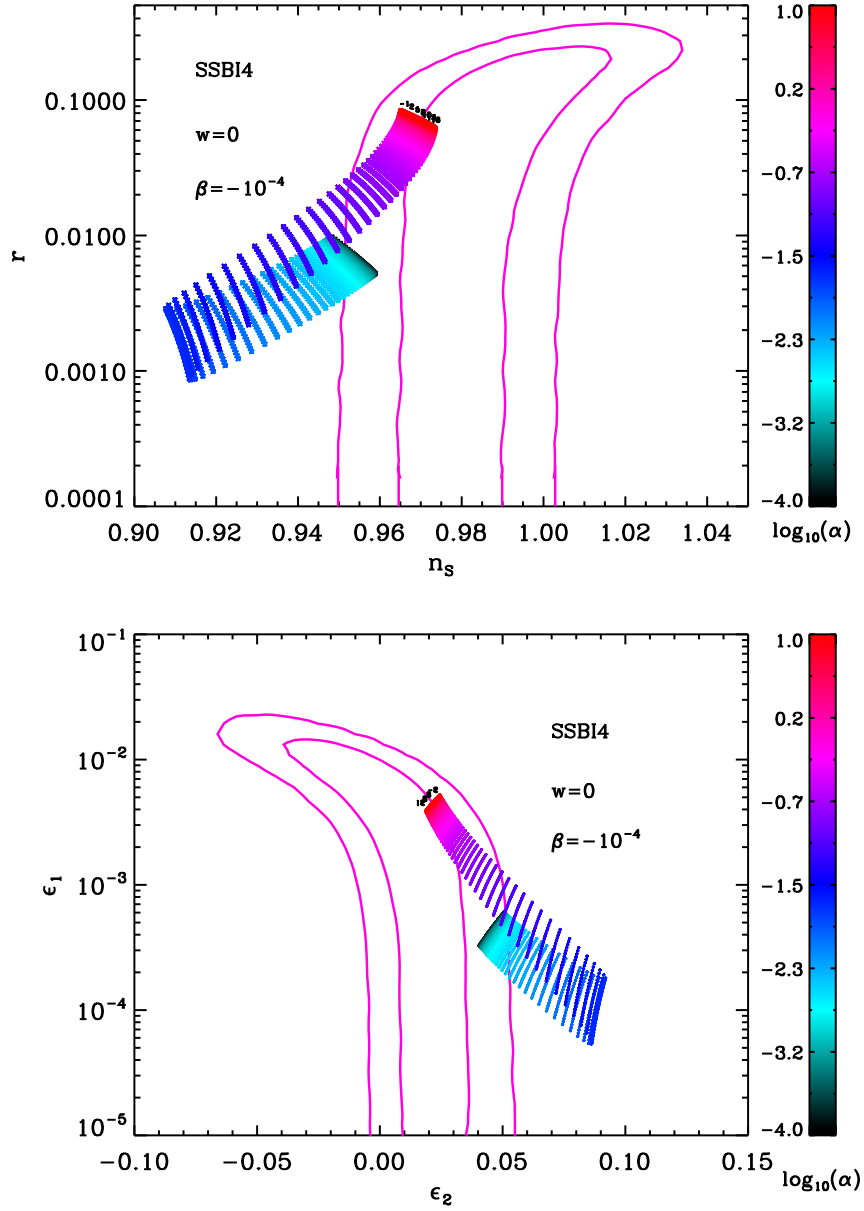


Figure 134. Reheating consistent slow-roll predictions for the spontaneous symmetry breaking 4 inflation [$\alpha > 0, \beta < 0, x^2 > -\alpha/(2\beta)$] models for $\beta = -10^{-4}$, in the plane (n_s, r) (top panel) and the plane (ϵ_1, ϵ_2) (bottom panel). The two pink solid contours are the one and two-sigma WMAP confidence intervals (marginalized over second order slow-roll). The annotations trace the energy scale at which reheating ends and correspond to $\log(g_*^{1/4} T_{\text{reh}}/\text{GeV})$.

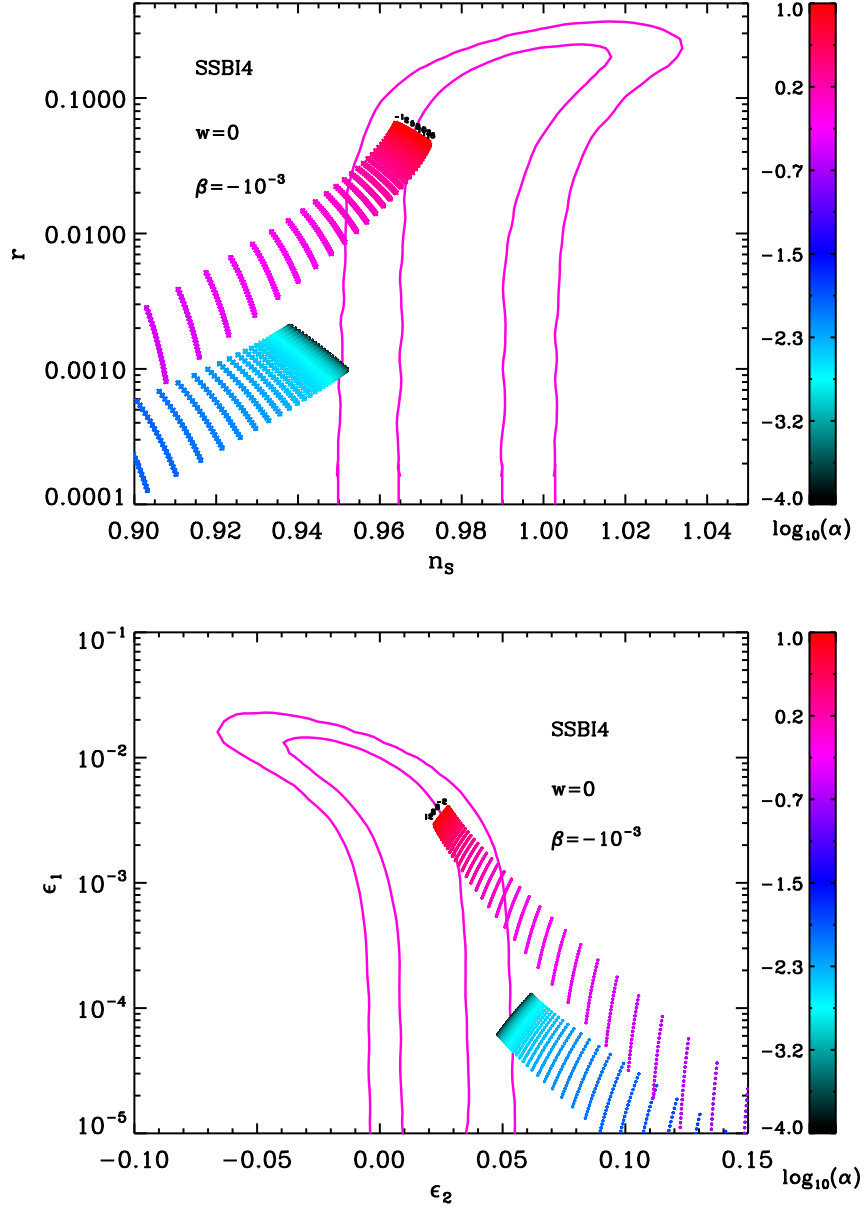


Figure 135. Reheating consistent slow-roll predictions for the spontaneous symmetry breaking 4 inflation [$\alpha > 0, \beta < 0, x^2 > -\alpha/(2\beta)$] models for $\beta = -10^{-3}$, in the plane (n_s, r) (top panel) and the plane (ϵ_1, ϵ_2) (bottom panel). The two pink solid contours are the one and two-sigma WMAP confidence intervals (marginalized over second order slow-roll). The annotations trace the energy scale at which reheating ends and correspond to $\log(g_*^{1/4} T_{\text{reh}}/\text{GeV})$.

A.41 Spontaneous Symmetry Breaking Inflation 5 (SSBI5)

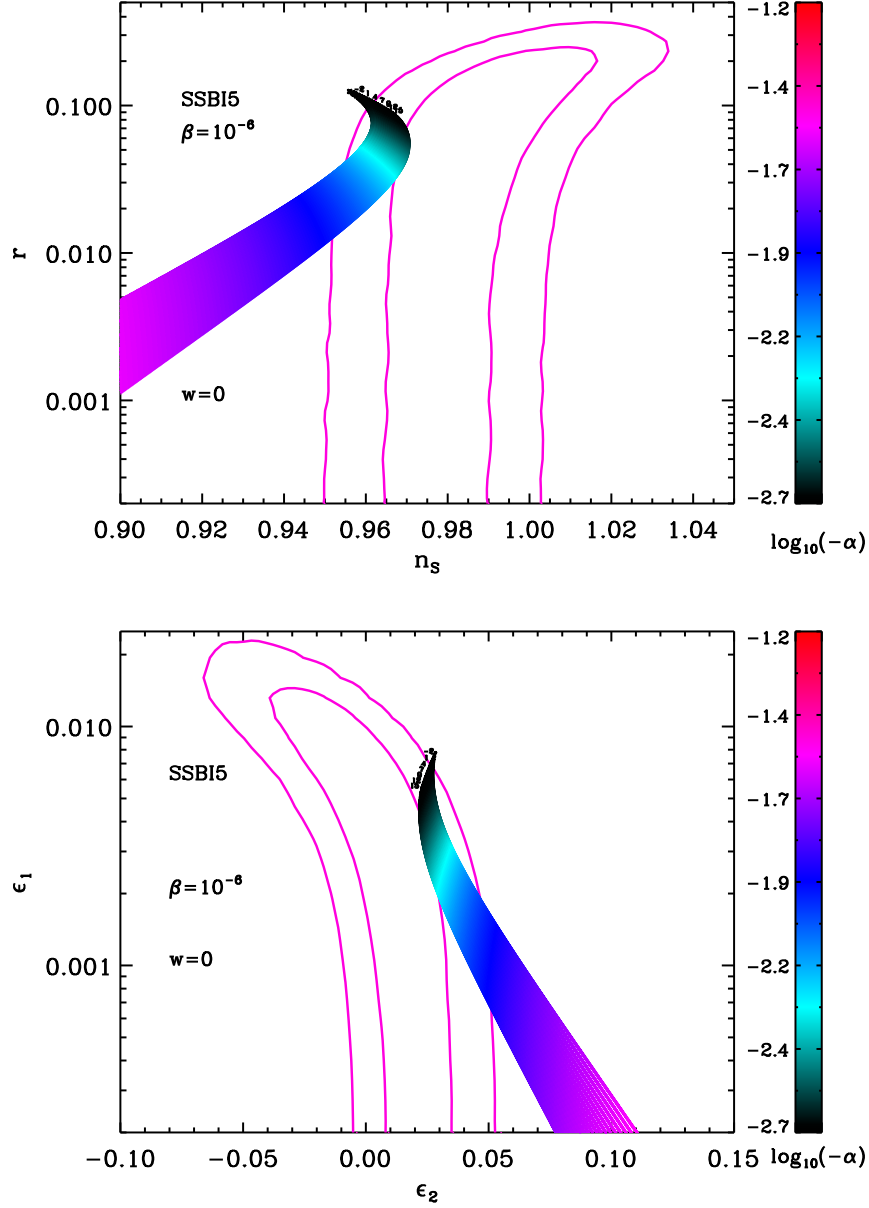


Figure 136. Reheating consistent slow-roll predictions for the spontaneous symmetry breaking 5 inflation [$\alpha < 0, \beta > 0, x^2 < -\alpha/(2\beta)$] models for $\beta = 10^{-6}$, in the plane (n_s, r) (top panel) and the plane (ϵ_1, ϵ_2) (bottom panel). The two pink solid contours are the one and two-sigma WMAP confidence intervals (marginalized over second order slow-roll). The annotations trace the energy scale at which reheating ends and correspond to $\log(g_*^{1/4} T_{\text{reh}}/\text{GeV})$. The parameter α is varied between $|\alpha_{\text{min}}(\beta)| < |\alpha| < 10|\alpha_{\text{min}}(\beta)|$.

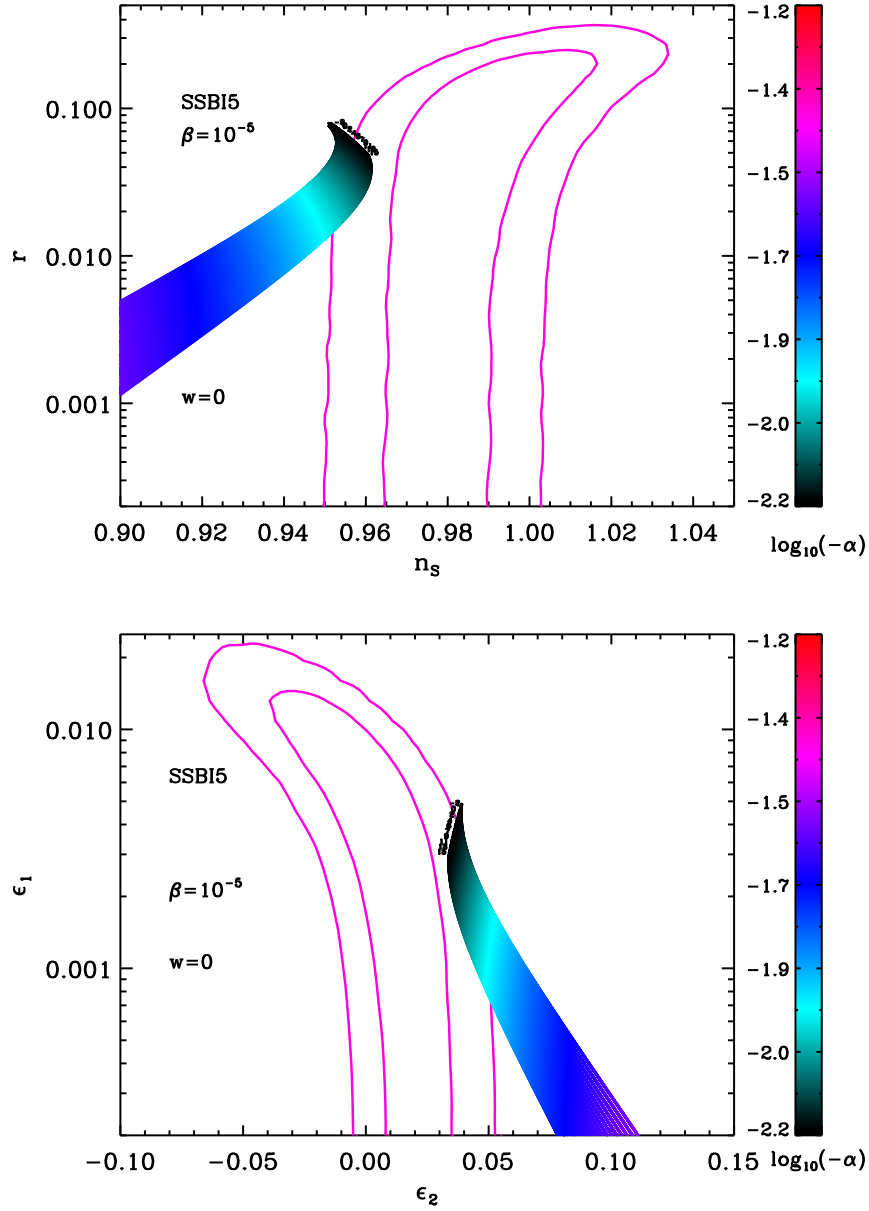


Figure 137. Reheating consistent slow-roll predictions for the spontaneous symmetry breaking 5 inflation [$\alpha < 0, \beta > 0, x^2 < -\alpha/(2\beta)$] models for $\beta = 10^{-5}$, in the plane (n_s, r) (top panel) and the plane (ϵ_1, ϵ_2) (bottom panel). The two pink solid contours are the one and two-sigma WMAP confidence intervals (marginalized over second order slow-roll). The annotations trace the energy scale at which reheating ends and correspond to $\log(g_*^{1/4} T_{\text{reh}}/\text{GeV})$. The parameter α is varied between $|\alpha_{\text{min}}(\beta)| < |\alpha| < 10|\alpha_{\text{min}}(\beta)|$.

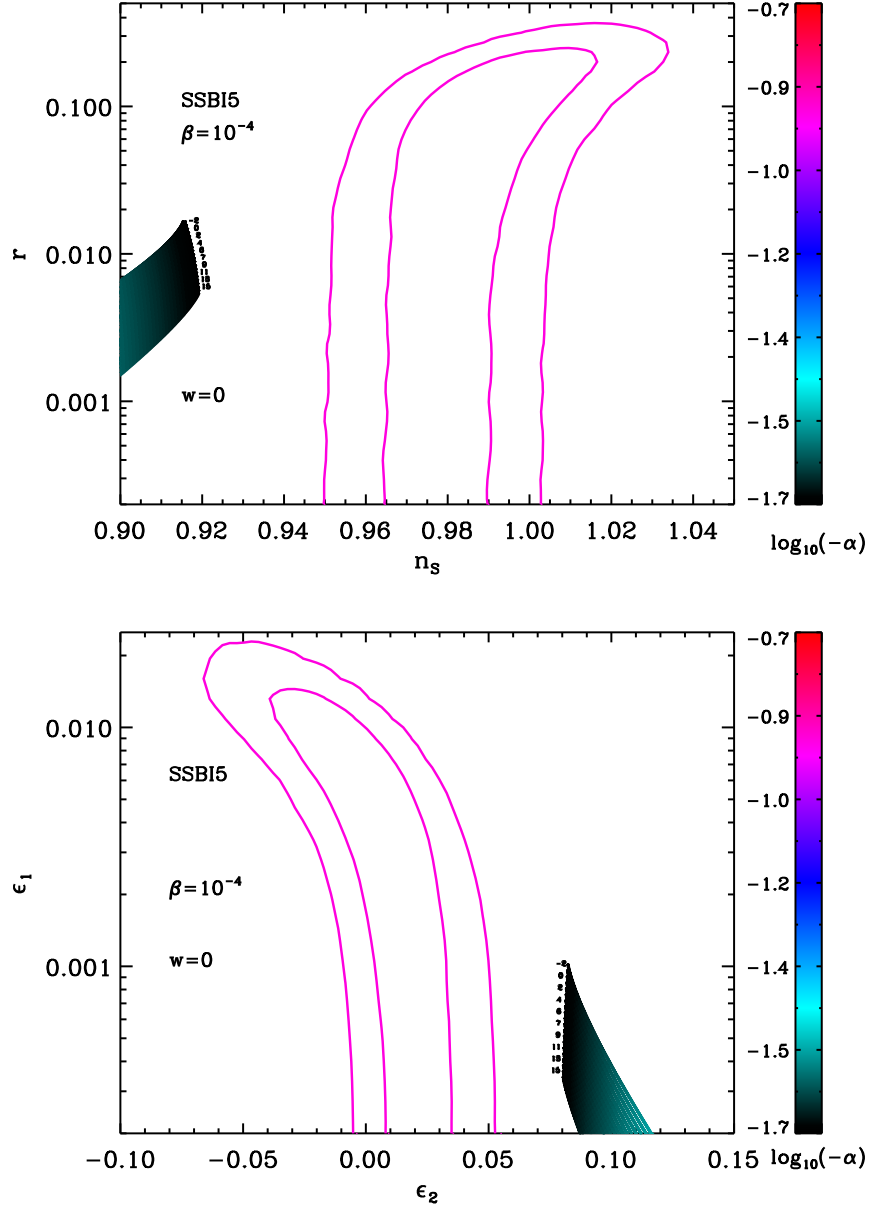


Figure 138. Reheating consistent slow-roll predictions for the spontaneous symmetry breaking 5 inflation [$\alpha < 0, \beta > 0, x^2 < -\alpha/(2\beta)$] models for $\beta = 10^{-4}$, in the plane (n_s, r) (top panel) and the plane (ϵ_1, ϵ_2) (bottom panel). The two pink solid contours are the one and two-sigma WMAP confidence intervals (marginalized over second order slow-roll). The annotations trace the energy scale at which reheating ends and correspond to $\log(g_*^{1/4} T_{\text{reh}}/\text{GeV})$. The parameter α is varied between $|\alpha_{\text{min}}(\beta)| < |\alpha| < 10|\alpha_{\text{min}}(\beta)|$.

A.42 Spontaneous Symmetry Breaking Inflation 6 (SSBI6)

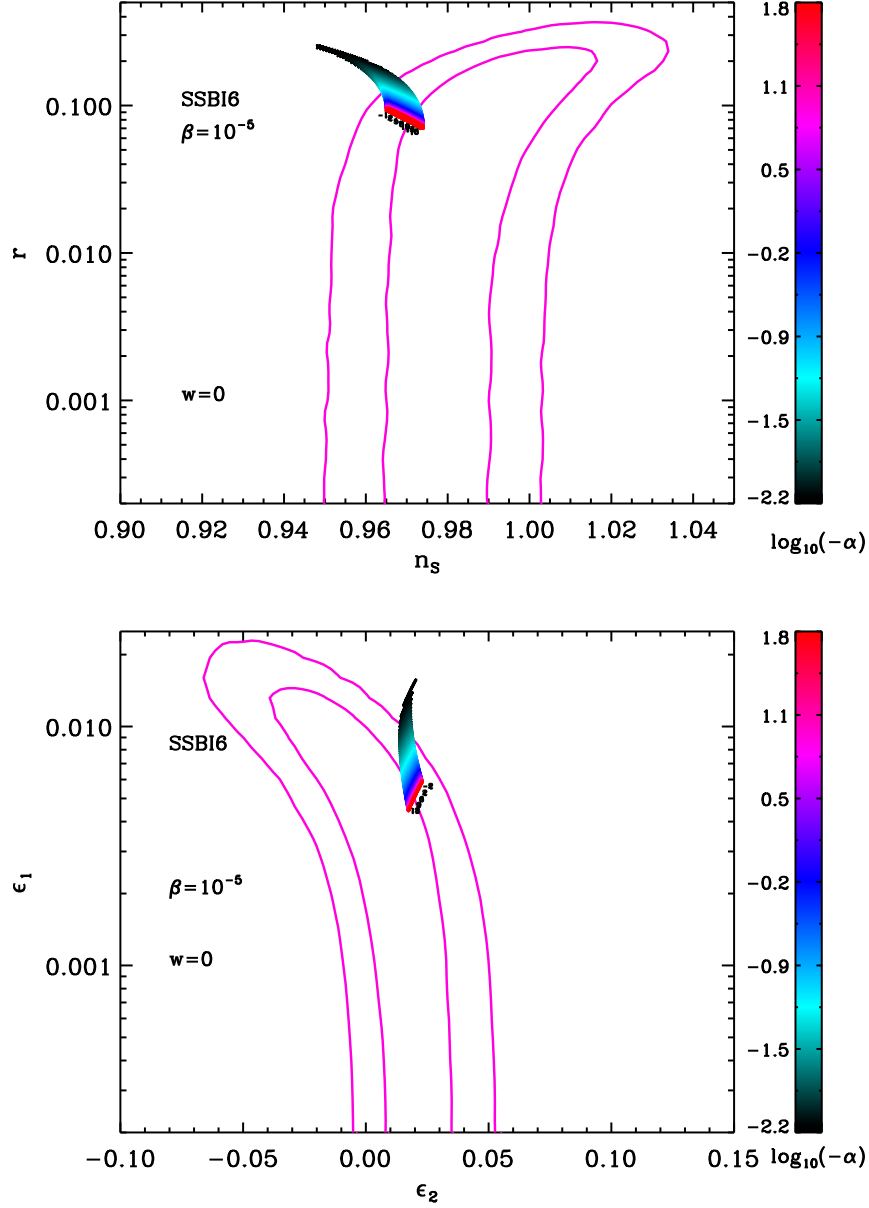


Figure 139. Reheating consistent slow-roll predictions for the spontaneous symmetry breaking 6 inflation [$\alpha < 0, \beta > 0, x^2 > -\alpha/(2\beta)$] models for $\beta = 10^{-5}$, in the plane (n_s, r) (top panel) and the plane (ϵ_1, ϵ_2) (bottom panel). The two pink solid contours are the one and two-sigma WMAP confidence intervals (marginalized over second order slow-roll). The annotations trace the energy scale at which reheating ends and correspond to $\log(g_*^{1/4} T_{\text{reh}}/\text{GeV})$. The parameter α is varied between $|\alpha_{\min}(\beta)| < |\alpha| < 10^4 |\alpha_{\min}(\beta)|$.

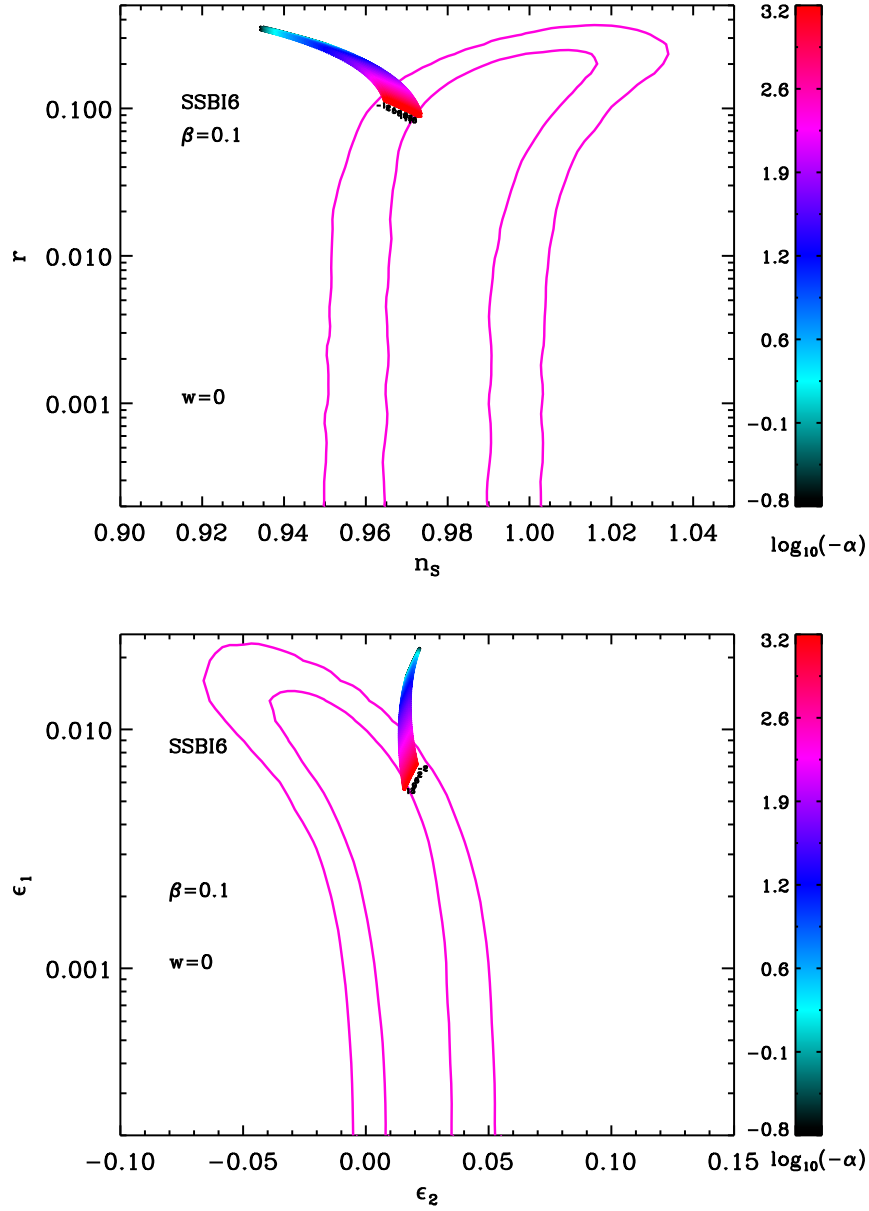


Figure 140. Reheating consistent slow-roll predictions for the spontaneous symmetry breaking 6 inflation [$\alpha < 0, \beta > 0, x^2 > -\alpha/(2\beta)$] models for $\beta = 10^{-1}$, in the plane (n_s, r) (top panel) and the plane (ϵ_1, ϵ_2) (bottom panel). The two pink solid contours are the one and two-sigma WMAP confidence intervals (marginalized over second order slow-roll). The annotations trace the energy scale at which reheating ends and correspond to $\log(g_*^{1/4} T_{\text{reh}}/\text{GeV})$. The parameter α is varied between $|\alpha_{\text{min}}(\beta)| < |\alpha| < 10^4 |\alpha_{\text{min}}(\beta)|$.

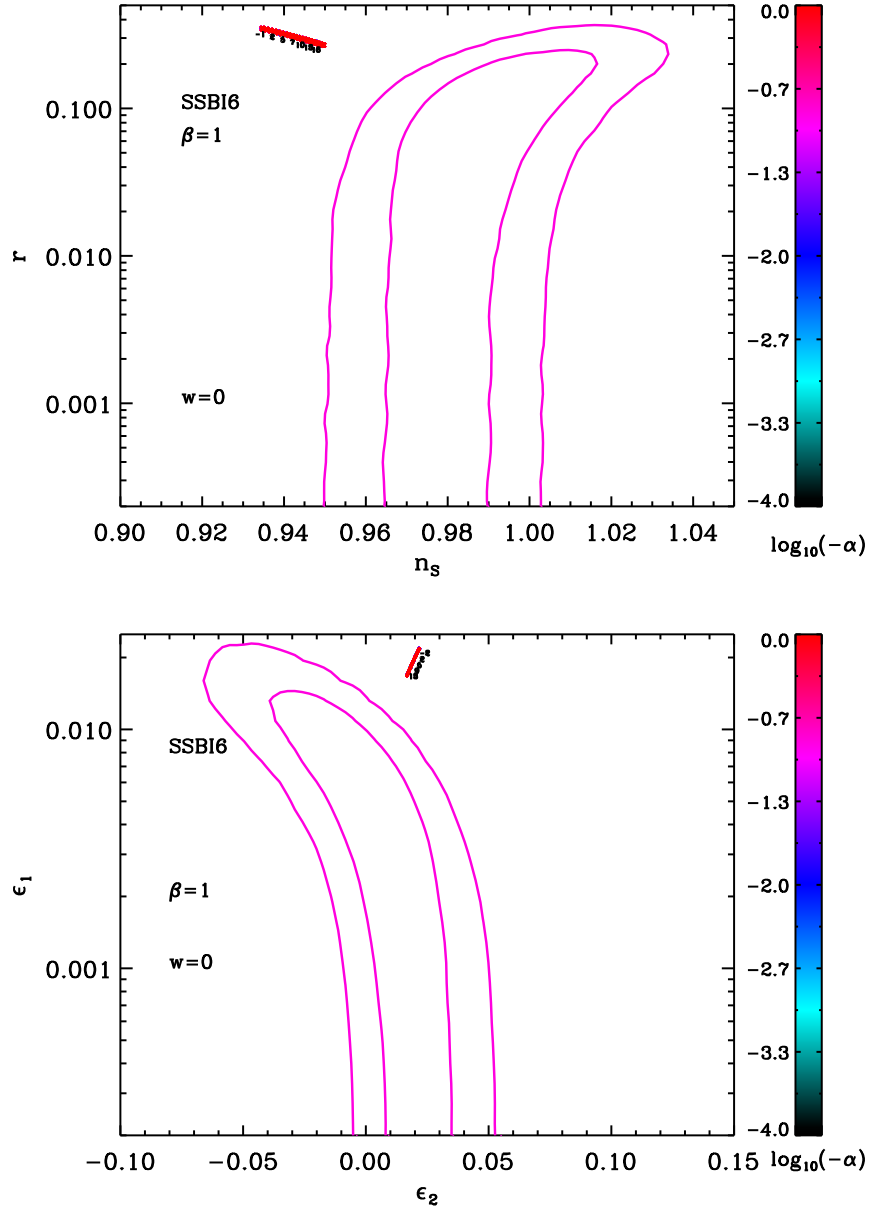


Figure 141. Reheating consistent slow-roll predictions for the spontaneous symmetry breaking 6 inflation [$\alpha < 0, \beta > 0, x^2 > -\alpha/(2\beta)$] models for $\beta = 1$, in the plane (n_s, r) (top panel) and the plane (ϵ_1, ϵ_2) (bottom panel). The two pink solid contours are the one and two-sigma WMAP confidence intervals (marginalized over second order slow-roll). The annotations trace the energy scale at which reheating ends and correspond to $\log(g_*^{1/4} T_{\text{reh}}/\text{GeV})$. The parameter α is varied between $|\alpha_{\min}(\beta)| < |\alpha| < 10^4 |\alpha_{\min}(\beta)|$.

A.43 Running Mass Inflation 1 (RMI1)

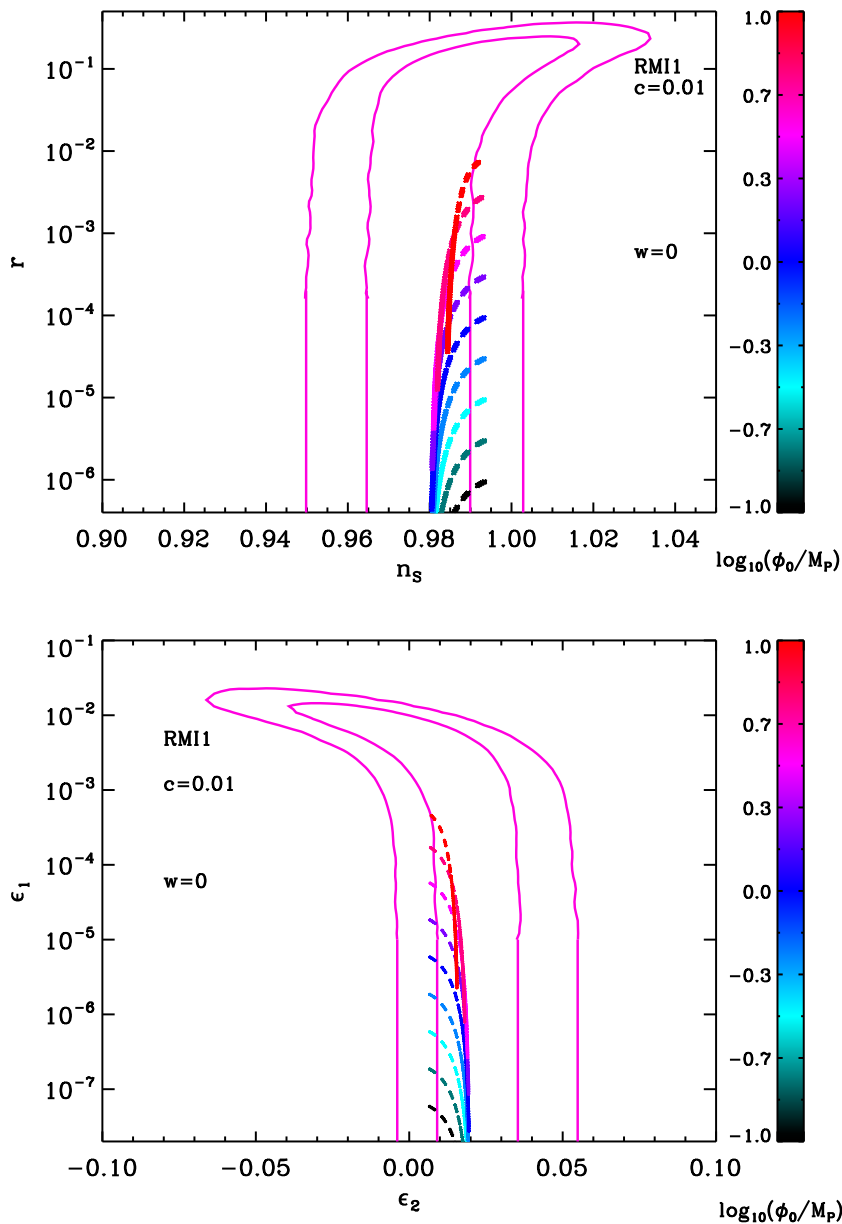


Figure 142. Reheating consistent slow-roll predictions for the running mass inflation 1 models ($c > 0$, $\phi < \phi_0$) with $c = 0.01$, $\phi_0/M_{\text{Pl}} < 1/\sqrt{c}$, $1/e < \phi_{\text{end}}/\phi_0 < 1$, in the plane (n_s, r) (top panel) and the plane (ϵ_1, ϵ_2) (bottom panel). The two pink solid contours are the one and two-sigma WMAP confidence intervals (marginalized over second order slow-roll). The energy scale at which reheating ends and the field vev when inflation stops ϕ_{end} are degenerated, which is the reason why they are not displayed.

A.44 Running Mass Inflation 2 (RMI2)

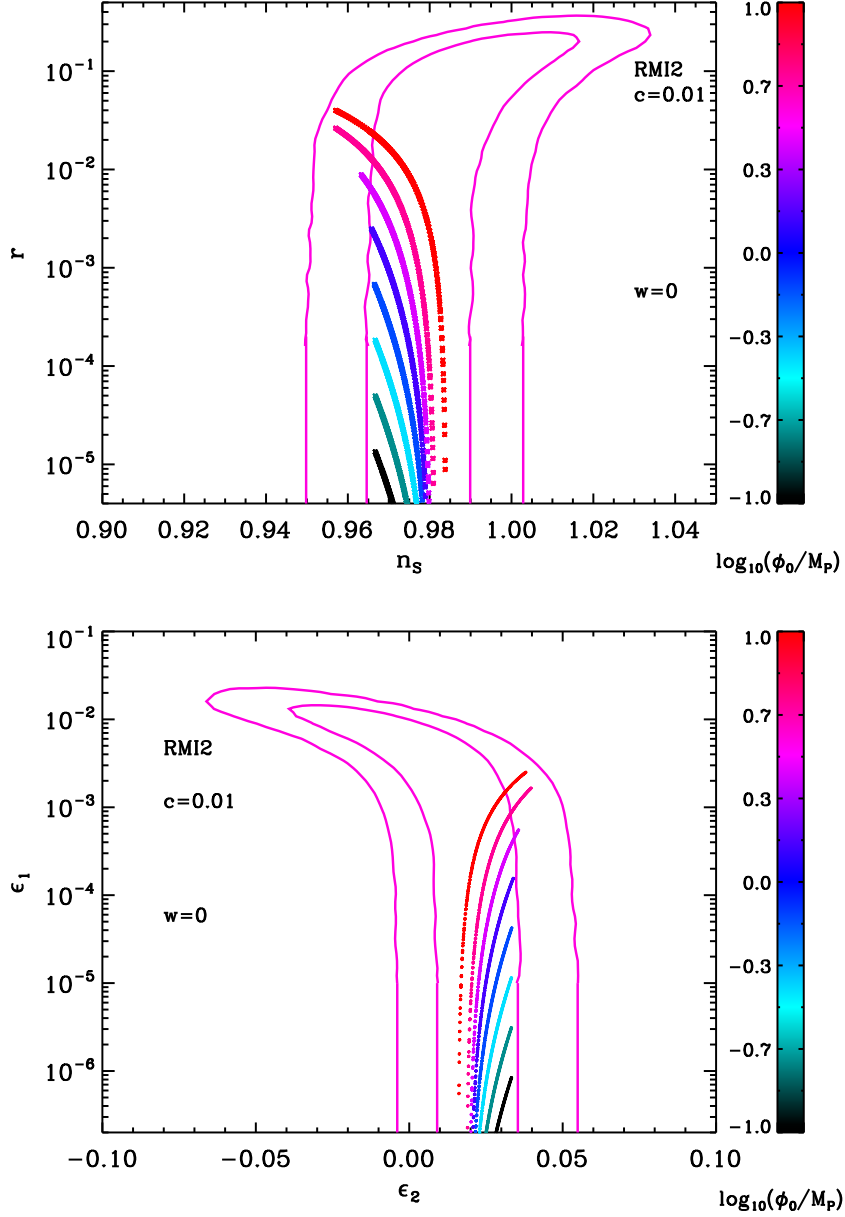


Figure 143. Reheating consistent slow-roll predictions for the running mass inflation 2 models ($c > 0$, $\phi > \phi_0$) with $c = 0.01$, $\phi_0/M_{\text{Pl}} < 1/\sqrt{c}$, $1 < \phi_{\text{end}}/\phi_0 < e$, in the plane (n_s, r) (top panel) and the plane (ϵ_1, ϵ_2) (bottom panel). The two pink solid contours are the one and two-sigma WMAP confidence intervals (marginalized over second order slow-roll). The energy scale at which reheating ends and the field vev when inflation stops ϕ_{end} are degenerated and not represented.

A.45 Running Mass Inflation 3 (RMI3)

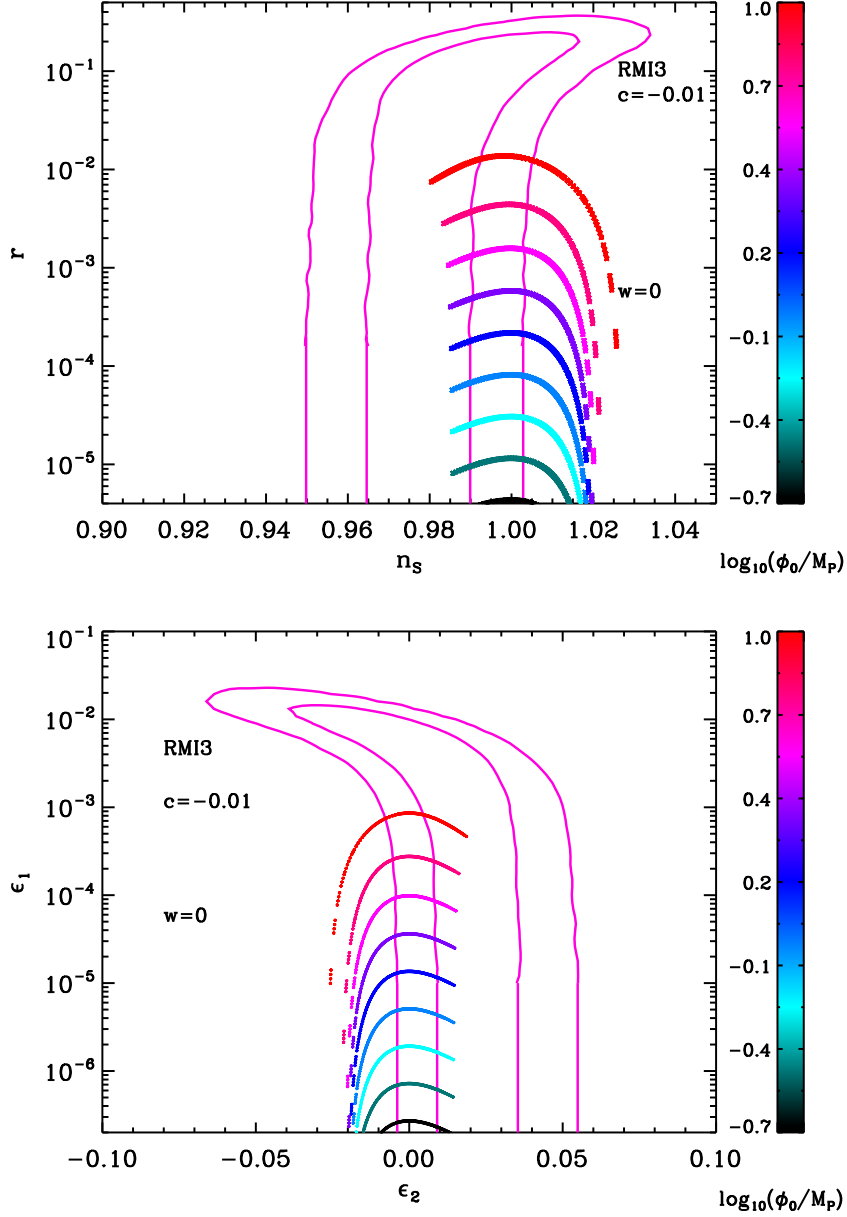


Figure 144. Reheating consistent slow-roll predictions for the running mass inflation 3 models ($c < 0$, $\phi < \phi_0$) with $c = -0.01$, $\phi_0/M_{\text{Pl}} < 1/\sqrt{-c}$, $1/e < \phi_{\text{end}}/\phi_0 < 1$, in the plane (n_s, r) (top panel) and the plane (ϵ_1, ϵ_2) (bottom panel). The two pink solid contours are the one and two-sigma WMAP confidence intervals (marginalized over second order slow-roll). The energy scale at which reheating ends and the field v_{ev} when inflation stops ϕ_{end} are degenerated and have not been represented.

A.46 Running Mass Inflation 4 (RMI4)

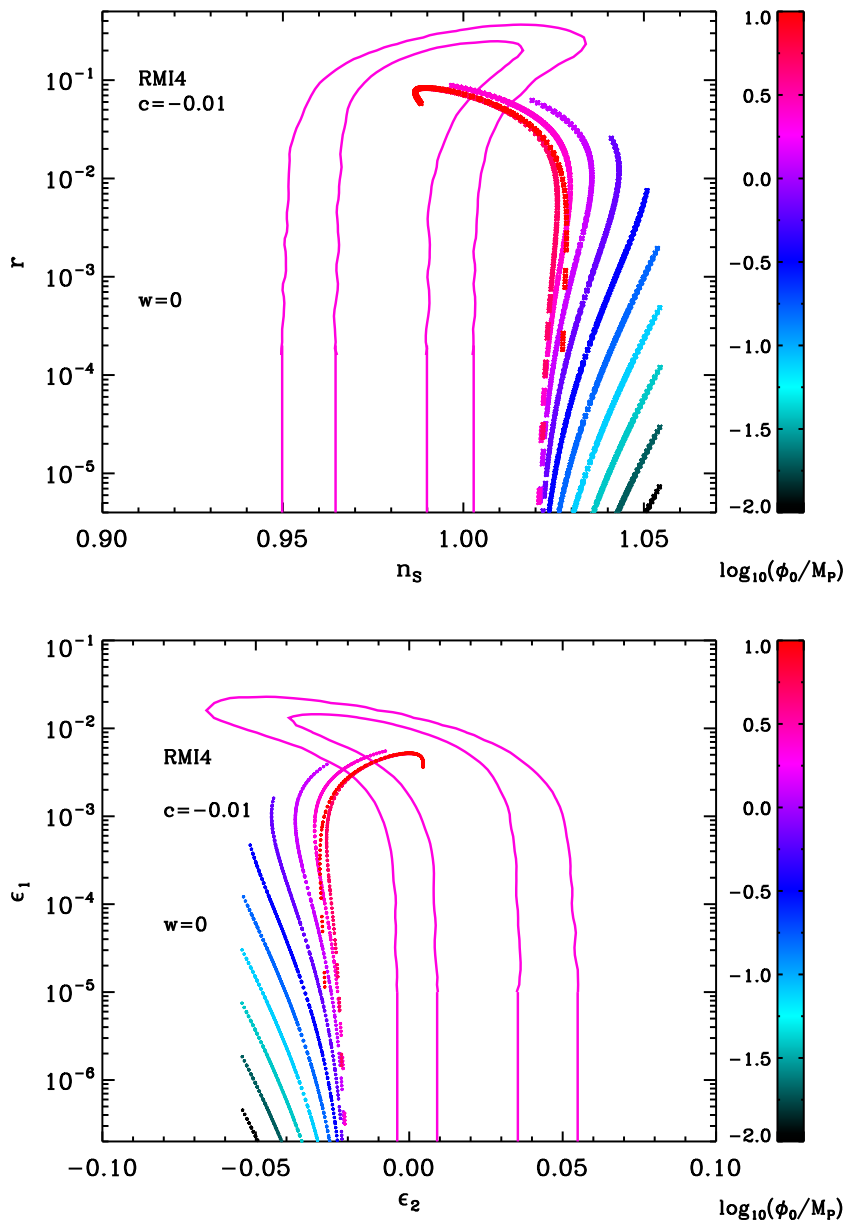


Figure 145. Reheating consistent slow-roll predictions for the running mass inflation 4 models ($c < 0$, $\phi > \phi_0$) with $c = -0.01$, $\phi_0/M_{\text{Pl}} < 1/\sqrt{-c}$, $1 < \phi_{\text{end}}/\phi_0 < e$, in the plane (n_s, r) (top panel) and the plane (ϵ_1, ϵ_2) (bottom panel). The two pink solid contours are the one and two-sigma WMAP confidence intervals (marginalized over second order slow-roll). The energy scale at which reheating ends and the field $v_{\text{ev}} \phi_{\text{end}}$ are degenerated and not displayed.

A.47 Valley Hybrid Inflation (VHI)

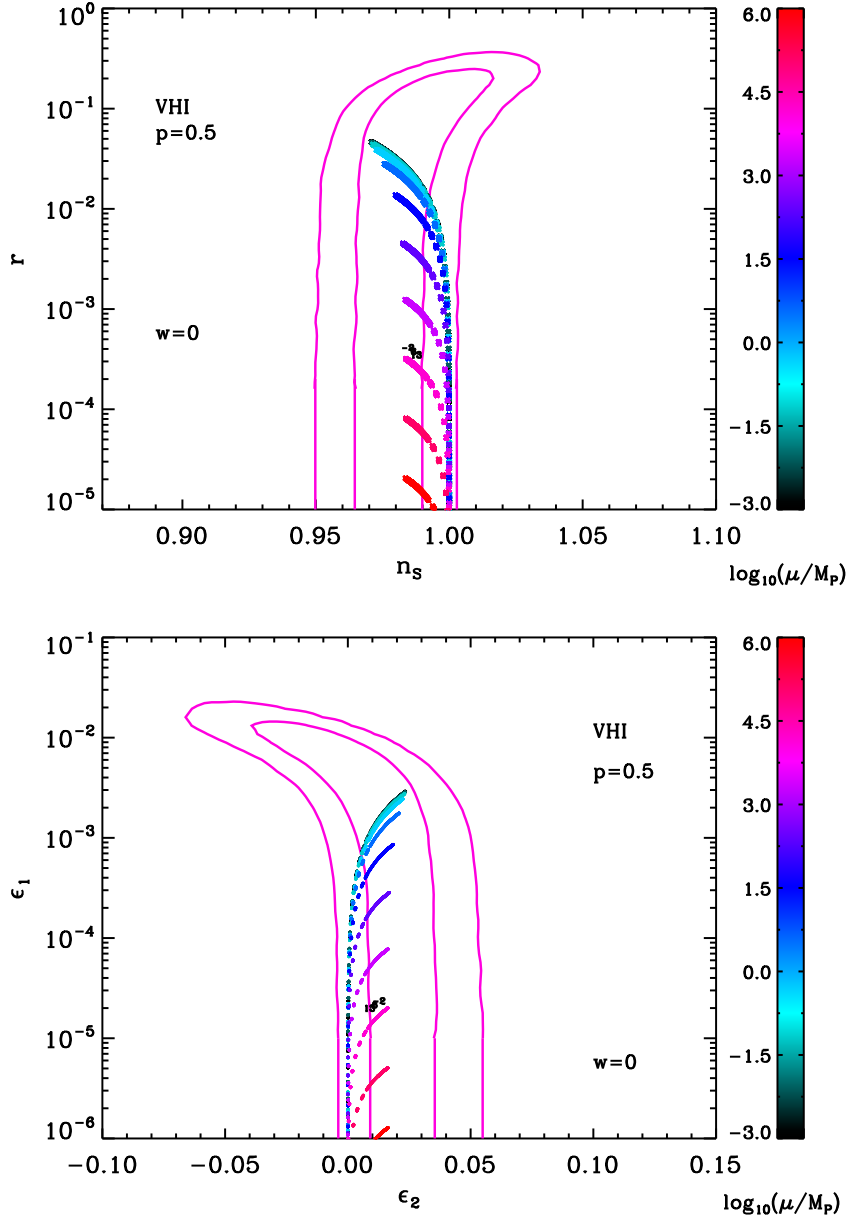


Figure 146. Reheating consistent slow-roll predictions for the valley hybrid inflation models with $p = 0.5$, in the plane (n_s, r) (top panel) and the plane (ϵ_1, ϵ_2) (bottom panel). The two pink solid contours are the one and two-sigma WMAP confidence intervals (marginalized over second order slow-roll). The color of the data points encodes the value of μ , while different data blocks correspond to different values of x_{end} . Inside a given block, the annotations trace the energy scale at which reheating ends and correspond to $\log(g_*^{1/4} T_{\text{reh}}/\text{GeV})$.

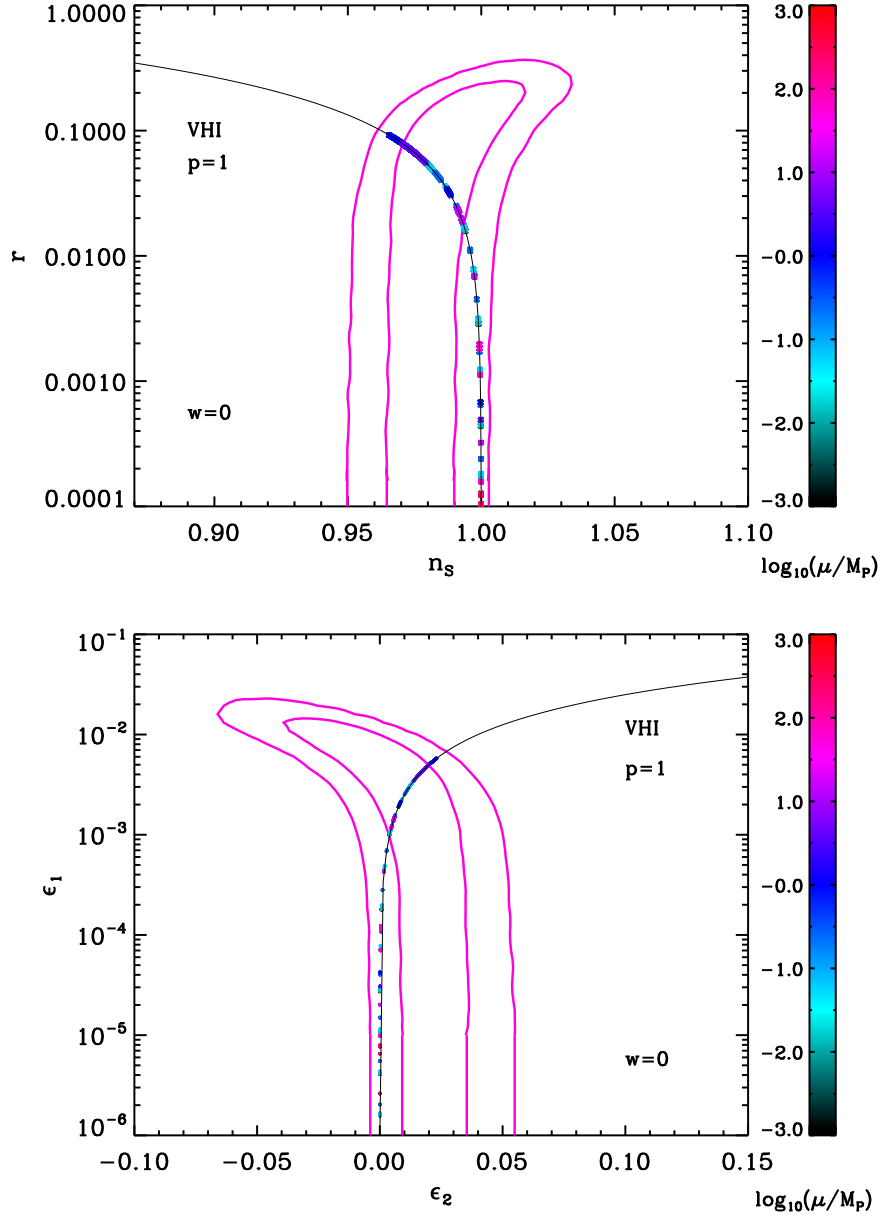


Figure 147. Reheating consistent slow-roll predictions for the valley hybrid inflation models with $p = 1$, in the plane (n_s, r) (top panel) and the plane (ϵ_1, ϵ_2) (bottom panel). The two pink solid contours are the one and two-sigma WMAP confidence intervals (marginalized over second order slow-roll). The color of the data points encodes the value of μ , while different data blocks correspond to different values of x_{end} . Inside a given block, the annotations trace the energy scale at which reheating ends and correspond to $\log(g_*^{1/4} T_{\text{reh}}/\text{GeV})$. The black solid line represent the locus of the points such that $\epsilon_2 = 4\epsilon_1$.

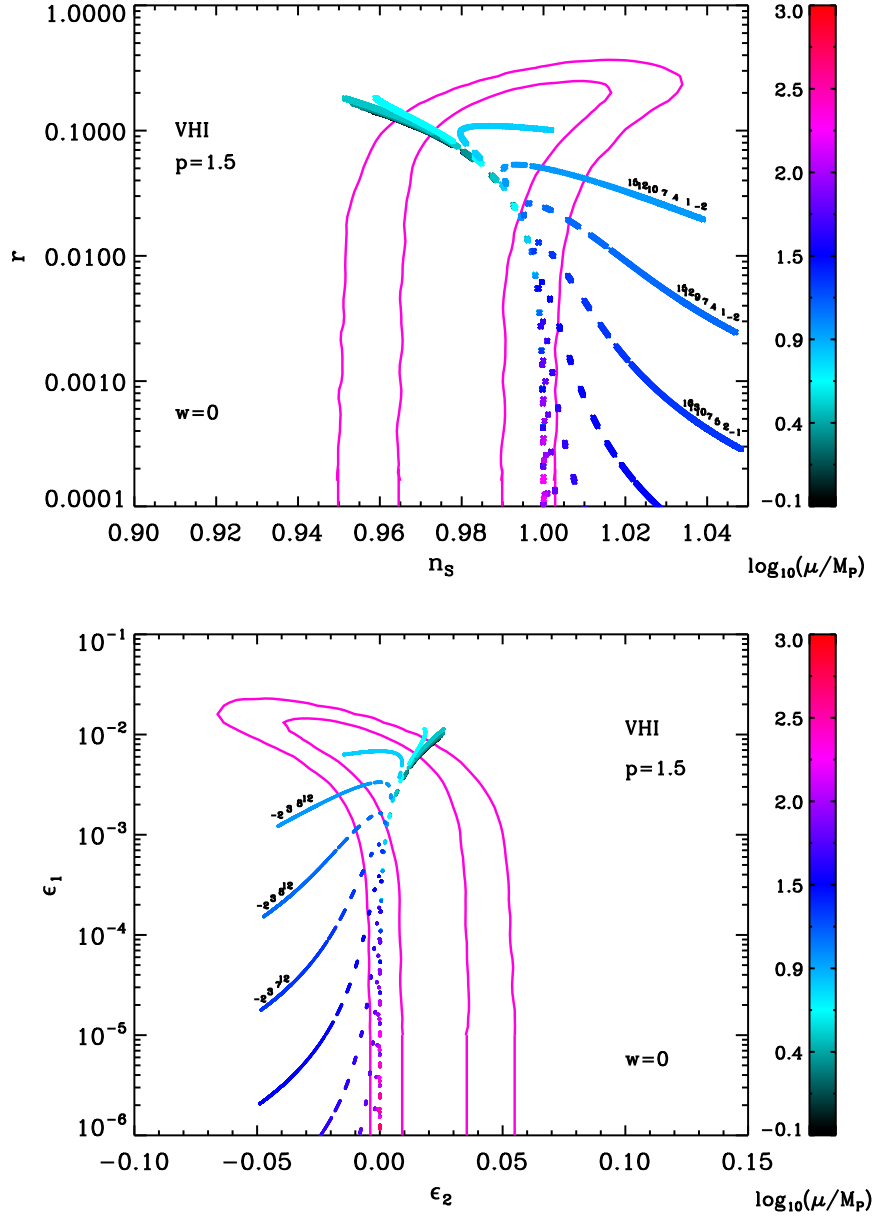


Figure 148. Reheating consistent slow-roll predictions for the valley hybrid inflation models with $p = 1.5$, in the plane (n_s, r) (top panel) and the plane (ϵ_1, ϵ_2) (bottom panel). The two pink solid contours are the one and two-sigma WMAP confidence intervals (marginalized over second order slow-roll). The color of the data points encodes the value of μ , while different data blocks correspond to different values of x_{end} . Inside a given block, the annotations trace the energy scale at which reheating ends and correspond to $\log(g_*^{1/4} T_{\text{reh}}/\text{GeV})$.

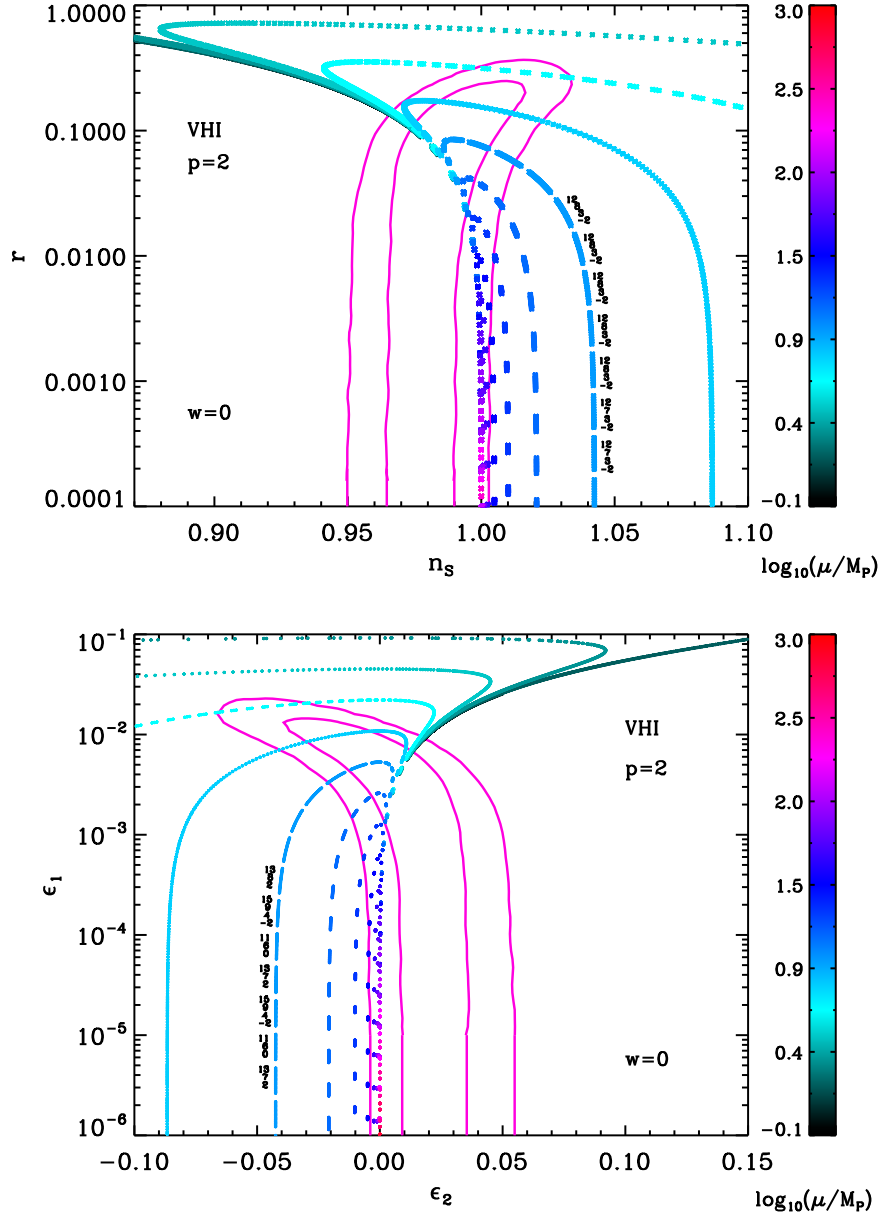


Figure 149. Reheating consistent slow-roll predictions for the valley hybrid inflation models with $p = 2$, in the plane (n_s, r) (top panel) and the plane (ϵ_1, ϵ_2) (bottom panel). The two pink solid contours are the one and two-sigma WMAP confidence intervals (marginalized over second order slow-roll). The color of the data points encodes the value of μ , while different data blocks correspond to different values of x_{end} . Inside a given block, the annotations trace the energy scale at which reheating ends and correspond to $\log(g_*^{1/4} T_{\text{reh}}/\text{GeV})$.

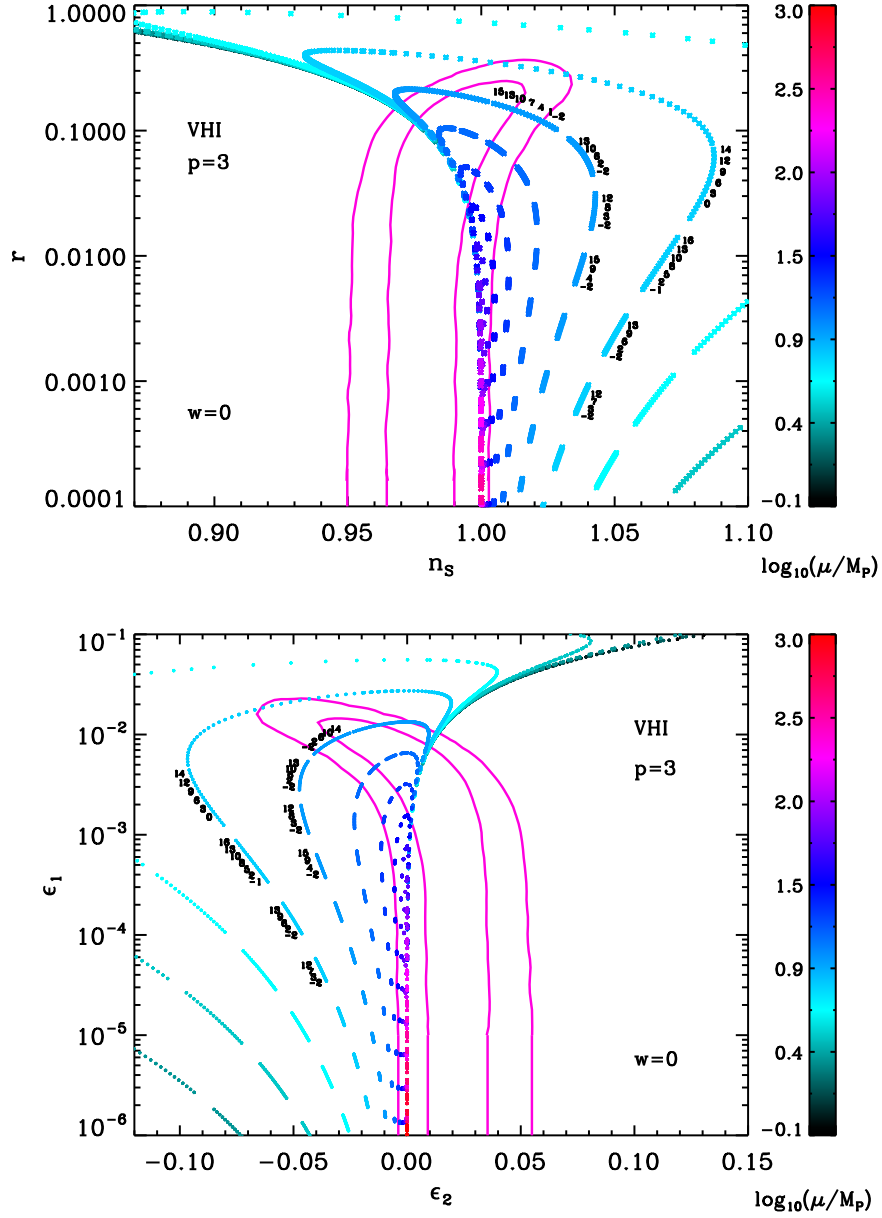


Figure 150. Reheating consistent slow-roll predictions for the valley hybrid inflation models with $p = 3$, in the plane (n_s, r) (top panel) and the plane (ϵ_1, ϵ_2) (bottom panel). The two pink solid contours are the one and two-sigma WMAP confidence intervals (marginalized over second order slow-roll). The color of the data points encodes the value of μ , while different data blocks correspond to different values of x_{end} . Inside a given block, the annotations trace the energy scale at which reheating ends and correspond to $\log(g_*^{1/4} T_{\text{reh}}/\text{GeV})$.

A.48 Dynamical Supersymmetric Inflation (DSI)

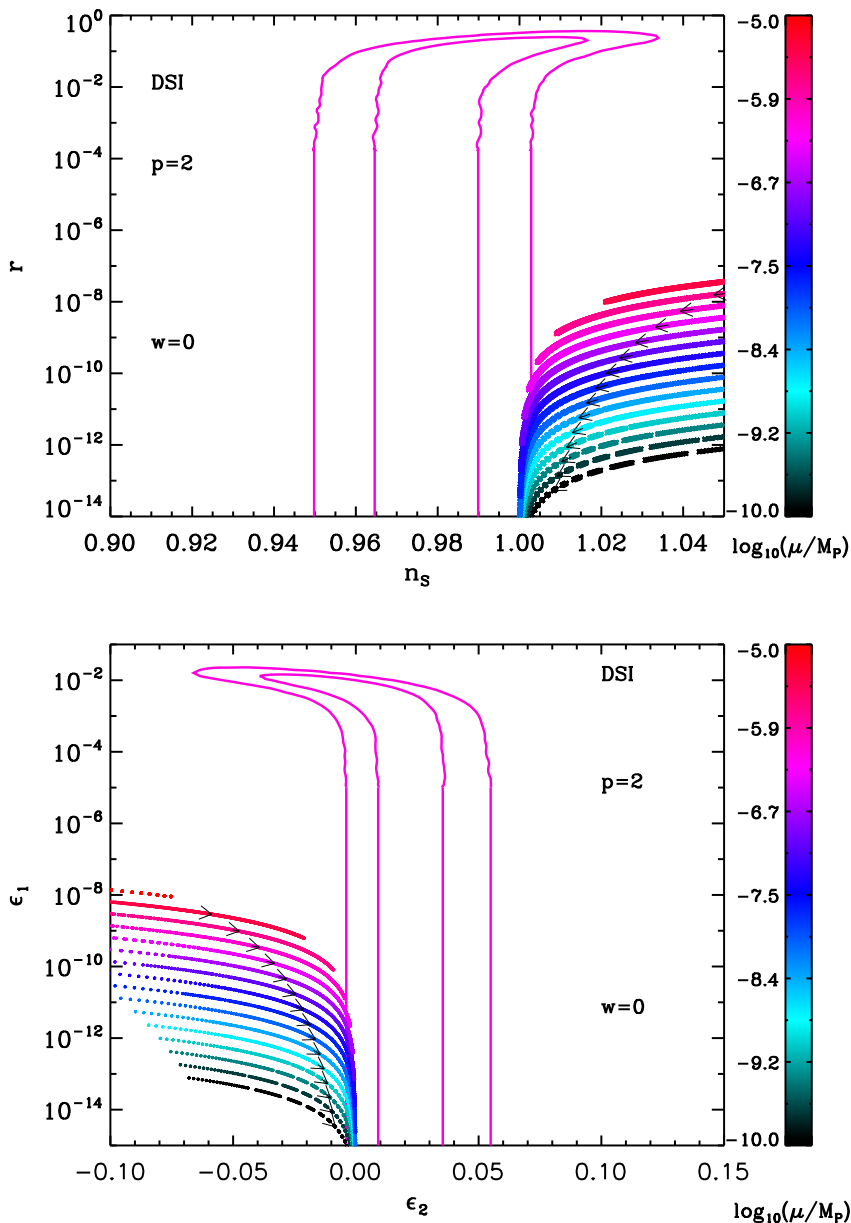


Figure 151. Reheating consistent slow-roll predictions for the dynamical supersymmetric inflation models with $p = 2$, $10^{-10} < \mu/M_{\text{Pl}} < \mu_{\text{max}}/M_{\text{Pl}}$, and $x_{\text{end}}^{\text{min}} < x_{\text{end}} < x_{\text{end}}^{\text{max}}$ in the plane (n_s, r) (top panel) and the plane (ϵ_1, ϵ_2) (bottom panel). The two pink solid contours are the one and two-sigma WMAP confidence intervals (marginalized over second order slow-roll). The parameter x_{end} increases along the direction specified by the arrows, and is degenerate with the energy scale at which reheating ends.

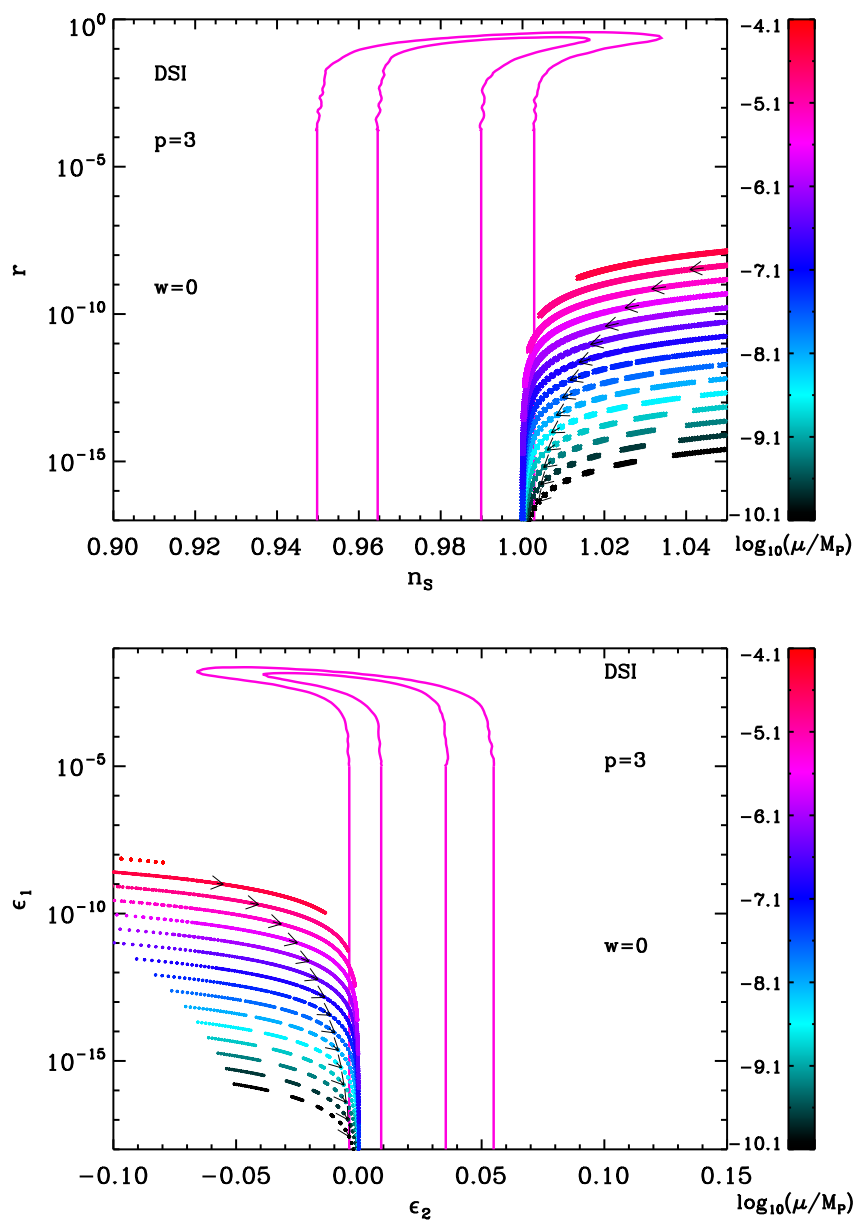


Figure 152. Reheating consistent slow-roll predictions for the dynamical supersymmetric inflation models with $p = 3$, $10^{-10} < \mu/M_{\text{Pl}} < \mu_{\text{max}}/M_{\text{Pl}}$, and $x_{\text{end}}^{\text{min}} < x_{\text{end}} < x_{\text{end}}^{\text{max}}$, in the plane (n_s, r) (top panel) and the plane (ϵ_1, ϵ_2) (bottom panel). The two pink solid contours are the one and two-sigma WMAP confidence intervals (marginalized over second order slow-roll). The parameter x_{end} increases along the direction specified by the arrows, and is degenerated with the energy scale at which reheating ends.

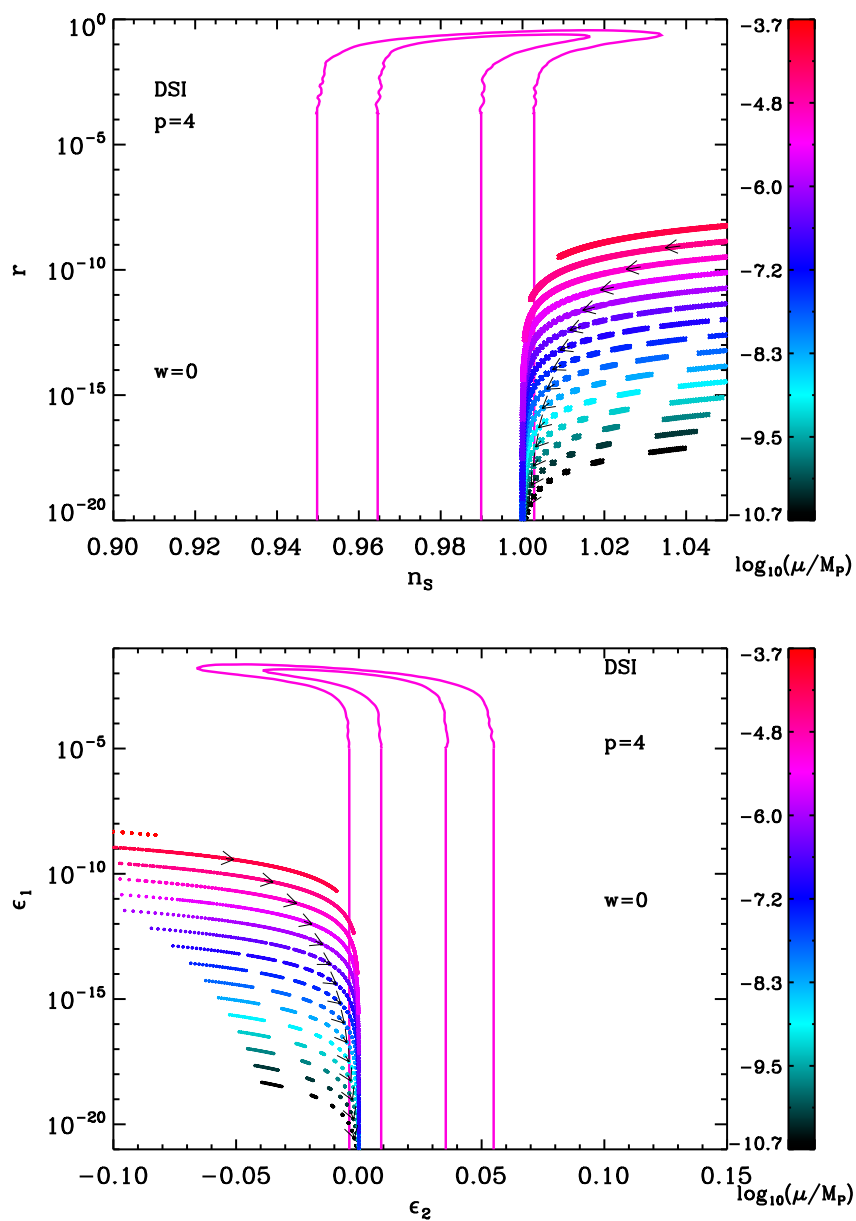


Figure 153. Reheating consistent slow-roll predictions for the dynamical supersymmetric inflation models with $p = 4$, $10^{-10} < \mu/M_{\text{Pl}} < \mu_{\text{max}}/M_{\text{Pl}}$, and the prior $x_{\text{end}}^{\text{min}} < x_{\text{end}} < x_{\text{end}}^{\text{max}}$ in the plane (n_s, r) (top panel) and the plane (ϵ_1, ϵ_2) (bottom panel). The two pink solid contours are the one and two-sigma WMAP confidence intervals (marginalized over second order slow-roll). The parameter x_{end} increases along the direction specified by the arrows and is degenerated with the energy scale at which reheating ends.

A.49 Generalized Mixed Inflation (GMLFI)

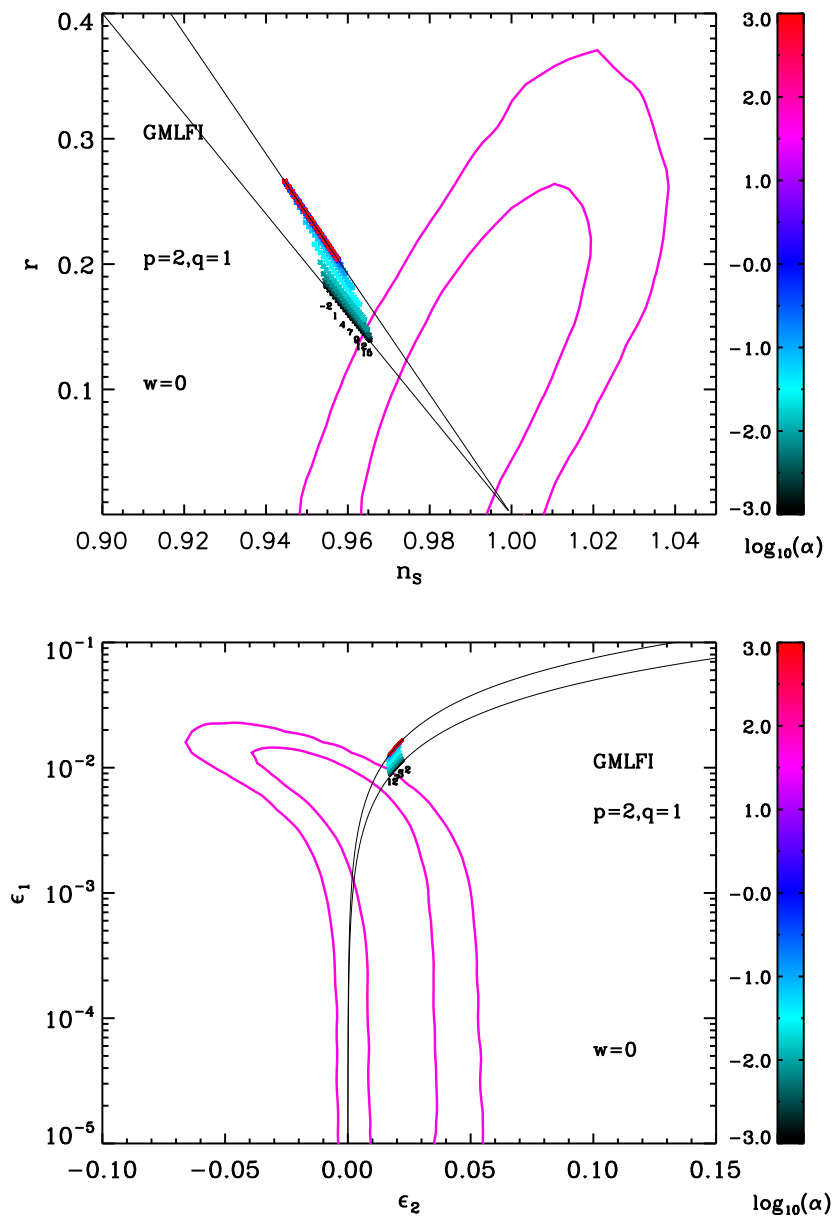


Figure 154. Reheating consistent slow-roll predictions for the generalized mixed inflation models with $p = 2$ and $q = 1$, in the plane (n_s, r) (top panel) and the plane (ϵ_1, ϵ_2) (bottom panel). The two pink solid contours are the one and two-sigma WMAP confidence intervals (marginalized over second order slow-roll). The annotations trace the energy scale at which reheating ends and correspond to $\log(g_*^{1/4} T_{\text{reh}}/\text{GeV})$. The black solid lines represent the locus of the LFI- p and LFI- $p + q$ models (for which $\epsilon_2 = (4/p)\epsilon_1$ and $\epsilon_2 = 4\epsilon_1/(p + q)$ respectively).

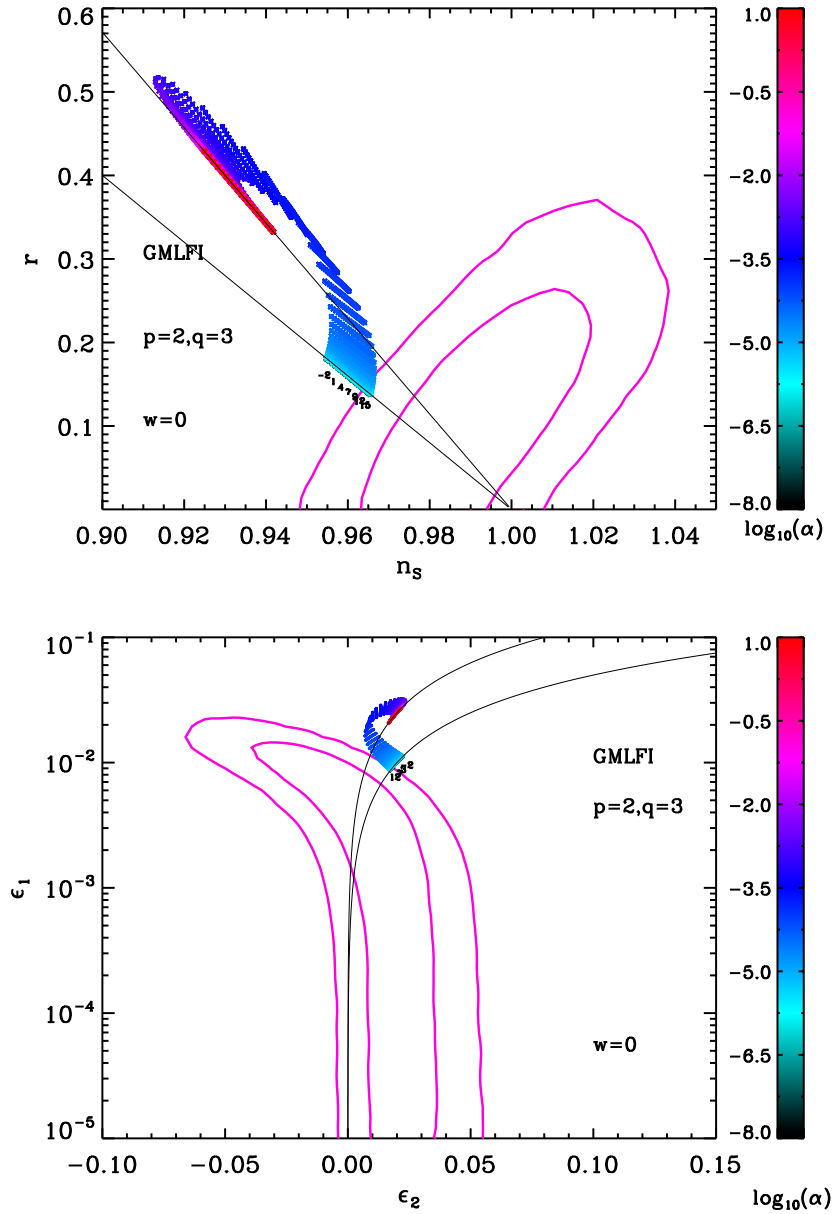


Figure 155. Reheating consistent slow-roll predictions for the generalized mixed inflation models with $p = 2$ and $q = 3$, in the plane (n_s, r) (top panel) and the plane (ϵ_1, ϵ_2) (bottom panel). The two pink solid contours are the one and two-sigma WMAP confidence intervals (marginalized over second order slow-roll). The annotations trace the energy scale at which reheating ends and correspond to $\log(g_*^{1/4} T_{\text{reh}}/\text{GeV})$. The black solid lines represent the locus of the LFI- p and LFI- $p + q$ models (for which $\epsilon_2 = (4/p)\epsilon_1$ and $\epsilon_2 = 4\epsilon_1/(p + q)$ respectively).

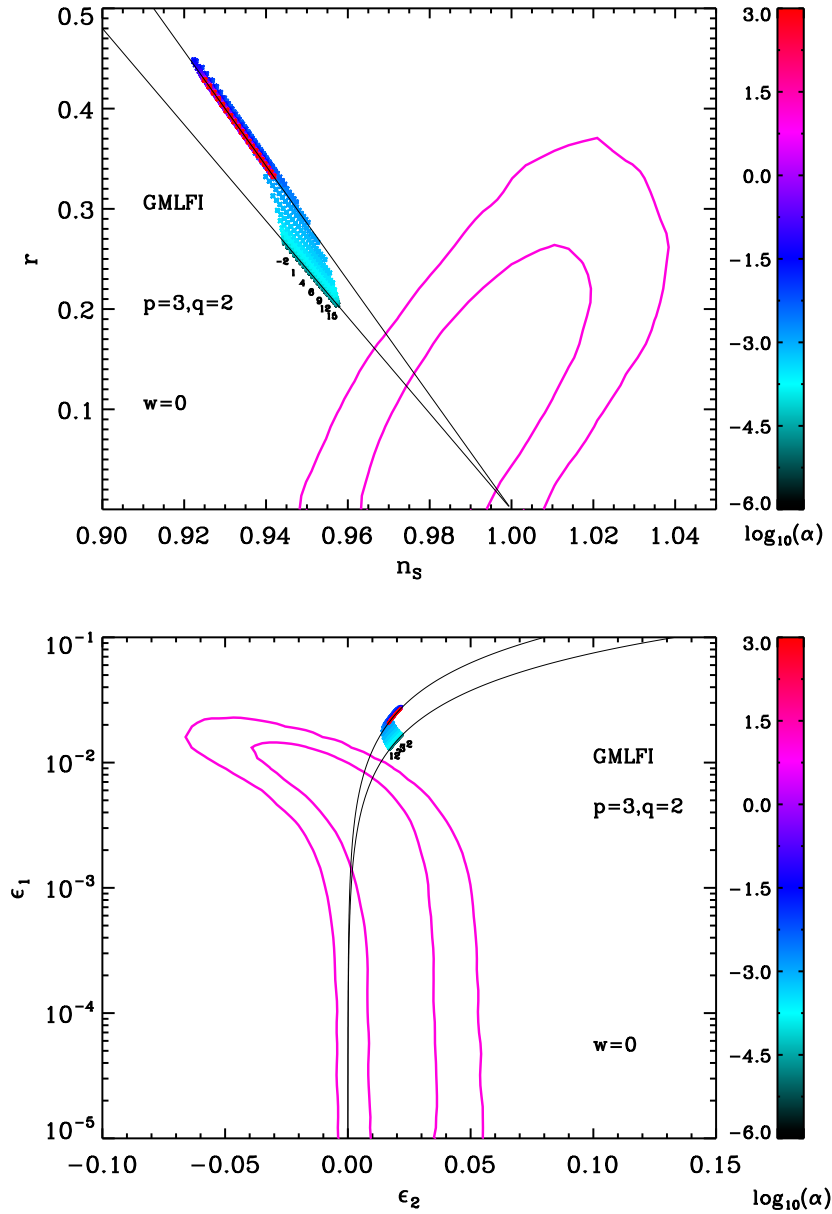


Figure 156. Reheating consistent slow-roll predictions for the generalized mixed inflation models with $p = 3$ and $q = 2$, in the plane (n_s, r) (top panel) and the plane (ϵ_1, ϵ_2) (bottom panel). The two pink solid contours are the one and two-sigma WMAP confidence intervals (marginalized over second order slow-roll). The annotations trace the energy scale at which reheating ends and correspond to $\log(g_*^{1/4} T_{\text{reh}}/\text{GeV})$. The black solid lines represent the locus of the LFI- p and LFI- $p + q$ models (for which $\epsilon_2 = (4/p)\epsilon_1$ and $\epsilon_2 = 4\epsilon_1/(p + q)$ respectively).

A.50 Logarithmic Potential Inflation 1 (LPI1)

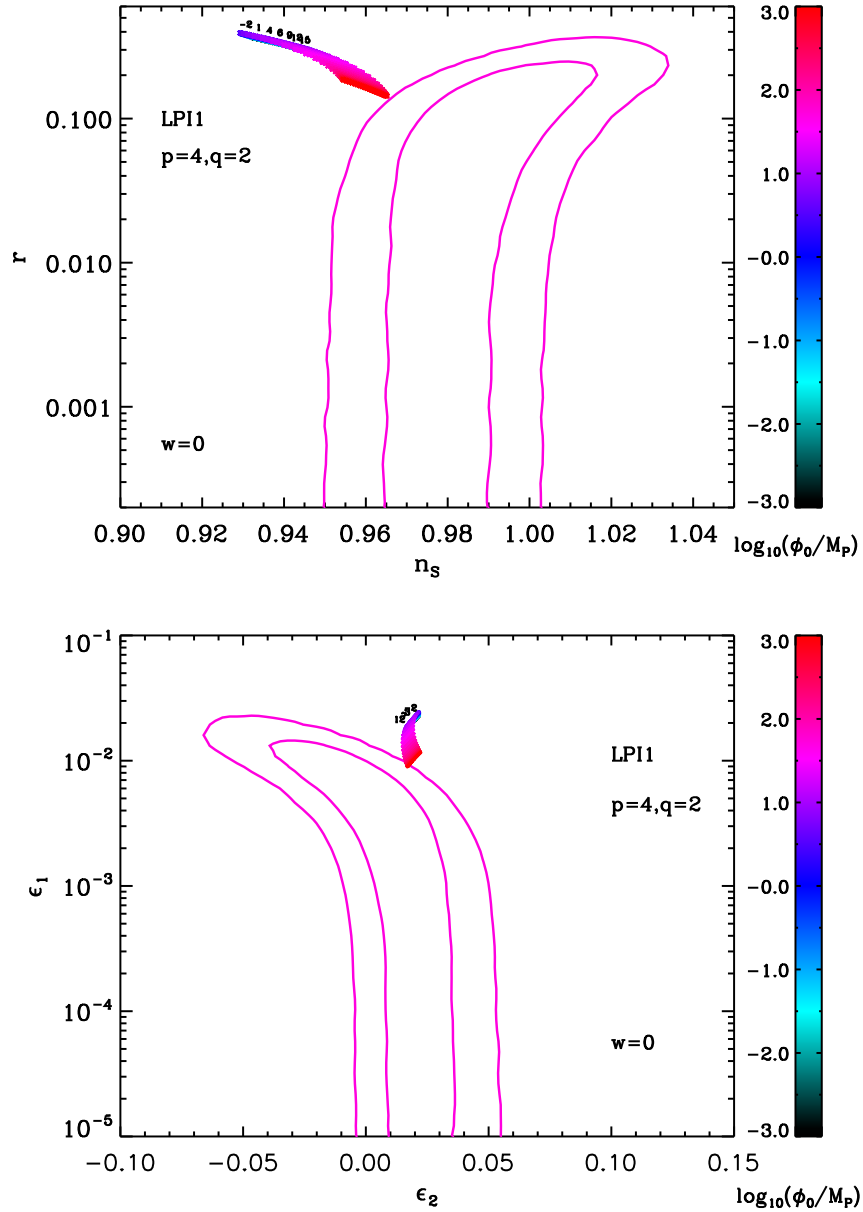


Figure 157. Reheating consistent slow-roll predictions for the logarithmic potential inflation 1 models for $p = 4$ and $q = 2$ in the plane (n_s, r) (top panel) and the plane (ϵ_1, ϵ_2) (bottom panel). The two pink solid contours are the one and two-sigma WMAP confidence intervals (marginalized over second order slow-roll). The annotations trace the energy scale at which reheating ends and correspond to $\log(g_*^{1/4} T_{\text{reh}}/\text{GeV})$.

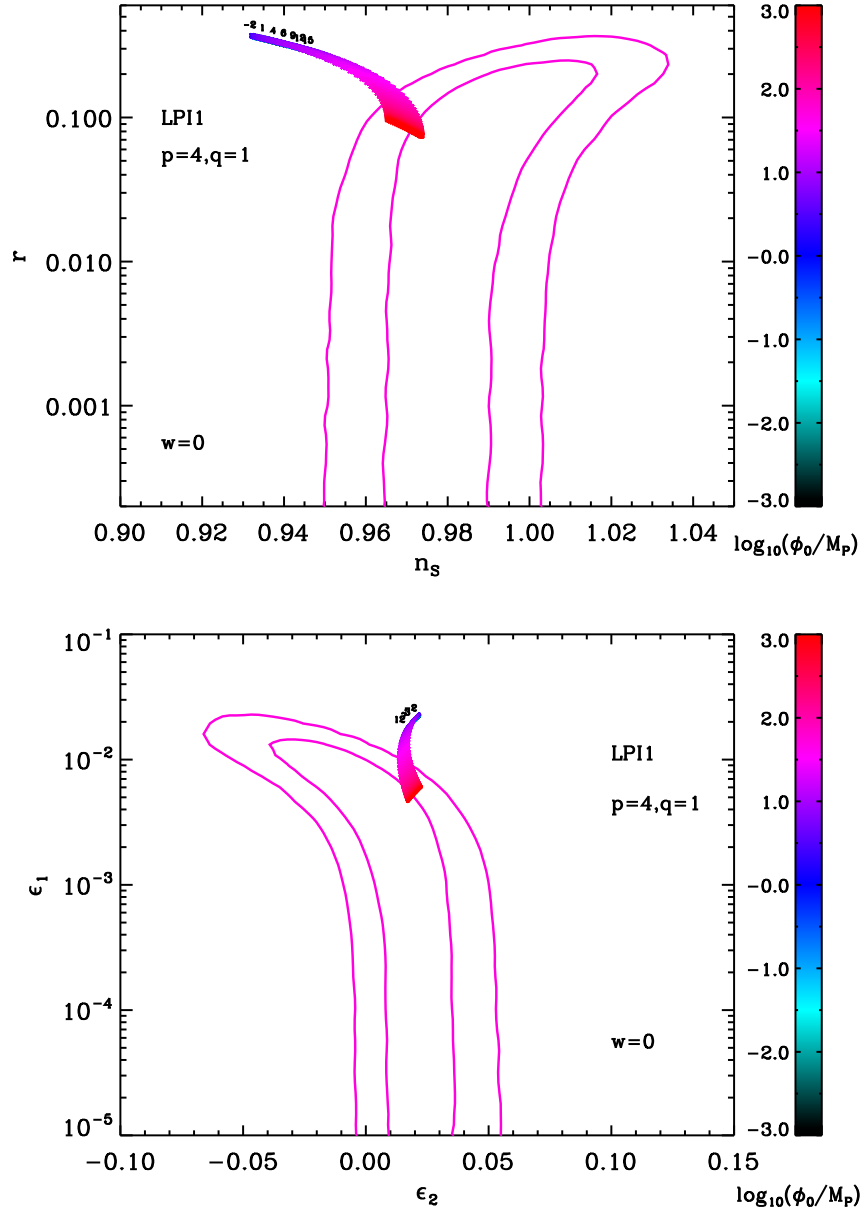


Figure 158. Reheating consistent slow-roll predictions for the logarithmic potential inflation 1 models for $p = 4$ and $q = 1$ in the plane (n_s, r) (top panel) and the plane (ϵ_1, ϵ_2) (bottom panel). The two pink solid contours are the one and two-sigma WMAP confidence intervals (marginalized over second order slow-roll). The annotations trace the energy scale at which reheating ends and correspond to $\log(g_*^{1/4} T_{\text{reh}}/\text{GeV})$.

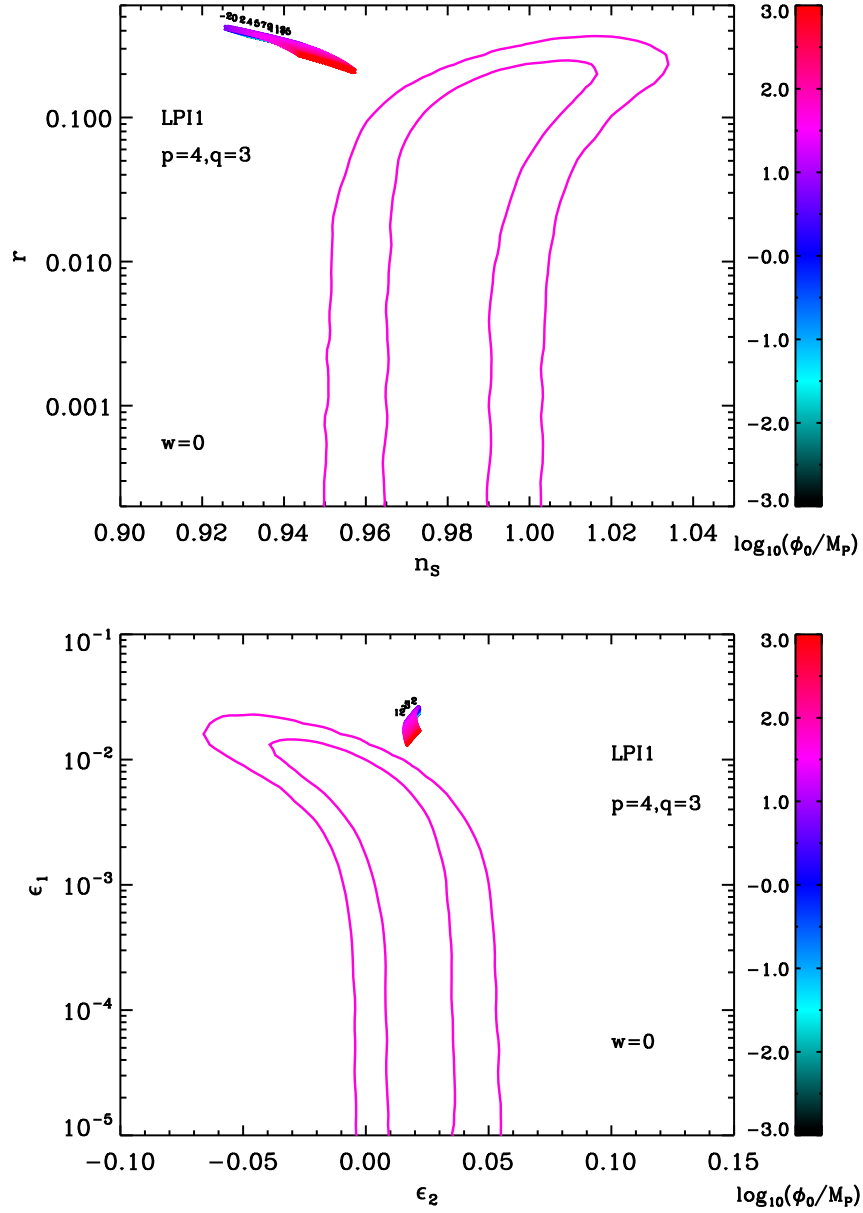


Figure 159. Reheating consistent slow-roll predictions for the logarithmic potential inflation 1 models for $p = 4$ and $q = 3$ in the plane (n_s, r) (top panel) and the plane (ϵ_1, ϵ_2) (bottom panel). The two pink solid contours are the one and two-sigma WMAP confidence intervals (marginalized over second order slow-roll). The annotations trace the energy scale at which reheating ends and correspond to $\log(g_*^{1/4} T_{\text{reh}}/\text{GeV})$.

A.51 Logarithmic Potential Inflation 2 (LPI2)

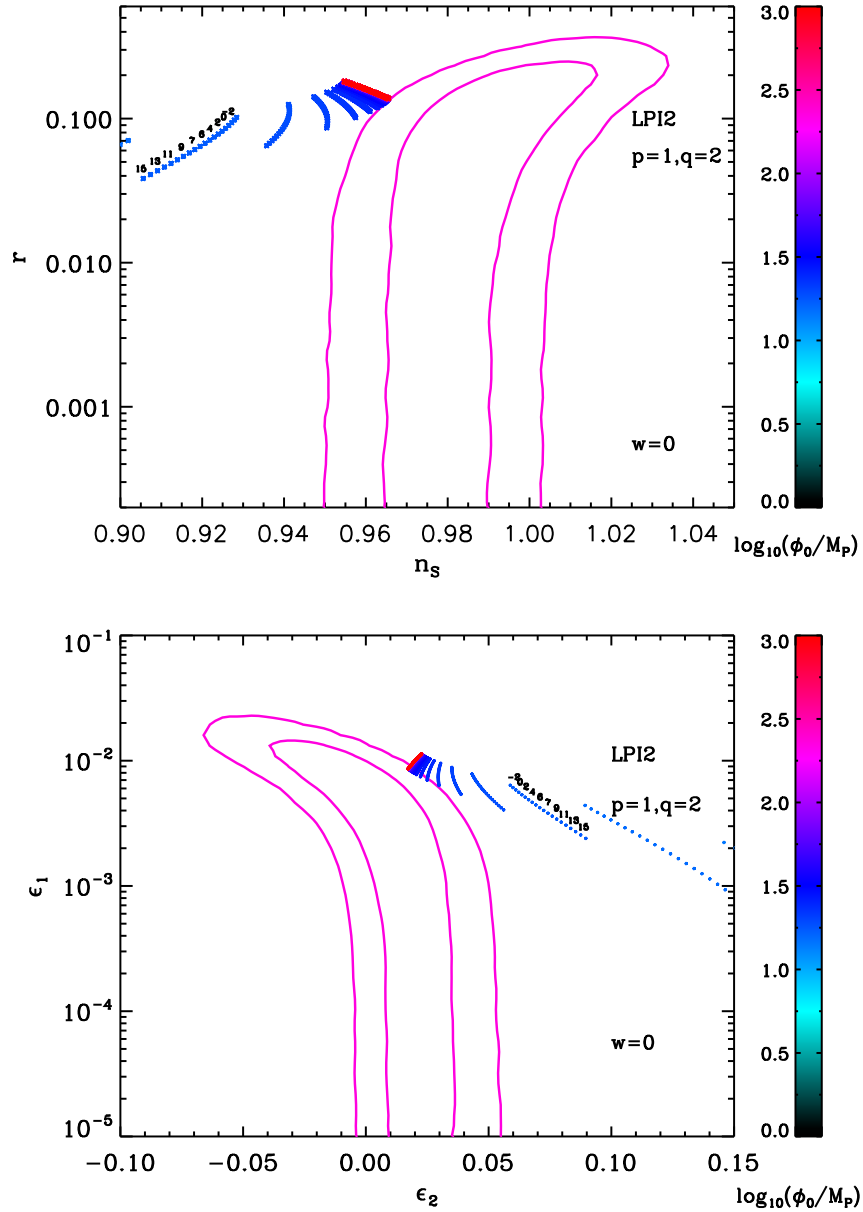


Figure 160. Reheating consistent slow-roll predictions for the logarithmic potential inflation 2 models for $p = 4$ and $q = 2$ in the plane (n_s, r) (top panel) and the plane (ϵ_1, ϵ_2) (bottom panel). The two pink solid contours are the one and two-sigma WMAP confidence intervals (marginalized over second order slow-roll). The annotations trace the energy scale at which reheating ends and correspond to $\log(g_*^{1/4} T_{\text{reh}}/\text{GeV})$.

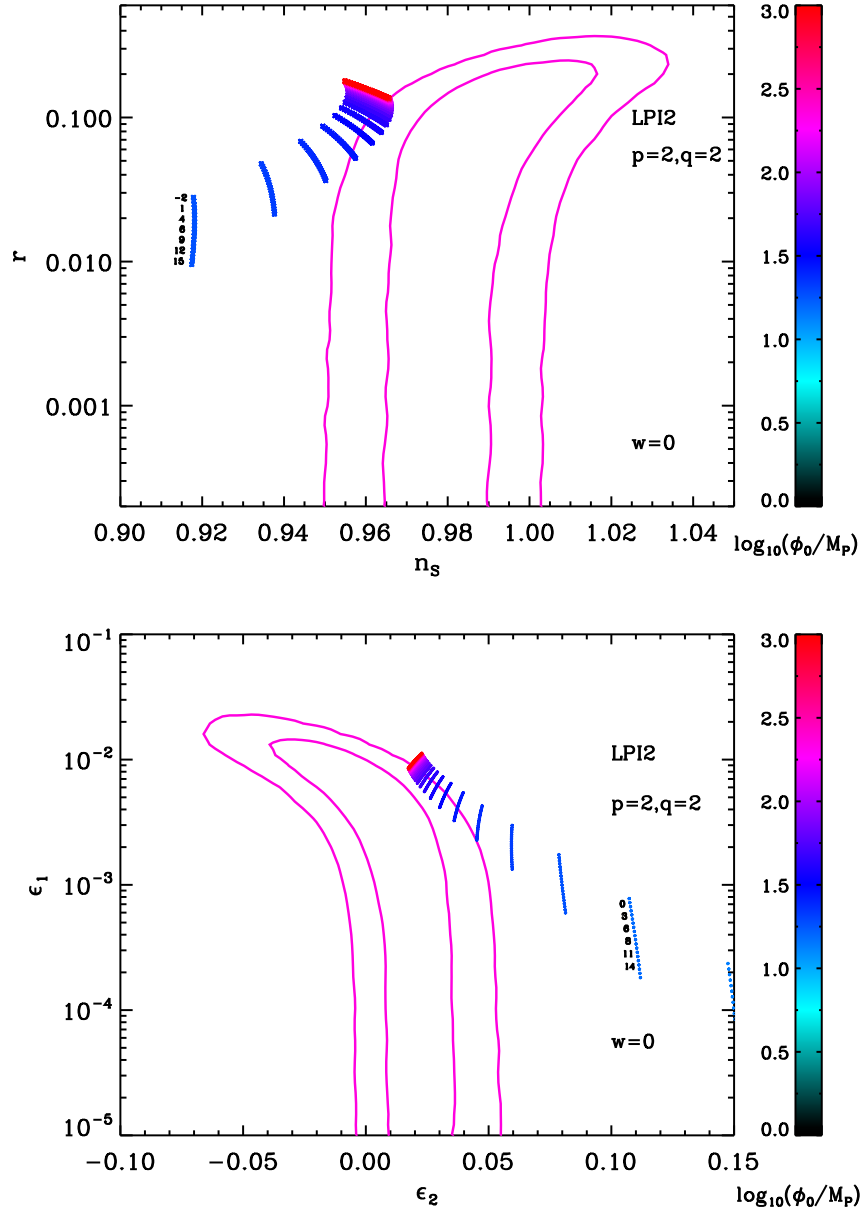


Figure 161. Reheating consistent slow-roll predictions for the logarithmic potential inflation 2 models for $p = 4$ and $q = 1$ in the plane (n_s, r) (top panel) and the plane (ϵ_1, ϵ_2) (bottom panel). The two pink solid contours are the one and two-sigma WMAP confidence intervals (marginalized over second order slow-roll). The annotations trace the energy scale at which reheating ends and correspond to $\log(g_*^{1/4} T_{\text{reh}}/\text{GeV})$.

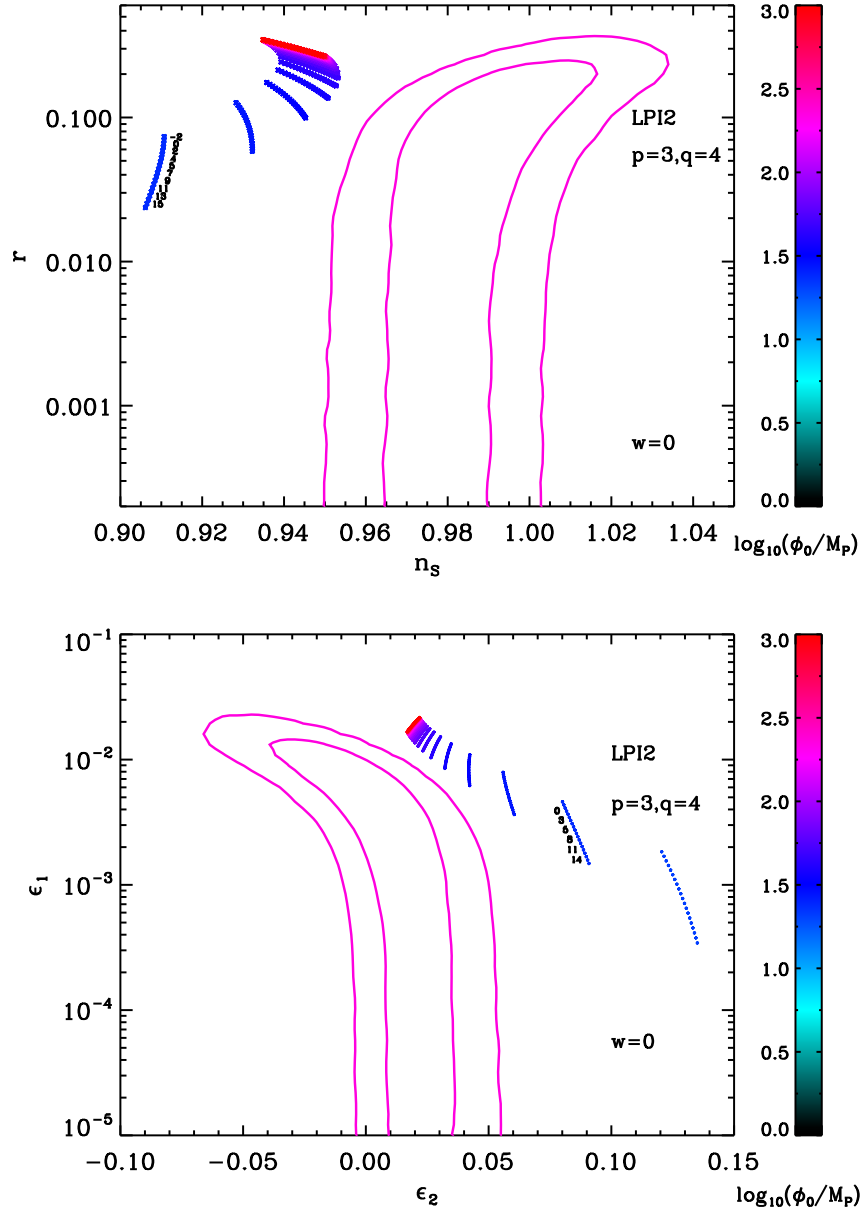


Figure 162. Reheating consistent slow-roll predictions for the logarithmic potential inflation 2 models for $p = 4$ and $q = 3$ in the plane (n_s, r) (top panel) and the plane (ϵ_1, ϵ_2) (bottom panel). The two pink solid contours are the one and two-sigma WMAP confidence intervals (marginalized over second order slow-roll). The annotations trace the energy scale at which reheating ends and correspond to $\log(g_*^{1/4} T_{\text{reh}}/\text{GeV})$.

A.52 Logarithmic Potential Inflation 3 (LPI3)

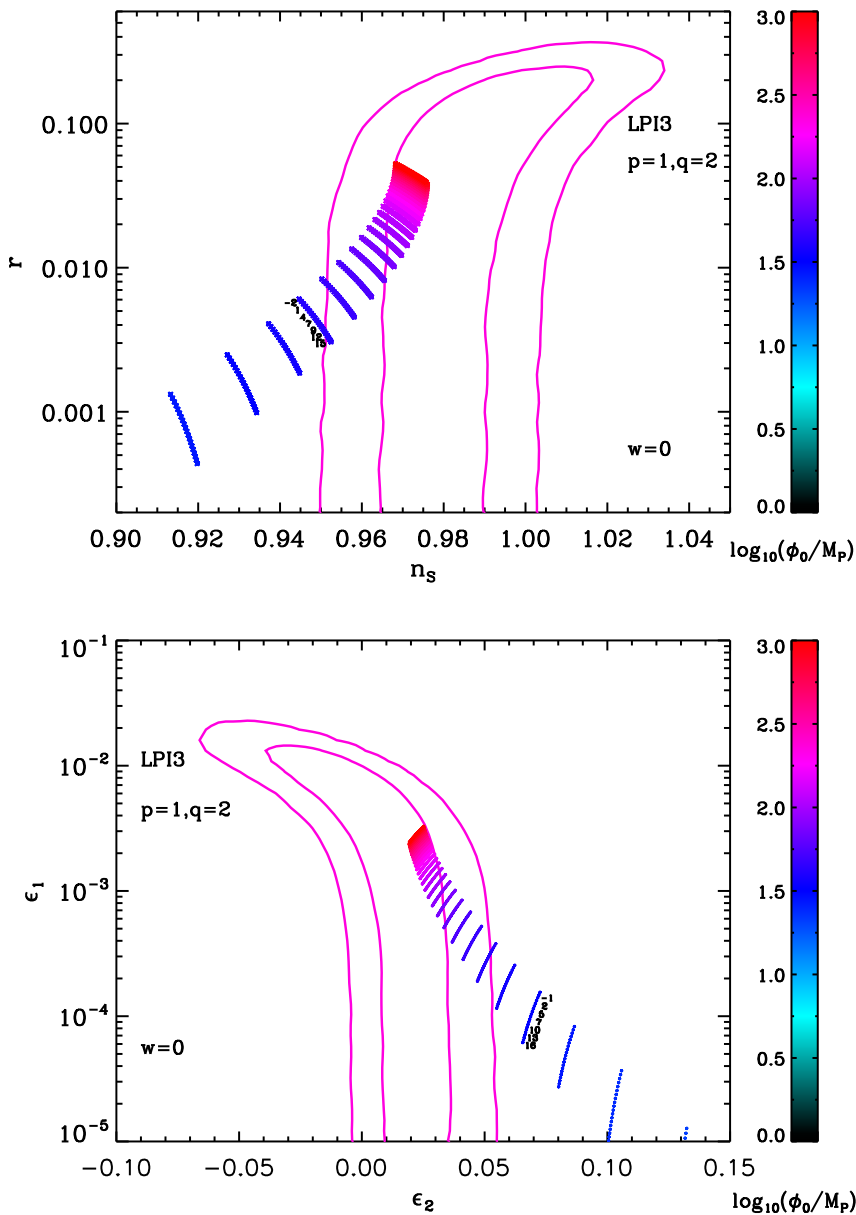


Figure 163. Reheating consistent slow-roll predictions for the logarithmic potential inflation 3 models for $p = 4$ and $q = 2$ in the plane (n_s, r) (top panel) and the plane (ϵ_1, ϵ_2) (bottom panel). The two pink solid contours are the one and two-sigma WMAP confidence intervals (marginalized over second order slow-roll). The annotations trace the energy scale at which reheating ends and correspond to $\log(g_*^{1/4} T_{\text{reh}}/\text{GeV})$.

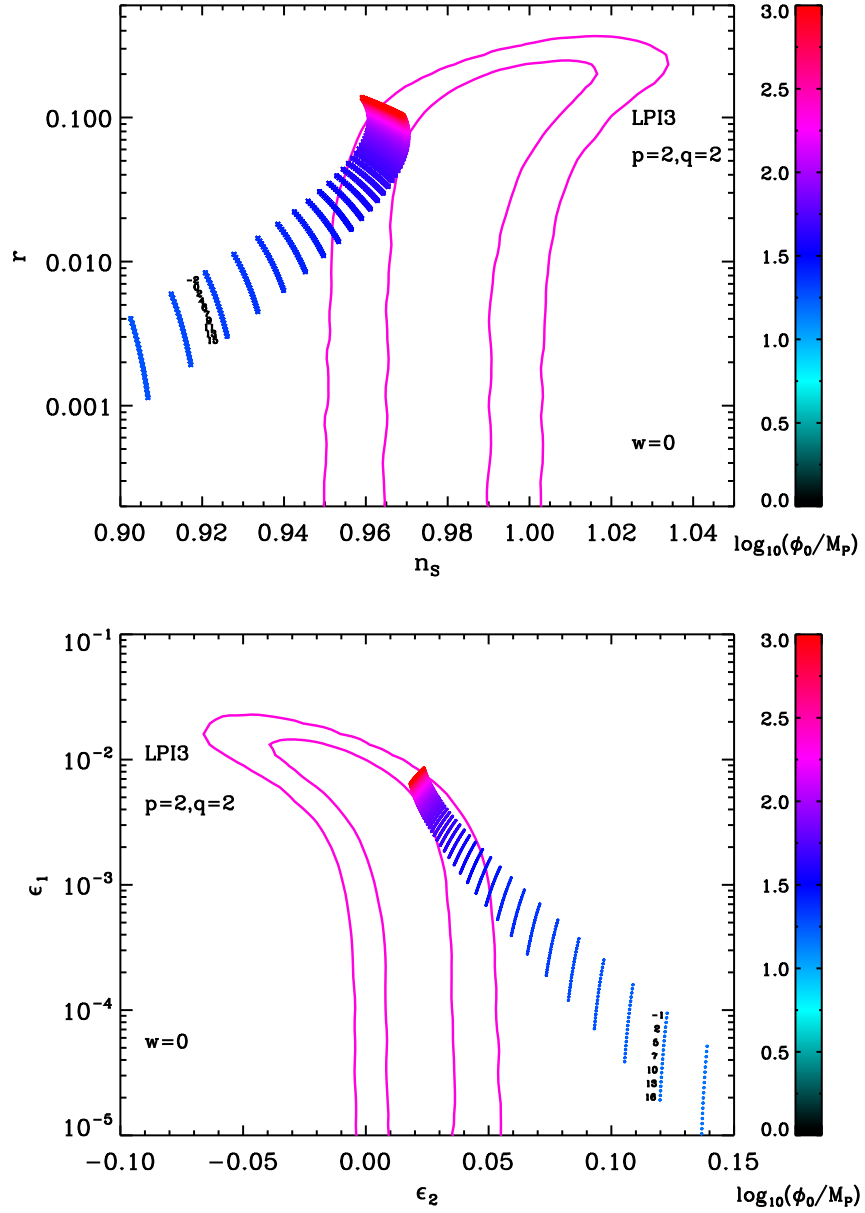


Figure 164. Reheating consistent slow-roll predictions for the logarithmic potential inflation 3 models for $p = 4$ and $q = 1$ in the plane (n_s, r) (top panel) and the plane (ϵ_1, ϵ_2) (bottom panel). The two pink solid contours are the one and two-sigma WMAP confidence intervals (marginalized over second order slow-roll). The annotations trace the energy scale at which reheating ends and correspond to $\log(g_*^{1/4} T_{\text{reh}}/\text{GeV})$.

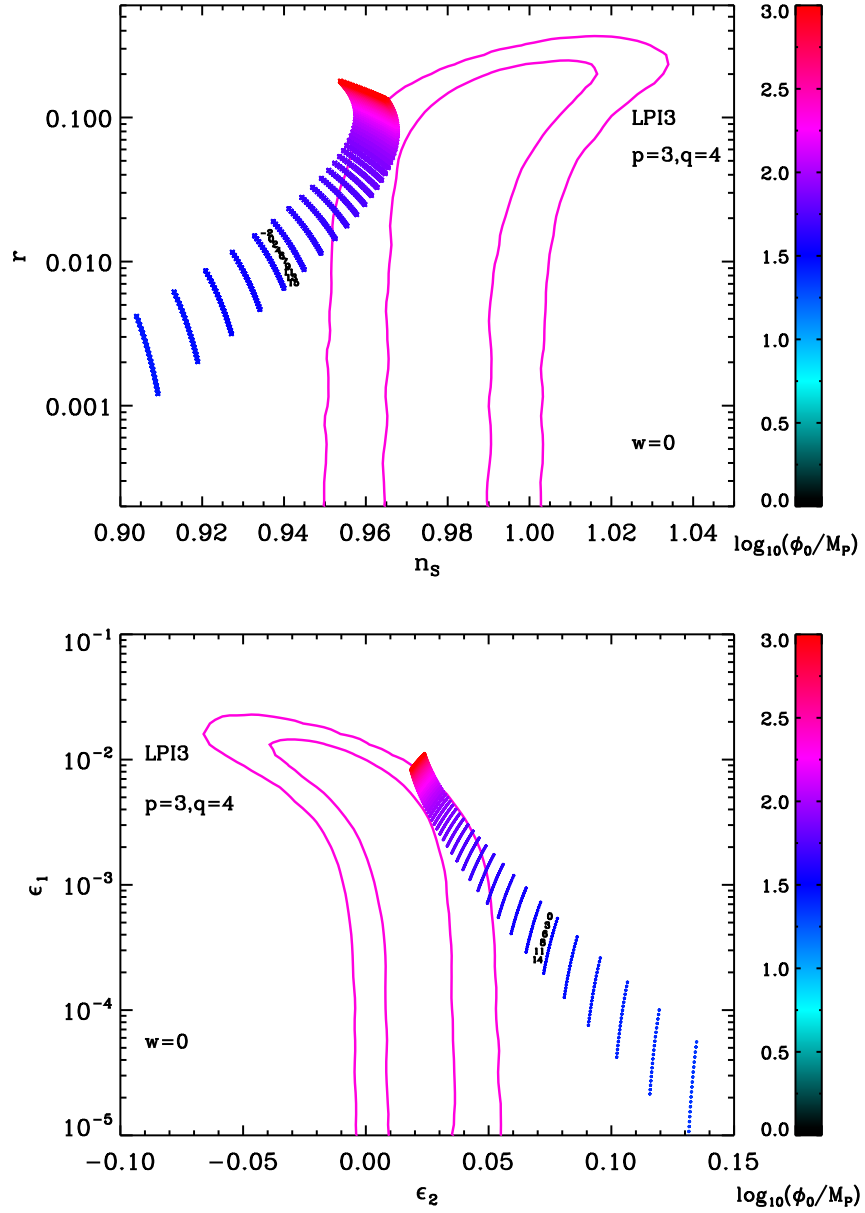


Figure 165. Reheating consistent slow-roll predictions for the logarithmic potential inflation 3 models for $p = 4$ and $q = 3$ in the plane (n_s, r) (top panel) and the plane (ϵ_1, ϵ_2) (bottom panel). The two pink solid contours are the one and two-sigma WMAP confidence intervals (marginalized over second order slow-roll). The annotations trace the energy scale at which reheating ends and correspond to $\log(g_*^{1/4} T_{\text{reh}}/\text{GeV})$.

A.53 Constant n_s D Inflation (CNDI)

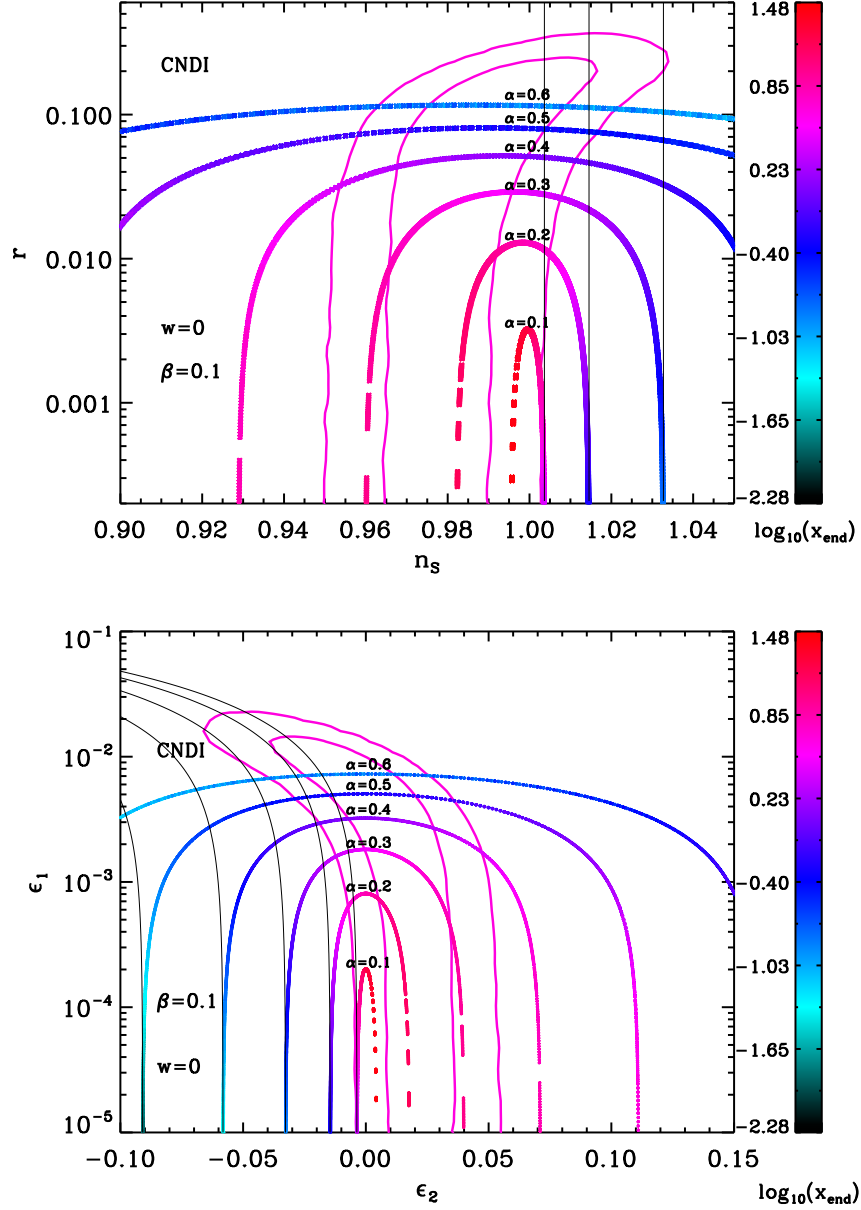


Figure 166. Reheating consistent slow-roll predictions for the constant n_s D inflation models for $\beta = 0.1$ in the plane (n_s, r) (top panel) and the plane (ϵ_1, ϵ_2) (bottom panel). The two pink solid contours are the one and two-sigma WMAP confidence intervals (marginalized over second order slow-roll). The energy scale at which reheating ends is not annotated since it is degenerated with the parameter x_{end} . The black solid lines stand for the points such that $n_s = 1 + 4\alpha^2\beta/(\beta + 1)$.

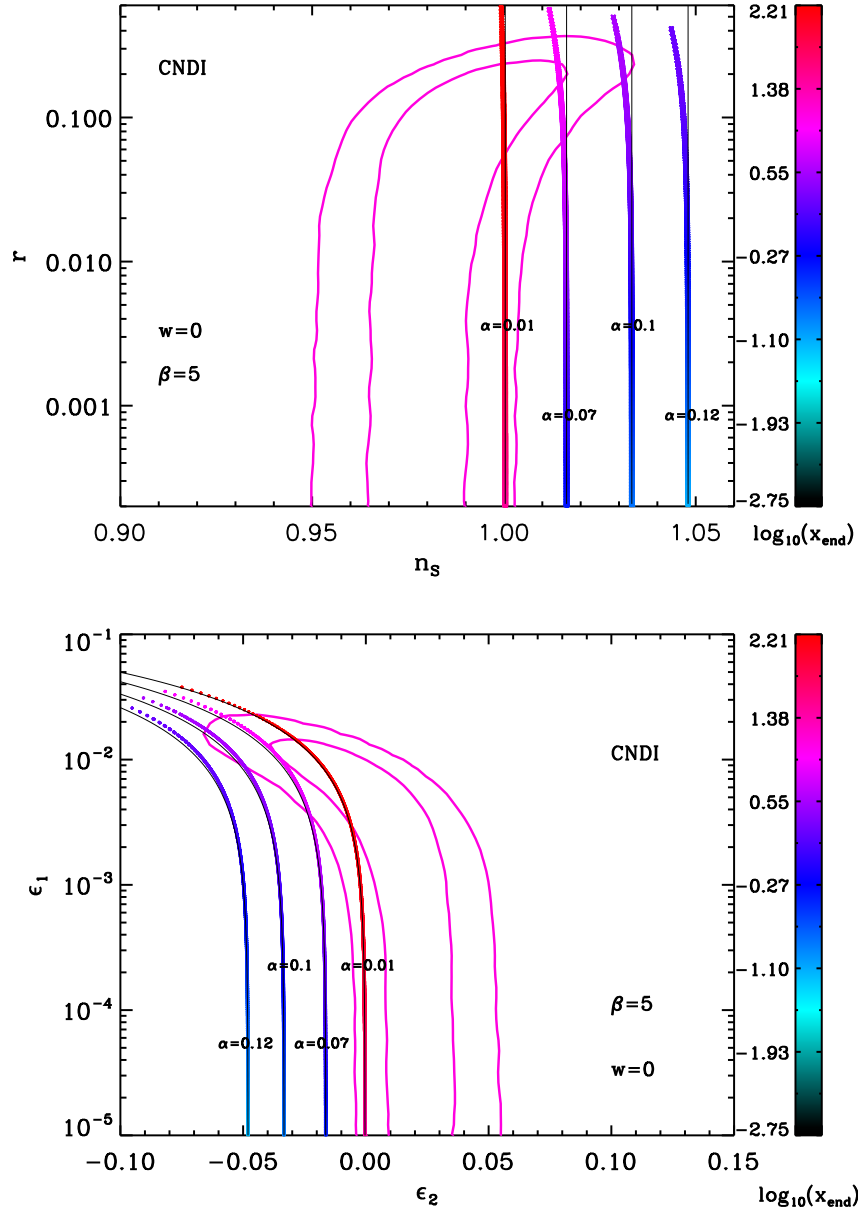


Figure 167. Reheating consistent slow-roll predictions for the constant n_s D inflation models for $\beta = 5$ in the plane (n_s, r) (top panel) and the plane (ϵ_1, ϵ_2) (bottom panel). The two pink solid contours are the one and two-sigma WMAP confidence intervals (marginalized over second order slow-roll). The energy scale at which reheating ends is not annotated since it is degenerated with the parameter x_{end} . The black solid lines stand for the points such that $n_s = 1 + 4\alpha^2\beta/(\beta + 1)$.

Acknowledgments

This work is partially supported by the ESA Belgian Federal PRODEX Grant No. 4000103071 and the Wallonia-Brussels Federation grant ARC No. 11/15-040. We would like to thank EvaluatorIAP for his everyday encouragements.

References

- [1] A. H. Guth, *The Inflationary Universe: A Possible Solution to the Horizon and Flatness Problems*, *Phys. Rev.* **D23** (1981) 347–356.
- [2] A. D. Linde, *A New Inflationary Universe Scenario: A Possible Solution of the Horizon, Flatness, Homogeneity, Isotropy and Primordial Monopole Problems*, *Phys.Lett.* **B108** (1982) 389–393.
- [3] A. Albrecht and P. J. Steinhardt, *Cosmology for Grand Unified Theories with Radiatively Induced Symmetry Breaking*, *Phys.Rev.Lett.* **48** (1982) 1220–1223.
- [4] A. D. Linde, *Chaotic Inflation*, *Phys. Lett.* **B129** (1983) 177–181.
- [5] A. D. Linde, *Inflationary Cosmology*, *Lect. Notes Phys.* **738** (2008) 1–54, [[arXiv:0705.0164](#)].
- [6] J. Martin, *Inflation and precision cosmology*, *Braz. J. Phys.* **34** (2004) 1307–1321, [[astro-ph/0312492](#)].
- [7] J. Martin, *Inflationary cosmological perturbations of quantum- mechanical origin*, *Lect. Notes Phys.* **669** (2005) 199–244, [[hep-th/0406011](#)].
- [8] J. Martin, *Inflationary perturbations: The cosmological Schwinger effect*, *Lect. Notes Phys.* **738** (2008) 193–241, [[arXiv:0704.3540](#)].
- [9] A. A. Starobinsky, *Relict Gravitation Radiation Spectrum and Initial State of the Universe. (In Russian)*, *JETP Lett.* **30** (1979) 682–685.
- [10] V. F. Mukhanov and G. Chibisov, *Quantum Fluctuation and Nonsingular Universe. (In Russian)*, *JETP Lett.* **33** (1981) 532–535.
- [11] S. Hawking, *The Development of Irregularities in a Single Bubble Inflationary Universe*, *Phys. Lett.* **B115** (1982) 295. Revised version.
- [12] A. A. Starobinsky, *Dynamics of Phase Transition in the New Inflationary Universe Scenario and Generation of Perturbations*, *Phys. Lett.* **B117** (1982) 175–178.
- [13] A. H. Guth and S. Y. Pi, *Fluctuations in the New Inflationary Universe*, *Phys. Rev. Lett.* **49** (1982) 1110–1113.
- [14] J. M. Bardeen, P. J. Steinhardt, and M. S. Turner, *Spontaneous Creation of Almost Scale - Free Density Perturbations in an Inflationary Universe*, *Phys. Rev.* **D28** (1983) 679.
- [15] E. D. Stewart and D. H. Lyth, *A More accurate analytic calculation of the spectrum of cosmological perturbations produced during inflation*, *Phys. Lett.* **B302** (1993) 171–175, [[gr-qc/9302019](#)].
- [16] V. F. Mukhanov, H. A. Feldman, and R. H. Brandenberger, *Theory of cosmological perturbations. Part 1. Classical perturbations. Part 2. Quantum theory of perturbations. Part 3. Extensions*, *Phys. Rept.* **215** (1992) 203–333.
- [17] A. R. Liddle, P. Parsons, and J. D. Barrow, *Formalizing the slow roll approximation in inflation*, *Phys. Rev.* **D50** (1994) 7222–7232, [[astro-ph/9408015](#)].
- [18] L. Grishchuk and Y. Sidorov, *Squeezed quantum states of relic gravitons and primordial density fluctuations*, *Phys.Rev.* **D42** (1990) 3413–3421.
- [19] D. Polarski and A. A. Starobinsky, *Semiclassicality and decoherence of cosmological perturbations*, *Class.Quant.Grav.* **13** (1996) 377–392, [[gr-qc/9504030](#)].
- [20] C. Kiefer, D. Polarski, and A. A. Starobinsky, *Quantum to classical transition for fluctuations in the early universe*, *Int.J.Mod.Phys.* **D7** (1998) 455–462, [[gr-qc/9802003](#)].
- [21] C. Kiefer and D. Polarski, *Why do cosmological perturbations look classical to us?*, *Adv.Sci.Lett.* **2** (2009) 164–173, [[arXiv:0810.0087](#)].

- [22] D. Sudarsky, *Shortcomings in the Understanding of Why Cosmological Perturbations Look Classical*, *Int.J.Mod.Phys.* **D20** (2011) 509–552, [[arXiv:0906.0315](#)].
- [23] J. Martin, V. Vennin, and P. Peter, *Cosmological Inflation and the Quantum Measurement Problem*, *Phys.Rev.* **D86** (2012) 103524, [[arXiv:1207.2086](#)].
- [24] J. Martin, *The Quantum State of Inflationary Perturbations*, *J.Phys.Conf.Ser.* **405** (2012) 012004, [[arXiv:1209.3092](#)].
- [25] S. Alexander, R. H. Brandenberger, and D. Easson, *Brane gases in the early universe*, *Phys.Rev.* **D62** (2000) 103509, [[hep-th/0005212](#)].
- [26] P. J. Steinhardt and N. Turok, *Cosmic evolution in a cyclic universe*, *Phys.Rev.* **D65** (2002) 126003, [[hep-th/0111098](#)].
- [27] J. Khoury, B. A. Ovrut, N. Seiberg, P. J. Steinhardt, and N. Turok, *From big crunch to big bang*, *Phys.Rev.* **D65** (2002) 086007, [[hep-th/0108187](#)].
- [28] J. Khoury, B. A. Ovrut, P. J. Steinhardt, and N. Turok, *The Ekpyrotic universe: Colliding branes and the origin of the hot big bang*, *Phys.Rev.* **D64** (2001) 123522, [[hep-th/0103239](#)].
- [29] J. Martin, P. Peter, N. Pinto Neto, and D. J. Schwarz, *Passing through the bounce in the ekpyrotic models*, *Phys.Rev.* **D65** (2002) 123513, [[hep-th/0112128](#)].
- [30] P. Steinhardt and N. Turok, *A cyclic model of the universe*, *Science* **296** (2002) 1436–1439.
- [31] F. Finelli and R. Brandenberger, *On the generation of a scale invariant spectrum of adiabatic fluctuations in cosmological models with a contracting phase*, *Phys.Rev.* **D65** (2002) 103522, [[hep-th/0112249](#)].
- [32] R. Brandenberger, D. A. Easson, and D. Kimberly, *Loitering phase in brane gas cosmology*, *Nucl.Phys.* **B623** (2002) 421–436, [[hep-th/0109165](#)].
- [33] R. Kallosh, L. Kofman, and A. D. Linde, *Pyrotechnic universe*, *Phys.Rev.* **D64** (2001) 123523, [[hep-th/0104073](#)].
- [34] J. Martin, P. Peter, N. Pinto-Neto, and D. J. Schwarz, *Comment on ‘Density perturbations in the ekpyrotic scenario’*, *Phys.Rev.* **D67** (2003) 028301, [[hep-th/0204222](#)].
- [35] P. Peter and N. Pinto-Neto, *Primordial perturbations in a non singular bouncing universe model*, *Phys.Rev.* **D66** (2002) 063509, [[hep-th/0203013](#)].
- [36] S. Tsujikawa, R. Brandenberger, and F. Finelli, *On the construction of nonsingular pre - big bang and ekpyrotic cosmologies and the resulting density perturbations*, *Phys.Rev.* **D66** (2002) 083513, [[hep-th/0207228](#)].
- [37] L. Kofman, A. D. Linde, and V. F. Mukhanov, *Inflationary theory and alternative cosmology*, *JHEP* **0210** (2002) 057, [[hep-th/0206088](#)].
- [38] J. Khoury, P. J. Steinhardt, and N. Turok, *Designing cyclic universe models*, *Phys.Rev.Lett.* **92** (2004) 031302, [[hep-th/0307132](#)].
- [39] J. Martin and P. Peter, *On the causality argument in bouncing cosmologies*, *Phys.Rev.Lett.* **92** (2004) 061301, [[astro-ph/0312488](#)].
- [40] J. Martin and P. Peter, *Parametric amplification of metric fluctuations through a bouncing phase*, *Phys.Rev.* **D68** (2003) 103517, [[hep-th/0307077](#)].
- [41] J. Martin and P. Peter, *On the properties of the transition matrix in bouncing cosmologies*, *Phys.Rev.* **D69** (2004) 107301, [[hep-th/0403173](#)].
- [42] A. Nayeri, R. H. Brandenberger, and C. Vafa, *Producing a scale-invariant spectrum of perturbations in a Hagedorn phase of string cosmology*, *Phys.Rev.Lett.* **97** (2006) 021302, [[hep-th/0511140](#)].

- [43] P. Peter, E. J. Pinho, and N. Pinto-Neto, *A Non inflationary model with scale invariant cosmological perturbations*, *Phys.Rev.* **D75** (2007) 023516, [[hep-th/0610205](#)].
- [44] F. Finelli, P. Peter, and N. Pinto-Neto, *Spectra of primordial fluctuations in two-perfect-fluid regular bounces*, *Phys.Rev.* **D77** (2008) 103508, [[arXiv:0709.3074](#)].
- [45] L. R. Abramo and P. Peter, *K-Bounce*, *JCAP* **0709** (2007) 001, [[arXiv:0705.2893](#)].
- [46] F. T. Falciano, M. Lilley, and P. Peter, *A Classical bounce: Constraints and consequences*, *Phys.Rev.* **D77** (2008) 083513, [[arXiv:0802.1196](#)].
- [47] A. Linde, V. Mukhanov, and A. Vikman, *On adiabatic perturbations in the ekpyrotic scenario*, *JCAP* **1002** (2010) 006, [[arXiv:0912.0944](#)].
- [48] L. R. Abramo, I. Yasuda, and P. Peter, *Non singular bounce in modified gravity*, *Phys.Rev.* **D81** (2010) 023511, [[arXiv:0910.3422](#)].
- [49] R. Brandenberger, *Matter Bounce in Horava-Lifshitz Cosmology*, *Phys.Rev.* **D80** (2009) 043516, [[arXiv:0904.2835](#)].
- [50] R. H. Brandenberger, *String Gas Cosmology: Progress and Problems*, *Class.Quant.Grav.* **28** (2011) 204005, [[arXiv:1105.3247](#)].
- [51] R. H. Brandenberger, *The Matter Bounce Alternative to Inflationary Cosmology*, [arXiv:1206.4196](#).
- [52] Y.-F. Cai, D. A. Easson, and R. Brandenberger, *Towards a Nonsingular Bouncing Cosmology*, *JCAP* **1208** (2012) 020, [[arXiv:1206.2382](#)].
- [53] Y.-F. Cai, R. Brandenberger, and P. Peter, *Anisotropy in a Nonsingular Bounce*, [arXiv:1301.4703](#).
- [54] M. S. Turner, *Coherent Scalar Field Oscillations in an Expanding Universe*, *Phys. Rev.* **D28** (1983) 1243.
- [55] L. Kofman, A. D. Linde, and A. A. Starobinsky, *Towards the theory of reheating after inflation*, *Phys. Rev.* **D56** (1997) 3258–3295, [[hep-ph/9704452](#)].
- [56] B. A. Bassett, S. Tsujikawa, and D. Wands, *Inflation dynamics and reheating*, *Rev. Mod. Phys.* **78** (2006) 537–589, [[astro-ph/0507632](#)].
- [57] A. Mazumdar and J. Rocher, *Particle physics models of inflation and curvaton scenarios*, *Phys. Rept.* **497** (2011) 85–215, [[arXiv:1001.0993](#)].
- [58] F. Finelli and R. H. Brandenberger, *Parametric amplification of gravitational fluctuations during reheating*, *Phys.Rev.Lett.* **82** (1999) 1362–1365, [[hep-ph/9809490](#)].
- [59] B. A. Bassett, D. I. Kaiser, and R. Maartens, *General relativistic preheating after inflation*, *Phys.Lett.* **B455** (1999) 84–89, [[hep-ph/9808404](#)].
- [60] F. Finelli and R. H. Brandenberger, *Parametric amplification of metric fluctuations during reheating in two field models*, *Phys. Rev.* **D62** (2000) 083502, [[hep-ph/0003172](#)].
- [61] K. Jedamzik, M. Lemoine, and J. Martin, *Collapse of Small-Scale Density Perturbations during Preheating in Single Field Inflation*, *JCAP* **1009** (2010) 034, [[arXiv:1002.3039](#)].
- [62] K. Jedamzik, M. Lemoine, and J. Martin, *Generation of gravitational waves during early structure formation between cosmic inflation and reheating*, *JCAP* **1004** (2010) 021, [[arXiv:1002.3278](#)].
- [63] R. Easther, R. Flauger, and J. B. Gilmore, *Delayed Reheating and the Breakdown of Coherent Oscillations*, *JCAP* **1104** (2011) 027, [[arXiv:1003.3011](#)].
- [64] J. Martin and C. Ringeval, *First CMB Constraints on the Inflationary Reheating Temperature*, *Phys. Rev.* **D82** (2010) 023511, [[arXiv:1004.5525](#)].

- [65] J.-M. Lamarre, J.-L. Puget, P. A. R. Ade, F. Bouchet, G. Guyot, A. E. Lange, F. Pajot, A. Arondel, K. Benabed, J.-L. Beney, A. Benoît, J.-P. Bernard, R. Bhatia, Y. Blanc, J. J. Bock, E. Bréelle, T. W. Bradshaw, P. Camus, A. Catalano, J. Charra, M. Charra, S. E. Church, F. Couchot, A. Coulais, B. P. Crill, M. R. Crook, K. Dassas, P. de Bernardis, J. Delabrouille, P. de Marcillac, J.-M. Delouis, F.-X. Désert, C. Dumesnil, X. Dupac, G. Efstathiou, P. Eng, C. Evesque, J.-J. Fourmond, K. Ganga, M. Giard, R. Gispert, L. Guglielmi, J. Haissinski, S. Henrot-Versillé, E. Hivon, W. A. Holmes, W. C. Jones, T. C. Koch, H. Lagardère, P. Lami, J. Landé, B. Leriche, C. Leroy, Y. Longval, J. F. Macías-Pérez, T. Maciaszek, B. Maffei, B. Mansoux, C. Marty, S. Masi, C. Mercier, M.-A. Miville-Deschênes, A. Moneti, L. Montier, J. A. Murphy, J. Narbonne, M. Nexon, C. G. Paine, J. Pahn, O. Perdereau, F. Piacentini, M. Piat, S. Plaszczynski, E. Pointecouteau, R. Pons, N. Ponthieu, S. Prunet, D. Rambaud, G. Recouvreur, C. Renault, I. Ristorcelli, C. Rosset, D. Santos, G. Savini, G. Serra, P. Stassi, R. V. Sudiwala, J.-F. Sygnet, J. A. Tauber, J.-P. Torre, M. Tristram, L. Vibert, A. Woodcraft, V. Yurchenko, and D. Yvon, *Planck pre-launch status: The HFI instrument, from specification to actual performance*, *Astron. & Astrophys.* **520** (Sept., 2010) A9.
- [66] C. Bennett, D. Larson, J. Weiland, N. Jarosik, G. Hinshaw, et al., *Nine-Year Wilkinson Microwave Anisotropy Probe (WMAP) Observations: Final Maps and Results*, [arXiv:1212.5225](#).
- [67] G. Hinshaw, D. Larson, E. Komatsu, D. Spergel, C. Bennett, et al., *Nine-Year Wilkinson Microwave Anisotropy Probe (WMAP) Observations: Cosmological Parameter Results*, [arXiv:1212.5226](#).
- [68] **Supernova Search Team** Collaboration, J. L. Tonry et al., *Cosmological results from high- z supernovae*, *Astrophys.J.* **594** (2003) 1–24, [[astro-ph/0305008](#)].
- [69] **Supernova Search Team** Collaboration, A. G. Riess et al., *Type Ia supernova discoveries at $z \lesssim 1$ from the Hubble Space Telescope: Evidence for past deceleration and constraints on dark energy evolution*, *Astrophys.J.* **607** (2004) 665–687, [[astro-ph/0402512](#)].
- [70] A. G. Riess, L.-G. Strolger, S. Casertano, H. C. Ferguson, B. Mobasher, et al., *New Hubble Space Telescope Discoveries of Type Ia Supernovae at $z \lesssim 1$: Narrowing Constraints on the Early Behavior of Dark Energy*, *Astrophys.J.* **659** (2007) 98–121, [[astro-ph/0611572](#)].
- [71] A. G. Riess, L. Macri, S. Casertano, H. Lampeitl, H. C. Ferguson, et al., *A 3Telescope and Wide Field Camera 3*, *Astrophys.J.* **730** (2011) 119, [[arXiv:1103.2976](#)].
- [72] **SDSS Collaboration** Collaboration, J. K. Adelman-McCarthy et al., *The Sixth Data Release of the Sloan Digital Sky Survey*, *Astrophys.J.Suppl.* **175** (2008) 297–313, [[arXiv:0707.3413](#)].
- [73] **SDSS Collaboration** Collaboration, K. N. Abazajian et al., *The Seventh Data Release of the Sloan Digital Sky Survey*, *Astrophys.J.Suppl.* **182** (2009) 543–558, [[arXiv:0812.0649](#)].
- [74] **Euclid collaboration** Collaboration, J. Amiaux et al., *Euclid Mission: building of a Reference Survey*, [arXiv:1209.2228](#).
- [75] J. Dunkley, E. Calabrese, J. Sievers, G. Addison, N. Battaglia, et al., *The Atacama Cosmology Telescope: likelihood for small-scale CMB data*, [arXiv:1301.0776](#).
- [76] J. L. Sievers, R. A. Hlozek, M. R. Nolta, V. Acquaviva, G. E. Addison, et al., *The Atacama Cosmology Telescope: Cosmological parameters from three seasons of data*, [arXiv:1301.0824](#).
- [77] Z. Hou, C. Reichardt, K. Story, B. Follin, R. Keisler, et al., *Constraints on Cosmology from the Cosmic Microwave Background Power Spectrum of the 2500-square degree SPT-SZ Survey*, [arXiv:1212.6267](#).
- [78] K. Story, C. Reichardt, Z. Hou, R. Keisler, K. Aird, et al., *A Measurement of the Cosmic Microwave Background Damping Tail from the 2500-square-degree SPT-SZ survey*, [arXiv:1210.7231](#).

- [79] M. Zaldarriaga, S. R. Furlanetto, and L. Hernquist, *21 Centimeter fluctuations from cosmic gas at high redshifts*, *Astrophys.J.* **608** (2004) 622–635, [[astro-ph/0311514](#)].
- [80] A. Lewis and A. Challinor, *The 21cm angular-power spectrum from the dark ages*, *Phys. Rev.* **D76** (2007) 083005, [[astro-ph/0702600](#)].
- [81] M. Tegmark and M. Zaldarriaga, *The Fast Fourier Transform Telescope*, *Phys. Rev.* **D79** (2009) 083530, [[arXiv:0805.4414](#)].
- [82] V. Barger, Y. Gao, Y. Mao, and D. Marfatia, *Inflationary Potential from 21 cm Tomography and Planck*, *Phys. Lett.* **B673** (2009) 173–178, [[arXiv:0810.3337](#)].
- [83] Y. Mao, M. Tegmark, M. McQuinn, M. Zaldarriaga, and O. Zahn, *How accurately can 21 cm tomography constrain cosmology?*, *Phys. Rev.* **D78** (2008) 023529, [[arXiv:0802.1710](#)].
- [84] P. Adshead, R. Easther, J. Pritchard, and A. Loeb, *Inflation and the Scale Dependent Spectral Index: Prospects and Strategies*, *JCAP* **1102** (2011) 021, [[arXiv:1007.3748](#)].
- [85] S. Clesse, L. Lopez-Honorez, C. Ringeval, H. Tashiro, and M. H. Tytgat, *Background reionization history from omniscopes*, *Phys.Rev.* **D86** (2012) 123506, [[arXiv:1208.4277](#)].
- [86] A. Golovnev, V. Mukhanov, and V. Vanchurin, *Vector Inflation*, *JCAP* **0806** (2008) 009, [[arXiv:0802.2068](#)].
- [87] P. Adshead and M. Wyman, *Chromo-Natural Inflation: Natural inflation on a steep potential with classical non-Abelian gauge fields*, *Phys.Rev.Lett.* **108** (2012) 261302, [[arXiv:1202.2366](#)].
- [88] M. Alishahiha, E. Silverstein, and D. Tong, *DBI in the sky*, *Phys.Rev.* **D70** (2004) 123505, [[hep-th/0404084](#)].
- [89] D. Langlois, S. Renaux-Petel, D. A. Steer, and T. Tanaka, *Primordial perturbations and non-Gaussianities in DBI and general multi-field inflation*, *Phys.Rev.* **D78** (2008) 063523, [[arXiv:0806.0336](#)].
- [90] D. Langlois, S. Renaux-Petel, and D. A. Steer, *Multi-field DBI inflation: Introducing bulk forms and revisiting the gravitational wave constraints*, *JCAP* **0904** (2009) 021, [[arXiv:0902.2941](#)].
- [91] A. Gangui, F. Lucchin, S. Matarrese, and S. Mollerach, *The Three point correlation function of the cosmic microwave background in inflationary models*, *Astrophys.J.* **430** (1994) 447–457, [[astro-ph/9312033](#)].
- [92] A. Gangui, *NonGaussian effects in the cosmic microwave background from inflation*, *Phys.Rev.* **D50** (1994) 3684–3691, [[astro-ph/9406014](#)].
- [93] A. Gangui and J. Martin, *Cosmic microwave background bispectrum and slow roll inflation*, *Mon.Not.Roy.Astron.Soc.* (1999) [[astro-ph/9908009](#)].
- [94] L.-M. Wang and M. Kamionkowski, *The Cosmic microwave background bispectrum and inflation*, *Phys.Rev.* **D61** (2000) 063504, [[astro-ph/9907431](#)].
- [95] J. M. Maldacena, *Non-Gaussian features of primordial fluctuations in single field inflationary models*, *JHEP* **0305** (2003) 013, [[astro-ph/0210603](#)].
- [96] D. Seery and J. E. Lidsey, *Primordial non-Gaussianities in single field inflation*, *JCAP* **0506** (2005) 003, [[astro-ph/0503692](#)].
- [97] X. Chen, *Running non-Gaussianities in DBI inflation*, *Phys.Rev.* **D72** (2005) 123518, [[astro-ph/0507053](#)].
- [98] X. Chen, M.-x. Huang, S. Kachru, and G. Shiu, *Observational signatures and non-Gaussianities of general single field inflation*, *JCAP* **0701** (2007) 002, [[hep-th/0605045](#)].
- [99] X. Chen, *Primordial Non-Gaussianities from Inflation Models*, *Adv.Astron.* **2010** (2010) 638979, [[arXiv:1002.1416](#)].

- [100] X. Chen, R. Easther, and E. A. Lim, *Large Non-Gaussianities in Single Field Inflation*, *JCAP* **0706** (2007) 023, [[astro-ph/0611645](#)].
- [101] X. Chen, R. Easther, and E. A. Lim, *Generation and Characterization of Large Non-Gaussianities in Single Field Inflation*, *JCAP* **0804** (2008) 010, [[arXiv:0801.3295](#)].
- [102] S. Hannestad, T. Haugbolle, P. R. Jarnhus, and M. S. Sloth, *Non-Gaussianity from Axion Monodromy Inflation*, *JCAP* **1006** (2010) 001, [[arXiv:0912.3527](#)].
- [103] R. Flauger and E. Pajer, *Resonant Non-Gaussianity*, *JCAP* **1101** (2011) 017, [[arXiv:1002.0833](#)].
- [104] P. Adshead, C. Dvorkin, W. Hu, and E. A. Lim, *Non-Gaussianity from Step Features in the Inflationary Potential*, *Phys.Rev.* **D85** (2012) 023531, [[arXiv:1110.3050](#)]. Typos fixed, supersedes journal version.
- [105] J. Martin and L. Sriramkumar, *The scalar bi-spectrum in the Starobinsky model: The equilateral case*, *JCAP* **1201** (2012) 008, [[arXiv:1109.5838](#)].
- [106] X. Chen, *Folded Resonant Non-Gaussianity in General Single Field Inflation*, *JCAP* **1012** (2010) 003, [[arXiv:1008.2485](#)].
- [107] A. Gangui, J. Martin, and M. Sakellariadou, *Single field inflation and non-Gaussianity*, *Phys.Rev.* **D66** (2002) 083502, [[astro-ph/0205202](#)].
- [108] R. Holman and A. J. Tolley, *Enhanced Non-Gaussianity from Excited Initial States*, *JCAP* **0805** (2008) 001, [[arXiv:0710.1302](#)].
- [109] W. Xue and B. Chen, *alpha-vacuum and inflationary bispectrum*, *Phys.Rev.* **D79** (2009) 043518, [[arXiv:0806.4109](#)].
- [110] P. D. Meerburg, J. P. van der Schaar, and P. S. Corasaniti, *Signatures of Initial State Modifications on Bispectrum Statistics*, *JCAP* **0905** (2009) 018, [[arXiv:0901.4044](#)].
- [111] J.-L. Lehners and S. Renaux-Petel, *Multifield Cosmological Perturbations at Third Order and the Ekpyrotic Trispectrum*, *Phys.Rev.* **D80** (2009) 063503, [[arXiv:0906.0530](#)].
- [112] S. Renaux-Petel, S. Mizuno, and K. Koyama, *Primordial fluctuations and non-Gaussianities from multifield DBI Galileon inflation*, *JCAP* **1111** (2011) 042, [[arXiv:1108.0305](#)].
- [113] R. Trotta, *Bayes in the sky: Bayesian inference and model selection in cosmology*, *Contemp.Phys.* **49** (2008) 71–104, [[arXiv:0803.4089](#)].
- [114] J. Martin, C. Ringeval, and V. Vennin, *K-inflationary Power Spectra at Second Order*, [[arXiv:1303.2120](#)].
- [115] J. B. Jimenez, M. Musso, and C. Ringeval, *Exact Mapping between Tensor and Most General Scalar Power Spectra*, [[arXiv:1303.2788](#)].
- [116] S. M. Leach and A. R. Liddle, *Constraining slow - roll inflation with WMAP and 2dF*, *Phys.Rev.* **D68** (2003) 123508, [[astro-ph/0306305](#)].
- [117] J. Martin and C. Ringeval, *Inflation after WMAP3: Confronting the slow-roll and exact power spectra to CMB data*, *JCAP* **0608** (2006) 009, [[astro-ph/0605367](#)].
- [118] L. Lorenz, J. Martin, and C. Ringeval, *Constraints on Kinetically Modified Inflation from WMAP5*, *Phys. Rev.* **D78** (2008) 063543, [[arXiv:0807.2414](#)].
- [119] F. Finelli, J. Hamann, S. M. Leach, and J. Lesgourgues, *Single-field inflation constraints from CMB and SDSS data*, *JCAP* **1004** (2010) 011, [[arXiv:0912.0522](#)].
- [120] D. K. Hazra, L. Sriramkumar, and J. Martin, *BINGO: A code for the efficient computation of the scalar bi-spectrum*, [[arXiv:1201.0926](#)].
- [121] C. Ringeval, P. Brax, C. van de Bruck, and A.-C. Davis, *Boundary Inflation and the WMAP Data*, *Phys. Rev.* **D73** (2006) 064035, [[astro-ph/0509727](#)].

- [122] C. Ringeval, *The exact numerical treatment of inflationary models*, *Lect.Notes Phys.* **738** (2008) 243–273, [[astro-ph/0703486](#)].
- [123] L. Lorenz, J. Martin, and C. Ringeval, *Brane inflation and the WMAP data: a Bayesian analysis*, *JCAP* **0804** (2008) 001, [[arXiv:0709.3758](#)].
- [124] M. J. Mortonson, H. V. Peiris, and R. Easther, *Bayesian Analysis of Inflation: Parameter Estimation for Single Field Models*, *Phys.Rev.* **D83** (2011) 043505, [[arXiv:1007.4205](#)].
- [125] A. R. Liddle and S. M. Leach, *How long before the end of inflation were observable perturbations produced?*, *Phys. Rev.* **D68** (2003) 103503, [[astro-ph/0305263](#)].
- [126] R. Easther and H. V. Peiris, *Bayesian Analysis of Inflation II: Model Selection and Constraints on Reheating*, *Phys.Rev.* **D85** (2012) 103533, [[arXiv:1112.0326](#)].
- [127] A. A. Starobinsky, *Spectrum of adiabatic perturbations in the universe when there are singularities in the inflation potential*, *JETP Lett.* **55** (1992) 489–494.
- [128] J. Silk and M. S. Turner, *Double Inflation*, *Phys.Rev.* **D35** (1987) 419.
- [129] P. Peter, D. Polarski, and A. A. Starobinsky, *Confrontation of double inflationary models with observations*, *Phys.Rev.* **D50** (1994) 4827–4834, [[astro-ph/9403037](#)].
- [130] D. Polarski and A. A. Starobinsky, *Structure of primordial gravitational waves spectrum in a double inflationary model*, *Phys.Lett.* **B356** (1995) 196–204, [[astro-ph/9505125](#)].
- [131] D. Parkinson, S. Tsujikawa, B. A. Bassett, and L. Amendola, *Testing for double inflation with WMAP*, *Phys.Rev.* **D71** (2005) 063524, [[astro-ph/0409071](#)].
- [132] S. Tsujikawa, D. Parkinson, and B. A. Bassett, *Correlation - consistency cartography of the double inflation landscape*, *Phys.Rev.* **D67** (2003) 083516, [[astro-ph/0210322](#)].
- [133] A. D. Linde, *Hybrid inflation*, *Phys.Rev.* **D49** (1994) 748–754, [[astro-ph/9307002](#)].
- [134] D. H. Lyth and E. D. Stewart, *More varieties of hybrid inflation*, *Phys.Rev.* **D54** (1996) 7186–7190, [[hep-ph/9606412](#)].
- [135] J. Martin, C. Ringeval, and R. Trotta, *Hunting Down the Best Model of Inflation with Bayesian Evidence*, *Phys. Rev.* **D83** (2011) 063524, [[arXiv:1009.4157](#)].
- [136] J. Martin and D. J. Schwarz, *WKB approximation for inflationary cosmological perturbations*, *Phys.Rev.* **D67** (2003) 083512, [[astro-ph/0210090](#)].
- [137] R. Casadio, F. Finelli, M. Luzzi, and G. Venturi, *Improved WKB analysis of cosmological perturbations*, *Phys.Rev.* **D71** (2005) 043517, [[gr-qc/0410092](#)].
- [138] R. Casadio, F. Finelli, M. Luzzi, and G. Venturi, *Higher order slow-roll predictions for inflation*, *Phys.Lett.* **B625** (2005) 1–6, [[gr-qc/0506043](#)].
- [139] R. Casadio, F. Finelli, M. Luzzi, and G. Venturi, *Improved WKB analysis of slow-roll inflation*, *Phys.Rev.* **D72** (2005) 103516, [[gr-qc/0510103](#)].
- [140] J.-O. Gong and E. D. Stewart, *The Density perturbation power spectrum to second order corrections in the slow roll expansion*, *Phys.Lett.* **B510** (2001) 1–9, [[astro-ph/0101225](#)].
- [141] J. Choe, J.-O. Gong, and E. D. Stewart, *Second order general slow-roll power spectrum*, *JCAP* **0407** (2004) 012, [[hep-ph/0405155](#)].
- [142] S. M. Leach, A. R. Liddle, J. Martin, and D. J. Schwarz, *Cosmological parameter estimation and the inflationary cosmology*, *Phys.Rev.* **D66** (2002) 023515, [[astro-ph/0202094](#)].
- [143] A. G. Riess, L. Macri, S. Casertano, M. Sosey, H. Lampeitl, et al., *A Redetermination of the Hubble Constant with the Hubble Space Telescope from a Differential Distance Ladder*, *Astrophys.J.* **699** (2009) 539–563, [[arXiv:0905.0695](#)].

- [144] C. Ringeval, T. Suyama, and J. Yokoyama, *Magneto-reheating constraints from curvature perturbations*, [arXiv:1302.6013](#).
- [145] **ATLAS Collaboration** Collaboration, G. Aad et al., *Observation of a new particle in the search for the Standard Model Higgs boson with the ATLAS detector at the LHC*, *Phys.Lett. B* **716** (2012) 1–29, [[arXiv:1207.7214](#)].
- [146] **CMS Collaboration** Collaboration, S. Chatrchyan et al., *Observation of a new boson at a mass of 125 GeV with the CMS experiment at the LHC*, *Phys.Lett. B* **716** (2012) 30–61, [[arXiv:1207.7235](#)].
- [147] F. Bezrukov and M. Shaposhnikov, *The Standard Model Higgs boson as the inflaton*, *Phys.Lett. B* **659** (2008) 703–706, [[arXiv:0710.3755](#)].
- [148] F. L. Bezrukov, A. Magnin, and M. Shaposhnikov, *Standard Model Higgs boson mass from inflation*, *Phys.Lett. B* **675** (2009) 88–92, [[arXiv:0812.4950](#)].
- [149] F. Bezrukov and M. Shaposhnikov, *Standard Model Higgs boson mass from inflation: Two loop analysis*, *JHEP* **0907** (2009) 089, [[arXiv:0904.1537](#)].
- [150] N. D. Birrell and P. C. W. Davies, *Quantum Fields In Curved Space*. Cambridge Univ. Pr., 1982.
- [151] G. Esposito-Farese and D. Polarski, *Scalar tensor gravity in an accelerating universe*, *Phys.Rev. D* **63** (2001) 063504, [[gr-qc/0009034](#)].
- [152] J. Garcia-Bellido, D. G. Figueroa, and J. Rubio, *Preheating in the Standard Model with the Higgs-Inflaton coupled to gravity*, *Phys.Rev. D* **79** (2009) 063531, [[arXiv:0812.4624](#)].
- [153] O. Bertolami, P. Frazao, and J. Paramos, *Reheating via a generalized non-minimal coupling of curvature to matter*, *Phys.Rev. D* **83** (2011) 044010, [[arXiv:1010.2698](#)].
- [154] H. Motohashi and A. Nishizawa, *Reheating after $f(R)$ inflation*, *Phys.Rev. D* **86** (2012) 083514, [[arXiv:1204.1472](#)].
- [155] A. Barvinsky, A. Y. Kamenshchik, and A. Starobinsky, *Inflation scenario via the Standard Model Higgs boson and LHC*, *JCAP* **0811** (2008) 021, [[arXiv:0809.2104](#)].
- [156] A. De Simone, M. P. Hertzberg, and F. Wilczek, *Running Inflation in the Standard Model*, *Phys.Lett. B* **678** (2009) 1–8, [[arXiv:0812.4946](#)].
- [157] A. Barvinsky, A. Y. Kamenshchik, C. Kiefer, A. Starobinsky, and C. Steinwachs, *Higgs boson, renormalization group, and naturalness in cosmology*, *Eur.Phys.J. C* **72** (2012) 2219, [[arXiv:0910.1041](#)].
- [158] F. Bezrukov, A. Magnin, M. Shaposhnikov, and S. Sibiryakov, *Higgs inflation: consistency and generalisations*, *JHEP* **1101** (2011) 016, [[arXiv:1008.5157](#)].
- [159] C. F. Steinwachs and A. Y. Kamenshchik, *Non-minimal Higgs Inflation and Frame Dependence in Cosmology*, [arXiv:1301.5543](#).
- [160] M. Abramowitz and I. A. Stegun, *Handbook of mathematical functions with formulas, graphs, and mathematical tables*. National Bureau of Standards, Washington, US, ninth ed., 1970.
- [161] I. S. Gradshteyn and I. M. Ryzhik, *Table of Integrals, Series, and Products*. Academic Press, New York and London, 1965.
- [162] A. Vilenkin, *Eternal inflation and chaotic terminology*, [gr-qc/0409055](#).
- [163] A. D. Linde, *Chaotic Inflating Universe*, *JETP Lett.* **38** (1983) 176–179.
- [164] M. Madsen and P. Coles, *CHAOTIC INFLATION*, *Nucl.Phys. B* **298** (1988) 701–725.
- [165] G. Lazarides and Q. Shafi, *A Predictive inflationary scenario without the gauge singlet*, *Phys.Lett. B* **308** (1993) 17–22, [[hep-ph/9304247](#)].

- [166] L. Kofman, A. D. Linde, and A. A. Starobinsky, *Reheating after inflation*, *Phys.Rev.Lett.* **73** (1994) 3195–3198, [[hep-th/9405187](#)].
- [167] G. Lazarides and Q. Shafi, *Topological defects and inflation*, *Phys.Lett.* **B372** (1996) 20–24, [[hep-ph/9510275](#)].
- [168] D. Baumann, A. Dymarsky, I. R. Klebanov, and L. McAllister, *Towards an Explicit Model of D-brane Inflation*, *JCAP* **0801** (2008) 024, [[arXiv:0706.0360](#)].
- [169] E. Silverstein and A. Westphal, *Monodromy in the CMB: Gravity Waves and String Inflation*, *Phys.Rev.* **D78** (2008) 106003, [[arXiv:0803.3085](#)].
- [170] R. H. Brandenberger, A. Knauf, and L. C. Lorenz, *Reheating in a Brane Monodromy Inflation Model*, *JHEP* **0810** (2008) 110, [[arXiv:0808.3936](#)].
- [171] K. Nakayama and F. Takahashi, *Higgs Chaotic Inflation in Standard Model and NMSSM*, *JCAP* **1102** (2011) 010, [[arXiv:1008.4457](#)].
- [172] A. Vilenkin, *Quantum Fluctuations in the New Inflationary Universe*, *Nucl. Phys.* **B226** (1983) 527.
- [173] A. Vilenkin, *The Birth of Inflationary Universes*, *Phys. Rev.* **D27** (1983) 2848.
- [174] A. Goncharov, A. D. Linde, and V. F. Mukhanov, *The Global Structure of the Inflationary Universe*, *Int. J. Mod. Phys.* **A2** (1987) 561–591.
- [175] A. D. Linde, D. A. Linde, and A. Mezhlumian, *From the Big Bang theory to the theory of a stationary universe*, *Phys. Rev.* **D49** (1994) 1783–1826, [[gr-qc/9306035](#)].
- [176] A. A. Starobinsky, *Stochastic De Sitter (Inflationary) Stage in the Early Universe*, .
- [177] J. Martin and M. Musso, *Solving stochastic inflation for arbitrary potentials*, *Phys. Rev.* **D73** (2006) 043516, [[hep-th/0511214](#)].
- [178] J. Martin and M. Musso, *On the reliability of the Langevin perturbative solution in stochastic inflation*, *Phys. Rev.* **D73** (2006) 043517, [[hep-th/0511292](#)].
- [179] R. Mohapatra, A. Perez-Lorenzana, and C. A. de Sousa Pires, *Inflation in models with large extra dimensions driven by a bulk scalar field*, *Phys.Rev.* **D62** (2000) 105030, [[hep-ph/0003089](#)].
- [180] F. Cao, *Generalized chaotic inflation*, [astro-ph/0205207](#).
- [181] M. Bellini, *Fresh inflation with nonminimally coupled inflaton field*, *Gen.Rel.Grav.* **34** (2002) 1953–1961, [[hep-ph/0205171](#)].
- [182] M. Bellini, *Fresh inflation with increasing cosmological parameter*, *Phys.Rev.* **D67** (2003) 027303, [[gr-qc/0211044](#)].
- [183] C.-S. Chen and C.-M. Lin, *Type II Seesaw Higgs Triplet as the inflaton for Chaotic Inflation and Leptogenesis*, *Phys.Lett.* **B695** (2011) 9–12, [[arXiv:1009.5727](#)].
- [184] A. Bouaouda, R. Zarrouki, H. Chakir, and M. Bennai, *F-term braneworld inflation in light of five-year WMAP observations*, *Int.J.Mod.Phys.* **A25** (2010) 3445–3451, [[arXiv:1010.4884](#)].
- [185] V. N. Senoguz and Q. Shafi, *Chaotic inflation, radiative corrections and precision cosmology*, *Phys. Lett.* **B668** (2008) 6–10, [[arXiv:0806.2798](#)].
- [186] K. Freese, J. A. Frieman, and A. V. Olinto, *Natural inflation with pseudo - Nambu-Goldstone bosons*, *Phys.Rev.Lett.* **65** (1990) 3233–3236.
- [187] F. C. Adams, J. R. Bond, K. Freese, J. A. Frieman, and A. V. Olinto, *Natural inflation: Particle physics models, power law spectra for large scale structure, and constraints from COBE*, *Phys.Rev.* **D47** (1993) 426–455, [[hep-ph/9207245](#)].

- [188] R. Peccei and H. R. Quinn, *Constraints Imposed by CP Conservation in the Presence of Instantons*, *Phys.Rev.* **D16** (1977) 1791–1797.
- [189] R. Peccei and H. R. Quinn, *CP Conservation in the Presence of Instantons*, *Phys.Rev.Lett.* **38** (1977) 1440–1443.
- [190] D. Lyth, *Axions and inflation: Sitting in the vacuum*, *Phys.Rev.* **D45** (1992) 3394–3404.
- [191] L. Knox and A. Olinato, *Initial conditions for natural inflation*, *Phys.Rev.* **D48** (1993) 946–949.
- [192] J. Garcia-Bellido, A. D. Linde, and D. Wands, *Density perturbations and black hole formation in hybrid inflation*, *Phys. Rev.* **D54** (1996) 6040–6058, [[astro-ph/9605094](#)].
- [193] D. H. Lyth and A. Riotto, *Particle physics models of inflation and the cosmological density perturbation*, *Phys. Rept.* **314** (1999) 1–146, [[hep-ph/9807278](#)].
- [194] S. Tsujikawa and T. Torii, *Spinodal effect in the natural inflation model*, *Phys.Rev.* **D62** (2000) 043505, [[hep-ph/9912499](#)].
- [195] X. Wang, B. Feng, M. Li, X.-L. Chen, and X. Zhang, *Natural inflation, Planck scale physics and oscillating primordial spectrum*, *Int.J.Mod.Phys.* **D14** (2005) 1347, [[astro-ph/0209242](#)].
- [196] K. Freese and W. H. Kinney, *On: Natural inflation*, *Phys.Rev.* **D70** (2004) 083512, [[hep-ph/0404012](#)].
- [197] C. Savage, K. Freese, and W. H. Kinney, *Natural Inflation: Status after WMAP 3-year data*, *Phys.Rev.* **D74** (2006) 123511, [[hep-ph/0609144](#)].
- [198] G. Panotopoulos, *Cosmic strings and natural inflation*, *JHEP* **0706** (2007) 080, [[arXiv:0706.2747](#)].
- [199] T. W. Grimm, *Axion inflation in type II string theory*, *Phys.Rev.* **D77** (2008) 126007, [[arXiv:0710.3883](#)].
- [200] K. Freese, C. Savage, and W. H. Kinney, *Natural Inflation: The Status after WMAP 3-year data*, *Int.J.Mod.Phys.* **D16** (2008) 2573–2585, [[arXiv:0802.0227](#)].
- [201] S. Mohanty and A. Nautiyal, *Natural inflation at the GUT scale*, *Phys.Rev.* **D78** (2008) 123515, [[arXiv:0807.0317](#)].
- [202] A. Ashoorioon, K. Freese, and J. T. Liu, *Slow nucleation rates in Chain Inflation with QCD Axions or Monodromy*, *Phys.Rev.* **D79** (2009) 067302, [[arXiv:0810.0228](#)].
- [203] G. G. Ross and G. German, *Hybrid natural inflation from non Abelian discrete symmetry*, *Phys.Lett.* **B684** (2010) 199–204, [[arXiv:0902.4676](#)].
- [204] M. E. Olsson, *Inflation assisted by heterotic axions*, *JCAP* **0704** (2007) 019, [[hep-th/0702109](#)].
- [205] D. Maity, *Kinetic Gravity Braiding and axion inflation*, [[arXiv:1209.6554](#)].
- [206] K. Freese, *A Coupling of pseudoNambu-Goldstone bosons to other scalars and role in double field inflation*, *Phys.Rev.* **D50** (1994) 7731–7734, [[astro-ph/9405045](#)].
- [207] W. H. Kinney and K. Mahanthappa, *Natural inflation from Fermion loops*, *Phys.Rev.* **D52** (1995) 5529–5537, [[hep-ph/9503331](#)].
- [208] W. H. Kinney and K. T. Mahanthappa, *Inflation at Low Scales: General Analysis and a Detailed Model*, *Phys. Rev.* **D53** (1996) 5455–5467, [[hep-ph/9512241](#)].
- [209] M. Kawasaki, M. Yamaguchi, and T. Yanagida, *Natural chaotic inflation in supergravity*, *Phys.Rev.Lett.* **85** (2000) 3572–3575, [[hep-ph/0004243](#)].
- [210] G. German, A. Mazumdar, and A. Perez-Lorenzana, *Angular inflation from supergravity*, *Mod.Phys.Lett.* **A17** (2002) 1627–1634, [[hep-ph/0111371](#)].

- [211] N. Arkani-Hamed, H.-C. Cheng, P. Creminelli, and L. Randall, *Extra natural inflation*, *Phys.Rev.Lett.* **90** (2003) 221302, [[hep-th/0301218](#)].
- [212] N. Arkani-Hamed, H.-C. Cheng, P. Creminelli, and L. Randall, *Pseudonatural inflation*, *JCAP* **0307** (2003) 003, [[hep-th/0302034](#)].
- [213] D. E. Kaplan and N. J. Weiner, *Little inflatons and gauge inflation*, *JCAP* **0402** (2004) 005, [[hep-ph/0302014](#)].
- [214] H. Firouzjahi and S. H. Tye, *Closer towards inflation in string theory*, *Phys.Lett.* **B584** (2004) 147–154, [[hep-th/0312020](#)].
- [215] J. P. Hsu and R. Kallosh, *Volume stabilization and the origin of the inflaton shift symmetry in string theory*, *JHEP* **0404** (2004) 042, [[hep-th/0402047](#)].
- [216] R. Gonzalez Felipe and N. Santos, *Natural inflation in 5-D warped backgrounds*, *Phys.Rev.* **D78** (2008) 023519, [[arXiv:0711.0022](#)].
- [217] B. A. Ovrut and S. Thomas, *Instanton induced periodic potentials in nonlinear sigma models*, *Phys.Lett.* **B267** (1991) 227–232.
- [218] J. E. Kim, *Axion and almost massless quark as ingredients of quintessence*, *JHEP* **9905** (1999) 022, [[hep-ph/9811509](#)].
- [219] S. C. Park, *Orbifold GUT inflation*, *JCAP* **0711** (2007) 001, [[arXiv:0704.3920](#)].
- [220] J. Preskill, M. B. Wise, and F. Wilczek, *Cosmology of the Invisible Axion*, *Phys.Lett.* **B120** (1983) 127–132.
- [221] L. Abbott and P. Sikivie, *A Cosmological Bound on the Invisible Axion*, *Phys.Lett.* **B120** (1983) 133–136.
- [222] M. Dine and W. Fischler, *The Not So Harmless Axion*, *Phys.Lett.* **B120** (1983) 137–141.
- [223] A. D. Linde, *Inflation and Axion Cosmology*, *Phys.Lett.* **B201** (1988) 437.
- [224] J. E. Kim, H. P. Nilles, and M. Peloso, *Completing natural inflation*, *JCAP* **0501** (2005) 005, [[hep-ph/0409138](#)].
- [225] S. Dimopoulos, S. Kachru, J. McGreevy, and J. G. Wacker, *N-flation*, *JCAP* **0808** (2008) 003, [[hep-th/0507205](#)].
- [226] Y. N. Obukhov, *Spin driven inflation*, *Phys.Lett.* **A182** (1993) 214–216, [[gr-qc/0008015](#)].
- [227] E. D. Stewart, *Inflation, supergravity and superstrings*, *Phys.Rev.* **D51** (1995) 6847–6853, [[hep-ph/9405389](#)].
- [228] G. Dvali and S. H. Tye, *Brane inflation*, *Phys.Lett.* **B450** (1999) 72–82, [[hep-ph/9812483](#)].
- [229] M. Cicoli, C. Burgess, and F. Quevedo, *Fibre Inflation: Observable Gravity Waves from IIB String Compactifications*, *JCAP* **0903** (2009) 013, [[arXiv:0808.0691](#)].
- [230] G. F. Giudice and H. M. Lee, *Unitarizing Higgs Inflation*, *Phys.Lett.* **B694** (2011) 294–300, [[arXiv:1010.1417](#)].
- [231] B. Ratra and P. Peebles, *Cosmological Consequences of a Rolling Homogeneous Scalar Field*, *Phys.Rev.* **D37** (1988) 3406.
- [232] P. G. Ferreira and M. Joyce, *Cosmology with a primordial scaling field*, *Phys.Rev.* **D58** (1998) 023503, [[astro-ph/9711102](#)].
- [233] D. La and P. J. Steinhardt, *Extended Inflationary Cosmology*, *Phys.Rev.Lett.* **62** (1989) 376.
- [234] E. W. Kolb, *First order inflation*, *Phys.Scripts* **T36** (1991) 199–217.
- [235] Y. Kitada and K.-i. Maeda, *Cosmic no hair theorem in power law inflation*, *Phys.Rev.* **D45** (1992) 1416–1419.

- [236] L. E. Mendes and A. B. Henriques, *Inflation in a simple Kantowski-Sachs model*, *Phys.Lett.* **B254** (1991) 44–48.
- [237] N. Banerjee and S. Sen, *Power law inflation and scalar field cosmology with a causal viscous fluid*, *Phys.Rev.* **D57** (1998) 4614–4619.
- [238] M. Fairbairn and M. H. Tytgat, *Inflation from a tachyon fluid?*, *Phys.Lett.* **B546** (2002) 1–7, [[hep-th/0204070](#)].
- [239] M. Sami, P. Chingangbam, and T. Qureshi, *Aspects of tachyonic inflation with exponential potential*, *Phys.Rev.* **D66** (2002) 043530, [[hep-th/0205179](#)].
- [240] V. H. Cardenas, *Tachyonic quintessential inflation*, *Phys.Rev.* **D73** (2006) 103512, [[gr-qc/0603013](#)].
- [241] J. M. Aguirregabiria, L. P. Chimento, A. S. Jakubi, and R. Lazkoz, *Symmetries leading to inflation*, *Phys.Rev.* **D67** (2003) 083518, [[gr-qc/0303010](#)].
- [242] K. Becker, M. Becker, and A. Krause, *M-theory inflation from multi M5-brane dynamics*, *Nucl.Phys.* **B715** (2005) 349–371, [[hep-th/0501130](#)].
- [243] M. Bennai, H. Chakir, and Z. Sakhi, *On Inflation Potentials in Randall-Sundrum Braneworld Model*, *Eur.J.Phys.* **9** (2006) 84–93, [[arXiv:0806.1137](#)].
- [244] F. Lucchin and S. Matarrese, *Power Law Inflation*, *Phys.Rev.* **D32** (1985) 1316.
- [245] J. Yokoyama and K.-i. Maeda, *On the Dynamics of the Power Law Inflation Due to an Exponential Potential*, *Phys.Lett.* **B207** (1988) 31.
- [246] A. R. Liddle, *POWER LAW INFLATION WITH EXPONENTIAL POTENTIALS*, *Phys.Lett.* **B220** (1989) 502.
- [247] B. Ratra, *INFLATION IN AN EXPONENTIAL POTENTIAL SCALAR FIELD MODEL*, *Phys.Rev.* **D45** (1992) 1913–1952.
- [248] B. Ratra, *QUANTUM MECHANICS OF EXPONENTIAL POTENTIAL INFLATION*, *Phys.Rev.* **D40** (1989) 3939.
- [249] H.-J. Schmidt, *New exact solutions for power law inflation Friedmann models*, *Astron.Nachr.* **311** (1990) 165, [[gr-qc/0109004](#)].
- [250] R. Maartens, D. Taylor, and N. Roussos, *Exact inflationary cosmologies with exit*, *Phys.Rev.* **D52** (1995) 3358–3364.
- [251] E. J. Copeland, A. R. Liddle, and D. Wands, *Exponential potentials and cosmological scaling solutions*, *Phys.Rev.* **D57** (1998) 4686–4690, [[gr-qc/9711068](#)].
- [252] S. Hirai and T. Takami, *Length of inflation and WMAP data in the case of power-law inflation*, [[astro-ph/0506479](#)].
- [253] J. M. Heinzle and A. D. Rendall, *Power-law inflation in spacetimes without symmetry*, *Commun.Math.Phys.* **269** (2007) 1–15, [[gr-qc/0506134](#)].
- [254] J. P. Conlon and F. Quevedo, *Kahler moduli inflation*, *JHEP* **0601** (2006) 146, [[hep-th/0509012](#)].
- [255] J. R. Bond, L. Kofman, S. Prokushkin, and P. M. Vaudrevange, *Roulette inflation with Kahler moduli and their axions*, *Phys.Rev.* **D75** (2007) 123511, [[hep-th/0612197](#)].
- [256] H.-X. Yang and H.-L. Ma, *Two-field Kahler moduli inflation on large volume moduli stabilization*, *JCAP* **0808** (2008) 024, [[arXiv:0804.3653](#)].
- [257] S. Krippendorff and F. Quevedo, *Metastable SUSY Breaking, de Sitter Moduli Stabilisation and Kahler Moduli Inflation*, *JHEP* **0911** (2009) 039, [[arXiv:0901.0683](#)].

- [258] J. J. Blanco-Pillado, D. Buck, E. J. Copeland, M. Gomez-Reino, and N. J. Nunes, *Kahler Moduli Inflation Revisited*, *JHEP* **1001** (2010) 081, [[arXiv:0906.3711](#)].
- [259] M. Kawasaki and K. Miyamoto, *Kahler moduli double inflation*, *JCAP* **1102** (2011) 004, [[arXiv:1010.3095](#)].
- [260] S. Lee and S. Nam, *Kähler moduli inflation and WMAP7*, *Int. J. Mod. Phys. A* **26** (2011) 1073–1096, [[arXiv:1006.2876](#)].
- [261] A. R. Liddle, *On the inflationary flow equations*, *Phys. Rev. D* **68** (2003) 103504, [[astro-ph/0307286](#)].
- [262] E. J. Copeland, I. J. Grivell, E. W. Kolb, and A. R. Liddle, *On the reliability of inflaton potential reconstruction*, *Phys. Rev. D* **58** (1998) 043002, [[astro-ph/9802209](#)].
- [263] E. Ramirez and A. R. Liddle, *Stochastic approaches to inflation model building*, *Phys. Rev. D* **71** (2005) 123510, [[astro-ph/0502361](#)].
- [264] S. R. Coleman and E. J. Weinberg, *Radiative Corrections as the Origin of Spontaneous Symmetry Breaking*, *Phys.Rev. D* **7** (1973) 1888–1910.
- [265] P. M. Stevenson, *The Gaussian Effective Potential. 1. Quantum Mechanics*, *Phys.Rev. D* **30** (1984) 1712.
- [266] P. M. Stevenson, *The Gaussian Effective Potential. 2. Lambda phi**4 Field Theory*, *Phys.Rev. D* **32** (1985) 1389–1408.
- [267] P. M. Stevenson and I. Roditi, *THE GAUSSIAN EFFECTIVE POTENTIAL. III. PHI**6 THEORY AND BOUND STATES*, *Phys.Rev. D* **33** (1986) 2305–2315.
- [268] P. M. Stevenson, *DIMENSIONAL CONTINUATION AND THE TWO lambda phi**4 in four-dimensions THEORIES*, *Z.Phys. C* **35** (1987) 467.
- [269] P. M. Stevenson and R. Tarrach, *The Return of Lambda phi**4*, *Phys.Lett. B* **176** (1986) 436.
- [270] P. M. Stevenson, B. Alles, and R. Tarrach, *O(n) Symmetric Lambda phi**4 Theory: The Gaussian Effective Potential Approach*, *Phys.Rev. D* **35** (1987) 2407.
- [271] P. M. Stevenson, G. Hajj, and J. Reed, *FERMIONS AND THE GAUSSIAN EFFECTIVE POTENTIAL*, *Phys.Rev. D* **34** (1986) 3117.
- [272] G. Hajj and P. M. Stevenson, *FINITE TEMPERATURE EFFECTS ON THE GAUSSIAN EFFECTIVE POTENTIAL*, *Phys.Rev. D* **37** (1988) 413.
- [273] R. Ibanez-Meier, I. Stancu, and P. M. Stevenson, *Gaussian effective potential for the U(1) Higgs model*, *Z.Phys. C* **70** (1996) 307–320, [[hep-ph/9207276](#)].
- [274] L. Abbott, *GRAVITATIONAL EFFECTS ON THE SU(5) BREAKING PHASE TRANSITION FOR A COLEMAN-WEINBERG POTENTIAL*, *Nucl.Phys. B* **185** (1981) 233.
- [275] A. Albrecht, L. G. Jensen, and P. J. Steinhardt, *INFLATION IN SU(5) GUT MODELS COUPLED TO GRAVITY*, *Nucl.Phys. B* **239** (1984) 290.
- [276] A. Albrecht and R. H. Brandenberger, *ON THE REALIZATION OF NEW INFLATION*, *Phys.Rev. D* **31** (1985) 1225.
- [277] J. R. Ellis, D. V. Nanopoulos, K. A. Olive, and K. Tamvakis, *PRIMORDIAL SUPERSYMMETRIC INFLATION*, *Nucl.Phys. B* **221** (1983) 524.
- [278] Q. Shafi and A. Vilenkin, *Inflation with SU(5)*, *Phys.Rev.Lett.* **52** (1984) 691–694.
- [279] R. Langbein, K. Langfeld, H. Reinhardt, and L. von Smekal, *Natural slow roll inflation*, *Mod.Phys.Lett. A* **11** (1996) 631–646, [[hep-ph/9310335](#)].
- [280] P. Gonzalez-Diaz, *PRIMORDIAL KALUZA-KLEIN INFLATION*, *Phys.Lett. B* **176** (1986) 29–32.

- [281] J. Yokoyama, *Chaotic new inflation and primordial spectrum of adiabatic fluctuations*, *Phys.Rev.* **D59** (1999) 107303.
- [282] Y.-g. Gong, *Constraints on inflation in Einstein-Brans-Dicke frame*, *Phys.Rev.* **D59** (1999) 083507, [[gr-qc/9808057](#)].
- [283] M. U. Rehman, Q. Shafi, and J. R. Wickman, *GUT Inflation and Proton Decay after WMAP5*, *Phys.Rev.* **D78** (2008) 123516, [[arXiv:0810.3625](#)].
- [284] C. Vayonakis, *NATURAL VALUES OF COUPLING CONSTANTS AND COSMOLOGICAL INFLATION IN A SUPERSYMMETRIC MODEL*, *Phys.Lett.* **B123** (1983) 396.
- [285] A.-C. Davis and M. Majumdar, *Inflation in supersymmetric cosmic string theories*, *Phys.Lett.* **B460** (1999) 257–262, [[hep-ph/9904392](#)].
- [286] L. Covi, *Models of inflation, supersymmetry breaking and observational constraints*, [[hep-ph/0012245](#)].
- [287] G. Dvali, Q. Shafi, and S. Solganik, *D-brane inflation*, [[hep-th/0105203](#)].
- [288] N. T. Jones, H. Stoica, and S. H. Tye, *Brane interaction as the origin of inflation*, *JHEP* **0207** (2002) 051, [[hep-th/0203163](#)].
- [289] M. Kawasaki and F. Takahashi, *Inflation model with lower multipoles of the CMB suppressed*, *Phys.Lett.* **B570** (2003) 151–153, [[hep-ph/0305319](#)].
- [290] A. Safsafi, A. Bouaouda, R. Zarrouki, H. Chakir, and M. Bennai, *Supersymmetric braneworld inflation in light of WMAP7 observations*, *Int.J.Theor.Phys.* **51** (2012) 1774–1782.
- [291] P. Binetruy and G. Dvali, *D term inflation*, *Phys.Lett.* **B388** (1996) 241–246, [[hep-ph/9606342](#)].
- [292] E. Halyo, *Hybrid inflation from supergravity D terms*, *Phys.Lett.* **B387** (1996) 43–47, [[hep-ph/9606423](#)].
- [293] T. Matsuda, *Successful D term inflation with moduli*, *Phys.Lett.* **B423** (1998) 35–39, [[hep-ph/9705448](#)].
- [294] J. Espinosa, A. Riotto, and G. G. Ross, *D - term inflation in superstring theories*, *Nucl.Phys.* **B531** (1998) 461–477, [[hep-ph/9804214](#)].
- [295] C. F. Kolda and D. H. Lyth, *D term inflation and M theory*, [[hep-ph/9812234](#)].
- [296] E. Halyo, *D term inflation in type I string theory*, *Phys.Lett.* **B454** (1999) 223–227, [[hep-ph/9901302](#)].
- [297] D. Suematsu, *D term inflation and neutrino mass*, *JHEP* **0210** (2002) 014, [[hep-ph/0207041](#)].
- [298] M. Gomez-Reino and I. Zavala, *Recombination of intersecting D-branes and cosmological inflation*, *JHEP* **0209** (2002) 020, [[hep-th/0207278](#)].
- [299] E. Halyo, *Inflation on fractional branes: D-brane inflation as D term inflation*, *JHEP* **0407** (2004) 080, [[hep-th/0312042](#)].
- [300] J. Urrestilla, A. Achucarro, and A. Davis, *D term inflation without cosmic strings*, *Phys.Rev.Lett.* **92** (2004) 251302, [[hep-th/0402032](#)].
- [301] K. Dasgupta, J. P. Hsu, R. Kallosh, A. D. Linde, and M. Zagermann, *D3/D7 brane inflation and semilocal strings*, *JHEP* **0408** (2004) 030, [[hep-th/0405247](#)].
- [302] E. Halyo, *P-term inflation on D-branes*, [[hep-th/0405269](#)].
- [303] G. Panotopoulos, *D-term inflation in D-brane cosmology*, *Phys.Lett.* **B623** (2005) 185–191, [[hep-ph/0503071](#)].

- [304] C.-M. Lin and J. McDonald, *Supergravity modification of D-term hybrid inflation: Solving the cosmic string and spectral index problems via a right-handed sneutrino*, *Phys.Rev.* **D74** (2006) 063510, [[hep-ph/0604245](#)].
- [305] C.-M. Lin and J. McDonald, *Supergravity and two-field inflation effects in right-handed sneutrino modified D-term inflation*, *Phys.Rev.* **D77** (2008) 063529, [[arXiv:0710.4273](#)].
- [306] J. McDonald, *F term hybrid inflation, the eta problem and extra dimensions*, *JHEP* **0212** (2002) 029, [[hep-ph/0201016](#)].
- [307] A. Hebecker, S. C. Kraus, D. Lust, S. Steinfurt, and T. Weigand, *Fluxbrane Inflation*, *Nucl.Phys.* **B854** (2012) 509–551, [[arXiv:1104.5016](#)].
- [308] G. Dvali, *Natural inflation in SUSY and gauge mediated curvature of the flat directions*, *Phys.Lett.* **B387** (1996) 471–477, [[hep-ph/9605445](#)].
- [309] E. Halyo, *Inflation in Wess–Zumino Models*, [arXiv:1001.4812](#).
- [310] A. A. Starobinsky, *A new type of isotropic cosmological models without singularity*, *Phys. Lett.* **B91** (1980) 99–102.
- [311] K. Stelle, *Classical Gravity with Higher Derivatives*, *Gen.Rel.Grav.* **9** (1978) 353–371.
- [312] P. Teyssandier and P. Tournenc, *The Cauchy problem for the $R+R^{**2}$ theories of gravity without torsion*, *J.Math.Phys.* **24** (1983) 2793.
- [313] K.-i. Maeda, *Towards the Einstein-Hilbert Action via Conformal Transformation*, *Phys. Rev.* **D39** (1989) 3159.
- [314] D. Wands, *Extended gravity theories and the Einstein-Hilbert action*, *Class.Quant.Grav.* **11** (1994) 269–280, [[gr-qc/9307034](#)].
- [315] A. De Felice, S. Tsujikawa, J. Elliston, and R. Tavakol, *Chaotic inflation in modified gravitational theories*, *JCAP* **1108** (2011) 021, [[arXiv:1105.4685](#)].
- [316] A. De Felice and S. Tsujikawa, *$f(R)$ theories*, *Living Rev.Rel.* **13** (2010) 3, [[arXiv:1002.4928](#)].
- [317] L. Kofman, A. D. Linde, and A. A. Starobinsky, *Inflationary Universe Generated by the Combined Action of a Scalar Field and Gravitational Vacuum Polarization*, *Phys.Lett.* **B157** (1985) 361–367.
- [318] S. Kaneda, S. V. Ketov, and N. Watanabe, *Slow-roll inflation in $(R+R^*4)$ gravity*, *Class.Quant.Grav.* **27** (2010) 145016, [[arXiv:1002.3659](#)].
- [319] S. V. Ketov and A. A. Starobinsky, *Embedding $(R+R^2)$ -Inflation into Supergravity*, *Phys.Rev.* **D83** (2011) 063512, [[arXiv:1011.0240](#)].
- [320] J. Goldstone, *Field Theories with Superconductor Solutions*, *Nuovo Cim.* **19** (1961) 154–164.
- [321] A. D. Linde and D. A. Linde, *Topological defects as seeds for eternal inflation*, *Phys.Rev.* **D50** (1994) 2456–2468, [[hep-th/9402115](#)].
- [322] A. Vilenkin, *Topological inflation*, *Phys.Rev.Lett.* **72** (1994) 3137–3140, [[hep-th/9402085](#)].
- [323] A. M. Green and A. R. Liddle, *Open inflationary universes in the induced gravity theory*, *Phys.Rev.* **D55** (1997) 609–615, [[astro-ph/9607166](#)].
- [324] J. Garcia-Bellido and A. R. Liddle, *Complete power spectrum for an induced gravity open inflation model*, *Phys.Rev.* **D55** (1997) 4603–4613, [[astro-ph/9610183](#)].
- [325] A. D. Linde, *SUPERGRAVITY AND INFLATIONARY UNIVERSE. (IN RUSSIAN)*, *Pisma Zh.Eksp.Teor.Fiz.* **37** (1983) 606–608.
- [326] A. D. Linde, *PRIMORDIAL INFLATION WITHOUT PRIMORDIAL MONOPOLES*, *Phys.Lett.* **B132** (1983) 317–320.
- [327] J. Casas and C. Munoz, *INFLATION FROM SUPERSTRINGS*, *Phys.Lett.* **B216** (1989) 37.

- [328] J. Casas, J. Moreno, C. Munoz, and M. Quiros, *COSMOLOGICAL IMPLICATIONS OF AN ANOMALOUS $U(1)$: INFLATION, COSMIC STRINGS AND CONSTRAINTS ON SUPERSTRING PARAMETERS*, *Nucl.Phys.* **B328** (1989) 272.
- [329] J. Cervantes-Cota and H. Dehnen, *Induced gravity inflation in the standard model of particle physics*, *Nucl.Phys.* **B442** (1995) 391–412, [[astro-ph/9505069](#)].
- [330] S. H. Alexander, *Inflation from D - anti- D -brane annihilation*, *Phys.Rev.* **D65** (2002) 023507, [[hep-th/0105032](#)].
- [331] R. Easther, J. Khoury, and K. Schalm, *Tuning locked inflation: Supergravity versus phenomenology*, *JCAP* **0406** (2004) 006, [[hep-th/0402218](#)].
- [332] J.-O. Gong, *Modular thermal inflation without slow-roll approximation*, *Phys.Lett.* **B637** (2006) 149–155, [[hep-ph/0602106](#)].
- [333] R. Kallosh and A. D. Linde, *Testing String Theory with CMB*, *JCAP* **0704** (2007) 017, [[arXiv:0704.0647](#)].
- [334] G. Lazarides and A. Vamvasakis, *Standard-smooth hybrid inflation*, *Phys.Rev.* **D76** (2007) 123514, [[arXiv:0709.3362](#)].
- [335] M. U. Rehman and Q. Shafi, *Higgs Inflation, Quantum Smearing and the Tensor to Scalar Ratio*, *Phys.Rev.* **D81** (2010) 123525, [[arXiv:1003.5915](#)].
- [336] F. Bauer and D. A. Demir, *Higgs-Palatini Inflation and Unitarity*, *Phys.Lett.* **B698** (2011) 425–429, [[arXiv:1012.2900](#)].
- [337] A. O. Barvinsky, *Standard Model Higgs Inflation: CMB, Higgs Mass and Quantum Cosmology*, *Prog.Theor.Phys.Suppl.* **190** (2011) 1–19, [[arXiv:1012.4523](#)].
- [338] G. Barenboim, *Inflation might be caused by the right: Handed neutrino*, *JHEP* **0903** (2009) 102, [[arXiv:0811.2998](#)].
- [339] R. Kallosh and A. Linde, *New models of chaotic inflation in supergravity*, *JCAP* **1011** (2010) 011, [[arXiv:1008.3375](#)].
- [340] L. Boubekeur and D. Lyth, *Hilltop inflation*, *JCAP* **0507** (2005) 010, [[hep-ph/0502047](#)].
Latex, 20 pages, 5 figures. Minor changes, references added.
- [341] K. Tzirakis and W. H. Kinney, *Inflation over the hill*, *Phys.Rev.* **D75** (2007) 123510, [[astro-ph/0701432](#)].
- [342] B. K. Pal, S. Pal, and B. Basu, *Mutated Hilltop Inflation : A Natural Choice for Early Universe*, *JCAP* **1001** (2010) 029, [[arXiv:0908.2302](#)].
- [343] B. K. Pal, S. Pal, and B. Basu, *A semi-analytical approach to perturbations in mutated hilltop inflation*, *Int.J.Mod.Phys.* **D21** (2012) 1250017, [[arXiv:1010.5924](#)].
- [344] M. Fairbairn, L. Lopez Honorez, and M. Tytgat, *Radion assisted gauge inflation*, *Phys.Rev.* **D67** (2003) 101302, [[hep-ph/0302160](#)].
- [345] A. de la Macorra and S. Lola, *Inflation in S dual superstring models*, *Phys.Lett.* **B373** (1996) 299–305, [[hep-ph/9511470](#)].
- [346] T. Gherghetta, C. F. Kolda, and S. P. Martin, *Flat directions in the scalar potential of the supersymmetric standard model*, *Nucl.Phys.* **B468** (1996) 37–58, [[hep-ph/9510370](#)].
- [347] R. Allahverdi, K. Enqvist, J. Garcia-Bellido, and A. Mazumdar, *Gauge invariant MSSM inflaton*, *Phys.Rev.Lett.* **97** (2006) 191304, [[hep-ph/0605035](#)].
- [348] J. Garcia-Bellido, *Flat direction MSSM (A -term) inflation*, *AIP Conf.Proc.* **878** (2006) 277–283, [[hep-ph/0610152](#)].
- [349] R. Allahverdi, *MSSM flat direction inflation*, *eConf* **C0605151** (2006) 0020, [[hep-ph/0610180](#)].

- [350] D. H. Lyth, *MSSM inflation*, *JCAP* **0704** (2007) 006, [[hep-ph/0605283](#)].
- [351] R. Allahverdi and A. Mazumdar, *Spectral tilt in A-term inflation*, [hep-ph/0610069](#).
- [352] R. Allahverdi, B. Dutta, and A. Mazumdar, *Probing the parameter space for an MSSM inflation and the neutralino dark matter*, *Phys.Rev.* **D75** (2007) 075018, [[hep-ph/0702112](#)].
- [353] K. Enqvist, L. Mether, and S. Nurmi, *Supergravity origin of the MSSM inflation*, *JCAP* **0711** (2007) 014, [[arXiv:0706.2355](#)].
- [354] R. Allahverdi, B. Dutta, and A. Mazumdar, *Attraction towards an inflection point inflation*, *Phys.Rev.* **D78** (2008) 063507, [[arXiv:0806.4557](#)].
- [355] K. Kamada and J. Yokoyama, *On the realization of the MSSM inflation*, *Prog.Theor.Phys.* **122** (2010) 969–986, [[arXiv:0906.3402](#)].
- [356] R. Allahverdi, B. Dutta, and Y. Santoso, *MSSM inflation, dark matter, and the LHC*, *Phys.Rev.* **D82** (2010) 035012, [[arXiv:1004.2741](#)].
- [357] K. Enqvist, A. Mazumdar, and P. Stephens, *Inflection point inflation within supersymmetry*, *JCAP* **1006** (2010) 020, [[arXiv:1004.3724](#)].
- [358] K. Kohri and C.-M. Lin, *Hilltop Supernatural Inflation and Gravitino Problem*, *JCAP* **1011** (2010) 010, [[arXiv:1008.3200](#)].
- [359] A. D. Linde and A. Mezhlumian, *Inflation with Omega not = 1*, *Phys.Rev.* **D52** (1995) 6789–6804, [[astro-ph/9506017](#)].
- [360] A. D. Linde, *A Toy model for open inflation*, *Phys.Rev.* **D59** (1999) 023503, [[hep-ph/9807493](#)].
- [361] R. K. Jain, P. Chingangbam, J.-O. Gong, L. Sriramkumar, and T. Souradeep, *Punctuated inflation and the low CMB multipoles*, *JCAP* **0901** (2009) 009, [[arXiv:0809.3915](#)].
- [362] R. K. Jain, P. Chingangbam, L. Sriramkumar, and T. Souradeep, *The tensor-to-scalar ratio in punctuated inflation*, *Phys.Rev.* **D82** (2010) 023509, [[arXiv:0904.2518](#)].
- [363] D. A. Lowe and S. Roy, *Punctuated eternal inflation via AdS/CFT*, *Phys.Rev.* **D82** (2010) 063508, [[arXiv:1004.1402](#)].
- [364] S. Hotchkiss, A. Mazumdar, and S. Nadathur, *Inflection point inflation: WMAP constraints and a solution to the fine-tuning problem*, *JCAP* **1106** (2011) 002, [[arXiv:1101.6046](#)].
- [365] C. S. Aulakh and I. Garg, *Supersymmetric Seesaw Inflation*, *Phys.Rev.* **D86** (2012) 065001, [[arXiv:1201.0519](#)].
- [366] C. S. Aulakh, *Susy Seesaw Inflation and NMSO(10)GUT*, [arXiv:1210.2042](#).
- [367] L.-M. Wang, V. F. Mukhanov, and P. J. Steinhardt, *On the problem of predicting inflationary perturbations*, *Phys.Lett.* **B414** (1997) 18–27, [[astro-ph/9709032](#)].
- [368] M. Drees and E. Erfani, *Running Spectral Index and Formation of Primordial Black Hole in Single Field Inflation Models*, *JCAP* **1201** (2012) 035, [[arXiv:1110.6052](#)].
- [369] M. Drees and E. Erfani, *Dark Matter Primordial Black Holes and Inflation Models*, [arXiv:1205.4012](#).
- [370] A. Vallinotto, E. J. Copeland, E. W. Kolb, A. R. Liddle, and D. A. Steer, *Inflationary potentials yielding constant scalar perturbation spectral indices*, *Phys.Rev.* **D69** (2004) 103519, [[astro-ph/0311005](#)].
- [371] D. Veberic, *Lambert w function for applications in physics*, *CoRR* **abs/1209.0735** (2012).
- [372] P. Binetruy and M. Gaillard, *Candidates for the Inflaton Field in Superstring Models*, *Phys.Rev.* **D34** (1986) 3069–3083.

- [373] W. H. Kinney and K. Mahanthappa, *Inflation from symmetry breaking below the Planck scale*, *Phys.Lett.* **B383** (1996) 24–27, [[hep-ph/9511460](#)].
- [374] M. Kawasaki and M. Yamaguchi, *A Supersymmetric topological inflation model*, *Phys.Rev.* **D65** (2002) 103518, [[hep-ph/0112093](#)].
- [375] K. Kumekawa, T. Moroi, and T. Yanagida, *Flat potential for inflaton with a discrete R invariance in supergravity*, *Prog.Theor.Phys.* **92** (1994) 437–448, [[hep-ph/9405337](#)].
- [376] J. A. Adams, G. G. Ross, and S. Sarkar, *Natural supergravity inflation*, *Phys.Lett.* **B391** (1997) 271–280, [[hep-ph/9608336](#)].
- [377] K.-I. Izawa and T. Yanagida, *Natural new inflation in broken supergravity*, *Phys.Lett.* **B393** (1997) 331–336, [[hep-ph/9608359](#)].
- [378] K. Izawa, M. Kawasaki, and T. Yanagida, *R invariant topological inflation*, *Prog.Theor.Phys.* **101** (1999) 1129–1133, [[hep-ph/9810537](#)].
- [379] W. Buchmuller, K. Hamaguchi, M. Ratz, and T. Yanagida, *Gravitino and goldstino at colliders*, [[hep-ph/0403203](#)].
- [380] T. Banks, M. Berkooz, S. Shenker, G. W. Moore, and P. Steinhardt, *Modular cosmology*, *Phys.Rev.* **D52** (1995) 3548–3562, [[hep-th/9503114](#)].
- [381] Y. Himemoto and M. Sasaki, *Brane world inflation without inflaton on the brane*, *Phys.Rev.* **D63** (2001) 044015, [[gr-qc/0010035](#)].
- [382] N. Sago, Y. Himemoto, and M. Sasaki, *Quantum fluctuations in brane world inflation without inflaton on the brane*, *Phys.Rev.* **D65** (2002) 024014, [[gr-qc/0104033](#)].
- [383] X. Chen, *Inflation from warped space*, *JHEP* **0508** (2005) 045, [[hep-th/0501184](#)].
- [384] J. D. Barrow, *Graduated Inflationary Universes*, *Phys. Lett.* **B235** (1990) 40–43.
- [385] J. D. Barrow and P. Saich, *The Behavior of intermediate inflationary universes*, *Phys. Lett.* **B249** (1990) 406–410.
- [386] J. D. Barrow and A. R. Liddle, *Perturbation spectra from intermediate inflation*, *Phys. Rev.* **D47** (1993) 5219–5223, [[astro-ph/9303011](#)].
- [387] J. D. Barrow, A. R. Liddle, and C. Pahud, *Intermediate inflation in light of the three-year WMAP observations*, *Phys. Rev.* **D74** (2006) 127305, [[astro-ph/0610807](#)].
- [388] J. D. Barrow, *String-Driven Inflationary and Deflationary Cosmological Models*, *Nucl.Phys.* **B310** (1988) 743–763.
- [389] S. del Campo, R. Herrera, and A. Toloza, *Tachyon Field in Intermediate Inflation*, *Phys.Rev.* **D79** (2009) 083507, [[arXiv:0904.1032](#)].
- [390] H. Farajollahi and A. Ravanpak, *Tachyon Field in Intermediate Inflation on the Brane*, *Phys.Rev.* **D84** (2011) 084017, [[arXiv:1106.2211](#)].
- [391] S. del Campo and R. Herrera, *Warm-Intermediate inflationary universe model*, *JCAP* **0904** (2009) 005, [[arXiv:0903.4214](#)].
- [392] S. del Campo, R. Herrera, and J. Saavedra, *Tachyon warm inflationary universe model in the weak dissipative regime*, *Eur.Phys.J.* **C59** (2009) 913–916, [[arXiv:0812.1081](#)].
- [393] R. Herrera and N. Videla, *Intermediate inflation in Gauss-Bonnet braneworld*, *Eur.Phys.J.* **C67** (2010) 499–505, [[arXiv:1003.5645](#)].
- [394] A. Cid and S. del Campo, *Constraints from CMB in the intermediate Brans-Dicke inflation*, *JCAP* **1101** (2011) 013, [[arXiv:1101.4588](#)].
- [395] A. Cid and S. del Campo, *Intermediate Inflation in the Jordan-Brans-Dicke Theory*, *AIP Conf.Proc.* **1471** (2012) 114–117, [[arXiv:1210.5273](#)].

- [396] J. D. Barrow and N. J. Nunes, *Dynamics of Logamediate Inflation*, *Phys. Rev.* **D76** (2007) 043501, [[arXiv:0705.4426](#)].
- [397] P. Parsons and J. D. Barrow, *Generalized scalar field potentials and inflation*, *Phys.Rev.* **D51** (1995) 6757–6763, [[astro-ph/9501086](#)].
- [398] L. Kofman and A. D. Linde, *Problems with tachyon inflation*, *JHEP* **0207** (2002) 004, [[hep-th/0205121](#)].
- [399] J. L. Davis, T. S. Levi, M. Van Raamsdonk, and K. R. L. Whyte, *Twisted Inflation*, *JCAP* **1009** (2010) 032, [[arXiv:1004.5385](#)].
- [400] D. H. Lyth and A. Riotto, *Generating the Curvature Perturbation at the End of Inflation in String Theory*, *Phys.Rev.Lett.* **97** (2006) 121301, [[astro-ph/0607326](#)].
- [401] J. Bueno Sanchez, K. Dimopoulos, and D. H. Lyth, *A-term inflation and the MSSM*, *JCAP* **0701** (2007) 015, [[hep-ph/0608299](#)].
- [402] A. Chatterjee and A. Mazumdar, *Tuned MSSM Higgses as an inflaton*, *JCAP* **1109** (2011) 009, [[arXiv:1103.5758](#)].
- [403] R. Allahverdi, K. Enqvist, J. Garcia-Bellido, A. Jokinen, and A. Mazumdar, *MSSM flat direction inflation: Slow roll, stability, fine tuning and reheating*, *JCAP* **0706** (2007) 019, [[hep-ph/0610134](#)].
- [404] E. Dudas, N. Kitazawa, S. Patil, and A. Sagnotti, *CMB Imprints of a Pre-Inflationary Climbing Phase*, [arXiv:1202.6630](#).
- [405] J. Trudeau and J. M. Cline, *Warped Radion Inflation*, *JHEP* **1202** (2012) 081, [[arXiv:1111.4257](#)].
- [406] E. Pajer, *Inflation at the Tip*, *JCAP* **0804** (2008) 031, [[arXiv:0802.2916](#)].
- [407] J. S. Alcaniz and F. Carvalho, *Beta-exponential inflation*, *Europhys.Lett.* **79** (2007) 39001, [[astro-ph/0612279](#)].
- [408] C. Panagiotakopoulos, *Hybrid inflation with quasicanonical supergravity*, *Phys.Lett.* **B402** (1997) 257–262, [[hep-ph/9703443](#)].
- [409] C. Panagiotakopoulos, *Blue perturbation spectra from hybrid inflation with canonical supergravity*, *Phys.Rev.* **D55** (1997) 7335–7339, [[hep-ph/9702433](#)].
- [410] L. M. Hall and H. V. Peiris, *Cosmological Constraints on Dissipative Models of Inflation*, *JCAP* **0801** (2008) 027, [[arXiv:0709.2912](#)].
- [411] B. Kyae, *Spectral Index and Non-Gaussianity in Supersymmetric Hybrid Inflation*, *Eur.Phys.J.* **C72** (2012) 1857, [[arXiv:0910.4092](#)].
- [412] H. Hodges and G. Blumenthal, *Arbitrariness of inflationary fluctuation spectra*, *Phys.Rev.* **D42** (1990) 3329–3333.
- [413] P. Channuie, J. Joergensen, and F. Sannino, *Composite Inflation from Super Yang-Mills, Orientifold and One-Flavor QCD*, [arXiv:1209.6362](#).
- [414] S. Choudhury and S. Pal, *Brane inflation in background supergravity*, *Phys.Rev.* **D85** (2012) 043529, [[arXiv:1102.4206](#)].
- [415] S. Choudhury and S. Pal, *Brane inflation: A field theory approach in background supergravity*, [arXiv:1209.5883](#).
- [416] I. Moss, *PRIMORDIAL INFLATION WITH SPONTANEOUS SYMMETRY BREAKING*, *Phys.Lett.* **B154** (1985) 120.
- [417] B. Hu and D. O’Connor, *MIXMASTER INFLATION*, *Phys.Rev.* **D34** (1986) 2535.

- [418] M. Dine and A. Riotto, *An Inflaton candidate in gauge mediated supersymmetry breaking*, *Phys.Rev.Lett.* **79** (1997) 2632–2635, [[hep-ph/9705386](#)].
- [419] A. Riotto, *Inflation and the nature of supersymmetry breaking*, *Nucl.Phys.* **B515** (1998) 413–435, [[hep-ph/9707330](#)].
- [420] D. Cormier and R. Holman, *Spinodal inflation*, *Phys.Rev.* **D60** (1999) 041301, [[hep-ph/9812476](#)].
- [421] D. Cormier and R. Holman, *Spinodal decomposition and inflation: Dynamics and metric perturbations*, *Phys.Rev.* **D62** (2000) 023520, [[hep-ph/9912483](#)].
- [422] S. Bhattacharya, D. Choudhury, D. P. Jatkar, and A. A. Sen, *Brane dynamics in the Randall-Sundrum model, inflation and graceful exit*, *Class.Quant.Grav.* **19** (2002) 5025–5038, [[hep-th/0103248](#)].
- [423] W.-F. Wang, *Exact solution in the cosmological chaotic inflation model with induced gravity*, *Phys.Lett.* **A328** (2004) 255–260.
- [424] T. Fukuyama, T. Kikuchi, and W. Naylor, *Electroweak inflation and reheating in the NMSSM*, [[hep-ph/0511105](#)].
- [425] S. Antusch, *Sneutrino hybrid inflation*, *AIP Conf.Proc.* **878** (2006) 284–290, [[hep-ph/0608261](#)].
- [426] P. Brax, S. C. Davis, and M. Postma, *The Robustness of $n(s) \approx 0.95$ in racetrack inflation*, *JCAP* **0802** (2008) 020, [[arXiv:0712.0535](#)].
- [427] J.-O. Gong and N. Sahu, *Inflation in minimal left-right symmetric model with spontaneous D -parity breaking*, *Phys.Rev.* **D77** (2008) 023517, [[arXiv:0705.0068](#)].
- [428] L.-Y. Lee, K. Cheung, and C.-M. Lin, *Comments on SUSY inflation models on the brane*, *Mod.Phys.Lett.* **A25** (2010) 2105–2110, [[arXiv:0912.5423](#)].
- [429] C.-M. Lin and K. Cheung, *Reducing the Spectral Index in Supernatural Inflation*, *Phys.Rev.* **D79** (2009) 083509, [[arXiv:0901.3280](#)].
- [430] C.-M. Lin, *Hilltop Supernatural Inflation*, *Prog.Theor.Phys.Suppl.* **190** (2011) 20–25, [[arXiv:1012.2647](#)].
- [431] S. Khalil and A. Sil, *Right-handed Sneutrino Inflation in SUSY B - L with Inverse Seesaw*, *Phys.Rev.* **D84** (2011) 103511, [[arXiv:1108.1973](#)].
- [432] S. Khalil and A. Sil, *Sneutrino inflation in supersymmetric B - L with inverse seesaw*, *AIP Conf.Proc.* **1467** (2012) 294–297.
- [433] S. Antusch and D. Nolde, *Kähler-driven Tribrid Inflation*, [[arXiv:1207.6111](#)].
- [434] E. D. Stewart, *Flattening the inflaton’s potential with quantum corrections*, *Phys.Lett.* **B391** (1997) 34–38, [[hep-ph/9606241](#)].
- [435] E. D. Stewart, *Flattening the inflaton’s potential with quantum corrections. 2.*, *Phys.Rev.* **D56** (1997) 2019–2023, [[hep-ph/9703232](#)].
- [436] L. Covi, D. H. Lyth, and L. Roszkowski, *Observational constraints on an inflation model with a running mass*, *Phys.Rev.* **D60** (1999) 023509, [[hep-ph/9809310](#)].
- [437] L. Covi and D. H. Lyth, *Running-mass models of inflation, and their observational constraints*, *Phys. Rev.* **D59** (1999) 063515, [[hep-ph/9809562](#)].
- [438] S. M. Leach, I. J. Grivell, and A. R. Liddle, *Black hole constraints on the running mass inflation model*, *Phys.Rev.* **D62** (2000) 043516, [[astro-ph/0004296](#)].
- [439] D. H. Lyth, *Observational constraints on models of inflation from the density perturbation and gravitino production*, [[hep-ph/0012065](#)].

- [440] L. Covi, D. H. Lyth, and A. Melchiorri, *New constraints on the running-mass inflation model*, *Phys. Rev.* **D67** (2003) 043507, [[hep-ph/0210395](#)].
- [441] K. Kadota and E. D. Stewart, *Inflation on moduli space and cosmic perturbations*, *JHEP* **0312** (2003) 008, [[hep-ph/0311240](#)].
- [442] L. Covi, D. H. Lyth, A. Melchiorri, and C. J. Odman, *The running-mass inflation model and WMAP*, *Phys. Rev.* **D70** (2004) 123521, [[astro-ph/0408129](#)].
- [443] G. German, G. G. Ross, and S. Sarkar, *Implementing quadratic supergravity inflation*, *Phys.Lett.* **B469** (1999) 46–54, [[hep-ph/9908380](#)].
- [444] A. D. Linde, *Axions in inflationary cosmology*, *Phys. Lett.* **B259** (1991) 38–47.
- [445] E. J. Copeland, A. R. Liddle, D. H. Lyth, E. D. Stewart, and D. Wands, *False vacuum inflation with Einstein gravity*, *Phys. Rev.* **D49** (1994) 6410–6433, [[astro-ph/9401011](#)].
- [446] C. Panagiotakopoulos, *Hybrid inflation and supergravity*, [hep-ph/0011261](#).
- [447] G. Lazarides, *Supersymmetric hybrid inflation*, [hep-ph/0011130](#).
- [448] S. Clesse and J. Rocher, *Avoiding the blue spectrum and the fine-tuning of initial conditions in hybrid inflation*, *Phys. Rev.* **D79** (2009) 103507, [[arXiv:0809.4355](#)].
- [449] S. Clesse, C. Ringeval, and J. Rocher, *Fractal initial conditions and natural parameter values in hybrid inflation*, *Phys. Rev.* **D80** (2009) 123534, [[arXiv:0909.0402](#)].
- [450] S. Clesse, *Hybrid inflation along waterfall trajectories*, *Phys. Rev.* **D83** (2011) 063518, [[arXiv:1006.4522](#)].
- [451] H. Kodama, K. Kohri, and K. Nakayama, *On the waterfall behavior in hybrid inflation*, *Prog.Theor.Phys.* **126** (2011) 331–350, [[arXiv:1102.5612](#)].
- [452] M. Bento, O. Bertolami, and A. Sen, *Supergravity inflation on the brane*, *Phys.Rev.* **D67** (2003) 023504, [[gr-qc/0204046](#)].
- [453] J. Rocher and M. Sakellariadou, *Constraints on Supersymmetric Grand Unified Theories from Cosmology*, *JCAP* **0503** (2005) 004, [[hep-ph/0406120](#)].
- [454] M. Bastero-Gil, S. F. King, and Q. Shafi, *Supersymmetric hybrid inflation with non-minimal Kaehler potential*, *Phys. Lett.* **B651** (2007) 345–351, [[hep-ph/0604198](#)].
- [455] J. Martin and V. Vennin, *Stochastic Effects in Hybrid Inflation*, *Phys.Rev.* **D85** (2012) 043525, [[arXiv:1110.2070](#)].
- [456] W. H. Kinney and A. Riotto, *Dynamical supersymmetric inflation*, *Astropart. Phys.* **10** (1999) 387–395, [[hep-ph/9704388](#)].
- [457] W. H. Kinney and A. Riotto, *A Signature of inflation from dynamical supersymmetry breaking*, *Phys.Lett.* **B435** (1998) 272–276, [[hep-ph/9802443](#)].
- [458] C. Burgess, M. Majumdar, D. Nolte, F. Quevedo, G. Rajesh, et al., *The Inflationary brane anti-brane universe*, *JHEP* **0107** (2001) 047, [[hep-th/0105204](#)].
- [459] G. Shiu and S. H. Tye, *Some aspects of brane inflation*, *Phys.Lett.* **B516** (2001) 421–430, [[hep-th/0106274](#)].
- [460] J. Garcia-Bellido, *Inflation from branes at angles*, [astro-ph/0306195](#).
- [461] L. Pogosian, S. H. Tye, I. Wasserman, and M. Wyman, *Observational constraints on cosmic string production during brane inflation*, *Phys.Rev.* **D68** (2003) 023506, [[hep-th/0304188](#)].
- [462] T. Matsuda, *F term, D term and hybrid brane inflation*, *JCAP* **0311** (2003) 003, [[hep-ph/0302078](#)].
- [463] T. Matsuda, *Brane Q ball, branonium and brane Q ball inflation*, *JCAP* **0410** (2004) 014, [[hep-ph/0402223](#)].

- [464] H.-X. Yang, *D3/D7 inflation in a Type-0B string background*, [hep-th/0504096](#).
- [465] Q.-G. Huang, M. Li, and J.-H. She, *Brane Inflation After WMAP Three Year Results*, *JCAP* **0611** (2006) 010, [[hep-th/0604186](#)].
- [466] R. Bean, S. E. Shandera, S. Henry Tye, and J. Xu, *Comparing brane inflation to WMAP*, *JCAP* **0705** (2007) 004, [[hep-th/0702107](#)].
- [467] R. A. Battye, B. Garbrecht, A. Moss, and H. Stoica, *Constraints on Brane Inflation and Cosmic Strings*, *JCAP* **0801** (2008) 020, [[arXiv:0710.1541](#)].
- [468] S.-H. Henry Tye, *Brane inflation: String theory viewed from the cosmos*, *Lect.Notes Phys.* **737** (2008) 949–974, [[hep-th/0610221](#)].
- [469] R. H. Brandenberger, A. R. Frey, and L. C. Lorenz, *Entropy fluctuations in brane inflation models*, *Int.J.Mod.Phys.* **A24** (2009) 4327–4354, [[arXiv:0712.2178](#)].
- [470] L. Lorenz, *Constraints on brane inflation from WMAP3*, [arXiv:0801.4891](#).
- [471] Y.-Z. Ma and X. Zhang, *Brane inflation revisited after WMAP five year results*, *JCAP* **0903** (2009) 006, [[arXiv:0812.3421](#)].
- [472] K. L. Panigrahi and H. Singh, *Assisted Inflation from Geometric Tachyon*, *JHEP* **0711** (2007) 017, [[arXiv:0708.1679](#)].
- [473] P. S. Kwon, G. Y. Jun, K. L. Panigrahi, and M. Sami, *Inflation driven by single geometric tachyon with D-brane orbiting around NS5-branes*, *Phys.Lett.* **B712** (2012) 10–15, [[arXiv:1106.4118](#)].
- [474] P. Brax, C. A. Savoy, and A. Sil, *SQCD Inflation & SUSY Breaking*, *JHEP* **0904** (2009) 092, [[arXiv:0902.0972](#)].
- [475] P. Peebles and B. Ratra, *Cosmology with a Time Variable Cosmological Constant*, *Astrophys.J.* **325** (1988) L17.
- [476] G. Huey and J. E. Lidsey, *Inflation, brane worlds and quintessence*, *Phys.Lett.* **B514** (2001) 217–225, [[astro-ph/0104006](#)].
- [477] J. D. Barrow and P. Parsons, *Inflationary models with logarithmic potentials*, *Phys.Rev.* **D52** (1995) 5576–5587, [[astro-ph/9506049](#)].
- [478] F. Bezrukov, P. Channuie, J. J. Joergensen, and F. Sannino, *Composite Inflation Setup and Glueball Inflation*, *Phys.Rev.* **D86** (2012) 063513, [[arXiv:1112.4054](#)].
- [479] D. J. Schwarz and C. A. Terrero-Escalante, *Primordial fluctuations and cosmological inflation after WMAP 1.0*, *JCAP* **0408** (2004) 003, [[hep-ph/0403129](#)].